

University of Warwick institutional repository: <http://go.warwick.ac.uk/wrap>

A Thesis Submitted for the Degree of PhD at the University of Warwick

<http://go.warwick.ac.uk/wrap/34794>

This thesis is made available online and is protected by original copyright.

Please scroll down to view the document itself.

Please refer to the repository record for this item for information to help you to cite it. Our policy information is available from the repository home page.

The use of frequency domain parameters
to predict structural fatigue

by

N. W. M. Bishop

A Dissertation submitted for the Degree of
Doctor of Philosophy

Department of Engineering
University of Warwick

December 1988

Summary

The work in this thesis outlines the use of power spectral density data for estimating the Fatigue Damage of structures or components subjected to random loading. Since rainflow cycle counting has been accepted as the best way of estimating the fatigue damage caused by random loadings, an obvious target was a method of obtaining the rainflow range distribution from the PSD. Such a solution is derived in this thesis. It forms the major part of the work presented and appears in chapter 5. The rest of the thesis deals with the following topics;

Chapter 3 first presents some empirical solutions developed by other authors for the prediction of rainflow ranges from PSD's. An empirical solution developed by Dirlik in 1985 is then used to investigate the effect that stresses contained within a given frequency range have on fatigue damage when there are other frequencies present in the PSD plot. This can be thought of as 'fatigue damage potential'. Interactions between stresses in different frequency intervals are investigated and it is shown that the fatigue damage potential of one frequency interval is dependent not only on the magnitude of that interval but on the magnitudes of other frequency intervals present. This 'Interaction' effect within the PSD plot, is of specific interest because it can be used to determine the change of fatigue damage for any given structure or component when parts of the signal or PSD plot are altered.

Chapter 4 is concerned with methods of regenerating a signal from a PSD in the form of a set of peaks and troughs. Work by Kowalewski in 1963 is introduced which gives a solution for the joint distribution of peaks and troughs. This distribution can be used to generate a continuous set of adjacent peaks and troughs, of any length, using Monte-Carlo techniques. Approximations in this result are discussed, in comparison with the (distribution of times between) zero crossings problem. An improvement to this joint distribution of peak and troughs is given which uses an empirical solution for the distribution of 'ordinary ranges' (ranges between adjacent peaks and troughs).

Chapter 5 forms the major part of the original work presented in this thesis and outlines a theoretical solution for the prediction of rainflow ranges using statistics computed directly from the power spectral density plot. The rainflow range mechanism is broken down into a set of logical criteria which can be analyzed using Markov process theory. The dependence between extremes in this instance is modelled using the prediction of the joint distribution of peaks and troughs proposed by Kowalewski, and shown in chapter 4.

Chapter 6 deals with the fatigue damage assessment and stress history determination of components when only limited samples of the service data are available. An investigation is carried out into the relative merits of time and frequency domain techniques. In particular, the effect of finite sample length was investigated with particular reference to the variance of fatigue predictions using both a rainflow count on a limited time sample and a rainflow count produced directly from a PSD of the same time sample. The frequency domain approach is shown to be at least as accurate as the direct time domain approach.

Chapter 7 deals with one specific area where the methods presented in this thesis are applicable, namely, dynamically sensitive offshore structures. Various methods of fatigue damage assessment are highlighted, followed by a detailed description of the 'deterministic/spectral' approach. Many factors which have not previously been recognised are investigated and shown to have significant effect, for instance, tidal effects.

Table of contents

	Summary	(i)
	Table of contents	(ii)
	List of tables and figures	(v)
	List of abbreviations and symbols	(xi)
	Acknowledgements	(xvi)
	Declaration	(xvii)
1.0	Introduction	1
1.1	References	7
2.0	Theoretical tools for the statistical and fatigue damage analysis of random signals	9
2.1	Basic fatigue theory	9
2.2	Cycle counting methods	10
2.3	Probability theory and random variables	13
2.3.1	General assumptions	13
2.3.2	One random variable	14
2.3.3	Two random variables	15
2.4	Power spectra	16
2.5	Random variables which follow a Gaussian (normal) distribution	19
2.6	The statistical analysis of signals which are stationary, ergodic, Gaussian and random using the joint distributions of x , $\frac{dx}{dt}$, $\frac{d^2x}{dt^2}$ and $\frac{d^3x}{dt^3}$	20
2.7	The narrow band solution for calculating the fatigue damage from frequency domain statistics	22
2.8	The distribution of times between zero crossings	24
2.9	References	27
3.0	An investigation of the fatigue damage potential of individual frequency components within any power spectral density plot using an empirical solution for the prediction of 'ordinary' and 'rainflow' ranges	35
3.1	Introduction	35
3.2	Previous solutions to the rainflow range program	36
3.3	A general solution for fatigue damage including the wide band case	38
3.4	Computer programs used for investigation	39
3.4.1	Stage 1. Computation of fatigue damage using narrow band, rainflow range and ordinary range solutions	40
3.4.2	Stage 2. Fatigue damage potential of individual frequency components	42
3.4.3	Stage 3. Interactions between discrete frequency components within the PSD.	43
3.5	Conclusions	44
3.6	References	46

4.0	Signal regeneration using Markov matrices - an improved solution to Kowalewski's joint peak-trough probability density function.	66
4.1	Introduction	66
4.2	Kowalewski's solution for the joint distribution of peaks and troughs.	68
4.2.1	The distribution of maxima	69
4.2.2	The number of points of inflection per second	71
4.2.3	Kowalewski's joint distribution of peaks and troughs	72
4.3	An improvement to Kowalewski's solution for the joint distribution of peaks and troughs.	76
4.4	Generating time signals in the form of a set of peaks and troughs	77
4.5	Cycle counting from a series of peaks and troughs	78
4.6	Results and conclusions	80
4.7	References	83
5.0	A theoretical solution for the prediction of 'rainflow' ranges from power spectral density data	102
5.1	Introduction	102
5.2	Historical background to the theory of rainflow range predictions from power spectral density plots.	103
5.3	A new theoretical solution for the prediction of rainflow ranges.	105
5.4	Markov chains.	107
5.5	Modelling the problem	108
5.6	Outline of computational solution	112
5.6.1	Generation and acquisition of 'real data'	112
5.6.2	Rainflow range count on original signal	112
5.6.3	Power spectral density computation	112
5.6.4	A rainflow count from a set of peaks and troughs generated from Kowalewski's joint probability density function	113
5.6.5	A rainflow range density function produced using the new theoretical solution	113
5.7	Results and discussion.	113
5.8	References	116
6.0	The use of frequency domain techniques to characterise the amplitude content of short lengths of signal.	133
6.1	Introduction	133
6.2	Generating realistic data	135
6.3	Data acquisition	135
6.4	Data qualification	136
6.5	Cycle counting from time signals, with particular reference to short lengths of signal	138
6.6	Frequency domain analysis of time signals	140

6.7	Computational procedure for estimating the fatigue damage from both time and frequency domain information	141
6.8	The variance of fatigue predictions from limited sample sizes using both time and frequency domain methods	142
6.9	Conclusions	144
6.10	References	145
7.0	The dynamic fatigue damage analysis of fixed offshore platforms, with some examination of structures subjected to wind loading.	179
7.1	Introduction	179
7.2	Recap of other Authors work and relevant theory	181
7.2.1	Sea Environment Characterisation	181
7.2.2	Wave Model	183
7.2.3	Member Force Calculation	186
7.2.4	Structural Behaviour	188
7.2.5	Spectral Analysis	190
7.2.6	Fatigue Damage Model	192
7.3	Present Methods of Analysing Wave Loadings	192
7.3.1	Deterministic	193
7.3.2	Transient	195
7.3.3	Spectral	197
7.3.4	Deterministic/Spectral	200
7.3.5	Transient/Spectral	201
7.3.6	Probabilistic	202
7.4	One approach to the analysis of wind loading	202
7.5	Analysis used for this investigation	206
7.5.1	ASAS#G	207
7.5.2	ASAS#WAVE	208
7.5.3	ASAS#RESPONSE	210
7.5.4	ASAS#FATJACK	210
7.5.5	N2	211
7.5.6	N12	212
7.6	Results	212
7.7	Conclusions	216
7.8	References	221
8.0	Conclusions and suggestions for future research	276
9.0	Appendices	281

List of tables and figures

Figure 1.1. A typical stress response PSD plot from a location in a component or structure which exhibits dynamic response.	8
Figure 2.1. A typical stress-life (S-N) diagram.	30
Figure 2.2. The time response which results from the mixture of a low and high frequency.	31
Figure 2.3. The four different types of pattern which are considered in the Pattern Classification Procedure.	32
Figure 2.4. An example of the use of the Pattern Classification Procedure for rainflow cycle counting a short length of time signal.	33
Figure 2.5. The process of obtaining a PSD from a time sample and its use for calculating the spectral moments.	34
Table 3.1. Fatigue damage calculations using the narrow band, ordinary range and rainflow range methods for 11 sea states which are typical of the environmental conditions experienced in the north sea.	48
Table 3.2. A numerical example of the application of equation 3.13, showing 'primary' interactions between frequency components within a rectangular PSD as shown in figure 3.17.	49
Table 3.3. The numerical results for primary interactions at moving strip 11 showing that the sum of the effects of the interacting strips is approximately equal to the fatigue damage potential of strip 11.	50
Table 3.4. Damage results for different values of the following; the number of frequency points used (M), the number of points used in the range probability function (L) and the range probability function integration limit (JN times the rms).	51
Figure 3.1. Basic outline of the three stages of programs used for the investigation.	52
Figure 3.2(a)-3.12(a). Sea state 1-11	53-58
Figure 3.2(b)-3.12(b). Narrow band, ordinary and rainflow range probability density functions computed from sea state 1-11 using equations 2.57, 3.4, 3.5.	53-58
Figure 3.13. The fatigue damage caused by one isolated strip which does not take into account the effect of interactions between frequencies.	59
Figure 3.14. The fatigue damage potential of particular frequencies within sea state 1 calculated with the narrow band, ordinary range and rainflow range methods.	59
Figure 3.15(a). A rectangular PSD with a thin strip removed from a location which is stepped along the frequency axis and called a 'moving strip'.	60
Figure 3.15(b). The effect on fatigue damage of removing one small strip from the PSD.	60
Figure 3.16(a). A rectangular PSD which also has an additional strip present at some remote point.	61
Figure 3.16(b). The effect on fatigue damage of removing one small strip from the PSD is now seen to be affected by the additional strip present at some remote point.	61

Figure 3.17. The method used to assess the effect of primary interactions.	62
Figure 3.18. The effect of an interacting strip on the fatigue damage potential of a particular moving strip computed using rainflow ranges.	63
Figure 3.19. The effect of an interacting strip on the fatigue damage potential of a particular moving strip computed using ordinary ranges.	64
Figure 3.20. The effect of an interacting strip on the fatigue damage potential of a particular moving strip computed using the narrow band assumption.	65
Figure 4.1(a). Kowalewski's peak-trough joint probability density function (equation 4.38), for sea state 1.	85
Figure 4.1(b). A contour plot of Kowalewski's peak-trough joint probability density function (equation 4.38), for sea state 1.	85
Figure 4.2(a). Kowalewski's peak-range joint probability density function (equation 4.42), for sea state 1.	86
Figure 4.2(b). A contour plot of Kowalewski's peak-range joint probability density function (equation 4.42), for sea state 1.	86
Figure 4.3(a). The authors modified peak-range joint probability density function (equation 4.44), for sea state 1.	87
Figure 4.3(b). A contour plot of the authors peak-range joint probability density function (equation 4.44), for sea state 1.	87
Figure 4.4. The use of a peak-range joint probability density function for generating a time history of peaks and troughs.	88
Figure 4.5. The first 251 points in a peak-trough series generated from Kowalewski's peak-range joint probability density function, for sea state 1.	89
Figure 4.6. The narrow band, ordinary and rainflow range probability density functions computed from sea state 1 using equations 2.57, 3.4, 3.5.	90
Figure 4.7. The peak distributions computed from time series of Kowalewski's and the modified peak-range joint distributions compared with the theoretical prediction (equation 2.53), for sea state 1.	90
Figure 4.8. Dirlik's ordinary range solution compared with the ordinary range predictions computed from both the Kowalewski and the modified joint distributions (equations 4.42 and 4.44), for sea state 1.	91
Figure 4.9. Dirlik's rainflow range solution compared with the rainflow range predictions computed from both the Kowalewski and the modified joint distributions (equations 4.42 and 4.44), for sea state 1.	91
Figure 4.10. Kowalewski's peak-range joint probability density function (equation 4.42), for sea state 7.	92
Figure 4.11. The first 251 points in a peak-trough series generated from Kowalewski's peak-range joint probability density function, for sea state 7.	92
Figure 4.12. The narrow band, ordinary and rainflow range probability density functions computed from sea state 7 using equations 2.57, 3.4, 3.5.	93
Figure 4.13. The peak distributions computed from time series of Kowalewski's and the modified peak-range joint distributions compared with the theoretical prediction (equation 2.53), for sea state 7.	93

Figure 4.14. Dirlik's ordinary range solution compared with the ordinary range predictions computed from both the Kowalewski and the modified joint distributions (equations 4.42 and 4.44), for sea state 7.	94
Figure 4.15. Dirlik's rainflow range solution compared with the rainflow range predictions computed from both the Kowalewski and the modified joint distributions (equations 4.42 and 4.44), for sea state 7.	94
Figure 4.16. Kowalewski's peak-range joint probability density function (equation 4.42), for sea state 11.	95
Figure 4.17. The first 251 points in a peak-trough series generated from Kowalewski's peak-range joint probability density function, for sea state 11.	95
Figure 4.18. The narrow band, ordinary and rainflow range probability density functions computed from sea state 11 using equations 2.57, 3.4, 3.5.	96
Figure 4.19. The peak distributions computed from time series of Kowalewski's and the modified peak-range joint distributions compared with the theoretical prediction (equation 2.53), for sea state 11.	96
Figure 4.20. Dirlik's ordinary range solution compared with the ordinary range predictions computed from both the Kowalewski and the modified joint distributions (equations 4.42 and 4.44), for sea state 11.	97
Figure 4.21. Dirlik's rainflow range solution compared with the rainflow range predictions computed from both the Kowalewski and the modified joint distributions (equations 4.42 and 4.44), for sea state 11.	97
Figure 4.22. The b_{th} moment of the ordinary range density functions computed from both the Kowalewski and the modified joint distributions after being normalised by the b_{th} moment of Dirlik's ordinary range density function, for sea state 1.	98
Figure 4.23. The b_{th} moment of the rainflow range density functions computed from both the Kowalewski and the modified joint distributions after being normalised by the b_{th} moment of Dirlik's rainflow range density function, for sea state 1.	98
Figure 4.24(a)-4.26(a) The effect on the normalised 5_{th} moment of the rainflow range density function computed from Kowalewski's joint distribution of varying the sample size, for a matrix size $L=33, 65$ and 101 .	99-101
Figure 4.24(b)-4.26(b) The effect on the normalised 5_{th} moment of the rainflow range density function computed from the modified joint distribution of varying the sample size, for a matrix size $L=33, 65$ and 101 .	99-101
Figure 5.1. The concept of upper and lower bounds on damage compared with that computed using rainflow ranges.	118
Figure 5.2. Rychlik's definition of a rainflow range cycle.	119
Figure 5.3. Discrete form of the authors definition of a rainflow range cycle.	120
Figure 5.4(a). Kowalewski's expression for the dependence between adjacent extremes.	121
Figure 5.4(b). Kowalewski's expression for the dependence between adjacent extremes after both the peak-trough and the trough-peak parts have been normalised to 1.	122
Figure 5.5(a). The peak-trough part of kowalewski's expression (equation 2), for a 16 by 16 element matrix.	123

Figure 5.5(b). The trough-peak part of Kowalewski's expression (equation 2) for a 16 by 16 element matrix.	123
Figure 5.6. The Markov process model used to characterise the steps of figure 2 which are necessary to fully define a rainflow range cycle for a particular peak.	124
Figure 5.7(a). Transition matrix representing peak-trough (1 step) movements for the particular configuration of $ip=10$ and $kp=3$.	125
Figure 5.7(b). Transition matrix representing trough-peak (1 step) movements for the particular configuration of $ip=10$ and $kp=3$.	125
Figure 5.8(a). Transition matrix representing peak-trough-peak (2 step) movements for the particular configuration of $ip=10$ and $kp=3$.	126
Figure 5.8(b). Condensed transition matrix representing peak-trough-peak (2 step) movements for the particular configuration of $ip=10$ and $kp=3$.	126
Figure 5.8(c). Condensed transition matrix after it has been squared enough times to ensure state 4 is empty (2^n steps, where n is the number of times the matrix is squared).	126
Figure 5.9(a-c). A comparison of the rainflow range distributions obtained (data set 2 with 16, 32 and 63 element matrices) using equation 1 (new theoretical solution) with a distribution obtained from a peak-trough count of, (1) the original signal, and (2) a signal regenerated from a Kowalewski peak-trough matrix.	127-129
Figures 5.9(d-f). A comparison of the rainflow range distributions obtained (data sets 1, 3 and 5 and 32 element matrix) using equation 1 (new theoretical solution) with a distribution obtained from a peak-trough count of, (1) the original signal, and (2) a signal regenerated from a Kowalewski peak-trough matrix.	130-132
Tables 6.1-6.5. qualification tests carried out on data sets 1-5	147-156
Table 6.6. Results showing the effect of quantisation on accuracy.	157
Figure 6.1. The output characteristics of the Brüel and Kjaer random signal generator	158
Figure 6.2. The output of one of the low pass filters set to 250 Hz.	159
Figure 6.3(a-e). Power Spectral Density plot computed from data sets 1-5	160-164
Figure 6.4. The effect of quantisation of the signal on the range distributions.	165
Figure 6.5. A study of the percentage error caused by the moment integration elemental strip width (DX), for various values of (b), the slope of the S-N curve, (X) the range value and (A) and (D), the vertical and horizontal axis intersections with a straight line representing the range distribution.	166
Figure 6.6. The eighth possible combinations of the signal tails shown along with the most justifiable method of joining the ends together.	167
Figure 6.7(a). Comparison of ordinary ranges computed directly from full data set with ordinary ranges computed from PSD of full data set using equation 3.4.	168
Figure 6.7(b). Comparison of rainflow ranges computed directly from full data set with rainflow ranges computed from PSD of full data set using equation 3.5.	168
Figure 6.8(a). Moments of ordinary ranges shown in figure 6.7(a)	169
Figure 6.8(b). Moments of rainflow ranges shown in figure 6.7(b)	169
Figures 6.9-6.12. Moments of rainflow ranges from data sets 2-5	170-171
Figure 6.13(a). Mean signal value of sample, normalised by population mean	172

Figure 6.13(b). Narrow band frequency domain prediction of fatigue (using equation 2.58), normalised by rainflow range prediction of time signal ... plotted against sample size	172
Figure 6.14(a). rms computed from PSD of time sample, normalised by population rms ... plotted against sample size	173
Figure 6.14(b). rms computed from time sample, normalised by population rms	173
Figure 6.15(a) Number of peaks per second calculated from PSD of time sample (using equation 2.8), normalised by population number of peaks per second ... plotted against sample size	174
Figure 6.15(b) Number of peaks per second calculated from time sample, normalised by population number of peaks per second ... plotted against sample size	174
Figure 6.16(a). Ordinary range frequency domain prediction of fatigue (using equation 3.4), normalised by ordinary range prediction from PSD of full time signal ... plotted against sample size	175
Figure 6.16(b). Ordinary range time domain prediction of fatigue, directly from time signal, normalised by ordinary range prediction on full time signal ... plotted against sample size	175
Figure 6.17(a). Rainflow range frequency domain prediction of fatigue (using equation 3.5), normalised by rainflow range prediction from PSD of full time signal ... plotted against sample size	176
Figure 6.17(b). Rainflow range time domain prediction of fatigue, directly from time signal, normalised by rainflow range prediction on full time signal ... plotted against sample size	176
Figure 6.18(a). Ordinary range prediction of fatigue from Kowalewski's regenerated signal, normalised by ordinary range prediction on full time signal ... plotted against sample size	177
Figure 6.18(b). Ordinary range prediction of fatigue using the authors regenerated signal, normalised by ordinary range prediction on full time signal ... plotted against sample size	177
Figure 6.19(a). Rainflow range prediction of fatigue from Kowalewski's regenerated signal, normalised by rainflow range prediction on full time signal ... plotted against sample size	178
Figure 6.19(b). Rainflow range prediction of fatigue using the authors regenerated signal, normalised by rainflow range prediction on full time signal ... plotted against sample size	178
Table 7.1. Statistical properties and damage expectations computed from Wirsching's data	225
Table 7.2(i). base wave cases used in ASAS#WAVE	225
Table 7.2(ii). Full ASAS results	226
Table 7.3. N12 results for fatigue damage caused by sea states 1 to 11	228
Table 7.4. N12 results for fatigue damage potential estimation.	231
Table 7.5. The variation of D_N with A_w and B_w	232
Table 7.6. The variation of D_N with b , the slope of the S-N curve, for $A_w=500$ and $B_w=1200$	233

Figure 7.1. The variation of force with depth for different wave periods	234
Figure 7.2(a). Velocity, acceleration and force curves along the wave profile	235
Figure 7.2(b). Results for one vertical member from an ASAS#WAVE run	236
Figure 7.3. The relative effects of the drag and inertia terms on the wave force	237
Figure 7.4. Frequency response plot for a one degree of freedom system	238
Figure 7.5. The interaction effects within any PSD plot	239
Figures 7.6(a-c). Velocity, acceleration and force spectra for sea states 1,6 and 11	240-242
Figure 7.6(d). Velocity, acceleration and force spectra for sea state 6, with various member diameters	243
Figure 7.7. An example of the Deterministic/spectral method	244
Figure 7.8. The effects of varying the parameters A_w and B_w on fatigue damage	245
Figure 7.9. A flow chart of the programs used for analysis	246
Figure 7.10. Plots of structures A and B using ASAS#ASDIS	247
Figure 7.11. The first eight mode shapes for structure B	248
Figure 7.12(a). The sin fitting process with 12, 6 and 4 phase increments for an inertia dominated wave	249
Figure 7.12(b). The sin fitting process for a drag dominated wave	250
Figure 7.12(c). The sin fitting process for a drag dominated wave in the splash zone	250
Figure 7.13(a). Height against force. Conservative linearisation	251
Figure 7.13(b). Height against force. Unconservative linearisation	251
Figure 7.14. The process of obtaining the transfer function	252
Figure 7.15. The variation of fundamental frequency with added mass	253
Figure 7.16. The variation of fatigue life with critical damping	254
Figures 7.17(a-k). Results for sea states 1-11 with transfer function H3	255-265
Figures 7.18(a-k). Fatigue damage potential for sea states 1-11	255-265
Figure 7.19. Different methods of estimating the fatigue damage potential of any response plot	266
Figure 7.20. The variation of fatigue life with a wave angle of 0 degrees representing waves square on to the side	267
Figure 7.21. The variation of fatigue life or damage with elevation of water level at 0.0, representing a water level at a horizontal bracing level	268
Figure 7.22. The maximum response of a structure comprising of a 3 by 3 array of piles for varying wavelength	269
Figure 7.23. The maximum response of a structure comprising of a 3 by 3 array of piles for varying wavelength and waveangle	270
Figures 7.24(a-j). Results for sea state 7 with transfer function D1, D5, D15, D18, E1, E4, G1, G2, G3, and H3	271-275

List of abbreviations and symbols

This section lists the more common symbols and notation used throughout this thesis along with a reference to the first use in the text.

- | | |
|--|--|
| a = factor used in equation 4.7. | $c(b)$ = coefficient in Wirsching's correction factor (3.2). |
| a = water particle acceleration (7.6(b)). | C = sub determinant of A (4.29) |
| a_{ij} = covariance of x_1x_j (2.33). | C = factor in equation 4.9. |
| $a(b)$ = coefficient in Wirsching's correction factor (3.2). | C = sub matrix of P (5.7). |
| A = matrix in n dimensional normal distribution (2.31). | C = factor used in equation 7.118. |
| A = intersection of S-N curve line with vertical axis. | C = damping factor (7.28). |
| A = coefficient in equation 3.9. | $C(f)$ = characteristic function (2.10). |
| A = sub matrix of P (5.7). | $C(f,g)$ = joint characteristic function (2.20). |
| A = factor used in equation 7.118. | C_1, C_2 = coefficients in Dirlik's expression for ordinary ranges (3.4). |
| A = area of incremental section of member (7.15). | $C_{\max}(\eta)$ = characteristic function of maxima (4.31). |
| A = factor in equation 7.25. | $C_{inflex}(\eta)$ = characteristic function of points of inflection (4.32). |
| A_{ij} = cofactor of a_{ij} (2.33). | C_i = factor used in equation 4.44. |
| A_1, A_2 = factors used in program N2. | C_I = inertia coefficient (7.13). |
| A_i = factor used in equation 4.44. | C_D = drag coefficient (7.14). |
| A_1, A_2 = factors used in equation 7.38. | C_1, C_2 = factors used in equation 7.16. |
| a_N = normal acceleration (7.55). | C_c = critical damping factor (7.28) |
| a_T = tangential acceleration (7.55). | C_i = multiplying weighting constant (7.60). |
| $A(t)$ = factor given by equation 7.58(f). | d = factor used in equation 4.9. |
| A_w = factor used in equation 7.88. | d = depth to mean water level. |
| b = slope of S-N curve. | dN = increment of H-N curve. |
| b = factor in equation 4.7. | D = intersection of S-N curve line with horizontal axis. |
| B = factor used in equation 4.7. | D diameter of incremental section of member (7.15). |
| B = sub matrix of P (5.7). | D = sub determinant of A (4.29). |
| B = factor used in equation 7.118. | D = fatigue damage (7.49). |
| B_i = factor used in equation 4.44. | D_1, D_2, D_3 = coefficients in Dirlik's expression for rainflow ranges (3.5). |
| B_j = factor used in equation 4.44. | $dh=Dh$ = stress range interval width. |
| b_2 = slope of H-N curve (7.44). | |
| $B(t)$ = factor given by equation 7.58(g). | |
| B_w = factor used in equation 7.88. | |
| c = wave celerity (7.7). | |

D_i = factor used in equation 4.44.

D_j = factor used in equation 4.44.

D_i = total damage in i_{th} sea state.

D_N = normalised damage (7.100).

$erf(x)$ = error function

$e^{j\omega t} = (\cos\omega t - j\sin\omega t)$ (7.35).

$E[\]$ = expected or mean value (2.5).

$E[P]$ = expected number of peaks per unit time (2.50).

$E[PI]$ = expected number of points of inflection per unit time (2.51).

$E[0]$ = expected number of zeros per unit time (2.49).

$E[\alpha]$ = expected number of level crossings per unit time (2.48).

$E[D]_{NB}$ = fatigue damage based on the narrow band assumption (2.56).

$E[D]_{OR}$ = fatigue damage calculated using ordinary ranges (3.8).

$E[D]_{RR}$ = fatigue damage calculated using rainflow ranges (3.6).

f = frequency in Hertz.

f_n = natural frequency (3.9).

f_{ik}^* = long term transition probability.

f_i = expected frequency of observations (6.1).

f_D = frequency of wave spectrum peak (7.2(b)).

$f(t)$ = fluctuating force (7.87).

$f_R = \sqrt{\frac{1}{B_w}}$ (7.88).

$f_u = \frac{zL_u f}{V_z}$ (7.89).

F = load or force (7.29).

FFT = Fast Fourier Transform.

F_1, F_2 = factors used in program N2.

F_i = observed frequency of observations (6.1).

F_I = inertia component of force (7.12).

F_D = drag component of force (7.12).

F_T = total force (7.12).

F_{TAPP} = approximation to F_T (7.16).

F_0 = maximum load or force (7.29).

$F(t)$ load or force as function of time (7.36)

$\bar{F}(t)$ factor given by equation 7.58(e).

$F_n(z, t)$ = force at depth z on member n at time t .

\bar{F} = static force (7.87).

F_{DN} = denormalising factor (7.100).

F_{T1} = force on one pile (7.120).

F_{TN} = force on N piles (7.120).

g = gravity.

$g(\alpha)$ = probability density function of peaks (2.53).

$G(r)$ = factor given by equation 7.70).

$G_k(f) = G(f)$ = single sided PSD in units of Hertz (2.27).

h = stress range (see section 3.2).

H = wave height.

H_s = significant wave height (3.9)

$H(j\omega)$ = transfer function (7.37).

H_m = maximum wave height in 100 years (7.44).

ip = level of point 1 (see section 5.3).

JN = integration limit for range functions.

k = coefficient from S-N curve.

kp = level of point 2 (see section 5.3).

k = wave number (7.5).

K = factor in equation 4.7.

K = stiffness (7.20).

K = factor used in equation 7.86.

\bar{K} = factor given by equation 7.58(d).

l = factor used in equation 7.68.

L = wave length.

L = matrix size (see section 4.4).

L_s = time sample duration.

*L_u = length scale (7.91).

$m(s)$ = moment generating function (2.8).

$m(s,t)$ = joint moment generating function (2.18).

$m_n = n_{th}$ moment of $G(f)$ (2.28(a)).

M = mass (7.20).

M_G = factor used in equation 7.97).

n = number of cycles at a particular stress range.

n_c = number of sinusoidal components used to fit wave profile (7.54).

N = allowable number of cycles at a particular stress range.

N_m = number of waves in 100 years (7.44).

N_i = number of waves in the i_{th} sea state (7.52).

N_G = total number of wind speed fluctuations (7.94).

$p(x)$ = probability density function (2.3).

$p(x,y)$ = joint probability density function (2.14).

p_{OR} = probability density function of ordinary ranges (3.4).

p_{RR} = probability density function of rainflow ranges (3.5).

$p(x_1, x_2, x_3, \dots, x_n)$ = n dimensional probability density function.

$p(s)$ = probability density function of stress ranges (2.55).

$p_{amp}(\alpha_a)$ = probability density function of amplitudes (4.37).

$p_{min,max}(\alpha_1, \alpha_2)$ = joint probability density function of peaks and troughs (4.38).

$p_{m,amp}(\alpha_m, \alpha_a)$ = joint probability density function of means and amplitudes (4.39).

$p_{m,rng}(\alpha_m, \alpha_{rng})$ = joint probability density function of means and ranges (4.40).

$p_{max,amp}(\alpha_2, \alpha_a)$ = joint probability density function of peaks and amplitudes (4.41).

$p_{max,rng}(\alpha_2, \alpha_{rng})$ = joint probability density function of peaks and ranges (4.42).

$p_{elam}(i,j)$ = joint probability density function calculated from elemental probabilities.

$p(S_n)$ = probability density function of normalised stress range (7.96).

PSD = Power Spectral Density.

P = transition matrix (5.4).

$P(x,y)$ = joint probability distribution function (2.12).

$P(x)$ = probability distribution function (2.2).

P_1, P_2, P_4 = sub matrices of P (5.6).

$P(R,Q)$ = empirical distribution for the heights of sea waves (7.4).

$p(H)$ = Rayleigh distribution (7.51).

Q = coefficient used in Dirlik's expression for rainflow ranges (3.5).

Q_1, Q_2 = factors used in program N2

Q_i = sub matrix of P (5.6).

Q = normalised wave period (7.4).

$Q(t)$ = total force on structure (7.77).

r = wave amplitude (7.4).

rms = root mean square value.

$R_{xy}(\tau)$ = cross correlation function (2.22).

$R_{xx}(\tau) = R(\tau)$ = auto correlation function (2.23).

R = coefficient in Dirlik's expression for rainflow ranges (3.5).

R_{31}, R_{32}, R_{34} = sub matrices of P (5.6).

R = normalised wave height (7.4).

R_{FF} = auto correlation function of wave force on one pile (7.69).

R_{FF}^N = auto correlation of wave force on N piles (7.78).

s = stress range (2.55).

S = stress range (3.6).

$S(\omega)$ = double sided PSD in units of radians (2.24(a)).

$S_{RR}(h)$ = rainflow range probability density function (5.1).

$S_{xy}(\omega)$ = cross spectral density function (2.25(a)).

$S_{\eta\eta}(f)$ = Pierson Moskowitz sea state spectrum (7.2(a)).

$S_{RR}(f)$ = response PSD (7.40).

$S_{FF}(f)$ = force PSD (7.41).

$S_{DD}(f)$ = displacement PSD (7.42).

$S_{\sigma\sigma}(f)$ = stress response PSD (7.43).

$S(H) = a_1H + a_2H^2$

S_d = dynamic response including a dynamic amplification function (7.50).

$S_{gg}(f)$ = PSD representing the sum of a number of random processes (7.60).

$S_{f_i f_i}(f)$ = PSD of generalised forces (7.64).

$S_{z_i z_i}(f)$ = PSD of generalised modal coordinates (7.65).

$S_{x_i x_i}(f)$ = PSD after transformation back into original coordinates (7.66).

$S_{FF}(f)$ = PSD of loading component (7.75).

$S_{uu}(f)$ = PSD of water particle velocities (7.72(a)).

$S_{uu}(f)$ = PSD of wind speed fluctuations (7.88).

$S_{aa}(f)$ = PSD of water particle accelerations (7.72(b)).

$S_{\theta\theta}^N(f)$ = PSD of wave forces on N piles (7.79).

$S_{FF}(f)$ = PSD of loading component (7.75).

$S_{FF}(f)$ = PSD of loading component (7.75).

$S_{FF}(f)$ = PSD of loading component (7.75).

S_n = normalised stress range (7.95).

T = wave period (7.4).

T_D = dominant wave period.

T_z = zero crossing period (7.3).

T_{\min} = lowest natural period of structure (7.59).

$T_{MP}^N(f)$ = transfer function between PSD of force on one pile and the PSD of force on N piles (7.82).

$T(f)$ = transfer function (7.83).

u = stress range level at $y(t)$ (see section 5.3).

u = water particle velocity (7.6(a)).

u_{rms} = rms of velocity fluctuations (7.19).

$V(t)$ = fluctuating wind velocity (7.87).

\bar{V} = mean wind velocity (7.87).

V_z = hourly-mean wind speed (7.91).

$V_{3\beta}$ = sub matrices of P (5.12).

$w_n = n_{th}$ moment of $S(\omega)$ (2.28(b)).

w_1 = circular frequency of oscillation of a one degree of freedom system (7.22).

$x(t)$ = variable as function of time.

$x(k)$ = discrete samples taken of $x(t)$.

\bar{x} = mean value of $x(k)$.

X_k = FFT of $x(k)$ (2.26).

${}^m x = \frac{d^m x}{dt^m}$

x_{var} = coefficient used in Dirlik's expressions (3.4,3.5).

x_m = coefficient used in Dirlik's expressions (3.4,3.5).

x_0 = maximum displacement (7.31).

x_n = horizontal space coordinate for the n_{th} pile in an N pile array measured in the direction of wave travel (7.79).

x_l = horizontal distance from some reference point (7.120).

z = water depth at calculation point (7.6(a)).

z = transformed variable given by equation 7.26.

Z = normalised variable (3.7).

$\lim_{n \rightarrow \infty} P_{\alpha}^n > 0$ (5.10).

ΔD = damage at a particular wave height (7.48).

Δt = increment of time.

Δ_n = number of segment lengths (see section 4.4).

$$\Omega = \frac{w}{w_1} \quad (7.33).$$

Φ = phase shift (7.32).

$$\Pi_\alpha = \lim_{n \rightarrow \infty} P_\alpha^n \quad (5.10).$$

Ψ_{true} = correct estimate (6.2).

Ψ_z = approximate estimate (6.2).

Θ = angle of attack of waves onto side of structure (7.82).

Y_1 = condition 1 of rainflow range test.

Y_2 = condition 2 of rainflow range test.

Y_3 = condition 3 of rainflow range test.

$$Y(v) = 1 + 0.25v^2 \quad (7.4).$$

α = Philips constant (7.2(a)).

α = factor used in equation 7.56.

α_n = n_{th} moment (2.6).

α = variable used for displacement (2.34).

α_1 = trough value.

α_2 = peak value.

α_m = mean value.

α_a = amplitude value.

β = variable used for velocity (2.34).

β = a constant used in equation 7.2(a).

β = factor used in equation 7.56.

$$\beta_a = \frac{1}{\sqrt{\pi}}(\beta_2 - \beta_1) \quad (4.24).$$

$$\beta_m = \frac{1}{\sqrt{\pi}}(\beta_2 + \beta_1) \quad (4.24).$$

χ^2 = chi squared value (6.1).

δ = wave orbit (7.11).

δ_x = elemental probability box size (see section 4.4).

δ_t = time between samples (see section 6.1(a)).

δ_{err} = error in estimation (6.2).

$$\varepsilon = \sqrt{1 - \gamma^2}.$$

η = distance of sea surface elevation from mean water level (7.2(a)).

η_i = critical damping in the i_{th} mode (7.57).

γ = irregularity factor (2.52).

γ_f = factor used in equation 7.16.

$\lambda(b, \varepsilon)$ = Wirsching's correction factor (3.2).

μ = variable used for derivative of acceleration.

ν = factor used in equation 7.4.

ω = circular frequency.

ϕ = coefficient (3.9).

ϕ = variable used for coordinate transformation (7.26).

${}^n \psi_0$ = n_{th} moment of $R_{xx}(\tau)$ at $\tau=0$ (2.59).

${}^n \psi_\tau$ = n_{th} moment of $R_{xx}(\tau)$ (2.59).

ψ = factor used in equation 7.68.

ρ = mass density of water (7.15).

σ_x^2 = variance of $x(k)$ (2.7).

σ_x = standard deviation.

σ = rms (for zero mean valued variable = σ_x).

σ_w^2 = variance of wind speed fluctuations (7.89).

σ_S = rms of stress ranges (7.95).

τ = time separation.

τ = coefficient in Dirlik's expression for ordinary ranges (3.4)

$\bar{\tau}$ = factor used in equation 7.4.

ξ = damping factor (3.9).

ζ = variable used for acceleration (4.5).

$$\zeta_a = \frac{1}{\sqrt{2}}(\zeta_2 - \zeta_1) \quad (4.25).$$

$$\zeta_m = \frac{1}{\sqrt{2}}(\zeta_2 + \zeta_1) \quad (4.25).$$

Acknowledgements

First of all I would like to thank SERC, the University of Warwick and the Department of Engineering for their financial support during the period of this research.

My supervisor was Dr Frank Sherratt and I would like to express my deep appreciation for his encouragement, guidance and advice over the past three and a half years.

This thesis is dedicated to Bella, without whom it would not have been possible.

Declaration

This dissertation is submitted in support of an application for the Degree of Doctor of Philosophy in Engineering Science, from the University of Warwick.

No part of the work contained in the thesis has been submitted for other Degrees or Diplomas from this University or any other Institution.

The work contained in this thesis is original and my own unless otherwise stated in the text.

I declare that this declaration is true in every respect.

N.W.M. Bishop

1. Introduction

The work in this thesis outlines the use of power spectral density data for estimating the Fatigue Damage of structures or components subjected to random loading. Fatigue has been defined as (ref.1.1);

The process of progressive localized permanent structural change occurring in a material subjected to conditions which produce fluctuating stresses and strains at some point or points and which may culminate in cracks or complete fracture after a sufficient number of fluctuations.

Most basic research into material fatigue has been concerned with metals. In these, the fundamental process of crack formation is now known to result from an intensification of slip lines, or dislocations within crystals, caused by repeated loading. These cracks may propagate until total collapse of the component or structure occurs. Despite the fact that a thorough understanding of the physics underlying these processes is now available (refs.1.2,1.3), most engineering design is based on an empirical approach.

The particular empirical approach used will depend on the type of component being designed. For instance, a nuclear plant pressure vessel will have been classified as failed after the appearance of a crack. However, in an offshore platform tubular joint it may be acceptable for the structure to remain in service with cracks of much greater size than the minimum which can be detected, perhaps of 5mm or more. This leads to the idea of cracks appearing and growing in size without impeding the integrity of the structure or component.

Various analysis techniques have emerged to deal with such differing design requirements. These include;

- (a) The nominal stress approach. The amplitude of some representative stress in the component is used to predict its life. The stress is often a nominal stress based on, for example, simple bending formulae, in which case local features such as holes and notches will be dealt with by introducing stress concentration factors. Failure may be taken as the appearance of a crack, a specific length of crack, or total failure depending on the test data available.

- (b) The fracture mechanics approach. Crack propagation is assumed to depend on a fracture mechanics parameter, usually the range of crack tip stress ΔK . Life is then calculated by assuming an initial crack length and finding how many cycles are needed to make this crack grow to an unacceptable size.
- (c) The local stress-strain or critical location approach. The strain history of some critical location is estimated from the loading history, including plasticity effects. Life is then estimated from test data taken under strain controlled conditions. Prediction of life to crack initiation is the objective.

The nominal stress approach was used for the work described in this thesis whenever a particular choice of methods was necessary, therefore parts of the thesis which deal specifically with aspects of fatigue analysis have direct relevance to this method. It was chosen because methods such as the ones described above, either have no relevant influence on the focus of the present study, or are unsuitable for dealing with the loading problems investigated. Loading problems arise because there is a need to define a stress (or strain) 'cycle' of loading. This is required whenever the loading conditions are more complex than constant amplitude. The main purpose of the work in this thesis is to investigate such loading conditions using modern ideas on cycle counting.

Wöhler (ref.1.4) first pointed out many very important aspects of fatigue behaviour, the most important being that fatigue depends more on the range of stress than the maximum stress. He also suggested that the fatigue life of specimens reduces when the amplitudes of repeated loading increases, introducing the concept of stress versus life (S-N) diagrams. Because of the apparent simplicity of this relationship it has formed the basis of much present day fatigue design. The diagram is traditionally produced using results from tests carried out at constant load amplitudes.

When a structure or component is subjected to normal service loadings this approach has to be adapted to account for the fact that the loadings will not be of constant amplitude. Miner's rule (ref. 1.5) is commonly used and is an empirical relationship which assumes that fatigue damage accumulates linearly according to the magnitude and number of stress cycles present. This rule is linear because it assumes that similar cycles cause similar damage regardless of whether they occur at the start or end of the service loading history, and non-interactive because the damage caused by one stress range is

unaffected by the presence of a different stress range. Having ignored the possible consequences of the above assumptions there is still a problem to be solved when the loading is irregular, because of the way different frequencies and magnitudes of the signal are mixed together. This makes it difficult to extract cycles of stress on which to apply Miner's rule. This is typical of random vibrations in a car body shell or where dynamic responses are present in structures such as offshore oil platforms.

The appearance of 'rainflow cycle counting' (ref.1.6) has provided an answer to the problem of what constitutes a 'cycle'. It has now generally been accepted that rainflow cycle ranges give the best agreement with actual fatigue lives (ref.1.7). Furthermore, when the service loading history is specified in the time domain it is then a relatively simple task to compute the fatigue life of the component (ref.1.8).

It is, however, common for the service loading to be specified in the frequency domain as a power spectral density (PSD) plot. This could be because of the nature of the structural inputs, such as earthquakes, where a frequency domain measurement is easier to perform or where the structure being designed has many input-output (transfer function) relationships which are dealt with most efficiently using frequency domain techniques. Wind turbines, automobiles, aeroplanes and lattice type steel structures are just a few examples of where frequency domain service loading histories may be encountered.

Recently, considerable attention has focused on the spectral fatigue damage approach to offshore structures. However, previous design work has tended to rely on the deterministic or time domain solutions, for several reasons; The bulk of the data required for this sort of analysis is already available and the structural analysis techniques are much simpler. Also, dynamic responses were less significant because the design depths required in the past were shallower. Another reason was that most offshore structures have many degrees of freedom and this, until recently, inhibited the structural analysis technique. However, deeper water depths and the advent of Finite Element Analysis has made the use of frequency domain analysis viable. A frequency domain analysis has many advantages. For instance, a PSD plot is the best way of reducing random output from structures subject to random input, and often the PSD output is directly obtainable from a Finite Element Package. In addition, only the frequency domain

analysis is able to take full account of the truly random nature of the sea because a deterministic approach loses the frequency composition of the sea waves, and is therefore flawed if the structure exhibits significant dynamic response.

Because of its widely applicable use, much work has been done on the frequency domain technique. However, the majority of the work has been for situations where the loading is narrow band, or of one predominant frequency. There is evidence to show that many structures, including offshore structures, exhibit wide band response. This is often a two peaked PSD output.(see figure 1.1)

Work by S.O.Rice (ref.1.9) and then J.S.Bendat (ref.1.10) produced relationships for calculating the number of peaks and zero crossings per second from frequency domain representations of the loading. In certain circumstances, where the loading is narrow band, a fatigue damage result can be obtained by noting that the density of peaks is the same as the density of ranges, and for a narrow band process this is given by the Rayleigh function. However, in situations where the service loading has more than one predominant frequency, the so called 'wide band' case, there was no satisfactory solution. Many design methods, without justification, continued to use the narrow band approach, modified by some features of the wide band statistics.

Since rainflow cycle counting has been accepted as the best way of estimating the fatigue damage caused by random loadings, the obvious way forward was to search for a method of obtaining the rainflow range distribution from the PSD. This could then be fed directly into the Miner's rule assumption to obtain a prediction of fatigue damage. Empirically based solutions of this problem have appeared recently (refs.1.11,1.12), with varying amounts of justification. These solutions were obtained using computer modelling, and curve fitting, and had no significant theoretical input. Therefore, although useful, these results were not substantial enough to influence the design practices of structures such as offshore oil platforms. Before such a change in design practices could take place more substantial theoretical backing was needed. Such a solution is derived in this thesis. It forms the major part of the work presented and appears in chapter 5. The rest of the thesis deals with the following topics;

Chapter 2 gives a brief summary of some of the statistical techniques and aspects of fatigue analysis which are encountered throughout the thesis.

Chapter 3 first presents some empirical solutions developed by other authors for the prediction of rainflow ranges from PSD's. Dirlik's solution (ref.1.11) is then used to investigate the effect that stresses contained within a given frequency range have on fatigue damage when there are other frequencies present in the PSD plot. This can be envisaged as 'fatigue damage potential', which for the narrow band case is a simple concept because there are no other frequencies present. Interactions between stresses in different frequency intervals are investigated and it is shown that the fatigue damage potential of one frequency interval is dependent not only on the magnitude of that interval but on the magnitudes of other frequency intervals present. This 'Interaction' effect within the PSD plot, is of specific interest because it can be used to determine the change of fatigue damage for any given structure or component when parts of the signal or PSD plot are altered.

Chapter 4 is concerned with methods of regenerating a signal from a PSD in the form of a set of peaks and troughs. Only the peaks and troughs are needed when a fatigue damage estimation is required, because only the magnitude of stress (and sometimes the mean) has any influence on the fatigue behaviour, and not the form of the segments adjoining the peaks and troughs. Work by Kowalewski (ref.1.13) is introduced which gives a solution for the joint distribution of peaks and troughs. This distribution can be used to generate a continuous set of adjacent peaks and troughs, of any length, using Monte-Carlo techniques. Approximations in this result are discussed, in comparison with the (distribution of times between) zero crossings problem highlighted by S.O.Rice (ref.1.9). An improvement to this joint distribution of peak and troughs is given which uses an empirical solution for the distribution of 'ordinary ranges' (ranges between adjacent peaks and troughs).

Chapter 5 forms the major part of the original work presented in this thesis and outlines a theoretical solution for the prediction of rainflow ranges using statistics computed directly from the power spectral density plot. The rainflow range mechanism is broken down into a set of logical criteria which can be analyzed using Markov process theory. The dependence between extremes in this instance is modelled using the prediction of the joint distribution of peaks and adjacent troughs proposed by Kowalewski, and shown in chapter 4.

Chapter 6 deals with the fatigue damage assessment and stress history determination of components when only limited samples of the service data are available. An investigation is carried out into the relative merits of time and frequency domain techniques. In particular, the effect of finite sample length was investigated with particular reference to the variance of fatigue predictions using both a rainflow count on a limited time sample and a rainflow count produced directly from a PSD of the same time sample. The frequency domain approach is shown to be at least as accurate as the direct time domain approach. This has many interesting implications, for instance, frequency domain calculations may be preferred to time domain for reasons of slower data acquisition rates or smaller data storage space.

Chapter 7 deals with one specific area where the methods presented in this thesis are applicable, namely, dynamically sensitive offshore structures. Various methods of fatigue damage assessment are highlighted, followed by a detailed description of the 'deterministic/spectral' approach. This description has been used because although a spectral analysis approach appears to be the main tool, a deterministic technique is used to obtain the transfer functions. Many factors which have not previously been recognised are investigated and shown to have significant effect, for instance, tidal effects. Refinements to the loading problem are proposed for future research and a method of linearising the non linear system is discussed.

Chapter 8 gives a summary of the conclusions from each chapter, an overall discussion of the work and future direction the research can take.

1.1. References

- (1.1) Standard definitions of terms relating to fatigue testing and statistical analysis of data, ASTM Designation E206-72.
- (1.2) H.O.Fuchs and R.I.Stevens, Metal fatigue in engineering, John Wiley & Sons, 1980.
- (1.3) Dieter, Mechanical Metallurgy, Mcgraw Hill, 3rd ed., 1986.
- (1.4) Wöhler's experiments on the strength of metals, Engineering, August 23, 1967 p160.
- (1.5) M.A. Miner. Cumulative Damage in Fatigue, Journal of applied mechanics, A.S.M.E. Vol 12, p. A-159, 1945.
- (1.6) M.Matsuishi and T.Endo, Fatigue of metals subject to varying stress, paper presented to Japan Soc Mech Engrs (Jukvoka, Japan, 1968)
- (1.7) N.E.Dowling, Fatigue predictions for complicated stress strain histories, J Mater 1, pp 71-87, 1972.
- (1.8) S.D.Downing and D.F.Socie, Simple rainflow counting algorithms, Int J Fatigue 4 No 1, pp 31-40, 1982.
- [1.9] S.O.Rice, Mathematical Analysis of Random Noise, Selected Papers on Noise and Stochastic Processes (Dover, New York), 1954.
- [1.10] J.S.Bendat, Probability Functions for Random Responses, NASA Report on Contract NAS-5-4590, 1964.
- (1.11) P.H.Wirsching et al, Fatigue Under Wide Band Random Loading, J Structural Div, July 1980.
- (1.12) T.Dirlik, Application of computers in Fatigue Analysis, University of Warwick Thesis, Jan 1985.
- (1.13) J.Kowalewski, On the relationship Between Component Life Under Irregularly Fluctuating and Ordered Load sequences. Part 2, DVL Report 249, 1963. MIRA Translation no 60/66.

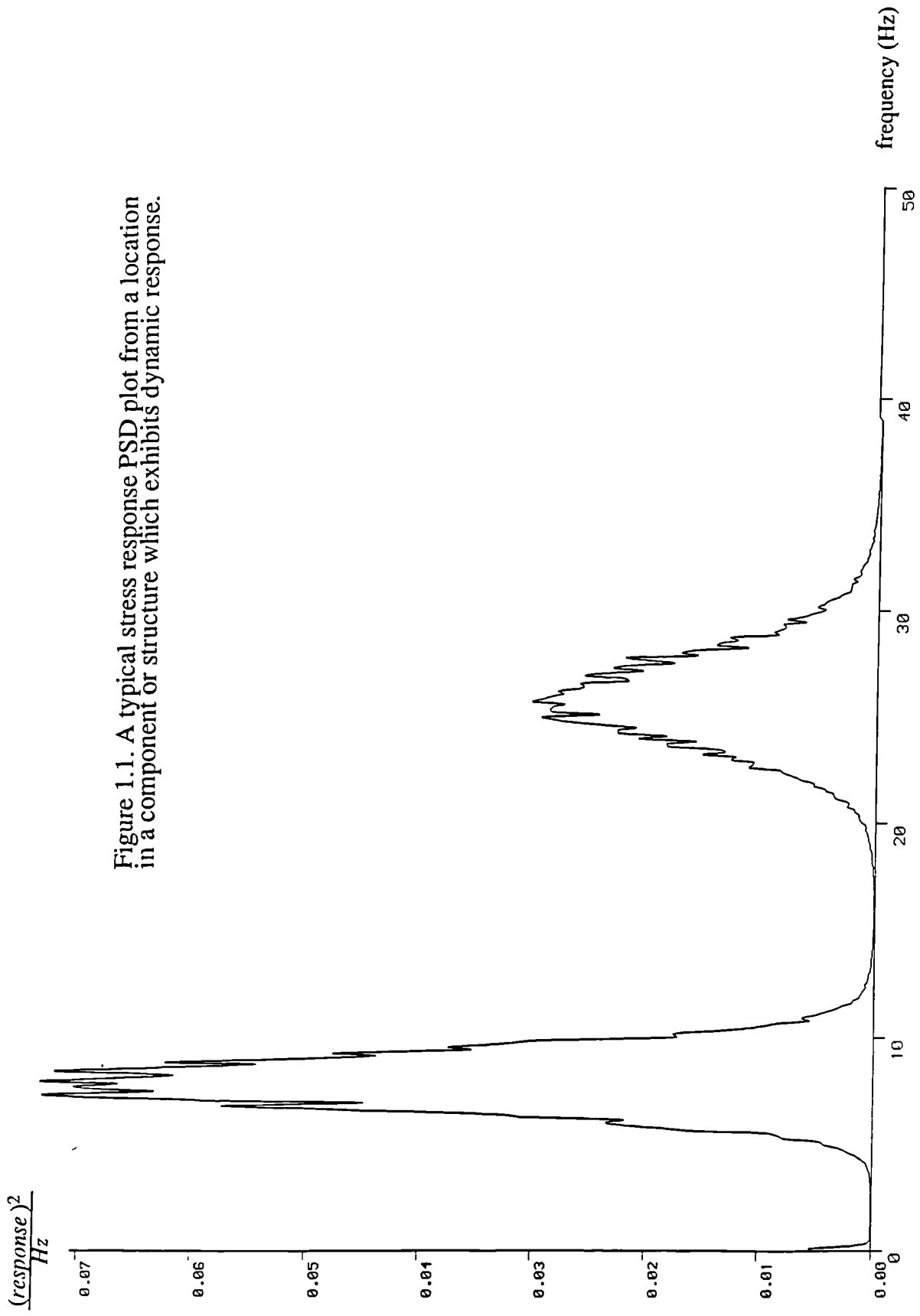


Figure 1.1. A typical stress response PSD plot from a location in a component or structure which exhibits dynamic response.

2. Theoretical tools for the statistical and fatigue damage analysis of random signals.

This chapter presents a summary of the general theory which is required in later chapters. This is given to avoid the need to consult texts. If a more detailed treatment of any topic is required readers can refer to references quoted at the start of each section.

2.1. Basic fatigue theory

A good general review of present day fatigue analysis methods is contained in four papers by Sherratt (refs.2.1,2.2,2.3,2.4). Traditional methods of fatigue damage analysis are covered as well as the local stress-strain and fracture mechanics methods. As explained in chapter one, various methods are available for obtaining a fatigue life estimation from service data. The particular method chosen will depend on the available data and type of component as well as other factors. Because this study was concerned mainly with obtaining a rainflow range distribution from frequency domain data, a nominal stress approach was used to obtain fatigue damage estimations, where required. It should be noted, however, that the type of fatigue analysis method used is quite separate from the main focus of this investigation. Every fatigue damage calculation requires some form of loading function, but, the nominal stress approach is a more convenient choice as a fatigue damage method than, say, fracture mechanics when the loading function is a rainflow range distribution. This is because there is no simple method of applying the rainflow range distribution in correct sequence. Research work (1982,ref.2.5) has been carried out on methods of regenerating load histories from rainflow range distributions, but this area of work is not covered in this investigation.

A traditional S-N curve as shown in figure 2.1 is used to model the material properties of the components being analysed. This simply shows that under constant amplitude cyclic loading, a linear relationship exists between cycles to failure N and applied stress range S when plotted on log-log paper. At low stresses, an endurance limit is sometimes included, indicating that stresses below a certain level cause no fatigue damage. Obviously, scatter will be seen in test results. Therefore the S-N curve is a probabilistic representation of the test results, usually plotted to give, say, 5% probability of failure.

Because 'real' signals rarely conform to the ideal constant amplitude situation, an empirical approach has to be adopted for calculating the damage caused by stress signals of varying amplitudes. Despite its limitations, Miner's rule (1945,ref.2.6) is generally used for this purpose. Miner's work was a generalisation of work done by Palmgren (1924,ref.2.7) who first proposed a linear damage law for the estimation of roller bearing life. The law states that;

$$\sum \frac{n}{N} = 1.0 \text{ at failure.} \quad (2.1)$$

This linear relationship assumes that the damage caused by parts of a stress signal with a particular range can be calculated and accumulated to the total damage separately from that caused by other amplitudes. A ratio is calculated for each stress range, equal to the number of actual cycles at a particular stress range n divided by the allowable number of cycles to failure at that stress N (obtained from the $S-N$ curve). Failure is assumed to occur when the sum of these ratios, for all stress ranges, equals 1.0.

2.2. Cycle counting methods

The basic aim of counting methods is to reduce complicated time domain stress histories into a form more amenable to analysis from a fatigue point of view. At least twelve types of counting methods have been reported in the literature (refs.2.8,2.9,2.10). The relevant aspects of each are listed below, starting first with the less important methods;

- (i) **Peak count method.** The number of peaks and/or troughs at particular levels are counted.
- (ii) **Mean-crossing peak count method.** As (i) above except that only the maximum peak or minimum trough is counted between each zero crossing.
- (iii) **Ordinary range count.** The height of ranges between adjacent peaks and troughs is counted. From this a probability density of ordinary ranges can be calculated.
- (iv) **Range-mean count.** This method is identical to (iii), except that the mean values of each ordinary range are also counted.

- (v) **Level crossing count.** The number of upwards (or downwards) crossings of particular levels are counted.
- (vi) **Fatiguemeter count.** A technique developed in the aeronautics industry (1953,ref.2.11) to measure variations of acceleration. This is a similar technique to (v) except that small variations in the signal, such as noise, are removed by using a gate or trigger level. Signal excursions from the previous recorded level are only recorded if the trigger level is exceeded.

Several more important counting methods have emerged in the last twenty years. The importance of these techniques can be seen by considering a time signal consisting predominantly of two frequencies, such as a low frequency wave with a high frequency ripple along it (see figure 2.2). Material fatigue data, represented by the S-N curve, shows that the relationship between stress range and fatigue damage is nonlinear. Therefore, techniques such as the ordinary range counting technique will underestimate the fatigue damage by ignoring the low frequency fluctuations in the stress history. On the other hand, using a peak count to predict ranges by pairing opposite peaks and troughs results in an overestimation of the fatigue damage. The other methods described above all suffer from similar drawbacks. The methods listed below have generally been accepted as better methods of calculating fatigue damage from random signals (1972,ref.2.12);

(vii) **Range-pair count** (1972,ref.2.8).

(viii) **Wetzel's method** (1971,ref.2.13).

(ix) **Rainflow method.**

version (ix.(a)), **Pagoda Roof method** (1968,ref.2.14).

version (ix.(b)), **Maximum-Minimum Procedure** (1974,ref.2.15).

version (ix.(c)), **Pattern Classification Procedure** (1974,ref.2.15).

These methods properly account for global stress fluctuations, in addition to the smaller and medium sized fluctuations. Material stress-strain concepts like hysteresis loops are sometimes used to justify their use. In chapter five an upper bound-lower bound approach is used when asserting their importance.

Methods (vii),(viii),(ix.(a)),(ix.(b)) and (ix.(c)) require fairly complicated descriptions. For instance, the original version of the rainflow method, version ix.(a), uses an obscure definition involving rain dripping down rooftops. Hence the name 'Pagoda Roof Method'. However, all five methods are essentially the same and give identical cycle counts if the time history starts and ends at either the highest peak or the lowest trough. Therefore, a description will be given of only one method, the Pattern Classification Procedure. This is the definition often used for writing computer code (ref.2.16). The references can be consulted for details of the other methods.

The rules for this technique are as follows. The first four peaks/troughs of the signal are analysed and the pattern formed is classified as one of four types (see figure 2.3);

(D-I)The interrupting cycle (2-3) is counted as one full cycle, point 4 is turned into point 2 and the next two peaks/troughs in the time history are considered.

(I-I) Two half cycles are counted (1-2 and 2-3), and then points 3-4-5-6 are checked next.

(I-D)The first range 1-2 is counted as a half cycle and then points 2-3-4-5 are checked.

(D-D)No cycle is formed and so points 3-4-5-6 are checked next. If a (D-I) cycle then occurs, the interrupting cycle (4-5) is counted as a full cycle, point 6 is changed to point 4 and then points 1-2-3-4 are checked. But, if a (D-D) pattern is encountered again, then points 5-6-7-8 are checked, and so on until a cycle is formed.

This procedure is continued until the end of the time signal is reached. It is possible to make the signal start and end at the highest peak, or lowest trough, by manipulating the signal (see chapter 4). This means that no odd bits of signal are left at the end of the count. It also means that only the D-D and D-I types of classifications need to be considered, which considerably simplifies the procedure. An example of the use of this procedure is given in figure 2.4.

A completely new definition of the rainflow cycle counting method, which is easier to analyse statistically, is developed by the author and used in chapter five.

2.3. Probability theory and random variables

This section will give a brief summary of the more important aspects of stochastic processes or random processes. Several texts can be consulted for a more complete presentation of the subject (refs.2.17,2.18,2.19,2.20,2.21,2.22). For convenience, all processes described in the following sections will be assumed to be time varying, unless otherwise stated.

2.3.1. General assumptions

The assumptions that will be used throughout this thesis about the processes being investigated are that they are stationary, ergodic, Gaussian and random.

In general terms, any data representing a physical process can be classified as either **deterministic** or **random**. A deterministic process can be thought of as one where future states into which the process may fall can be predicted accurately, and with certainty. Such data is then either periodic or non periodic. A sine wave is one example of deterministic periodic data. A random process is one where the future movements of the process cannot be represented by any mathematical expression with certainty at any particular time. For example, the ground movement caused by earthquakes or wind buffeting on a telegraph mast. In particular situations, however, we can make predictions about the process.

A **stationary** random process is one where the statistical properties measured across a set of records, or ensemble, at a particular time, say t_0 , are identical with the statistics measured across the ensemble at any other time say t_τ . Weak stationarity is assumed if the first few moments conform to the stationarity test, and strong stationarity is assumed if all the moments satisfy the required conditions.

In addition to being stationary, the process can be termed **ergodic** if the statistics measured along any one sample or record are representative of the statistics measured along any other sample. It is very useful if the ergodicity assumption is valid because it means that one long sample can be used to compute any desired statistics, instead of having to measure many different records.

Random variables which follow a **Gaussian** distribution are described in section 2.5.

2.3.2. One random variable

Firstly consider one random variable $x(t)$, sampled at discrete points in time and represented by $x(k)$. The **probability distribution function** is given by;

$$P(x) = Prob[x(k) \leq x] \quad (2.2)$$

Where,

$$P(-\infty) = 0.0 \quad P(\infty) = 1.0 \quad P(a) \leq P(b), \text{ if } a \leq b$$

In a similar way the **probability density function** is given by;

$$p(x) = \frac{dP(x)}{dx} \quad (2.3)$$

or;

$$p(x) = \lim_{\Delta x \rightarrow 0} \left[\frac{Prob[x < x(k) \leq x + \Delta x]}{\Delta x} \right] \quad (2.4)$$

The **expected value** or mean value, is given by;

$$E[x(k)] = \int_{-\infty}^{\infty} x p(x) dx = \bar{x} \quad (2.5)$$

which is assumed to be zero throughout this thesis.

The **nth moment** of x_k is given by;

$$E[x^n(k)] = \int_0^{\infty} x^n p(x) dx = \alpha_n \quad (2.6)$$

The mean square value of $x(k)$ is then given by $E[x^2(k)]$. The mean square value of $x(k)$ about its mean represents the **variance** of $x(k)$ and is given by;

$$E[(x(k) - \bar{x})^2] = \int_{-\infty}^{\infty} (x - \bar{x})^2 p(x) dx = \alpha_2 - (\bar{x})^2 = \sigma_x^2 \quad (2.7)$$

Where σ_x is the **standard deviation**, which for zero mean signals equals the **root mean square value** (rms).

The **moment generating function** of $x(k)$ is defined as;

$$m(s) = E[e^{sx}] = \int_{-\infty}^{\infty} e^{sx} p(x) dx \quad (2.8)$$

and so the moments of $x(k)$ are then;

$$E[x^n] = \int_{-\infty}^{\infty} x^n p(x) dx = m^{(n)}(0) \quad (2.9)$$

Where $m^{(n)}$ represents the n_{th} derivative of $m(s)$

The **Characteristic function** $C(f)$ of $x(k)$ is given by;

$$C(f) = E[e^{j2\pi fx}] = \int_{-\infty}^{\infty} e^{j2\pi fx} p(x) dx \quad (2.10)$$

Therefore $C(f)$ is an inverse fourier transform of $p(x)$, and;

$$p(x) = \int_{-\infty}^{\infty} e^{-j2\pi fx} C(f) df \quad (2.11)$$

2.3.3. Two random variables

Consider now two random variables $x(t)$ and $y(t)$, represented in discrete form by $x(k)$ and $y(k)$. Their **joint probability distribution function** is given by;

$$P(x, y) = Prob[x(k) \leq x \text{ and } y(k) \leq y] \quad (2.12)$$

The **joint density function** is then;

$$p(x, y) = \frac{\partial}{\partial y} \left[\frac{\partial P(x, y)}{\partial x} \right] \quad (2.13)$$

Or;

$$p(x, y) = \lim_{\substack{\Delta x \rightarrow 0 \\ \Delta y \rightarrow 0}} \left[\frac{Prob[x < x(k) \leq x + \Delta x \text{ and } y < y(k) \leq y + \Delta y]}{\Delta x \Delta y} \right] \quad (2.14)$$

Where;

$$P(-\infty, y) = P(x, -\infty) = 0.0, \quad P(\infty, \infty) = 1.0$$

The **second order moments** of $x(k)$ and $y(k)$ are defined by;

$$E [x(k)^n . y(k)^m] = \int_{-\infty}^{\infty} \int_{-\infty}^{\infty} x^n y^m p(x,y) dx dy = \alpha_{nm} \quad (2.15)$$

If $x(k)$ and $y(k)$ are statistically **independent**, then;

$$p(x,y) = p(x) . p(y) \quad (2.16)$$

and;

$$E [x(k),y(k)] = E [x(k)] . E [y(k)] \quad (2.17)$$

The **joint moment generating function** of $x(k)$ and $y(k)$ is given by;

$$m(s,t) = E [e^{sx+ty}] = \int_{-\infty}^{\infty} \int_{-\infty}^{\infty} e^{sx+ty} p(x,y) dx dy \quad (2.18)$$

We then get, at $s,t=0$ a result for the mixed moments of $x(k)$ and $y(k)$;

$$E [x^r y^n] = \int_{-\infty}^{\infty} \int_{-\infty}^{\infty} x^r y^n p(x,y) dx dy = \frac{\partial^{r+n} m(s,t)}{\partial s^r \partial t^n} \quad (2.19)$$

The **joint characteristic function** $C(f,g)$ is defined by;

$$C(f,g) = E [e^{j2\pi(fx+gy)}] = \int_{-\infty}^{\infty} \int_{-\infty}^{\infty} e^{j2\pi(fx+gy)} p(x,y) dx dy \quad (2.20)$$

Which is the double inverse fourier transform of $p(x,y)$, and so;

$$p(x,y) = \int_{-\infty}^{\infty} \int_{-\infty}^{\infty} e^{-j2\pi(fx+gy)} C(f,g) df dg \quad (2.21)$$

2.4. Power spectra

An earlier section gave details of counting methods which can be used to compress a stress time history into a form more easily analysed using fatigue analysis techniques. It will be shown in later sections that an alternative route can be taken by first transforming the data into the frequency domain, from which the relevant fatigue damage statistics can then be calculated. This section will summarise the more important aspects of frequency domain analysis. Because the material comes from a very large and detailed area, readers are referred to other texts for a complete treatment of the subject (see refs.2.17,2.23,2.24).

A **cross-correlation function** gives a measure of the amount by which two functions are related to each other. If we have two random variables $x(t)$ and $y(t)$, their cross-correlation function is given by:

$$R_{xy}(\tau) = \lim_{T \rightarrow \infty} \frac{1}{2T} \int_{-T}^T x(t)y(t+\tau)dt \quad (2.22)$$

An **autocorrelation function** defines how a signal is correlated with itself:

$$R_{xx}(\tau) = \lim_{T \rightarrow \infty} \frac{1}{2T} \int_{-T}^T x(t)x(t+\tau)dt = R(\tau) \quad (2.23)$$

The **Power Spectral Density (PSD)** or autospectral density function of a signal gives an indication of the average power contained in particular frequencies. It can be expressed in units of radians as a two sided function $S(\omega)$, or in units of hertz as a one sided function $G(f)$.

The autocorrelation function and power spectral density are related by a **Fourier transform pair**:

$$S(\omega) = \frac{1}{2\pi} \int_{-\infty}^{\infty} R(\tau)e^{-j\omega\tau}d\tau \quad (2.24(a))$$

$$R(\tau) = \int_{-\infty}^{\infty} S(\omega)e^{j\omega\tau}d\omega \quad (2.24(b))$$

Because S_{xx} is a real valued quantity we get;

$$R(\tau) = \int_{-\infty}^{\infty} \cos\omega\tau S(\omega)d\omega \quad (2.24(c))$$

Similarly, the cross-correlation function and its inverse the **cross spectral density** function are related by;

$$S_{xy}(\omega) = \frac{1}{2\pi} \int_{-\infty}^{\infty} R_{xy}(\tau)e^{-j\omega\tau}d\tau \quad (2.25(a))$$

$$R_{xy}(\tau) = \int_{-\infty}^{\infty} S_{xy}(\omega) e^{j\omega\tau} d\omega \quad (2.25(b))$$

The PSD is usually computed directly from a time sample using the **Fast Fourier Transform (FFT)** given by;

$$X_k = \frac{1}{N} \sum_{r=0}^{N-1} x_r e^{-i2\pi(\frac{kr}{N})}, \quad k=0,1,2,\dots,N-1 \quad (2.26)$$

Where N is the number of points used for the FFT, x_r is the r_{th} point in the sample on which the FFT is being computed and X_k is the k_{th} point of the complex valued FFT.

A set of $\frac{N}{2}$ points representing the discrete form of the one sided PSD in units of hertz, $G_k(f)$, is then given by;

$$G_k(f) = 2L_s \left[(\text{real } X_k)^2 + (\text{imag } X_k)^2 \right] \quad (2.27)$$

Where, L_s is the sample length equal to $N \cdot \Delta t$, Δt is the distance between values of x_r and the term enclosed in square brackets represents the square of the k_{th} complex term of the FFT.

From the above we can define two versions of the very important **nth moment** of the PSD function:

$$m_n = \int_0^{\infty} f^n G(f) df \quad (2.28(a))$$

or, in a form which is strictly correct;

$$w_n = \int_{-\infty}^{\infty} \omega^n S(\omega) d\omega = m_n \cdot (2\pi)^n \quad (2.28(b))$$

The form of m_n has had the $(2\pi)^n$ factor removed, as shown in equation 2.28(b). This is because it provides more elegant solutions for the number of zeros and peaks per second derived in section 2.6. The use of equation 2.28(a) is highlighted in figure 2.5, along with the method used for converting a sequence representing a time signal into an FFT and then a PSD.

The zeroth moment w_0 can then be used as an alternative method of computing the root mean square value which is a good indication of the intensity of a process:

$$\text{root mean square} = \sigma = (w_0)^{1/2} \quad (2.29)$$

2.5. Random variables which follow a Gaussian (normal) distribution

A zero mean random variable is said to be **Gaussian** if its probability density function is in the following form;

$$p(x) = \frac{1}{\sigma_x \sqrt{2\pi}} e^{-\frac{x^2}{2\sigma_x^2}} \quad (2.30)$$

The reason that the normal or Gaussian distribution finds so many applications in areas such as engineering can be explained using the **central limit theorem**. This states, in general terms, that any random variable which is the sum of a number of independent random variables will follow a Gaussian distribution if the number of random variables contributing to the sum is reasonably large and no individual random variable dominates the distribution. This theorem does not require that the individual random variables be Gaussian themselves.

Equation 2.30 can be extended to give the n dimensional normal distribution;

$$p(x_1, x_2, x_3, \dots, x_n) = (2\pi)^{-\frac{n}{2}} |A|^{-\frac{1}{2}} e^{-\frac{1}{2} \left(\frac{-1}{|A|} \sum_{i,j=1}^n A_{ij} x_i x_j \right)} \quad (2.31)$$

Where;

$$A = \begin{pmatrix} a_{11} & a_{1j} & a_{1n} \\ \cdot & \cdot & \cdot \\ \cdot & \cdot & \cdot \\ a_{i1} & a_{ij} & a_{in} \\ \cdot & \cdot & \cdot \\ \cdot & \cdot & \cdot \\ \cdot & \cdot & \cdot \\ a_{n1} & a_{nj} & a_{nn} \end{pmatrix} \quad (2.32)$$

and;

$$a_{ij} = E[x_i x_j] = a_{ji} \quad (2.33)$$

a_{ij} is the covariance or second moment of $x_i x_j$, $|A|$ is the determinant of A and A_{ij} is the cofactor of a_{ij} .

This expression will be used to derive several important equations in the next section which are used to analyse components subjected to vibration.

2.6. The statistical analysis of signals which are stationary, ergodic, Gaussian and random using the joint distributions of x , $\frac{dx}{dt}$, $\frac{d^2x}{dt^2}$ and $\frac{d^3x}{dt^3}$

Much of the work being carried out on Fatigue Damage of structures subject to random loading relies heavily on the work of S.O.Rice (1954, ref.2.25) and J.S.Bendat (1964, ref.2.26). Results were produced for the number of peaks and zero crossings per unit time. Kowalewski (1963,ref.2.27) later extended the analysis to cover the numbers of points of inflection per unit time. We will start with the two parameter distribution of x and \dot{x} , where $x = x(t)$ and $\dot{x} = \frac{dx}{dt}$. In later sections we will use the terminology $\ddot{x} = \frac{d^2x}{dt^2}$, $\dddot{x} = \frac{d^3x}{dt^3}$, and generally, $x^{(m)} = \frac{d^m x}{dt^m}$.

The average number of level crossings per unit time will be derived. Consider the two dimensional distribution of x and \dot{x} ;

$$Prob [\alpha < x(t) \leq \alpha + d\alpha ; \beta < \dot{x}(t) \leq \beta + d\beta] \approx p(\alpha, \beta) d\alpha d\beta \quad (2.34)$$

This represents the period of time that x is between α and $\alpha + d\alpha$ when the velocity \dot{x} is between β and $\beta + d\beta$. If we define the time to cross one interval as Δt , we get;

$$\Delta t \approx \frac{d\alpha}{\beta} \quad (2.35)$$

From which we can obtain the expected total number of positive crossings of level α by dividing 2.34 by Δt and integrating over all positive values of β ;

$$E[\alpha] = \int_0^{\infty} \beta p(\alpha, \beta) d\beta \quad (2.36)$$

By setting $\alpha = 0$ we get the required number of zero crossings per unit time.

$$E[0] = \int_0^{\infty} \beta p(0, \beta) d\beta \quad (2.37)$$

The joint probability function in equation 2.36 is obtained from equation 2.31.

$$p(\alpha, \beta) = (2\pi)^{-1} |A|^{-\frac{1}{2}} e^{-\frac{1}{2|A|} (A_{11}\alpha^2 + 2A_{12}\alpha\beta + A_{22}\beta^2)} \quad (2.38)$$

Elements in the matrix A are;

$$\text{from equation 2.23} \quad a_{11} = E[x(t)x(t+\tau)]_{\tau=0} = R(0) \quad (2.39)$$

Similarly;

$$a_{12} = E[x(t) \cdot \dot{x}(t+\tau)]_{\tau=0} = \left[\lim_{T \rightarrow \infty} \frac{1}{2T} \int_{-T}^T x(t) \cdot \dot{x}(t+\tau) dt \right]_{\tau=0} \quad (2.40)$$

It can be shown that (ref.2.27);

$$\dot{x}(t+\tau) = \frac{dx(t+\tau)}{dt} = \frac{dx(t+\tau)}{d\tau} \quad (2.41)$$

Then;

$$\lim_{T \rightarrow \infty} \frac{1}{2T} \int_{-T}^T x(t) \cdot \dot{x}(t+\tau) dt = \frac{d}{d\tau} \left[\lim_{T \rightarrow \infty} \frac{1}{2T} \int_{-T}^T x(t) \cdot x(t+\tau) dt \right] \quad (2.42)$$

Therefore;

$$a_{12} = a_{21} = \left[\frac{dR(\tau)}{d\tau} = \int_0^{\infty} 2\pi f G(f) \sin \omega \tau df \right]_{\tau=0} = w_1 = 0 \quad (2.43)$$

Finally we get;

$$a_{22} = E[\dot{x}(t) \cdot \dot{x}(t+\tau)]_{\tau=0} \quad (2.44)$$

$$\begin{aligned} E[\dot{x}(t) \cdot \dot{x}(t+\tau)] &= \lim_{T \rightarrow \infty} \frac{1}{2T} \int_{-T}^T \dot{x}(t) \cdot \dot{x}(t+\tau) dt \\ &= \lim_{T \rightarrow \infty} \left[\frac{1}{2T} \left[\dot{x}(t+\tau) \cdot x(t) \right]_{-T}^T - \frac{1}{2T} \int_{-T}^T \ddot{x}(t+\tau) \cdot x(t) dt \right] \end{aligned} \quad (2.45)$$

The first term in brackets tends to zero in the limit, since we are assuming that $x(t)$ and its derivatives remain finite. Hence, using arguments similar to those in equation 2.41 it can be proved that;

$$a_{22} = \frac{-d^2R(0)}{d\tau^2} = \int_0^{\infty} (2\pi f)^2 G(f) df = w_2 \quad (2.46)$$

The matrix A is then;

$$A = \begin{bmatrix} a_{11} & 0 \\ 0 & a_{22} \end{bmatrix} = \begin{bmatrix} w_0 & 0 \\ 0 & w_2 \end{bmatrix} \quad (2.47)$$

Then from 2.35 we get, after carrying out the required integration, a result for the number of upwards level crossings per unit time.

$$E[\alpha] = \frac{1}{2\pi} \left[\frac{w_2}{w_0} \right]^{1/2} e^{\frac{-\alpha^2}{2w_0}} \quad (2.48)$$

If we set α equal to 0 we get the important result for the number of zero crossings per unit time.

$$E[0] = \frac{1}{2\pi} \left[\frac{w_2}{w_0} \right]^{1/2} = \left[\frac{m_2}{m_0} \right]^{1/2} \quad (2.49)$$

Similar results can be derived for the number of peaks, and the number of points of inflection per unit time (see chapter 4).

$$E[P] = \left[\frac{m_4}{m_2} \right]^{1/2} \quad (2.50)$$

$$E[PI] = \left[\frac{m_6}{m_4} \right]^{1/2} \quad (2.51)$$

2.7. The narrow band solution for calculating the fatigue damage from frequency domain statistics

A term which is useful when interpreting the type of response is the **irregularity factor**.

$$\gamma = \frac{E[0]}{E[P]} \quad (2.52)$$

The irregularity factor varies between 1 and 0. As it approaches 1 the signal becomes more like a regular sine wave. In this limiting case the signal is said to be **narrow band**. As it approaches 0 the signal becomes more like shot noise. In this limiting case the signal is said to be **wide band**.

The theoretical expressions for these cases can be considered by looking at the equation for the probability density of peaks (see chapter 4), which for Gaussian signals with any irregularity factor is given by;

$$g(\alpha) = \frac{1}{(2\pi w_0)^{\frac{1}{2}}} (1-\gamma^2)^{1/2} e^{-\alpha^2 [2w_0(1-\gamma^2)]^{-1}} \quad (2.53)$$

$$+ \frac{\alpha}{2w_0} \gamma \left[1 + \operatorname{erf} \left[\frac{\alpha}{(w_0)^{\frac{1}{2}}} (2\gamma^2 - 2)^{-1/2} \right] \right] e^{-\frac{\alpha^2}{2w_0}}$$

When the irregularity factor approaches 1 the probability density of peaks becomes **Rayleigh**.

$$g(\alpha) = \frac{\alpha}{w_0} e^{-\frac{\alpha^2}{2w_0}} \quad (2.54(a))$$

When it approaches 0 the probability density of peaks becomes Gaussian.

$$g(\alpha) = \frac{1}{(2\pi w_0)^{\frac{1}{2}}} e^{-\frac{\alpha^2}{2w_0}} \quad (2.54(b))$$

In practice for many structures the response is neither narrow nor wide band but somewhere between. Designers have tended to lean towards a narrow band approach which assumes that the distribution of peaks is equal to the distribution of stress amplitudes or stress ranges.

$$p(s) = g(\alpha) \quad (2.55)$$

This is because it has been simpler to implement and gives a conservative result. Such approaches have been highlighted by Miles (1954, ref.2.28), Williams and Rinne (1977, ref.2.29) and Hallam (1979, ref.2.30). Below is a similar derivation based on stress range rather than amplitude and in units of hertz. It starts from an expression for Fatigue Damage quoted by Bendat (1964 ref.2.26).

$$E[D]_{NB} = E[P] \frac{T}{k} \int_0^{\infty} s^b p(s) ds \quad (2.56)$$

Converting to stress range units and noting that for narrow band the number of peaks is equal to the number of positive zero crossings.

$$E[D]_{NB} = E[0] \frac{T}{k} \int_0^{\infty} S^b p(S) dS \quad (2.57)$$

$$=E [0] \frac{T}{k} \int_0^{\infty} S^b \frac{S}{4m_0} e^{-\frac{S^2}{8m_0}} dS \quad (2.58)$$

k and b are material parameters obtained from the $S-N$ curve, S is the stress range and T is the time duration over which the fatigue damage is being calculated. m_0 is calculated using equation 2.28(a).

There are, however, a number of flaws involved with this solution. By using the Rayleigh distribution, it assumes the signal is narrow band. Therefore, positive troughs and negative peaks are ignored. In addition, all positive peaks are matched with corresponding troughs of similar magnitude regardless of whether they actually form stress cycles. This is similar to the upper bound idea discussed in sections 2.2 and 5.1. When the response is wide band, the method overestimates the probability of large stress ranges. Any damage calculated will therefore be overconservative. In many situations an attempt is made to reduce the degree of conservatism involved by using the number of peaks per unit time instead of the number of zero crossings. This modified form of the narrow band solution has no theoretical basis when applied to wide band signals. Experimental work by Tunna has compared the fatigue lives of specimens with various prediction techniques which use rainflow ranges and the narrow band solution (ref.2.33). He concluded that the rainflow range method gave the best agreement with test results.

2.8. The distribution of times between zero crossings

The problem of predicting the distribution of times between zero crossings is still unsolved. Rice (ref.2.25) developed a solution for the probability of a noise current passing through zero in the interval $\tau, \tau+d\tau$ with a negative slope, when it is known that the current passes through zero at $\tau = 0$ with a positive slope. No attempt is made to derive the results, but they are quoted below in order to discuss the problems involved with Kowalewski's solution for the joint distribution of peaks and troughs given in chapter 4. The solution is;

$$\frac{d\tau}{2\pi} \left[\frac{\psi_0}{-2\psi_0} \right] \frac{1}{2} \left[\frac{A_{23}}{H} \right] (\psi_0^2 - \psi_\tau^2)^{-\frac{3}{2}} \left[1 + H \cot^{-1}(-H) \right] \quad (2.59)$$

Where;

$$H = A_{23} \left[A_{22}^2 - A_{23}^2 \right]^{-\frac{1}{2}} \quad (2.60)$$

The covariances of $x(t)$, $\dot{x}(t)$, $\dot{x}(t+\tau)$ and $x(t+\tau)$ in that order are (using the terminology of section 2.6);

$$A = \begin{bmatrix} \psi_0 & 0 & {}^1\psi_\tau & \psi_\tau \\ 0 & -{}^2\psi_0 & -{}^2\psi_\tau & -{}^1\psi_\tau \\ {}^1\psi_\tau & -{}^2\psi_\tau & -{}^2\psi_0 & 0 \\ \psi_\tau & -{}^1\psi_\tau & 0 & \psi_0 \end{bmatrix} \quad (2.61)$$

With $\cot^{-1}(-H)$ chosen in the range $0 \leq \cot^{-1}(-H) \leq \pi$, and $\cot^{-1}(-H) = \pi$ at $\tau = 0$ and $\cot^{-1}(-H) = \frac{\pi}{2}$ as $\tau \rightarrow \infty$. Also, the elements of equation 2.61 are given by;

$${}^n\psi_\tau = (-2\pi)^2 \int_0^\infty f^2 G(f) \text{var } 2\pi f \tau df \quad (2.62)$$

Where the factor *var* is cos for even n and sin for odd n . Rice considered the behaviour of equation 2.59, and concluded that it approaches the following values, as τ goes to both 0 and ∞ ;

$$\frac{d\tau}{2\pi} \left[\frac{-{}^2\psi_0}{\psi_0} \right]^{\frac{1}{2}} \text{ as } \tau \rightarrow \infty \quad (2.63)$$

$$d\tau \frac{\tau}{8} \left[\frac{\psi_0^4 \psi_0 - {}^2\psi_0^2}{-{}^2\psi_0^2 \psi_0} \right] \text{ as } \tau \rightarrow 0 \quad (2.64)$$

Equation 2.63 is identical to equation 2.49. This is as expected because Rice's solution (equation 2.59) is the distribution function of distances between zero crossings of opposite sign, but not necessarily adjacent zeros. Therefore, for large τ the distribution simply represents the probability of a zero in the chosen interval $d\tau$.

Rice derived a similar expression to equation 2.59 for the distribution function of the distance between zero crossings of equal or opposite sign. By comparing the discrepancies between this function and equation 2.59 he concluded that for a low pass filter cutting off at f_b , equation 2.59 was a good approximation of the true distribution up to $\tau = \frac{0.64}{f_b}$. For larger τ the method of 'inclusion and exclusion' was described as one

method to obtain an approximate solution. This involves extensive multiple numerical integration and does not provide a satisfactory solution.

Longuit-Higgins carried out similar work resulting in solutions which converged slightly faster. However, for large τ , it appears that the problem still remains unsolved, and Bendat (ref.2.20) states that;

the question of determining the complete distribution function for the distance between successive zeros is not solved by Rice and, in fact, is still one of the outstanding open problems in random noise theory

2.9. References.

- (2.1) F.Sherratt, Fatigue life estimation: A review of traditional methods, Journal of the Society of Environmental Engineers, December 1982.
- (2.2) F.Sherratt, Fatigue life estimation using simple fracture mechanics, Journal of the Society of Environmental Engineers, March 1983.
- (2.3) F.Sherratt and D.Eaton, Fatigue life estimation by local stress-strain methods, Journal of the Society of Environmental Engineers, September 1983.
- (2.4) F.Sherratt, Vibration and fatigue: Basic life estimation methods, Journal of the Society of Environmental Engineers, December 1983.
- (2.5) D.M.Holford, Synthesis of loading sequences from a range mean pairs (rainflow) count or fatigue load meter data, RAE tech. report no. 82080, July 1982.
- (2.6) M.A. Miner. Cumulative Damage in Fatigue, Journal of applied mechanics, A.S.M.E. Vol 12, p. A-159, 1945.
- (2.7) A.Palmgren, The service life of ball bearings, a technical translation, NASA TT F-13460.
- (2.8) J.Livesey and D.Webber, Recording and interpretation of strain measurements in military bridges, J.B.C.S.A. conference, 1972.
- (2.9) T.Haas, Loading statistics as a basis of structural and mechanical design, Engineers Digest, vol. 23, nos. 3, 4 and 5, 1962.
- (2.10) J.Schijve, The analysis of random load-time histories with relation to fatigue tests and life calculations, 2nd ICAF-AGARD symposium, Paris, 16-18 May 1961.
- (2.11) J.Taylor, Measurement of gust loads in aircraft, J. Roy. Aero. Soc. 57, 78, 1953.
- (2.12) N.E.Dowling, Fatigue predictions for complicated stress strain histories, J Mater 1, pp 71-87, 1972.
- (2.13) R.M.Wetzel, A method of fatigue damage analysis, PhD thesis, University of Waterloo, Canada, 1971.
- (2.14) M.Matsuishi and T.Endo, Fatigue of metals subject to varying stress, paper presented to Japan Soc Mech Engrs (Jukvoka, Japan, 1968)

- (2.15) T. Endo et al, Damage evaluation of metals for random or varying loads, procs. symposium on mech. behaviour of materials, Soc Mats. Sci., Kyoto, Japan, Aug 1974.
- (2.16) S.D. Downing and D.F. Socie, Simple rainflow counting algorithms, Int J Fatigue 4 No 1, pp 31-40, 1982.
- (2.17) D.E. Newland, An introduction to random vibrations and spectral analysis (2nd edition), Longman Inc., New York, 1984.
- (2.18) A. Papoulis, Probability, random variables, and stochastic processes (2nd edition), McGraw Hill Inc., New York, 1984.
- (2.19) S.H. Crandall and W.D. Mark, Random vibration in mechanical systems, Academic press Inc., London, 1963.
- (2.20) J.S. Bendat, Principles and Applications of Random Noise Theory, John Wiley & Sons, Inc., New York 1958.
- (2.21) J.S. Bendat and A.G. Piersol, Random data, analysis and measurement procedures (2nd edition), John Wiley & Sons, Inc., New York 1986.
- (2.22) Y.K. Lin, Probabilistic Theory of Structural Dynamics, McGraw Hill Inc., New York, 1967.
- (2.23) P.E. Wellstead, Methods and applications of digital spectral analysis, tech. report no. 008/83, Solartron Instruments, 1984.
- (2.24) P.E. Wellstead, Theory and statistical accuracy of spectral analysis, tech. report no. 009/83, Solartron Instruments, 1984.
- (2.25) S.O. Rice, Mathematical Analysis of Random Noise, Selected Papers on Noise and Stochastic Processes (Dover, New York), 1954.
- (2.26) J.S. Bendat, Probability Functions for Random Responses, NASA Report on Contract NAS-5-4590, 1964.
- (2.27) J. Kowalewski, On the relationship Between Component Life Under Irregularly Fluctuating and Ordered Load sequences. Part 2, DVL Report 249, 1963. MIRA Translation no 60/66.

- (2.28) J.W. Miles, On Structural Fatigue Under Random Loading, Journal of the Aeronautical Sciences, Nov 1954.
- (2.29) A.K. Williams and J.E. Rinne, Fatigue Analysis of Steel Offshore Structures, Procs I.C.E., Part 1, Nov 1976.
- (2.30) M.G. Hallam, Fatigue Analysis of Offshore Oil Platforms, SEECO '78' conference "Application of Computers in Fatigue", April 1978.
- (2.31) M.S. Longuet-Higgins, On the intervals between successive zeros of a random function, Proc. Roy. Soc. A, vol. 246, 1958.
- (2.32) M.S. Longuet-Higgins, The distribution of intervals between zeros of a stationary random function, Proc. Roy. Soc. A, vol. 254, 1962.
- (2.33) J.M. Tunna, Fatigue life predictions for Gaussian random loads at the design stage, Fatigue and Fracture of Engineering Materials and Structures, Vol. 9, No. 3, 1986.

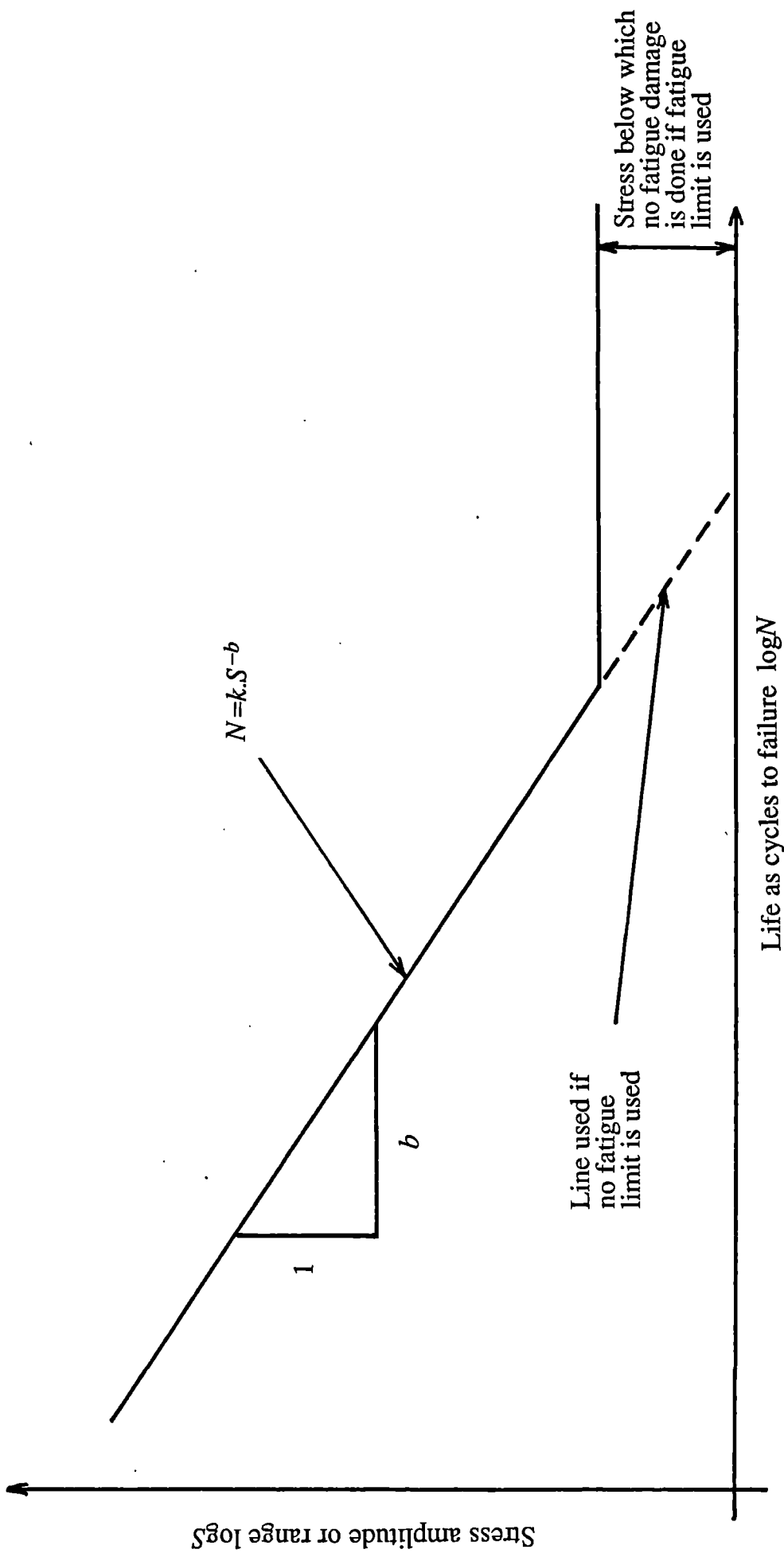


Figure 2.1.1. A typical stress-life (S-N) diagram.

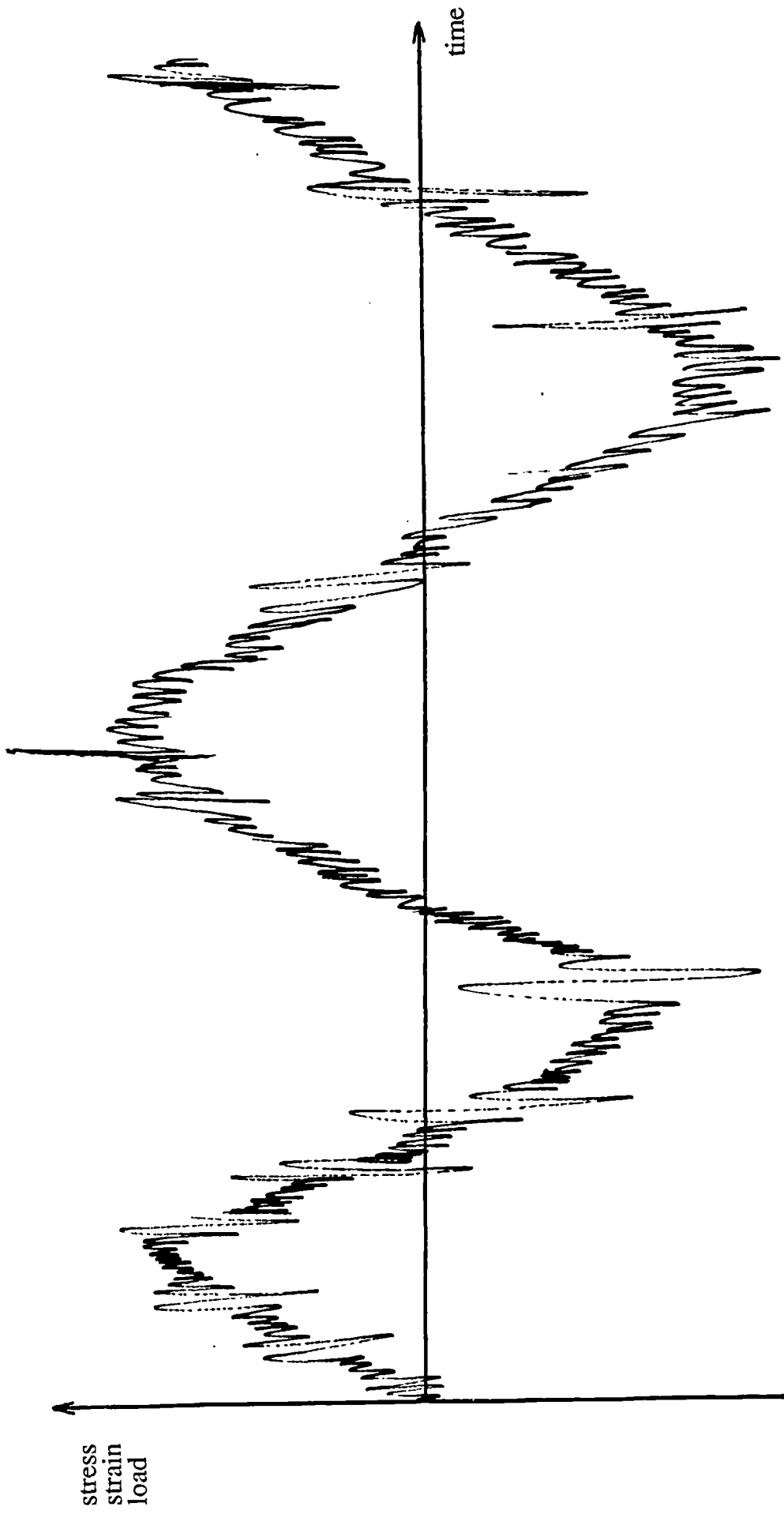


Figure 2.2. The time response which results from the mixture of a low and high frequency.

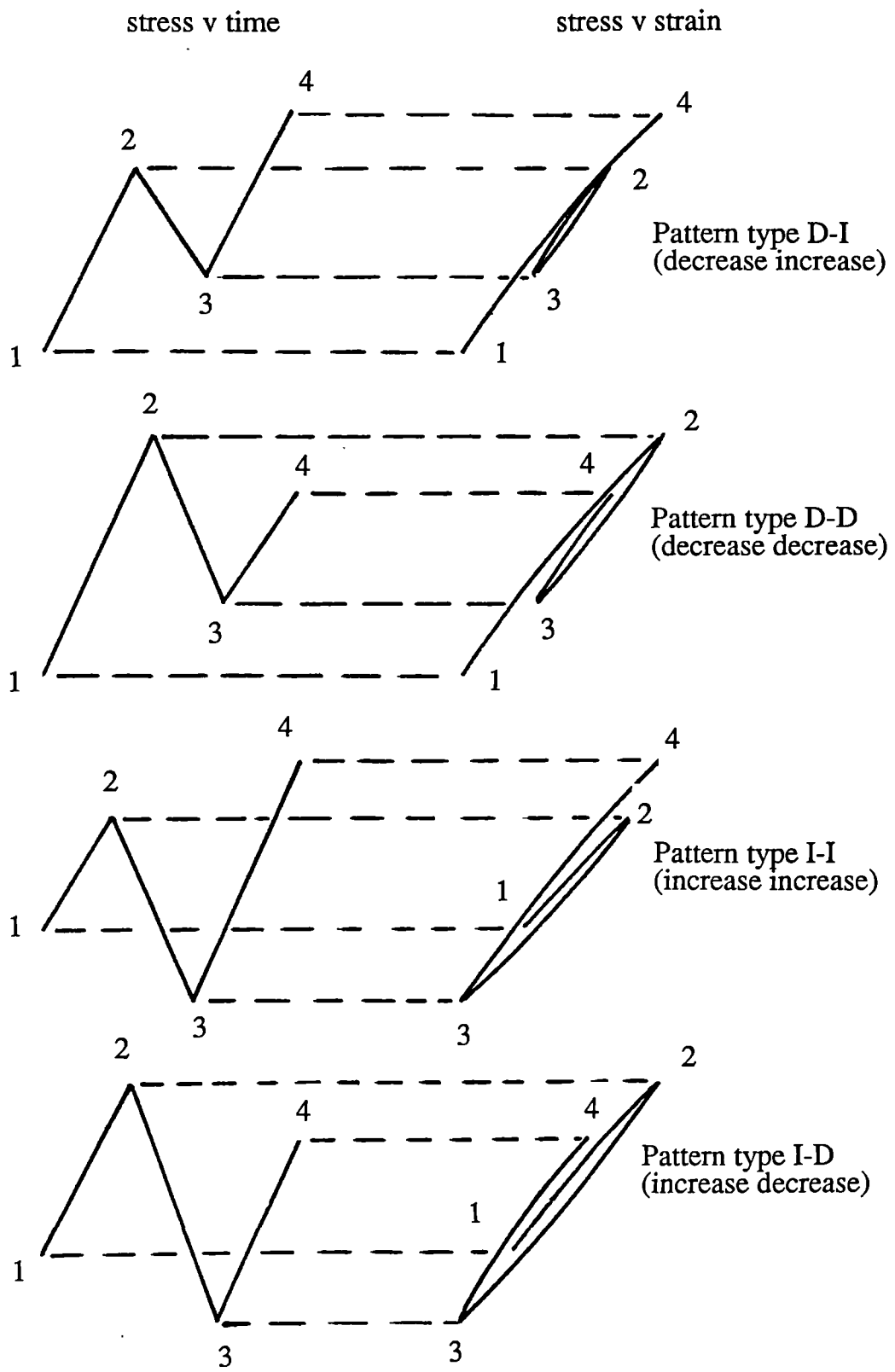
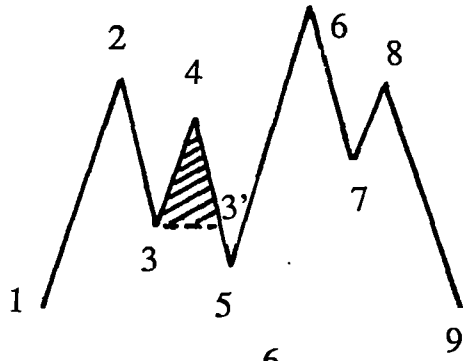
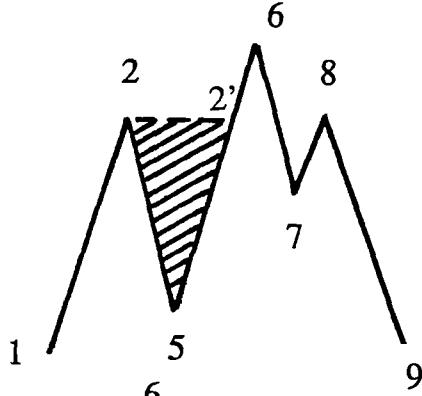


Figure 2.3. The four different types of pattern which are considered in the Pattern Classification Procedure.

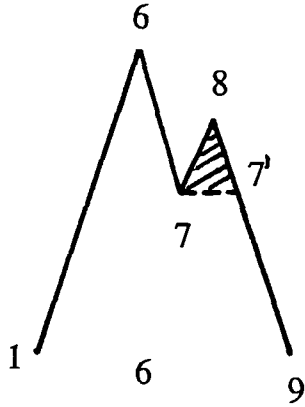
load/stress/strain v time



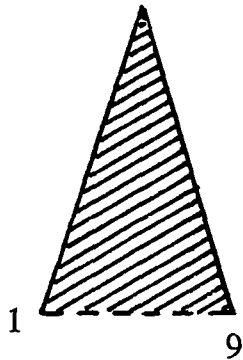
(i) time history showing first possible cycle to be extracted



+  (ii) first extracted cycle and 2nd possible cycle to be extracted



+  (iii) second extracted cycle and 3rd possible cycle to be extracted



+  (iv) third extracted cycle and 4th possible cycle to be extracted

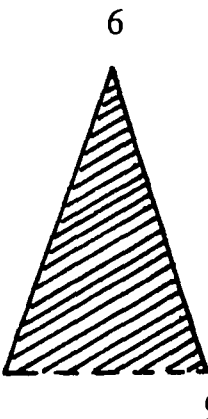
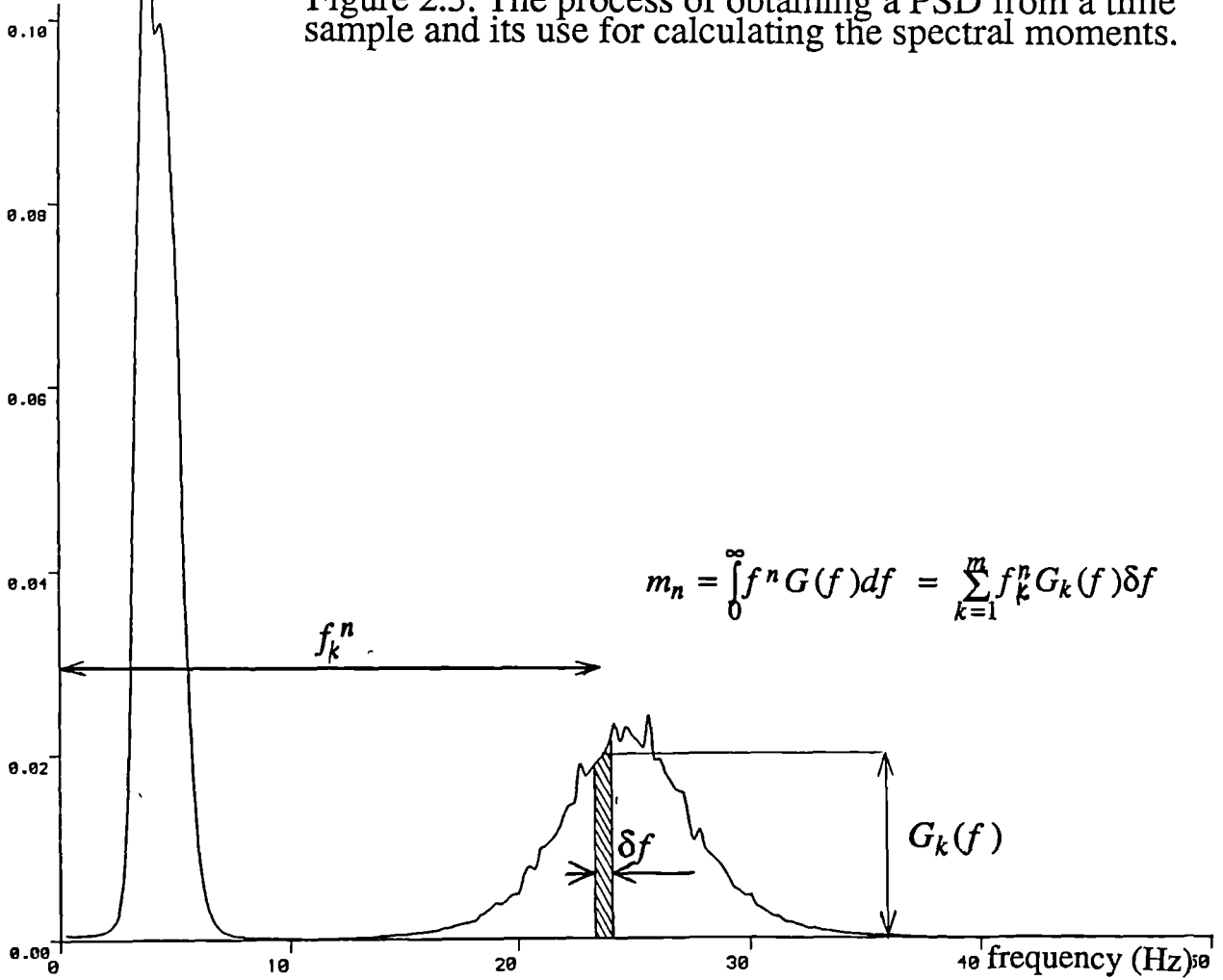
+  (v) last extracted cycle

Figure 2.4. An example of the use of the Pattern Classification Procedure for rainflow cycle counting a short length of time signal.

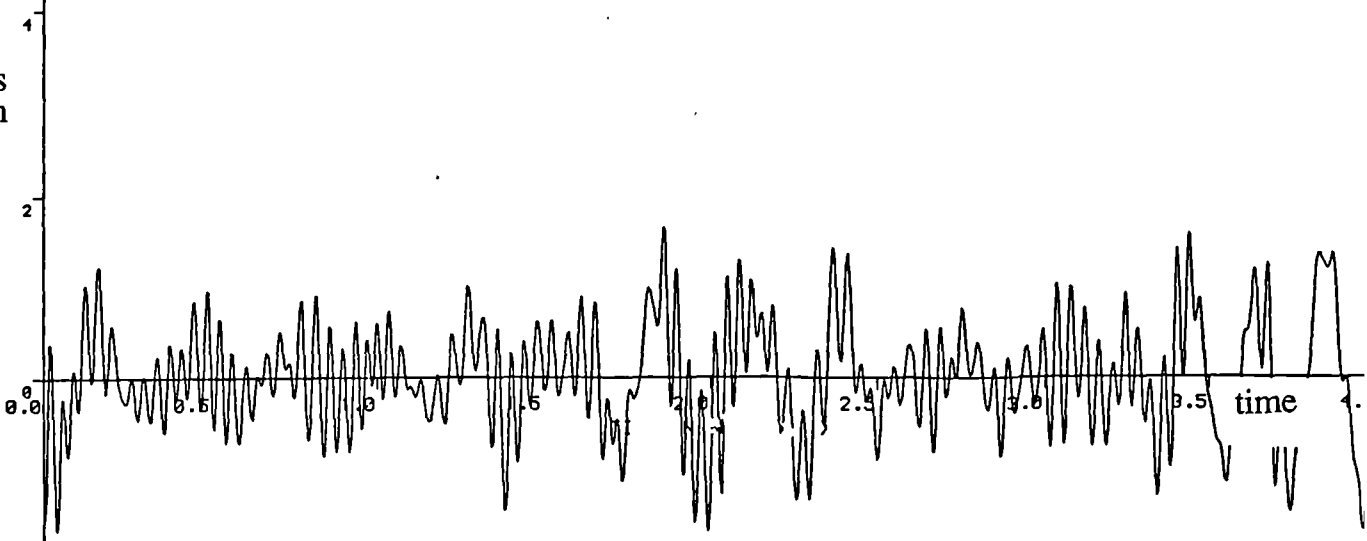
$\frac{(\text{response})^2}{\text{Hz}}$

Figure 2.5. The process of obtaining a PSD from a time sample and its use for calculating the spectral moments.



$$m_n = \int_0^{\infty} f^n G(f) df = \sum_{k=1}^m f_k^n G_k(f) \delta f$$

stress
strain
load



$$X_k = \frac{1}{N} \sum_{r=0}^{N-1} x_r e^{-i2\pi(\frac{kr}{N})}, \quad k=0,1,2,\dots,N-1$$

$$G_k(f) = 2L_s \left[(\text{real} X_k)^2 + (\text{imag} X_k)^2 \right]$$

3. An investigation of the fatigue damage potential of individual frequency components within any power spectral density data using an empirical solution for the prediction of 'ordinary' and 'rainflow' ranges.

3.1. Introduction

This chapter describes an investigation which was carried out to assess fatigue damage "interaction effects" between discrete bands within Power Spectral Density (PSD) data. The terminology used should not be confused with fundamental interaction effects within the fatigue process (Booth,1972,ref.3.1).

Dirlik's (1985,ref.3.2) empirical solutions for ordinary and rainflow ranges are used to obtain the range probability density functions from PSD's. Therefore, the first part of this chapter will give details of the modelling process used to obtain these. An earlier, and less complete, empirical solution by Wirsching (refs.3.3,3.4,3.5) is also described, along with its limitations, because it is the more widely known of the two solutions.

Dirlik's solution is used to establish what effect stresses contained within a given frequency range have on fatigue damage when there are other frequencies present in the PSD data. This 'fatigue damage potential', is a simple concept for the narrow band case because there are no other frequencies present. However, for the wide band case, stresses contained in one frequency band have an influence on stresses contained within other frequency bands. These interactions between different frequency intervals are investigated and it is shown that the fatigue damage potential of one PSD interval is dependent not only on the magnitude of that interval but on the magnitudes of other frequency intervals present.

This 'Interaction' effect can be used to determine the change of fatigue damage for any given structure or component when parts of the signal or PSD data are altered. In the automotive industry a technique called 'remote parameter control'(RPC) has been used extensively to simulate service loadings in the test laboratory (refs,3.6-3.16). No standard method has been generally adopted for checking the equivalence of 'test' and 'desired' loading signals. Often, time or frequency domain information is checked only by eye. The 'fatigue damage potential' concept is shown to be one way of quantifying allowable variations from the desired test signal. Also, it is sometimes advantageous to remove

certain frequencies from the test signal. The effect on fatigue damage can again be quantified using this technique.

3.2. Previous solutions to the rainflow range program

Wirsching's solution has the form of a correction factor to be applied to the narrow band solution (equation 2.58) where;

$$E[D]_{RR} = E[D]_{NB} \lambda(b, \epsilon) \quad (3.1)$$

$\lambda(b, \epsilon)$, it is claimed, is a function of the irregularity factor γ (equation 2.52) and b , the slope of the S-N curve (figure 2.1). The full correction factor is;

$$\lambda(b, \epsilon) = a(b) + [1 - a(b)](1 - \epsilon)^{c(b)} \quad (3.2)$$

Where,

$$a(b) = 0.926 - 0.033b \quad ; \quad c(b) = 1.587b - 2.323 \quad ; \quad \epsilon = \sqrt{1 - \gamma^2} \quad (3.3)$$

This empirical solution was obtained by digital simulation of time samples from various PSD's. Seventeen unimodal and seventeen bimodal PSD's were used in the simulation. The parameters considered were, $b = 3, 4, 5, 6$ and 10 , for γ in the range 0.45 to 1.0 . No indication was given about the number of frequencies used or the minimum number of time points per cycle, although approximately 8000 cycles were generated per simulation. Factors such as the minimum number of time points per time cycle and the number of cycles used to carry out the simulation have a significant effect on the range predictions obtained. This is discussed in chapter 6, and it is shown that, particularly for the larger values of b , 8000 cycles may not be enough.

L.D.Lutes (1984, ref.3.17) compared the results obtained using this solution with other simulation studies (refs.3.18,3.19). Considerable scatter about the line representing equation 3.2, was observed from which it was concluded that the rainflow range function is not simply a function of γ and b , as suggested by Wirsching.

Dirlik has produced expressions which produce similar damage results, and in this study it was claimed that the rainflow range function is also dependent on the first moment of the PSD plot in addition to the factors mentioned above. This is not however the most important difference between the two sets of work. Dirlik did not obtain a

correction factor, but instead obtained expressions for the range probability functions, which are useful in determining the fatigue behaviour of structures. This was done using computer simulations to model the signals using the Monte Carlo technique. Seventy PSD's were considered of various shapes. 20480 time points were used for each simulation with an average number of points per cycle of 10 which gave approximately 2000 cycles per simulation. Again, the work in chapter 6 shows that this number of cycles may be insufficient to quantify the range distributions with reasonable accuracy. Also, 10 samples per cycle may slightly underestimate some ranges by missing the true peak value. However, the errors involved with too low a sampling rate will be greatest for the higher frequencies which tend to have lower amplitudes. The effect on damage will therefore be minimal and so will not be considered further in this chapter although a full discussion of this topic is given in chapter 6.

The range distributions of these signals were compared to the zeroth, first, second and fourth moments of the PSD, and a least cost technique applied to the modelled expressions. Dirlik showed that the scatter in the results seen by Wirsching was considerably reduced by including the first moment in the modelling process. Two different empirical solutions were obtained, one for ordinary Ranges, and the other for rainflow ranges. Rainflow cycle counting will be covered in detail in chapter 5 and a historical perspective of rainflow and ordinary range counting techniques was given in chapter 2. Therefore at this point it is sufficient to briefly describe the main points of both (see sections 2.2 and 5.3).

Range cycle counting methods which identify and record ordinary ranges, extract the magnitude of the signal between each peak/trough and the next trough/peak.

Rainflow range counting techniques identify different parts of the signal which form complete stress-strain hysteresis loops. By removing the smaller closed loop cycles from the sample, eventually only larger cycles are left to be counted. The Rainflow method therefore identifies the larger variations in the signal which methods like the ordinary range technique miss. Individual rainflow range cycles can therefore be made up from different parts of the sample.

Dirlik's expression for ordinary ranges is;

$$P_{OR}(S) = \frac{\frac{C_1}{\tau} e^{-\frac{Z}{\tau}} + \frac{C_2 Z}{\alpha^2} e^{-\frac{Z^2}{2\alpha^2}}}{2\sqrt{m_o}} \quad (3.4)$$

Where m_n is obtained from equation 2.28(a), and;

$$C_1 = \frac{x_{var}}{\gamma^2} \quad \tau = 0.02 + \frac{2x_{var}}{\gamma} \quad C_2 = 1 - C_1 \quad \alpha = \gamma + \frac{x_{var}}{\gamma} \quad \gamma = \left[\frac{m_2^2}{m_0 m_4} \right]^{1/2}$$

$$S = 2\sqrt{m_0} Z \quad x_{var} = x_m - x_{min} \quad x_m = \frac{m_1}{m_0} \left[\frac{m_2}{m_4} \right]^{1/2} \quad x_{min} = \frac{\gamma}{1.0 + 1.25(1.0 - \gamma)}$$

And the expression for rainflow ranges is;

$$P_{RR}(S) = \frac{\frac{D_1}{Q} e^{-\frac{Z}{Q}} + \frac{D_2 Z}{R^2} e^{-\frac{Z^2}{2R^2}} + D_3 Z e^{-\frac{Z^2}{2}}}{2\sqrt{m_0}} \quad (3.5)$$

Where;

$$D_1 = \frac{2(x_m - \gamma^2)}{1 + \gamma^2} \quad D_2 = \frac{(1 - \gamma - D_1 + D_1^2)}{1 - R} \quad D_3 = 1 - D_1 - D_2$$

$$Q = \frac{1.25(\gamma - D_3 - (D_2 R))}{D_1} \quad R = \frac{\gamma - x_m - D_1^2}{1 - \gamma - D_1 + D_1^2}$$

3.3. A general solution for fatigue damage including the wide band case

From equations 3.4 and 3.5 the damage can be obtained in a similar way to section 2.7, where;

$$E[D]_{RR} = E[P] \frac{T}{k} \int_0^\infty S^b P_{RR}(S) dS \quad (3.6)$$

Equations 3.4, 3.5 and 3.6 have been expressed in terms of stress range (S). Dirlik's original expression was in terms of normalised variable;

$$Z = \frac{S}{2\sigma} \quad (3.7)$$

$E[D]_{RR}$ can be used to compute the fatigue damage directly from any PSD. The limitations of the narrow band solution $E[D]_{NB}$ no longer apply because the damage computation is based on rainflow ranges which, as explained earlier, give the best indication of fatigue damage for a wide band random signal.

$E[D]_{OR}$ represents the fatigue damage computed using ordinary ranges and is included for comparison purposes;

$$E[D]_{OR} = E[P] \frac{T}{k} \int_0^{\infty} S^b p_{OR}(S) dS \quad (3.8)$$

3.4. Computer programs used for analysis

The data used for this investigation was obtained from the following expression (Wirsching,1980,ref.3.20):

$$G(f) = A.H_s^\phi \frac{e^{\left[\frac{-1050}{(2\pi T_D f)^4} \right]}}{T_D^A (2\pi f)^5 \left\{ \left[1 - (f/f_n)^2 \right]^2 + \left[\frac{2\xi f}{f_n} \right]^2 \right\}^{1/2}} \quad (3.9)$$

This equation is useful for generating PSD shapes which are typical of the type of response experienced by offshore structures in the North Sea. T_D and H_s represent the dominant wave period and significant wave height (see chapter 7). The other factors in equation 3.9 are given by $\phi=3.25$, $A=5580$, $f_n=0.286$ and $\xi=0.02$.

The computer program was developed in three stages. The basic outline of the program is given in figure 3.1.

- [1] The first stage of the program calculates the fatigue damage of any structure or component given the input in the form of power spectral density data.
- [2] The second stage assesses the fatigue damage capabilities of stresses at particular frequencies.
- [3] Finally, with the ability developed in [2] to scan any given PSD plot for its fatigue damage potential, it was required to assess the interaction effects within any PSD data. This was performed by a 2 dimensional scanning technique.

The program was developed in a way that was able to deal with four types of input. They are;

- (a) A one or two peaked spectrum with peak heights A1 and A2, at frequencies F1 and F2 with slopes up to the first peak and away from the second peak of Q1

and Q2.

- (b) A manually input spectrum.
- (c) A two blocked rectangular spectrum of heights A1 and A2 spanning frequencies F1 to F2 and Q1 to Q2.
- (d) A two peaked spectrum based on dominant wave period and significant wave height.

A full list of the program is given in appendix 1.

3.4.1. Stage 1. Computation of fatigue damage using narrow band, rainflow range and ordinary range solutions

Three types of fatigue damage were calculated which were based on the narrow band solution (equation 2.58), and the wide band solutions using the ordinary and rainflow range density functions produced by Dirlik. The results are based on a traditional S-N curve approach. The values used for the material constants are $k=1.23 \times 10^{15}$ (MPa units) and $b=4.38$. These values are taken from ref.3.20, so that comparisons can be made with other work which used the same data (ref.3.21).

The process of calculation was similar for all three and is as follows;

- [1] Calculate moments of PSD plot using subroutine SIMP1.
- [2] Construct range probability density function using Dirlik's expressions or a Rayleigh function based on stress ranges.
- [3] Compute damage using equations 2.58, 3.6 or 3.8.

Damage calculations were carried out on the data used in ref.3.21. Numerical results are given in table 3.1 . The results show the following lives for the narrow band and wide band approaches.

$$LIFE_{NB} = 28.05 \text{ years.} \quad (3.10)$$

$$LIFE_{OR} = 53.98 \text{ years.} \quad (3.11)$$

$$LIFE_{RR} = 36.23 \text{ years.} \quad (3.12)$$

These results correlate well with those published by Chaudhury (ref.3.21). Comparisons with range distributions calculated directly from generated time signals are given in chapter 6 and confirm the accuracy of equations 3.4 and 3.5. The individual sea states and computed range functions are provided in figures 3.2 to 3.12.

The rainflow method therefore predicts a life 35% greater than the narrow band approach. This result is for a material constant value for b of 4.38, which is typical of many offshore structures, but for many engineering components a higher value of b may be applicable. In such circumstances the discrepancy between the life predictions based on the narrow band and rainflow assumptions would be much greater. Care has to be taken when employing new methods of analysis which predict longer component lives. However, the rainflow technique is widely believed to be a more accurate method of reducing the loading history for the purpose of computing the fatigue damage of a component. This modification to any fatigue analysis is therefore acceptable. Dealing with offshore structures specifically, the significance of this increase in predicted life could easily be magnified by the need to recheck older structures. As any structure approaches the end of the fatigue life predicted by narrow band methods, this new approach could double or treble its predicted residual life. This is because any new prediction of life would be from the original construction date.

The range function shapes are interesting in many ways. The familiar Rayleigh function is present for the narrow band case, however, it is the difference between the rainflow range and ordinary range functions which is significant. The rainflow range function is higher at low and high stress ranges because the rainflow range technique extracts small range cycles leaving larger cycles to be counted later. This has the effect of increasing the probabilities at low and high ranges. This is important because it is the few extra high range cycles which cause greatest difference to the damage. It can be seen that the Rayleigh function has a higher probability at all high stress ranges, as expected, because it matches all peaks with corresponding troughs regardless of whether such cycles are present. Finally, note how the three range functions converge at high values of the irregularity factor. This would also be expected because, for a narrow band signal, the

three techniques extract the same information. This is the limiting case where all peaks are joined to adjacent troughs.

The ability to deal with an endurance limit was included in the program. However, for limits below 50MPa there is no significant change from the damage obtained without an endurance limit. Also, the endurance limit does not affect the rest of the work carried out and is not discussed further.

3.4.2. Stage 2. Fatigue damage potential of individual frequency components

The second stage of the program was developed to assess how much fatigue damage is caused by discrete sections of the PSD plot. It is not possible to obtain any information from a fatigue calculation on a thin strip such as in figure 3.13, because in using only one thin strip the statistics of the signal have been changed. Instead it is the fatigue damage potential of that strip with all other strips present that is required. One acceptable way of doing this is to perform two fatigue calculations, one on the whole spectra and one on the spectra with the thin strip removed. In this way, if the strip is sufficiently small the statistics of the signal would not be changed. This approach was used. A moving strip was passed through the spectra and the 'reductions in damage' calculated. However, the amount of reduction is dependent on the strip width and so these reductions had to be normalised by this width. The linearity of the reductions obtained from various strip widths was checked by comparing results for two runs. One with a strip width of .005Hz and the other with a strip width of 0.025Hz. After normalisation the results were within two or three percent. Therefore, for the rest of this investigation, strip widths of 0.025Hz were used.

As an initial trial, the program was then used on sea state 1. The result was a plot of normalised reduction in damage as the moving strip passed through the spectra. Figure 3.14 shows the results. This was an interesting, though not very useful exercise since the variable height of the spectra disguised any other information. Therefore a rectangular spectra 0.4Hz wide and 1000 units high was used for a similar run. The results are plotted on figure 3.15. It is obvious from the shape of the curves that there is an interaction effect. This was confirmed by figure 3.16, where an additional block was added further up the frequency band. The presence of this block increases the normalised reductions

obtained from the primary block. A more thorough investigation of this interaction effect was therefore undertaken.

3.4.3. Stage 3. Interactions between discrete frequency components within the PSD.

Figure 3.17 shows the proposed analysis method. As before a moving strip is passed through the block, but in addition, a secondary strip is removed. In this way a 'reduction in reduction' can be obtained for each moving strip in the presence of an 'interacting' strip at any position elsewhere in the block. Therefore for this example a 20x20 matrix can be set up as below;

$$\begin{bmatrix} D_{1-1} & * & D_{I-1} & * & D_{20-1} \\ * & * & * & * & * \\ D_{1-j} & * & D_{I-j} & * & D_{20-j} \\ * & * & * & * & * \\ D_{1-20} & * & D_{I-20} & * & D_{20-20} \end{bmatrix} \quad (3.13)$$

The notation used is that;

$$D_{IJ} = \text{damage at moving str pos } J, \text{ in the presence of int str } I \quad (3.14)$$

Table 3.2 gives a numerical example of this. The time scale used is not comparable with earlier examples so comparisons with those results cannot be made. The results for rainflow range, ordinary range and narrow band techniques are plotted in figures 3.18,3.19 and 3.20.

What we have investigated here is the effect of 'primary interaction'. It was necessary to assess if secondary interaction effects were significant. If no such secondary interaction effects were present then it should be possible to simply sum the primary interactions. For example, if a strip is chosen within the PSD plot, and then the interaction effects from all remaining strips taken away from the damage for the whole block, the result will be the damage attributable to that one isolated strip. The results, shown in table 3.3, confirm this assumption.

Before using this technique it would be necessary to assess "sizing effects" on the behaviour of this interaction. This is the effect of varying the height of the plot (This may be non-linear).

On the question of errors within the program used, it was found that the major source of error was using too small an integration limit for the range functions. Only small errors were induced by varying the number of points chosen for either the frequency plot or the range functions. This is shown in table 3.4. Double precision variables were used throughout the program.

3.5. Conclusions

A program has been developed that calculates the fatigue damage of a structure using three different methods. Rainflow range, ordinary range and narrow band techniques are used with the stress histories being input in the form of a power spectral density plot. The results obtained were in good agreement with those of Chaudhury (1985) (work in chapter 6 confirms that the empirical solutions developed by Dirlik provide accurate estimations of the ordinary and rainflow range distributions). Results obtained for typical North Sea conditions show that the Rainflow method predicts lives 35% greater than the narrow band approach for a material constant value b of 4.38.

Secondly a program was developed to determine the damage contributions from discrete frequency bands within the PSD plot. These damage contributions were seen to be not simply related to frequency, but dependent on other frequency bands within the PSD data.

This investigation shows that there is an interaction effect within PSD data. The results obtained indicate that it is possible to quantify this interaction. Furthermore, with the aid of Finite Element programs it may be possible to obtain a direct relationship between a small change in structural geometry and the overall fatigue damage without a completely new fatigue damage analysis. This will result in a considerable saving in time and money.

In addition to applications in the offshore industry, this work may be useful in areas such as automotive design and testing. One such example is Remote Parameter Control (RPC). This is where frequency domain control is used for the loading simulation of automotive components. It may be possible to clarify the amount by which the PSD input can vary for a maximum given error in the fatigue damage calculation.

More generally, this technique may be useful in any area where truncation of the input signal is necessary. One example is where cheaper signal reproduction costs are required by simplification of the loading.

3.6. References.

- (3.1) R.T.Booth, The effects of stress interaction and frequency composition in random load fatigue, PhD Warwick University, 1972.
- (3.2) T.Dirlik, Application of computers in Fatigue Analysis, University of Warwick Thesis, Jan 1985.
- (3.3) P.H.Wirsching and A.M.Shehata, Fatigue under wide band random stresses using the rain-flow method, Journal of Engineering Materials and Technology, ASME, Vol 99, July 1977.
- (3.4) P.H.Wirsching, Fatigue reliability for offshore structures, Journal of Structural Engineering, ASCE, Vol 110, No. 10, October 1984.
- (3.5) P.H.Wirsching, Fatigue reliability analysis in offshore structures, presented at the ASCE National Convention, held at St. Louis, Mo., 1981.
- (3.6) C.J.Dodds, The laboratory simulation of vehicle service stress, paper 73-DET-24 presented at the ASME Design Engineering Technical Conference, Cincinnati, Ohio, September 9-12, 1973.
- (3.7) B.W.Cryer and P.E.Nawrocki, A road simulation system for heavy duty vehicles, reprinted from Vol. 85, Section 2, 1976 SAE Transactions.
- (3.8) C.J.Dodds, Environmental testing under random loading, paper presented at the Symposium on Service Fatigue Loads Monitoring, Simulation and Analysis, Atlanta, Georgia, November 14-15, 1977.
- (3.9) R.A.Lund, Multiple environmental simulation techniques, paper presented at the Symposium on Experimental Simulation Testing of Motor Vehicles and Their Elements, Warsaw, Poland, October 1-2, 1979.
- (3.10) J.Peterson and G.Weißberger, The conception, description, and application of a new vehicle endurance test system at AUDI NSU, paper 820094 presented at SAE Automotive Engineering Congress and Exposition, Detroit, Michigan, February 22-26, 1982.
- (3.11) R.A.Lund and K.H.Donaldson,jr., Approaches to vehicle dynamics and durability testing, paper 820092 presented at SAE Automotive Engineering Congress and Exposition, Detroit, Michigan, February 22-26, 1982.

- (3.12) J. Peterson and G. Weißberger, Strain simulation on the complete vehicle... The Audi Road Simulator, Closed Loop (MTS publication), Summer 1984.
- (3.13) R.S. Stephens and F. Schuetz, Current and future technologies of fatigue laboratory automation, paper presented at International Seminar on Current and Future Techniques for Testing of Vehicles and Related Structural Components, Turin, Italy, June 7-8, 1984.
- (3.14) K.J. White, The Audi road simulator - a practical laboratory approach, C110/85, IMechE, 1985.
- (3.15) A.G. Herraty, Selection criteria for simulation test systems, C101/85. IMechE, 1985.
- (3.16) P. Grote and G. Grenier, Taking the test track to the lab, reprinted from 'Automotive Engineering', Vol. 95, No. 6, June 1987.
- (3.17) L.D. Lutes, Stochastic fatigue damage accumulation, Journal of Structural Engineering, ASCE, Vol. 110, No. 11, 1984
- (3.18) M. Corazao, Stress ranges produced by stochastic loads, MSc thesis presented to Rice University, Houston, Texas, 1981.
- (3.19) J.J. Zimmerman, Stochastic stress history simulation for fatigue analysis, MSc thesis presented to Rice University, Houston, Texas, 1983.
- (3.20) P.H. Wirsching and M.C. Light Fatigue under wide band random stresses, Journal of the Structural Division, ASCE, paper 15574, Vol 106, No. ST7, 1980.
- (3.21) G.K. Chaudhury and W.D. Dover, Fatigue Analysis of Offshore Platforms Subject to Sea Wave Loading, Int J Fatigue 7 No 1, Jan 1985.

sea state	sig. vv. ht.	dom. per.	fract. time in sea state i	exp. no. pks per sec.	exp. no. zero csgs. per sec.	irreg. fact.	root mean sq. value	rel. mean	RR dam. per sec. x 10 ⁻¹⁵	OR dam. per sec. x 10 ⁻¹⁵	NB dam. per sec. x 10 ⁻¹⁵
SS	H _s	T _D	T	E[P]	E[0]	γ	rms	X _m	D _{RR}	D _{OR}	D _{NB}
1	16.01	17.3	0.0000368	0.245	0.124	0.507	47.72	0.393	013422	004681	007926
2	14.48	16.5	0.0000932	0.247	0.132	0.534	41.32	0.419	019516	007495	025994
3	12.96	15.8	0.00037	0.250	0.140	0.559	35.19	0.445	041065	017298	054505
4	11.43	14.7	0.0022	0.254	0.153	0.603	29.81	0.491	130094	064776	171259
5	9.90	13.6	0.0073	0.257	0.168	0.651	24.78	0.543	211708	125812	275243
6	8.38	12.7	0.0135	0.260	0.180	0.693	19.89	0.592	160215	110360	205285
7	6.86	11.6	0.0265	0.264	0.197	0.746	15.54	0.656	124188	095935	155527
8	5.53	10.3	0.06	0.268	0.216	0.809	11.66	0.737	093291	081890	112576
9	3.81	9.1	0.21	0.271	0.234	0.863	7.87	0.810	064202	063103	074091
10	2.28	7.7	0.49	0.275	0.252	0.917	4.32	0.885	012658	012745	013878
11	0.76	4.4	0.19	0.283	0.279	0.986	1.69	0.982	000098	000099	000099
									870457	584194	1106383

Table 3.1. Fatigue damage calculations using the narrow band, ordinary range and rainflow range methods for 11 sea states which are typical of the environmental conditions experienced in the north sea.

interacting strip position

0.012	0.00000E+00	0.91669E-12	0.87396E-12	0.84748E-12	0.83363E-12	0.82972E-12	0.83364E-12	0.84355E-12	0.85765E-12	0.87409E-12
0.037	0.89067E-12	0.90475E-12	0.91283E-12	0.91003E-12	0.88924E-12	0.83966E-12	0.93421E-12	0.93421E-12	0.93421E-12	0.93421E-12
0.062	0.14630E-11	0.00000E+00	0.14076E-11	0.13667E-11	0.13748E-11	0.13702E-11	0.13715E-11	0.1373E-11	0.13661E-11	0.13963E-11
0.087	0.19036E-11	0.14143E-11	0.14178E-11	0.14135E-11	0.13966E-11	0.13934E-11	0.15025E-11	0.15025E-11	0.15025E-11	0.15025E-11
0.112	0.15367E-11	0.15021E-11	0.00000E+00	0.16573E-11	0.16454E-11	0.18394E-11	0.18381E-11	0.18403E-11	0.18449E-11	0.18503E-11
0.137	0.18554E-11	0.18584E-11	0.18583E-11	0.18522E-11	0.18371E-11	0.18066E-11	0.19970E-11	0.19970E-11	0.19970E-11	0.19970E-11
0.162	0.23262E-11	0.22971E-11	0.22732E-11	0.00000E+00	0.22419E-11	0.22338E-11	0.22299E-11	0.22291E-11	0.22301E-11	0.22317E-11
0.187	0.22328E-11	0.22321E-11	0.22285E-11	0.22202E-11	0.22047E-11	0.21765E-11	0.24129E-11	0.24129E-11	0.24129E-11	0.24129E-11
0.212	0.26504E-11	0.26232E-11	0.25994E-11	0.25799E-11	0.00000E+00	0.25548E-11	0.25483E-11	0.25447E-11	0.25427E-11	0.25412E-11
0.237	0.25390E-11	0.25380E-11	0.25282E-11	0.25172E-11	0.2497E-11	0.24705E-11	0.27510E-11	0.27510E-11	0.27510E-11	0.27510E-11
0.262	0.29113E-11	0.28835E-11	0.28582E-11	0.28367E-11	0.28196E-11	0.00000E+00	0.27979E-11	0.27916E-11	0.27870E-11	0.27828E-11
0.287	0.27779E-11	0.27712E-11	0.27415E-11	0.27475E-11	0.27267E-11	0.26941E-11	0.30158E-11	0.30158E-11	0.30158E-11	0.30158E-11
0.312	0.31143E-11	0.30839E-11	0.30560E-11	0.30319E-11	0.30122E-11	0.29969E-11	0.00000E+00	0.29769E-11	0.29700E-11	0.29663E-11
0.337	0.29566E-11	0.29474E-11	0.29353E-11	0.29182E-11	0.28936E-11	0.28562E-11	0.32148E-11	0.32148E-11	0.32148E-11	0.32148E-11
0.362	0.32674E-11	0.32329E-11	0.32015E-11	0.31743E-11	0.31518E-11	0.31339E-11	0.31201E-11	0.00000E+00	0.31066E-11	0.30926E-11
0.387	0.30839E-11	0.30732E-11	0.30589E-11	0.30391E-11	0.30166E-11	0.29679E-11	0.33581E-11	0.33581E-11	0.33581E-11	0.33581E-11
0.412	0.33808E-11	0.33410E-11	0.33053E-11	0.32746E-11	0.32491E-11	0.32286E-11	0.32125E-11	0.31999E-11	0.00000E+00	0.31804E-11
0.437	0.31707E-11	0.31390E-11	0.31343E-11	0.31215E-11	0.30899E-11	0.30427E-11	0.34574E-11	0.34574E-11	0.34574E-11	0.34574E-11
0.462	0.34661E-11	0.34200E-11	0.33796E-11	0.33450E-11	0.33164E-11	0.32933E-11	0.32750E-11	0.32607E-11	0.32492E-11	0.00000E+00
0.487	0.32291E-11	0.32012E-11	0.32012E-11	0.31786E-11	0.31452E-11	0.30956E-11	0.35262E-11	0.35262E-11	0.35262E-11	0.35262E-11
0.512	0.35362E-11	0.34833E-11	0.34341E-11	0.33994E-11	0.33677E-11	0.33419E-11	0.33214E-11	0.33055E-11	0.32930E-11	0.32826E-11
0.537	0.00000E+00	0.32613E-11	0.32462E-11	0.32243E-11	0.31917E-11	0.31437E-11	0.35797E-11	0.35797E-11	0.35797E-11	0.35797E-11
0.562	0.36052E-11	0.35465E-11	0.34963E-11	0.34539E-11	0.34187E-11	0.33901E-11	0.33674E-11	0.33498E-11	0.33363E-11	0.33256E-11
0.587	0.33163E-11	0.00000E+00	0.32933E-11	0.32745E-11	0.32464E-11	0.32064E-11	0.36347E-11	0.36347E-11	0.36347E-11	0.36347E-11
0.612	0.36893E-11	0.36260E-11	0.35720E-11	0.35262E-11	0.34879E-11	0.34564E-11	0.34312E-11	0.34115E-11	0.33967E-11	0.33857E-11
0.637	0.33771E-11	0.33693E-11	0.00000E+00	0.33474E-11	0.33294E-11	0.33081E-11	0.37107E-11	0.37107E-11	0.37107E-11	0.37107E-11
0.662	0.38080E-11	0.37432E-11	0.36875E-11	0.36395E-11	0.35985E-11	0.35639E-11	0.35356E-11	0.35132E-11	0.34964E-11	0.34845E-11
0.687	0.34768E-11	0.34720E-11	0.34689E-11	0.00000E+00	0.34683E-11	0.34683E-11	0.38322E-11	0.38322E-11	0.38322E-11	0.38322E-11
0.712	0.39892E-11	0.39283E-11	0.38742E-11	0.38259E-11	0.37828E-11	0.37451E-11	0.37129E-11	0.36866E-11	0.36667E-11	0.36531E-11
0.737	0.36462E-11	0.36458E-11	0.36529E-11	0.36703E-11	0.00000E+00	0.37931E-11	0.40341E-11	0.40341E-11	0.40341E-11	0.40341E-11
0.762	0.42787E-11	0.42301E-11	0.41829E-11	0.41369E-11	0.40928E-11	0.40516E-11	0.40146E-11	0.39831E-11	0.39585E-11	0.39426E-11
0.787	0.39372E-11	0.39450E-11	0.39707E-11	0.40248E-11	0.41322E-11	0.00000E+00	0.43732E-11	0.43732E-11	0.43732E-11	0.43732E-11
0.812	0.00000E+00									
0.837	0.00000E+00									
0.862	0.00000E+00									
0.887	0.00000E+00									
0.912	0.00000E+00									

moving strip position

Table 3.2. A numerical example of the application of equation 3.13, showing 'primary' interactions between frequency components within a rectangular PSD as shown in figure 3.17.

Frequency	Interacting Strip Number (I)	Damage at Moving Strip 11 with Interacting Strip at position (I)	Normalised Reduction in Damage
0.000→0.025	1	35362	435
0.025→0.050	2	34836	961
0.050→0.075	3	34381	1416
0.075→0.100	4	33996	1801
0.100→0.125	5	33677	2120
0.125→0.150	6	33419	2378
0.150→0.175	7	33214	2583
0.175→0.200	8	33055	2742
0.200→0.225	9	32930	2867
0.225→0.250	10	32826	2971
0.250→0.275	11	35797	0000
0.275→0.300	12	32613	3184
0.300→0.325	13	32462	3335
0.325→0.350	14	32243	3554
0.350→0.375	15	31917	3880
0.375→0.400	16	31437	4360
0.400→0.425	17	35797	0000
0.425→0.450	18	35797	0000
0.450→0.475	19	35797	0000
0.475→0.500	20	35797	0000
			38587

Table 3.3. The numerical results for primary interactions at moving strip 11 showing that the sum of the effects of the interacting strips is approximately equal to the fatigue damage potential of strip 11.

Conditions	Rainflow	Ordinary	NarrowBand
M=1000,L=1000,JN=11	14257	4692	19052
M=1000,L=1000,JN=10	14252	4692	19044
M=1000,L=1000,JN=9	14226	4691	19010
M=1000,L=1000,JN=8	14122	4689	18869
M=1000,L=1000,JN=7	13420	4681	17924
M=1000,L=1000,JN=10	14252	4692	19044
M=1000,L=500 ,JN=10	14252	4692	19044
M=1000,L=300 ,JN=10	14252	4692	19044
M=1000,L=200 ,JN=10	14252	4692	19044
M=1000,L=100 ,JN=10	14251	4692	19044
M=1000,L=50 ,JN=10	14251	4691	19043
M=1000,L=1000,JN=10	14252	4692	19045
M=500 ,L=1000,JN=10	14252	4692	19044
M=300 ,L=1000,JN=10	14252	4692	19044
M=200 ,L=1000,JN=10	14252	4692	19044
M=100 ,L=1000,JN=10	14247	4689	19037
M=50 ,L=1000,JN=10	14538	4839	19526

Table 3.4. Damage results for different values of the following; the number of frequency points used (M), the number of points used in the range probability function (L) and the range probability function integration limit (JN times the rms).

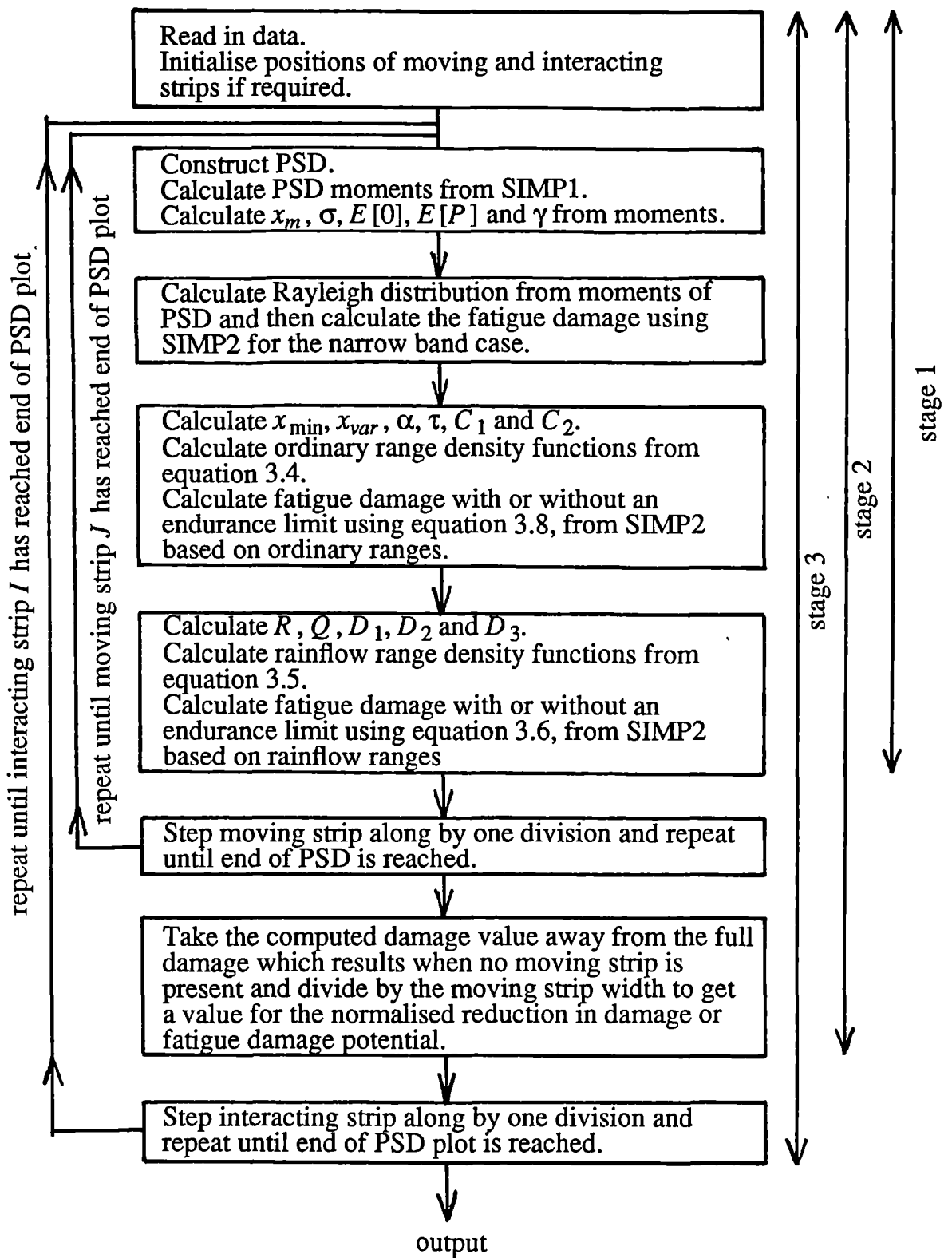


Figure 3.1. Basic outline of the three stages of programs used for the investigation.

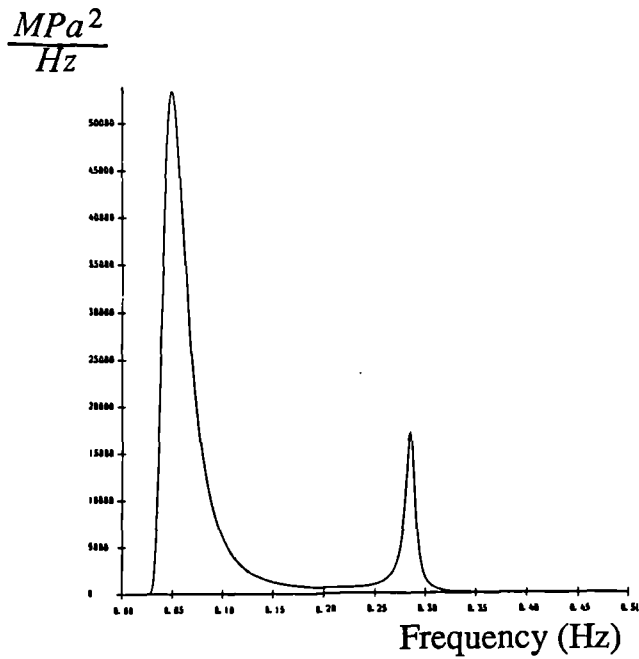


Figure 3.2(a). Sea state 1

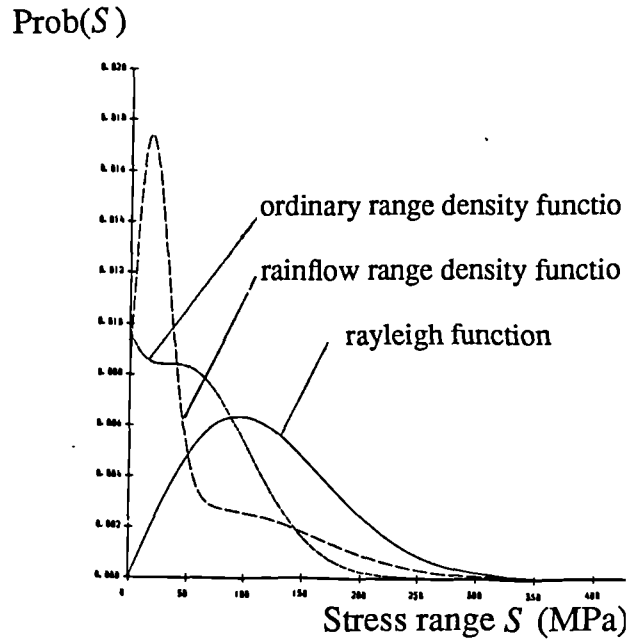


Figure 3.2(b). Narrow band, ordinary and rainflow range probability density functions computed from sea state 1 using equations 2.57, 3.4, 3.5.

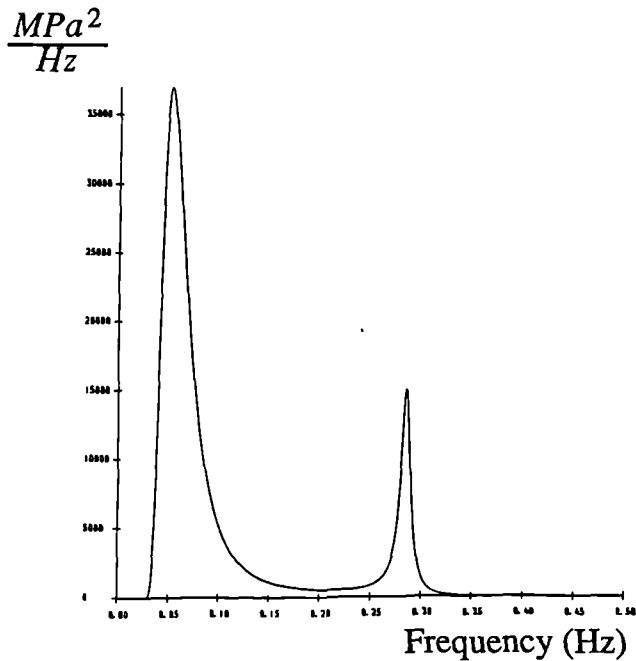


Figure 3.3(a). Sea state 2

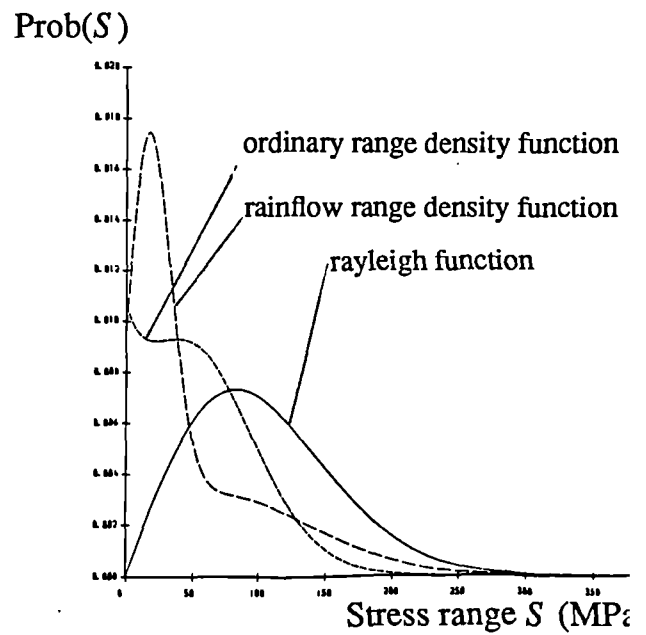


Figure 3.3(b). Narrow band, ordinary and rainflow range probability density functions computed from sea state 2 using equations 2.57, 3.4, 3.5.

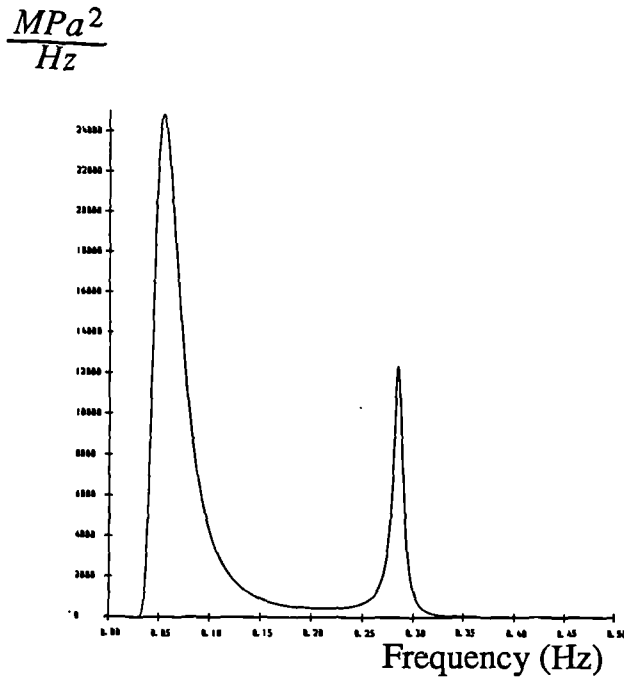


Figure 3.4(a). Sea state 3

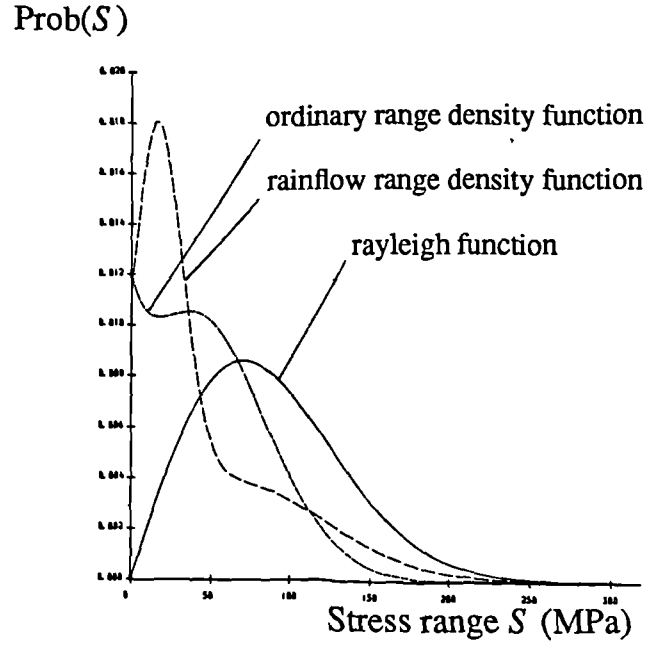


Figure 3.4(b). Narrow band, ordinary and rainflow range probability density functions computed from sea state 3 using equations 2.57, 3.4, 3.5.

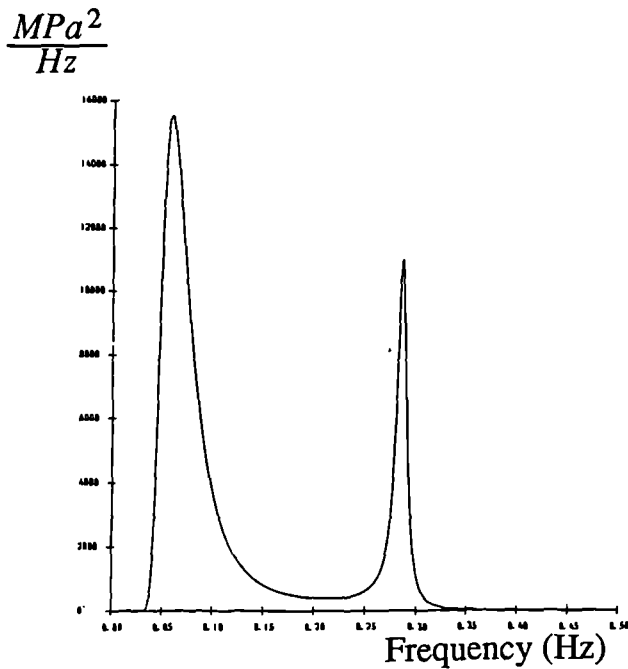


Figure 3.5(a). Sea state 4

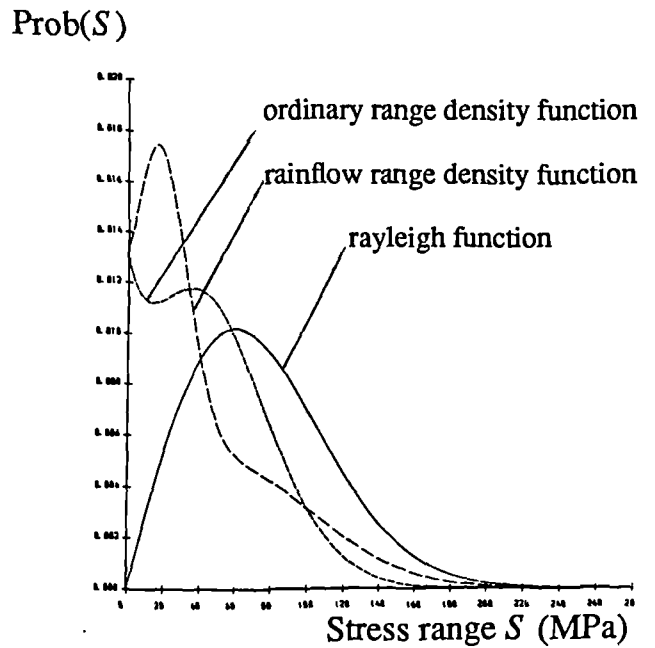


Figure 3.5(b). Narrow band, ordinary and rainflow range probability density functions computed from sea state 4 using equations 2.57, 3.4, 3.5.

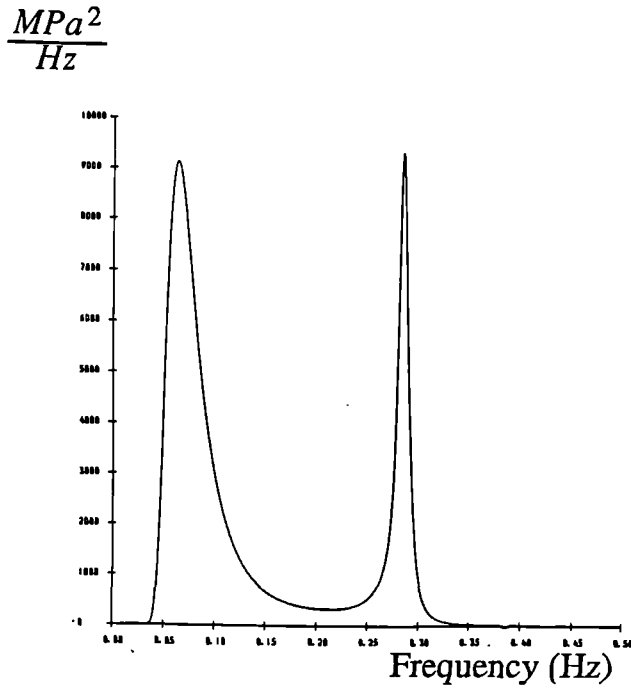


Figure 3.6(a). Sea state 5

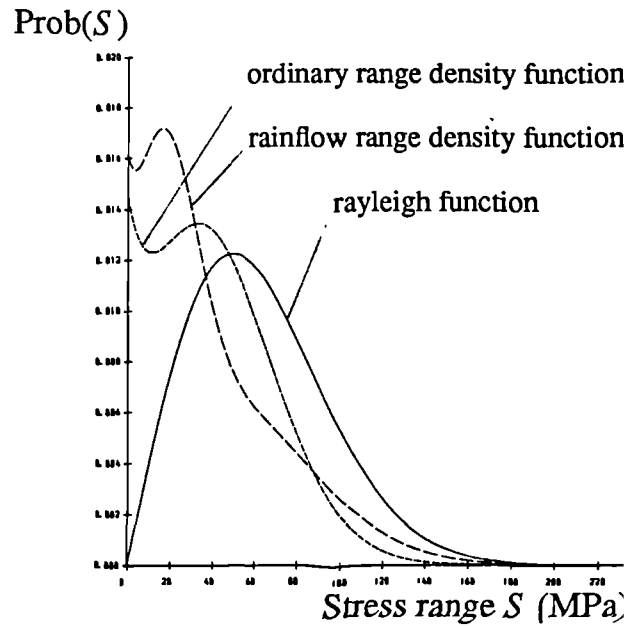


Figure 3.6(b). Narrow band, ordinary and rainflow range probability density functions computed from sea state 5 using equations 2.57, 3.4, 3.5.

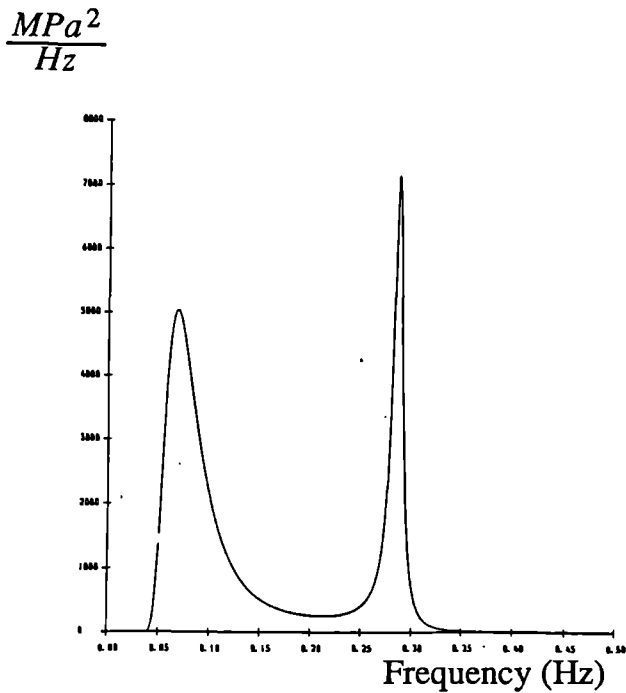


Figure 3.7(a). Sea state 6

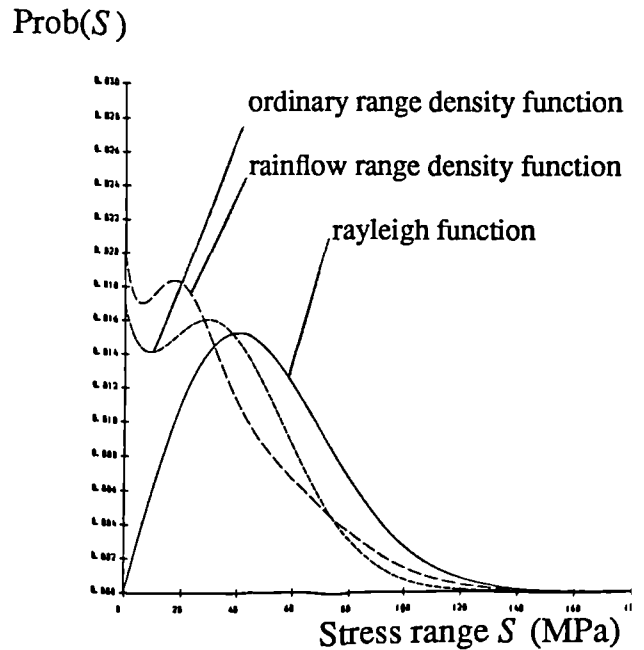


Figure 3.7(b). Narrow band, ordinary and rainflow range probability density functions computed from sea state 6 using equations 2.57, 3.4, 3.5.

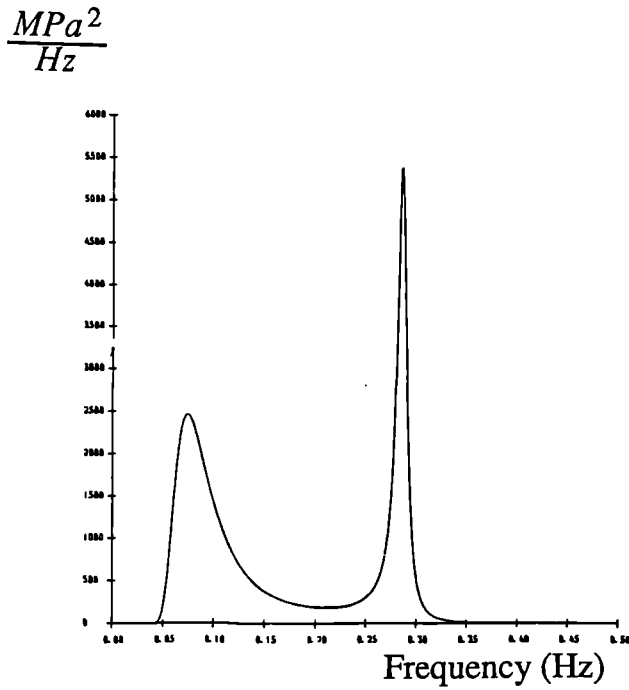


Figure 3.8(a). Sea state 7

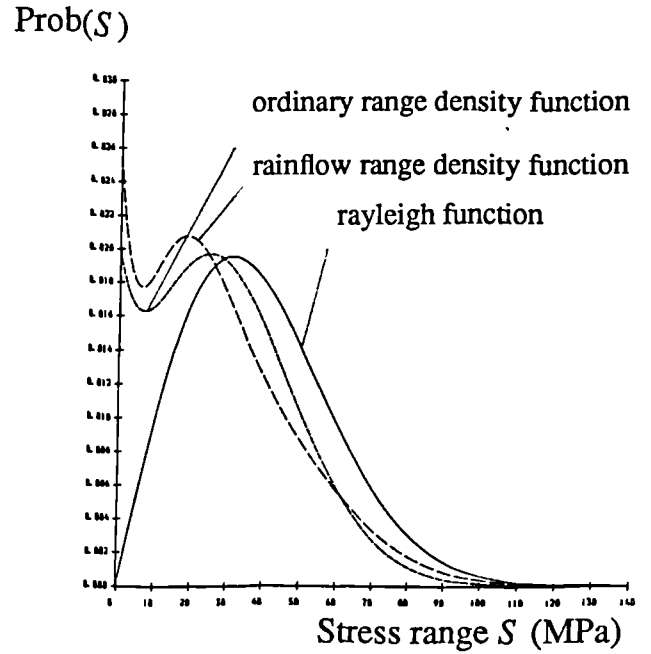


Figure 3.8(b). Narrow band, ordinary and rainflow range probability density functions computed from sea state 7 using equations 2.57, 3.4, 3.5.

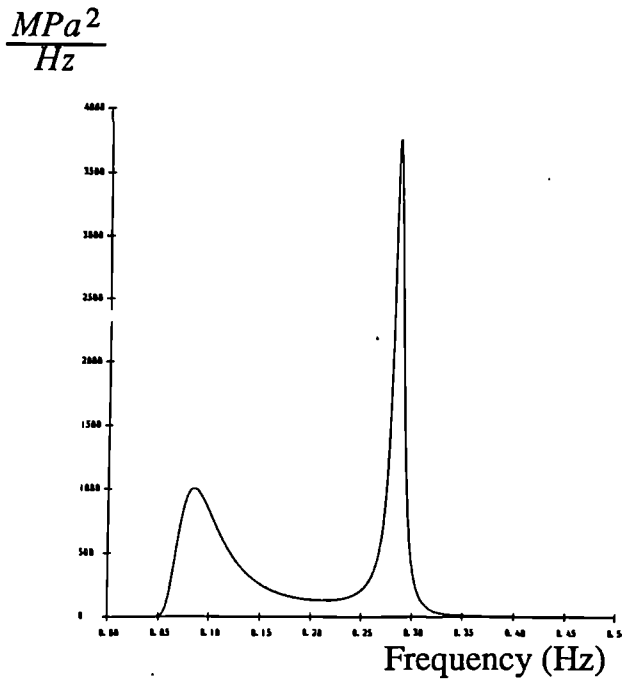


Figure 3.9(a). Sea state 8

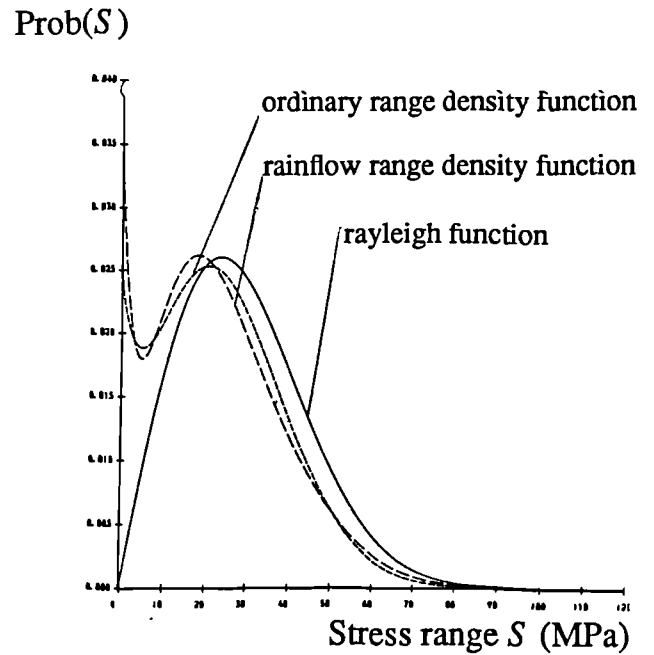


Figure 3.9(b). Narrow band, ordinary and rainflow range probability density functions computed from sea state 8 using equations 2.57, 3.4, 3.5.

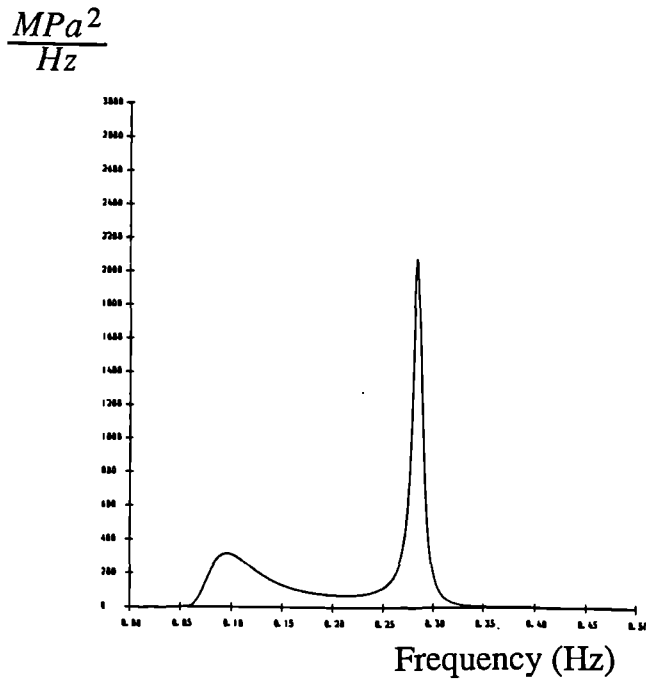


Figure 3.10(a). Sea state 9

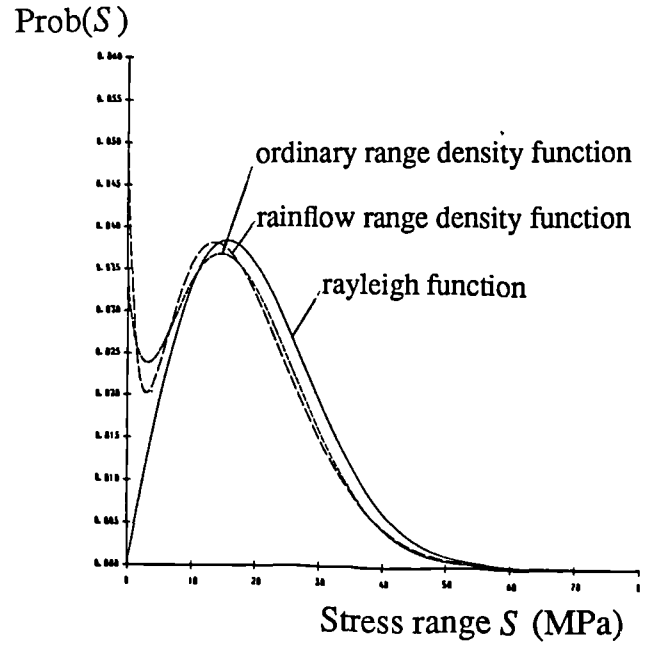


Figure 3.10(b). Narrow band, ordinary and rainflow range probability density functions computed from sea state 9 using equations 2.57, 3.4, 3.5.

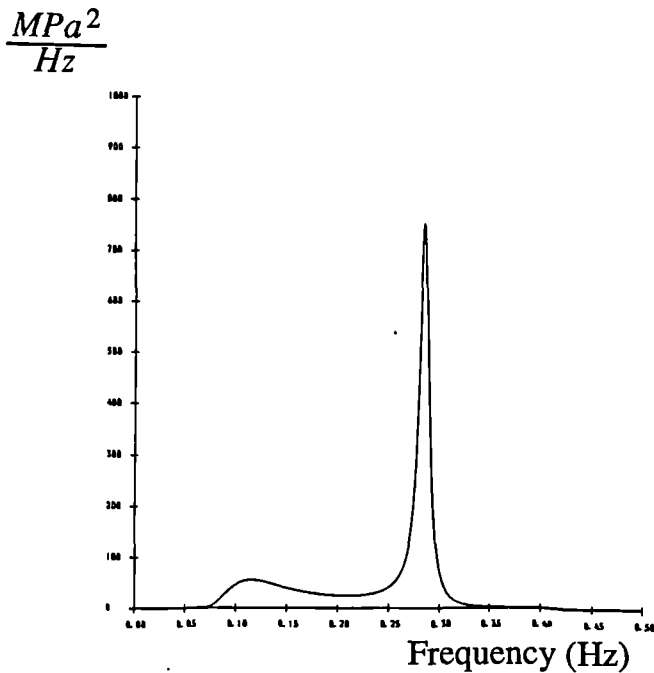


Figure 3.11(a). Sea state 10

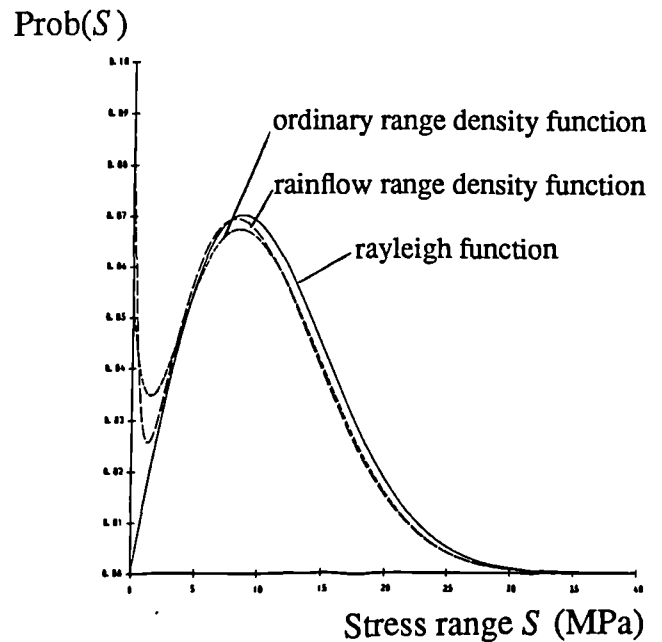


Figure 3.11(b). Narrow band, ordinary and rainflow range probability density functions computed from sea state 10 using equations 2.57, 3.4, 3.5.

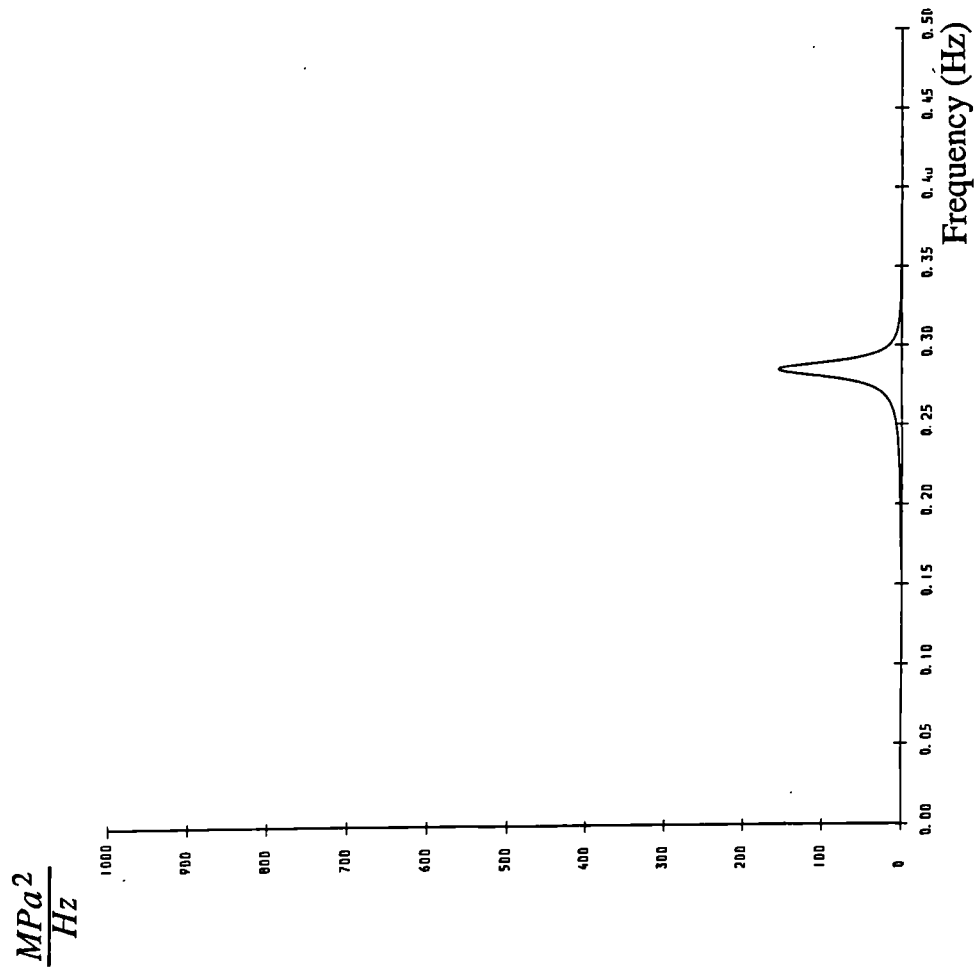


Figure 3.12(a). Sea state 11

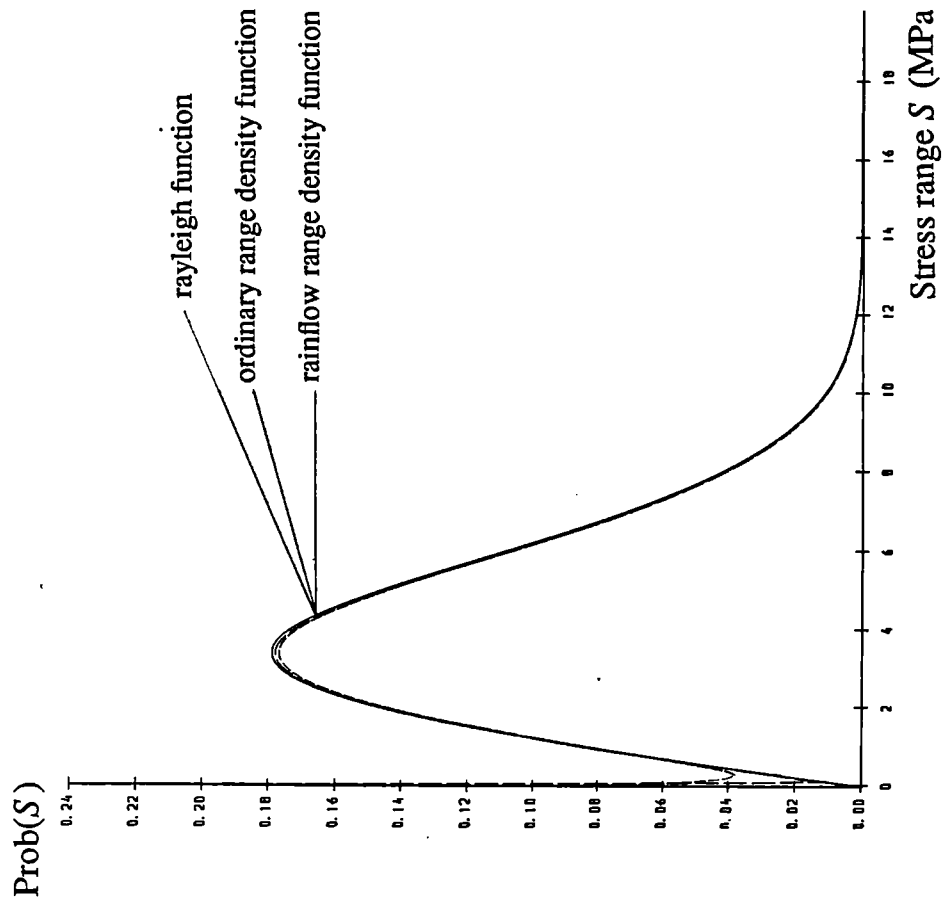


Figure 3.12(b). Narrow band, ordinary and rainflow range probability density functions computed from sea state 11 using equations 2.57, 3.4, 3.5.

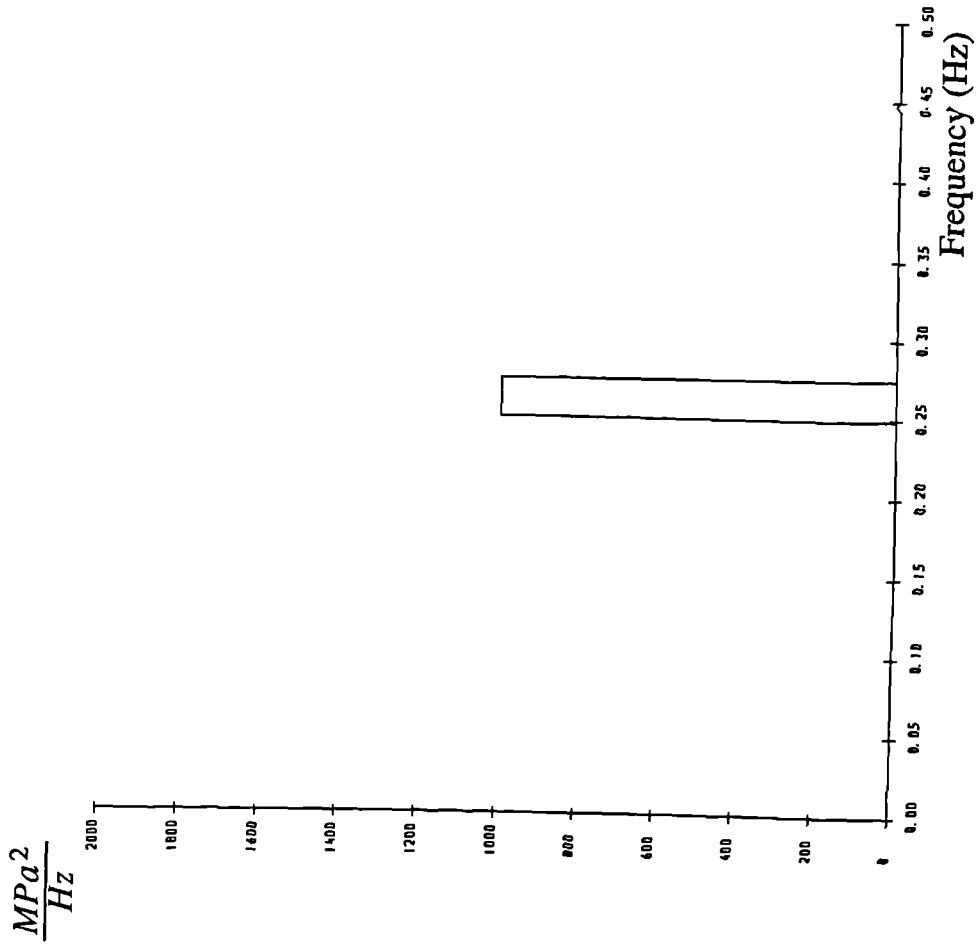


Figure 3.13. Isolated strip which does not take into account the effect of interactions between frequencies.

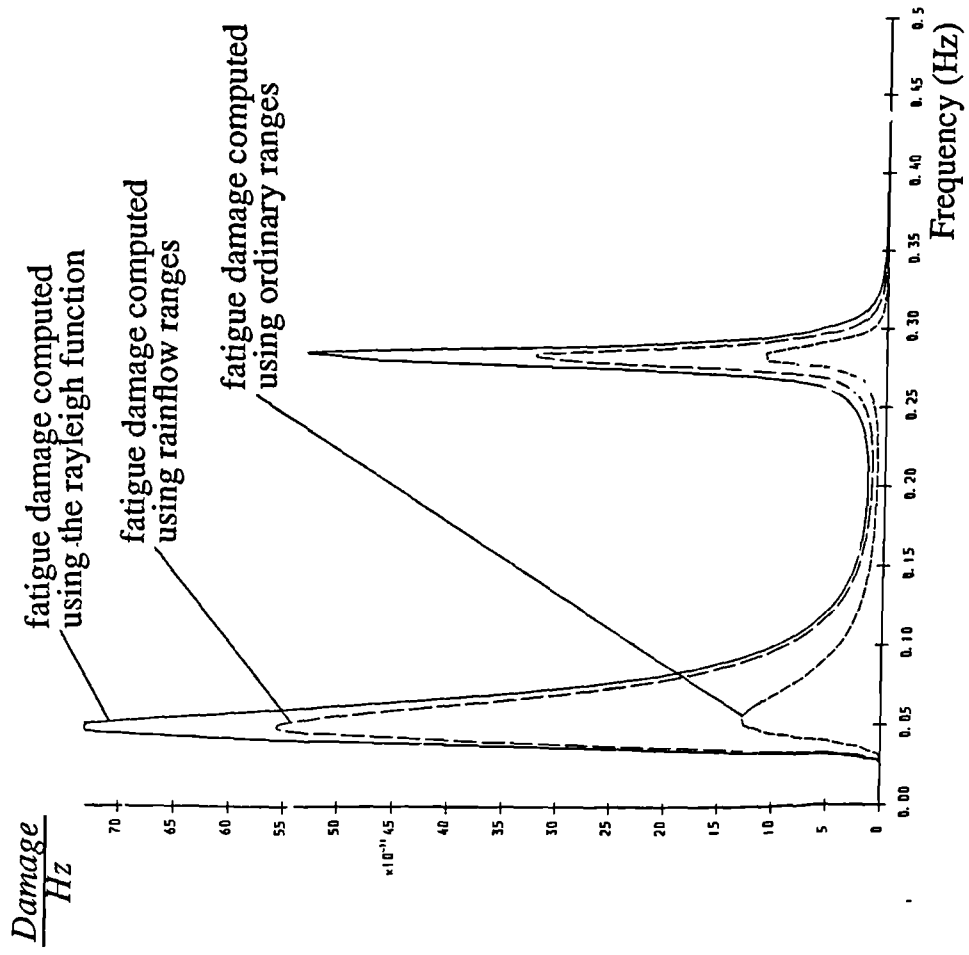


Figure 3.14. The fatigue damage potential of particular frequencies within sea state 1 calculated with the narrow band, ordinary range and rainflow range methods.

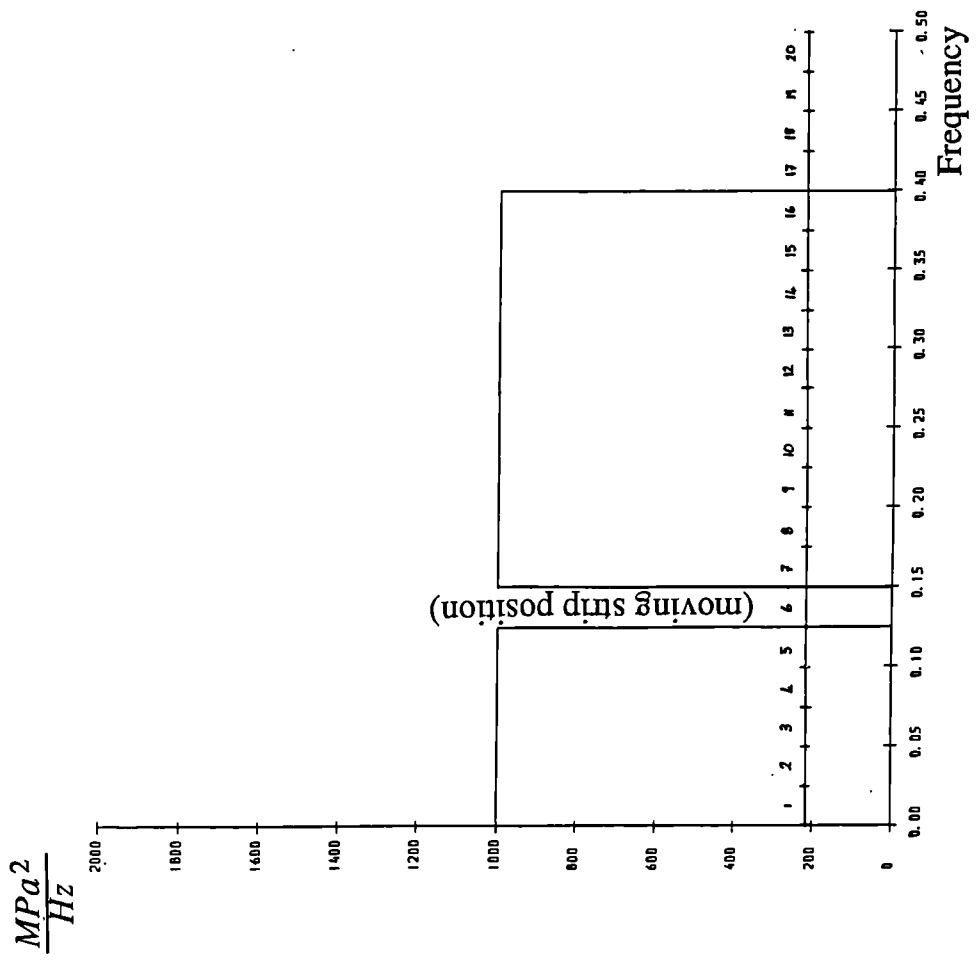


Figure 3.15(a). A rectangular PSD with a thin strip removed from a location which is stepped along the frequency axis and called a 'moving strip'.

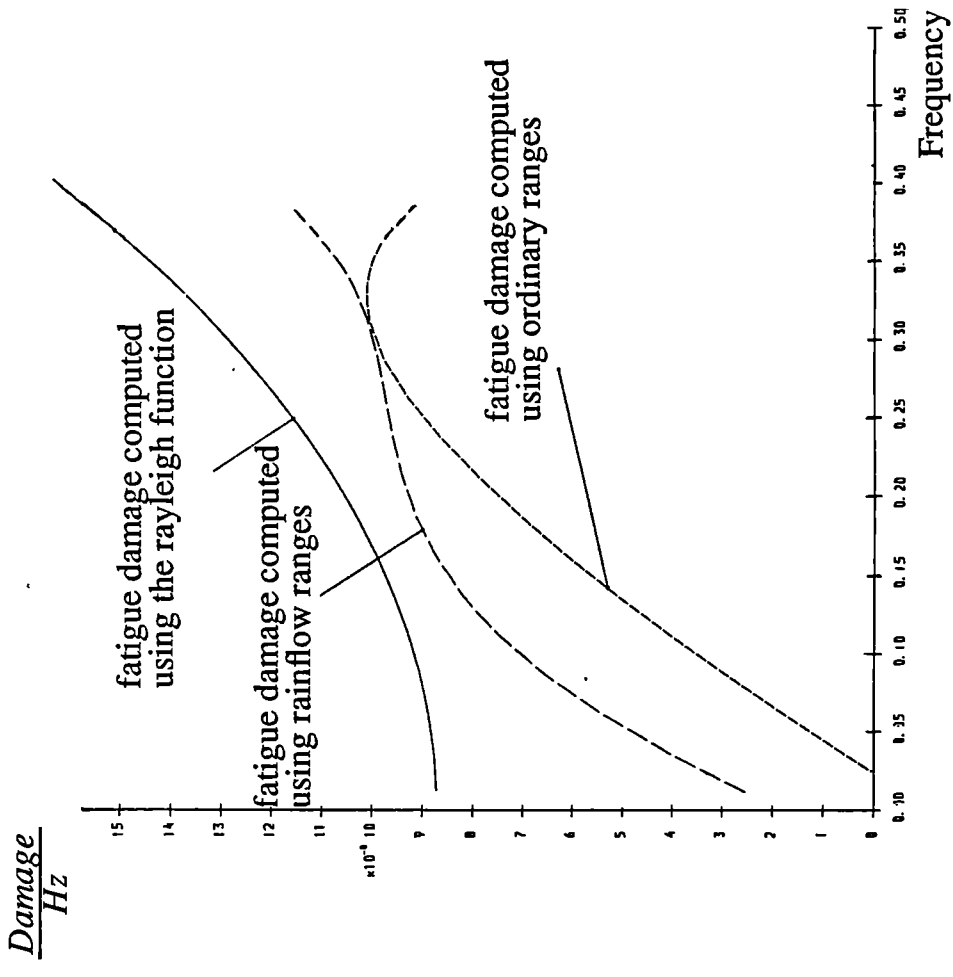


Figure 3.15(b). The effect on fatigue damage of removing one small strip from the PSD.

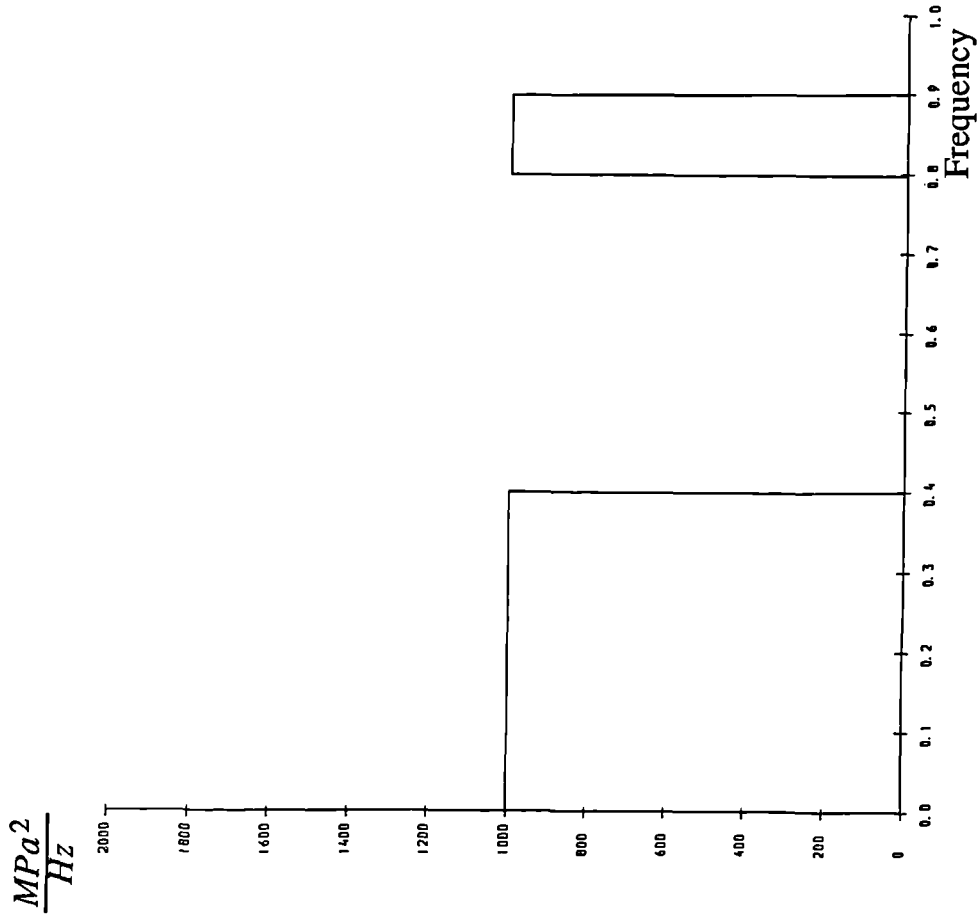


Figure 3.16(a). A rectangular PSD which also has an additional strip present at some remote point.

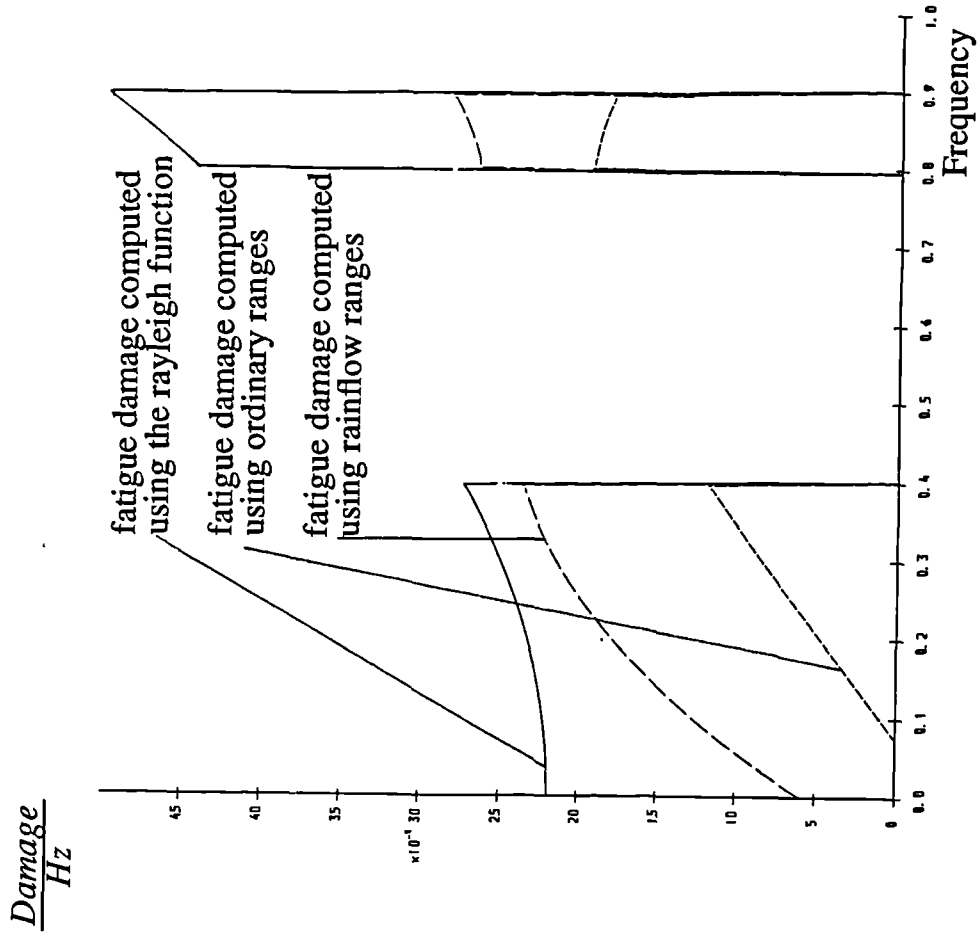


Figure 3.16(b). The effect on fatigue damage of removing one small strip from the PSD is now seen to be affected by the additional strip present at some remote point.

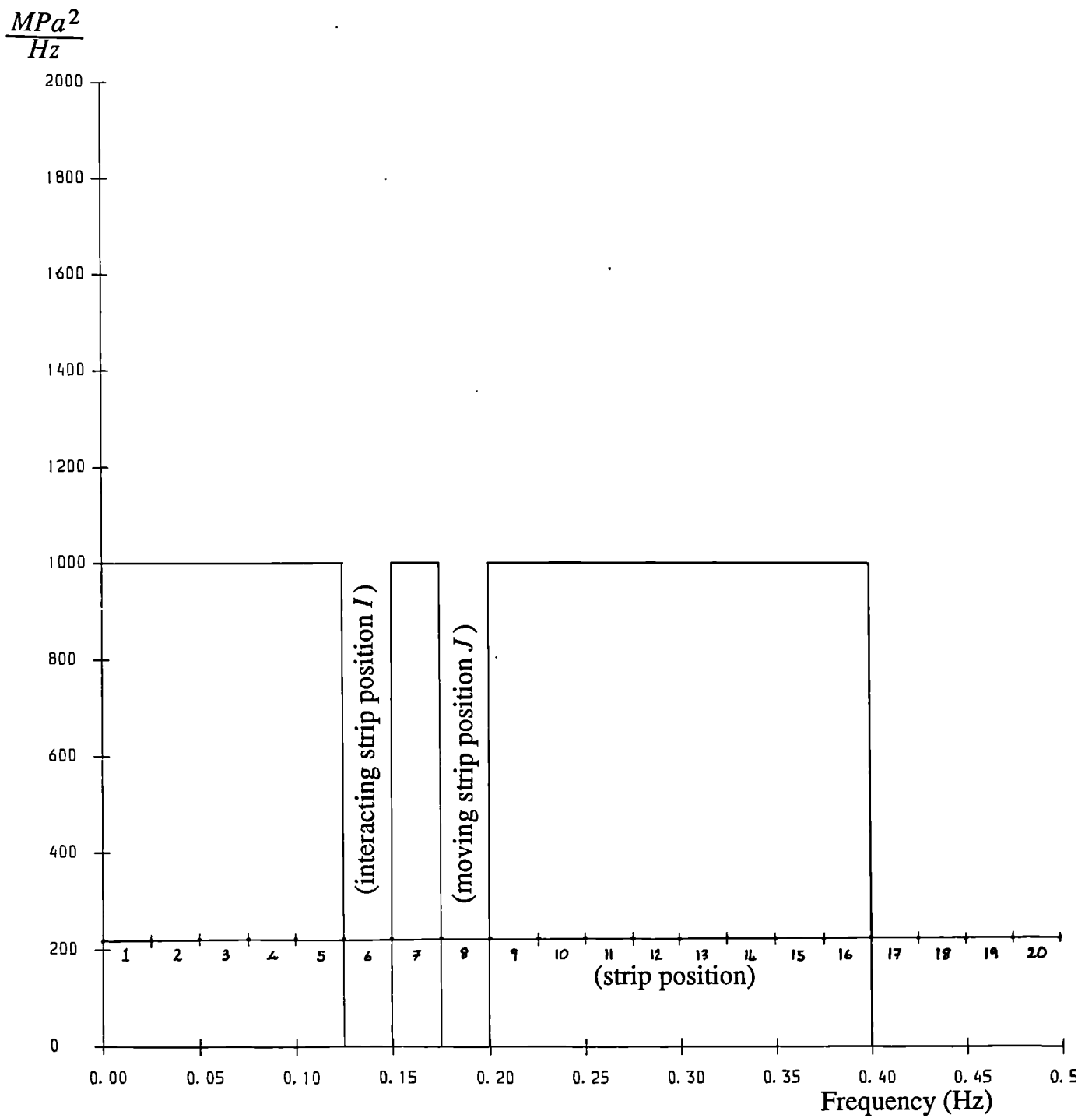


Figure 3.17. The method used to assess the effect of primary interactions.

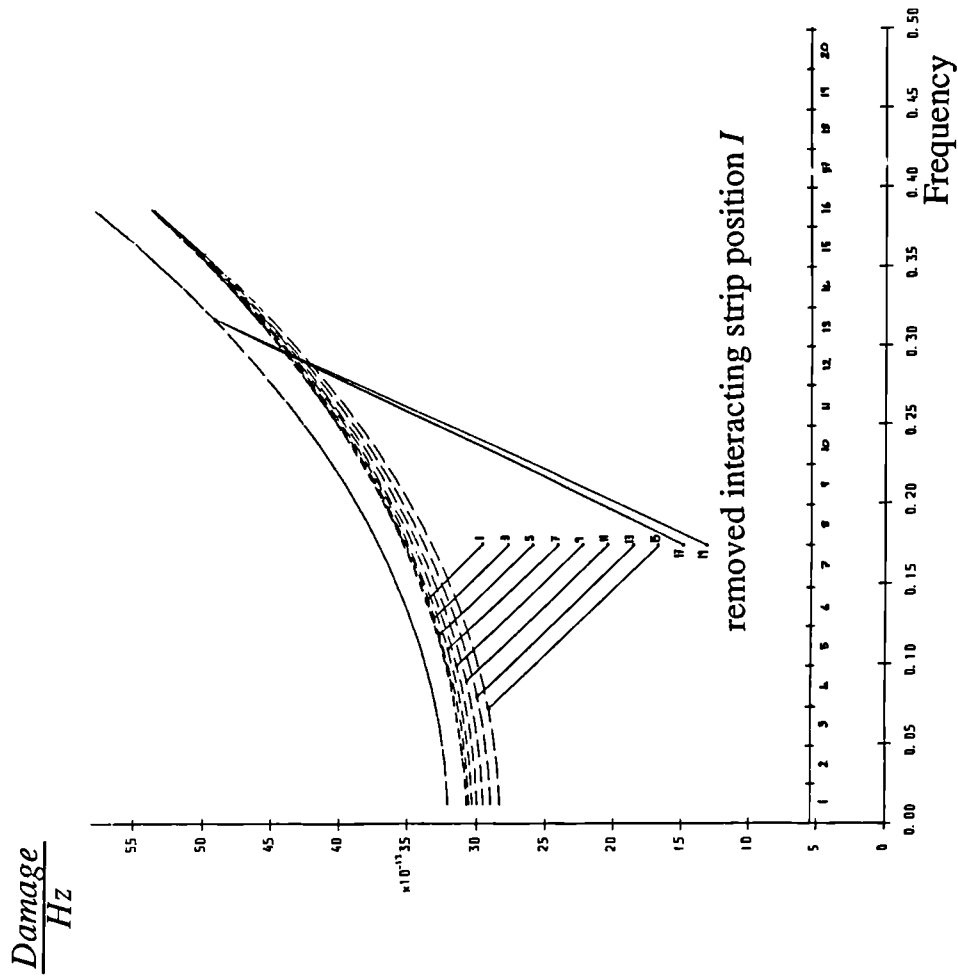
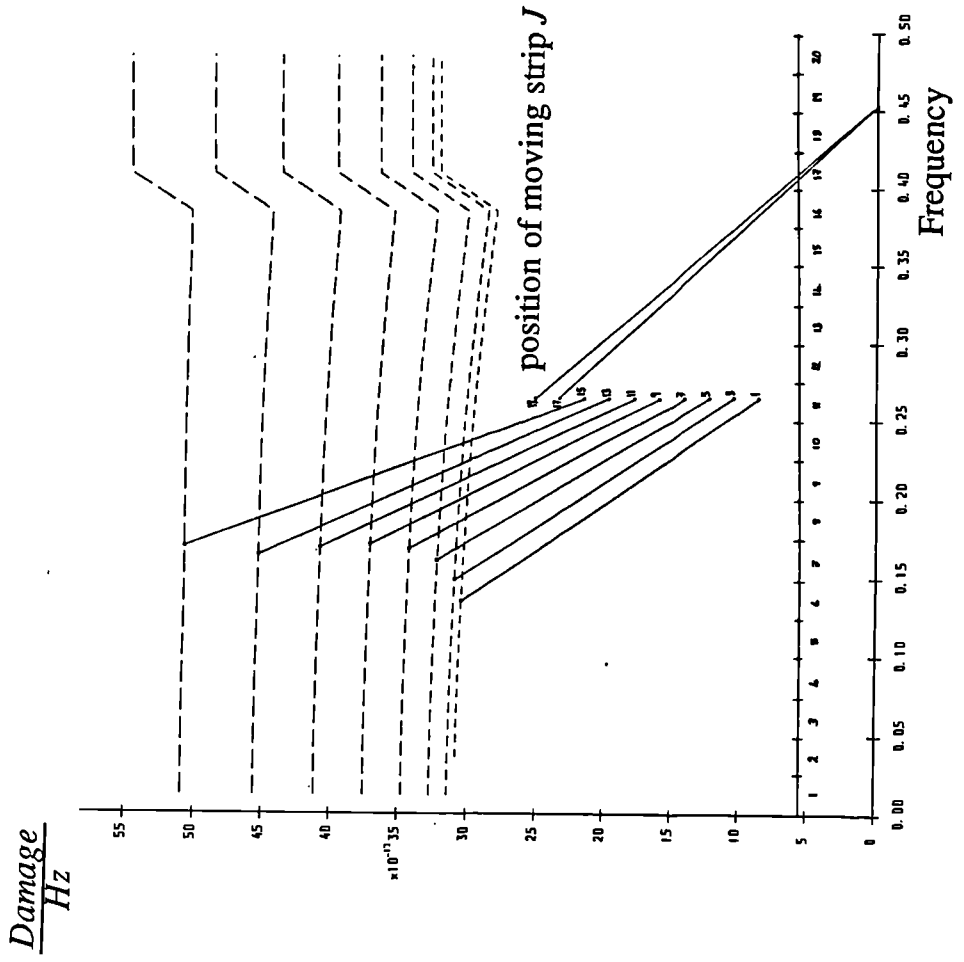


Figure 3.18. The effect of an interacting strip on the fatigue damage potential of a particular moving strip computed using rainfall ranges.

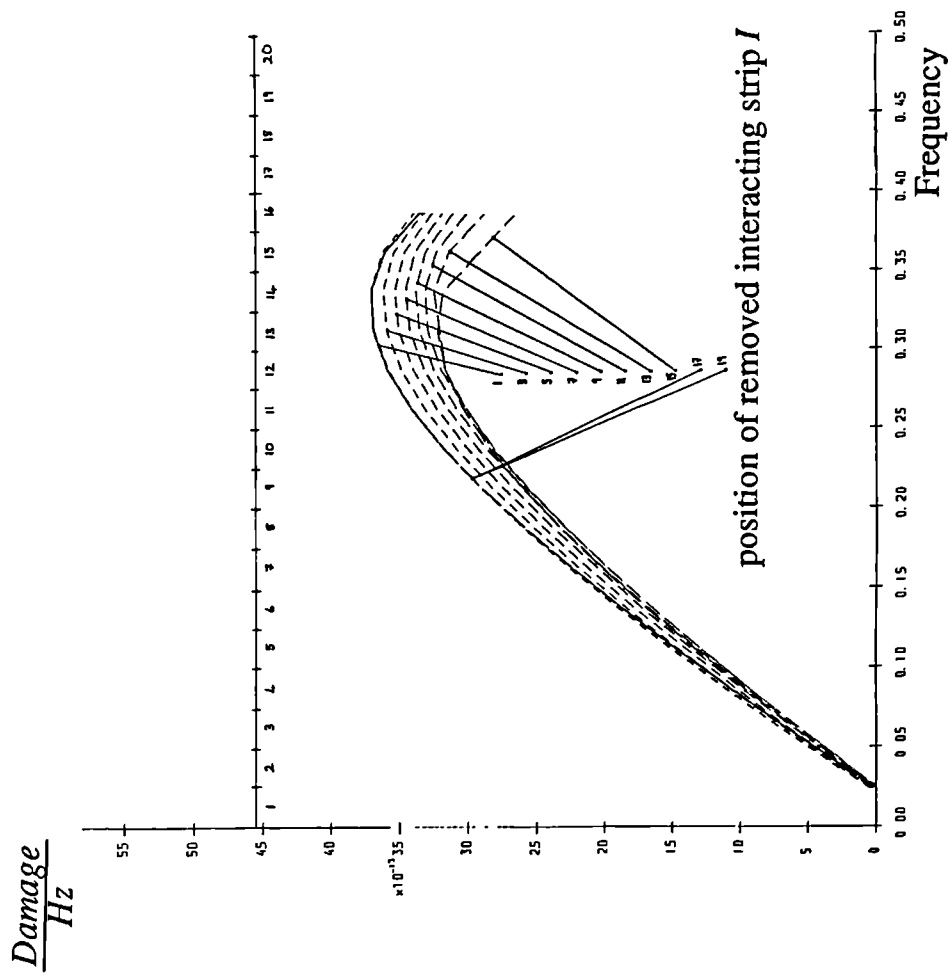
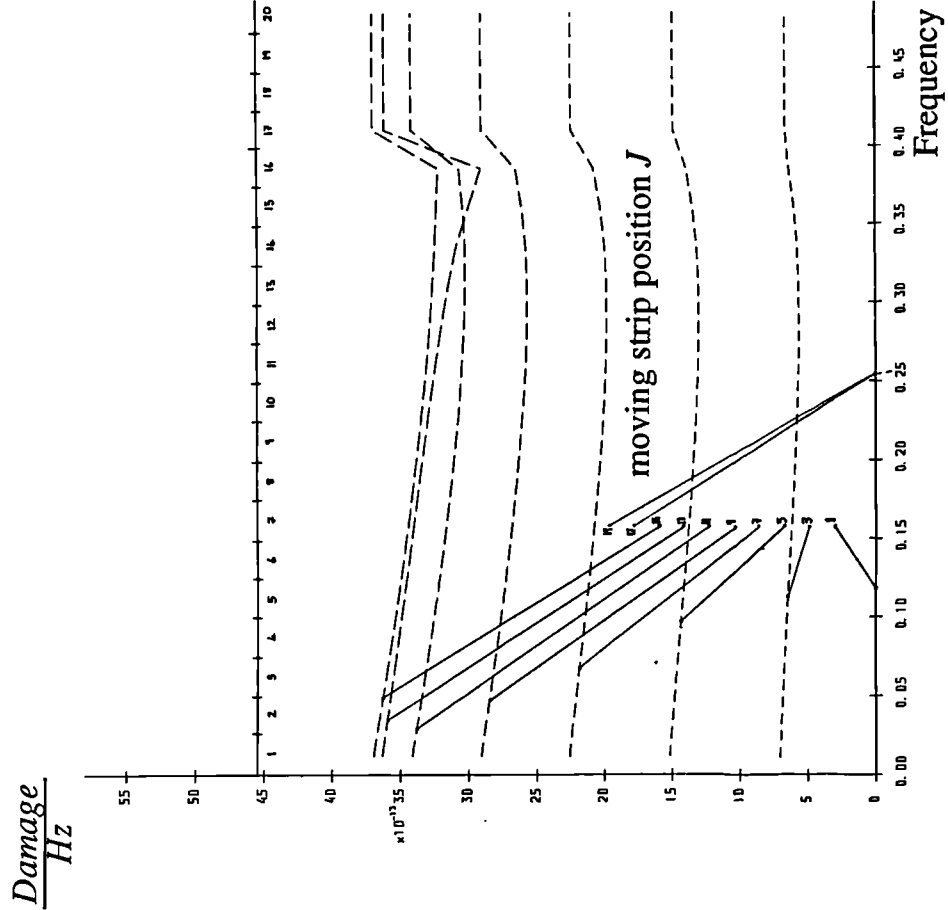


Figure 3.19. The effect of an interacting strip on the fatigue damage potential of a particular moving strip computed using ordinary ranges.

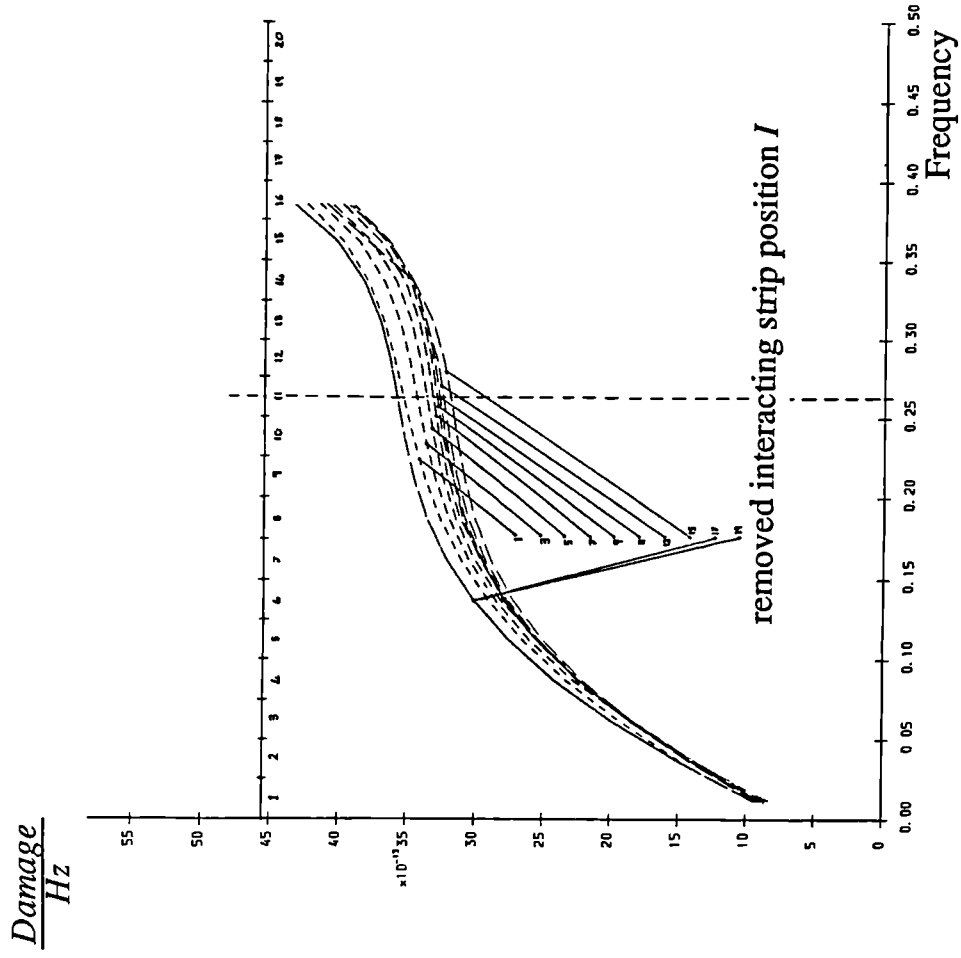
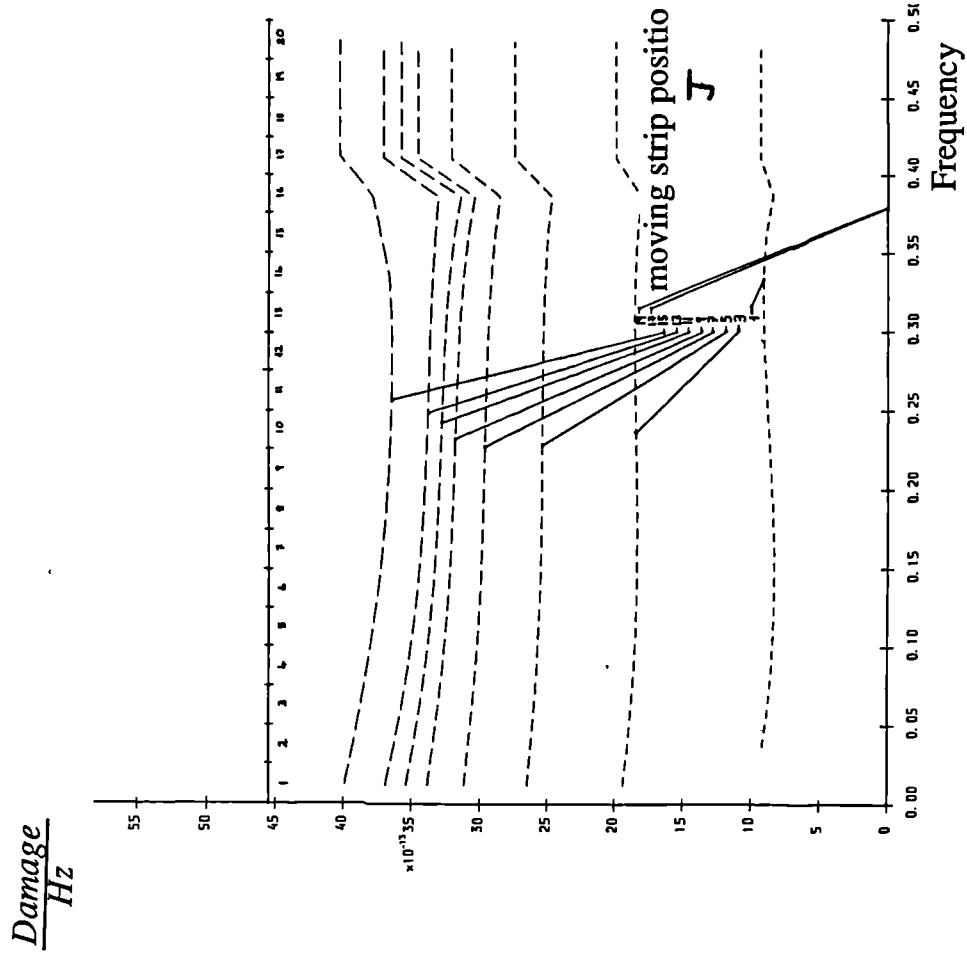


Figure 3.20. The effect of an interacting strip on the fatigue damage potential of a particular moving strip computed using the narrow band assumption.

4. Signal regeneration using Markov matrices - an improved solution to Kowalewski's joint peak-trough probability density function.

4.1. Introduction

It is now generally accepted that if one wishes to reproduce a loading sequence for a fatigue damage test, it is the magnitudes between adjacent peaks and troughs which is important and the form of the signal between these peaks and troughs can follow any shape (e.g., straight line or curve) necessitated by the particular testing device and software. Furthermore, for the vast majority of situations, the frequency content of the loading experienced by the specimen being tested can be ignored. However, we must make the distinction between the resultant loading conditions in a specimen and the applied loading to, say, an aircraft body where dynamic response means that the frequency of the applied loading might affect the final response at some desired location.

As well as the amplitudes between adjacent peaks and troughs, it has been recognised that the sequence of the loading affects fatigue damage. Therefore, it is important that as well as the peak distribution, the joint distribution between peaks and troughs must be accurately represented in any loading sequence. In the past, the complexity of such a loading sequence has been governed by both the availability of testing equipment which would perform the task and insufficient knowledge of the correct service loading on the other hand. Modern computer controlled servo-hydraulic testing equipment now means that any loading sequence can be applied to test specimens, so the remaining problem was one of quantifying what the correct loading sequence was and in what form it should be applied.

One of the earliest such sequences was Gassner's eight step program test (1959,ref.4.1), which might be considered to be the earliest standard loading sequence. In 1973 the Laboratorium für Betriebsfestigkeit (LBF) in Germany and the National Aerospace Laboratory (NLR) in the Netherlands introduced a proposal for a standardised loading sequence for describing the loading environment experienced at the wing root of a transport aircraft (ref.4.2). As part of another project in 1975 (refs.4.3,4.4,4.5,4.6) between Industrieanlagen Betriebsgesellschaft (IABG) in Germany, NLR, LBF and the Swiss Federal Aircraft factory (F+W), a standardised loading sequence called

FALSTAFF (Fighter Aircraft Loading STandard For Fatigue evaluation) was introduced. Actual measurements at the wing roots of fighter aircraft were recorded in the form of time histories of stress. These time histories were classified into mission types such as severe(regular) or severe(irregular). The recordings for each mission type were then collected together and decomposed into joint peak-trough number of occurrence matrices. These matrices were called Markov matrices (see section 5.4) because of their use for regeneration of peak trough series by methods used successfully by Sherratt and Fisher (1972,ref.4.7).

Although useful, these standard loading sequences were very specialised. However, in 1976 as part of a research project between IABG and LBF a more general standard random load sequence was recommended (ref.4.8) which came from an expression developed by Kowalewski in 1963 (ref.4.9). It allowed a sequence of peaks and troughs to be generated from a frequency domain representation of the loading. The work was based on the assumption that the joint distribution between peaks and troughs adequately represented the true service history. This requires that the Markov assumption holds and previous events have no effect on the next event. If this was not true then a three parameter or more joint distribution would be required (i.e., a peak-trough-peak distribution). The use of a three step peak-trough-peak distribution has been discussed by Conle and Topper (ref.4.10), but in most engineering situations there is no evidence to suggest that a two parameter peak-trough joint distribution is not sufficient to fully characterise the signal distribution. This is examined in detail in chapter 6.

Kowalewski's work is used later in this chapter. It is also used in chapter 5 as a 'building block' for obtaining a theoretical solution to the rainflow range problem. Therefore, the first part of this chapter will examine this work in detail in order to highlight the parts of the work which are only approximate. Section 4.3 will show one possible improvement to Kowalewski's work which was developed by the author. The improvement makes use of an empirical solution to the ordinary range problem developed by Dirlik and presented in chapter 3. Kowalewski's solution is used in preference to this solution in chapter 5 because the author did not want to make use of any empirical work for the derivation of the rainflow range solution in that chapter. It will be shown in chapter 5 that flaws in the section of work presented by Kowalewski for the joint distribution of

peaks and troughs do not affect the quality or usefulness of the work in chapter 5, since the two are essentially different problems. The joint distribution between peaks and troughs is effectively the same problem as the distribution of times between zero crossings discussed in chapter 2, and remains to this day unsolved. The work in chapter 5 represents a complete solution to the problem of obtaining rainflow ranges and any future improvement to the solution for the distribution of times between zero crossings would immediately result in the possibility of a complete solution to the joint distribution of peaks and troughs. This could then be fed directly into the work in chapter 5 without affecting, in any way, the form of the rainflow range solution.

Section 4.4 describes a method for regenerating test signals from Power Spectral Density plots (PSD's) in the form of a series of successive peaks and troughs. The method presented here will be shown to give significant improvement over previously available techniques in that the series is infinite and non repeating.

Section 4.5 gives details of the cycle counting techniques used to decompose the relevant time signals into range distributions for comparison purposes. Only simple techniques will be used in this chapter that require the signal to start and end at the highest possible maximum. Chapter 6 will use a more sophisticated technique because of the shorter lengths of signal being investigated. Computations on short lengths of signal are more susceptible to the errors in the range distribution which result from the approximation of making the signal start and end at the highest possible maximum.

Section 4.6 gives the results and conclusions for this chapter.

4.2. Kowalewski's solution for the joint distribution of peaks and troughs.

Before moving onto a discussion of Kowalewski's work we will look at the theoretical expressions for the distribution of maxima and the number of points of inflection per second. These expressions are used by Kowalewski to quantify the statistical situations where his solution is strictly valid. The whole of this chapter assumes that the signals under consideration are zero mean Gaussian variables.

4.2.1. The distribution of maxima

If we use the same terminology as in section 2.6 we need to consider the distribution of x , 1x and 2x , given by;

$$Prob[\alpha < x(t) \leq \alpha + d\alpha]; \quad (4.1)$$

$$\beta < {}^1x(t) \leq \beta + d\beta;$$

$$\zeta < {}^2x(t) \leq \zeta + d\zeta] \approx p(\alpha, \beta, \zeta) d\alpha d\beta d\zeta$$

Then by setting β to zero and carrying out the following integration over all negative values of ζ , we get the number of maxima in the interval α .

$$g(\alpha) d\alpha = -d\alpha \int_{-\infty}^0 p(\alpha, 0, \zeta) \zeta d\zeta \quad (4.2)$$

The distribution of x , 1x and 2x follows from equation 2.31, and is given by;

$$p(\alpha, \beta, \zeta) = \frac{(2\pi)^{-\frac{3}{2}}}{|A|^{\frac{1}{2}}} e^{\left[\frac{-1}{2|A|} (A_{11}\alpha^2 + 2A_{13}\alpha\zeta + A_{33}\zeta^2) \right]} \quad (4.3)$$

The elements of A are given in the same way as in section 2.6 from which we get;

$$A = \begin{bmatrix} w_0 & 0 & -w_2 \\ 0 & w_2 & 0 \\ -w_2 & 0 & w_4 \end{bmatrix} \quad (4.4)$$

We note that A_{11} , A_{13} and A_{33} are all positive therefore, from Schwartz's inequality, $|A|$ is always positive and is given by;

$$|A| = w_2(w_0w_4 - w_2^2) \quad (4.5)$$

Because the details of the integration required in equation 4.2 have not been found anywhere in the literature, the authors derivation is given below. In order to carry out this integration we must first note that it can be reduced to the following form;

$$g(\alpha) = -K \int_{-\infty}^0 \zeta e^{[-(a\zeta^2 + b\zeta)]} d\zeta \quad (4.6)$$

Where;

$$K = \frac{(2\pi)^{-\frac{3}{2}}}{|A|^{\frac{1}{2}}} e^{\left(\frac{-A_{11}\alpha}{2|A|} \right)}; \quad a = \frac{A_{33}}{2|A|}; \quad b = \frac{A_{13}\alpha}{|A|} \quad (4.7)$$

Then we can use integration by parts to get;

$$g(\alpha) = \frac{K}{2a} - \frac{Kb}{2a} \int_0^{\infty} e^{-(a\zeta^2+b\zeta)} d\zeta \quad (4.8)$$

Then we use;

$$((c\zeta+d)^2-d^2)=(a\zeta^2+b\zeta) \quad \text{where, } c=\sqrt{a} \text{ and } d=\frac{b}{2c} \quad (4.9)$$

From which, if we use $B=e^{d^2}$ we get;

$$g(\alpha) = \frac{K}{2a} - \frac{KBb}{2a} \int_0^{\infty} e^{-(c\zeta+d)^2} d\zeta \quad (4.10)$$

By transforming the variable of integration using $u = -(c\zeta+d)$, where, $\frac{du}{d\zeta} = -c$, $\zeta=0$ at $u=-d$ and $\zeta=\infty$ at $u=-\infty$, we finally get;

$$g(\alpha) = \frac{K}{2a} + \frac{KBb}{2ac} \int_{-d}^{\infty} e^{-u^2} du \quad (4.11)$$

$$= \frac{K}{2a} \left[1 + \frac{Bb}{c} \frac{\sqrt{\pi}}{2} (1 + \operatorname{erf}(d)) \right] \quad (4.12)$$

Which is identical, in form, to equation 2.53, which was converted into units of irregularity factor by Huston and Skopinski (ref.4.11).

To find the expected number of peaks per second equation 4.12 must be integrated over all possible values of α . However, it is more convenient to carry out the integration over α before the integration over ζ is carried out in equation 4.2 (see ref.4.12, for details of this);

$$E[P] = \int_0^{\infty} \zeta \left[\int_{-\infty}^{\infty} p(\alpha, 0, \zeta) d\alpha \right] d\zeta \quad (4.13)$$

$$= \int_0^{\infty} \zeta \left[\frac{1}{2\pi(w_2w_4)^{\frac{1}{2}}} e^{\left(\frac{-\zeta^2}{2w_4}\right)} \right] d\zeta \quad (4.14)$$

$$= \frac{1}{2\pi} \left[\frac{w_4}{w_2} \right]^{\frac{1}{2}} \quad (4.15)$$

$$= \left[\frac{m_4}{m_2} \right]^{\frac{1}{2}} \quad (4.16)$$

4.2.2. The number of points of inflection per second

If we again use the terminology as in section 2.6 we need to consider the distribution of x , 1x , 2x and 3x given by (see ref.4.9 for greater details of the derivation);

$$Prob [\alpha < x(t) \leq \alpha+d\alpha ; \quad (4.17)$$

$$\beta < {}^1x(t) \leq \beta+d\beta ;$$

$$\zeta < {}^2x(t) \leq \zeta+d\zeta ;$$

$$\mu < {}^3x(t) \leq \mu+d\mu] \approx p(\alpha, \beta, \zeta, \mu) d\alpha d\beta d\zeta d\mu$$

We get from equation 2.32;

$$A = \begin{bmatrix} w_0 & 0 & -w_2 & 0 \\ 0 & w_2 & 0 & -w_4 \\ -w_2 & 0 & w_4 & 0 \\ 0 & -w_4 & 0 & w_6 \end{bmatrix} \quad (4.18)$$

The probability density function of points of inflection regardless of slope, is;

$$h(\alpha) = - \int_{-\infty}^0 p(\alpha, 0, \mu) \mu d\mu$$

from which we get, after carrying out the desired integration (ref.4.9);

$$h(\alpha) = \frac{1}{(2\pi w_0(1-\gamma^2))^{\frac{1}{2}}} e^{-\frac{\alpha^2}{2w_0(1-\gamma^2)}} \quad (4.19)$$

To obtain the desired result for the number of points of inflection per unit time we need to carry out the following integration (again see ref.4.9);

$$q(\alpha) = - \int_{-\infty}^0 \int_{-\infty}^{\infty} p(\alpha, \beta, 0, \mu) \mu d\beta d\mu \quad (4.20)$$

By noting that;

$$q(\alpha) = E[PI] \cdot h(\alpha)$$

we get;

$$E[PI] = \frac{1}{2\pi} \left[\frac{w_6}{w_4} \right]^{\frac{1}{2}} \quad (4.21(a))$$

$$= \left[\frac{m_6}{m_4} \right]^{\frac{1}{2}} \quad (4.21(b))$$

4.2.3. Kowalewski's joint distribution of peaks and troughs

In 1963 Kowalewski (ref.4.9) developed an approximate solution for the distribution of adjacent peaks and troughs within a signal specified in the frequency domain. Other authors (refs.4.13,4.14) have attempted to obtain solutions to the problem of the distribution of ordinary ranges using similar information, without achieving a complete solution. Sjöström (ref.4.15) carried out similar work to Kowalewski, but did not quantify the approximations made in any way. The purpose of this section is to follow through Kowalewski's solution in order to identify the approximations made. We will start with a statement about the problem.

We will show shortly that it is a reasonably simple task to formulate an expression which gives the probability of a peak in the interval $t \rightarrow t+dt$ and a trough at some time $(t+\tau \rightarrow t+\tau+dt)$. However, it is not possible to ensure that the peak and trough are adjacent. In other words, that there are no intervening extremes. This is a very similar problem to the distribution of zero crossings problem discussed in section 2.8. In order to obtain a solution Kowalewski found it necessary to make certain assumptions about the signal under consideration. To do this he considered the six dimensional Gaussian probability of x , 1x and 2x at times t and $t+\tau$, given by;

$$\begin{aligned} Prob [\alpha_1 < x(t) \leq \alpha_1+d\alpha_1 ; & \quad (4.22) \\ \beta_1 < ^1x(t) \leq \beta_1+d\beta_1 ; & \\ \zeta_1 < ^2x(t) \leq \zeta_1+d\zeta_1 ; & \\ \alpha_2 < x(t+\tau) \leq \alpha_2+d\alpha_2 ; & \\ \beta_2 < ^1x(t+\tau) \leq \beta_2+d\beta_2 ; & \\ \zeta_2 < ^2x(t+\tau) \leq \zeta_2+d\zeta_2] \approx p(\alpha_1, \beta_1, \zeta_1, \alpha_2, \beta_2, \zeta_2, \tau) d\alpha_1 d\beta_1 d\zeta_1 d\alpha_2 d\beta_2 d\zeta_2 \end{aligned}$$

The six dimensional Gaussian probability density function given by equation 2.31 for the above contains a determinant with 36 elements of which 28 are present. Kowalewski used the following variable transformations to simplify this matrix in order to reduce the

number of non-zero elements to 18;

$$\frac{1}{\sqrt{2}}(\alpha_2 - \alpha_1) = \alpha_a \quad \frac{1}{\sqrt{2}}(\alpha_2 + \alpha_1) = \alpha_m \quad (4.23)$$

$$\frac{1}{\sqrt{2}}(\beta_2 - \beta_1) = \beta_a \quad \frac{1}{\sqrt{2}}(\beta_2 + \beta_1) = \beta_m \quad (4.24)$$

$$\frac{1}{\sqrt{2}}(\zeta_2 - \zeta_1) = \zeta_a \quad \frac{1}{\sqrt{2}}(\zeta_2 + \zeta_1) = \zeta_m \quad (4.25)$$

Then we get, for the probability of a trough in the interval $t \rightarrow t+dt$ and a peak in the interval $t+\tau \rightarrow t+\tau+dt$;

$$-dt dt d\alpha_a d\alpha_m \int_{-\infty}^{\infty} \int_{-\infty}^{\infty} p(\alpha_m, 0, \zeta_m, \zeta_a, 0, \alpha_a; \tau) \frac{1}{2}(\zeta_m^2 - \zeta_a^2) d\zeta_a d\zeta_m \quad (4.26)$$

and the desired six dimensional probability density function is given by;

$$p(\alpha_m, 0, \zeta_m, \zeta_a, 0, \alpha_a) = \frac{1}{(2\pi)^3 |A|^{1/2}} e^{-\frac{1}{2|C|}(C_{11}\alpha_m^2 + 2C_{13}\alpha_m\zeta_m + C_{33}\zeta_m^2) - \frac{1}{|2D|}(D_{11}\alpha_a^2 + 2D_{13}\alpha_a\zeta_a + D_{33}\zeta_a^2)} \quad (4.27)$$

where, if we use ${}^2R(\tau)$ to represent the second derivative of $R(\tau)$;

$$A = \begin{bmatrix} (w_0+R(\tau)) & 0 & ({}^2R(\tau)-w_2) & 0 & -{}^1R(\tau) & 0 \\ 0 & (w_2-{}^2R(\tau)) & 0 & {}^3R(\tau) & 0 & {}^1R(\tau) \\ ({}^2R(\tau)-w_2) & 0 & (w_4+{}^4R(\tau)) & 0 & -{}^3R(\tau) & 0 \\ 0 & {}^3R(\tau) & 0 & (w_4-{}^4R(\tau)) & 0 & (-w_2-{}^2R(\tau)) \\ -{}^1R(\tau) & 0 & -{}^3R(\tau) & 0 & (w_2+{}^2R(\tau)) & 0 \\ 0 & {}^1R(\tau) & 0 & (-w_2-{}^2R(\tau)) & 0 & (w_0-{}^1R(\tau)) \end{bmatrix} \quad (4.28)$$

$$|A| = |C| \cdot |D| = \begin{bmatrix} (w_0+R(\tau)) & -{}^1R(\tau) & ({}^2R(\tau)-w_2) \\ -r1 & (w_2+{}^2R(\tau)) & -{}^3R(\tau) \\ ({}^2R(\tau)-w_2) & -{}^3R(\tau) & (w_4+{}^4R(\tau)) \end{bmatrix} \cdot \begin{bmatrix} (w_0-{}^1R(\tau)) & {}^1R(\tau) & (-w_2-{}^2R(\tau)) \\ {}^1R(\tau) & (w_2-{}^2R(\tau)) & {}^3R(\tau) \\ (-w_2-{}^2R(\tau)) & {}^3R(\tau) & (w_4-{}^4R(\tau)) \end{bmatrix} \quad (4.29)$$

The elements of A are found as second moments of the relevant statistical variables and derivations of these are given elsewhere (ref.4.9).

It is important to note that although the above equations represent a solution to the problem of the joint probability between peaks and troughs separated by τ (with possible

intervening extremes), the elements are no longer just the simple moments of the PSD. Many of the terms which are present can only be evaluated by numerical integration. A process extensively used in references 4.13 and 4.14 for evaluating ordinary ranges.

Kowalewski compared a Taylor series expansion of the moments of the above joint distribution of peaks and troughs separated by τ with an equivalent expression for the joint distribution of two troughs. His argument for an approximate solution was as follows;

Look at the relative probabilities of two events, the first being the probability of a peak and a trough at some time τ later, and the second being the probability of two troughs separated by an interval of τ . As τ increases from zero, the probability of both the above events will start at zero. The relative probability of two troughs occurring will remain at zero until τ is greater than the value of τ at which the probability of a peak and a trough becomes non-zero. By only using terms in the Taylor series expansion for the moments of the peaks-trough distribution below the lowest term present in a similar series for the trough-trough distribution, we can assume that there are no intervening extremes. This is because, for there to be an intervening extreme the probability of two troughs must become non-zero.

Kowalewski then went on to show that for this modified distribution the mean values and amplitudes become independent and so;

$$P_{mean,amp}(\alpha_m, \alpha_a) = P_{mean}(\alpha_m) \cdot P_{amp}(\alpha_a) \quad (4.30)$$

and also that for the case when $E[P] \approx E[PI]$ the distribution of mean values is identical with the distribution of points of inflection. This is not as severe an assumption as the narrow band assumption which assumes that $E[0] \approx E[P]$.

The characteristic function for maxima is obtained from equations 2.10 and 4.12 as;

$$C_{\max}(\xi) = \left[e^{-\frac{\xi^2}{2} w_0 (1-\gamma^2)} \right] \cdot \left[1 + \sqrt{\frac{w_0 \pi}{2}} i \xi \gamma e^{-\frac{\xi^2}{2} w_0 \gamma^2} \left[1 + \operatorname{erf} \left(i \xi \gamma \sqrt{\frac{w_0}{2}} \right) \right] \right] \quad (4.31)$$

and the characteristic function of points of inflection is, from equation 4.19;

$$C_{inflex}(\xi) = e^{-\frac{\xi^2}{2} w_0 (1-\gamma^2)} \quad (4.32)$$

We define the trough and peak heights to be;

$$\text{trough height } \alpha_1 = \alpha_m - \alpha_a \quad (4.33)$$

$$\text{peak height } \alpha_2 = \alpha_m + \alpha_a \quad (4.34)$$

and so;

$$C_{\max}(\xi) = C_{\text{amp}}(\xi) \cdot C_{\text{inflex}}(\xi) \quad (4.35)$$

From which the characteristic function of amplitudes can be obtained;

$$C_{\text{amp}}(\xi) = 1 + \sqrt{\frac{w_0 \pi}{2}} i \xi \gamma e^{-\frac{\xi^2}{2} w_0 \gamma^2} \left[1 + \text{erf} \left(i \xi \gamma \sqrt{\frac{w_0}{2}} \right) \right] \quad (4.36)$$

which has the following probability density function;

$$p_{\text{amp}}(\alpha_a) = \frac{1}{w_0 \gamma^2} \alpha_a e^{-\frac{\alpha_a^2}{2w_0 \gamma^2}} \quad (4.37)$$

This can be identified as a Rayleigh type distribution. Using this equation and equations 4.12, 4.30, 4.33 and 4.34, we can finally obtain the desired joint probability density function of adjacent peaks and troughs;

$$p_{\min, \max}(\alpha_1 \alpha_2) = \left[\frac{\alpha_2 - \alpha_1}{4w_0 \gamma^2} \right] \left[\frac{1}{(2\pi w_0 (1 - \gamma^2))^{1/2}} \right] e^{\left(\frac{-1}{8w_0 \gamma^2 (1 - \gamma^2)} \left[\alpha_1^2 + \alpha_2^2 + 2\alpha_1 \alpha_2 (2\gamma^2 - 1) \right] \right)} \quad (4.38)$$

This is shown in figure 4.1(a) and 4.1(b). It is useful to note that the joint probability density function is symmetrical about both diagonals. Much useful information can be derived from this distribution, such as;

- (i) The number of peaks.
- (ii) The distribution of peaks.
- (iii) The distribution of ordinary ranges.
- (iv) The number of level crossings.
- (v) The number of zero crossings.
- (vi) The irregularity factor.

The following related expressions can be derived from equation 4.38):

The probability density function of means and amplitudes;

$$p_{m, \text{amp}}(\alpha_m, \alpha_a) = \left[\frac{\alpha_a}{4w_0 \gamma^2} \right] \left[\frac{1}{(2\pi w_0 (1 - \gamma^2))^{1/2}} \right] e^{\left(\frac{-\alpha_a^2}{8w_0 \gamma^2} + \frac{-\alpha_m^2}{2w_0 (1 - \gamma^2)} \right)} \quad (4.39)$$

and the probability density function of means and stress ranges, where $\alpha_{rng} = 2\alpha_a$, is;

$$p_{m,rng}(\alpha_m, \alpha_{rng}) = \left[\frac{\alpha_{rng}}{w_0 \gamma^2} \right] \left[\frac{1}{(2\pi w_0(1-\gamma^2))^{\frac{1}{2}}} \right] e^{\left(\frac{-\alpha_{rng}^2}{2w_0 \gamma^2} + \frac{-\alpha_m^2}{2w_0(1-\gamma^2)} \right)} \quad (4.40)$$

Similarly, for the probability density function of peaks and amplitudes we get;

$$p_{max,amp}(\alpha_2, \alpha_a) = \left[\frac{\alpha_a}{4w_0 \gamma^2} \right] \left[\frac{1}{(2\pi w_0(1-\gamma^2))^{\frac{1}{2}}} \right] e^{\left(\frac{-1}{2w_0(1-\gamma^2)} (\alpha_2^2 + \frac{\alpha_a^2}{4\gamma^2} - \alpha_{max} \alpha_a) \right)} \quad (4.41)$$

and the probability density function of peaks and stress ranges is;

$$p_{max,rng}(\alpha_2, \alpha_{rng}) = \left[\frac{\alpha_{rng}}{w_0 \gamma^2} \right] \left[\frac{1}{(2\pi w_0(1-\gamma^2))^{\frac{1}{2}}} \right] e^{\left(\frac{-1}{2w_0(1-\gamma^2)} (\alpha_2^2 + \frac{\alpha_{rng}^2}{\gamma^2} - 2\alpha_{max} \alpha_{rng}) \right)} \quad (4.42)$$

The joint probability density function of peaks and ranges described by equation 4.42 is shown in figures 4.2(a) and 4.2(b).

We will investigate the accuracy of these expressions in later sections.

4.3. An improvement to Kowalewski's solution for the joint distribution of peaks and troughs.

Kowalewski made two major assumptions in the process of deriving equation 4.38. The first was that the distribution of means and amplitudes are independent and the second was that, for $E[P] \approx E[PI]$, the characteristic function of the distribution of points of inflection is identical with the characteristic function of the distribution of means. Other authors have made the first assumption, but gave no theoretical backing in defence of the solution.

Both the assumptions made by Kowalewski introduce errors into the analysis. Later numerical analysis in chapter 6 will quantify the errors involved with the assumption of independence. Here we will identify errors introduced by the assumption that the number of peaks is approximately equal to the number of points of inflection. Firstly, if equation 4.41 is integrated over all amplitudes to obtain a peak distribution then an expression identical to 2.53 results, which is correct. However, when equation 4.42 is integrated over all peaks to obtain an expression for ordinary ranges, we get;

$$p_{rng}(\alpha_{rng}) = \frac{\alpha_{rng}}{4w_0\gamma^2} e^{\frac{-\alpha_{rng}^2}{8w_0\gamma^2}} \quad (4.43)$$

Which is very different from the form of equation 3.4.

Kowalewski had the problem of intervening extremes and so had to make some sweeping assumptions in the process of his solution which affected the ordinary range parameter. The appearance of an empirical solution to the ordinary range problem has enabled a more accurate result to be obtained. By replacing the ordinary range parameter in equation 4.42 we get;

$$p_{max,rng} = A_i B_j e^{-(C_i \alpha_{rng} + D_j (\alpha_2^2 + 0.25\alpha_{rng}^2 - \alpha_2 \alpha_{rng}))} + B_i B_j e^{-(D_i \alpha_{rng}^2 + D_j (\alpha_2^2 + 0.25\alpha_{rng}^2 - \alpha_2 \alpha_{rng}))} \quad (4.44)$$

Where;

$$A_i = \frac{c_1}{\tau} \quad B_i = \frac{C_2}{\alpha^2} \quad C_i = \frac{1}{\tau} \quad D_i = \frac{1}{2\alpha^2} \quad B_j = \left[\frac{1}{2\pi w_0(1-\gamma^2)} \right]^{1/2} \quad D_j = \frac{1}{2w_0(1-\gamma^2)} \quad (4.45)$$

and all the terms contained in the above expressions can be obtained using the terms in equation 3.4, from the moments of the PSD using equation 2.28. Figures 4.3(a), 4.3(b) and 4.3(c) show this modified joint distribution. Later in this chapter we will compare the results obtained from equations 4.42 and 4.44.

4.4. Generating time signals in the form of a set of peaks and troughs

Either equation 4.42 or 4.44 can be used to regenerate continuous non repetitive signals from any PSD in the following way (see figure 4.4);

- (1) Calculate the zeroth, first, second and fourth moments from equation 2.28, and hence obtain all of the coefficients of equations 4.42 and 4.44.
- (2) Calculate L by L point values of two dimensional peak range function $p_{max,rng}(\alpha_2, \alpha_{rng})$. That is $p_{max,rng}(i, j)$ for $i=1$ to L and $j=1$ to L where L is the maximum anticipated signal range.
- (3) Using these values calculate $(L-1)$ by $(L-1)$ elemental probabilities from the formula;

$$p_{elem}(i, j) = 0.25 \left[p_{max,rng}(i, j) + p_{max,rng}(i+1, j) + p_{max,rng}(i, j+1) + p_{max,rng}(i+1, j+1) \right] \delta_x^2$$

Where δ_x is the elemental probability box size.

- (4) Sum these elemental probabilities along the ordinary range axis to obtain the total probability of ranges for particular peak values.
- (5) Choose a starting point for the time signal (maximum anticipated stress is used in this chapter).
- (6) Generate a random number in the range 0 to 1 and multiply this value by the relevant total ordinary range probability for the present peak value position.
- (7) Use a search routine to locate the elemental probability box into which this randomly generated signal range falls
- (8) Turn this trough into the present peak position by inverting the signal.
- (9) Repeat steps 5 to 8 according to the required number of peaks and troughs, which must be odd because of the condition set in (10) below.
- (10) Set the last point equal to the highest possible maximum.

Results obtained using this process will be presented at the end of this chapter. Two sets of results are presented for distributions termed 'Kowalewski' or 'modified' which represent equations 4.42 and 4.44 respectively.

4.5. Cycle counting from a series of peaks and troughs

The load histories obtained by the methods described in section 4.4 are characterised by a set (with an odd number of elements) of loadings representing an alternating set of peaks and troughs. Each peak or trough takes on some discrete value of load for which the resolution is determined by the interval width δ_x (see section 4.4 part 3). The cycle counting methods described in this chapter are used to obtain the ordinary and rainflow ranges from this set of peaks and troughs and will therefore have a resolution equal to δ_x .

The techniques used in this chapter are less sophisticated than those used in later chapters. By ensuring that the set of peaks and troughs starts and ends at the highest possible maximum, the rainflow range counting procedure contains only half of the conditions necessary for any other signal (see section 2.2). Because we are mainly concerned in this chapter with long load histories, the effect (on the various range distributions) of making the signal start and end at the highest possible maximum becomes insignificant.

The procedure for calculating the ordinary range distribution is as follows;

- (1) Calculate the segment length between point i and $i+1$ as OR_i .
- (2) Divide the magnitude of OR_i by the interval width δ_x to obtain an integer value n .
- (3) Increment the value of the ordinary range distribution array element n by a value of $\frac{1}{\delta_x \cdot \Delta_n}$, where Δ_n is the number of segment lengths equal to the number of peaks and troughs minus 1.
- (4) Increase i by 1 and repeat steps 1-3 until the last peak has been considered.

The result of this process is an array of point values representing the ordinary range probability density function spaced at intervals of δ_x along the range axis going from $1 * \delta_x$ to $(L-2) * \delta_x$.

The procedure for counting rainflow ranges is slightly more complicated. The logic behind the process is as follows;

- (1) Consider the first four points from the set of peaks and troughs.
- (2) If a $D-D$ pattern is formed then Point 3 is converted to point 1, point 4 is converted to point 2 and the next two points from the set of peaks and troughs are considered as point 3 and point 4. The old points 1 and 2 are stored for later use. Step (2) is repeated. Otherwise proceed to step (3).
- (3) A $D-I$ pattern is formed by the three segments of signal between points 1,2,3 and 4 and so the distance between point 2 and point 3 is calculated. This value is divided by the interval width δ_x to obtain an integer value n .
- (4) The value of the rainflow range distribution array element n is incremented by a value of $\frac{1}{\delta_x \cdot \Delta_n}$, where Δ_n is the number of segment lengths equal to the number of peaks and troughs minus 1.
- (5) If any points remain stored then point 1 is converted to point 3, and the most recently stored pair of points are considered as points 1 and 2, before proceeding to step (2). Otherwise proceed to step (6)

- (6) If the last minus 1 point in the series of peaks and troughs has been considered, then the segment between the last minus 1 and the last peak is considered as the last rainflow range and processed as in steps (3) and (4) and hence, calculation of the rainflow range density function is completed. Otherwise proceed to step (7)
- (7) Convert point 4 to point 2 and consider two more points from the set of peaks and troughs as points 3 and 4, then go to step (2)

Again the result of this process is an array of point values representing the rainflow range probability density function spaced at intervals of δ_x along the range axis going from $1 * \delta_x$ to $(L-2) * \delta_x$.

4.6. Results and conclusions

For continuity, the work described in this chapter was used on the same data as in chapter 3. Sea states 1,7 and 11 were used from table 3.1. PSD functions were generated using equation 3.9 from which moments were generated using equation 2.28(b). No other information, apart from these moments, is required for evaluating either Kowalewski's or the modified joint distributions discussed below.

Figures 4.5 shows a short length of signal regenerated from Kowalewski's peak-range distribution, equation 4.42, for sea state 1. The signal obtained using the modified distribution shows no discernible differences when shown in this form and is therefore not included.

Figure 4.6 gives the narrow band, ordinary range and rainflow range distributions calculated directly from the PSD using the equations given in chapter 3. For the rest of the discussions in this chapter, the predictions obtained using Dirlik's solutions for ordinary and rainflow ranges will be assumed to be truly representative of the frequency domain information being used. This assumption implies that for the Gaussian random variables being considered, each stationary time signal has only one ordinary range distribution (and one rainflow range distribution) and one frequency domain representation. This topic will be discussed in great detail in chapter 6.

Figure 4.7 compares the peak distributions obtained from regenerated signals using both the Kowalewski expression (equations 4.38-4.42) and the modified solution (equation 4.44) with a theoretical prediction (equation 4.12). For this calculation, and that of the ordinary and rainflow ranges below, 60001 points were used for the peak trough series. A matrix size 101 by 101 was used to compute the elemental probabilities in section 4.4 part (3).

Both the Kowalewski and modified expressions show very good agreement with the theoretical prediction. However, at high peak values the discrepancies are larger with the modified solution. This is entirely expected because by changing the amplitude parameter in order to obtain a better range distribution, the peak parameter in the perpendicular direction is slightly affected.

Figure 4.8 shows the ordinary range density function predictions computed from regenerated time signals using both the Kowalewski and modified solutions. Also plotted is the ordinary range density function computed using Dirlik's solution. The prediction based on Kowalewski's solution shows significant errors at all ranges. However, the modified solution shows very good agreement with Dirlik's prediction.

Similar results are shown for rainflow ranges in figure 4.9. For this situation the results are less conclusive. However, it can still be identified that the modified solution gives a better prediction, particularly at the medium and high stress range values which are more important from a fatigue point of view because of the non linear fatigue damage mechanism.

Figures 4.10 to 4.21 give the results for sea states 7 and 11 which have increasing irregularity factor. Sea state 11 is effectively the narrow band situation.

It is the moments (b) of the range distribution which effect fatigue damage. Therefore, for sea state 1, these were calculated for both the ordinary and rainflow range density functions using equation 2.6. The results are shown in figures 4.22 and 4.23. In each case, the results have been normalised by the results from Dirlik's solution, that being assumed to be the correct distribution. Moments between $b=0$ and $b=7.5$ are shown.

The results for ordinary ranges show that the modified distribution results are much better than those from Kowalewski's solution. Again the results for rainflow ranges are

less conclusive. However, it is important to note that, for rainflow ranges, the results from the modified solution have errors on the conservative side, whereas the Kowalewski solution is unconservative.

Figures 4.24(a) shows the effect of changing the the number of signal points used. The 5_{th} moment of the rainflow range distribution obtained using Kowalewski's solution for a matrix size $L=33$ is shown. The plot shows the scatter obtained from five samples taken at each signal length. Five signal lengths were considered from 501 points to 60001 points. Comparative results are shown in figure 4.24(b) for the modified solution. These results confirm the earlier findings that the Kowalewski solution tends to be unconservative.

The scatter observed in the plots described above appears to increase with decreasing sample length. No other conclusions can be made about this relationship from data because of the low number of samples used at each sample length. More data is used in chapter 6 where this subject is covered in more detail.

Figures 4.25(a),4.25(b),4.26(a) and 4.26(b) give the results for matrix sizes of $L=65$ and $L=101$. This shows that a matrix size $L=33$ gives results which appear to be as good as those obtained from matrices of greater size. The tendency for the moments to increase at low sample sizes can be explained because of the approximation of making the signal start and end at the highest possible maximum. As expected, this only has an effect for small sample sizes.

4.7. References

- (4.1) E.Gassner, Review of investigations on aeronautical fatigue in Western Germany, minutes of the 6th ICAF conference, Amsterdam, June 1959.
- (4.2) J.B.de Jonge et al, A standardised load sequence for flight simulation tests on transport aircraft wing structures, LBF-Bericht FB-106, NLR TR 730 39 K, March 1973.
- (4.3) G.M.van Dijk and J.B.de Jonge, Introduction to fighter aircraft loading standard for fatigue evaluation "FALSTAFF", paper no.3.61 presented at the the 8th ICAF symposium, Lausanne, June 1975.
- (4.4) M.Huck and W.Schütz, Generating the FALSTAFF load history by small process computer, paper no.3.62 presented at the the 8th ICAF symposium, Lausanne, June 1975.
- (4.5) J.Branger, Influence of differences between genuine and generated load sequences, paper no.3.63 presented at the the 8th ICAF symposium, Lausanne, June 1975.
- (4.6) D.Schütz and H.Lowak, The application of the standardised test program for the fatigue life estimation of fighter wing components, paper no.3.64, presented at the the 8th ICAF symposium, Lausanne, June 1975.
- (4.7) F.Sherratt and B.C.Fisher, Extracting fatigue testing and design data from service loading records, JBCSA conference, Institute of Marine Engineers, London, April 1972.
- (4.8) E.Haibach et al, A Standard Random load Sequence of Gaussian Type Recommended for general Applications to Fatigue Testing; Its Mathematical Background and Digital Generation, SEECO 76, 1976.
- (4.9) J.Kowalewski, On the relationship Between Component Life Under Irregularly Fluctuating and Ordered Load sequences. Part 2, DVL Report 249, 1963. MIRA Translation no 60/66.
- (4.10) A.Conle and T.H.Topper, Fatigue service histories: Techniques for data collection and history reconstruction, paper 820093 presented at SAE Automotive Engineering Congress and Exposition, Detroit, Michigan, February 22-26, 1982.

- (4.11)W.B.Huston and T.H.Skopinski, Probability and frequency characteristics of some flight buffet loads, NACA TN 3733, August 1956.
- (4.12)J.S.Bendat, Principles and Applications of Random Noise Theory, John Wiley & Sons, Inc., New York 1958.
- (4.13)J.R.Rice, First-Occurrence Time of High-Level Crossings in a Continuous Random process, Journal of the Acoustic Society of America, 1965.
- (4.14)J.R.Rice, On the Distribution of Rises and Falls in a Continuous Random Process, Trans ASME, 1965.
- (4.15)S.Sjöström, On random load analysis, Transactions of the Royal Institute of Technology, Stockholm, Sweden, 1961.

Figure 4.1(a). Kowalewski's peak-trough joint probability density function (equation 4.38), for sea state 1.

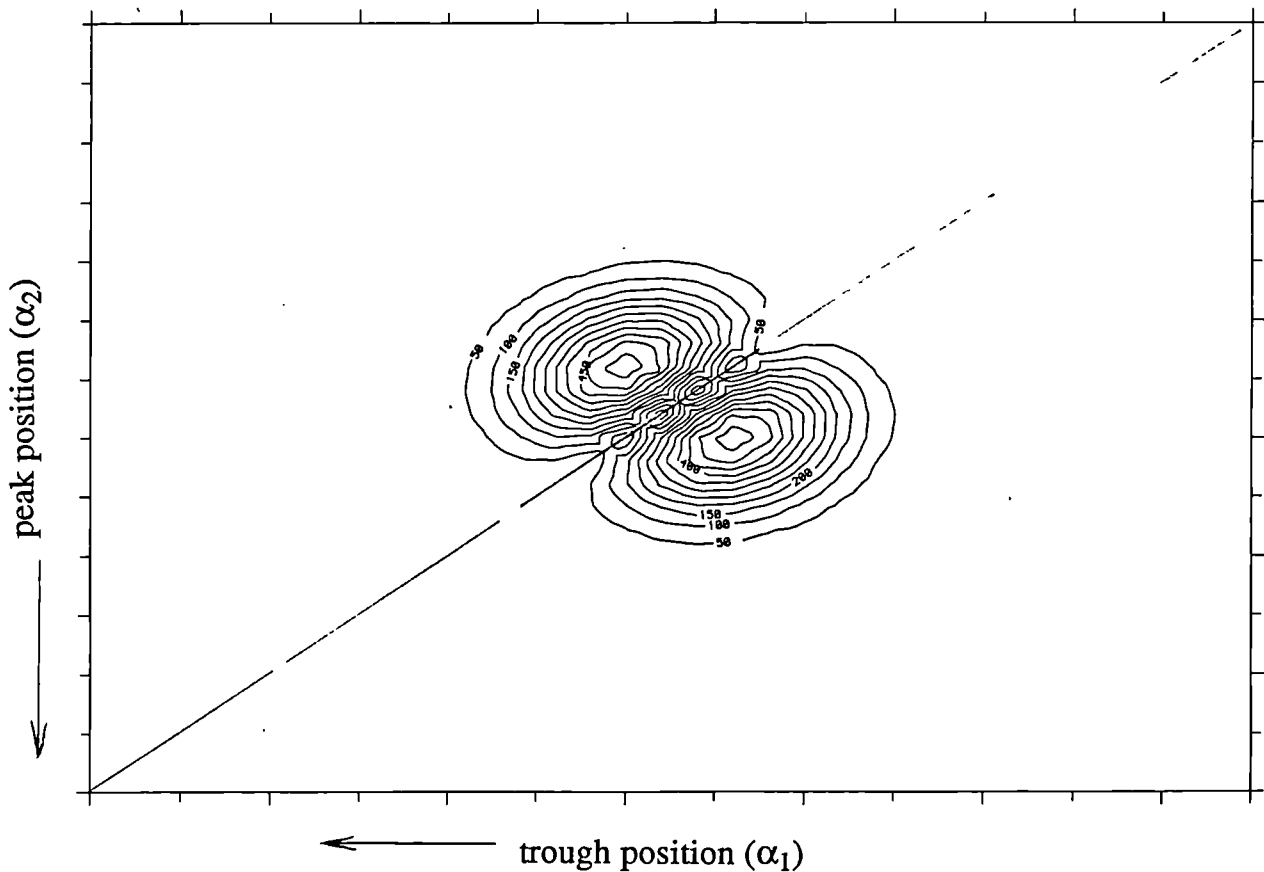
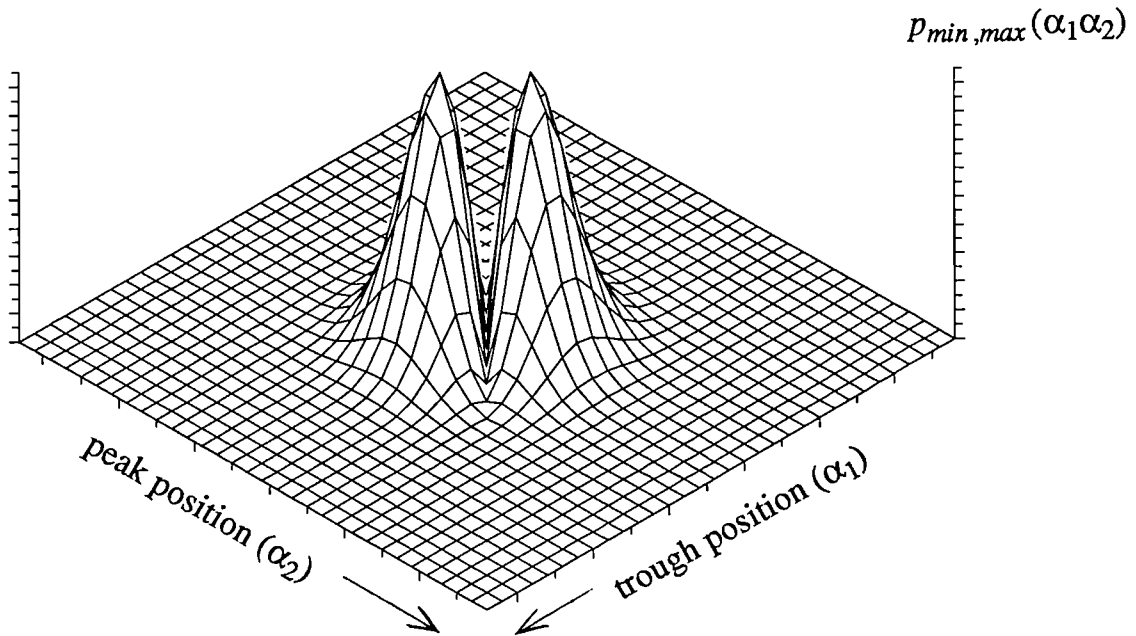


Figure 4.1(b). A contour plot of Kowalewski's peak-trough joint probability density function (equation 4.38), for sea state 1.

Figure 4.2(a). Kowalewski's peak-range joint probability density function (equation 4.42), for sea state 1.

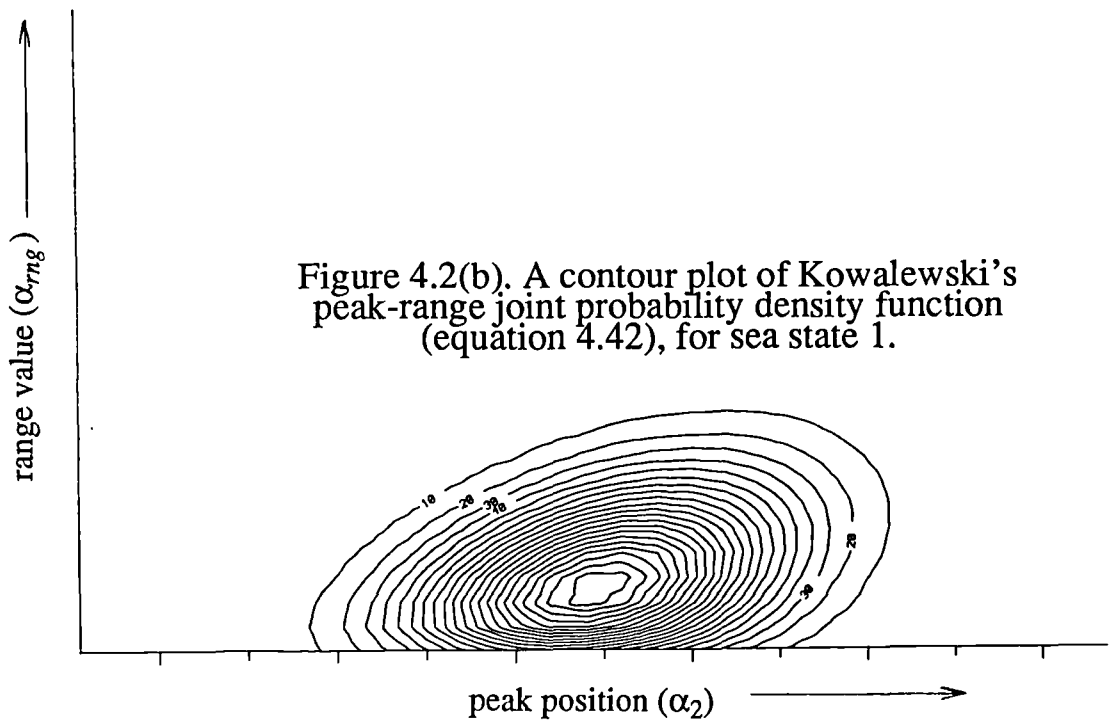
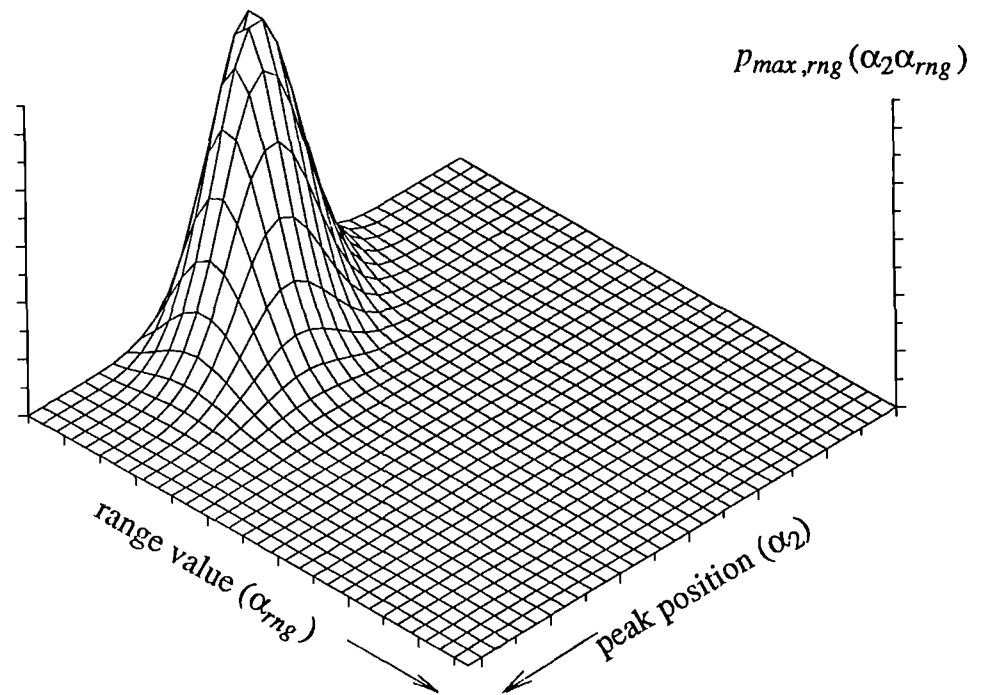
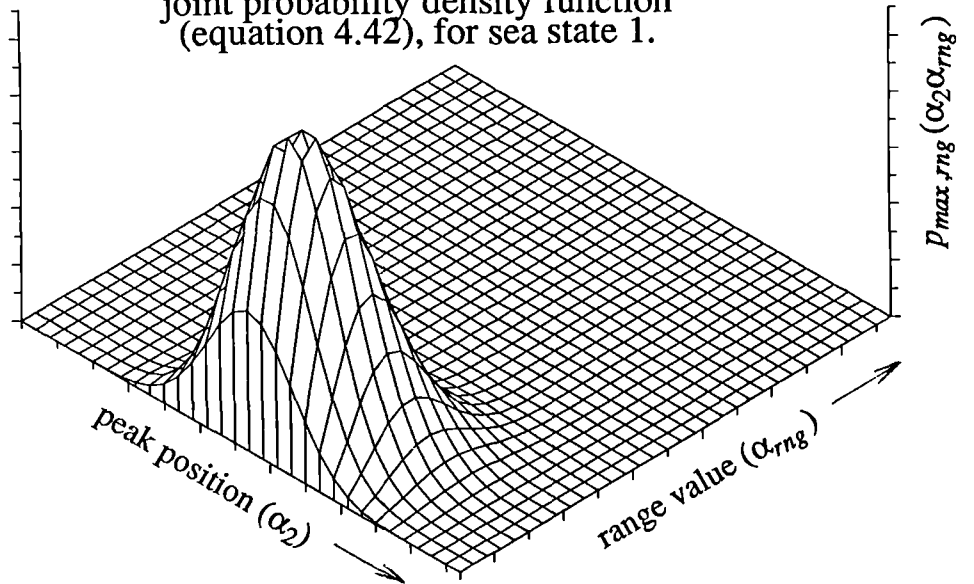


Figure 4.2(b). A contour plot of Kowalewski's peak-range joint probability density function (equation 4.42), for sea state 1.

Figure 4.3(a). The authors modified peak-range joint probability density function (equation 4.44), for sea state 1.

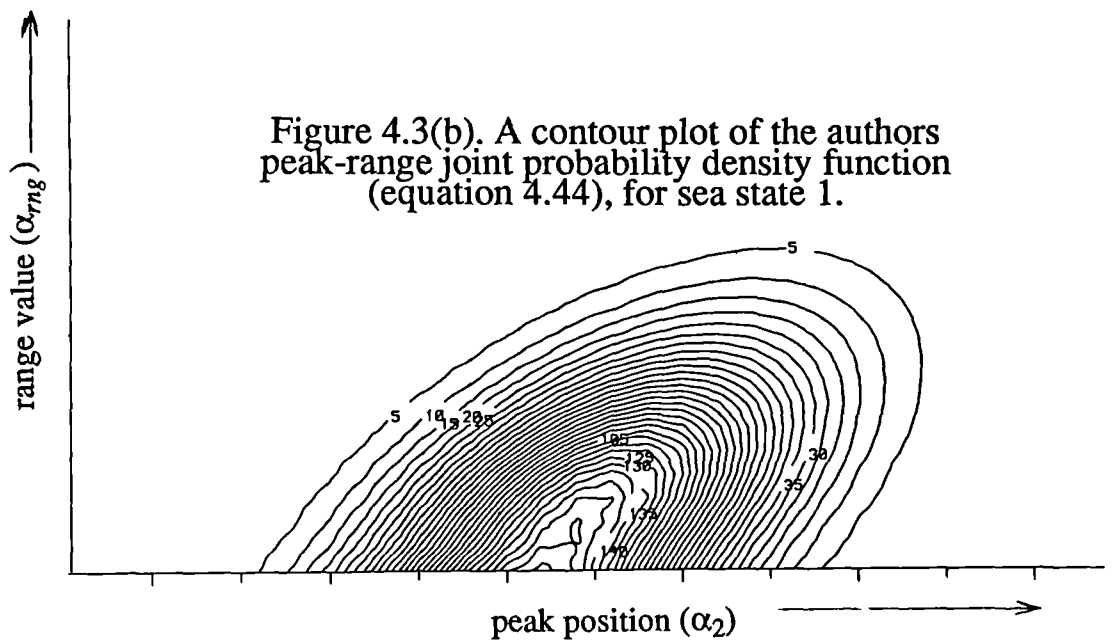
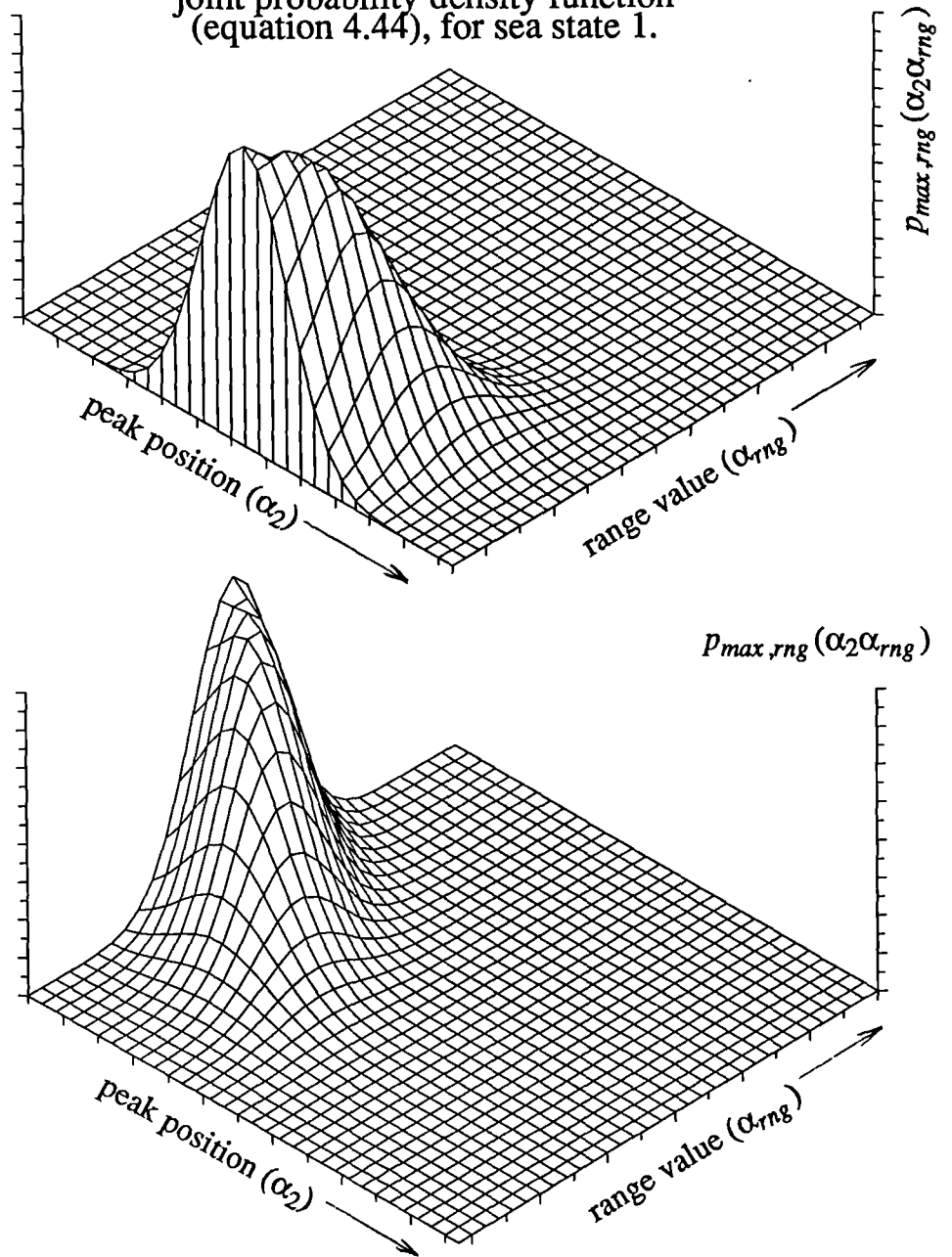


Figure 4.3(b). A contour plot of the authors peak-range joint probability density function (equation 4.44), for sea state 1.

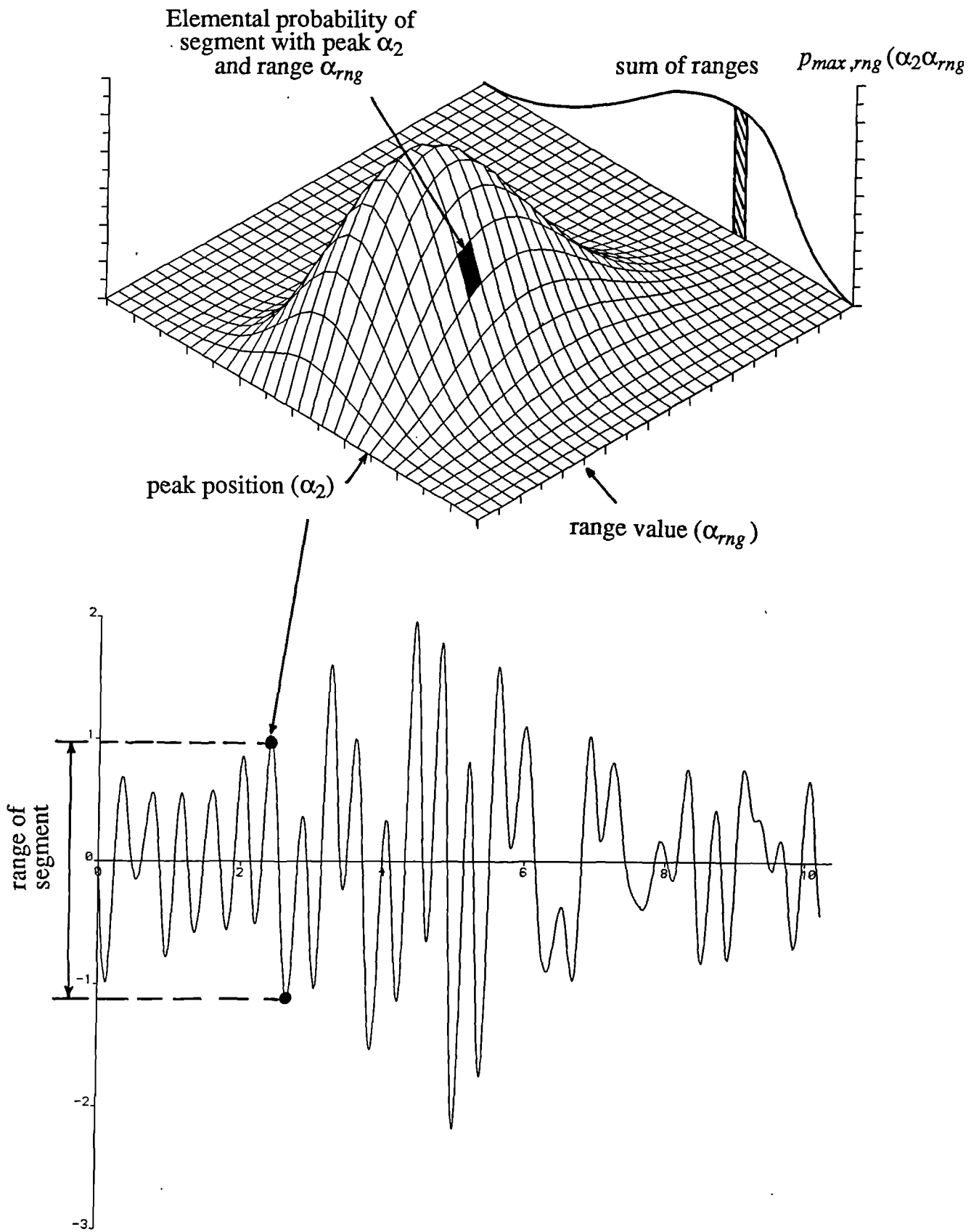
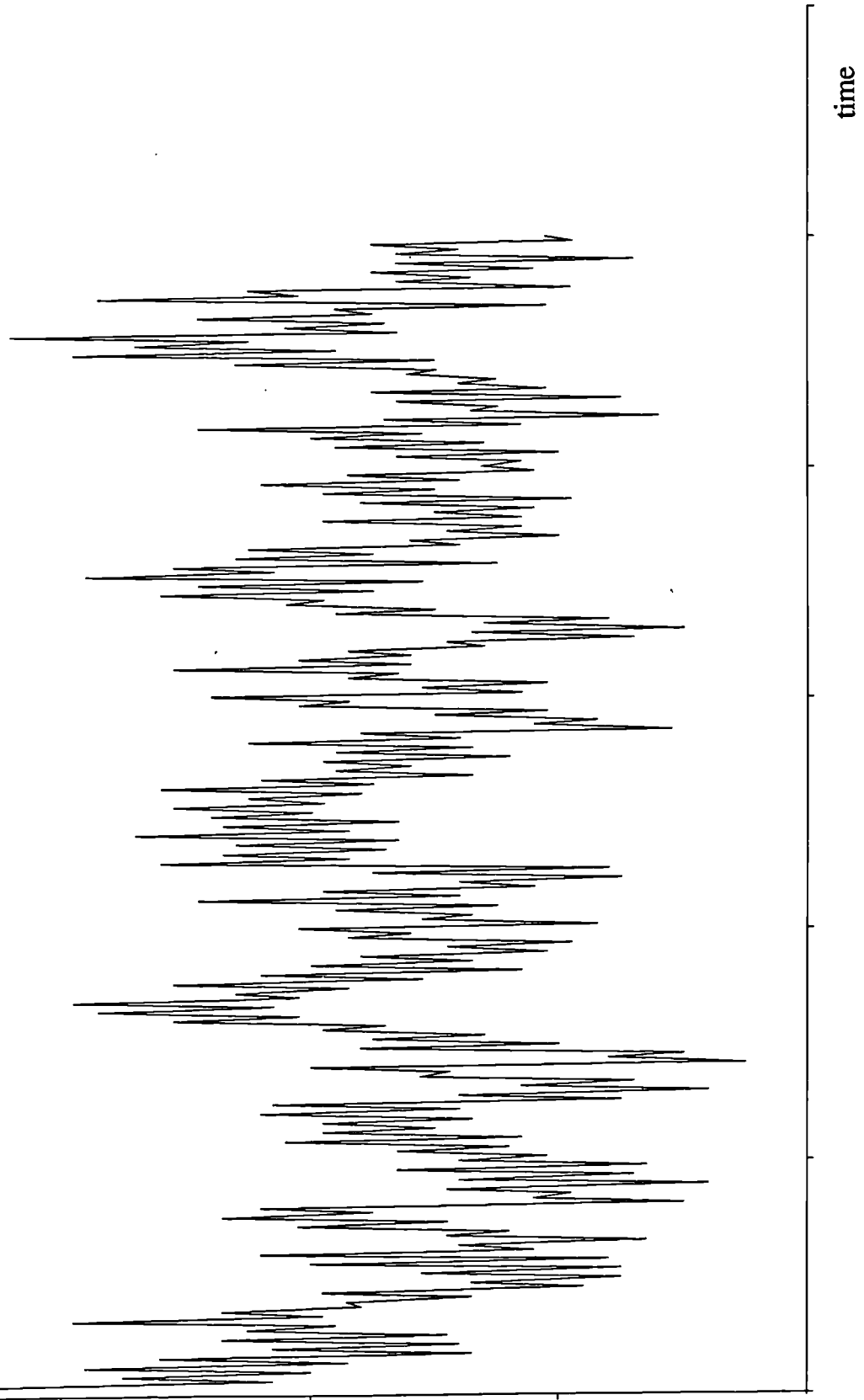
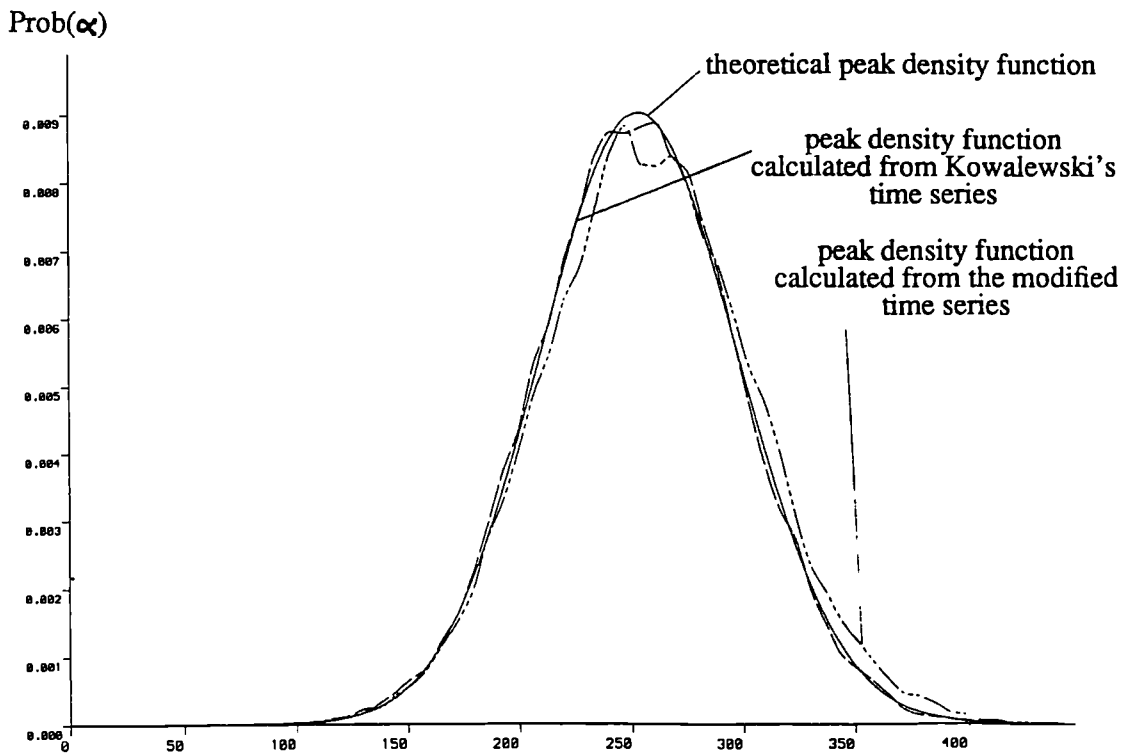
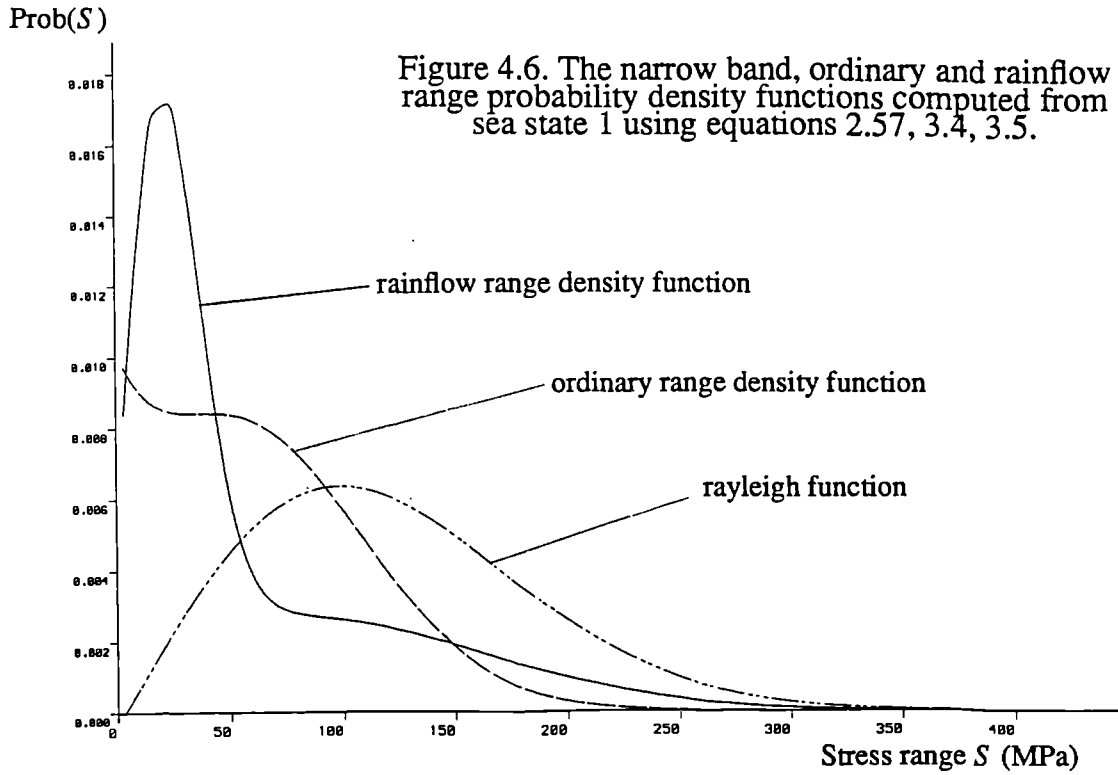


Figure 4.4. The use of a peak-range joint probability density function for generating a time history of peaks and troughs.

stress
strain
load

Figure 4.5. The first 251 points in a peak-trough series generated from Kowalewski's peak-range joint probability density function, for sea state 1.





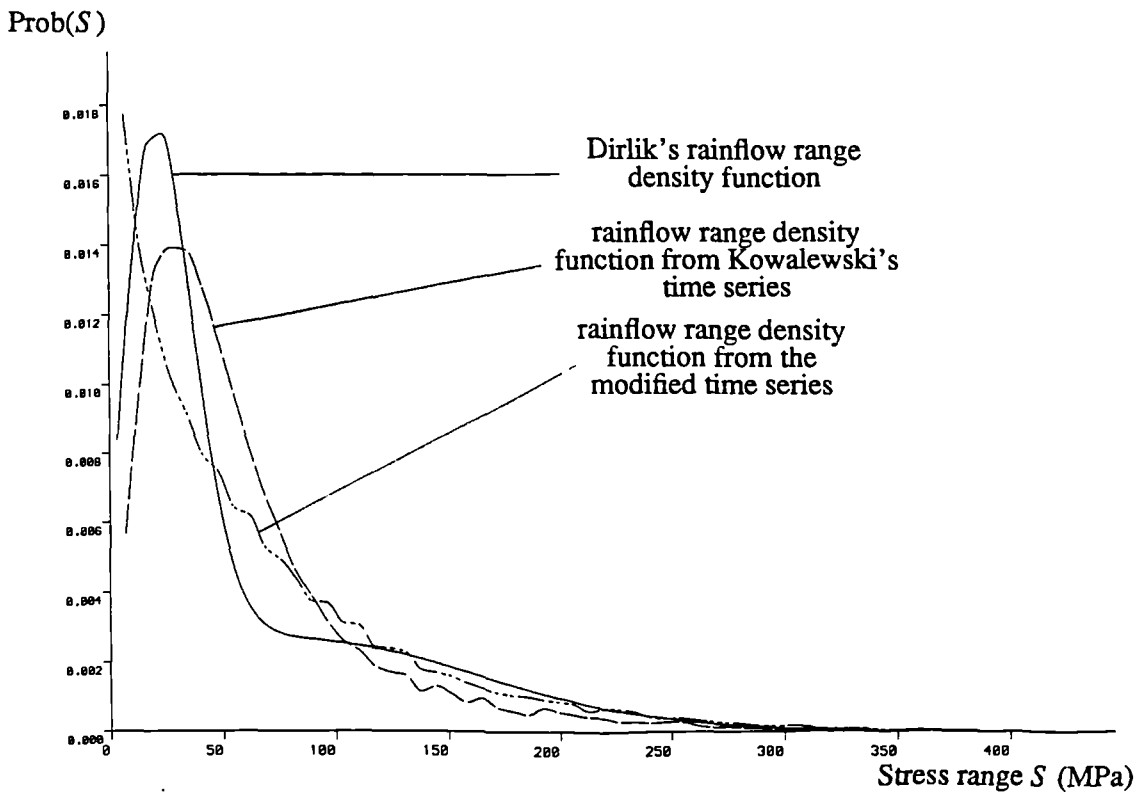
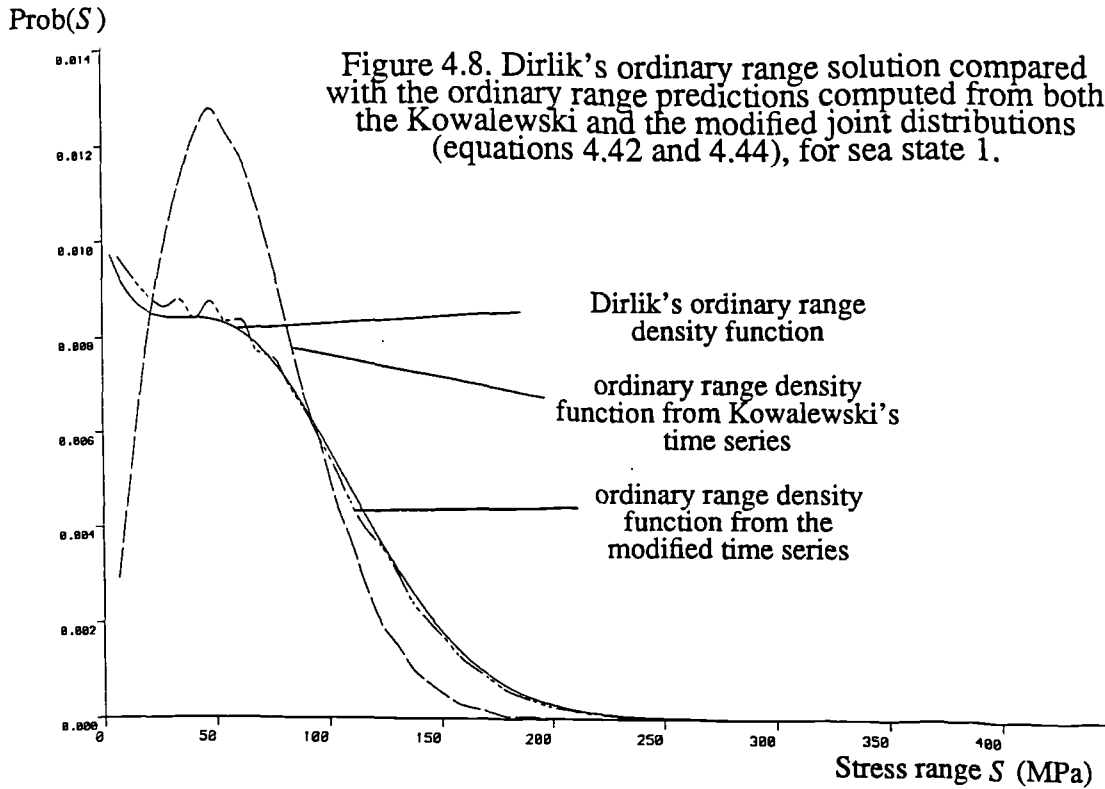


Figure 4.9. Dirlik's rainflow range solution compared with the rainflow range predictions computed from both the Kowalewski and the modified joint distributions (equations 4.42 and 4.44), for sea state 1.

Figure 4.10. Kowalewski's peak-range joint probability density function (equation 4.42), for sea state 7.

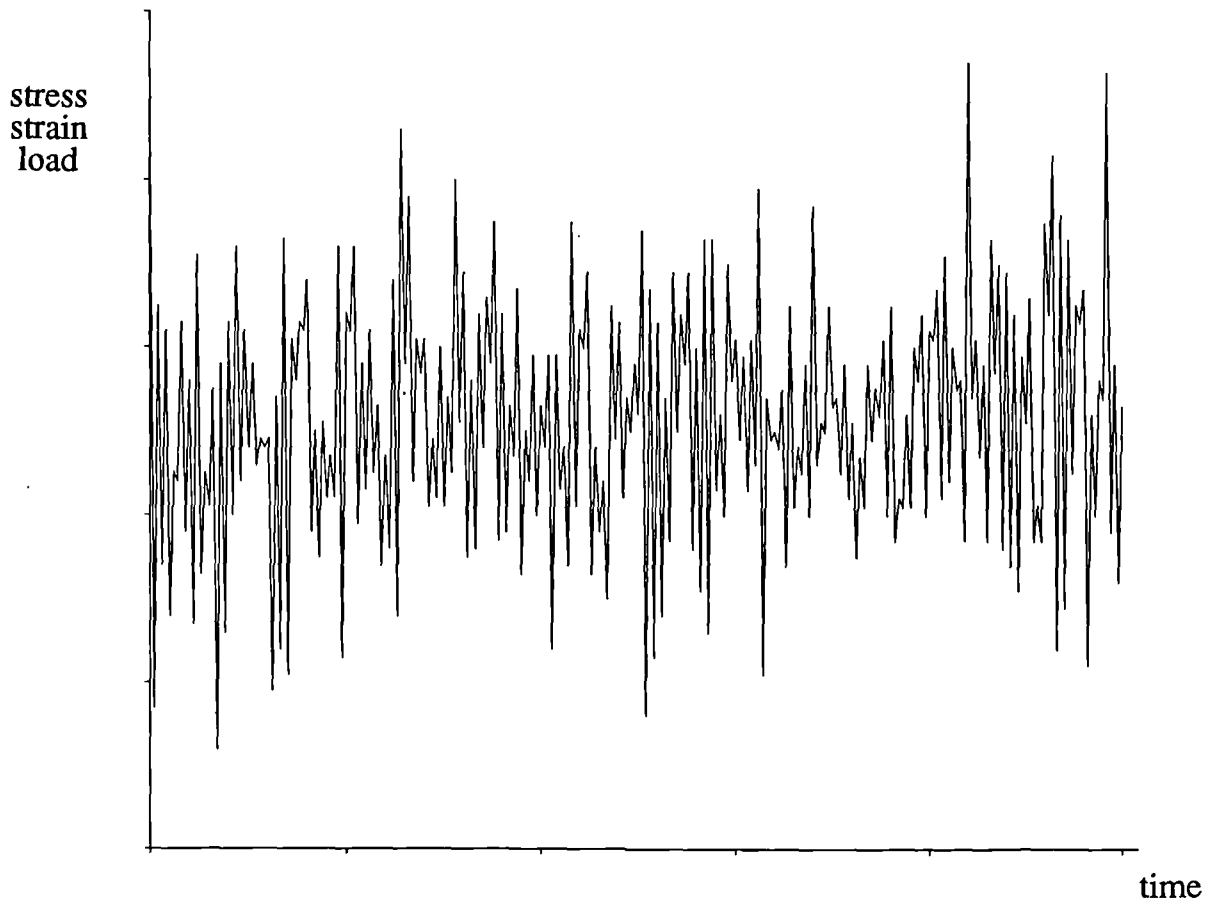
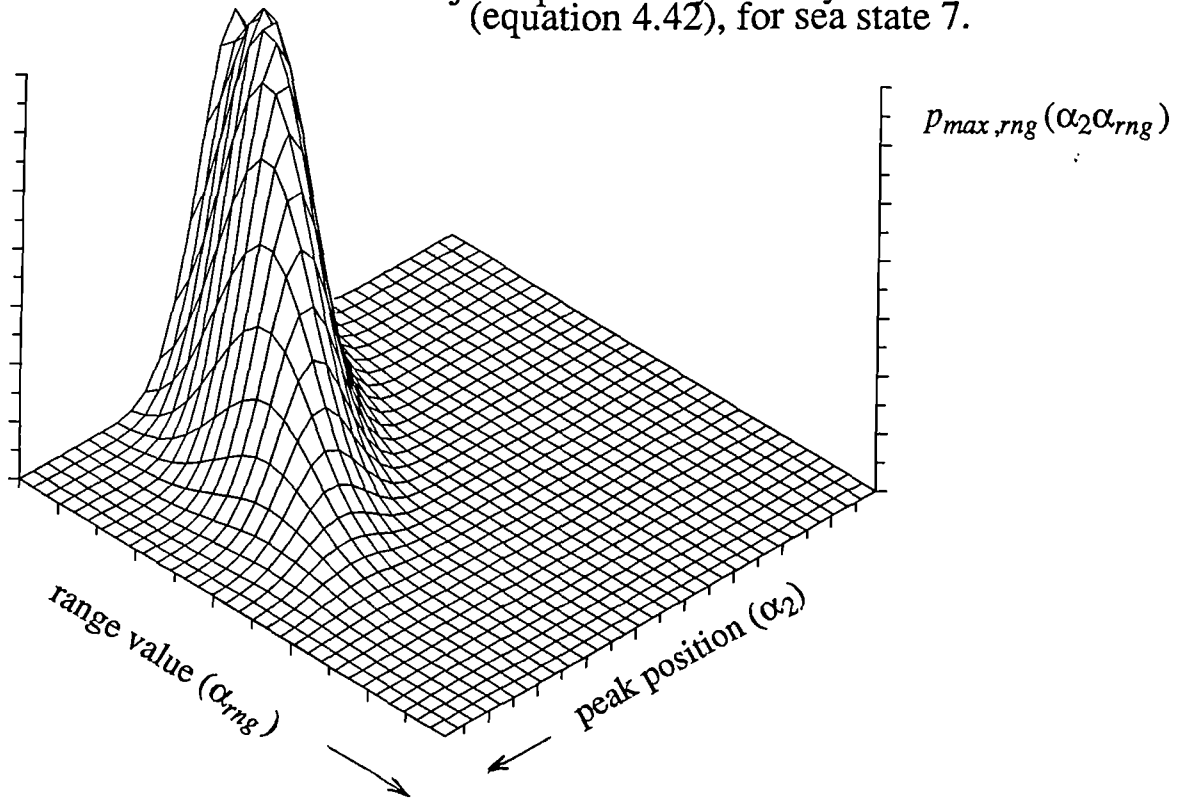


Figure 4.11. The first 251 points in a peak-trough series generated from Kowalewski's peak-range joint probability density function, for sea state 7.

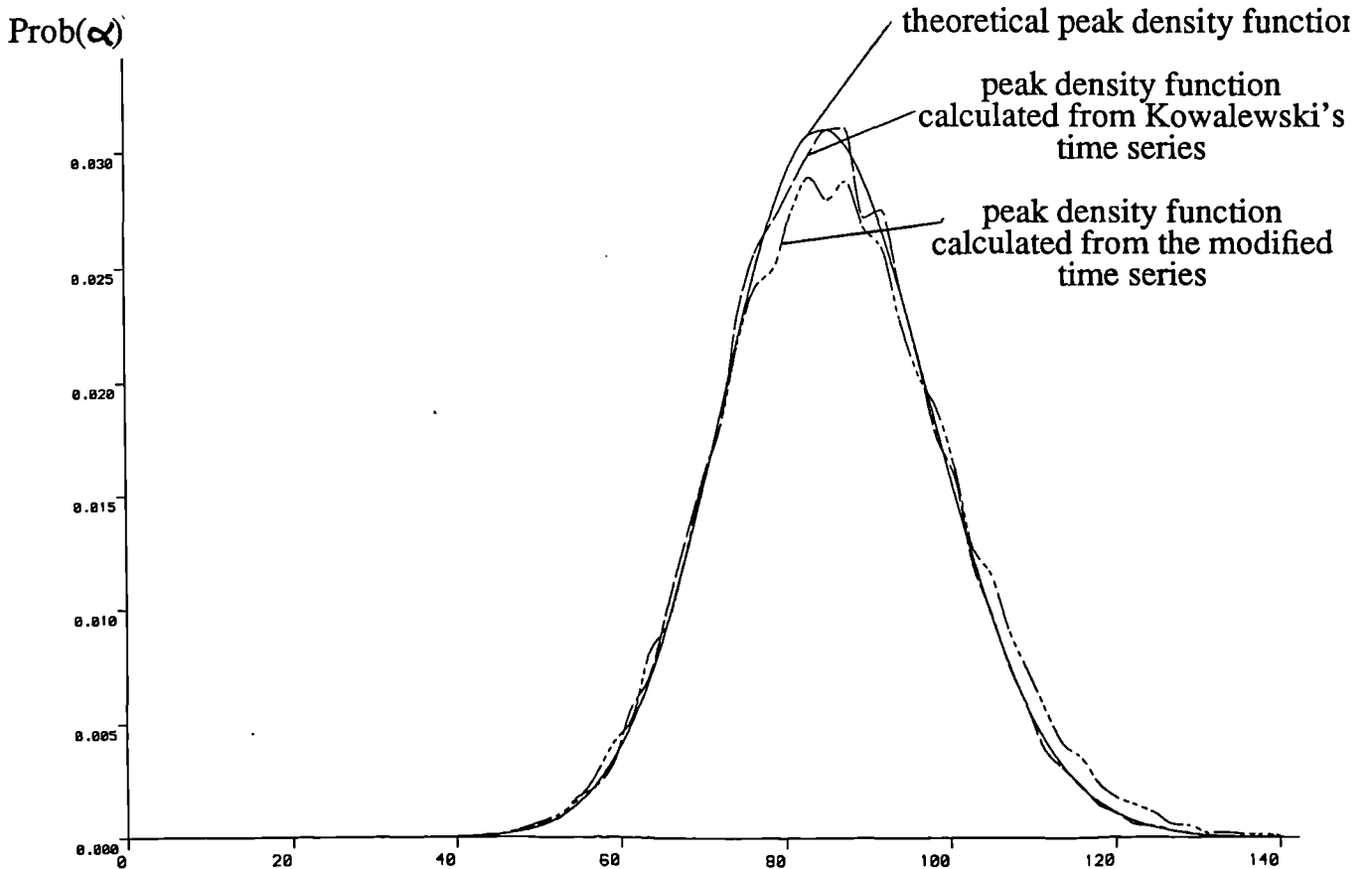
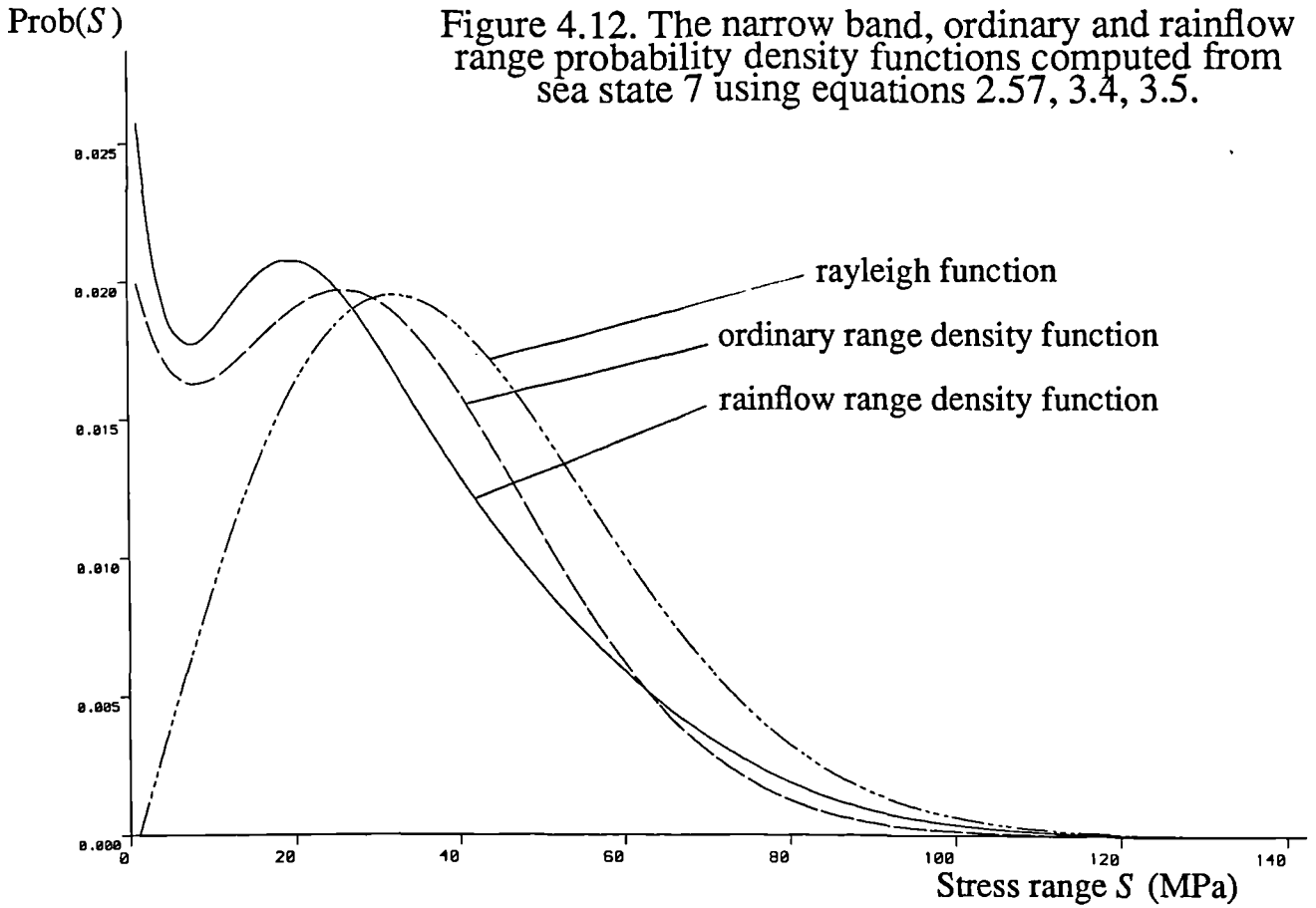


Figure 4.13. The peak distributions computed from time series of Kowalewski's and the modified peak-range joint distributions compared with the theoretical prediction (equation 2.53), for sea state 7.

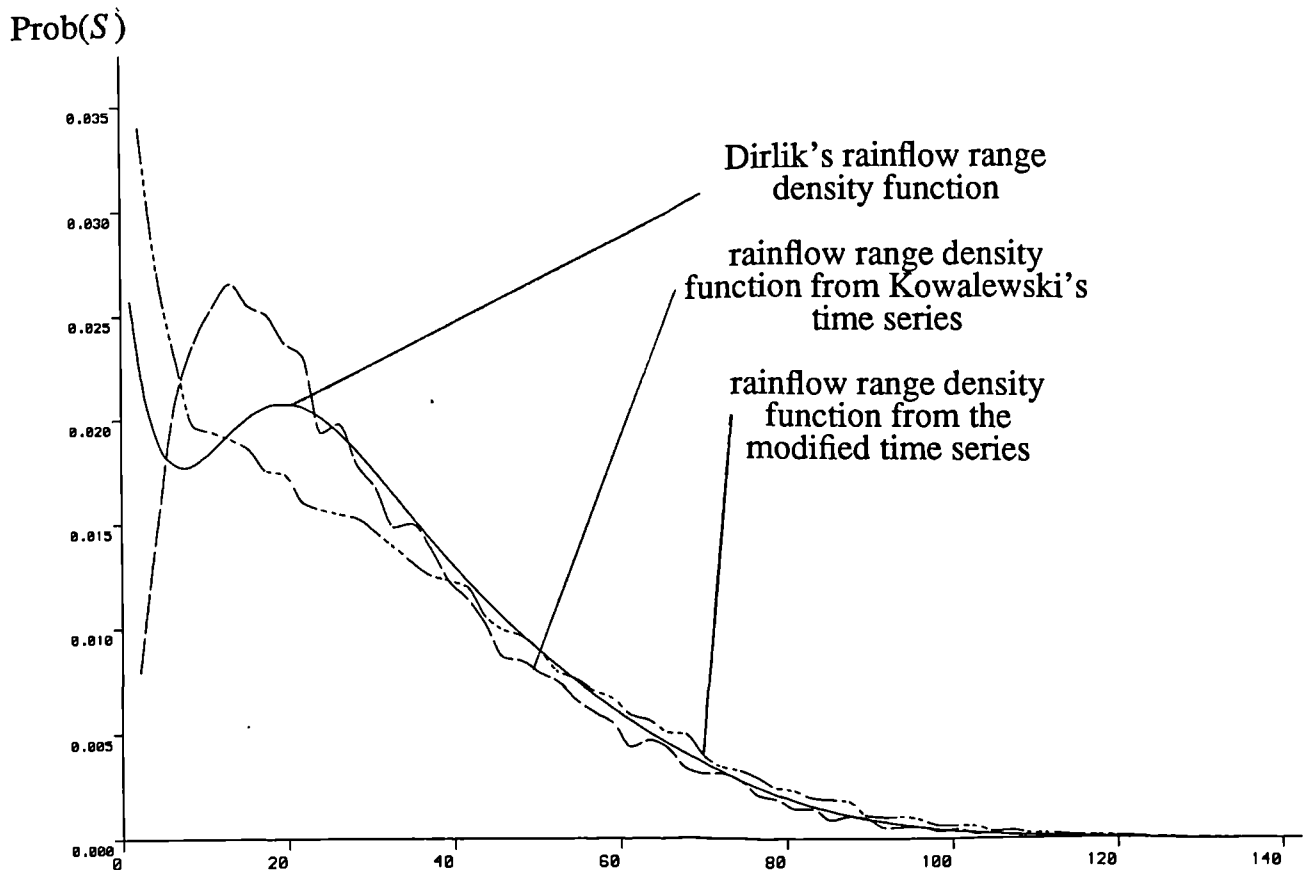
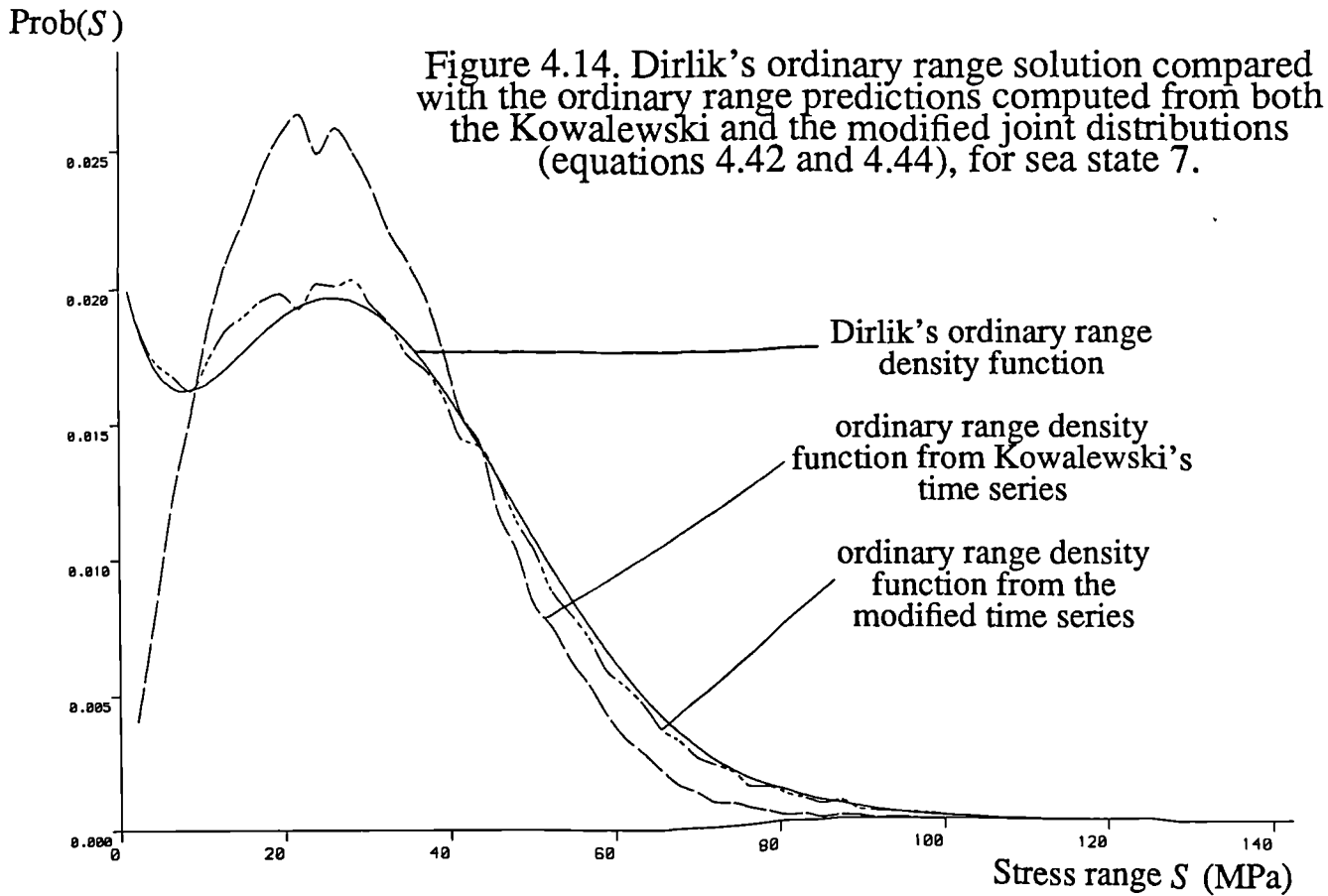


Figure 4.15. Dirlik's rainflow range solution compared with the rainflow range predictions computed from both the Kowalewski and the modified joint distributions (equations 4.42 and 4.44), for sea state 7.

Figure 4.16. Kowalewski's peak-range joint probability density function (equation 4.42), for sea state 11.

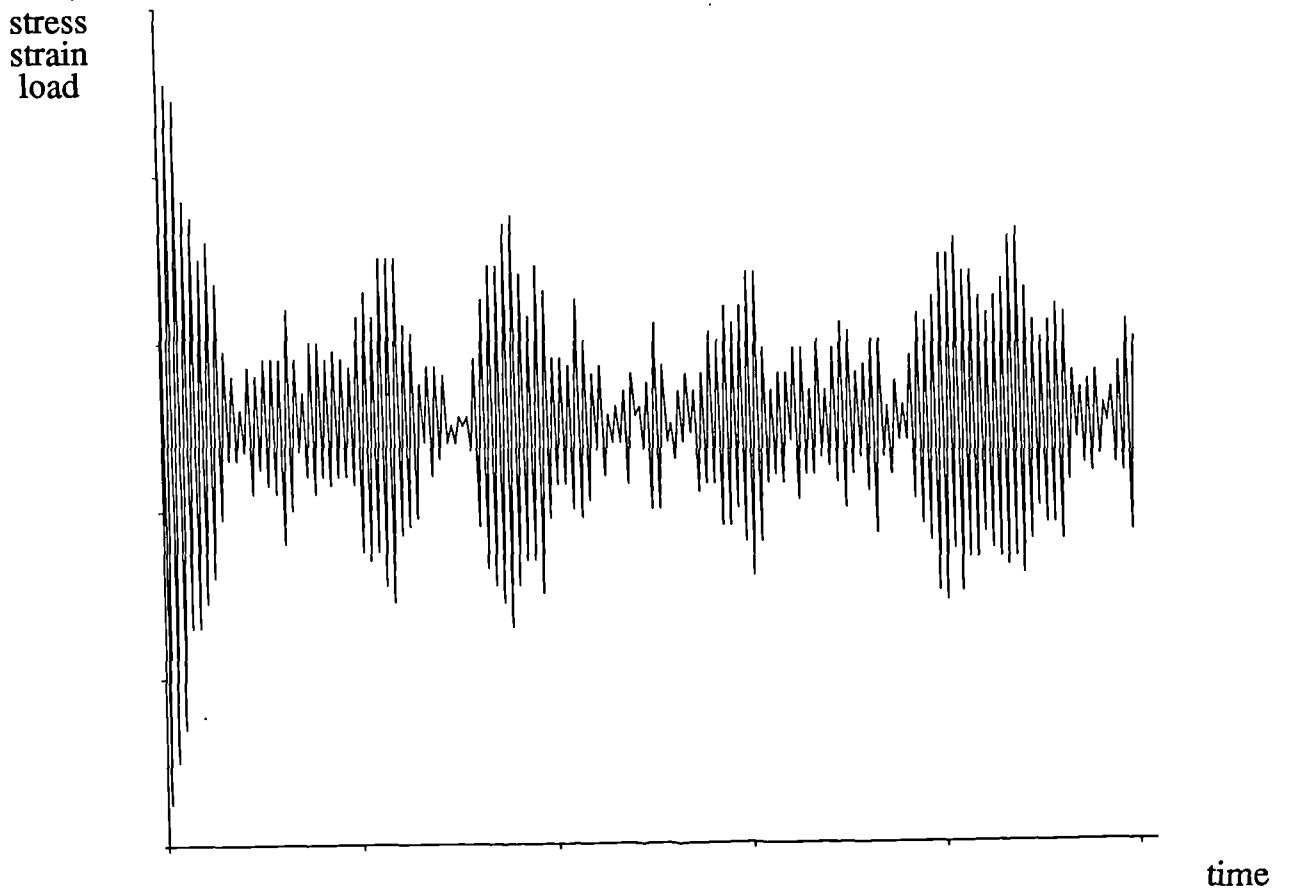
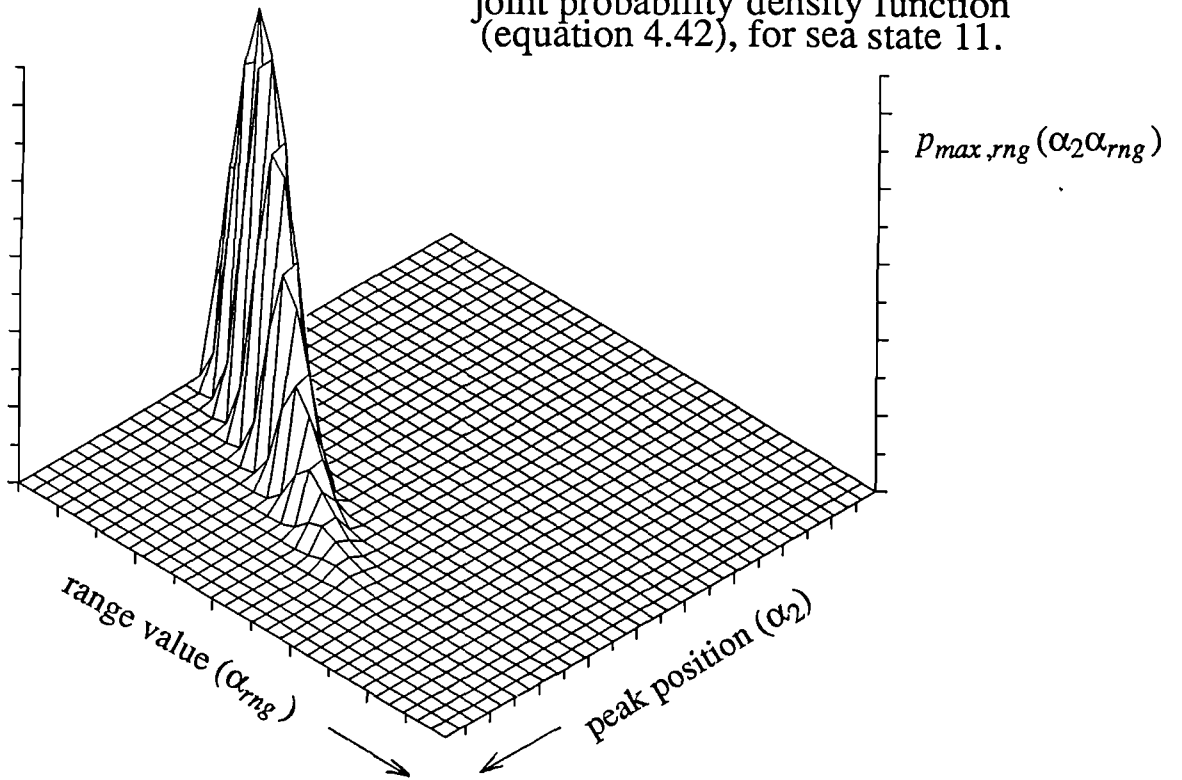


Figure 4.17. The first 251 points in a peak-trough series generated from Kowalewski's peak-range joint probability density function, for sea state 11.

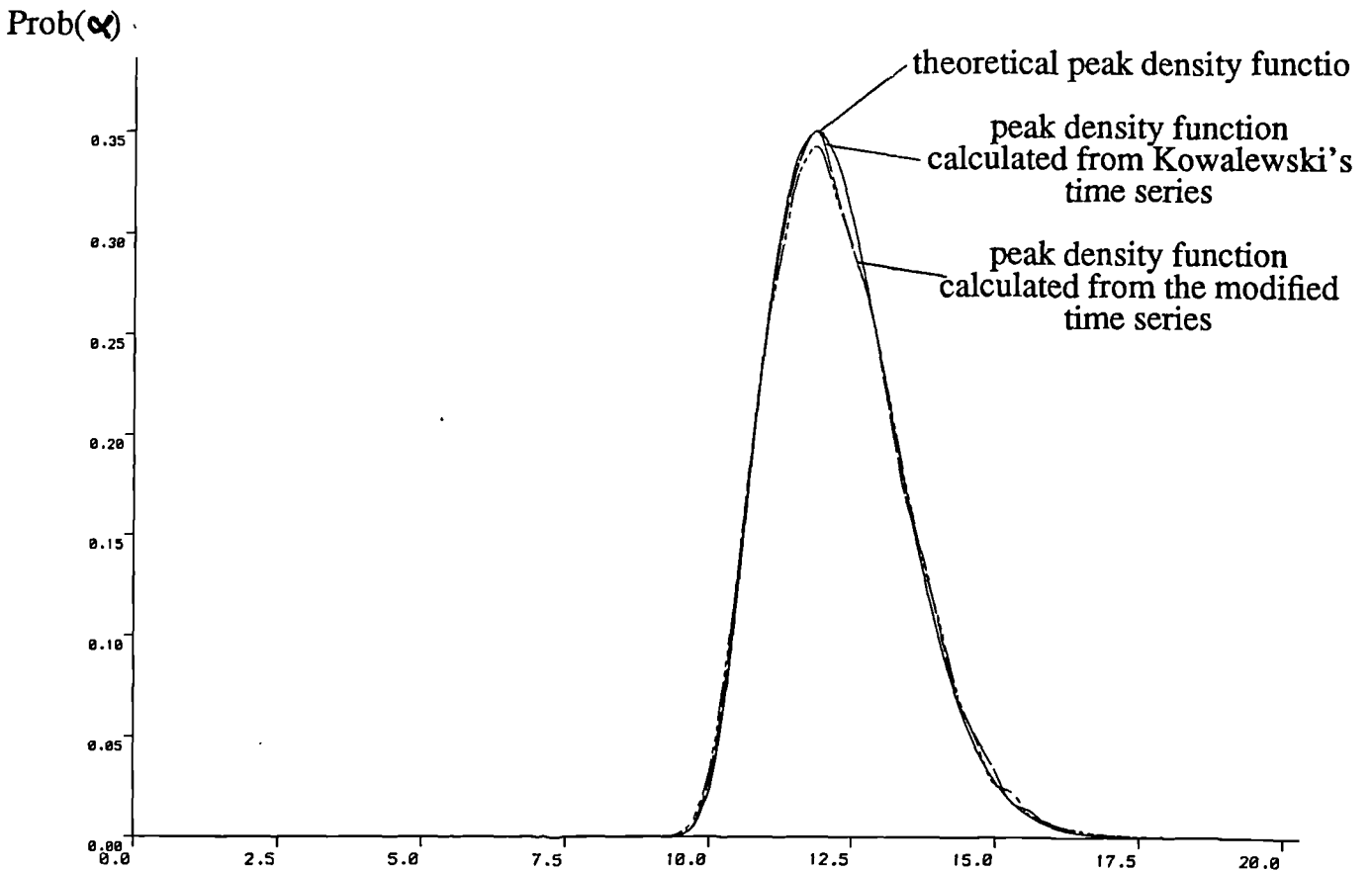
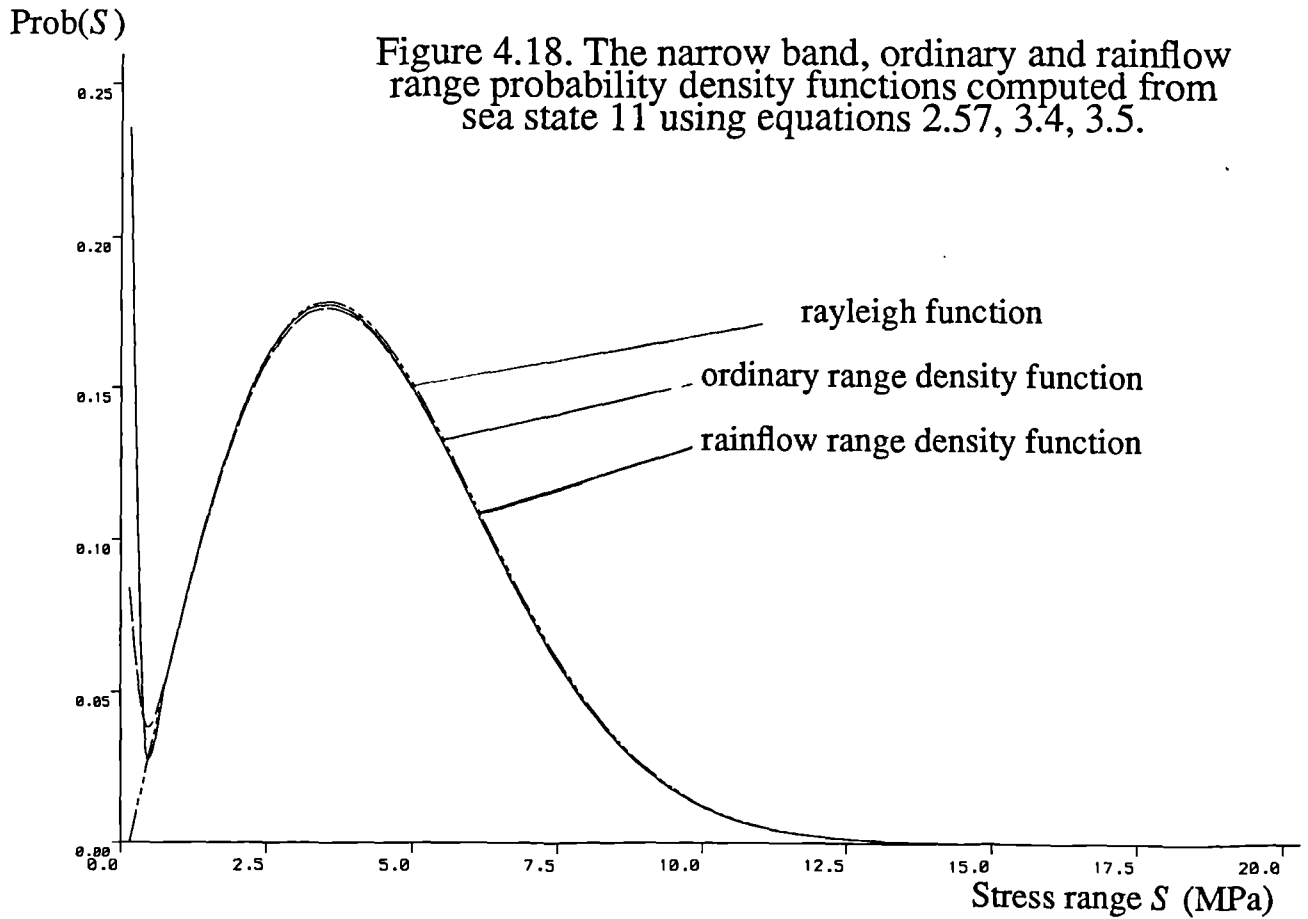


Figure 4.19. The peak distributions computed from time series of Kowalewski's and the modified peak-range joint distributions compared with the theoretical prediction (equation 2.53), for sea state 11.

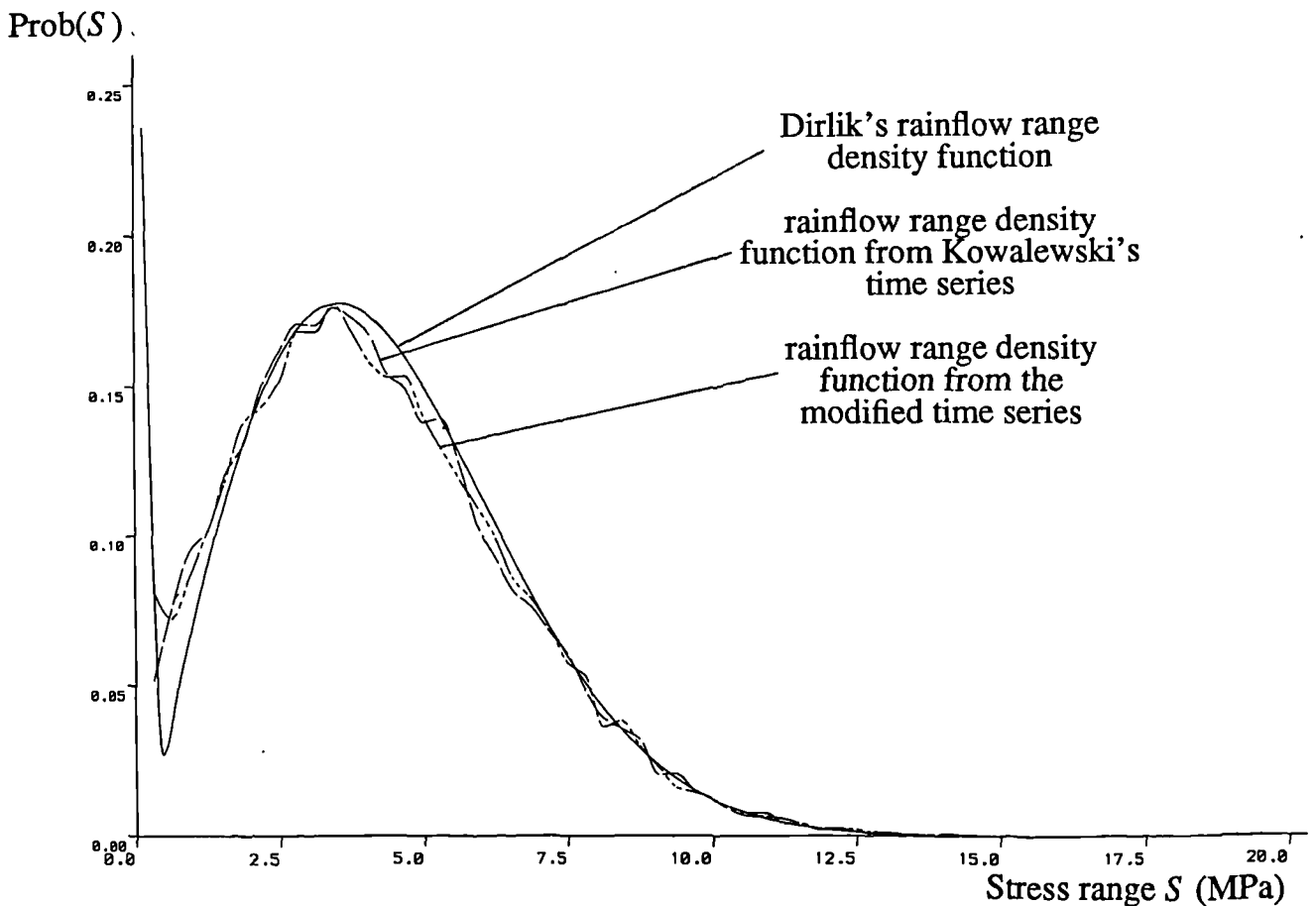
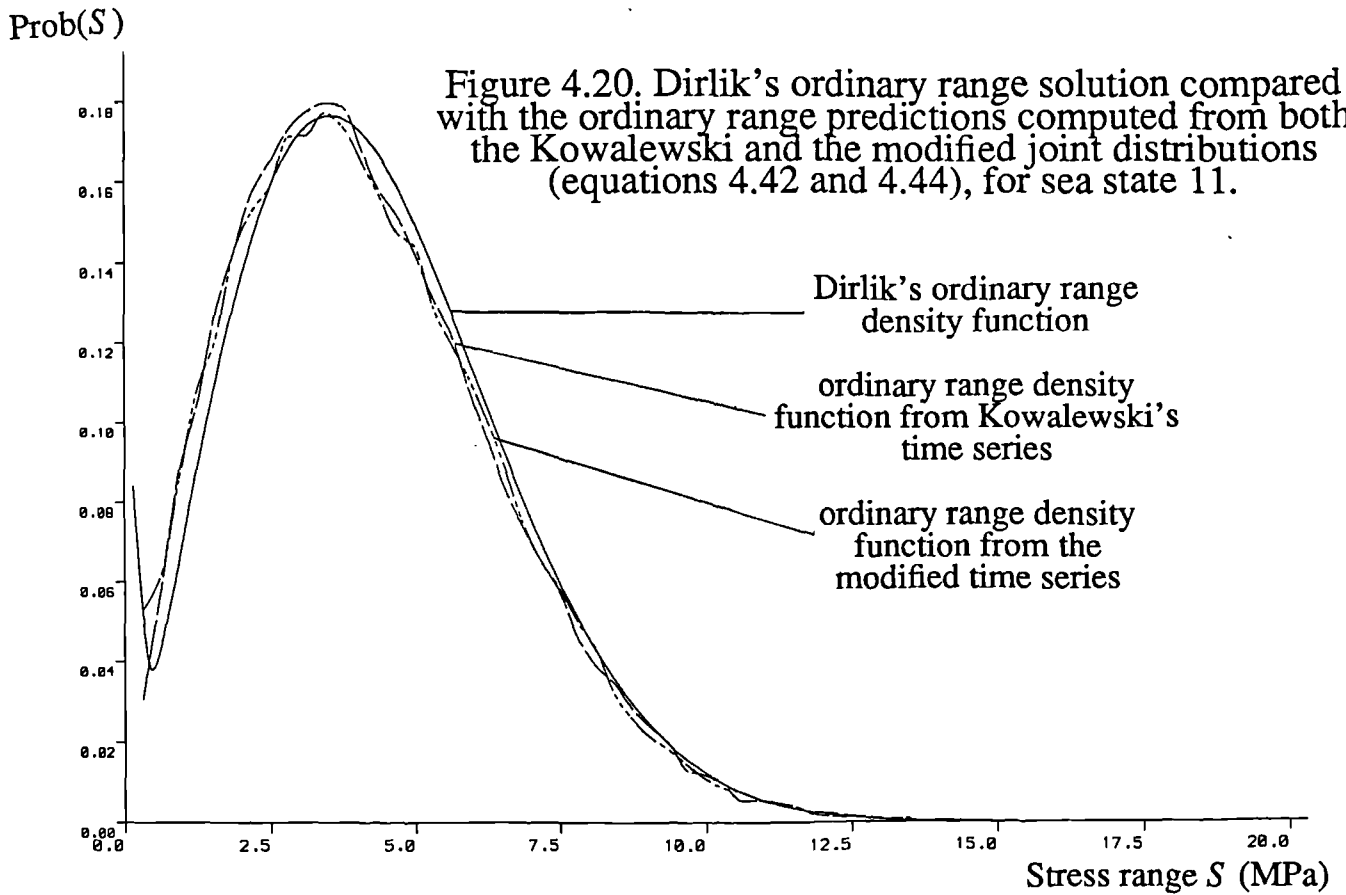


Figure 4.21. Dirlik's rainflow range solution compared with the rainflow range predictions computed from both the Kowalewski and the modified joint distributions (equations 4.42 and 4.44), for sea state 11.

Figure 4.22. The b_{th} moment of the ordinary range density functions computed from both the Kowalewski and the modified joint distributions after being normalised by the b_{th} moment of Dirlik's ordinary range density function, for sea state 1.

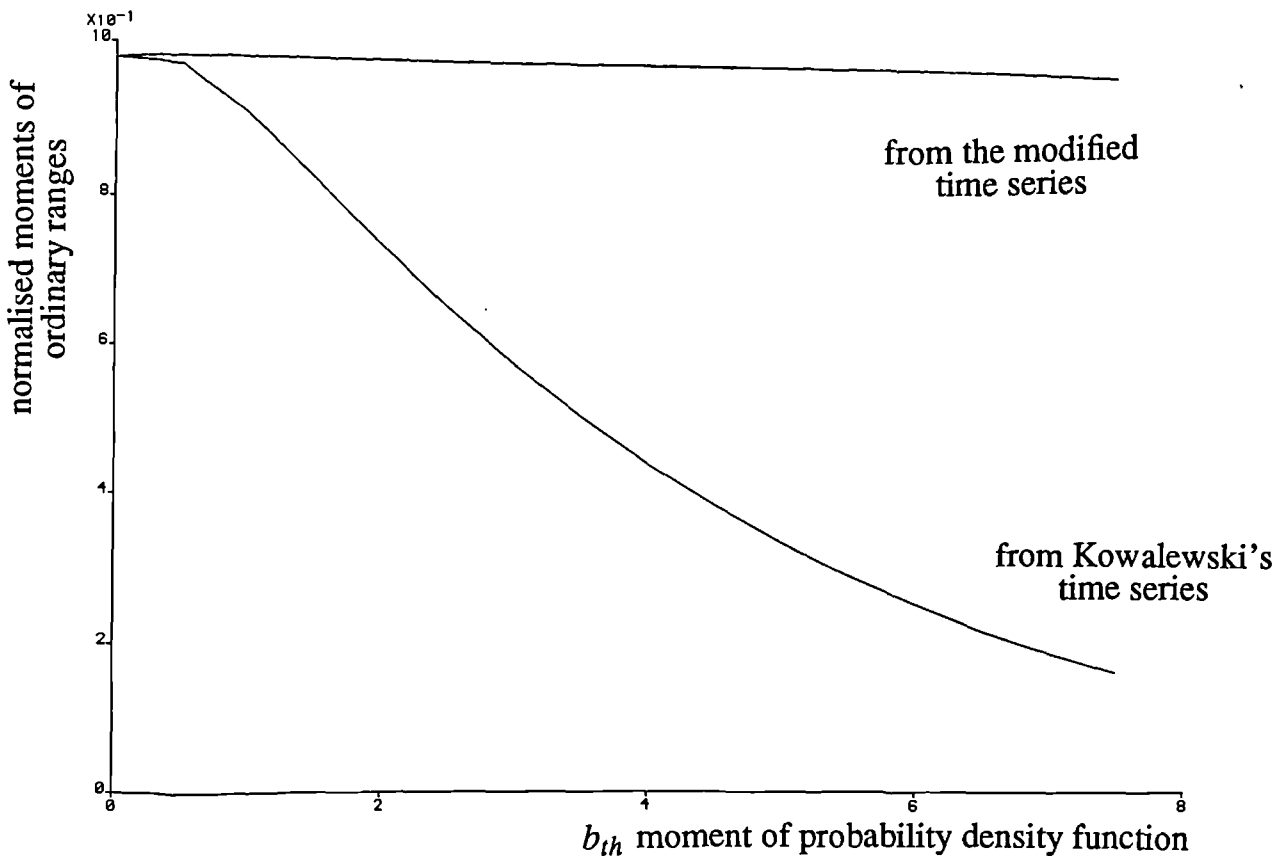


Figure 4.23. The b_{th} moment of the rainflow range density functions computed from both the Kowalewski and the modified joint distributions after being normalised by the b_{th} moment of Dirlik's rainflow range density function, for sea state 1.

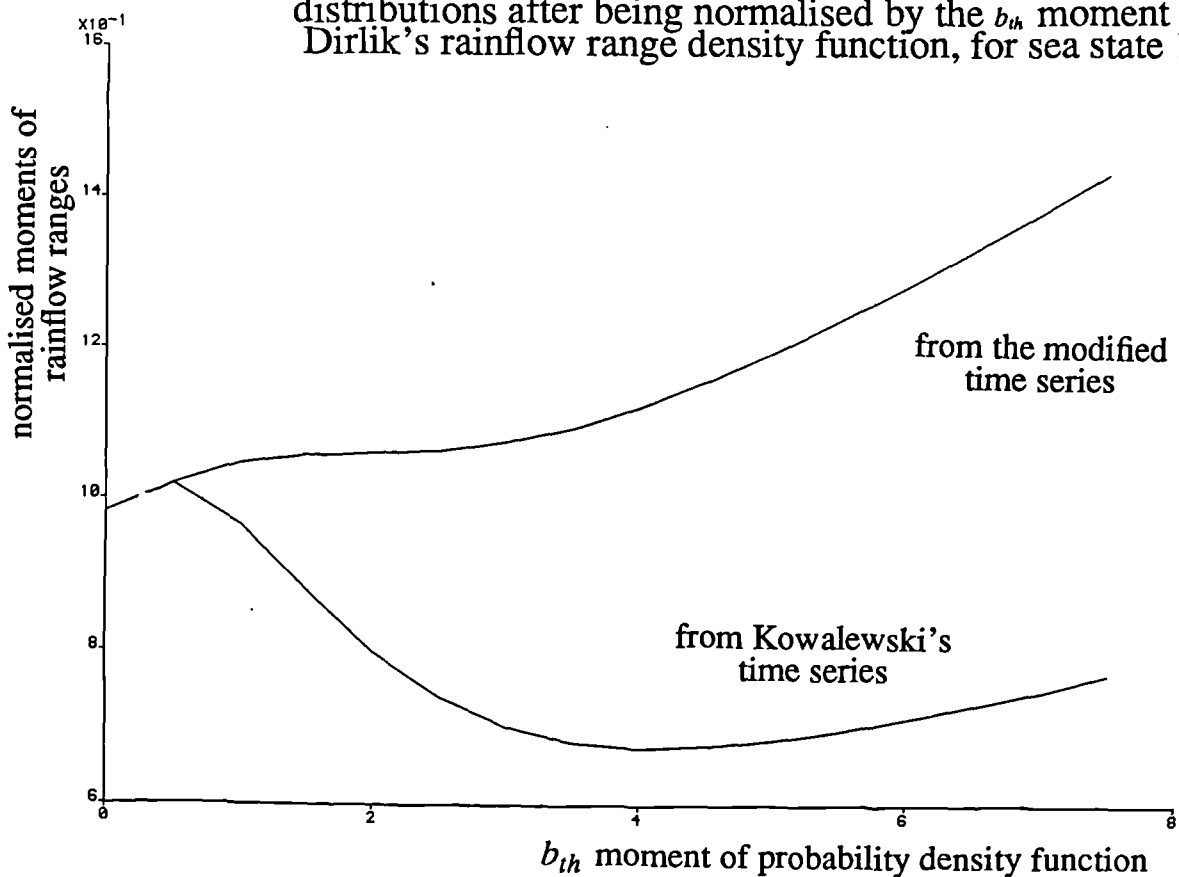


Figure 4.24(a) The effect on the normalised 5^{th} moment of the rainflow range density function computed from Kowalewski's joint distribution of varying the sample size, for a matrix size $L=33$.

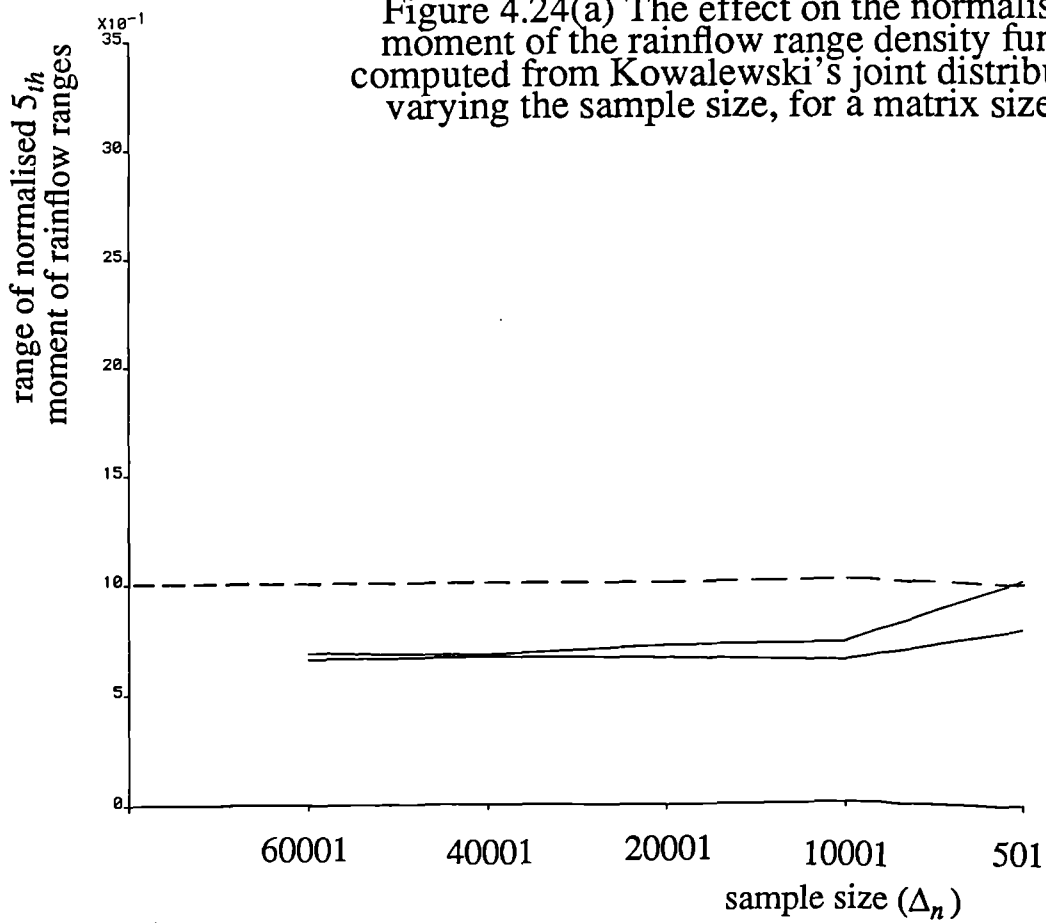
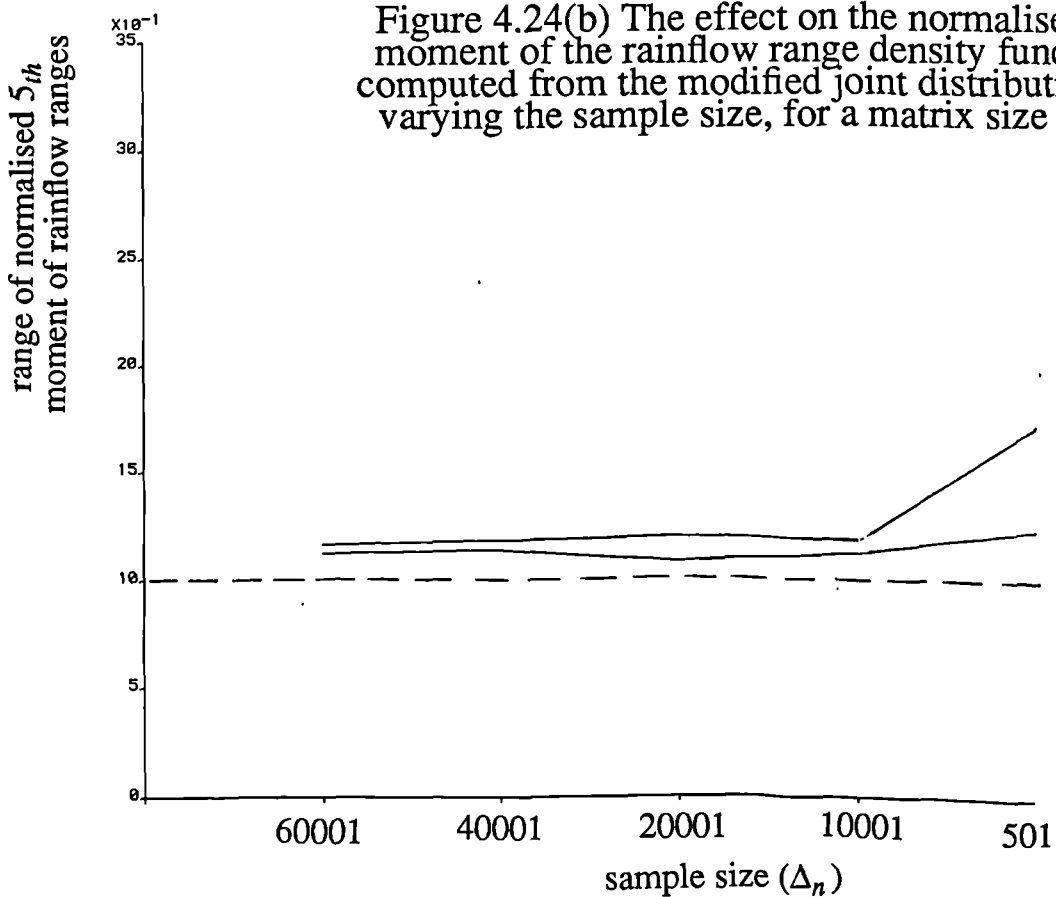
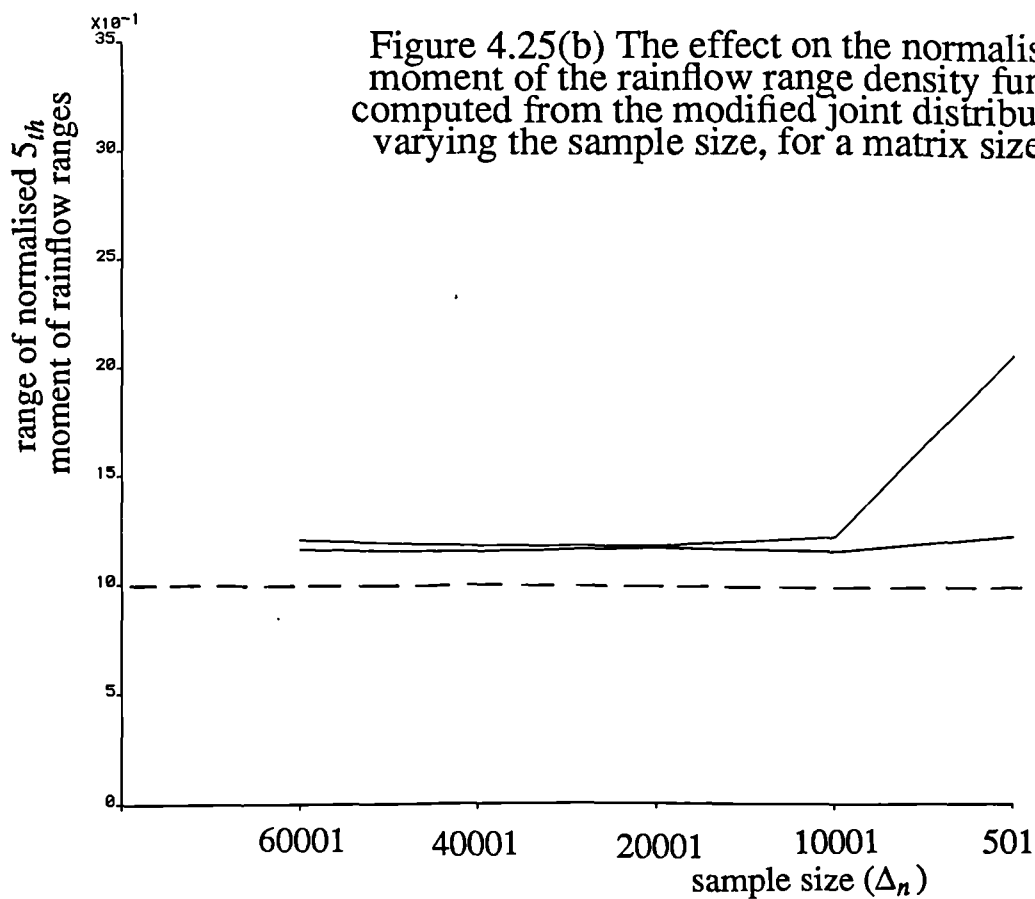
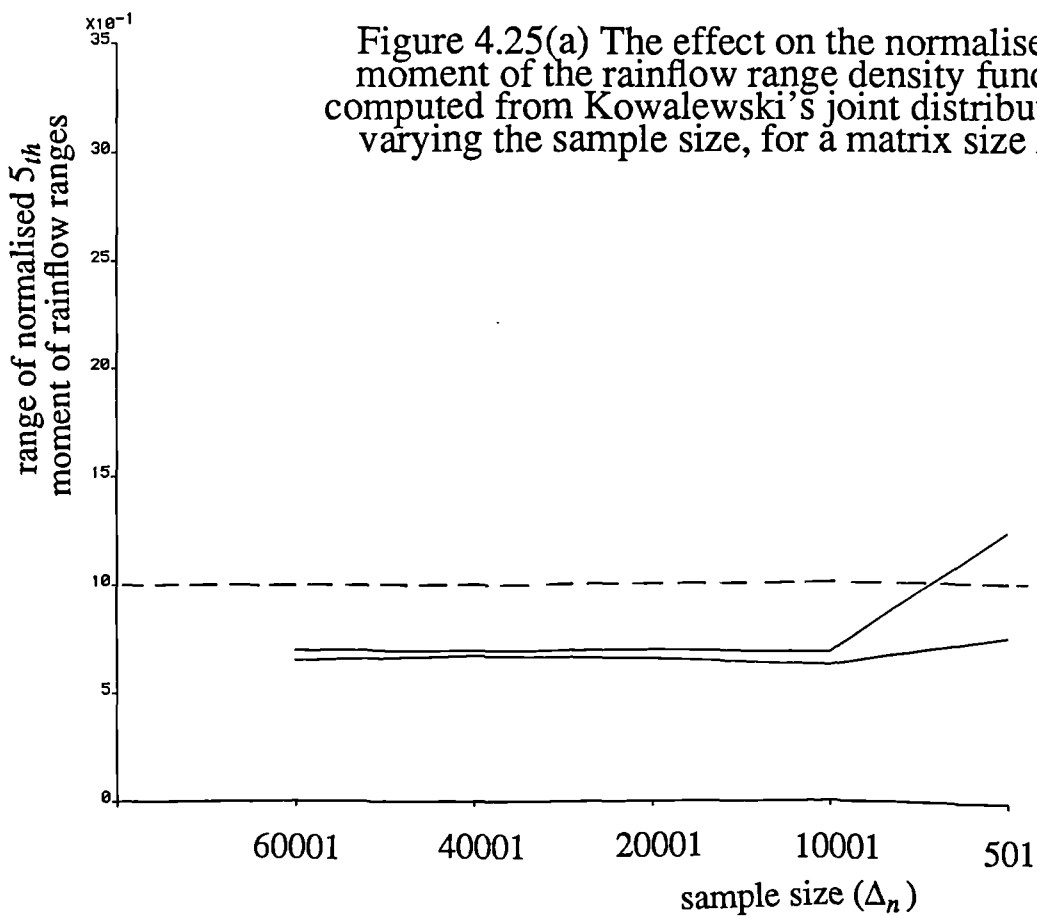
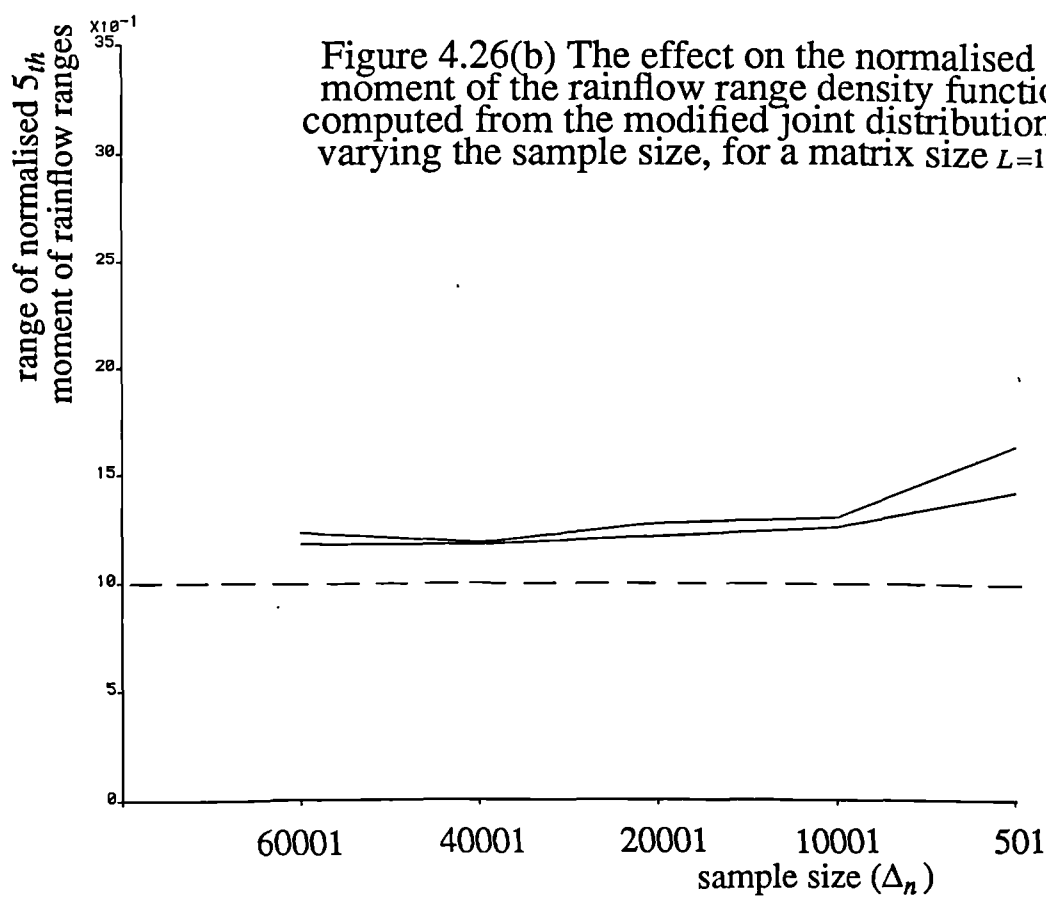
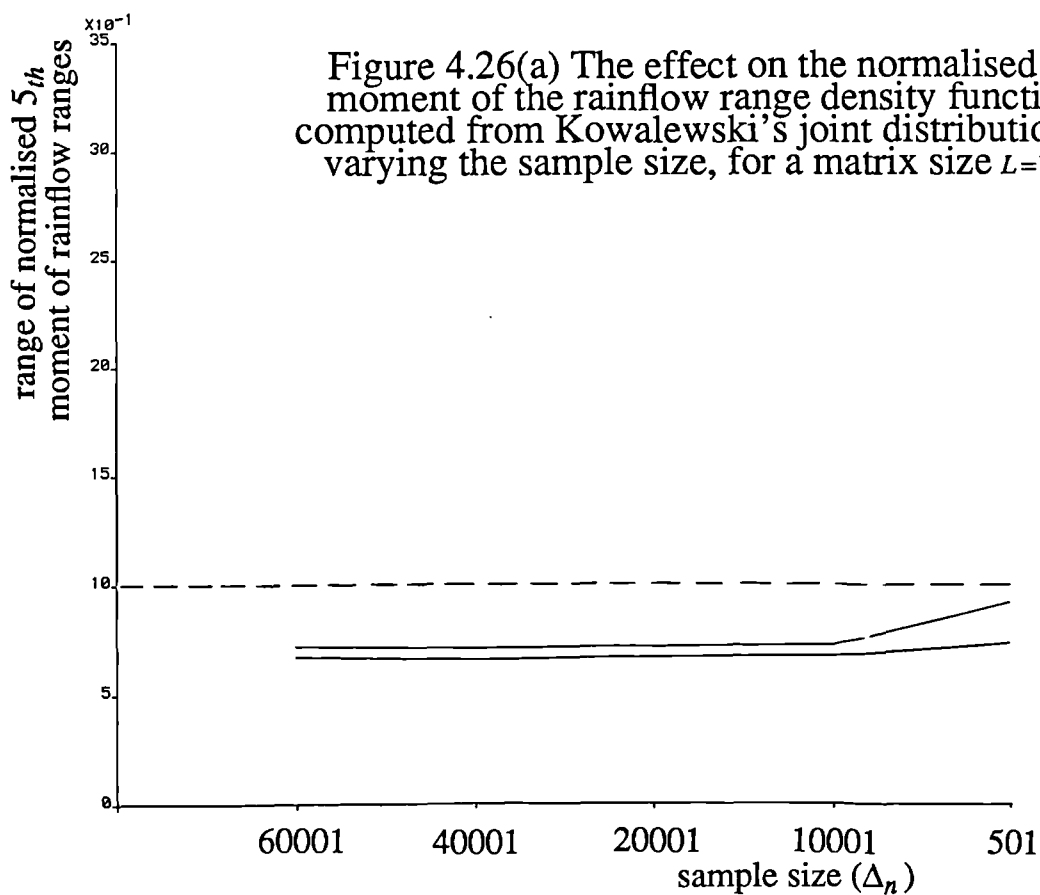


Figure 4.24(b) The effect on the normalised 5^{th} moment of the rainflow range density function computed from the modified joint distribution of varying the sample size, for a matrix size $L=33$.







5. A theoretical solution for the prediction of 'rainflow' ranges from power spectral density data.

5.1. Introduction

Since the rainflow cycle counting method was introduced 20 years ago it has become widely accepted as the best method of estimating the fatigue damage caused by randomly fluctuating loading conditions. A fatigue damage calculation which uses rainflow ranges can be thought of as giving a result for damage somewhere between an upper and lower bound. An upper bound on damage can be obtained by using the 'narrow band' assumption. This pairs each peak in the signal with a trough of equal but opposite magnitude. Because of the nonlinear nature of the fatigue damage mechanism, this will give a higher estimate of the damage than the lower bound approach of counting cycles between adjacent peaks and troughs. Rainflow cycle counting identifies trends in the signal which cause high fatigue damage. This is highlighted in figure 5.1.

In its original form it proved to be a reasonably efficient and simple exercise to write computer code to carry out the desired rainflow cycle count. However, in this form, the rainflow cycle counting definition required the whole time signal before the count could start. Furthermore, there was no way of obtaining the desired rainflow cycle distribution when the loading was specified in the frequency domain. In 1985, Dirlik (ref.5.1, see section 3.2) provided a solution to the latter based on computer modelling, although there was still a need for a theoretically based solution to the problem.

This chapter first provides a method of breaking down the rainflow range mechanism into logical steps which can be analysed using Markov process theory. Then, using the best available theoretically based relationship to define the dependence between peaks and troughs, the problem of obtaining rainflow ranges from power spectral density (PSD) data is solved.

Finally, the results are compared with actual rainflow counts on various 'real' signals, being the signals used to obtain the PSD's.

5.2. Historical background to the theory of rainflow range predictions from power spectral density data.

Matsuishi and Endo (ref.5.2) first proposed the rainflow cycle counting method in 1968. Since then it has become widely used for estimating the fatigue damage of materials subjected to random loadings. It is now generally thought to give the most consistent predictions when compared to actual fatigue life results (1972,ref.5.3). For a full definition of the rainflow cycle method defined in this way see reference 5.4.

This definition was of no use for frequency domain calculations. The definition of cycles was set up in terms which were not rigorously mathematical, and to obtain results the whole time signal was required before applying the method in order to establish the maximum range from the highest peak to the lowest trough.

Much interest has since been shown in the fatigue damage analysis and possibly, a rainflow range count, directly from the PSD (refs.5.5-5.13). The most useful contribution recently has been an alternative definition of the rainflow cycle counting method (1987,ref.5.14). This alternative method is shown in figure 5.2. The rules for the counting method are applied to each peak in the time signal. According to this new definition, for a rainflow range to exist the signal must recross the level of the peak from which it started (current peak) for both the negative and positive time directions. If we consider the signal to have been sampled with respect to time and set the current peak position equal to $t=0$, we have $+ve$ time to the right and $-ve$ time to the left. The current peak is paired with the lowest point in the signal in each of these directions, to give two ranges. The rainflow range is then defined as the smaller of these. This definition can be broken down into four stages. If we think of the signal travelling forwards and backwards from the current peak.

Stage 1 takes the signal forwards ($+ve$ time) from point 1 to point 2 a distance h below it.

Stage 2 takes the signal forwards from point 2 to point 3, some level at or above point 1 thus closing the rainflow cycle.

Stage 3 takes the signal backwards ($-ve$ time) from point 1 to point 4, some level at or below point 2.

Stage 4 takes the signal backwards from point 4 to point 5, some level at or above point 1.

It seems however, that when considering the long term distribution of the signal, stage 4 of the above definition is redundant, because once the signal has passed below the level of point 2 (part of stage 3) there is probability 1 that it will eventually go to a level above point 1 (given that it can go to any level below point 2 during this process).

In later papers Rychlik (refs.5.15-5.17) went on to use a modified form of the above definition which effectively removed both stages 3 and 4 from the analysis by proposing that the conditional rainflow range cycle for a particular peak at $y(t)$ is (refs 5.15,page 254 and 5.17,page 664);

"greater than h , if and only if $y(t+\tau)$ crosses the level $y(t)-h$ before it reaches the level $u=y(t)$ {the level of point 1 in figure 5.2}, as τ goes to both plus and minus infinity".

The implied assumption in the above statement that both the forwards and backwards traces of the signal must cross the level $y(t)-h$ is confirmed in ref.5.15, equation 4. In other words, the rainflow cycle is equal to some value between h and $h+dh$ if $y(t+\tau)$ crosses the level $y(t)-h$ but does not cross the level $y(t)-(h+dh)$ before it reaches the level $u=y(t)$, as $y(t)$ travels forwards and backwards. The effect of this modification is to underestimate the probability of a rainflow range because the rainflow range defining cycle (stages 3 and 4 above) would be restricted to finish within the interval $y(t)-h$ to $y(t)-(h+dh)$, where in fact it should be allowed to go to any point at or below this interval.

To fully define a rainflow range for a particular peak, stages 1,2, and 3 must be retained. Stages 1 and 2 to 'create' the rainflow cycle and stage 3 to 'define' it. The next section will develop a method for applying this new definition to frequency domain representations of the loading conditions.

5.3. A new theoretical solution for the prediction of rainflow ranges.

Using the above observations we can now formulate the following new rainflow range definition. For a rainflow range value h to be defined from a particular peak three events must happen. These events are highlighted in figure 5.3 in discrete form.

- (i) Y_1 . The signal must have come from a level at least h below the level of point 1 without at any time going above the level of point 1, (with any number of extreme points inbetween).
- (ii) Y_2 . The signal must then go from the level of point 1 to the level of point 2 without at any time between going back to the level of point 1 or below the level of point 2, (with any number of extreme points inbetween).
- (iii) Y_3 . The signal must then go from the level of point 2 to some point at or above the level of point 1 without at any time going back to the level of point 2, (with any number of extreme points inbetween). This is a minor approximation because for this leg of the definition to be rigorously correct, the signal should be allowed to travel back to, but not below, the level of point 2. The approximation was used because it allows considerable simplification of the problem at a later stage and appears to have no discernible effect on the results.

Because Y_1 , Y_2 and Y_3 can be considered as independent events, we can find the rainflow range density function by finding the probability of all three events occurring together and then normalising by the sum of the probabilities of all possible events. This can be expressed in the following way.

If the probability of being at a particular peak is defined as $P(ip)$ and a rainflow range of value $h=(ip)-(kp)$ is defined as $S_{RR}(h)$, where ip and kp are the levels at points 1 and 2 respectively, we have;

$$S_{RR}(h) = \sum_{ip=2}^{ip=\infty} \sum_{kp=1}^{kp=ip-1} \frac{2.0}{Dh} * Y_1(ip, kp) * Y_2(ip, kp) * Y_3(ip, kp) * P(ip) \quad (5.1)$$

Where; $Y_1(ip, kp)$ is the probability of event Y_1 happening with a peak at ip and a trough at kp , and so on for $Y_2(ip, kp)$ and $Y_3(ip, kp)$. Dh represents the interval width used to divide the total signal stress range. The value 2.0 comes from the fact that for a full set of events, rainflow ranges occurring with point 1 as a trough need to be

considered. In other words, for every configuration of $Y_1(ip, kp)$, $Y_2(ip, kp)$, and $Y_3(ip, kp)$ being considered, there is an equally likely configuration of the signal which is a rotation of the signal of 180° about an axis which represents the mean signal value.

Therefore the problem of obtaining a theoretical derivation to the rainflow range problem has become one of obtaining $Y_1(ip, kp)$, $Y_2(ip, kp)$, $Y_3(ip, kp)$ and $P(ip)$. Two areas of theory will be required for this. A suitable method is required to model the dependence between adjacent extremes, then a theory is required to extend this to model the dependence between extremes which are not adjacent. This will be required in order to obtain Y_1 , Y_2 and Y_3 because these events are not limited to adjacent extremes.

Firstly, adjacent extremes will be discussed. This topic is covered in detail in section 4.2.3 and the following represents a summary of that section.

In 1976 as part of a common research project between IABG and LBF in Germany, a standard random load sequence was recommended (ref.5.18) which came from an approximate expression developed by Kowalewski in 1963 (ref.5.19). The expression is approximate because, strongly tied up with the problem of obtaining this distribution is the one of obtaining the distribution of times between zero crossings. Until this problem is solved, a complete theoretical solution for the joint distribution of peaks and troughs will not exist. A modified version of Kowalewski's expression already exists (ref.5.20, see section 4.2.4) which gives improved results. This expression, however, is based on an empirical distribution for ordinary ranges (ordinary ranges are defined as the ranges joining adjacent peaks and troughs). Therefore, for the purposes of the work in this report Kowalewski's original expression will be used (equation 4.38). All of the factors which make up this expression can be obtained from the moments of the PSD obtained using equation 2.28(b).

From these moments we can get the number of zero crossings and the number of peaks per second. Using these, we can get a value for the irregularity factor from equation 2.52. Then from the above, we can now calculate the joint distribution of peaks and troughs given by equation 4.38. An example of this distribution is given in figure 5.4(a).

Having obtained an expression which models the dependence between a peak and the next trough, we now require a theory to describe the dependence between extremes

which are not adjacent. The application of Markov process theory appears to be the best way to solve this problem because it enables the probabilities of multiple events to be calculated once the single event probabilities are known. It is possible to construct a matrix model representing figure 3, including all the necessary absorbing states, which can be then be used to obtain the necessary probabilities of Y_1 , Y_2 and Y_3 ever happening. The fundamental assumption inherent in this technique, which appears to be reasonable, is that past events have no influence on future events. The next section gives a brief summary of the theory of Markov chains.

5.4. Markov Chains

A Markov chain is a special type of Markov process, which is itself a special type of stochastic process (see refs.5.21-5.22 for a detailed description of the subject). A Markov process is called a chain if the set of values the process can take are countably finite or discrete. A chain X_k satisfies the Markov property if for every k and all possible states i_1, i_2, \dots, i_n the following is true;

$$P\left[X_n=i_n | X_{n-1}=i_{n-1}, X_{n-2}=i_{n-2}, \dots, X_1=i_1\right] = P\left[X_n=i_n | X_{n-1}=i_{n-1}\right] \quad (5.2)$$

If we know that chain is at state i at time $n-1$, we wish to know the probability that it will be at state k at time n ;

$$p_{ik} = P\left[X_n=k | X_{n-1}=i\right] \quad (5.3)$$

This is the transitional probability of the process going from state i to state k , and it is independent of where the signal was before the process was at state i . If there are n possible states, then an n by n transition matrix exists denoted by P , equal to;

$$P = \begin{bmatrix} p_{11} & p_{12} & p_{13} & \cdot & \cdot & \cdot & p_{1n} \\ p_{21} & p_{22} & p_{23} & \cdot & \cdot & \cdot & p_{2n} \\ p_{31} & p_{32} & p_{33} & \cdot & \cdot & \cdot & p_{3n} \\ \cdot & \cdot & \cdot & \cdot & \cdot & \cdot & \cdot \\ \cdot & \cdot & \cdot & \cdot & \cdot & \cdot & \cdot \\ \cdot & \cdot & \cdot & \cdot & \cdot & \cdot & \cdot \\ p_{n1} & p_{n2} & p_{n3} & \cdot & \cdot & \cdot & p_{nn} \end{bmatrix} \quad (5.4)$$

If the above transition matrix represents the probabilities of going from state to state in one step, to find the probability of going from state to state in n steps one needs simply to find the n th power of the matrix.

$$p_{ik}^{(n)} = P^n \quad (5.5)$$

If the configuration of the transition matrix is such that the process can only travel into but not out of a given state or set of states, those states are defined as closed. They represent 'absorbing' states because they can only fill up and never empty. A Markov chain is termed 'irreducible' if all the states intercommunicate. Therefore, for the case where absorbing states are present the transition matrix is termed 'reducible'.

If we define the probability of ever going from state i to state k as f_{ik}^* , then state j is called 'persistent' if $f_{jj}^* = 1$ and 'transient' if $f_{jj}^* < 1$.

5.5. Modelling the problem

Firstly, a method will be shown for changing Kowalewski's peak-trough joint probability density function into a combined 2 step transition matrix (a peak-trough-peak transition matrix). One must first observe that peak-trough probabilities are separate from trough-peak probabilities. Figure 5.4(a) actually shows both on one plot. Initially these need to be converted into 1 step transition matrices and extracted separately. To do this, firstly the rows of both the upper and lower triangles of the probability density function must be normalised to 1 (see figure 5.4(b)). This is a fundamental requirement of transition matrices, and is obvious if one observes that the probability of going from one state to any other state must be 1 (i.e., going from a peak to any other trough). Once normalised, the upper and lower triangles can then be extracted to form the separate 1 step peak-trough and trough-peak transition matrices (see figures 5.5(a) and 5.5(b)).

Before the combined 2 step transition matrix can be formed, it is necessary to reconsider the problem to be solved.

Y_1 , Y_2 and Y_3 , are required for each peak and trough position to be considered. It will be shown that all the necessary information required to calculate these can be obtained if we set up transition matrices with absorption states which model the conditions shown in figure 5.6.

If we make the process start at ip , absorption state 1 models the probability of going from a level at ip to a level at kp at any time to infinity without going back to level ip . This represents $Y_2(ip, kp)$.

If we make the process start at ip , absorption state 2 models the probability of going to a level below kp at any time to infinity without going back to level ip . Because it is reasonable to assume that the process is both vertically and horizontally symmetrical, $Y_1(ip, kp)$ can be obtained by summing absorption states 1 and 2 (horizontal symmetry). $Y_3(ip, kp)$ can be obtained in a similar way by using the appropriate value of $Y_1(ip, kp)$ (vertical symmetry). In other words, once $Y_1(ip, kp)$ has been obtained, all the information required for $Y_3(ip, kp)$ is available.

Absorption state 3 models the probability of ever entering a level at or above ip . Absorption state 3 is unusual because although it does not include level ip it must include the probabilities of going to level ip . This keeps state ip empty and effectively does not allow probabilities to be accrued to absorption states 1 or 2 if the process at any time travels into state ip .

Transition state 4 represents the probabilities of travelling between states which are below state ip and above state kp .

We therefore need to obtain values for these 'long run' probabilities of going into absorption states 1 and 2 from state ip for each configuration of ip and kp .

The required 2 step transition matrix is obtained for each position of ip and kp by multiplying the peak-trough matrix by the trough-peak matrix. Before this is done, however, each of these matrices needs to be modified according to the specified positions of ip and kp . This is highlighted in figures 5.7(a) and 5.7(b). The absorption states described above are made into closed sets by putting 1's along the diagonal and zeros along the rest of the rows. The diagonals within the transition states are zero for both matrices highlighting the obvious fact that, for instance, a peak cannot go to a peak at the same level in one step (unless it has been made into an absorbing state). The trough-peak transition matrix shows arrows in row 10 (representing transitions into absorption state ip) indicating that the probabilities of transitions into this state have been added into state $ip + 1$. This is because the aim of the analysis is to model a process which starts

within state ip . ip cannot therefore be made into the type of closed state used for kp . One way of solving this problem is to turn the problem around. Instead of stopping transitions out of state ip , the transitions into state ip are moved to state $ip+1$. This has the same effect on the modelling process and does not effect the analysis because we are not interested in the states above ip .

The desired transition matrix is now obtained by multiplying these matrices together. This matrix is shown in figures 5.8(a) and 5.8(b) in its full and condensed form and represents two steps, a peak-trough step and a trough-peak step. The condensed form has had several simplifying modifications made. The row and column for state $kp+1$ has been removed since this is a null state because the process cannot reach state $kp+1$ without being absorbed into state kp . The states below kp have been condensed into 1 state and states above ip have been ignored because they have no effect on the desired elements of the 'long run' matrix (figure 5.8(c)).

Having obtained the two step peak-trough-peak transition matrix we now require a method of obtaining the desired probabilities of Y_1 , Y_2 and Y_3 after 2, 3, 4, 5 etc steps. In other words the probability of these events ever happening with any number of intervening extremes.

A simple way to now obtain the desired 'long run' absorption probabilities is to square and resquare the condensed matrix (figure 5.8(b)) until transition state 4 is empty. The values required to compute $Y_1(ip, kp)$ etc are then given by the bottom elements of rows 1 and 2 (equivalent to the bottom elements in R_{31} and R_{32} below). By choosing the bottom elements we are effectively forcing the process to start at ip . This process is repeated for all positions of ip and kp and hence the desired rainflow range distribution is obtained using equation 5.1.

An alternative method of obtaining these long run transition probabilities is given in reference 5.22, page 125. Although the method of squaring the matrix will be used to obtain the results in this study, a summary of this alternative method will be given below as it is possibly a more efficient method.

This method of solution is possible because the transition matrix can be reduced to the following condensed form.

$$P = \begin{bmatrix} P_1 & 0 & 0 & 0 \\ 0 & P_2 & 0 & 0 \\ R_{31} & R_{32} & Q_3 & R_{34} \\ 0 & 0 & 0 & P_4 \end{bmatrix} \quad (5.6)$$

Where;

P_1 represents transitions within abs. states lower than kp .(State 2)

P_2 represents transitions within abs. state kp .(State 1)

P_4 represents transitions within abs. states higher than ip .(State 3)

Q_3 represents trans. within states between $kp+1$ and ip .(State 4)

R_{31} represents transitions from $Q_3 \rightarrow P_1$.(States 4 to 2)

R_{32} represents transitions from $Q_3 \rightarrow P_2$.(States 4 to 1)

R_{34} represents transitions from $Q_3 \rightarrow P_4$.(States 4 to 3)

This is in the same form as figure 5.8(a).

For the method to be applicable, the following conditions must be satisfied;

- (1) P_α must be irreducible and primitive.
- (2) Q_3 must be irreducible.
- (3) $R_{31} + R_{32} + R_{34} \neq 0$

We may write equation 5.6 in the following way;

$$P = \begin{bmatrix} A & 0 \\ B & C \end{bmatrix} \quad P^n = \begin{bmatrix} A^n & 0 \\ B_n & C^n \end{bmatrix} \quad (5.7)$$

Where;

$$A = \begin{bmatrix} P_1 & 0 & 0 \\ 0 & P_2 & 0 \\ 0 & 0 & P_4 \end{bmatrix} \quad (5.8)$$

Then we get;

$$\lim_{n \rightarrow \infty} A^n = \begin{bmatrix} \Pi_1 & 0 & 0 \\ 0 & \Pi_2 & 0 \\ 0 & 0 & \Pi_4 \end{bmatrix} = \Pi \quad (5.9)$$

Where;

$$\Pi_{\alpha} = \lim_{n \rightarrow \infty} P_{\alpha}^n > 0, \quad \lim_{n \rightarrow \infty} C^n = 0 \quad (5.10)$$

and,

$$\lim_{n \rightarrow \infty} B_n = V = \begin{bmatrix} V_{31} & V_{32} & V_{34} \end{bmatrix} \quad (5.11)$$

and;

$$V_{3\beta} = (I - Q_3)^{-1} R_{3\beta} \Pi_{\beta} \quad (\beta = 1, 2, 4) \quad (5.12)$$

Then the required transitional probabilities are given by the appropriate elements of V_{31} and V_{32} .

5.6. Outline of computational solution

Sections (5.6.1), (5.6.2) and (5.6.3) deal with techniques for data generation, data acquisition, rainflow cycle counting and PSD computation which are covered in detail in chapter 6 and the following sections represent a summary of that work.

5.6.1. Generation and acquisition of 'real data'

- (1) White noise produced by a signal generator was filtered to produce a desired spectral shape.
- (2) 507904 points along each time signal were sampled at 0.001 samples/sec, giving 635 seconds of continuous data. 4096 stress range intervals were used to discretise each sample point.

5.6.2. Rainflow range count on original signal

- (3) All of these points were then used (approximately 20 per highest frequency) to extract peaks and troughs and hence get the rainflow range density functions. For this purpose, 192 stress intervals were used which is well in excess of the required interval resolution needed to give accurate peak/trough extraction.

5.6.3. Power spectral density computation

- (4) Every 8th point was used to perform Fast Fourier Transforms on the data using equation 2.26; The other seven points were discarded in order to prove that a lower sampling rate is needed for the frequency domain approach than for the time domain. Then $G(f)$ is given by equation 2.27; The above sampling rate gave a Nyquist frequency of 62.5HZ which was well above the highest frequencies of interest (approx 40HZ). 62 averages were carried out on FFTs of 1024 points. Therefore 63488 points were used to perform the final smoothed spectrum instead of the 507904 used for the peak/trough count, although the lengths of signal were the same.
- (5) The zeroth, first, second and fourth moments of the PSD were computed using equation 2.28(b).

5.6.4. A rainflow count from a set of peaks and troughs generated from Kowalewski's joint probability density function

- (6) Using the moments calculated above a set of peaks and troughs was generated from Kowalewski's peak-range joint distribution as detailed in section 4.2.3.

5.6.5. A rainflow range density function produced using the new theoretical solution

- (7) Elemental probabilities for the peak-trough and trough-peak matrices were calculated using equation 4.38.
- (8) For each position of ip and kp , these matrices were modified, a transition matrix calculated and hence, by squaring and resquaring the matrix until transition state 4 was empty values for $Y_1(ip, kp)$, $Y_2(ip, kp)$, and $Y_3(ip, kp)$ were produced.
- (9) Step (8) was repeated for all positions of ip and kp .
- (10) Equation 5.1 was the used to obtain a theoretical rainflow range distribution.

5.7. Results and discussion

Figures 5.9(a) to 5.9(f) show results for various analysis conditions. Two sets of curves are shown. A set representing a ten fold magnification of the densities is plotted in order to highlight the high stress range part of the curves.

The first three plots (5.9(a)-5.9(c)) highlight the effect of different stress range interval widths (Dh). As would be expected, the results for a very large element width (Figure 5.9(a), 16 elements total), are very approximate.

However, when the interval width is decreased, the results improve dramatically. Figures 5.9(b) and 5.9(c) show the results for 32 and 64 elements respectively. Several points can be identified from the plots.

- (i) Acceptable results are obtained using 32 elements and there is no discernible improvement when 64 elements are used.
- (ii) The results using the new theoretical method show very good agreement with both the rainflow range count from a regenerated signal using Kowalewski's peak-trough matrix and a rainflow range count on the original signal. However, agreement with the Kowalewski result is best. This is to be expected because the same matrix is used as a starting point for both the new technique and the Kowalewski peak-trough regeneration. Discrepancies between these curves and the actual rainflow range count of the original signal are due to the approximations in Kowalewski's work. Because the new theoretical method is a quite separate section of work to the actual peak-trough matrix used, whenever an improvement to the Kowalewski theory occurs, there will be an immediate improvement to this new theoretical method.
- (iii) The new theoretical method gives a very smooth prediction, whereas both the count of the actual signal and the regenerated signal are irregular. This is to be expected, because although a long time signal was used to extract peaks and troughs, earlier work shows that even long segments of signals show statistical fluctuations about a mean value (ref.5.20).
- (iv) The curve for the new theoretical method starts at point 2 along the stress axis. This is because a prediction cannot be made for a stress range of 1 interval

because of the nature of the definition, part of which requires that the signal travels between ip and kp . Obviously for a stress range of only 1 interval there would be no transition state (state 4).

Figures 5.9(d)-5.9(f) give results for various other spectral shapes using 32 elements. Again, all the results show good agreement with the actual signal and very good agreement with Kowalewski's regenerated signal.

In conclusion, therefore, it can be stated that a new theoretical solution has been obtained which predicts rainflow ranges from power spectral density data. The results have been shown to be good when compared to the original time signal from which the PSD was produced.

5.8. References

- (5.1) T.Dirlik, Application of computers in Fatigue Analysis, University of Warwick Thesis, Jan 1985.
- (5.2) M.Matsuishi and T.Endo, Fatigue of metals subject to varying stress, paper presented to Japan Soc Mech Engrs (Jukvoka, Japan, 1968)
- (5.3) N.E.Dowling, Fatigue predictions for complicated stress strain histories, J Mater 1, pp 71-87, 1972.
- (5.4) S.D.Downing and D.F.Socie, Simple rainflow counting algorithms, Int J Fatigue 4 No 1, pp 31-40, 1982.
- (5.5) J.R.Rice, First-Occurrence Time of High-Level Crossings in a Continuous Random process, Journal of the Acoustic Society of America, 1965.
- (5.6) J.R.Rice, On the Distribution of Rises and Falls in a Continuous Random Process, Trans ASME, 1965.
- (5.7) P.H.Wirsching et al, Fatigue Under Wide Band Random Loading, J Structural Div, ASCE, July 1980.
- (5.8) P.H.Wirsching et al, Fatigue Under Wide Band Random Stresses Using the Rain flow Method, J Eng Materials and Technology, Vol 99, No 3, ASME, July 1977.
- (5.9) J.M.Tunna, Random load fatigue: Theory and experiment, Proc IMechE, Vol 199, No C3, 1985.
- (5.10) J.M.Tunna, Fatigue life prediction for Gaussian random loads at the design stage, Fatigue Fract. Engng. Mater. Struct., Vol 9 No 3, pp 169-184, 1986.
- (5.11) M.G.Hallam, Fatigue Analysis of Offshore Oil Platforms, SEECO '78' conference "Application of Computers in Fatigue", April 1978.
- (5.12) G.K.Chaudhury and W.D.Dover, Fatigue Analysis of Offshore Platforms Subject to Sea Wave Loading, Int J Fatigue 7 No 1, Jan 1985.
- (5.13) N.Hay and C.J.Dodds, Vehicle Load Histories- The Duality of Vibration and Fatigue Spectra, SAE paper no. 871938, 1987.
- (5.14) I.Rychlik, A new definition of the rainflow cycle counting method, Int J Fatigue, 9 No 2, pp 119-121, April 1987.

- (5.15) I. Rychlik, Rainflow cycle distributions for fatigue life prediction under gaussian load processes, *Fatigue Fract. Engng. Mater. Struct.* Vol 10, No 3, pp 251-260, 1987.
- (5.16) I. Rychlik, Simple approximations of the rain-flow-cycle distribution for discretised random loads, Dept. Math. Stats., Univ. of Lund, May 1987.
- (5.17) I. Rychlik, Rain-flow-cycle distribution for ergodic load processes, Vol 48, No 3, June 1988.
- (5.18) E. Haibach et al, A Standard Random load Sequence of Gaussian Type Recommended for general Applications to Fatigue Testing; Its Mathematical Background and Digital Generation, SEECO 76, 1976.
- (5.19) J. Kowalewski, On the relationship Between Component Life Under Irregularly Fluctuating and Ordered Load sequences. Part 2, DVL Report 249, 1963. MIRA Translation no 60/66.
- (5.20) N.W.M. Bishop and F. Sherratt, Developments in the frequency domain approach to fatigue analysis and testing, submitted for publication, Society of Environmental Engineers, 1988.
- (5.21) D.L. Isaacson and R.W. Madsen, Markov chains theory and applications, John Wiley & Sons, New York, 1976.
- (5.22) D.R. Cox and H.R. Miller, The theory of stochastic processes, Methuen & Co Ltd, London, 1965.

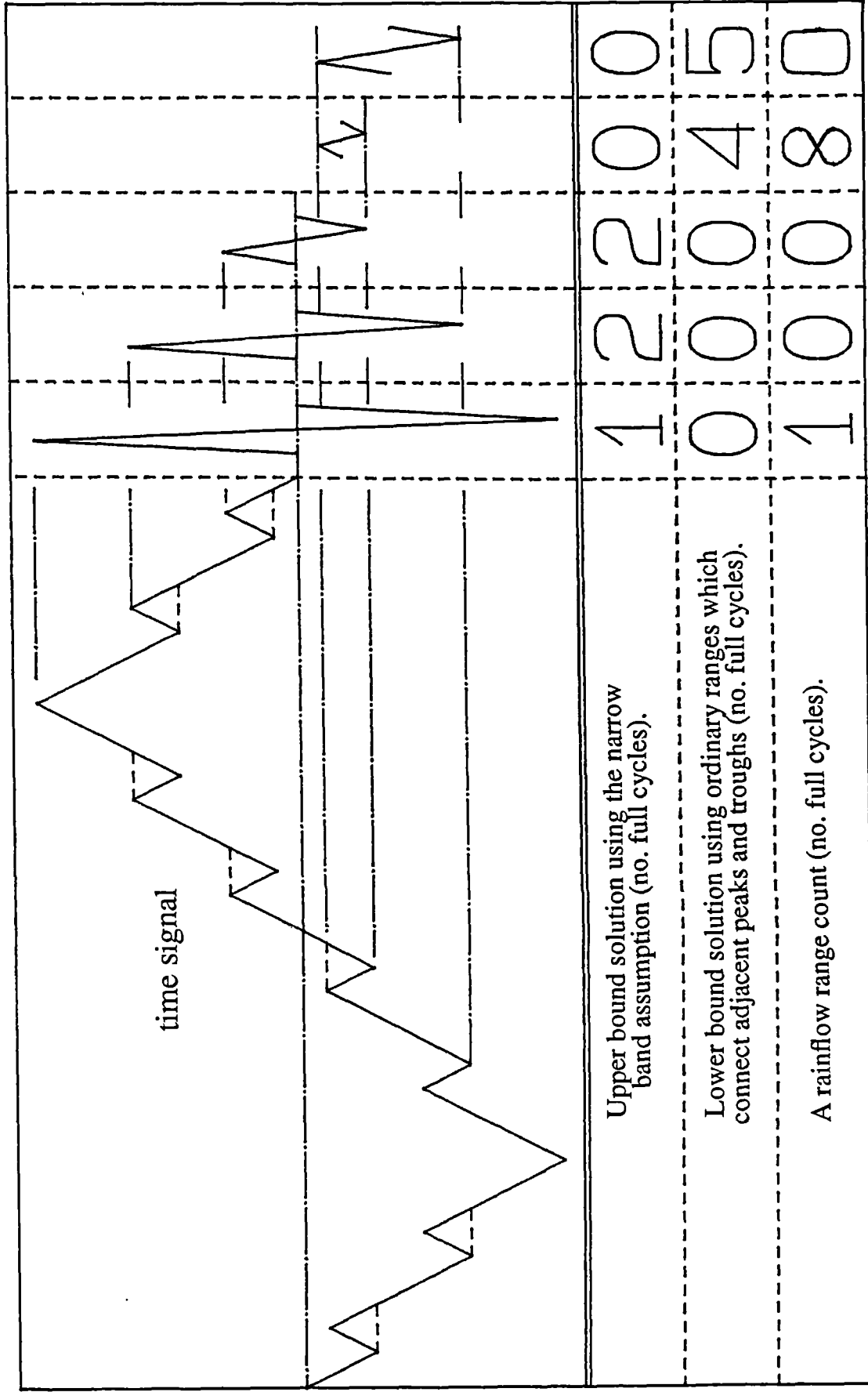


Figure 5.1. The concept of upper and lower bounds on damage compared with that computed using rainfall ranges.

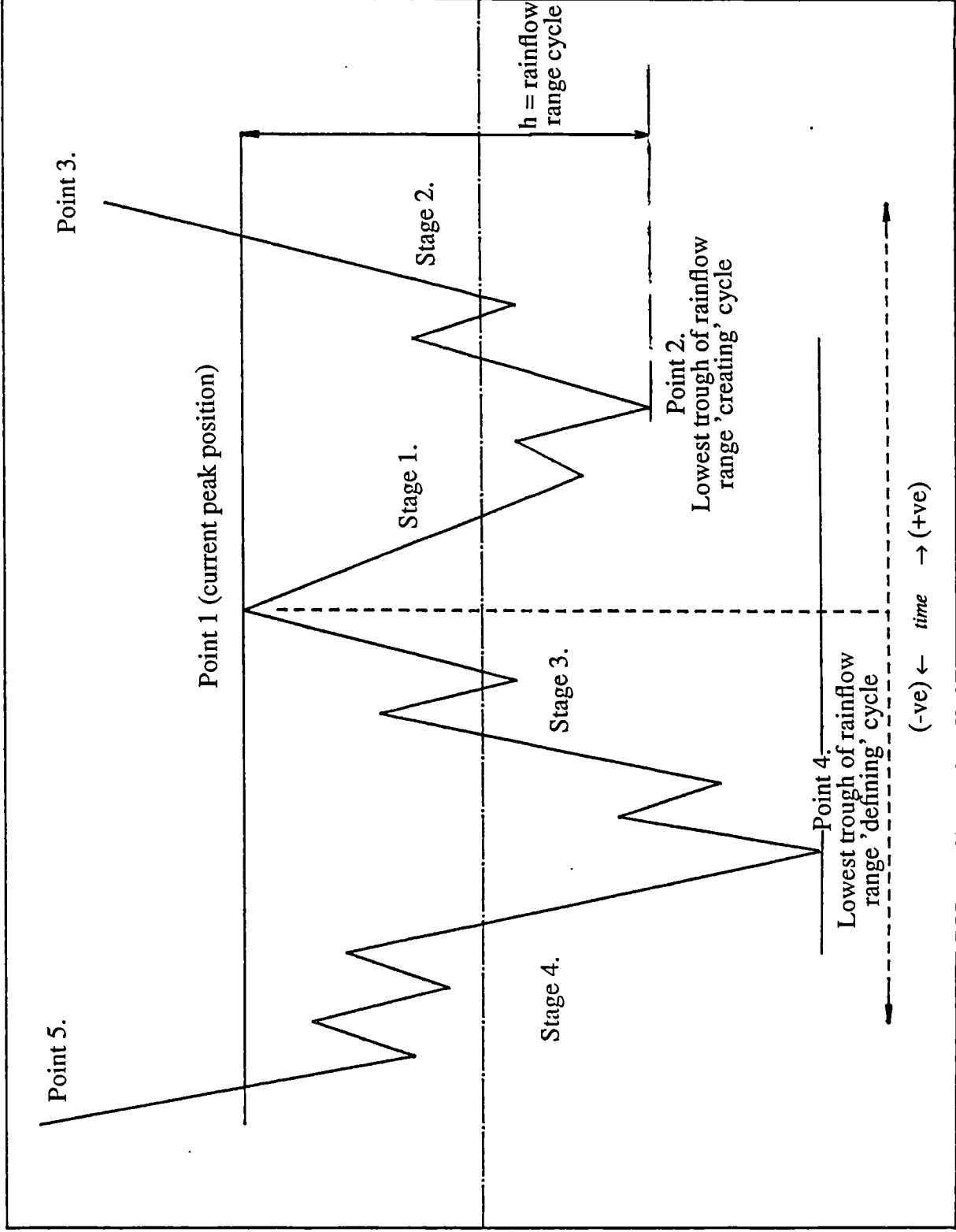


Figure 5.2. Rychlik's definition of a rainfall range cycle.

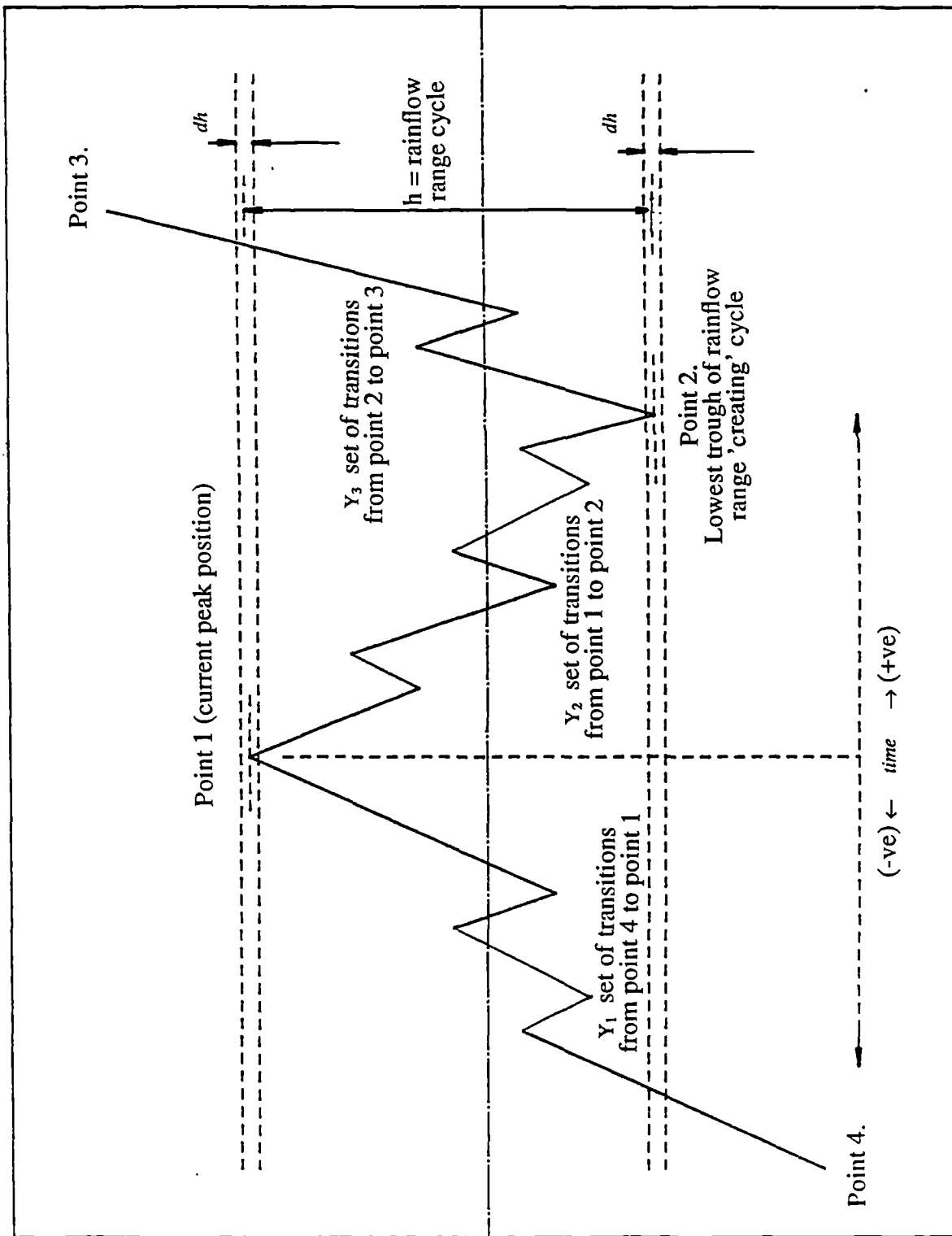


Figure 5.3. Discrete form of the authors definition of a rainfall range cycle.

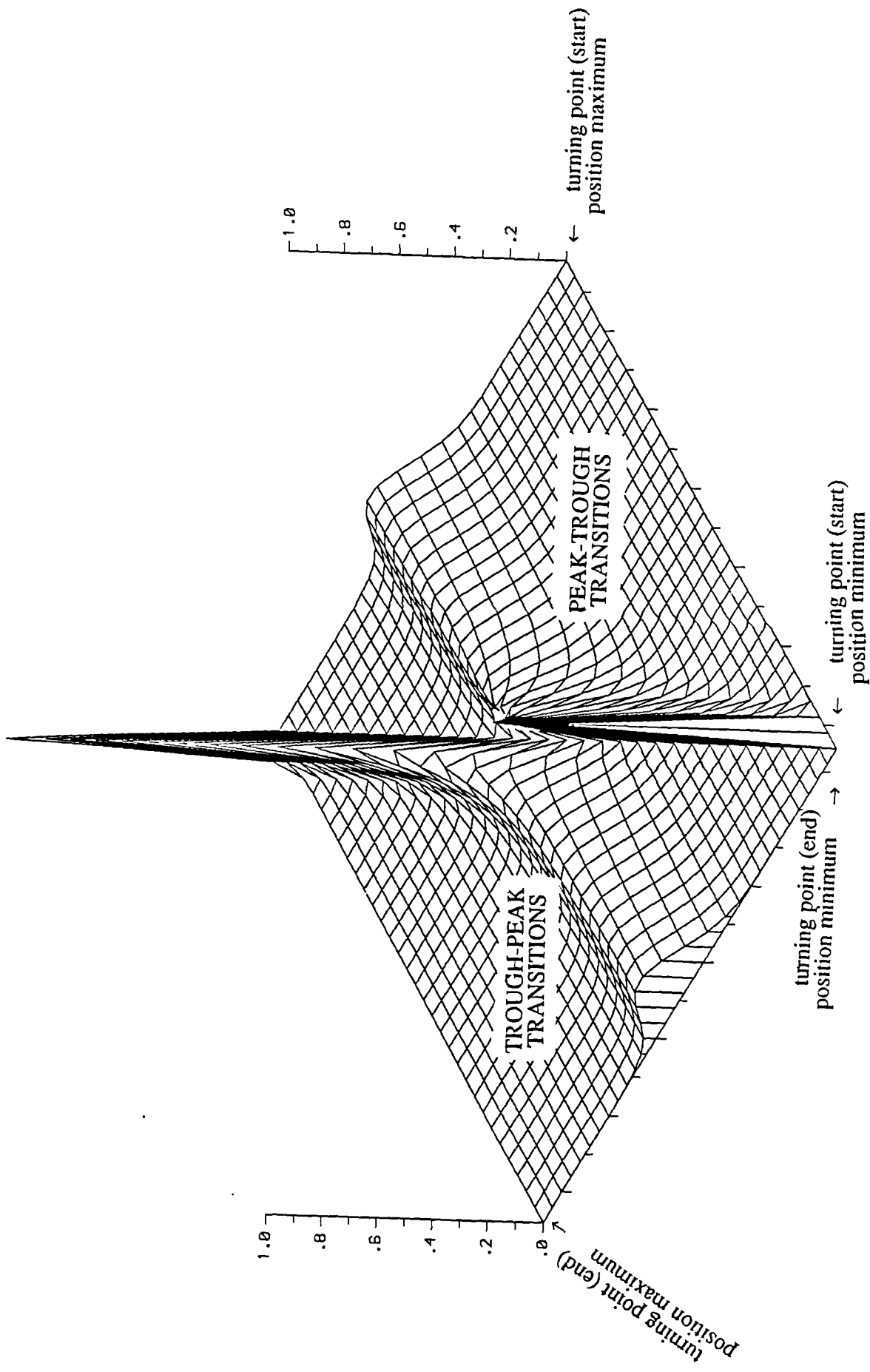


Figure 5.4(b). Kowalewski's expression for the dependence between adjacent extremes after both the peak-trough and the trough-peak parts have been normalised to 1.

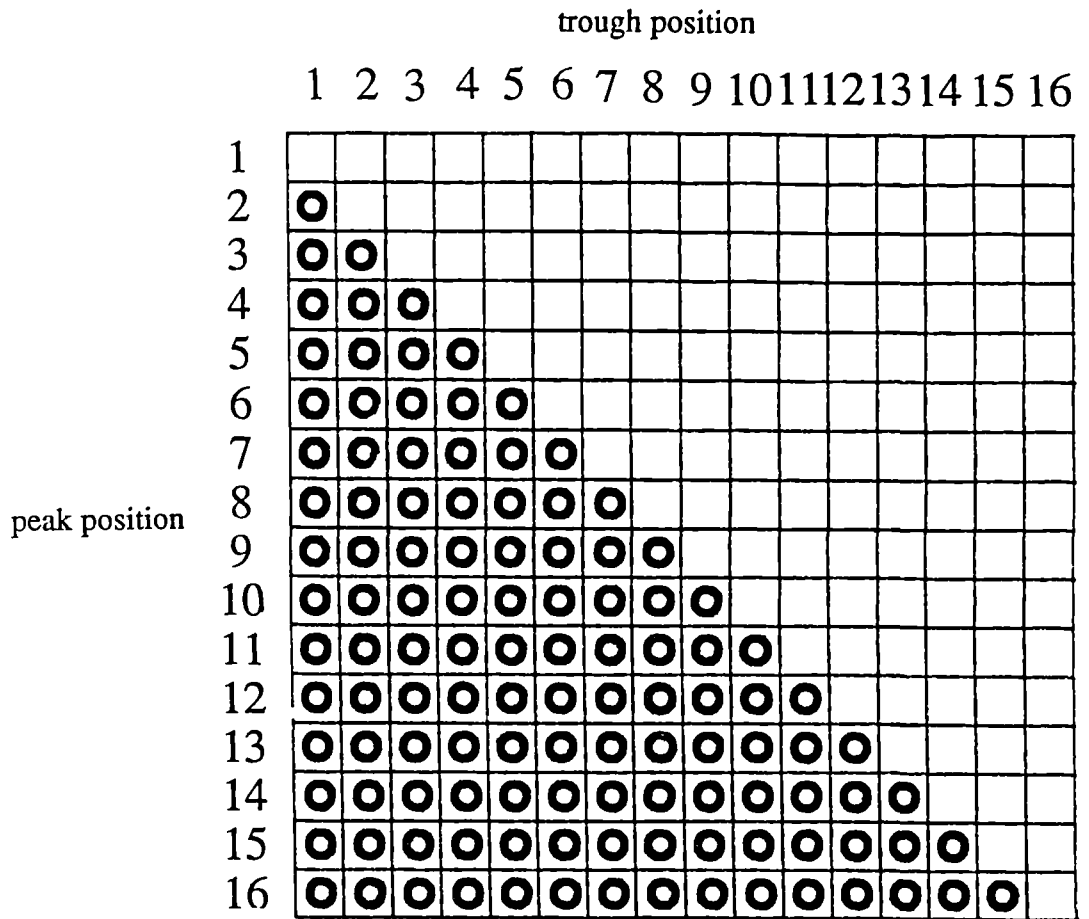


Figure 5.5(a). The peak-trough part of kowalewski's expression (equation 2) for a 16 by 16 element matrix.

○ represents full matrix element

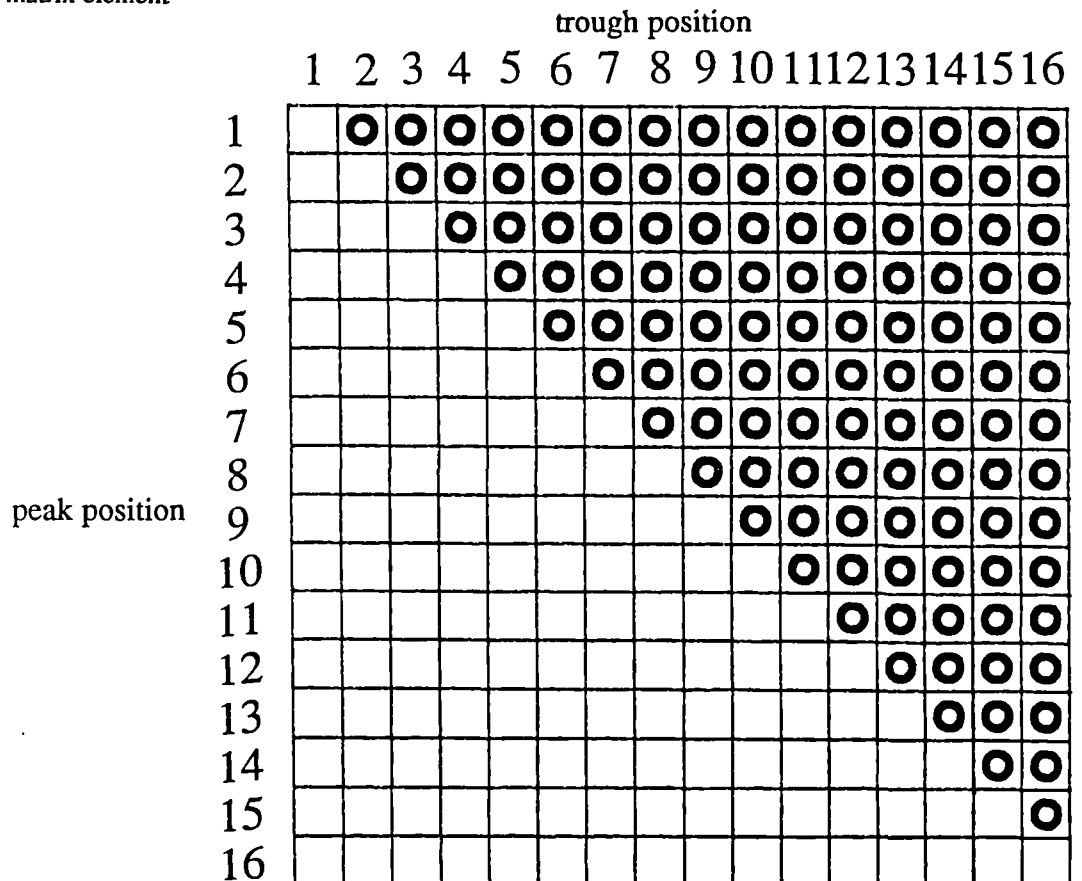


Figure 5.5(b). The trough-peak part of kowalewski's expression (equation 2) for a 16 by 16 element matrix.

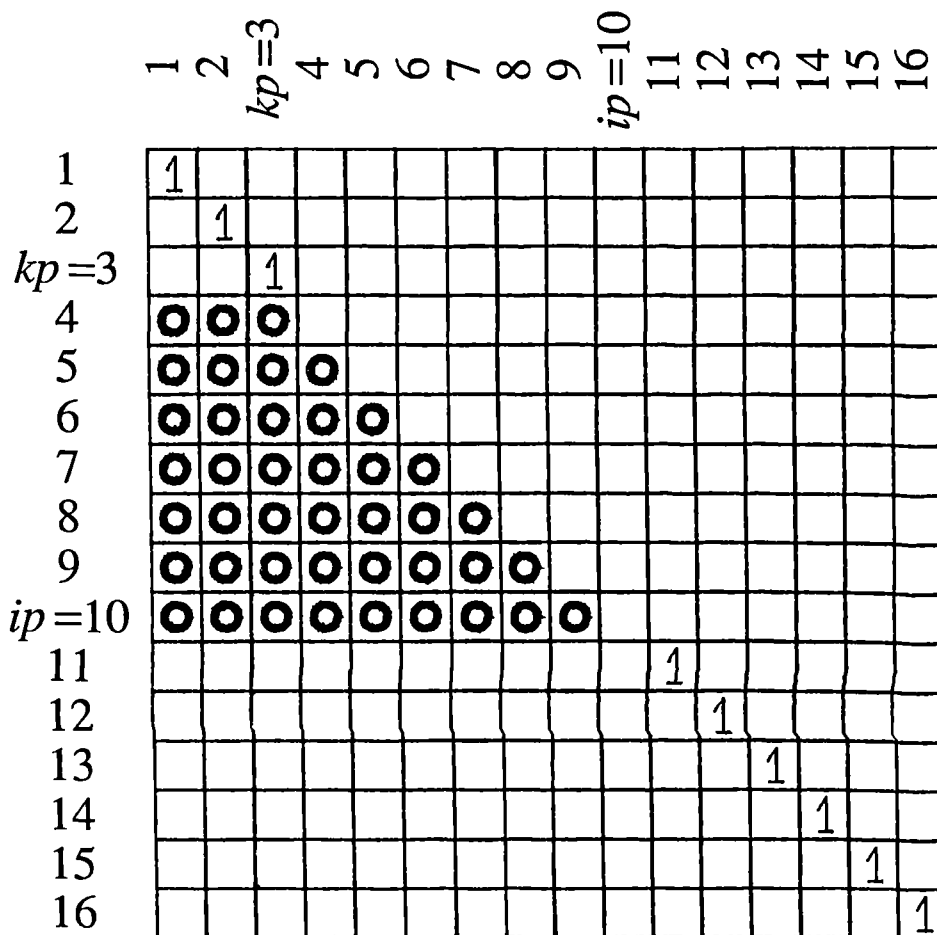


Figure 5.7(a). Transition matrix representing peak-trough (1 step) movements for the particular configuration of $ip=10$ and $kp=3$.

○ represents full matrix element

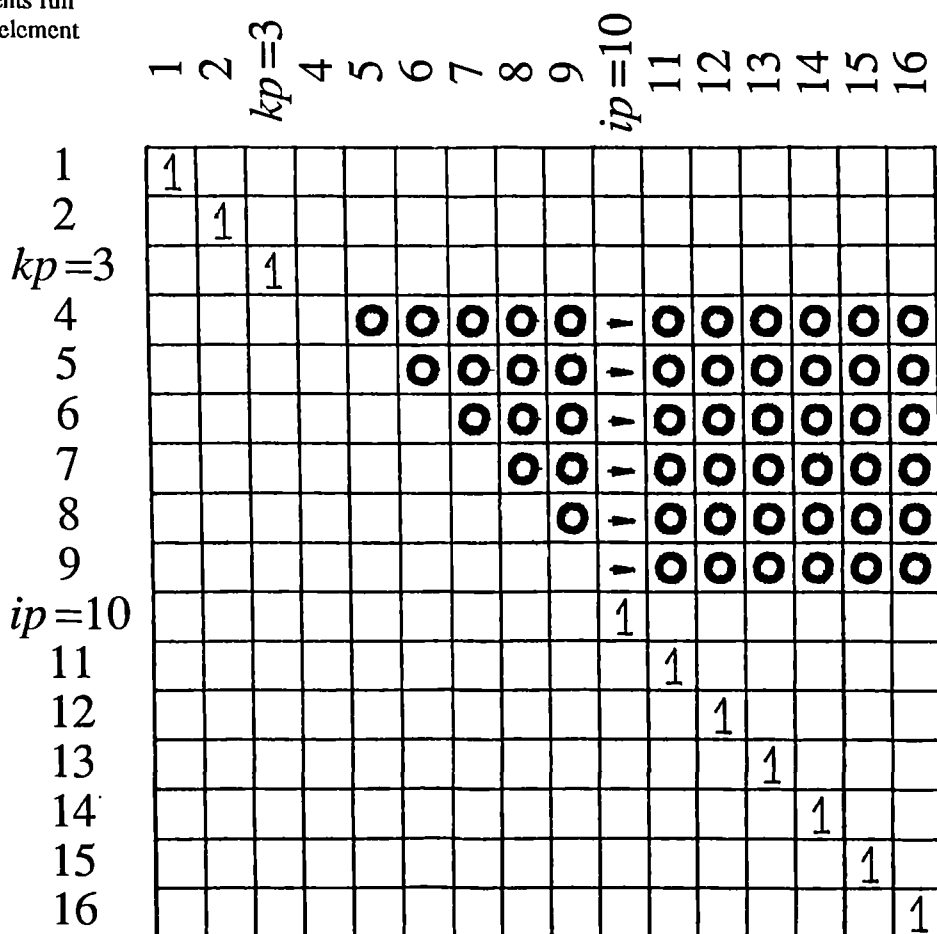


Figure 5.7(b). Transition matrix representing trough-peak (1 step) movements for the particular configuration of $ip=10$ and $kp=3$.

	state 2 ₁	state 2 ₂	state 1(k _p =3)	state 4 ₁	state 4 ₂	state 4 ₃	state 4 ₄	state 4 ₅	state 4 ₆	state 5(ip=10)	state 3 ₁	state 3 ₂	state 3 ₃	state 3 ₄	state 3 ₅	state 3 ₆
state 2 ₁	1															
state 2 ₂		1														
state 1(k _p =3)			1													
state 4 ₁	○	○	○													
state 4 ₂	○	○	○		○	○	○	○	○	↑	○	○	○	○	○	○
state 4 ₃	○	○	○		○	○	○	○	○	↑	○	○	○	○	○	○
state 4 ₄	○	○	○		○	○	○	○	○	↑	○	○	○	○	○	○
state 4 ₅	○	○	○		○	○	○	○	○	↑	○	○	○	○	○	○
state 4 ₆	○	○	○		○	○	○	○	○	↑	○	○	○	○	○	○
state 5(ip=10)	○	○	○		○	○	○	○	○	↑	○	○	○	○	○	○
state 3 ₁											1					
state 3 ₂												1				
state 3 ₃													1			
state 3 ₄														1		
state 3 ₅															1	
state 3 ₆																1

Figure 5.8(a). Transition matrix representing peak-trough-peak (2 step) movements for the particular configuration of $ip=10$ and $kp=3$.

○ represents full matrix element

	state 2	state 1	state 4 ₂	state 4 ₃	state 4 ₄	state 4 ₅	state 4 ₆	state 5
state 2	1							
state 1		1						
state 4 ₂	○	○	○	○	○	○	○	
state 4 ₃	○	○	○	○	○	○	○	
state 4 ₄	○	○	○	○	○	○	○	
state 4 ₅	○	○	○	○	○	○	○	
state 4 ₆	○	○	○	○	○	○	○	
state 5	○	○	○	○	○	○	○	

Figure 5.8(b). Condensed transition matrix representing peak-trough-peak (2 step) movements for the particular configuration of $ip=10$ and $kp=3$.

	state 2	state 1	state 4 ₂	state 4 ₃	state 4 ₄	state 4 ₅	state 4 ₆	state 5
state 2	1							
state 1		1						
state 4 ₂	○	○						
state 4 ₃	○	○						
state 4 ₄	○	○						
state 4 ₅	○	○						
state 4 ₆	○	○						
state 5	○	○						

Figure 5.8(c). Condensed transition matrix after it has been squared enough times to ensure state 4 is empty (2^n steps, where n is the number of times the matrix is squared).

Figure 5.9(a). A comparison of the rainflow range distributions obtained (data set 2 and 16 element matrix) using equation 1 (new theoretical solution) with a distribution obtained from a peak-trough count of, (1) the original signal, and (2) a signal regenerated from a Kowalewski peak-trough matrix.

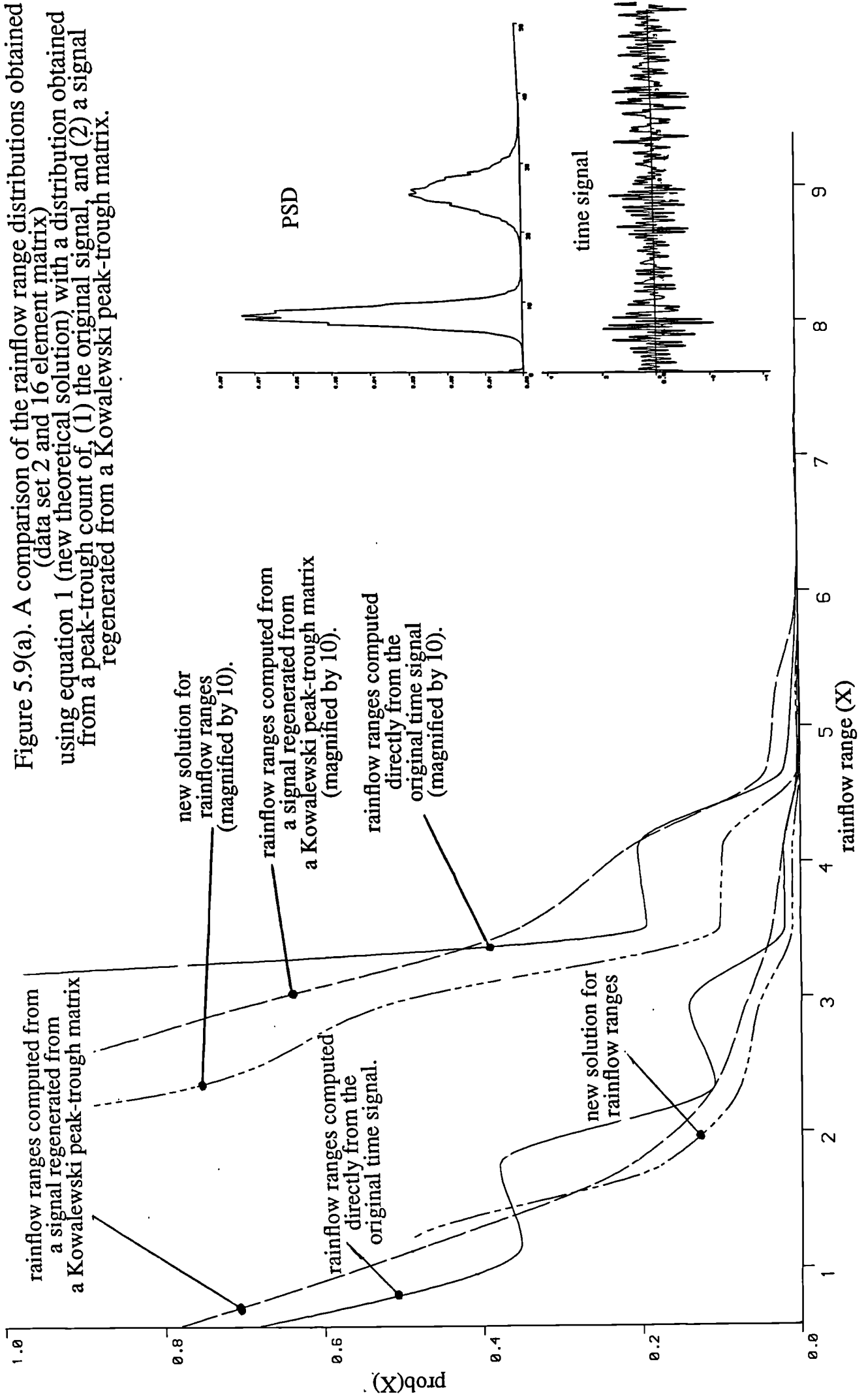


Figure 5.9(b). A comparison of the rainflow range distributions obtained using equation 1 (new theoretical solution) with a distribution obtained from a peak-trough count of, (1) the original signal, and (2) a signal regenerated from a Kowalewski peak-trough matrix.

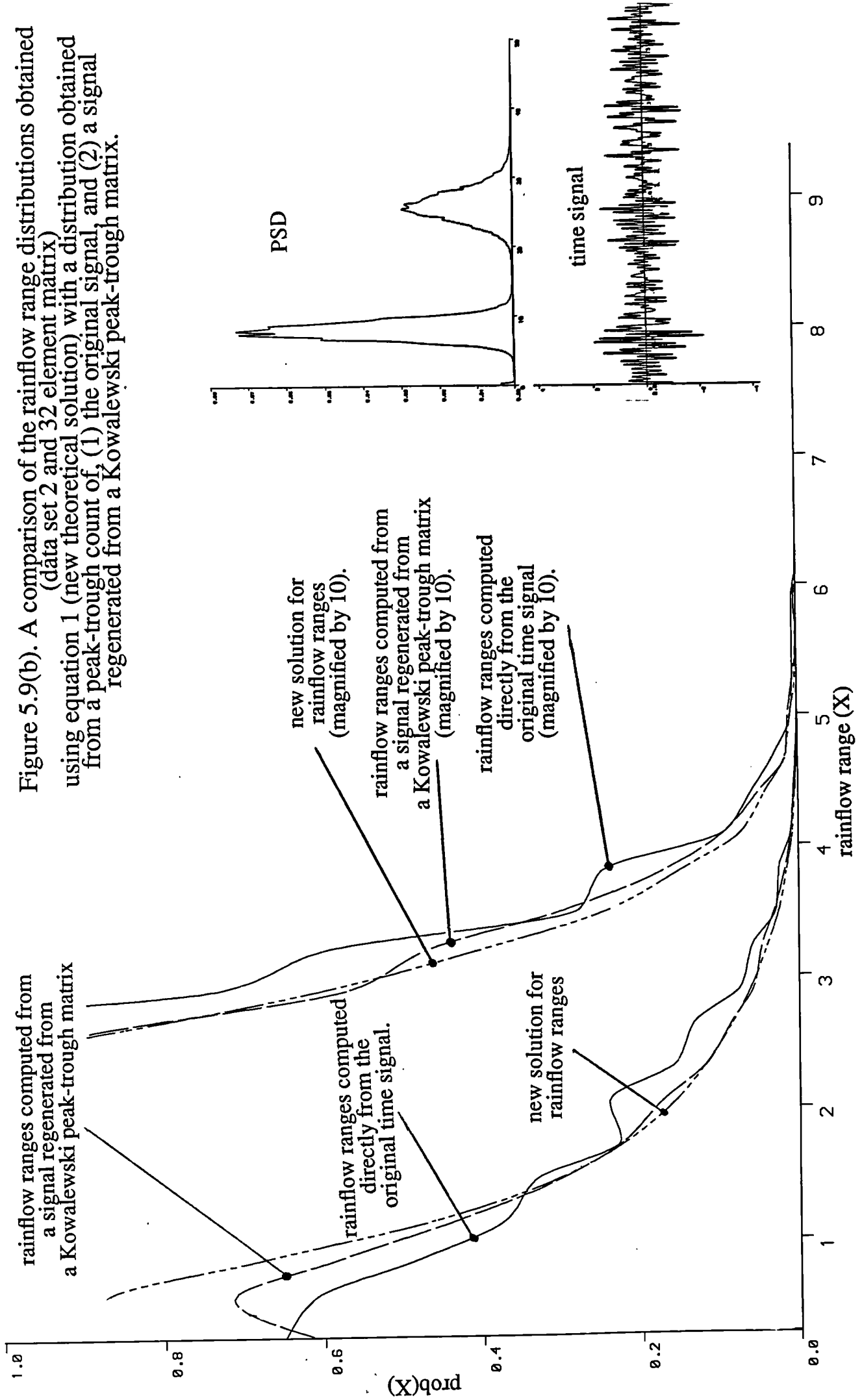


Figure 5.9(c). A comparison of the rainfall range distributions obtained using equation 1 (new theoretical solution) with a distribution obtained from a peak-trough count of, (1) the original signal, and (2) a signal regenerated from a Kowalewski peak-trough matrix.

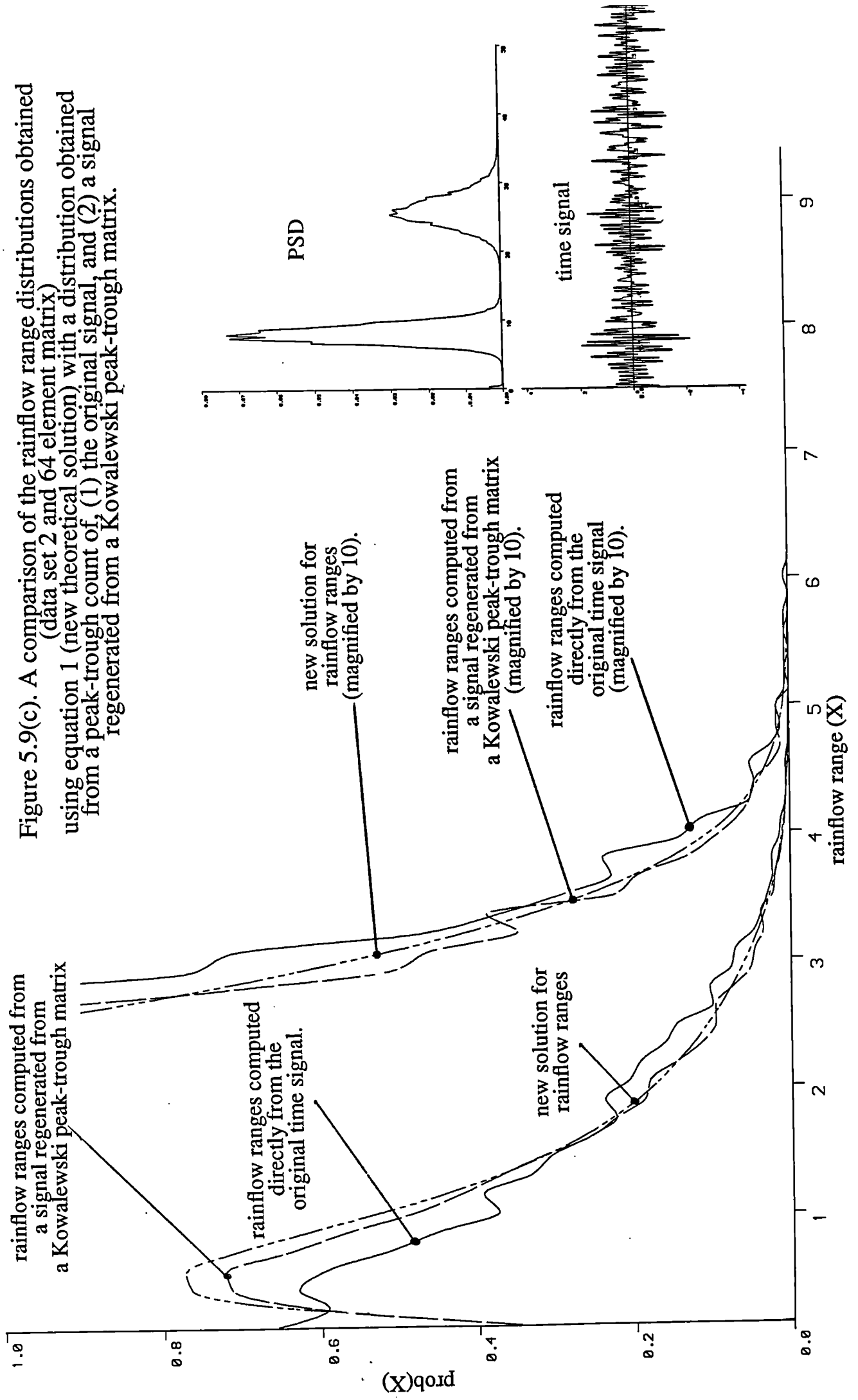


Figure 5.9(d). A comparison of the rainflow range distributions obtained (data set 1 and 32 element matrix) using equation 1 (new theoretical solution) with a distribution obtained from a peak-trough count of, (1) the original signal, and (2) a signal regenerated from a Kowalewski peak-trough matrix.

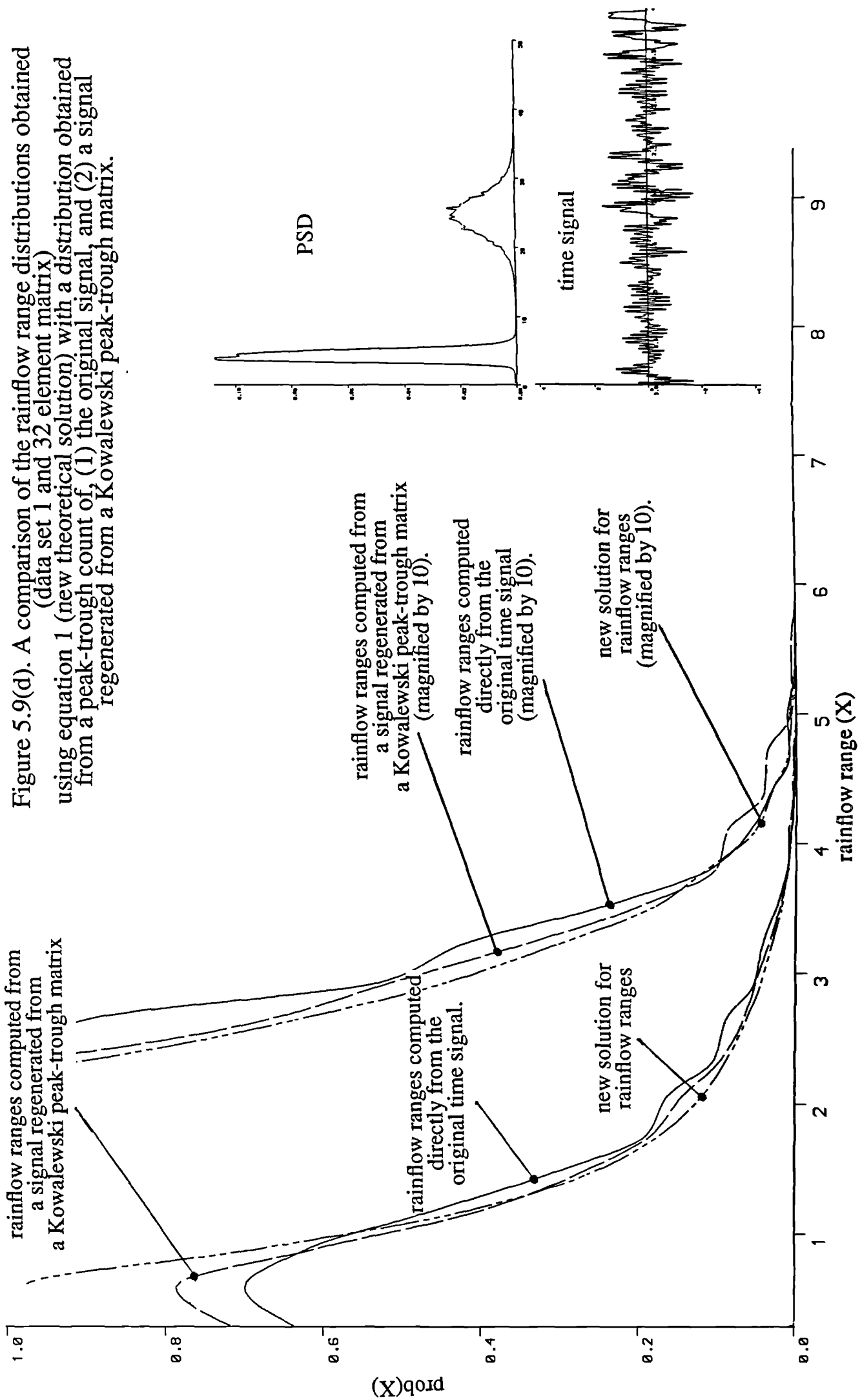


Figure 5.9(e). A comparison of the rainflow range distributions obtained using equation 1 (new theoretical solution) with a distribution obtained from a peak-trough count of, (1) the original signal, and (2) a signal regenerated from a Kowalewski peak-trough matrix.

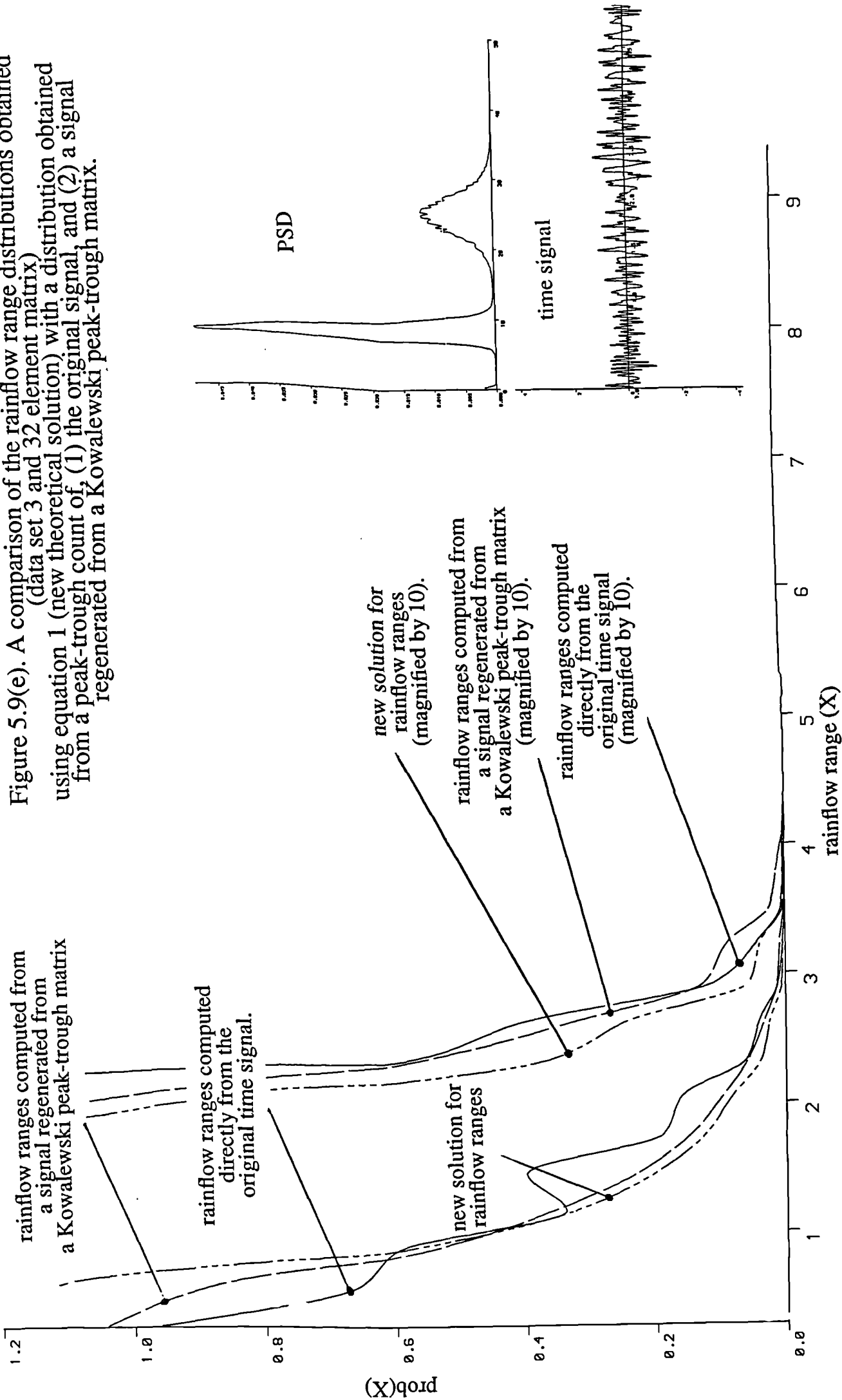
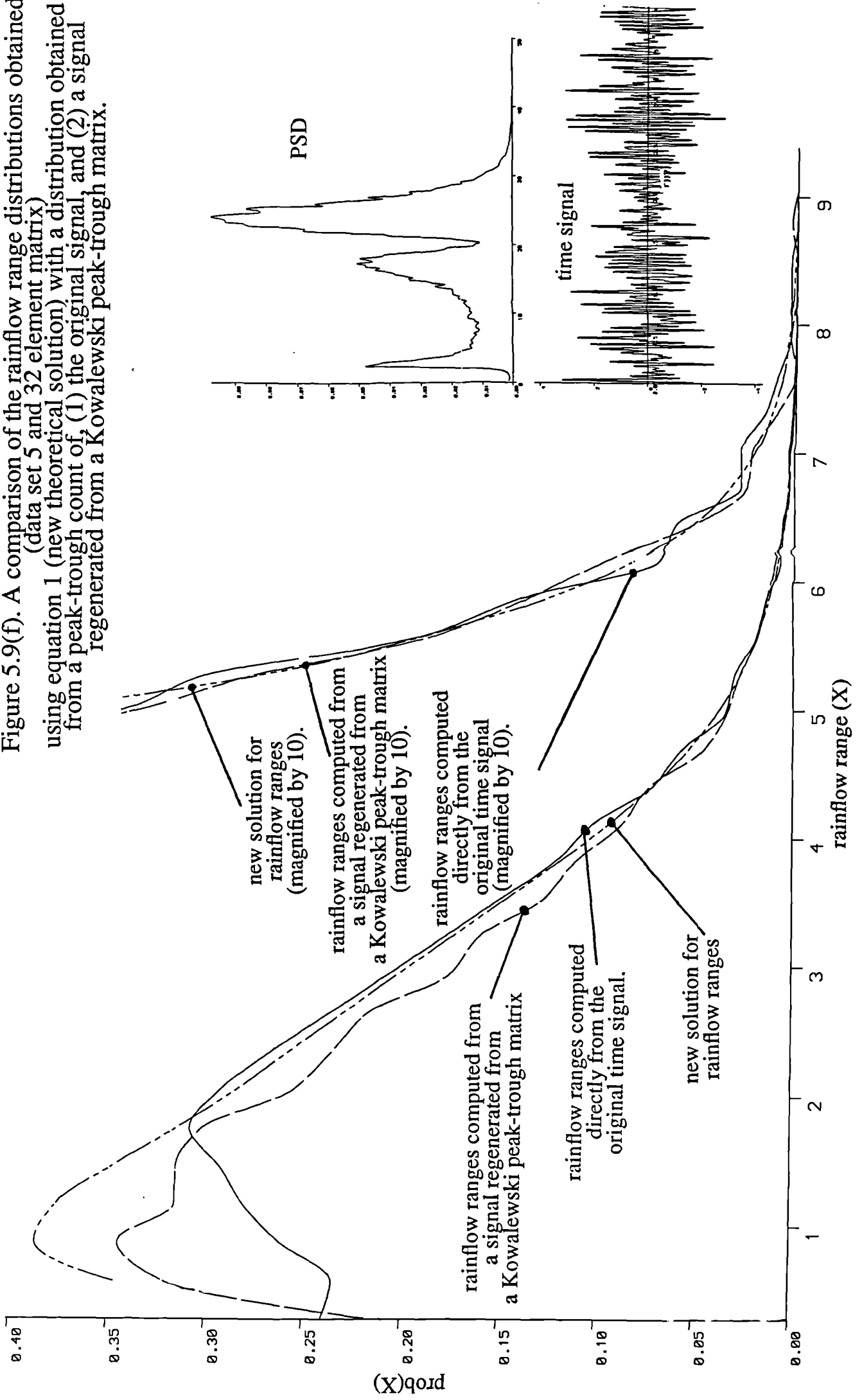


Figure 5.9(f). A comparison of the rainfall range distributions obtained (data set 5 and 32 element matrix) using equation 1 (new theoretical solution) with a distribution obtained from a peak-trough count of, (1) the original signal, and (2) a signal regenerated from a Kowalewski peak-trough matrix.



6. Developments in the frequency domain approach to fatigue analysis and testing

6.1. Introduction

Chapters 3 and 4 presented results which were produced using Dirlik's range distributions and peak-trough load history regeneration techniques. In each case the results were compared with data from other studies or with theoretical predictions, but no comparisons with 'real' data were given. One aim of this chapter is to check the results against such data. That is, data that originates from some physical process that has characteristics which might be expected in some typical engineering situations.

The second and more important objective of the work in this chapter was to investigate the effect of finite sample length on various statistical parameters, including fatigue damage. The results from such an investigation are of considerable interest to practicing engineers. Earlier chapters showed that the frequency domain approach to fatigue analysis and testing was a viable technique and data presented in this chapter will confirm this finding with comparisons on actual time recordings of physical processes. It will also investigate the relative merits of time and frequency domain approaches as well as highlighting some interesting and unexpected facts about the errors involved with predicting fatigue damage from short (or even not so short) lengths of signal, either in the time or frequency domain.

When time domain techniques are mentioned they refer to fatigue analysis predictions from data which can only represent one example of any expected service history. In other words, fatigue damage estimates on finite lengths of signal taken from a stationary time signal will show scatter. Similarly, fatigue damage estimates on PSD's taken from finite lengths of signal will also exhibit such scatter. A measured loading history may be truly representative of the expected service loading. It will not, however, generally give the expected value of damage. Measurements of damage or other statistical variables computed from the actual loading conditions will, in general, have a variance about its expected value and this chapter will investigate this phenomena, with particular reference to;

- (a) Variance of fatigue predictions using a rainflow count on a time sample of duration $L_s = (\Delta_n) * \delta_t$ where Δ_n is the number of points in the series of peaks

and troughs, and δ_t is the time between successive samples.

- (b) Variance of fatigue predictions using rainflow ranges produced from a PSD of the same time sample of duration L_s
- (c) Variance of fatigue predictions using a rainflow count on a sequence of peaks and troughs generated using Kowalewski's joint distribution, from the same PSD as in (b)
- (d) As (c) but using a modified solution for the joint distribution between peaks and troughs developed by the author.
- (e) Repetitions of (a) to (d) for ordinary ranges (segments joining successive peaks and troughs).

As well as determining whether to use time or frequency domain techniques, the work presented in this chapter is relevant to the problem of reliability. In the offshore industry, a considerable amount of work is being done on reliability analysis of offshore platforms (refs.6.1-6.5). Similar discussions have taken place in the automotive industry, concentrating more on the errors involved with the time domain data acquisition process (refs.6.6-6.10).

A Brüel and Kjaer random signal generator was used in conjunction with various analogue filtering devices for generating the data to be used for this investigation. This is described in section 6.2. A signal generator that produced shot noise using the arrival of electrons at the electrode of a valve was used in preference to a pseudo-random binary signal. It was thought that the signals derived from shot noise were less likely to be affected by mathematical bias of any kind which might be magnified because of the short lengths of signal being used for computation of the various range probability density functions.

Section 6.3 deals with the process of data acquisition using the ASYST data acquisition package. This was used to digitise the analogue signals produced by the Brüel and Kjaer random signal generator.

The validity of the data needed to be checked and this is covered in section 6.4. Various statistical tests such as the 'Goodness of Fit' normality test were used to establish that the signals being used were stationary and Gaussian. Other tests for phenomena

like periodicities were not needed because such statistics would show up in the later frequency domain analysis.

In section 6.5 cycle counting from time signals is described. In order to decompose the time signal into a set of peaks and troughs which is needed for cycle counting, a 2nd quantisation process was performed in addition to the one necessary for digitisation and the errors involved with this are discussed.

The extensive area of frequency domain analysis is briefly covered in section 6.6, in order to carry out a limited discussion on the merits of windowing, from a range distribution point of view.

Section 6.7 presents the computational procedure which was used to check the frequency domain approach against real data. Sections 6.8 details the work on the variance of fatigue predictions from limited sample sizes and 6.9 gives the conclusions.

6.2. Generating realistic data

A Brüel and Kjaer random signal generator was used to produce a broad band random signal with characteristics as shown in figure 6.1. Three separate signals were filtered using both low and high pass filters. This involved the use of three low pass and three high pass filters, all of which had variable cut off frequencies. The characteristics of one of the low pass filters is shown in figure 6.2. These signals were then combined using a signal adder device which ensured that the signals were correctly combined. Each signal loop had separate amplification control which was used to adjust the relative magnitudes of certain frequencies being generated. It was therefore possible to generate signals with various spectral shapes, as shown in figures 6.3(a) to 6.3(e).

6.3. Data acquisition

Large amounts of data were required for the investigation which was to be carried out. Five sets of data were generated with a maximum anticipated frequency of approximately 40Hz. The considerations which were imposed on this section of work were that the sampling rate needed to be fast enough to carry out an accurate peak-trough detection process (see section 6.5), and be well in excess of the highest frequency of interest. For a Nyquist frequency of 62.5Hz a sampling interval of 0.008 seconds is required. However

this is insufficient to give 25 samples per highest frequency which is required in order to ensure that the errors in the peak-trough detection process are reduced to a negligible level. At 2 samples per highest frequency, an upper bound on the error is given by $[1 - \cos(\frac{\pi}{2})] * 100 = 100\%$. At 4 samples per highest frequency we get an upper bound on the error of 29%, and for 10 the error is 4.9%, for 20 the error is 1.3% and for 25 samples per highest frequency the upper bound on the error is 0.8%. Therefore to get this upper bound on the error below 1%, we needed 25 samples per highest frequency, for which a sampling interval of 0.001 seconds was used. The length of the data sets was chosen as 1024000 points which required a storage space of 2 megabytes ASYST binary or 4 megabytes ASCII text.

The 64K memory space restriction imposed on desk top acquisition to RAM tasks meant that acquisition direct to hard disk was required. The performance characteristics of the ASYST 2.0 package more than satisfied the requirement listed above, with a maximum sampling rate of 50000 samples per second and a maximum continuous acquisition data set size restricted only by the disk space (20 megabytes in this case).

4096 intervals are used by the ASYST data acquisition package for the quantisation process. Signal values are recorded as integer values between 1 and 4096. All future analysis such as peak-trough detection and range density function computation is most easily carried out directly on these integer values. These results can be converted back into units of engineering significance after such analysis has been carried out. This number of levels is well in excess of the required number required for reasonable accuracy. A second quantisation process is described in section 6.5 where these 4096 levels are reduced to as low as 32 intervals. Errors involved with this process will be discussed in that section.

6.4. Data qualification

A maximum range of 10 volts was used for the quantisation process and the maximum and minimum values of every element within each set of integer data values was obtained to ensure that the range distributions were not distorted by clipping of the generated process.

Tests for normality and stationarity were carried out on the data, using the ‘Goodness of Fit’ and ‘Reverse Arrangements’ tests (1986,ref.6.11). In order to carry out the ‘goodness of fit’ test every 32nd data point was collected into 16 groups of 2000 points, thereby fully spanning the 1024000 points contained within each data set. For each of the 16 groups within each data set the mean, variance, rms, minimum, maximum and Chi-Squared value for the discrepancy between expected probability and actual probability of achieving a normal distribution were calculated. The Chi-Squared value is computed using the following expression;

$$\chi^2 = \sum_{i=1}^K \frac{(f_i - F_i)^2}{F_i} \quad (6.1)$$

Where; f_i and F_i represent the expected and observed frequency of observations in the K_{th} class interval respectively. The number of class intervals, K , was chosen as 43, giving a value of 40 for n the number of degrees of freedom.

The Reverse Arrangement test was applied to the means and rms’s of the 16 groups for each data set in order to test for stationarity. This involved considering the sequence of either mean values or rms’s as x_i for $i=1,16$ and counting the number of times $x_i < x_j$ for $i < j$.

The results for data sets 1-5 are given in tables 6.1-6.5. From these tables we can derive values for the average Chi-Square value and for the reverse arrangement test applied to the means and variances;

	average X^2	reverse arrangement test on means	reverse arrangement test on rms
data set 1	39.77	51	77
data set 2	40.49	61	77
data set 3	45.40	62	76
data set 4	39.34	52	53
data set 5	38.55	49	52

For a 0.05 level of significance we get a value of 55.75 for $\chi_{40,0.05}^2$ from reference 6.11, page 525,table A.3. Since all the average values of X^2 are lower and only 4 out of the 80

group values of the Chi-Square statistic are larger, it is reasonable to assume normality of the data.

Similarly, for a 0.05 level of significance we get an allowable range of 41 to 78 for the Reverse Arrangement test, from reference 6.11 page 533, table A.6. All five data sets satisfy this test. Therefore stationarity of the data can be assumed

6.5. Cycle counting from time signals, with particular reference to short lengths of signal

If one wishes to obtain cycle counts from data acquired using packages such as ASYST then three stages of operations are required;

- (1) A reduction of the number of intervals used for the first quantisation process from 4096 to as low as 32 levels.
- (2) A peak-trough detection operation resulting in the extraction of only those elements from the original time series which represent alternating peaks and troughs.
- (3) Application of the relevant cycle counting routine to determine either rainflow or ordinary ranges. When calculating rainflow ranges from short lengths of signal some manipulation of the tails of the peak-trough series is necessary, followed by a reordering of the series in order to apply the rainflow range cycle counting process described in section 2.2.

As mentioned in section 6.3, errors are introduced into the final fatigue damage results because of the quantisation process. However, because 4096 intervals are used, errors in the data acquisition process can be ignored. But a second quantisation process is required before the peak-trough detection process can be applied. Typically, 32, 64, 101, and 192 elements were used for this. Figure 6.4 highlights this problem. This shows that any range which is counted at a later stage in the analysis, actually involves two quantisations, one for the peak, and one for the trough. This means that counted ranges of predicted magnitude X , are actually of some magnitude between $X-DX$ and $X+DX$. It is the moments of such rainflow range distributions which are important from a fatigue point of view. Therefore, errors will result because the ranges between $X-DX$ and X

will be moved to X and so will be given larger weightings than they should actually have. Similarly, the ranges between X and $X+DX$ will be given smaller weightings than they should have.

We are actually interested in the following error;

$$\delta_{err} = (1 - \frac{\Psi_{true}}{\Psi_{\approx}}) \times 100 \quad (6.2)$$

where Ψ_{true} is the result which results when an infinitely small interval width DX is used and Ψ_{\approx} is the result which is produced when the ranges are lumped at the mid interval position. Therefore a negative value means that the damage is underestimated and a positive value that the damage is overestimated.

By using a simple model, the behaviour of δ_{err} can be investigated. The range distribution at a particular range value X is assumed to be linear, with a slope equal to $\frac{A}{D}$. A represents the value of the intersection point of the vertical axis and D the equivalent value for the horizontal axis. Nonlinear effects are not considered because for the important high ranges the linear assumption is reasonable. In addition to A , D , X and DX , δ_{err} is affected by b , the slope of the S-N curve.

The following expressions can be derived

$$\Psi_{\approx} = \left[\left(X + \frac{DX}{2} \right)^b \right] \left[\frac{A - A \left(X + \frac{DX}{2} \right)}{D} \right] DX \quad (6.3)$$

$$\begin{aligned} \Psi_{true} &= \int_X^{X+DX} X^b DX \left(A \left(1 - \frac{X}{D} \right) \right) \quad (6.4) \\ &= \frac{A}{D(b+2)} (X^{b+2} - (X+DX)^{b+2}) + \frac{A}{b+1} ((X+DX)^{b+1} - X^{b+1}) \end{aligned}$$

Table 6.6 gives results for which the values of A and D are meaningful for sea state 1 (figure 4.6). These results are plotted in figure 6.5. The behaviour of δ_{err} appears to be quite complicated. Several important points can be noticed. The top plot shows the variation or δ_{err} with increasing interval width DX at a relatively low range value. As would be expected, the error increases as the interval width increases. However, the third plot down shows that the sign of the error is dependent on the particular range value being considered. This is demonstrated in the bottom plot where we can observe that no error

occurs at approximately 250 MPa. Finally, note from the second plot down, that a maximum point occurs in the error when plotted against b the slope of the S-N curve. It would be expected that the position of this maximum would be dependent on the slope of the range distribution, that is, A and D . In conclusion it can be seen that none of the conditions considered give unreasonable accuracy, and so this topic will not be considered further.

Once the peak-trough detection process has been carried out, a time series of alternating maxima occurs to which the application of a rainflow count does not produce a complete distribution because the 'open ended' tails of the peak-trough series would almost certainly result in incomplete closure of all the relevant cycles. Therefore, the last remaining, largest and most important cycles would remain uncounted. The method used by the author for solving this problem was to consider all peak-trough series as falling into one of eight categories which are shown in figure 6.6. This figure also shows, for each case, the most justifiable methods of joining the end of the signal with the beginning. The series thus created could then be reordered to put the signal maximum at the beginning and therefore, also at the end of each signal. A conventional count can then be applied.

6.6. Frequency domain analysis of time signals

The methods described in section 2.4 were used to compute estimates of the PSD. FFT array sizes of between 512 and 4096 were used depending on the available data set size and the number of averages which were used.

Some work was done on the use of windows for improving the range density function estimates. No discernible improvement was observed. This might have been expected since the data being analysed tended to have slowly varying PSD functions with no sharp spikes to which some form of windowing might be applied for improved detection. However, even in such a situation, it is doubtful whether windowing could ever produce improved range density function predictions, since according to the modelling of Dirlík (ref.6.12) it is the moments of the PSD which completely define these distributions. Because windowing results in bias of the spectral estimates with decreasing scatter, the combined effect on the moments would almost certainly be detrimental.

6.7. Computational procedure for estimating the fatigue damage from both time and frequency domain information

The following sections describe the computational procedure used for this investigation;

- (1) White noise produced by the Brüel and Kjaer signal generator was filtered using various filters to produce any desired spectral shape (see figures 6.3(a), 6.3(b), 6.3(c), 6.3(d) and 6.3(e)).
- (2) 1024000 points along each time signal were acquired with a sampling interval of 0.001 seconds, giving 1024 seconds of continuous data. 4096 stress range intervals were used to discretise each sample point. Typical 4 seconds blocks of data are also shown in figures 6.3(a), 6.3(b), 6.3(c), 6.3(d) and 6.3(e).
- (3) All of these points were then used (approximately 20 per highest frequency) to extract peaks and troughs and hence, using the methods described in section 6.5 for manipulating the signal, get the rainflow and ordinary range density functions. For this purpose, 192 stress intervals were used which is well in excess of the required interval resolution needed to give accurate peak/trough extraction.
- (4) Every 8th point was used to perform Fast Fourier Transforms on the data using equation 2.26. This gave a Nyquist frequency of 62.5HZ which was well above the highest frequencies of interest (approx 40HZ). 250 averages were carried out on FFTs of 512 points. Therefore 128000 points were used to perform the final smoothed spectrum (using equation 2.5) instead of the 1024000 used for the peak/trough count, although the lengths of signal were the same.
- (5) The zeroth, first, second and forth moments of the PSD were computed using equation 2.28(b), and then used with equations 3.4 and 3.5 to produce the ordinary and rainflow range density functions shown in figures 6.7(a) and 6.7(b) for data set 1. The range functions computed directly from the peak/trough count are also shown for comparison.

The predictions using equations 3.4 and 3.5 are good, particularly at high ranges which are most important for fatigue computations. Figures 6.8(a) and 6.8(b) show the

b_{th} moments of these range functions, where 'b' is the slope of the S-N curve. Further examples of the moments of the rainflow range density function are shown for data sets 2-5 in figures 6.9, 6.10, 6.11 and 6.12.

6.8. The variance of fatigue predictions from limited sample sizes using both time and frequency domain methods

When collecting data on site it is important to know the length of data required to obtain a particular accuracy. This is true both for a straightforward peak-trough and then rainflow cycle count and also for the alternative frequency domain approach using equation 3.5. In this section results will be presented which highlight the change in the scatter of fatigue predictions for varying sample length L_s with particular reference to the following factors;

- (a) The 6th moment of the ordinary and rainflow range count of the actual time signal, meaning that the results relate to a typical machined component.
- (b) Mean, rms and number of peaks per second from the actual time signal.
- (c) Calculation of the PSD from the same length of sample (but with approximately one eighth of the sample rate required) from which the following can be calculated.
 - (c.i) 6th moment of the ordinary and rainflow ranges.
 - (c.ii) rms and number of peaks per second.
 - (c.iii) 6th moment of the ordinary and rainflow ranges from a set of peaks and troughs (same number of peaks as in time sample length L_s) generated according to equation 4.42.
 - (c.iv) As (c.iii) but using the improved solution developed by the author (equation 4.44).

For the following discussion, the method of calculating the parameters in sections (a) and (b) will be referred to as the 'time domain' approach. The method for sections (c.i) to (c.iv) will be called the 'frequency domain' approach for obvious reasons.

Steps (a) to (c.iv) above were carried out on the data shown in figure 3(a) for 11 different sample lengths L_s . For each sample length, 50 estimates of the various parameters

above were calculated. The results are shown in figures 6.12(a) to 6.18(b). All of the plots shown have been normalised by the 'population' values. These are the values computed on the full data sample length (i.e. 1024 seconds)

Figure 6.13(a) shows the reduction in scatter of the mean value as L_s increases. Figures 6.14(a) and 6.14(b) show the equivalent reductions in scatter of rms for the frequency and time domain approaches. There is negligible difference between these.

The number of peaks per second computed using the frequency and time domain methods are shown in figures 6.15(a) and 6.15(b). The time domain method predicts slightly lower rates for the number of peaks per second (approximately 5% less). This is because of the finite interval (192 levels) used for the peak-trough count. If adjacent peaks and troughs fall within the same interval they are ignored by the peak-trough extraction process. This will have little effect on the final fatigue result, however, because the range prediction for the important higher ranges is changed by this reduction in peaks per second to give almost identical fatigue predictions when the number of peaks per second is multiplied by the relevant range distribution moment (see equation 2.20).

Figure 6.13(b) shows the results obtained for the traditional narrow band approach. These results were normalised by the population time domain count of rainflow ranges. Noting the logarithmic units on the y axis it can be seen that this method is on average 100% conservative. The scatter at high sample lengths is +/- 20%.

Figures 6.16(a) and 6.16(b) show the frequency and time domain predictions for ordinary ranges. The interesting point here is that the scatter for the frequency domain approach is slightly less than for the time domain approach. Figures 6.17(a) and 6.17(b) show the comparison for rainflow ranges. Again, although smaller this time, the PSD approach shows a slight improvement in scatter. The important point is that the PSD approach is at least as good as the time domain approach.

Results for the peak-trough regeneration techniques described in section 4 are shown on figures 6.18(a), 6.18(b), 6.19(a) and 6.19(b). These plots were normalised by their respective time domain parameters. Figures 6.19(a) and 6.19(b) therefore show that for the 6th moment, Kowalewskis equation is on average approximately 40% unconservative. The authors improved solution, however, shows no significant overall error when

compared to the time domain result. The scatter for particular sample lengths is of the same order as the scatter in the time domain solutions.

The plots for the moments of the rainflow ranges (figures 6.17(a) and 6.17(b) show that for a limited sample length (one can never obtain an infinite sample) a factor of safety should be applied to the result to allow for unconservative scatter in the prediction. This applies to both time and frequency domain computations and also to regenerated signals using peak-trough Markov matrices. For example, with figures 6.17(a) and 6.17(b) for the moments of the rainflow ranges, the factor of safety would be 16% at 250 kbyte samples (256 seconds), 30% at 64 kbyte samples (66 seconds) and 40% at 32 kbytes (33 seconds).

6.9. Conclusions

- (1) The frequency domain approach to rainflow cycle counting has been shown to be a viable analysis technique. The acquisition rates and numbers of samples required are significantly less than the alternative time domain approach and this may result in significantly less computational time and storage space for on line fatigue analysis tests. Factors like the acquisition rate may be significant for high frequency fatigue work (ref.6.13).
- (2) The improved solution to Kowalewski's formulae for signal regeneration has been presented which shows significant improvements in terms of overall accuracy. Errors of 40% in the average value of fatigue predictions (based on the 6th moment of the rainflow ranges) have been removed by this improved solution.
- (3) Scatter in the fatigue predictions has been shown to reduce with sample size as would be expected. The results for the frequency domain approach indicate that it is at least as good as the time domain prediction in terms of scatter. Plots of this scatter show the need for a factor of safety to be applied to any fatigue prediction which is based on a limited sample size. This applies both to time domain calculations and frequency domain solutions where a probabilistic approach is being applied.

6.10. References

- (6.1) S.G.Martindale, Reliability-based progressive fatigue collapse, presented at the ASCE Structures '82 Congress and Exposition, New Orleans, LA, October 25-27 1982.
- (6.2) By the Committee on Reliability of Offshore Structures of the Committee on Structural Safety and Reliability of the Structural Division, Application of reliability method in design and analysis of offshore platforms, Journal of Structural Engineering, vol 109, no. 10, October 1983.
- (6.3) W.D.Anderson et al, Reliability procedure for fixed offshore platforms, Journal of the Structural Division, ASCE Vol 108, No. ST11, November 1982.
- (6.4) E.Vanmarcke, Risk assessment for offshore structures: A review, Journal of Structural Engineering, ASCE Vol 109, No. 2, February 1983.
- (6.5) R.G.Bea et al, Decision analysis approach to offshore platform design, Journal of Structural Engineering, Vol 110, No. 1, January 1984.
- (6.6) K.H.Donaldson, Field data classification and analysis techniques, paper presented at the SAE Automotive Engineering Congress and Exposition, Detroit, February 22-26, 1982.
- (6.7) G.C.Grenier et al, Integration of fatigue analysis and laboratory simulation requirements in the field data acquisition process, paper presented at the Earthquake Industry Conference, Peoria, Illinois, April 7-9, 1987.
- (6.8) G.Grenier, Sample rate expansion of random data for peak value determination, MTS internal report, July 1985.
- (6.9) G.Grenier, Sines, sampling, Shannon and Nyquist, alias, the alias, A^2 , the anti-alias, at random, "Whew"*, MTS internal report, 1986.
- (6.10) G.Grenier, Fatigue damage vs. sample rate, MTS internal report, 1986.
- (6.11) J.S.Bendat and A.G.Piersol, Random data, analysis and measurement procedures (2nd edition), John Wiley & Sons, Inc., New York 1986.
- (6.12) T.Dirlik, Application of computers in Fatigue Analysis, University of Warwick Thesis, Jan 1985.

(6.13)S.E.Stanzl, Fatigue testing at ultrasonic frequencies, paper read at joint SEE/EIS meeting, 23 October 1985, Journal of the Society of Environmental Engineers, March 1986

Table 6.1. qualification tests
carried out on data set 1

CUTOFF POINTS DEFINING CLASS INTERVALS
 -5.00000-1.99000-1.68000-1.48000-1.32000-1.19000-1.09000-0.98000
 -0.89000-0.81000-0.73000-0.66000-0.58000-0.52000-0.45000-0.39000
 -0.33000-0.27000-0.21000-0.15000-0.09000-0.03000 0.03000 0.09000
 0.15000 0.21000 0.27000 0.33000 0.39000 0.45000 0.52000 0.58000
 0.66000 0.73000 0.81000 0.89000 0.98000 1.09000 1.19000 1.32000
 1.48000 1.68000 1.99000 5.00000

PROBABILITIES WITHIN EACH CLASS INTERVAL
 0.02329 0.02319 0.02296 0.02398 0.02360 0.02084 0.02568 0.02319
 0.02224 0.02373 0.02193 0.02633 0.02057 0.02483 0.02191 0.02243
 0.02288 0.02325 0.02355 0.02376 0.02389 0.02394 0.02389 0.02376
 0.02355 0.02325 0.02288 0.02243 0.02191 0.02483 0.02057 0.02633
 0.02193 0.02373 0.02224 0.02319 0.02568 0.02084 0.02360 0.02398
 0.02296 0.02319 0.02329

GROUP	MEAN	VARIANCE	RMS	MIN	MAX	CHI.SQ
1	2362.62	65542.0	256.012	1518	3215	28.80
2	2365.71	67023.6	258.889	1416	3296	33.50
3	2360.56	69281.6	263.214	1498	3134	37.34
4	2363.54	66137.1	257.171	1566	3290	42.53
5	2365.30	58913.7	242.721	1572	3138	40.05
6	2364.16	61975.7	248.949	1409	3167	30.15
7	2367.81	62995.5	250.989	1603	3438	46.30
8	2362.33	60129.6	245.213	1479	3248	56.91
9	2364.69	63807.4	252.601	1377	3267	63.05
10	2361.70	65358.9	255.654	1493	3456	35.95
11	2366.62	66106.9	257.113	1445	3201	38.18
12	2364.57	65319.5	255.577	1558	3140	42.68
13	2364.49	66249.6	257.390	1479	3177	40.19
14	2365.00	60820.1	246.617	1578	3146	30.77
15	2363.45	60063.4	245.078	1516	3273	39.49
16	2365.88	59489.7	243.905	1472	3266	30.40

636.28

INT	INTUPLIM	EXPRB	EXPTED	OBSVED	DISC.NCY	CHI.SQ
1	1146.4	0.023	46.580	53.000	6.420	0.885
2	1880.5	0.023	46.380	40.000	-6.380	0.878
3	1956.1	0.023	45.920	41.000	-4.920	0.527
4	2004.9	0.024	47.960	48.000	0.040	0.000
5	2043.9	0.024	47.200	46.000	-1.200	0.031
6	2075.6	0.021	41.680	47.000	5.320	0.679
7	2100.0	0.026	51.360	58.000	6.640	0.858
8	2126.8	0.023	46.380	46.000	-0.380	0.003
9	2148.8	0.022	44.480	37.000	-7.480	1.258
10	2168.3	0.024	47.460	38.000	-9.460	1.886
11	2187.8	0.022	43.860	38.000	-5.860	0.783
12	2204.9	0.026	52.660	52.000	-0.660	0.008
13	2224.4	0.021	41.140	39.000	-2.140	0.111
14	2239.0	0.025	49.660	46.000	-3.660	0.270
15	2256.1	0.022	43.820	57.000	13.180	3.964
16	2270.8	0.022	44.860	39.000	-5.860	0.765
17	2285.4	0.023	45.760	50.000	4.240	0.393
18	2300.0	0.023	46.500	56.000	9.500	1.941
19	2314.7	0.024	47.100	51.000	3.900	0.323
20	2329.3	0.024	47.520	47.000	-0.520	0.006
21	2343.9	0.024	47.780	46.000	-1.780	0.066
22	2358.6	0.024	47.880	48.000	0.120	0.000
23	2373.2	0.024	47.780	55.000	7.220	1.091
24	2387.8	0.024	47.520	39.000	-8.520	1.528
25	2402.5	0.024	47.100	52.000	4.900	0.510
26	2417.1	0.023	46.500	52.000	5.500	0.651
27	2431.7	0.023	45.760	51.000	5.240	0.600
28	2446.4	0.022	44.860	48.000	3.140	0.220
29	2461.0	0.022	43.820	40.000	-3.820	0.333
30	2475.6	0.025	49.660	36.000	-13.660	3.757
31	2492.7	0.021	41.140	37.000	-4.140	0.417
32	2507.3	0.026	52.660	45.000	-7.660	1.114
33	2526.9	0.022	43.860	41.000	-2.860	0.186

34	2543.9	0.024	47.460	54.000	6.540	0.901
35	2563.4	0.022	44.480	52.000	7.520	1.271
36	2583.0	0.023	46.380	45.000	-1.380	0.041
37	2604.9	0.026	51.360	51.000	-0.360	0.003
38	2631.7	0.021	41.680	41.000	-0.680	0.011
39	2656.1	0.024	47.200	47.000	-0.200	0.001
40	2687.8	0.024	47.960	51.000	3.040	0.193
41	2726.9	0.023	45.920	45.000	-0.920	0.018
42	2775.6	0.023	46.380	54.000	7.620	1.252
43	2851.2	0.023	46.580	41.000	-5.580	0.668

INT	EXPT.TOT	OBSV.TOT
1	745.280	725.000
2	742.080	773.000
3	734.720	729.000
4	767.360	779.000
5	755.200	755.000
6	666.880	694.000
7	821.760	812.000
8	742.080	712.000
9	711.680	711.000
10	759.360	749.000
11	701.760	677.000
12	842.560	817.000
13	658.240	633.000
14	794.560	804.000
15	701.120	707.000
16	717.760	717.000
17	732.160	735.000
18	744.000	769.000
19	753.600	726.000
20	760.320	759.000
21	764.480	786.000
22	766.080	766.000
23	764.480	835.000
24	760.320	798.000
25	753.600	764.000
26	744.000	769.000
27	732.160	710.000
28	717.760	712.000
29	701.120	693.000
30	794.560	800.000
31	658.240	681.000
32	842.560	811.000
33	701.760	714.000
34	759.360	713.000
35	711.680	690.000
36	742.080	706.000
37	821.760	780.000
38	666.880	671.000
39	755.200	796.000
40	767.360	810.000
41	734.720	701.000
42	742.080	756.000
43	745.280	755.000

Table 6.2. qualification tests
carried out on data set 2

CUTOFF POINTS DEFINING CLASS INTERVALS

-5.00000-1.99000-1.68000-1.48000-1.32000-1.19000-1.09000-0.98000
 -0.89000-0.81000-0.73000-0.66000-0.58000-0.52000-0.45000-0.39000
 -0.33000-0.27000-0.21000-0.15000-0.09000-0.03000 0.03000 0.09000
 0.15000 0.21000 0.27000 0.33000 0.39000 0.45000 0.52000 0.58000
 0.66000 0.73000 0.81000 0.89000 0.98000 1.09000 1.19000 1.32000
 1.48000 1.68000 1.99000 5.00000

PROBABILITIES WITHIN EACH CLASS INTERVAL

0.02329 0.02319 0.02296 0.02398 0.02360 0.02084 0.02568 0.02319
 0.02224 0.02373 0.02193 0.02633 0.02057 0.02483 0.02191 0.02243
 0.02288 0.02325 0.02355 0.02376 0.02389 0.02394 0.02389 0.02376
 0.02355 0.02325 0.02288 0.02243 0.02191 0.02483 0.02057 0.02633
 0.02193 0.02373 0.02224 0.02319 0.02568 0.02084 0.02360 0.02398
 0.02296 0.02319 0.02329

GROUP	MEAN	VARIANCE	RMS	MIN	MAX	CHI.SQ
1	2183.80	67769.0	260.325	1257	3035	54.11
2	2184.37	70183.5	264.922	1228	3175	28.70
3	2184.11	66555.9	257.984	1271	2956	33.46
4	2179.74	67716.3	260.224	1263	3197	60.80
5	2187.15	72137.4	268.584	1021	3091	21.66
6	2182.02	65405.2	255.744	1350	3162	54.57
7	2188.53	70205.7	264.963	1278	3038	28.75
8	2183.67	65238.0	255.417	1056	3170	40.39
9	2186.42	58710.9	242.303	1290	2982	33.63
10	2184.43	60830.7	246.639	1170	2982	38.69
11	2185.82	68120.3	260.999	1070	3186	38.93
12	2181.96	59736.2	244.410	1220	3217	42.76
13	2184.61	72702.1	269.633	1385	3107	47.75
14	2177.39	63967.6	252.918	1081	3034	46.14
15	2183.63	67699.4	260.191	1139	3375	40.89
16	2186.07	62453.1	249.906	1304	2980	36.71
						647.95

INT	INTUPLIM	EXPRB	EXPTED	OBSVED	DISC.NCY	CHI.SQ
1	936.5	0.023	46.580	41.000	-5.580	0.668
2	1688.8	0.023	46.380	46.000	-0.380	0.003
3	1766.2	0.023	45.920	55.000	9.080	1.795
4	1816.2	0.024	47.960	53.000	5.040	0.530
5	1856.2	0.024	47.200	48.000	0.800	0.014
6	1888.7	0.021	41.680	44.000	2.320	0.129
7	1913.7	0.026	51.360	41.000	-10.360	2.090
8	1941.2	0.023	46.380	42.000	-4.380	0.414
9	1963.7	0.022	44.480	37.000	-7.480	1.258
10	1983.6	0.024	47.460	56.000	8.540	1.537
11	2003.6	0.022	43.860	46.000	2.140	0.104
12	2021.1	0.026	52.660	48.000	-4.660	0.412
13	2041.1	0.021	41.140	42.000	0.860	0.018
14	2056.1	0.025	49.660	47.000	-2.660	0.142
15	2073.6	0.022	43.820	40.000	-3.820	0.333
16	2088.6	0.022	44.860	44.000	-0.860	0.016
17	2103.6	0.023	45.760	46.000	0.240	0.001
18	2118.6	0.023	46.500	44.000	-2.500	0.134
19	2133.6	0.024	47.100	49.000	1.900	0.077
20	2148.6	0.024	47.520	46.000	-1.520	0.049
21	2163.6	0.024	47.780	51.000	3.220	0.217
22	2178.6	0.024	47.880	46.000	-1.880	0.074
23	2193.6	0.024	47.780	43.000	-4.780	0.478
24	2208.6	0.024	47.520	64.000	16.480	5.715
25	2223.6	0.024	47.100	44.000	-3.100	0.204
26	2238.5	0.023	46.500	54.000	7.500	1.210
27	2253.5	0.023	45.760	38.000	-7.760	1.316
28	2268.5	0.022	44.860	57.000	12.140	3.285
29	2283.5	0.022	43.820	47.000	3.180	0.231
30	2298.5	0.025	49.660	62.000	12.340	3.066
31	2316.0	0.021	41.140	38.000	-3.140	0.240
32	2331.0	0.026	52.660	56.000	3.340	0.212
33	2351.0	0.022	43.860	48.000	4.140	0.391

34	2368.5	0.024	47.460	45.000	-2.460	0.128
35	2388.5	0.022	44.480	42.000	-2.480	0.138
36	2408.5	0.023	46.380	39.000	-7.380	1.174
37	2431.0	0.026	51.360	42.000	-9.360	1.706
38	2458.5	0.021	41.680	32.000	-9.680	2.248
39	2483.5	0.024	47.200	35.000	-12.200	3.153
40	2515.9	0.024	47.960	49.000	1.040	0.023
41	2555.9	0.023	45.920	53.000	7.080	1.092
42	2605.9	0.023	46.380	48.000	1.620	0.057
43	2683.4	0.023	46.580	52.000	5.420	0.631

INT	EXPT.TOT	OBSV.TOT
1	745.280	778.000
2	742.080	719.000
3	734.720	703.000
4	767.360	746.000
5	755.200	723.000
6	666.880	629.000
7	821.760	822.000
8	742.080	704.000
9	711.680	752.000
10	759.360	789.000
11	701.760	682.000
12	842.560	854.000
13	658.240	696.000
14	794.560	786.000
15	701.120	698.000
16	717.760	723.000
17	732.160	711.000
18	744.000	771.000
19	753.600	757.000
20	760.320	785.000
21	764.480	760.000
22	766.080	761.000
23	764.480	817.000
24	760.320	774.000
25	753.600	772.000
26	744.000	797.000
27	732.160	742.000
28	717.760	713.000
29	701.120	698.000
30	794.560	808.000
31	658.240	630.000
32	842.560	878.000
33	701.760	684.000
34	759.360	755.000
35	711.680	731.000
36	742.080	710.000
37	821.760	796.000
38	666.880	645.000
39	755.200	741.000
40	767.360	759.000
41	734.720	730.000
42	742.080	710.000
43	745.280	761.000

Table 6.3. qualification tests
carried out on data set 3

CUTOFF POINTS DEFINING CLASS INTERVALS

-5.00000-1.99000-1.68000-1.48000-1.32000-1.19000-1.09000-0.98000
 -0.89000-0.81000-0.73000-0.66000-0.58000-0.52000-0.45000-0.39000
 -0.33000-0.27000-0.21000-0.15000-0.09000-0.03000 0.03000 0.09000
 0.15000 0.21000 0.27000 0.33000 0.39000 0.45000 0.52000 0.58000
 0.66000 0.73000 0.81000 0.89000 0.98000 1.09000 1.19000 1.32000
 1.48000 1.68000 1.99000 5.00000

PROBABILITIES WITHIN EACH CLASS INTERVAL

0.02329 0.02319 0.02296 0.02398 0.02360 0.02084 0.02568 0.02319
 0.02224 0.02373 0.02193 0.02633 0.02057 0.02483 0.02191 0.02243
 0.02288 0.02325 0.02355 0.02376 0.02389 0.02394 0.02389 0.02376
 0.02355 0.02325 0.02288 0.02243 0.02191 0.02483 0.02057 0.02633
 0.02193 0.02373 0.02224 0.02319 0.02568 0.02084 0.02360 0.02398
 0.02296 0.02319 0.02329

GROUP	MEAN	VARIANCE	RMS	MIN	MAX	CHI.SQ
1	2445.31	33145.8	182.060	1841	3052	51.74
2	2443.31	35272.8	187.811	1756	3104	44.10
3	2444.62	32560.0	180.444	1738	3177	42.15
4	2443.58	31845.5	178.453	1841	3000	49.89
5	2444.23	32415.6	180.043	1864	3014	25.01
6	2446.53	32090.3	179.138	1856	3053	48.65
7	2442.27	33212.5	182.243	1903	3011	49.08
8	2446.56	32062.6	179.060	1831	3062	74.06
9	2445.08	34126.0	184.732	1826	3164	33.42
10	2440.62	32439.2	180.109	1739	3052	41.57
11	2444.71	31233.4	176.730	1868	3047	50.00
12	2440.42	29186.1	170.839	1822	2969	50.24
13	2441.61	34429.9	185.553	1865	3133	34.90
14	2443.58	32366.2	179.906	1815	3119	51.86
15	2445.04	31747.8	178.179	1844	3108	30.12
16	2446.14	32095.5	179.152	1822	3009	49.63
						726.43

INT	INTUPLIM	EXPRB	EXPTED	OBSVED	DISC.NCY	CHI.SQ
1	1550.4	0.023	46.580	48.000	1.420	0.043
2	2089.6	0.023	46.380	36.000	-10.380	2.323
3	2145.2	0.023	45.920	49.000	3.080	0.207
4	2181.0	0.024	47.960	38.000	-9.960	2.068
5	2209.7	0.024	47.200	62.000	14.800	4.641
6	2233.0	0.021	41.680	36.000	-5.680	0.774
7	2250.9	0.026	51.360	58.000	6.640	0.858
8	2270.6	0.023	46.380	54.000	7.620	1.252
9	2286.7	0.022	44.480	35.000	-9.480	2.020
10	2301.0	0.024	47.460	56.000	8.540	1.537
11	2315.4	0.022	43.860	39.000	-4.860	0.539
12	2327.9	0.026	52.660	55.000	2.340	0.104
13	2342.2	0.021	41.140	37.000	-4.140	0.417
14	2353.0	0.025	49.660	51.000	1.340	0.036
15	2365.5	0.022	43.820	48.000	4.180	0.399
16	2376.3	0.022	44.860	50.000	5.140	0.589
17	2387.0	0.023	45.760	46.000	0.240	0.001
18	2397.8	0.023	46.500	41.000	-5.500	0.651
19	2408.5	0.024	47.100	46.000	-1.100	0.026
20	2419.3	0.024	47.520	46.000	-1.520	0.049
21	2430.0	0.024	47.780	46.000	-1.780	0.066
22	2440.8	0.024	47.880	62.000	14.120	4.164
23	2451.5	0.024	47.780	43.000	-4.780	0.478
24	2451.5	0.024	47.520	63.000	15.480	5.043
25	2462.3	0.024	47.100	42.000	-5.100	0.552
26	2473.0	0.024	46.500	46.000	-0.500	0.005
27	2483.8	0.023	45.760	44.000	-1.760	0.068
28	2494.5	0.023	45.760	44.000	-1.760	0.068
29	2505.3	0.022	44.860	35.000	-9.860	2.167
30	2516.0	0.022	43.820	43.000	-0.820	0.015
31	2526.8	0.025	49.660	44.000	-5.660	0.645
32	2539.3	0.021	41.140	49.000	7.860	1.502
33	2550.1	0.026	52.660	41.000	-11.660	2.582
33	2564.4	0.022	43.860	32.000	-11.860	3.207

34	2576.9	0.024	47.460	50.000	2.540	0.136
35	2591.3	0.022	44.480	41.000	-3.480	0.272
36	2605.6	0.023	46.380	53.000	6.620	0.945
37	2621.7	0.026	51.360	53.000	1.640	0.052
38	2641.4	0.021	41.680	40.000	-1.680	0.068
39	2659.3	0.024	47.200	64.000	16.800	5.980
40	2682.6	0.024	47.960	45.000	-2.960	0.183
41	2711.3	0.023	45.920	43.000	-2.920	0.186
42	2747.1	0.023	46.380	37.000	-9.380	1.897
43	2802.7	0.023	46.580	53.000	6.420	0.885

INT	EXPT.TOT	OBSV.TOT
1	745.280	762.000
2	742.080	729.000
3	734.720	729.000
4	767.360	716.000
5	755.200	786.000
6	666.880	691.000
7	821.760	787.000
8	742.080	760.000
9	711.680	677.000
10	759.360	748.000
11	701.760	746.000
12	842.560	802.000
13	658.240	660.000
14	794.560	876.000
15	701.120	681.000
16	717.760	740.000
17	732.160	744.000
18	744.000	738.000
19	753.600	739.000
20	760.320	711.000
21	764.480	738.000
22	766.080	805.000
23	764.480	812.000
24	760.320	764.000
25	753.600	765.000
26	744.000	738.000
27	732.160	781.000
28	717.760	651.000
29	701.120	714.000
30	794.560	775.000
31	658.240	672.000
32	842.560	807.000
33	701.760	732.000
34	759.360	759.000
35	711.680	687.000
36	742.080	728.000
37	821.760	837.000
38	666.880	678.000
39	755.200	771.000
40	767.360	740.000
41	734.720	765.000
42	742.080	707.000
43	745.280	752.000

Table 6.4. qualification tests
carried out on data set 4

CUTOFF POINTS DEFINING CLASS INTERVALS

-5.00000-1.99000-1.68000-1.48000-1.32000-1.19000-1.09000-0.98000
 -0.89000-0.81000-0.73000-0.66000-0.58000-0.52000-0.45000-0.39000
 -0.33000-0.27000-0.21000-0.15000-0.09000-0.03000 0.03000 0.09000
 0.15000 0.21000 0.27000 0.33000 0.39000 0.45000 0.52000 0.58000
 0.66000 0.73000 0.81000 0.89000 0.98000 1.09000 1.19000 1.32000
 1.48000 1.68000 1.99000 5.00000

PROBABILITIES WITHIN EACH CLASS INTERVAL

0.02329 0.02319 0.02296 0.02398 0.02360 0.02084 0.02568 0.02319
 0.02224 0.02373 0.02193 0.02633 0.02057 0.02483 0.02191 0.02243
 0.02288 0.02325 0.02355 0.02376 0.02389 0.02394 0.02389 0.02376
 0.02355 0.02325 0.02288 0.02243 0.02191 0.02483 0.02057 0.02633
 0.02193 0.02373 0.02224 0.02319 0.02568 0.02084 0.02360 0.02398
 0.02296 0.02319 0.02329

GROUP	MEAN	VARIANCE	RMS	MIN	MAX	CHI.SQ
1	2500.98131759.4	362.987	1227	3725	46.03	
2	2507.94129495.8	359.855	1380	3692	35.53	
3	2500.51130760.0	361.608	1312	3800	28.40	
4	2498.54132269.6	363.689	1411	3638	27.76	
5	2516.46130986.5	361.921	786	3766	53.69	
6	2503.84133906.1	365.932	1080	3782	43.14	
7	2496.88144307.2	379.878	1050	3913	35.94	
8	2514.77137235.6	370.453	1138	3788	31.16	
9	2502.01125412.6	354.136	1408	3807	37.31	
10	2504.18139309.5	373.242	1271	3683	39.02	
11	2507.12134053.5	366.133	1376	3679	38.36	
12	2511.80135056.6	367.500	1251	4039	57.97	
13	2501.14125126.9	353.733	1325	3813	30.40	
14	2495.24131848.4	363.109	1344	3561	39.41	
15	2509.94142114.3	376.981	1361	3927	43.67	
16	2510.97127119.0	356.538	1319	3523	41.72	

629.52

INT	INTUPLIM	EXPRB	EXPTED	OBSVED	DISC.NCY	CHI.SQ
1	728.3	0.023	46.580	44.000	-2.580	0.143
2	1801.5	0.023	46.380	58.000	11.620	2.911
3	1912.0	0.023	45.920	59.000	13.080	3.726
4	1983.3	0.024	47.960	35.000	-12.960	3.502
5	2040.3	0.024	47.200	39.000	-8.200	1.425
6	2086.7	0.021	41.680	39.000	-2.680	0.172
7	2122.3	0.026	51.360	40.000	-11.360	2.513
8	2161.6	0.023	46.380	48.000	1.620	0.057
9	2193.6	0.022	44.480	50.000	5.520	0.685
10	2222.2	0.024	47.460	45.000	-2.460	0.128
11	2250.7	0.022	43.860	43.000	-0.860	0.017
12	2275.7	0.026	52.660	54.000	1.340	0.034
13	2304.2	0.021	41.140	34.000	-7.140	1.239
14	2325.6	0.025	49.660	61.000	11.340	2.590
15	2350.5	0.022	43.820	47.000	3.180	0.231
16	2371.9	0.022	44.860	47.000	2.140	0.102
17	2393.3	0.023	45.760	40.000	-5.760	0.725
18	2414.7	0.023	46.500	49.000	2.500	0.134
19	2436.1	0.024	47.100	43.000	-4.100	0.357
20	2457.5	0.024	47.520	51.000	3.480	0.255
21	2478.9	0.024	47.780	49.000	1.220	0.031
22	2500.3	0.024	47.880	58.000	10.120	2.139
23	2521.7	0.024	47.780	39.000	-8.780	1.613
24	2521.7	0.024	47.520	40.000	-7.520	1.190
25	2543.1	0.024	47.100	50.000	2.900	0.179
26	2564.4	0.024	47.500	55.000	8.500	1.554
27	2585.8	0.023	46.500	33.000	-12.760	3.558
28	2607.2	0.023	45.760	50.000	5.140	0.589
29	2628.6	0.022	44.860	50.000	5.140	0.589
30	2650.0	0.022	43.820	52.000	8.180	1.527
31	2671.4	0.025	49.660	57.000	7.340	1.085
32	2696.4	0.021	41.140	35.000	-6.140	0.916
33	2717.8	0.026	52.660	50.000	-2.660	0.134
33	2746.3	0.022	43.860	44.000	0.140	0.000

34	2771.2	0.024	47.460	37.000	-10.460	2.305
35	2799.8	0.022	44.480	49.000	4.520	0.459
36	2828.3	0.023	46.380	44.000	-2.380	0.122
37	2860.4	0.026	51.360	61.000	9.640	1.809
38	2899.6	0.021	41.680	41.000	-0.680	0.011
39	2935.2	0.024	47.200	48.000	0.800	0.014
40	2981.6	0.024	47.960	49.000	1.040	0.023
41	3038.6	0.023	45.920	38.000	-7.920	1.366
42	3110.0	0.023	46.380	49.000	2.620	0.148
43	3220.5	0.023	46.580	46.000	-0.580	0.007

INT	EXPT.TOT	OBSV.TOT
1	745.280	731.000
2	742.080	741.000
3	734.720	725.000
4	767.360	768.000
5	755.200	744.000
6	666.880	648.000
7	821.760	795.000
8	742.080	750.000
9	711.680	736.000
10	759.360	749.000
11	701.760	731.000
12	842.560	905.000
13	658.240	600.000
14	794.560	783.000
15	701.120	691.000
16	717.760	728.000
17	732.160	758.000
18	744.000	785.000
19	753.600	768.000
20	760.320	798.000
21	764.480	776.000
22	766.080	800.000
23	764.480	737.000
24	760.320	708.000
25	753.600	767.000
26	744.000	733.000
27	732.160	742.000
28	717.760	781.000
29	701.120	695.000
30	794.560	789.000
31	658.240	638.000
32	842.560	815.000
33	701.760	706.000
34	759.360	745.000
35	711.680	722.000
36	742.080	704.000
37	821.760	825.000
38	666.880	681.000
39	755.200	719.000
40	767.360	733.000
41	734.720	739.000
42	742.080	751.000
43	745.280	760.000

Table 6.5. qualification tests
carried out on data set 5

CUTOFF POINTS DEFINING CLASS INTERVALS

-5.00000-1.99000-1.68000-1.48000-1.32000-1.19000-1.09000-0.98000
 -0.89000-0.81000-0.73000-0.66000-0.58000-0.52000-0.45000-0.39000
 -0.33000-0.27000-0.21000-0.15000-0.09000-0.03000 0.03000 0.09000
 0.15000 0.21000 0.27000 0.33000 0.39000 0.45000 0.52000 0.58000
 0.66000 0.73000 0.81000 0.89000 0.98000 1.09000 1.19000 1.32000
 1.48000 1.68000 1.99000 5.00000

PROBABILITIES WITHIN EACH CLASS INTERVAL

0.02329 0.02319 0.02296 0.02398 0.02360 0.02084 0.02568 0.02319
 0.02224 0.02373 0.02193 0.02633 0.02057 0.02483 0.02191 0.02243
 0.02288 0.02325 0.02355 0.02376 0.02389 0.02394 0.02389 0.02376
 0.02355 0.02325 0.02288 0.02243 0.02191 0.02483 0.02057 0.02633
 0.02193 0.02373 0.02224 0.02319 0.02568 0.02084 0.02360 0.02398
 0.02296 0.02319 0.02329

GROUP	MEAN	VARIANCE	RMS	MIN	MAX	CHI.SQ
1	2353.02157227.8	396.520	1133	3747	30.15	
2	2356.06151962.6	389.824	967	3964	35.73	
3	2356.54154607.7	393.202	1017	3634	36.40	
4	2352.64150797.5	388.327	1034	3789	26.63	
5	2357.34147731.9	384.359	904	3602	37.91	
6	2358.90169512.4	411.719	832	4074	48.21	
7	2358.00158471.6	398.085	855	3559	42.74	
8	2355.42158514.4	398.139	871	3631	50.16	
9	2355.60150103.3	387.432	796	3681	35.02	
10	2360.88140299.3	374.565	945	3550	47.39	
11	2360.22151305.4	388.980	896	3494	30.53	
12	2358.85152649.4	390.704	893	3618	45.28	
13	2363.71148498.7	385.355	814	3705	25.96	
14	2359.36153225.0	391.440	987	3653	33.26	
15	2355.06197401.5	444.299	800	3913	46.01	
16	2351.80219842.7	468.874	743	4027	45.50	
					616.88	

INT	INTUPLIM	EXPRB	EXPTED	OBSVED	DISC.NCY	CHI.SQ
1	7.4	0.023	46.580	37.000	-9.580	1.970
2	1418.7	0.023	46.380	54.000	7.620	1.252
3	1564.1	0.023	45.920	50.000	4.080	0.363
4	1657.9	0.024	47.960	43.000	-4.960	0.513
5	1732.9	0.024	47.200	47.000	-0.200	0.001
6	1793.8	0.021	41.680	50.000	8.320	1.661
7	1840.7	0.026	51.360	58.000	6.640	0.858
8	1892.3	0.023	46.380	59.000	12.620	3.434
9	1934.5	0.022	44.480	54.000	9.520	2.038
10	1972.0	0.024	47.460	47.000	-0.460	0.004
11	2009.5	0.022	43.860	31.000	-12.860	3.771
12	2042.3	0.026	52.660	48.000	-4.660	0.412
13	2079.8	0.021	41.140	43.000	1.860	0.084
14	2108.0	0.025	49.660	47.000	-2.660	0.142
15	2140.8	0.022	43.820	44.000	0.180	0.001
16	2168.9	0.022	44.860	38.000	-6.860	1.049
17	2197.1	0.023	45.760	53.000	7.240	1.145
18	2225.2	0.023	46.500	45.000	-1.500	0.048
19	2225.2	0.023	46.500	54.000	6.900	1.011
20	2253.3	0.024	47.100	41.000	-6.520	0.895
21	2281.5	0.024	47.520	49.000	1.220	0.031
22	2309.6	0.024	47.780	36.000	-11.880	2.948
23	2337.7	0.024	47.880	49.000	1.220	0.031
24	2365.9	0.024	47.780	49.000	1.480	0.046
25	2394.0	0.024	47.520	49.000	1.480	0.046
26	2422.1	0.024	47.100	51.000	3.900	0.323
27	2450.3	0.023	46.500	41.000	-5.500	0.651
28	2478.4	0.023	45.760	38.000	-7.760	1.316
29	2506.5	0.022	44.860	37.000	-7.860	1.377
30	2534.7	0.022	43.820	42.000	-1.820	0.076
31	2562.8	0.025	49.660	45.000	-4.660	0.437
32	2595.6	0.021	41.140	39.000	-2.140	0.111
33	2623.7	0.026	52.660	71.000	18.340	6.387
34	2661.3	0.022	43.860	49.000	5.140	0.602

34	2694.1	0.024	47.460	43.000	-4.460	0.419
35	2731.6	0.022	44.480	37.000	-7.480	1.258
36	2769.1	0.023	46.380	52.000	5.620	0.681
37	2811.3	0.026	51.360	49.000	-2.360	0.108
38	2862.9	0.021	41.680	32.000	-9.680	2.248
39	2909.8	0.024	47.200	51.000	3.800	0.306
40	2970.7	0.024	47.960	43.000	-4.960	0.513
41	3045.7	0.023	45.920	53.000	7.080	1.092
42	3139.5	0.023	46.380	59.000	12.620	3.434
43	3284.9	0.023	46.580	42.000	-4.580	0.450

INT	EXPT.TOT	OBSV.TOT
1	745.280	741.000
2	742.080	711.000
3	734.720	787.000
4	767.360	763.000
5	755.200	765.000
6	666.880	682.000
7	821.760	777.000
8	742.080	731.000
9	711.680	715.000
10	759.360	748.000
11	701.760	677.000
12	842.560	849.000
13	658.240	684.000
14	794.560	803.000
15	701.120	672.000
16	717.760	734.000
17	732.160	697.000
18	744.000	761.000
19	753.600	732.000
20	760.320	768.000
21	764.480	753.000
22	766.080	765.000
23	764.480	770.000
24	760.320	770.000
25	753.600	787.000
26	744.000	721.000
27	732.160	744.000
28	717.760	720.000
29	701.120	765.000
30	794.560	783.000
31	658.240	678.000
32	842.560	910.000
33	701.760	686.000
34	759.360	768.000
35	711.680	685.000
36	742.080	742.000
37	821.760	770.000
38	666.880	626.000
39	755.200	759.000
40	767.360	770.000
41	734.720	723.000
42	742.080	755.000
43	745.280	753.000

Table 6.6. Results showing the effect of quantisation on accuracy.

- 145 -

A	D	b	X	DX	δ_{err}
0.004	350.0	6.0	150.0	5.0	-0.09
0.004	350.0	6.0	150.0	10.0	-0.35
0.004	350.0	6.0	150.0	15.0	-0.76
0.004	350.0	6.0	150.0	20.0	-1.29
0.004	350.0	6.0	150.0	25.0	-1.93
0.004	350.0	6.0	150.0	30.0	-2.65
*	*	*	*	*	*
0.004	350.0	2.0	300.0	10.0	0.11
0.004	350.0	4.0	300.0	10.0	0.19
0.004	350.0	6.0	300.0	10.0	0.23
0.004	350.0	8.0	300.0	10.0	0.24
0.004	350.0	10.0	300.0	10.0	0.20
0.004	350.0	12.0	300.0	10.0	0.14
*	*	*	*	*	*
0.004	350.0	6.0	300.0	5.0	0.05
0.004	350.0	6.0	300.0	10.0	0.23
0.004	350.0	6.0	300.0	15.0	0.56
0.004	350.0	6.0	300.0	20.0	1.10
0.004	350.0	6.0	300.0	25.0	1.87
0.004	350.0	6.0	300.0	30.0	2.96
*	*	*	*	*	*
0.004	350.0	6.0	100.0	10.0	-0.94
0.004	350.0	6.0	200.0	10.0	-0.13
0.004	350.0	6.0	250.0	10.0	0.01
0.004	350.0	6.0	300.0	10.0	0.23

Figure 6.1. The output characteristics of the Brüel and Kjaer random signal generator

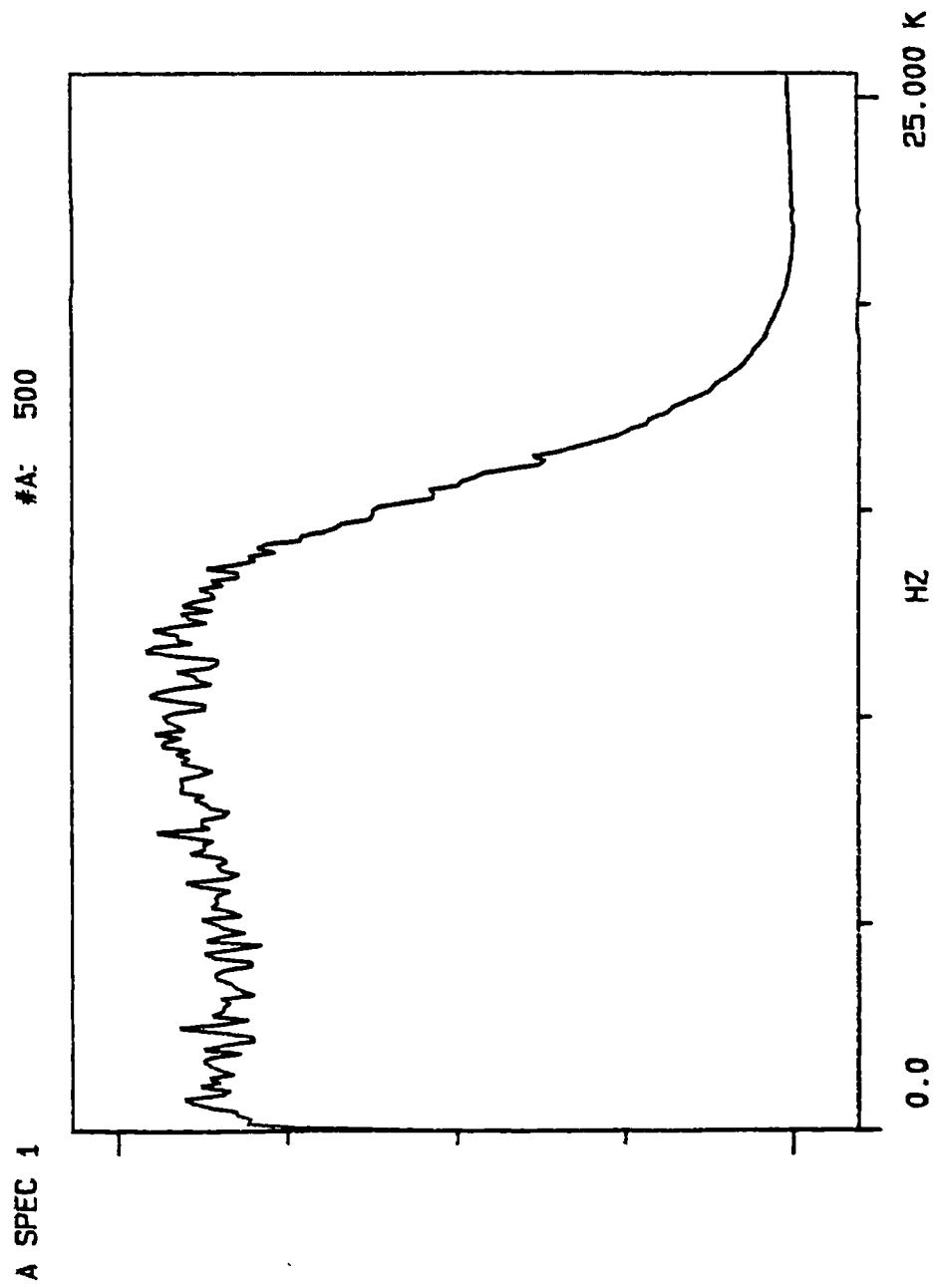


Figure 6.2. The output of one of the low pass filters set to 250 Hz.

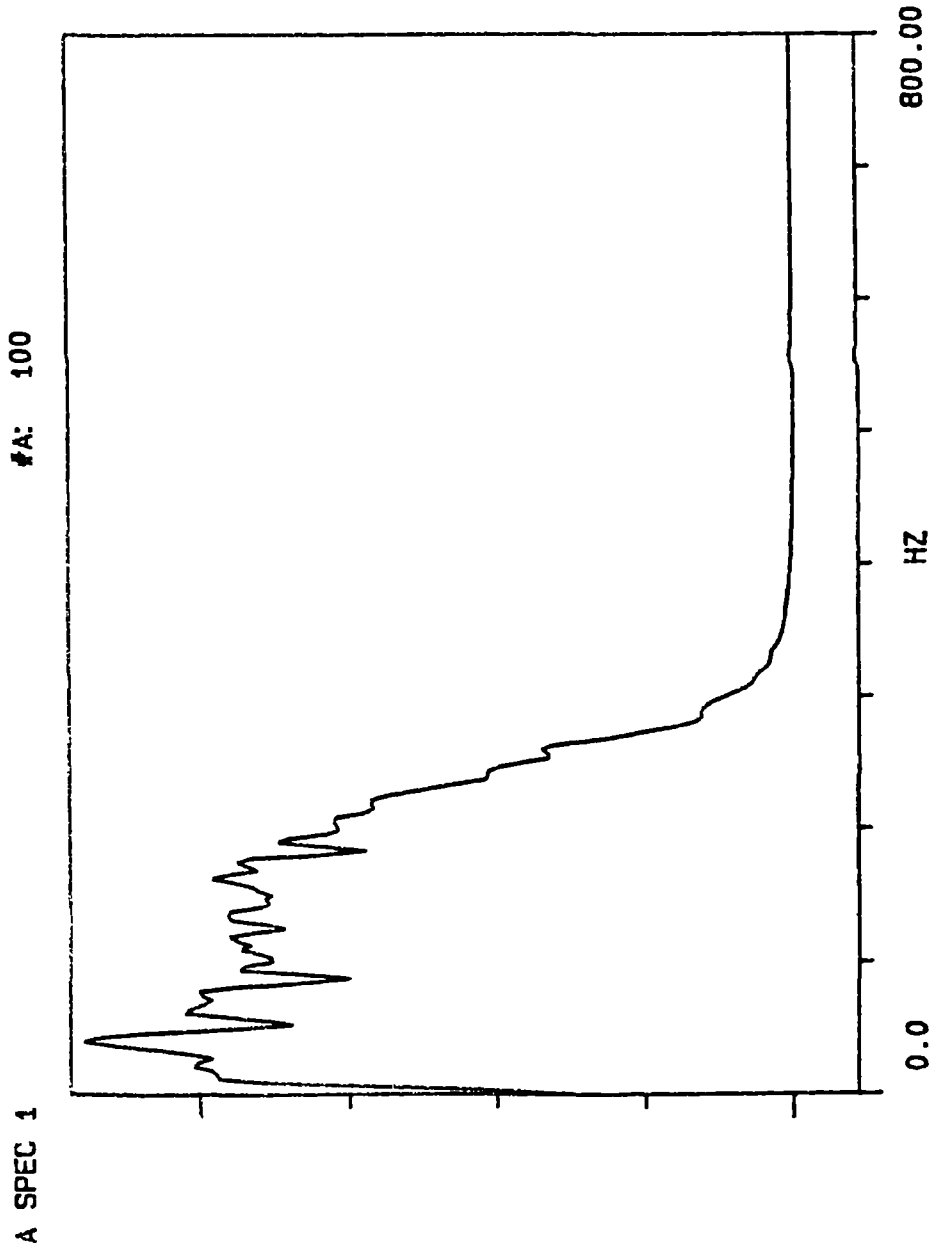
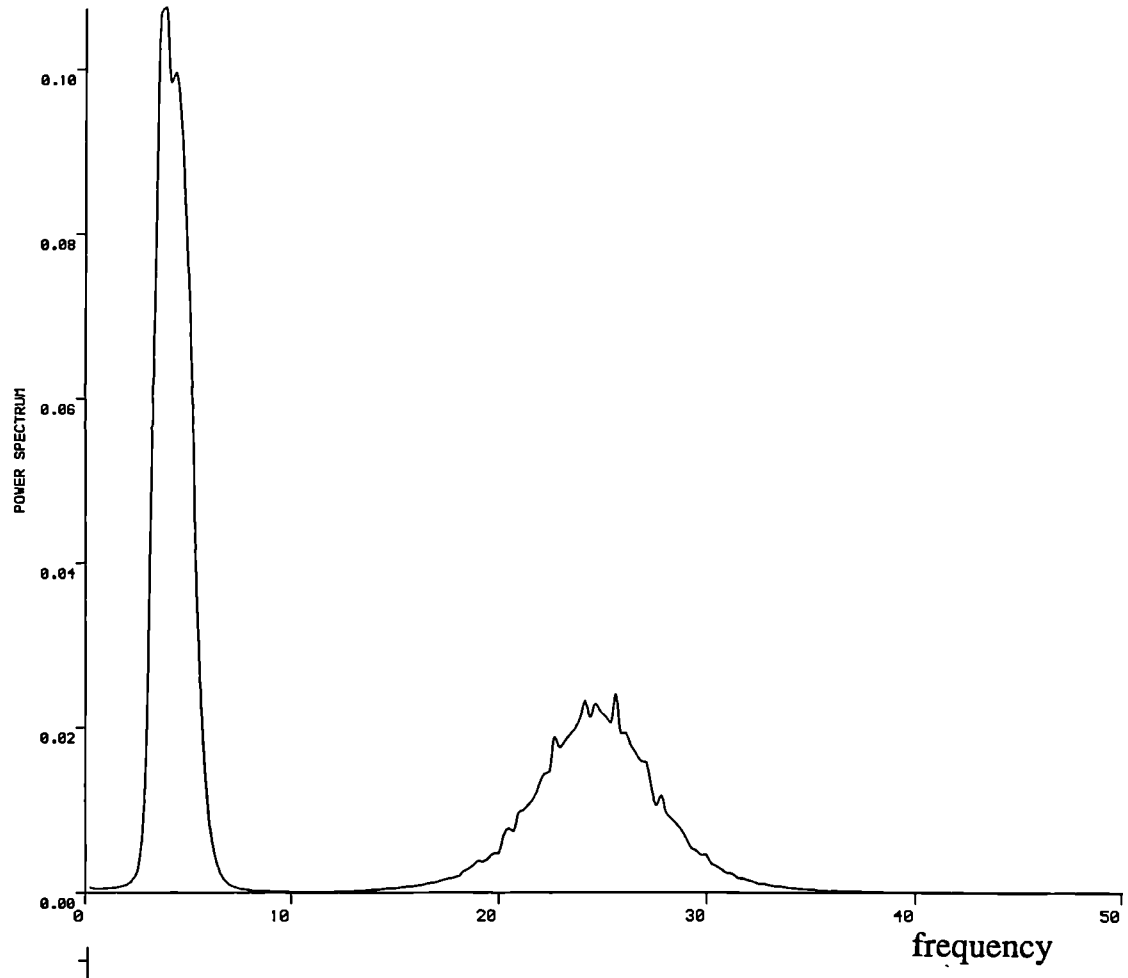


Figure 6.3(a). Power Spectral Density plot computed from data set 1

$$\frac{(\text{response})^2}{\text{Hz}}$$



First four seconds of data set 1

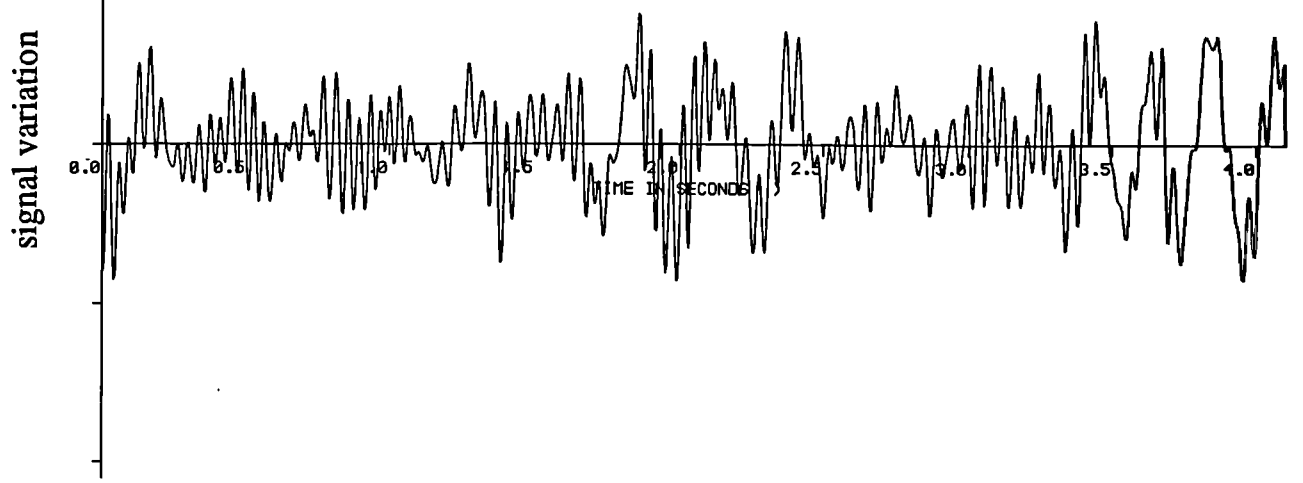
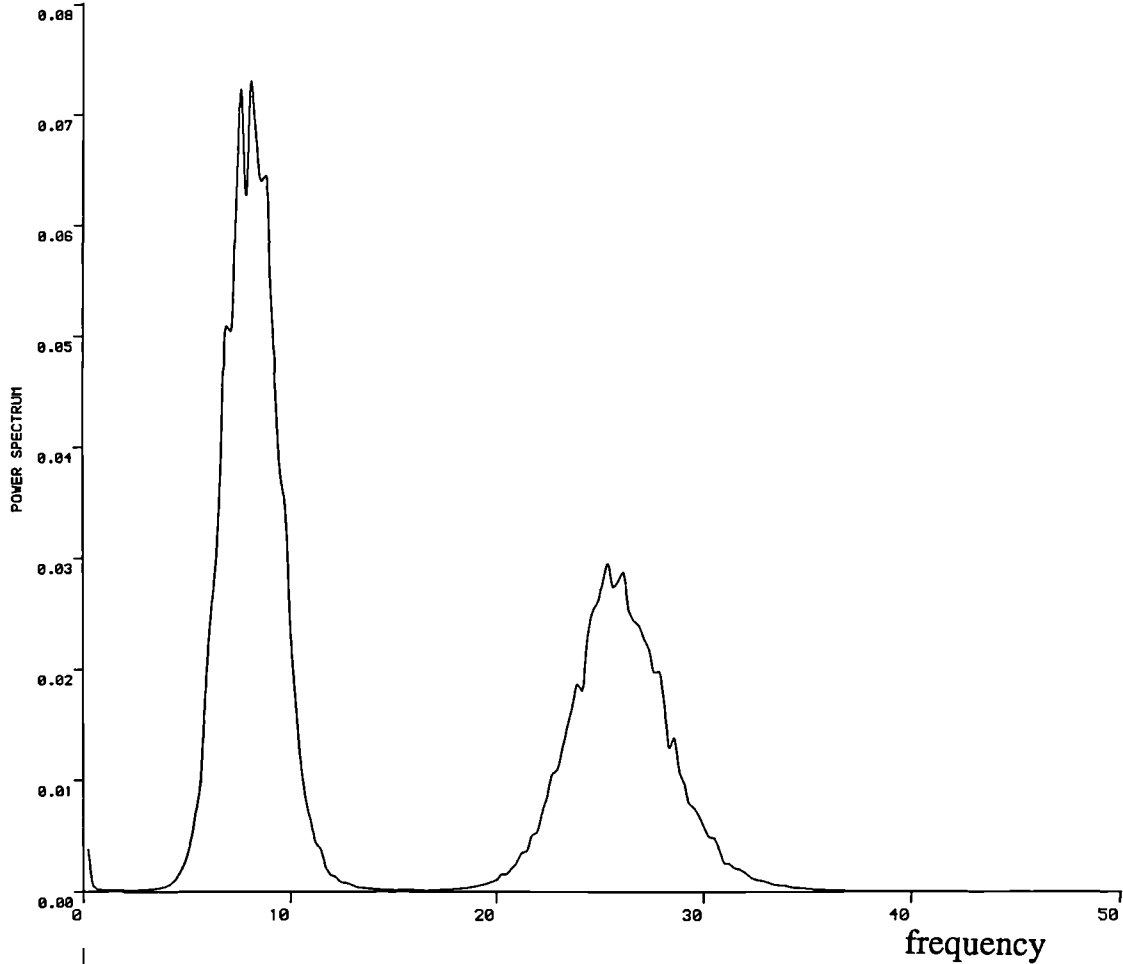


Figure 6.3(b). Power Spectral Density plot computed from data set 2

$$\frac{(\text{response})^2}{\text{Hz}}$$



First four seconds of data set 2

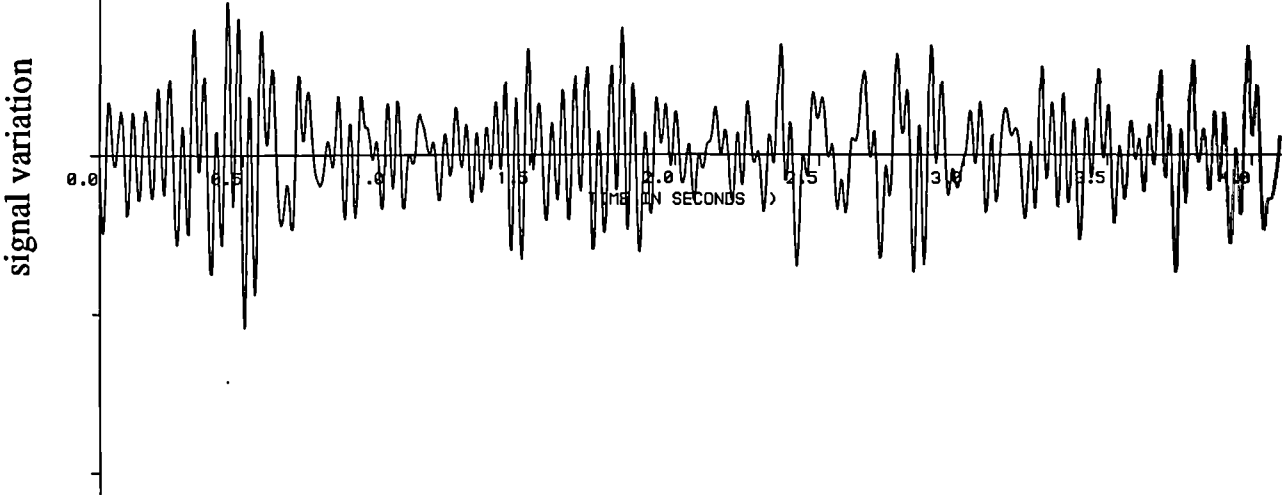
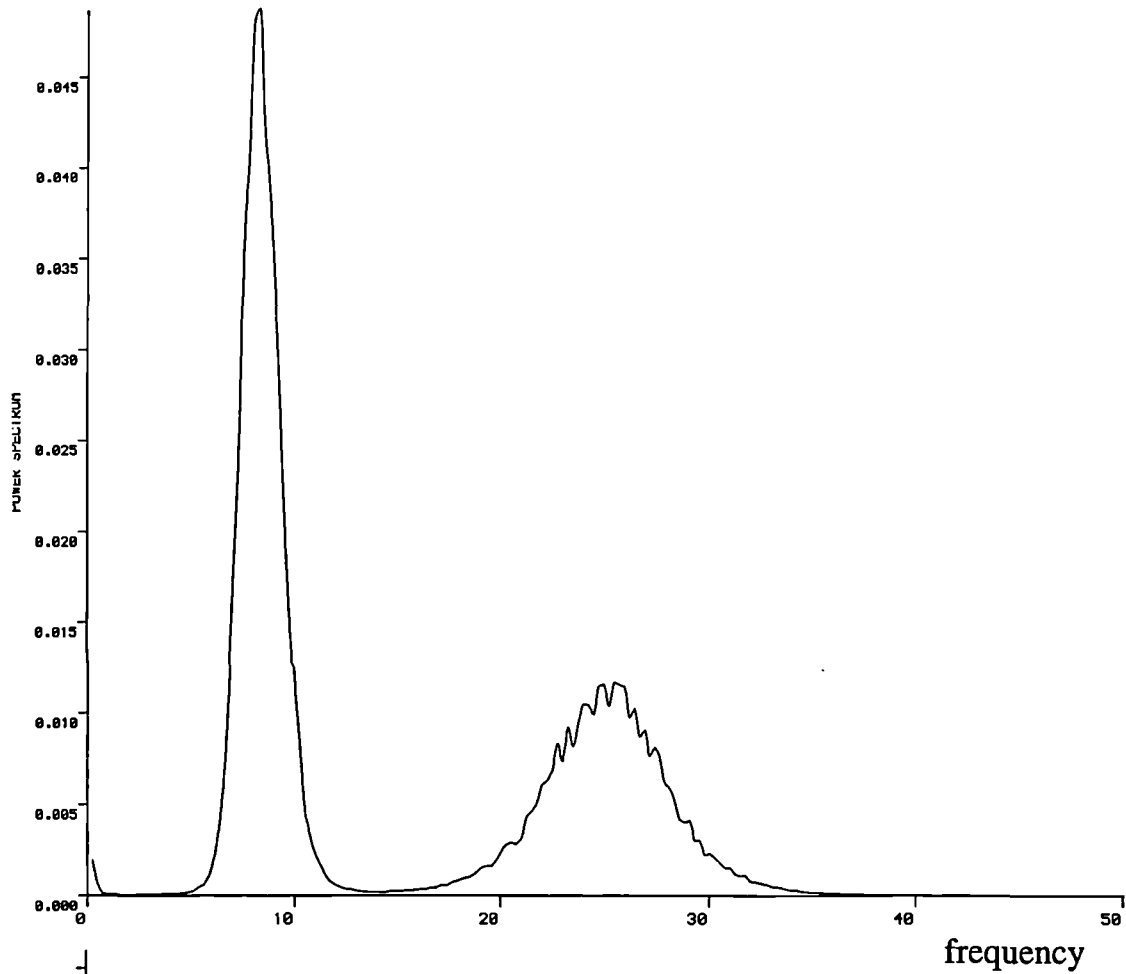


Figure 6.3(c). Power Spectral Density plot computed from data set 3

$$\frac{(\text{response})^2}{\text{Hz}}$$



First four seconds of data set 3

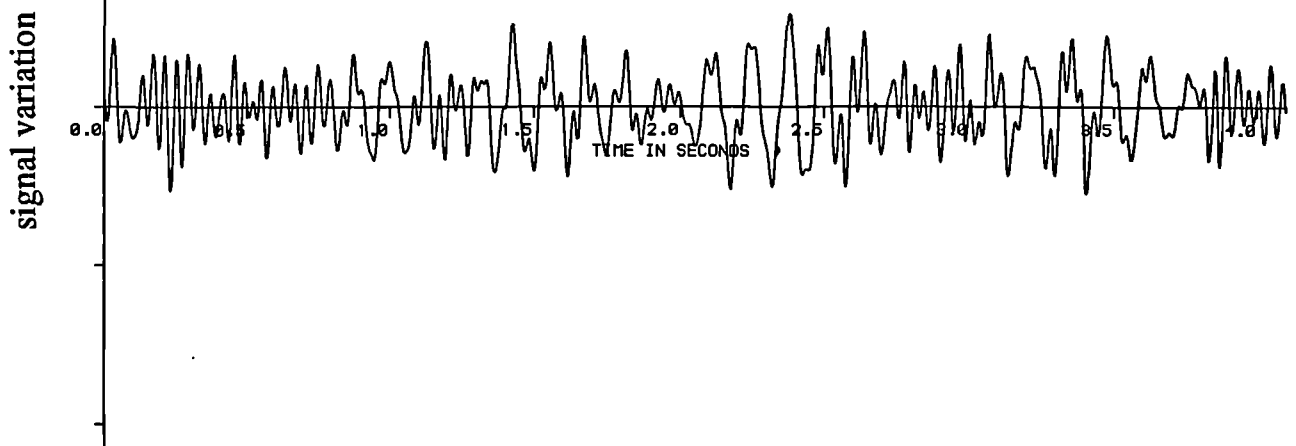
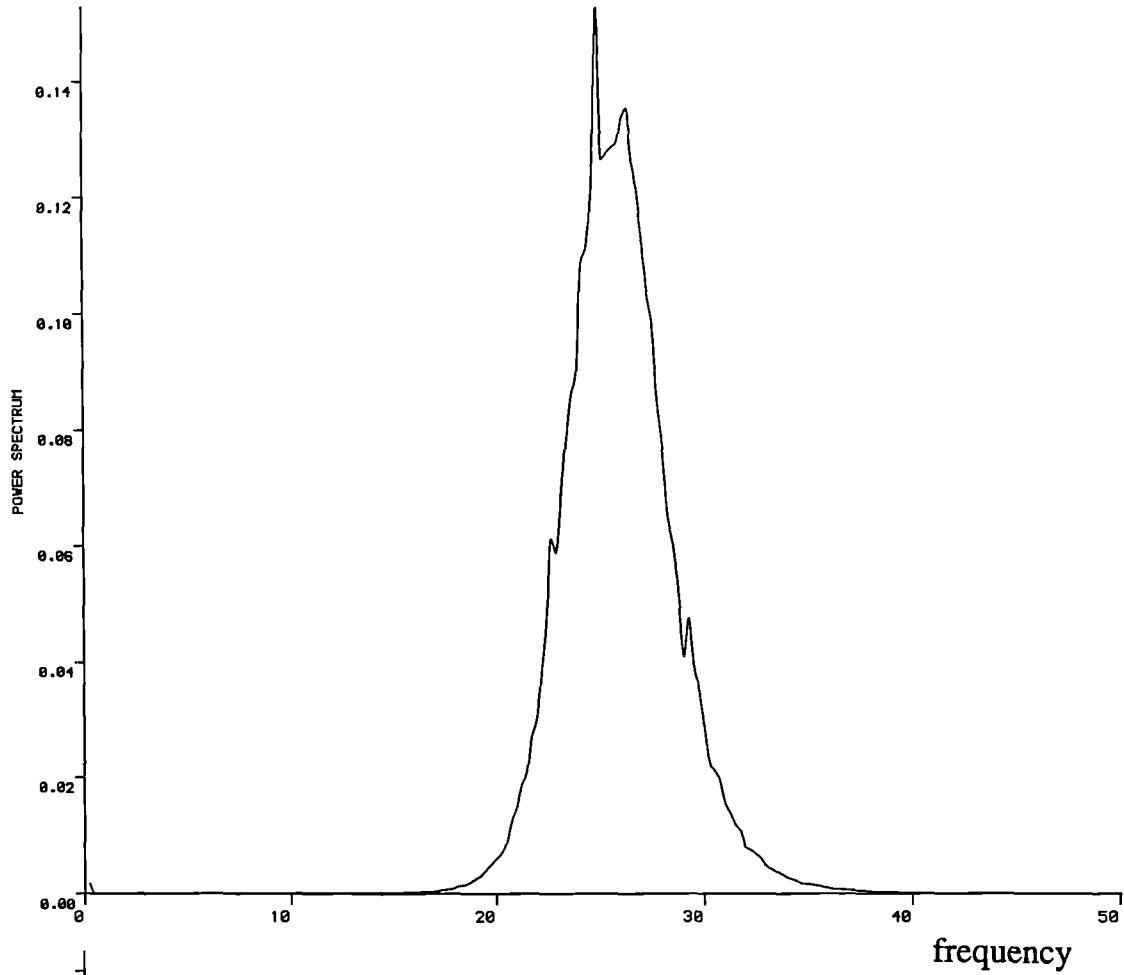


Figure 6.3(d). Power Spectral Density plot
computed from data set 4

$$\frac{(\text{response})^2}{\text{Hz}}$$



First four seconds of data set 4

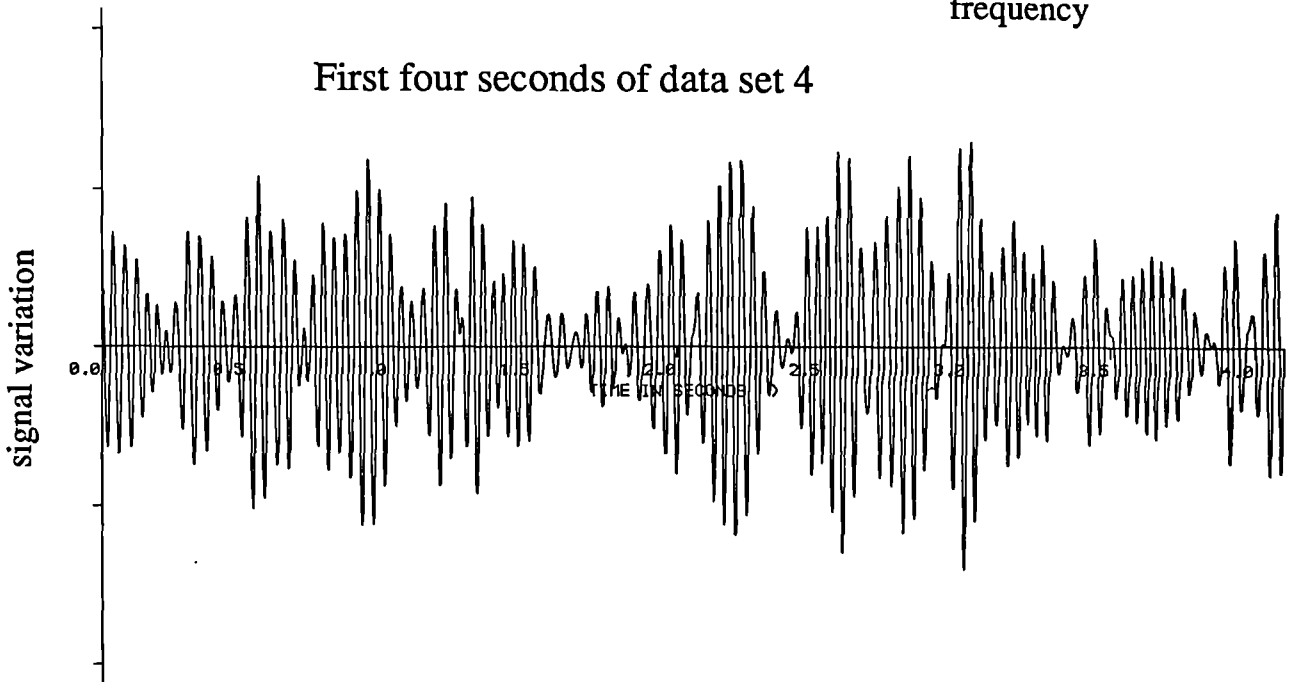
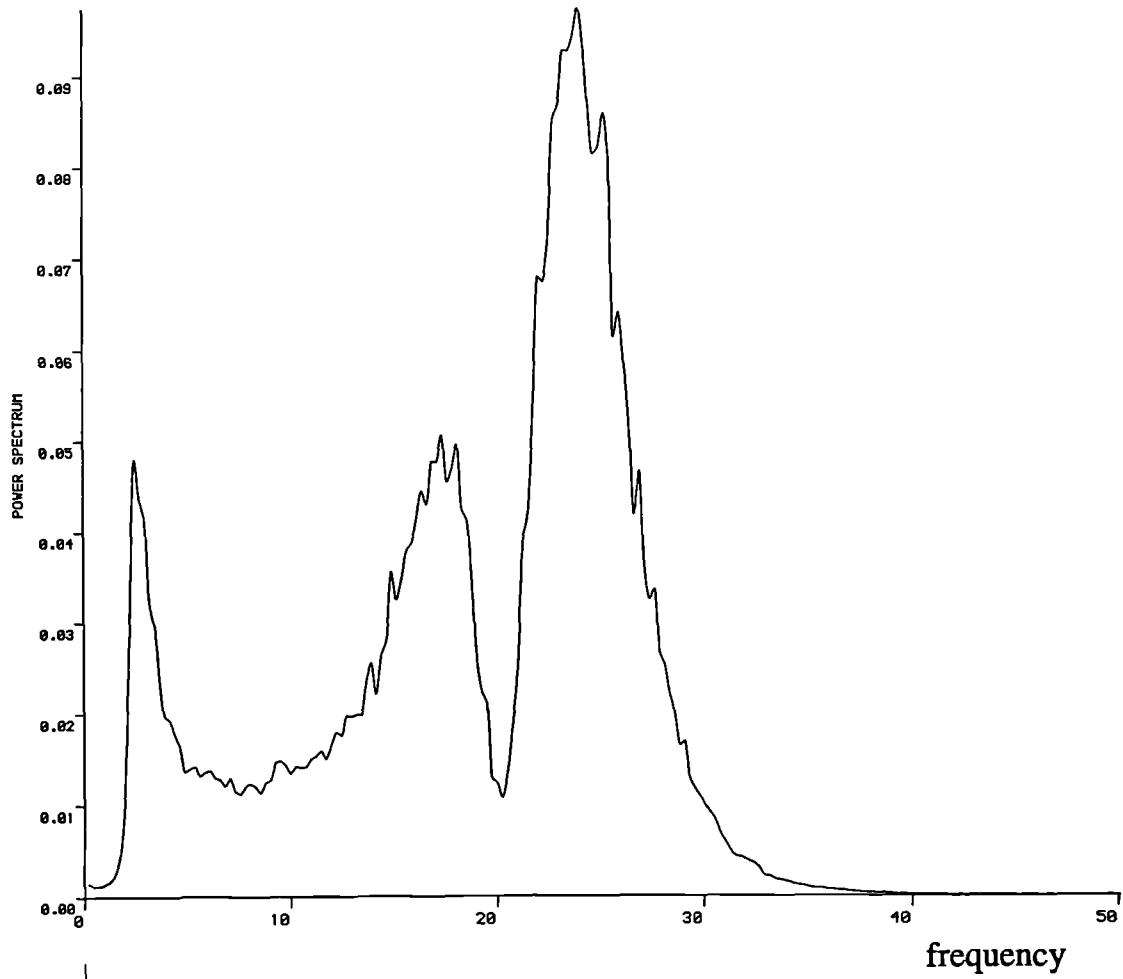


Figure 6.3(e). Power Spectral Density plot computed from data set 5

$$\frac{(\text{response})^2}{\text{Hz}}$$



First four seconds of data set 5

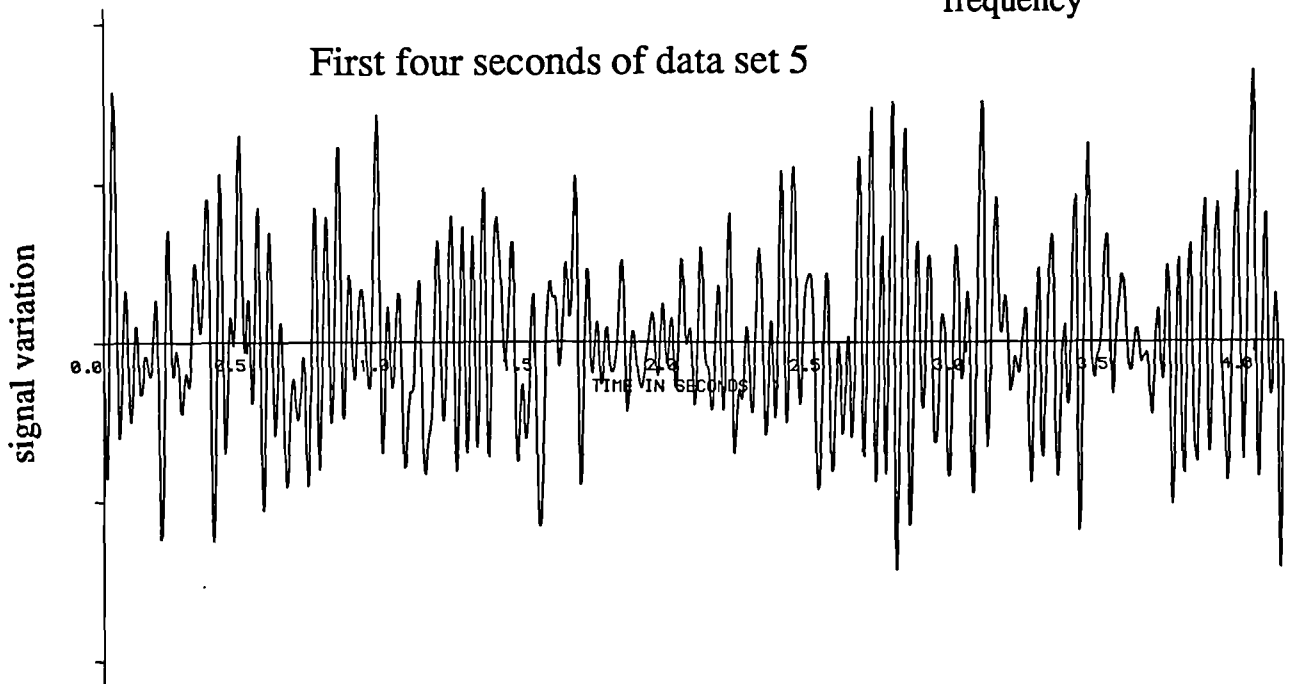
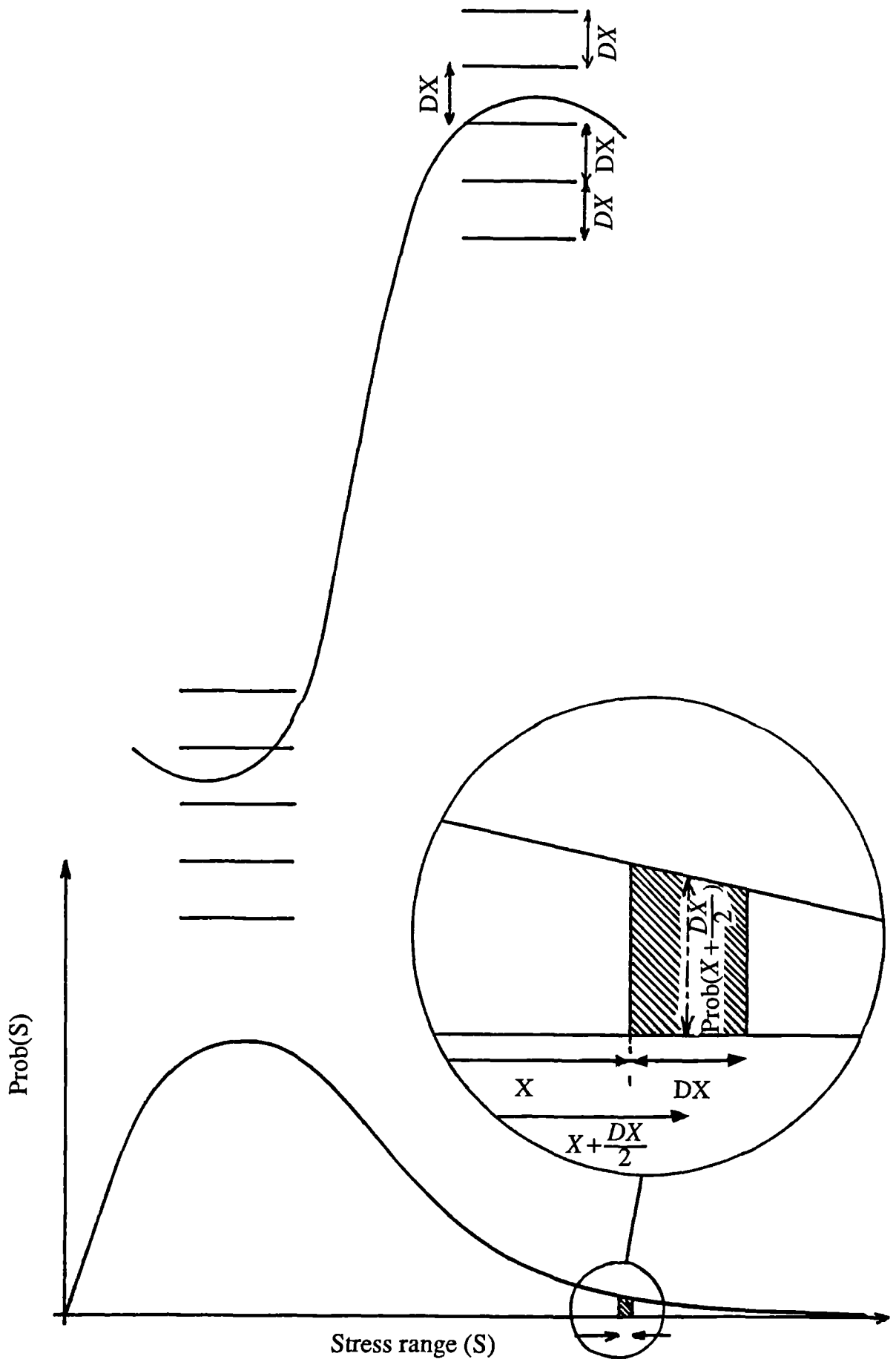


Figure 6.4. The effect of quantisation of the signal on the range distributions.



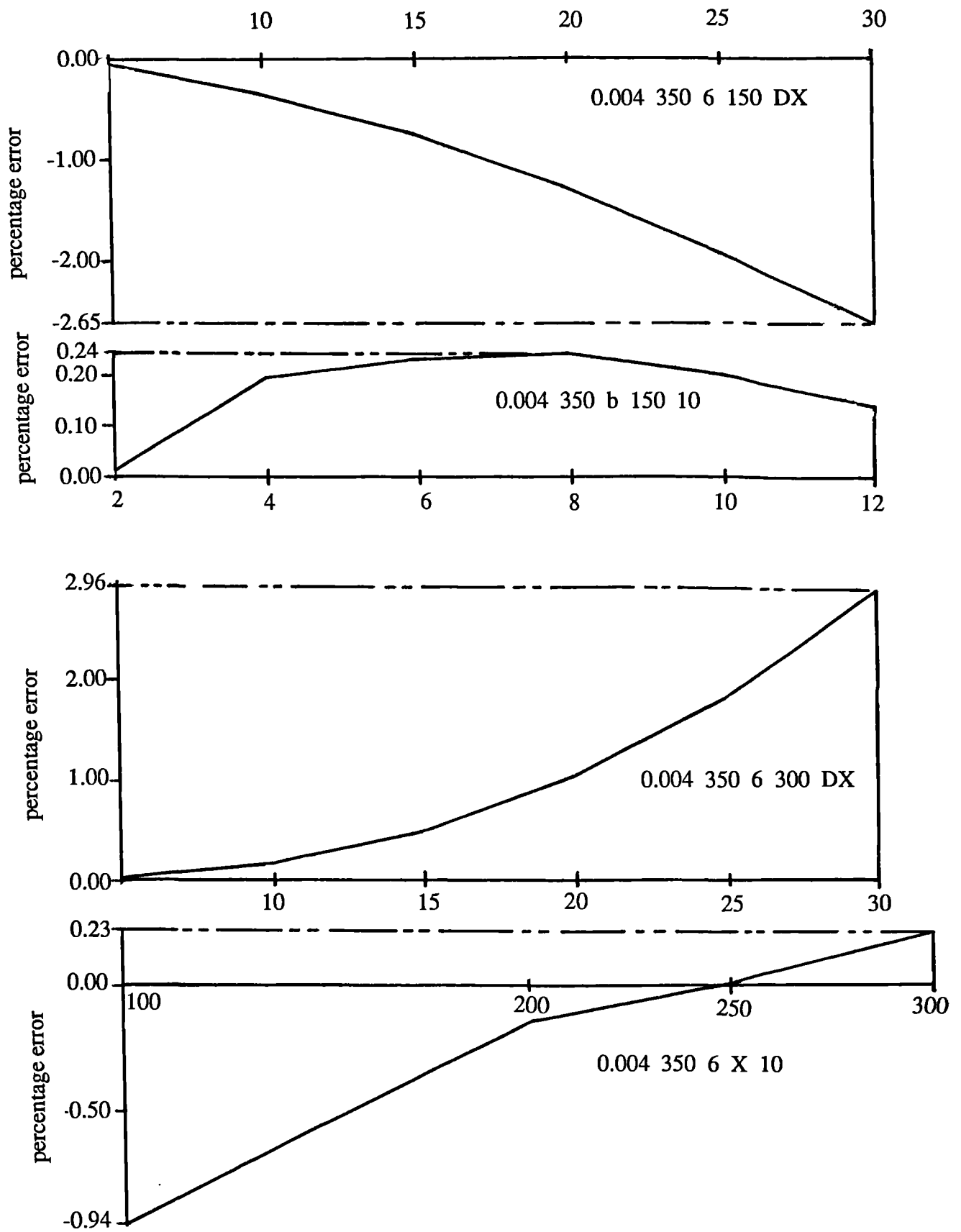


Figure 6.5. A study of the percentage error caused by the moment integration elemental strip width (DX), for various values of (b), the slope of the S-N curve, (x) the range value and (A) and (D), the vertical and horizontal axis intersections with a straight line representing the range distribution.

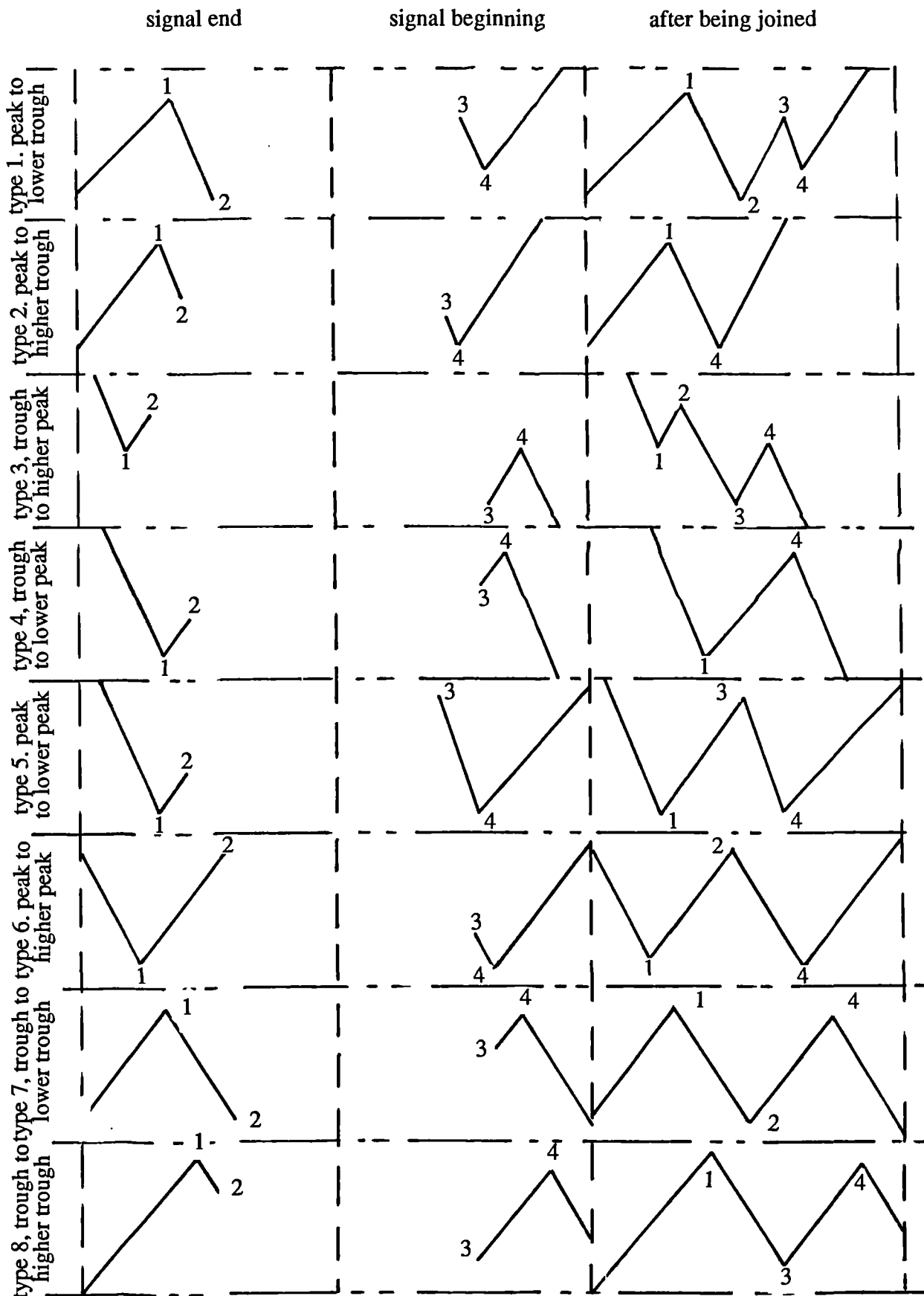


Figure 6.6. The eighth possible combinations of the signal tails shown along with the most justifiable method of joining the ends together.

Figure 6.7(a). Comparison of ordinary ranges computed directly from full data set with ordinary ranges computed from PSD of full data set using equation 3.4.

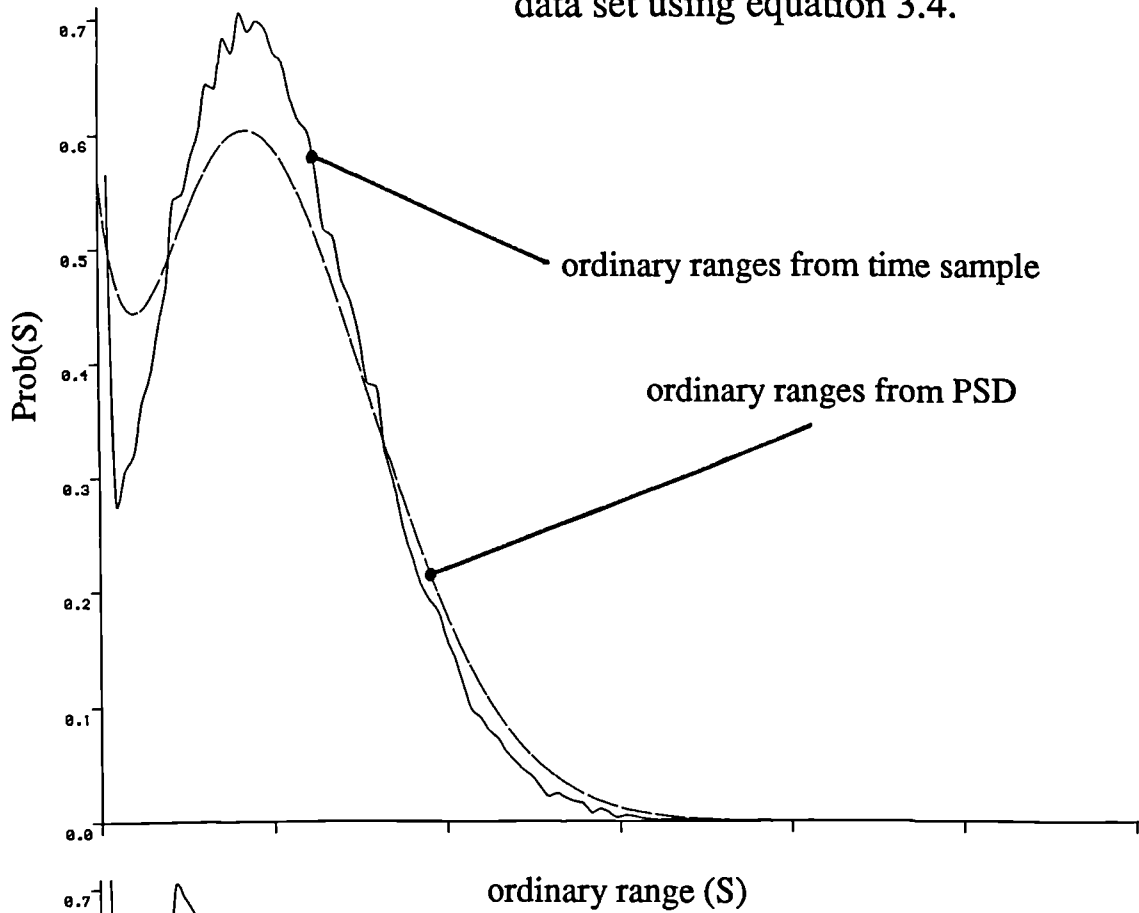


Figure 6.7(b). Comparison of rainflow ranges computed directly from full data set with rainflow ranges computed from PSD of full data set using equation 3.5.

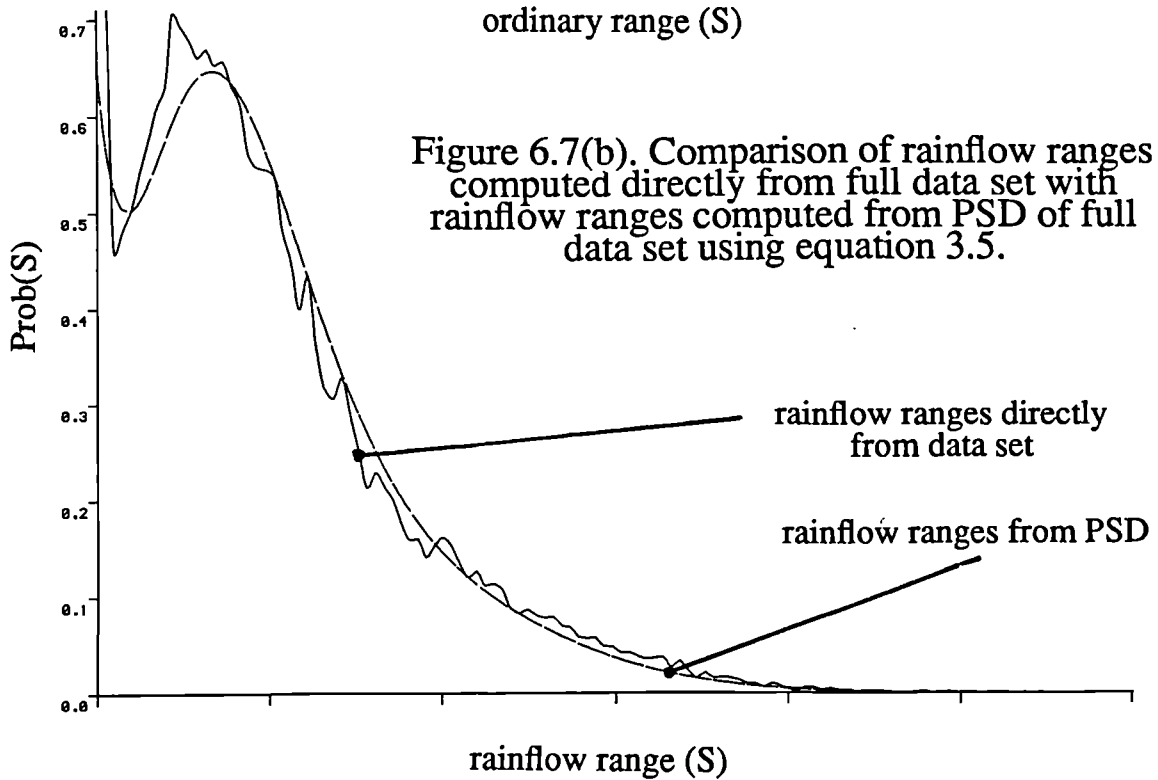


Figure 6.8(a). Moments of ordinary ranges shown in figure 6.7(a)

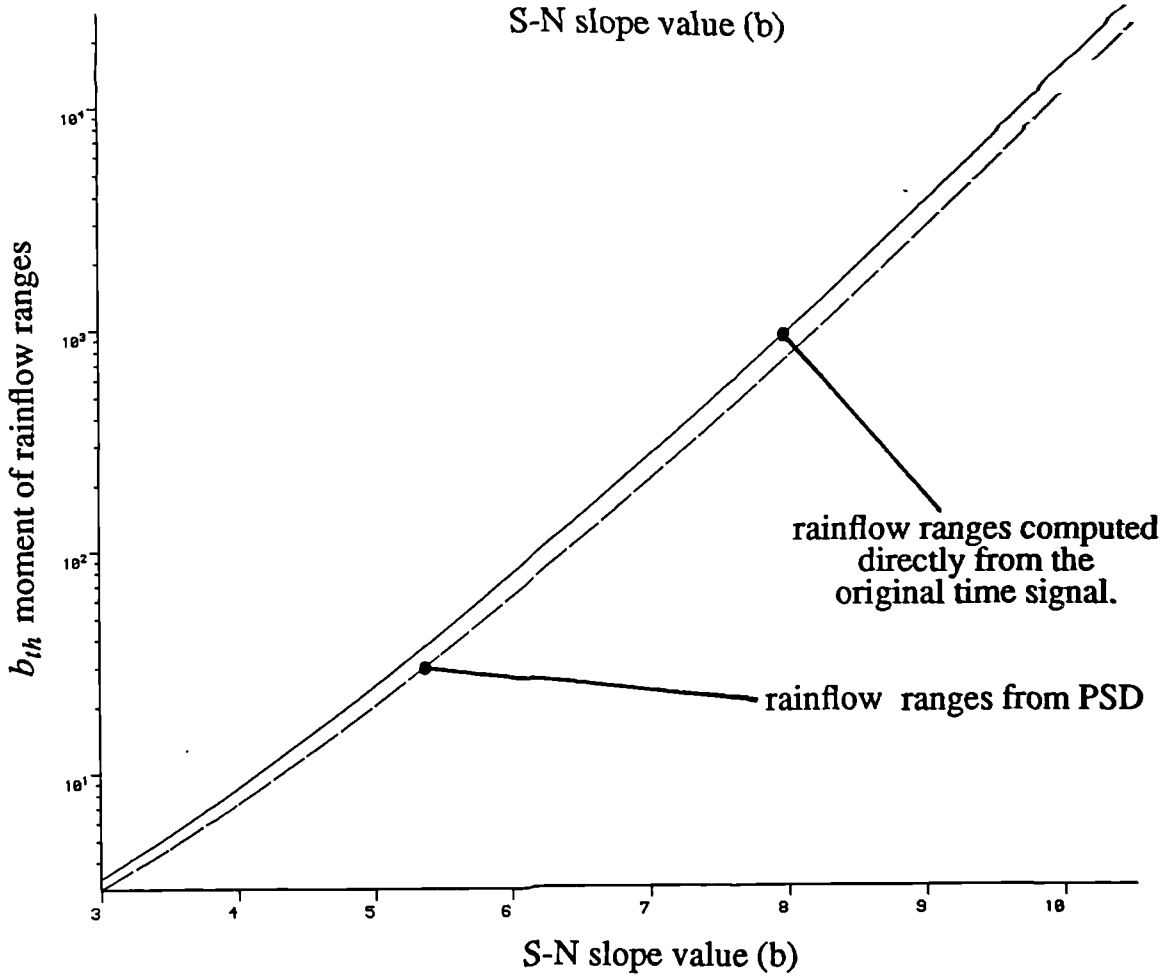
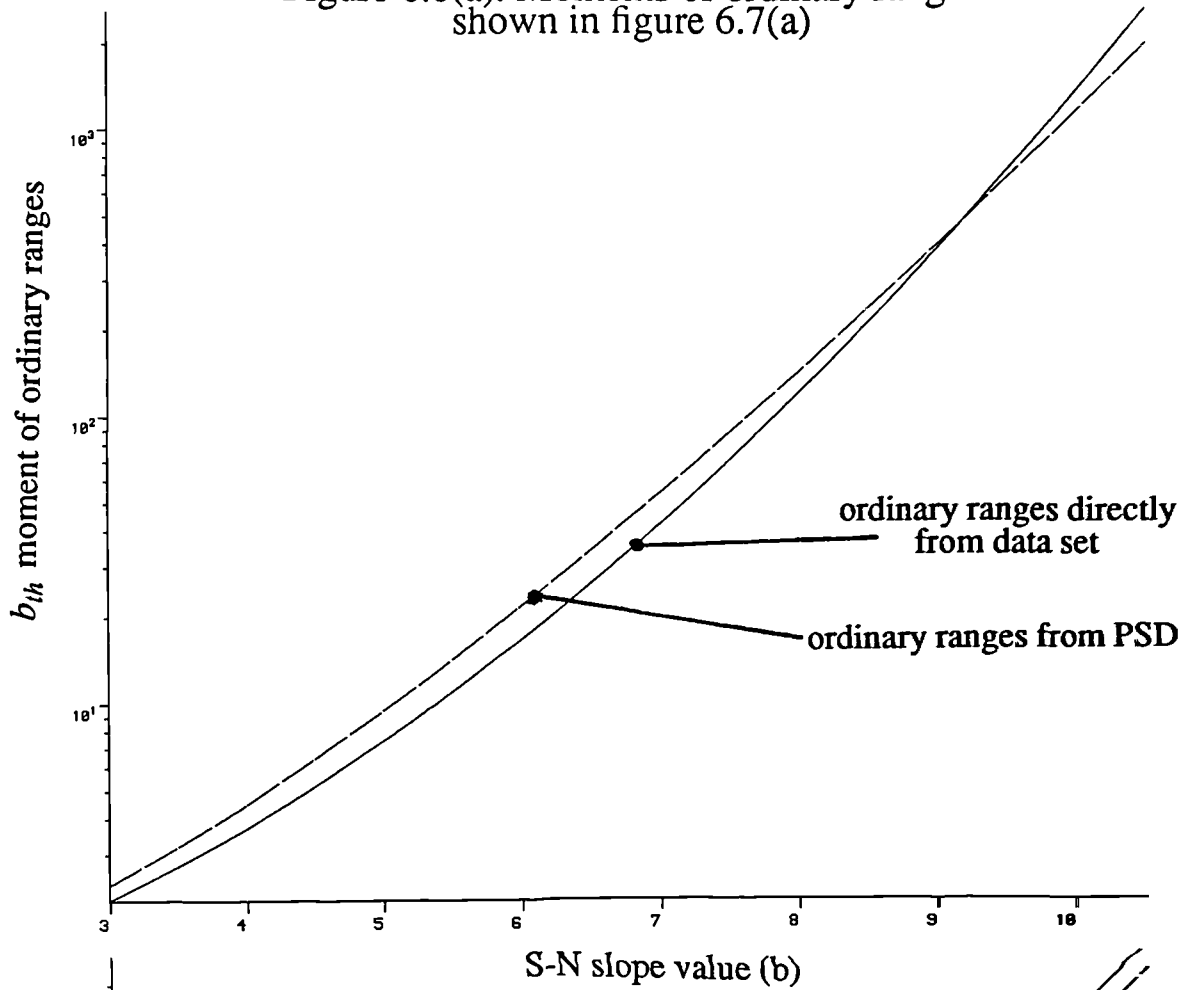


Figure 6.8(b). Moments of rainflow ranges shown in figure 6.7(h)

Figure 6.9. Moments of rainflow ranges from data set 2

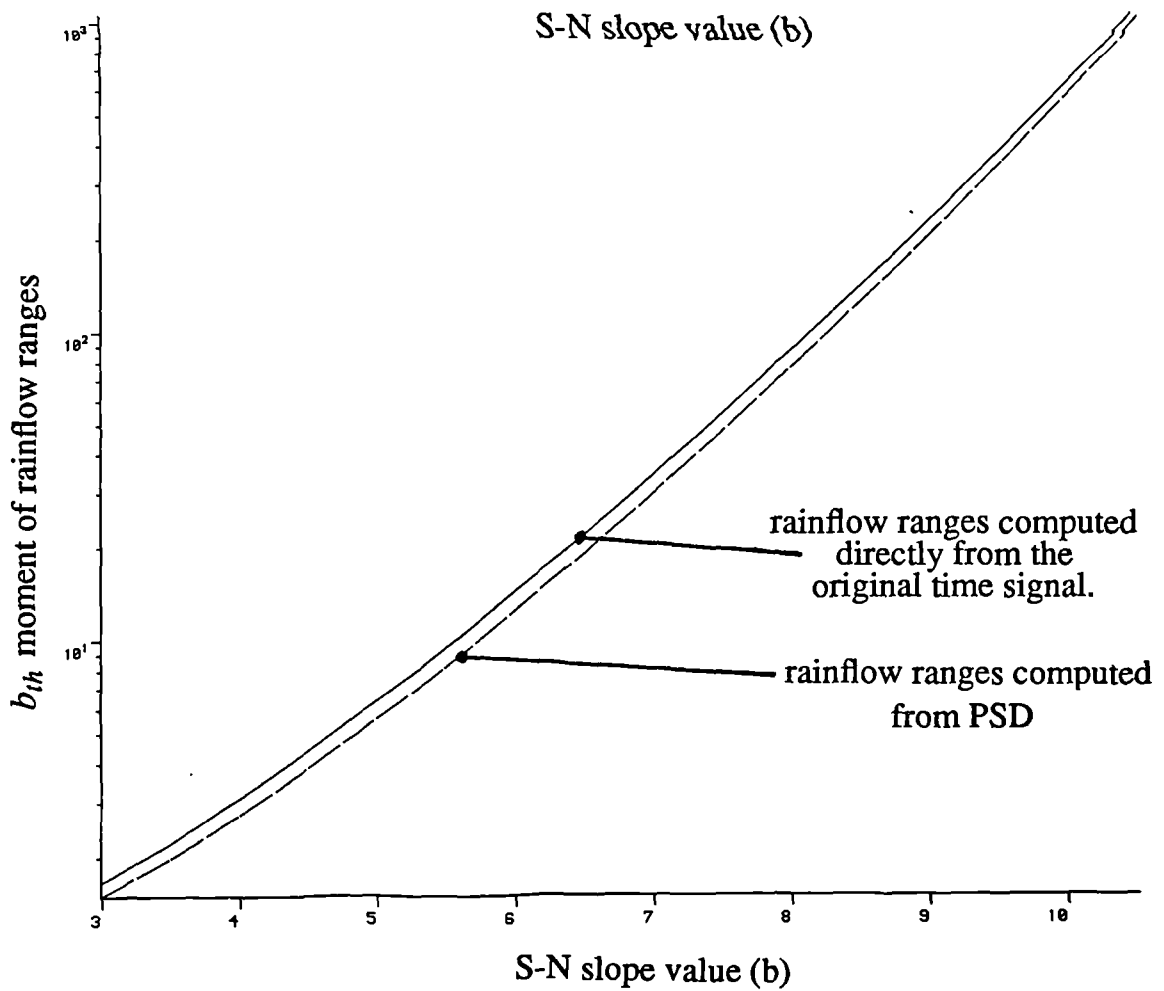
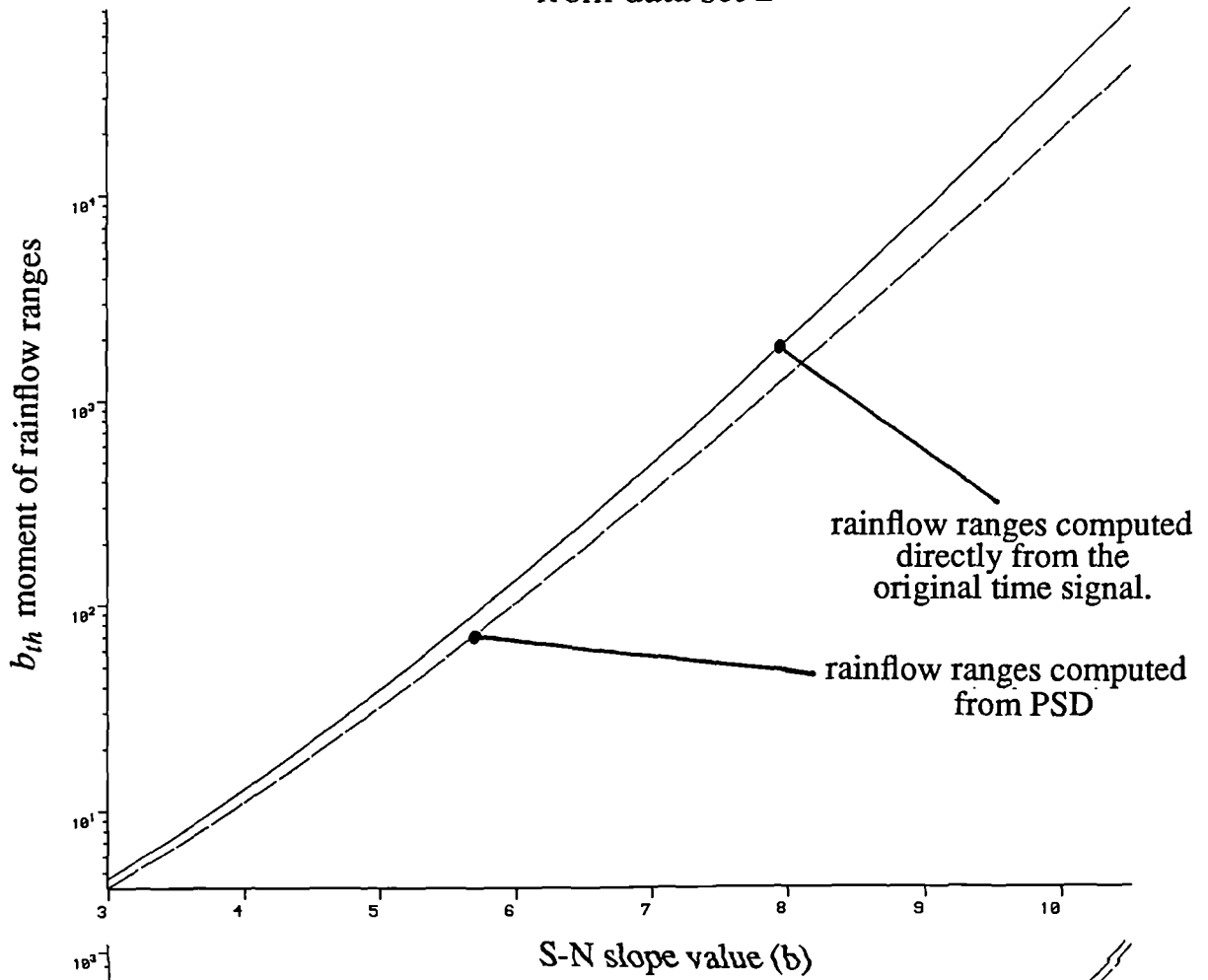


Figure 6.10. Moments of rainflow ranges from data set 2

Figure 6.11. Moments of rainflow ranges from data set 4

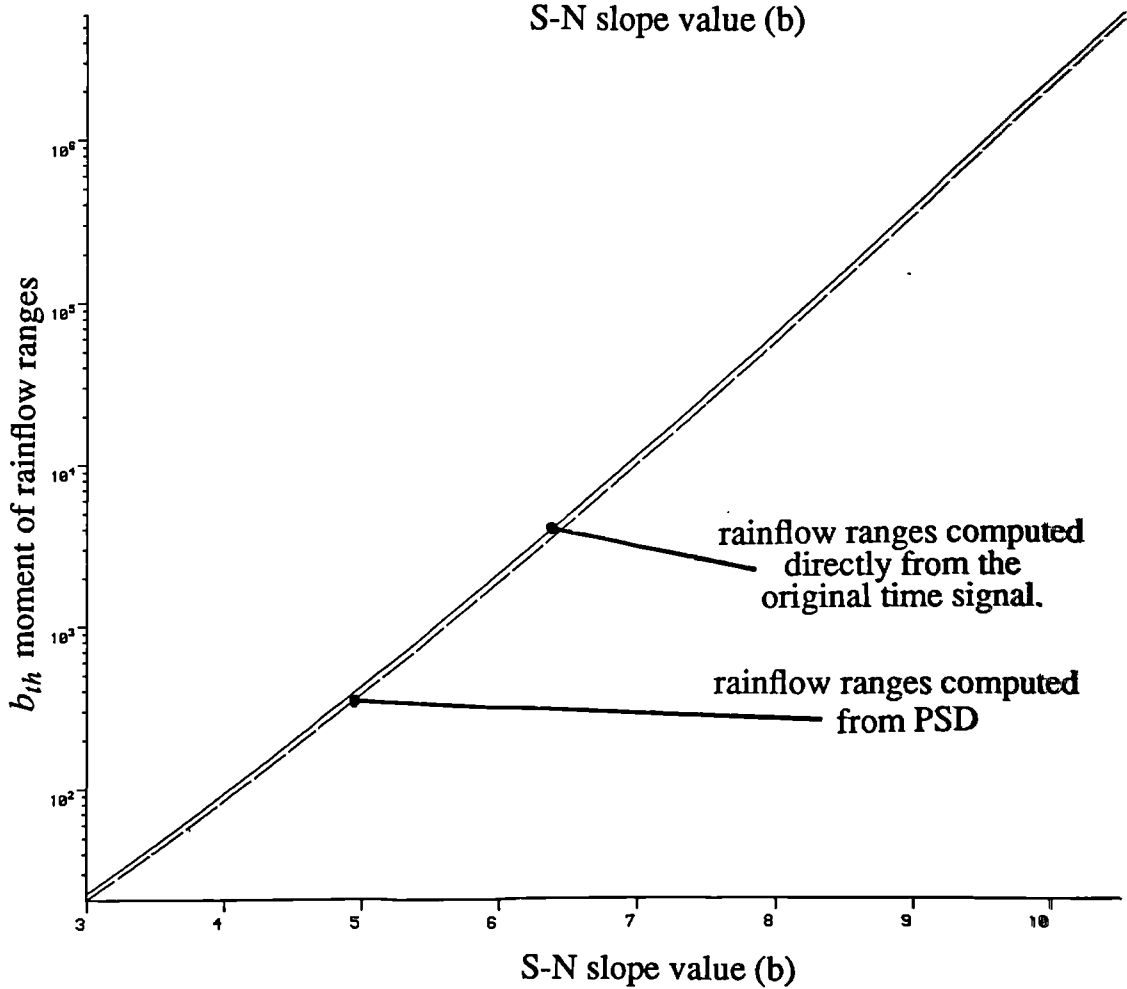
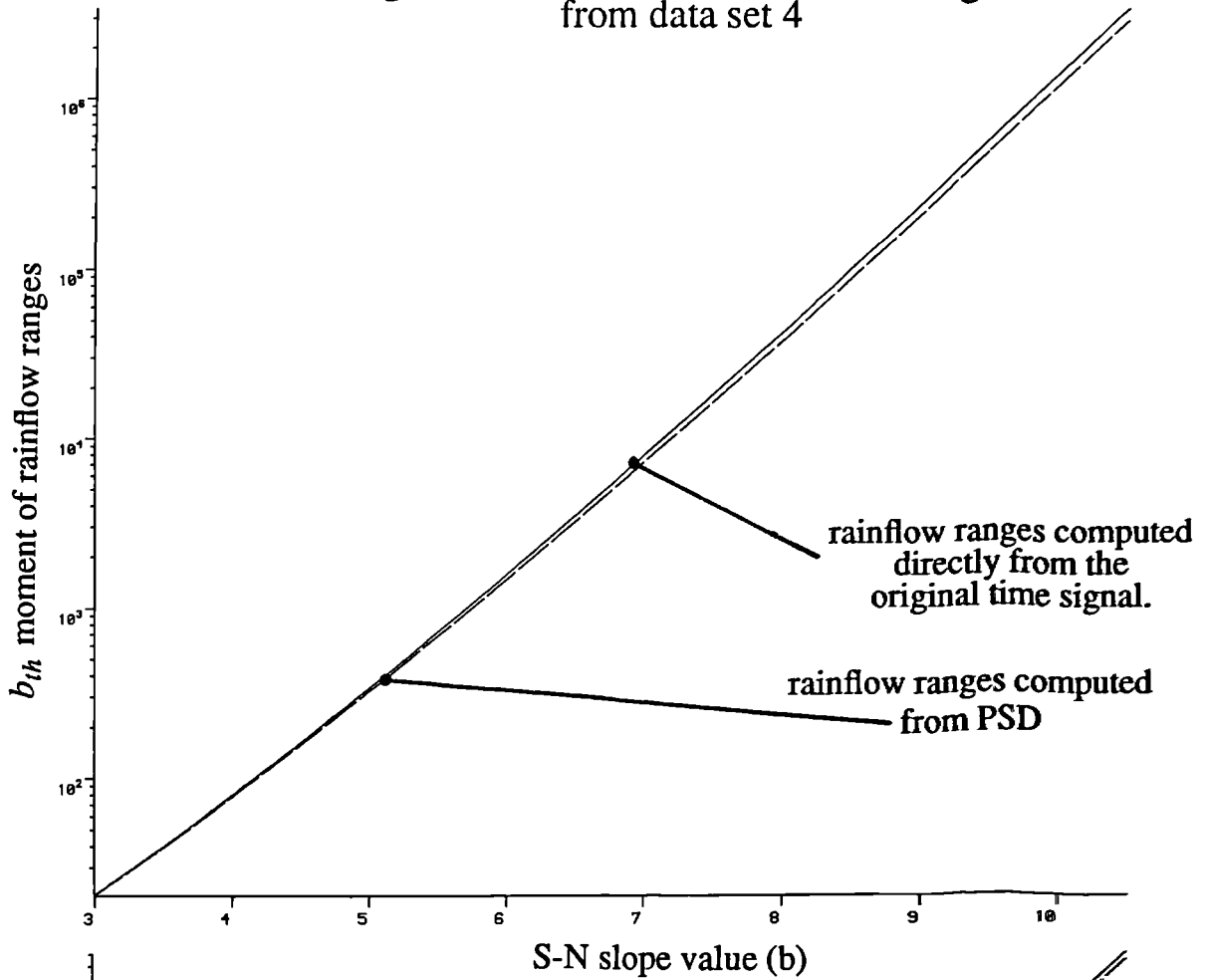


Figure 6.12. Moments of rainflow ranges from data set 5

Figure 6.13(a). Mean signal value of sample, normalised by population mean

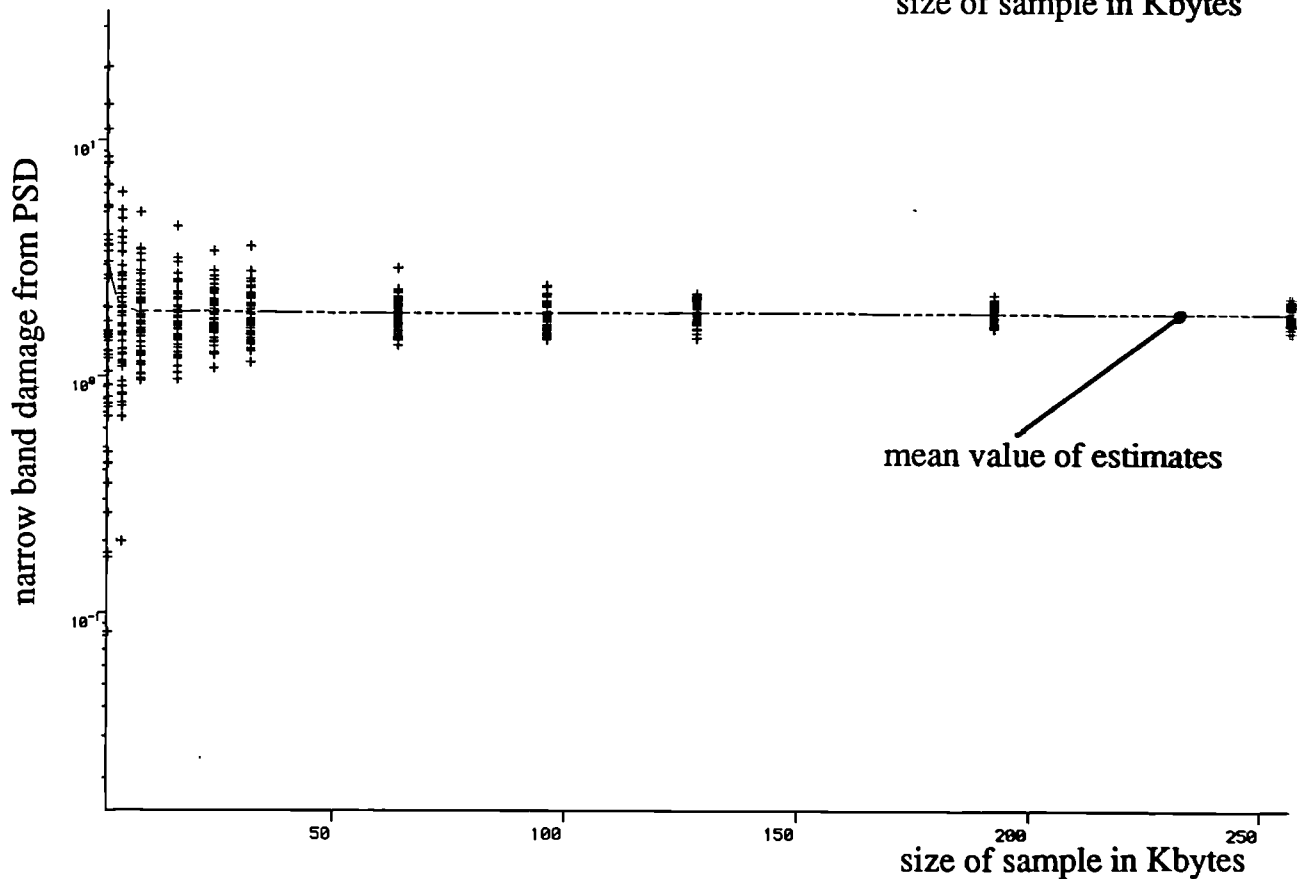
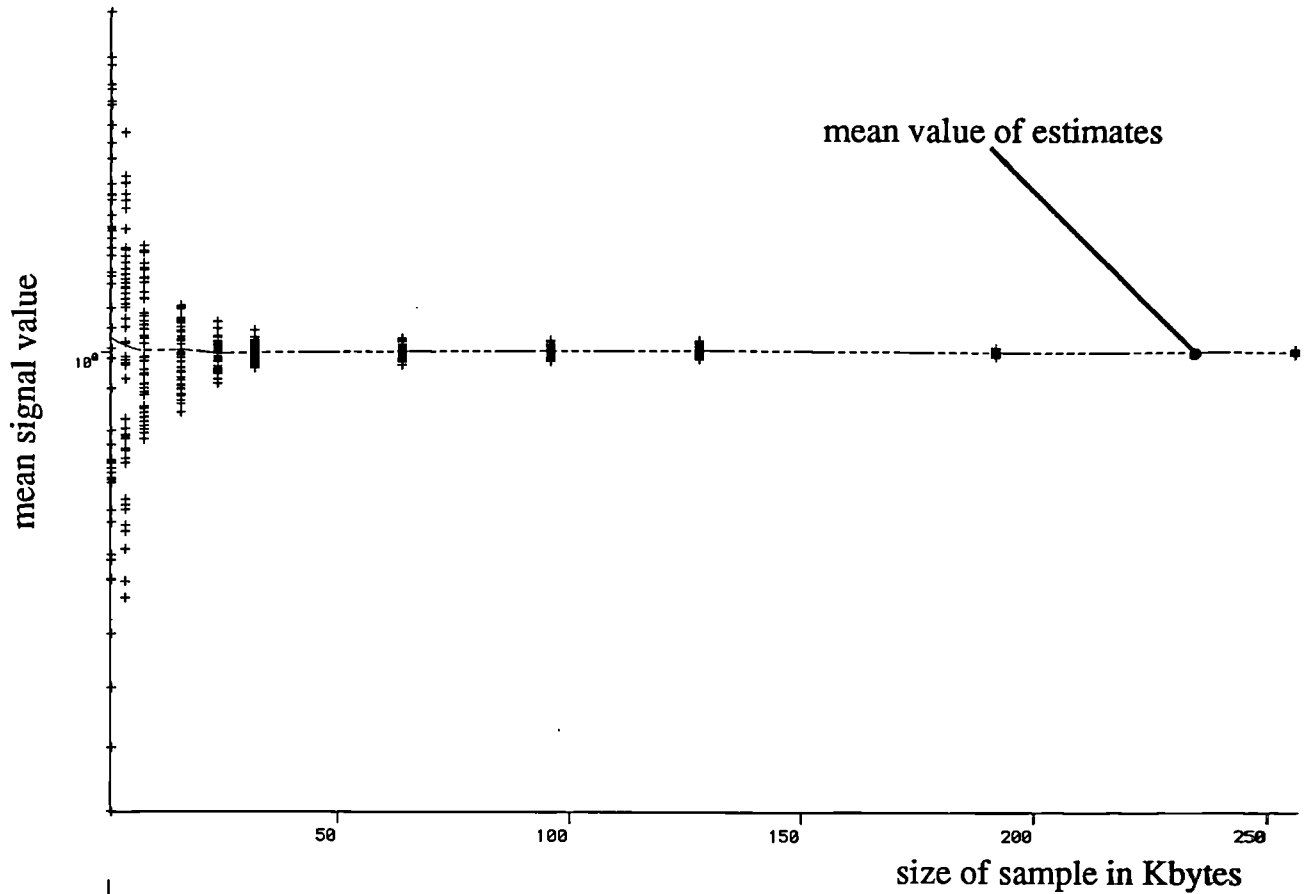


Figure 6.13(b). Narrow band frequency domain prediction of fatigue (using equation 2.58), normalised by rainflow range prediction of time signal ... plotted against sample size

Figure 6.14(a). rms computed from time sample, normalised by population rms ... plotted against sample size

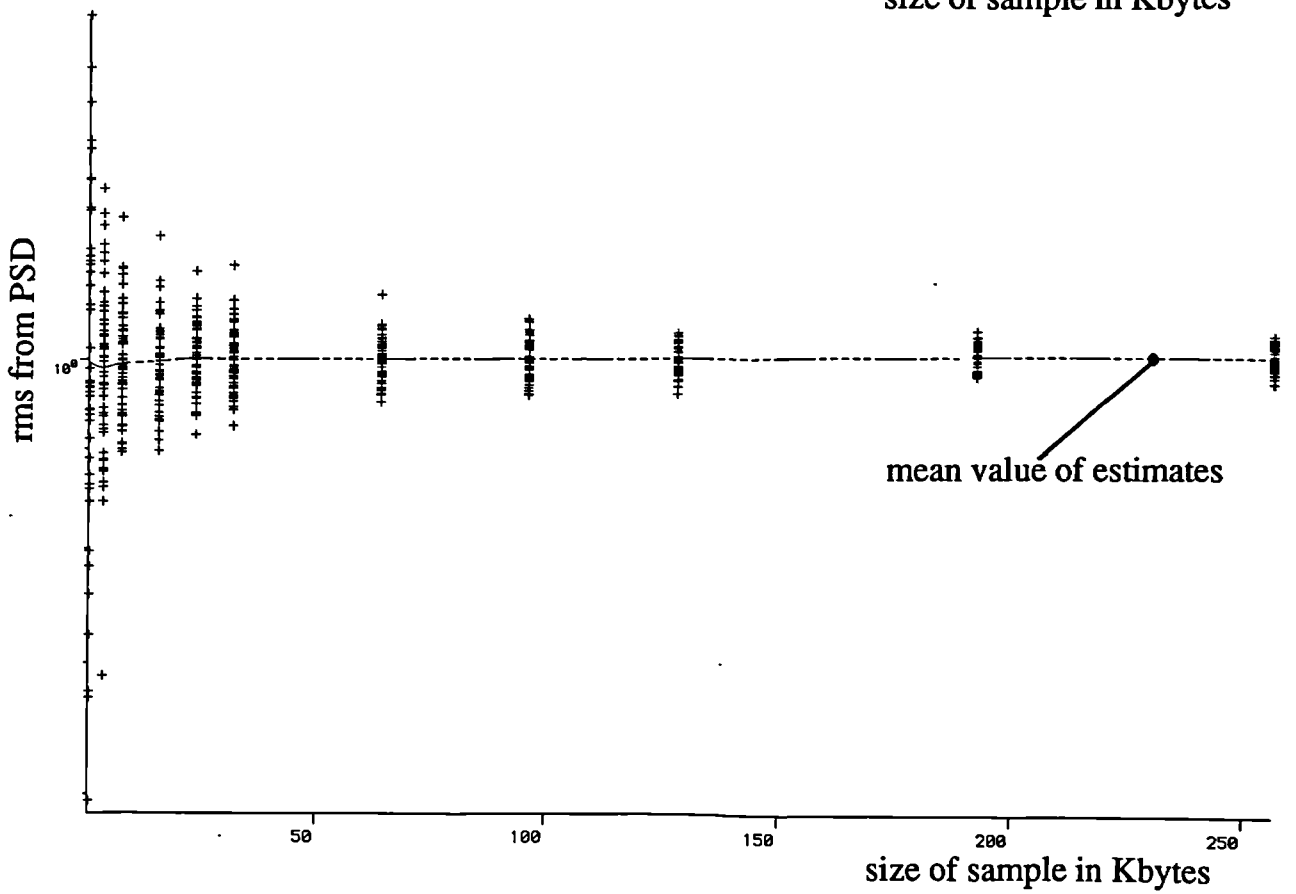
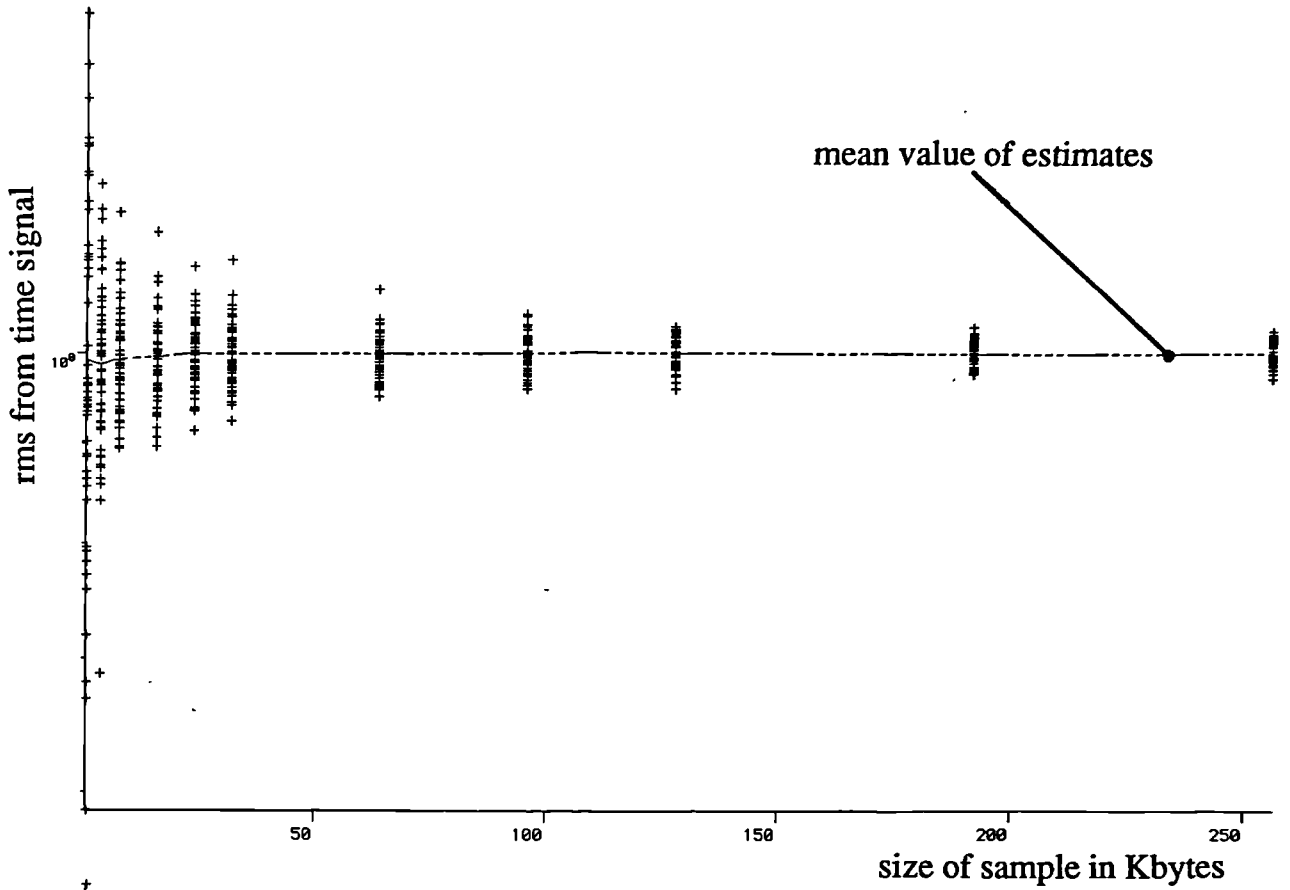


Figure 6.14(b). rms computed from PSD of time sample, normalised by population rms ... plotted against sample size

Figure 6.15(a) Number of peaks per second calculated from PSD of time sample (using equation 2.8), normalised by population number of peaks per second ... plotted against sample size

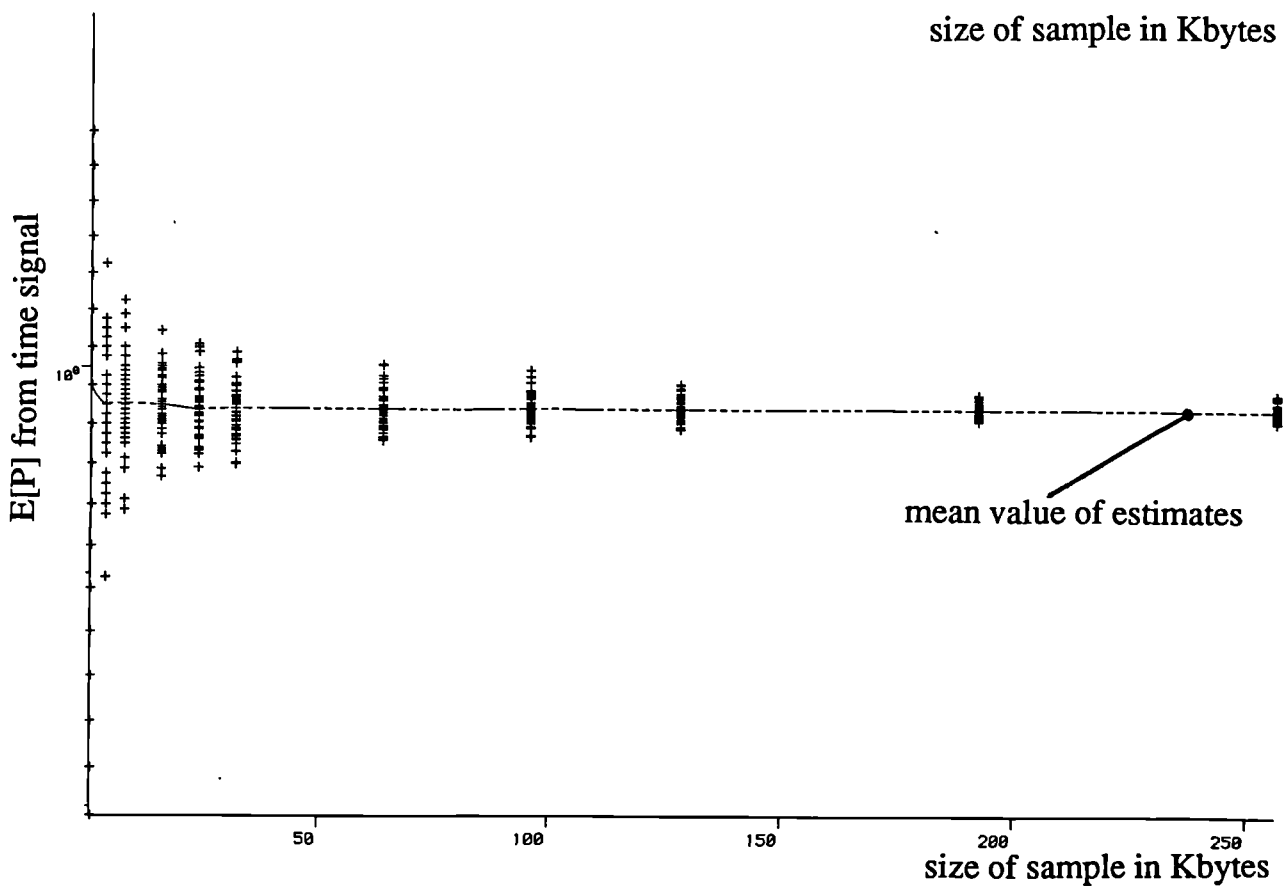
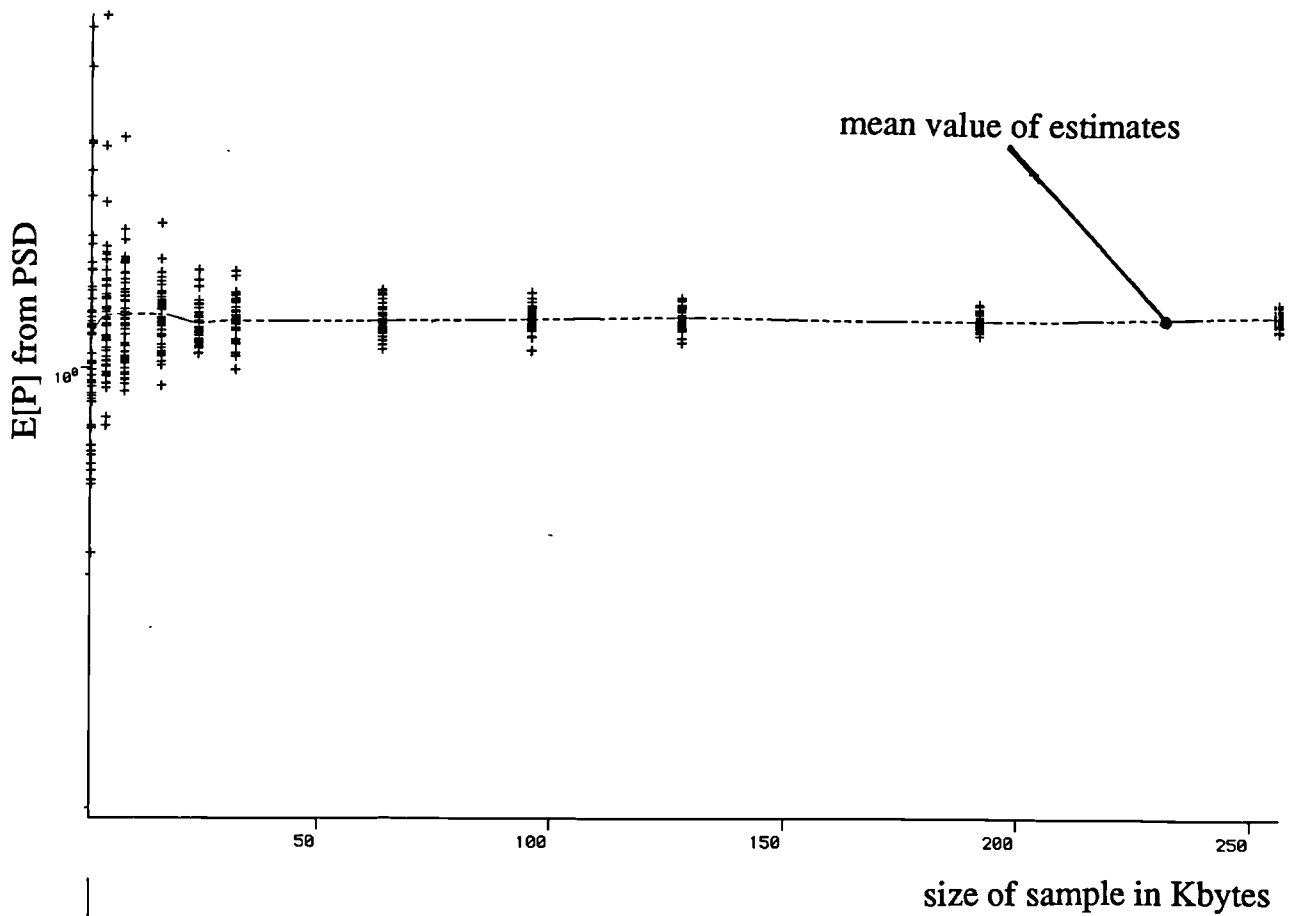


Figure 6.15(b) Number of peaks per second calculated from time sample, normalised by population number of peaks per second ... plotted against sample size

Figure 6.16(a). Ordinary range frequency domain prediction of fatigue (using equation 3.4), normalised by ordinary range prediction from PSD of full time signal ... plotted against sample size

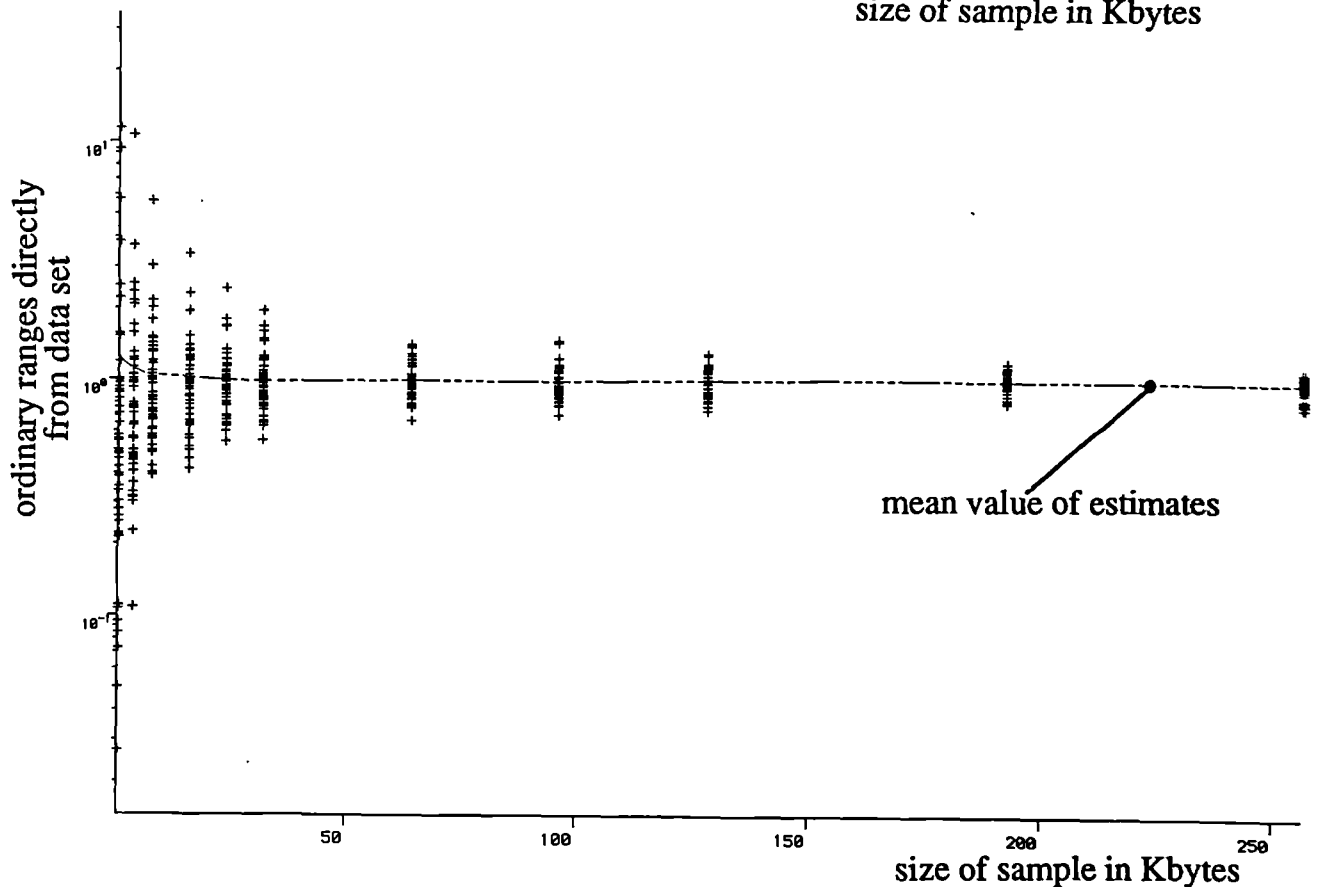
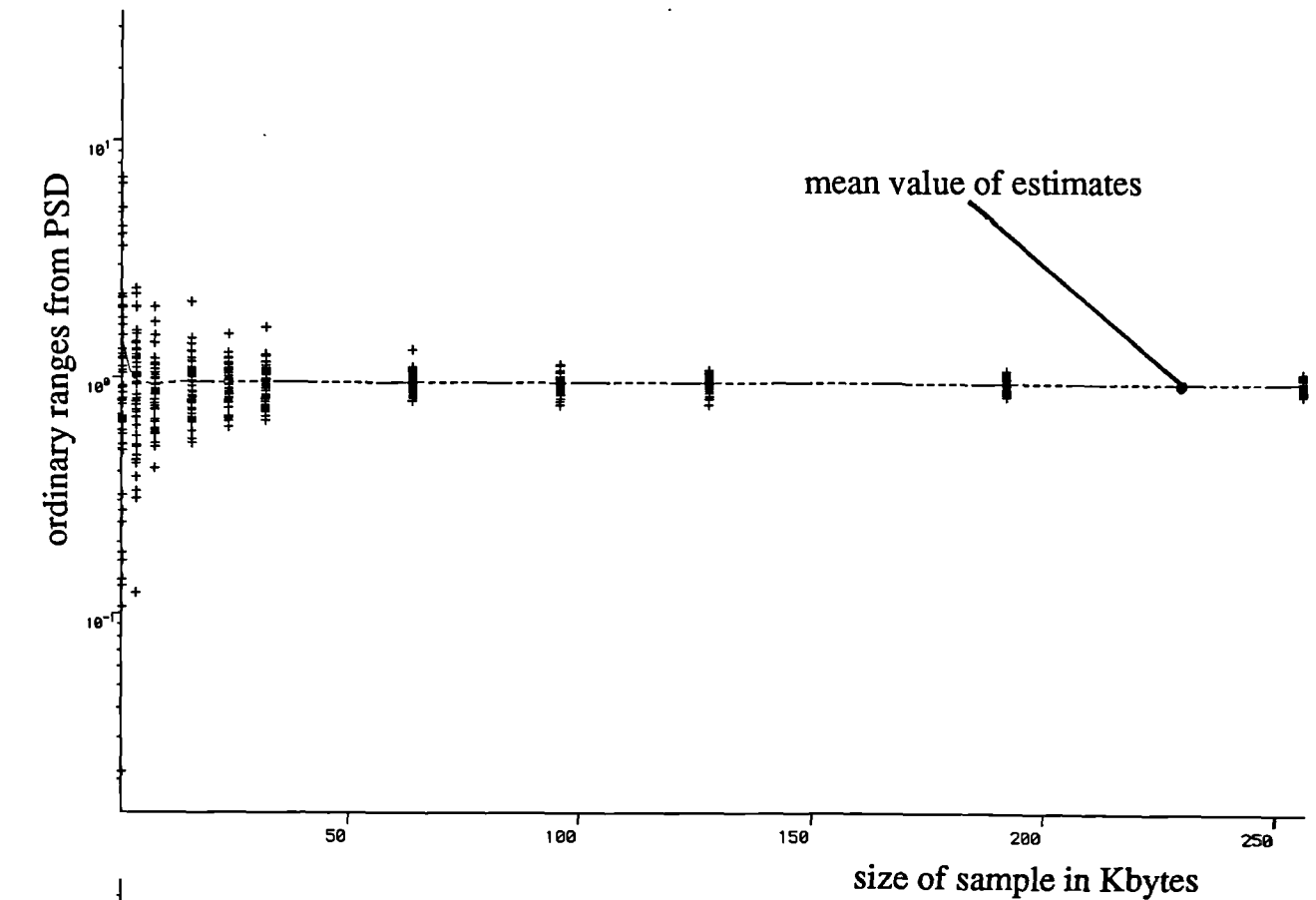


Figure 6.16(b). Ordinary range time domain prediction of fatigue, directly from time signal, normalised by ordinary range prediction on full time signal ... plotted against sample size

Figure 6.17(a). Rainflow range frequency domain prediction of fatigue (using equation 3.5), normalised by rainflow range prediction from PSD of full time signal ... plotted against sample size

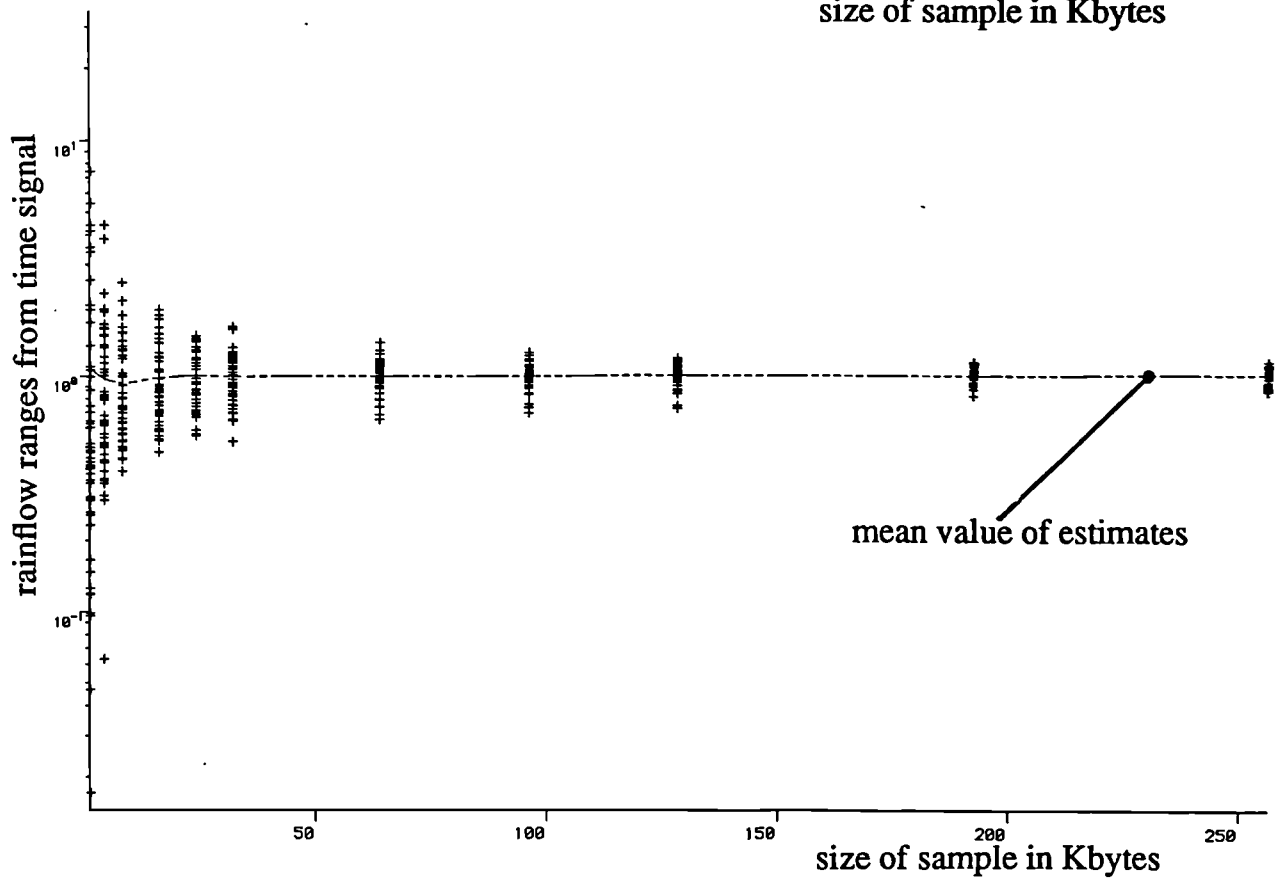
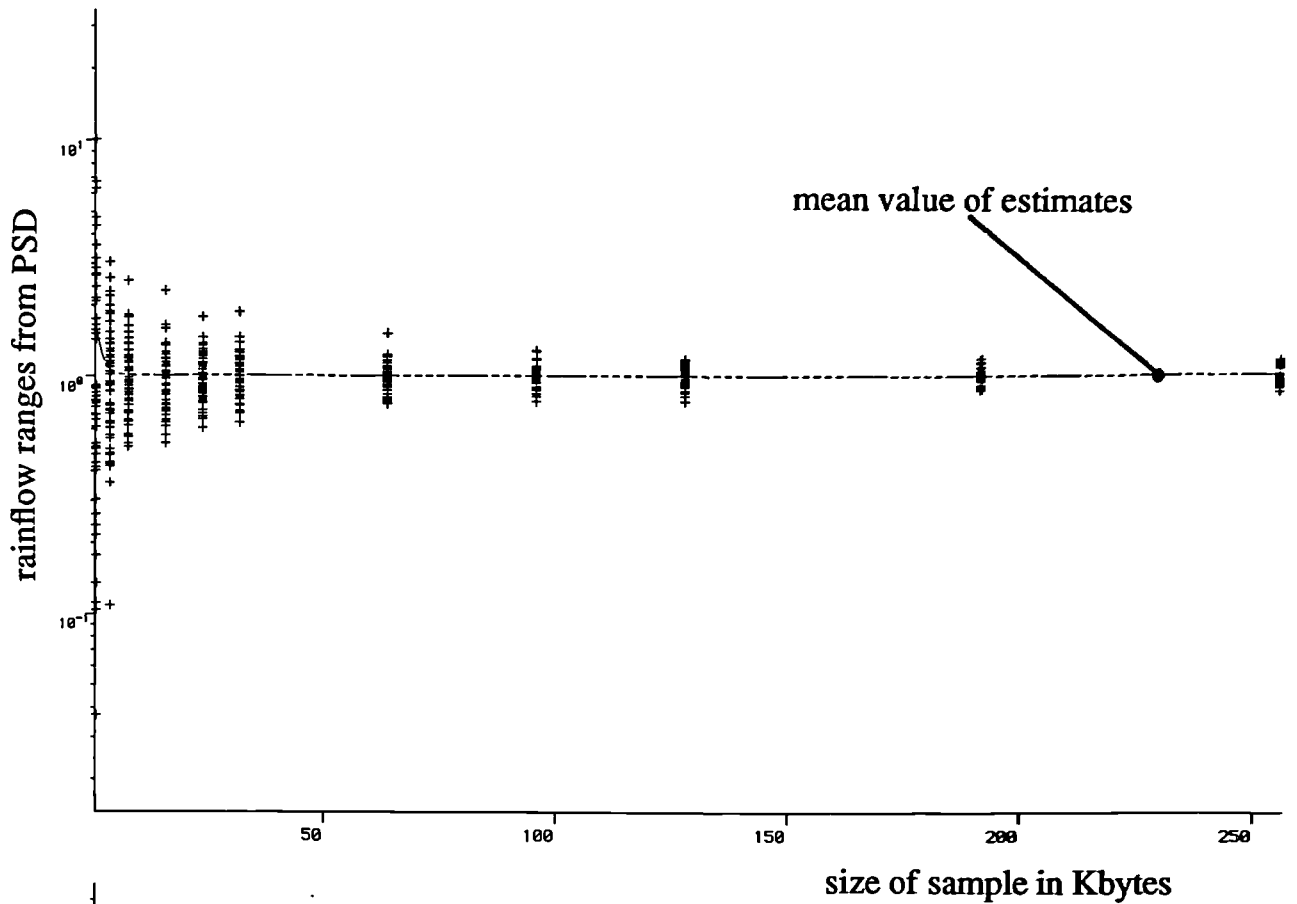


Figure 6.17(b). Rainflow range time domain prediction of fatigue, directly from time signal, normalised by rainflow range prediction on full time signal ... plotted against sample size

Figure 6.18(a). Ordinary range prediction of fatigue from Kowalewski's regenerated signal, normalised by ordinary range prediction on full time signal ... plotted against sample size

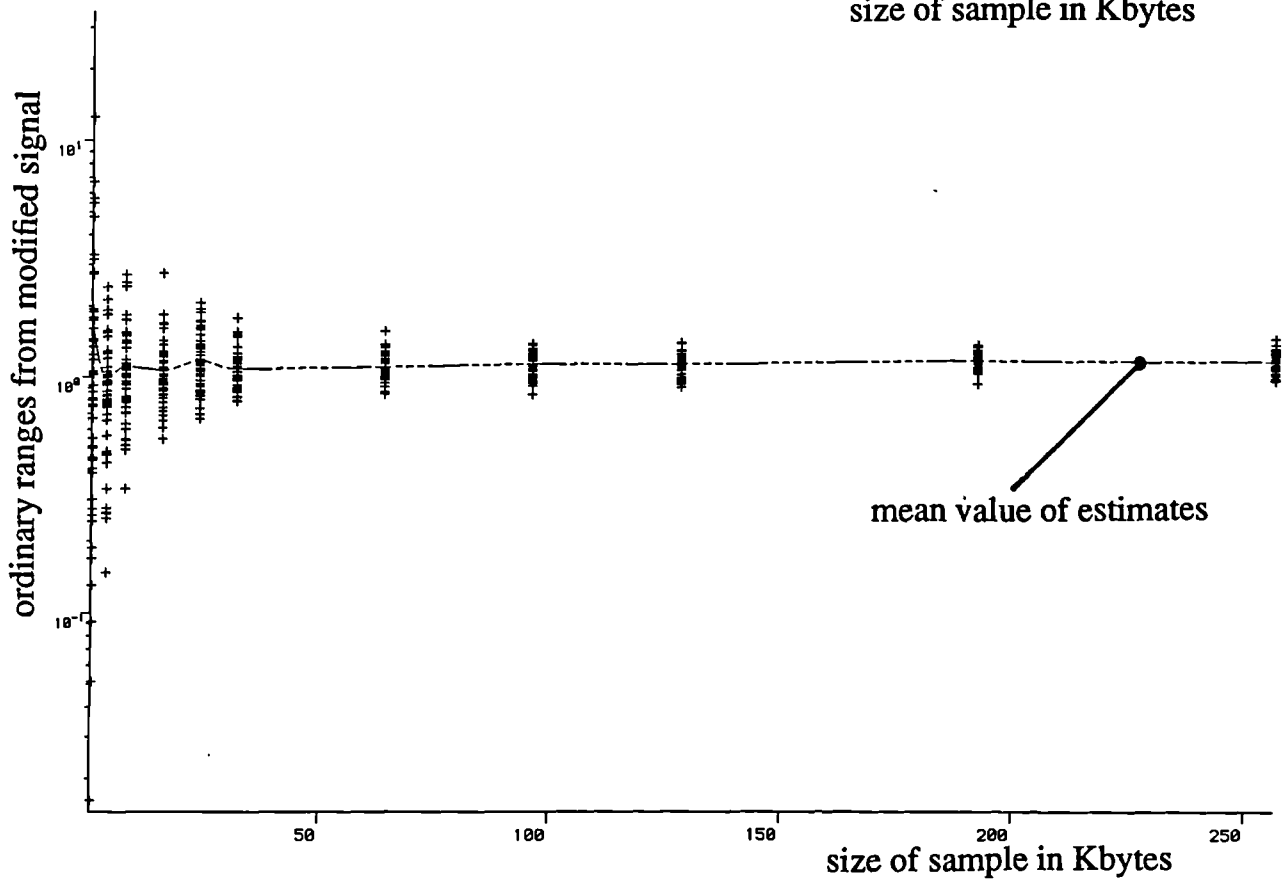
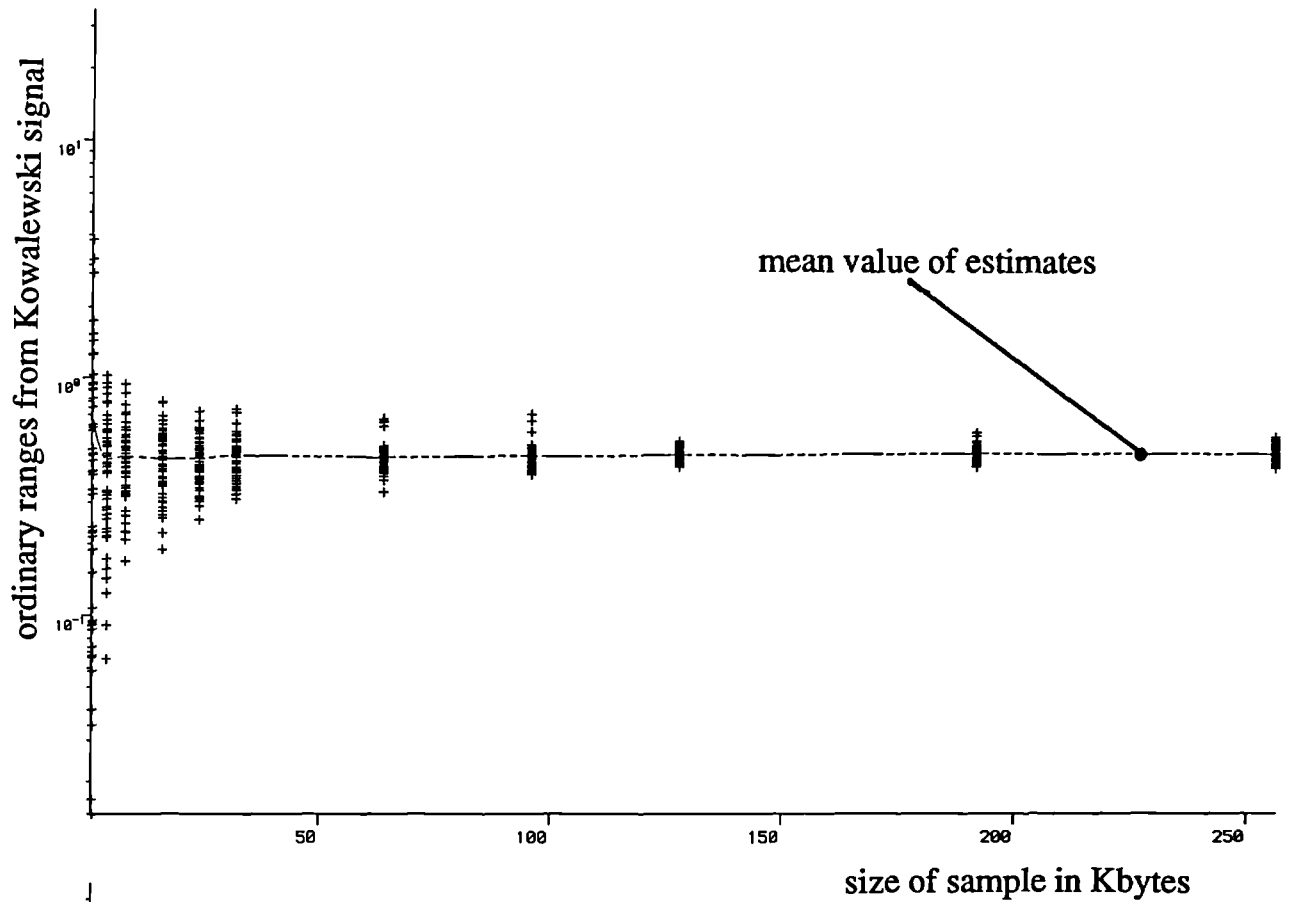


Figure 6.18(b). Ordinary range prediction of fatigue using the authors regenerated signal, normalised by ordinary range prediction on full time signal ... plotted against sample size

Figure 6.19(a). Rainflow range prediction of fatigue from Kowalewski's regenerated signal, normalised by rainflow range prediction on full time signal ... plotted against sample size

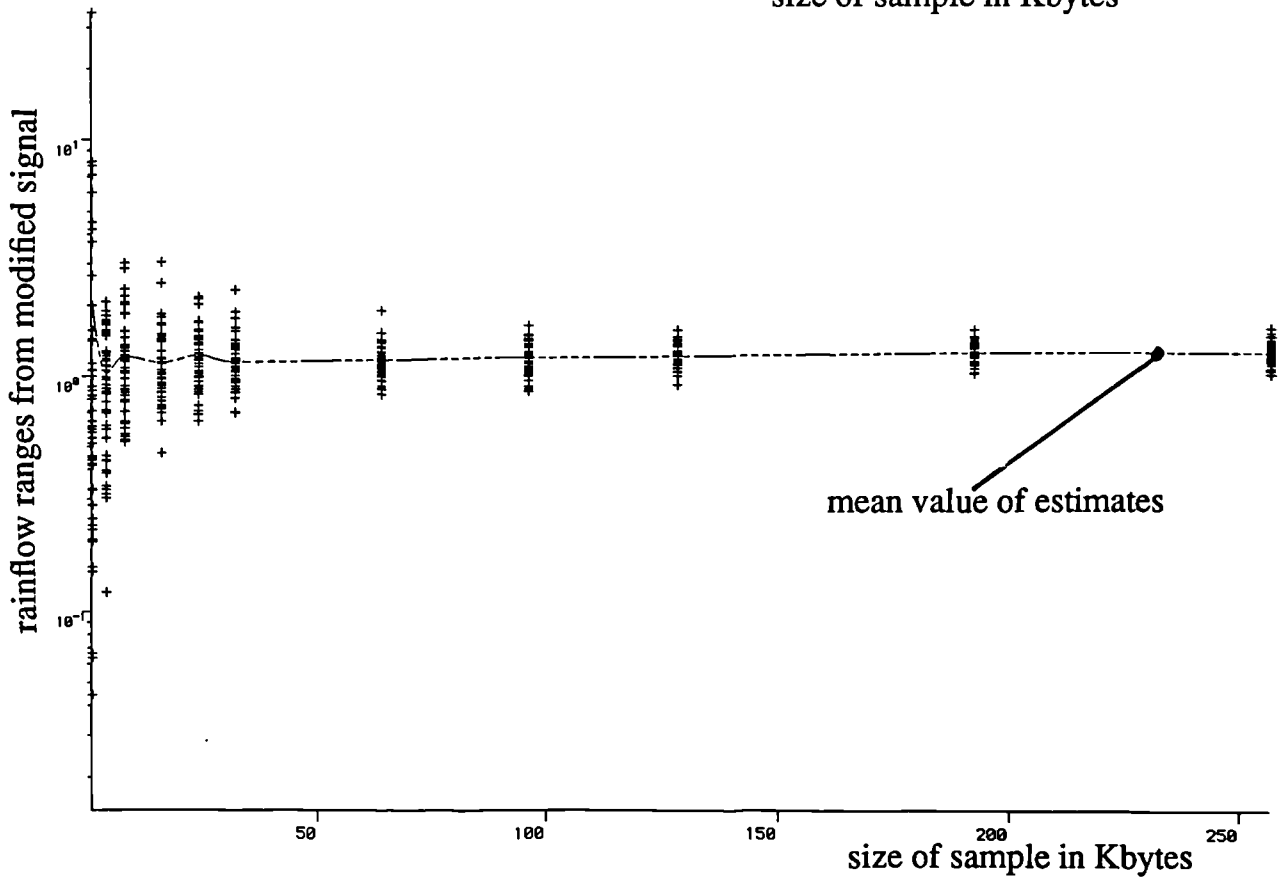
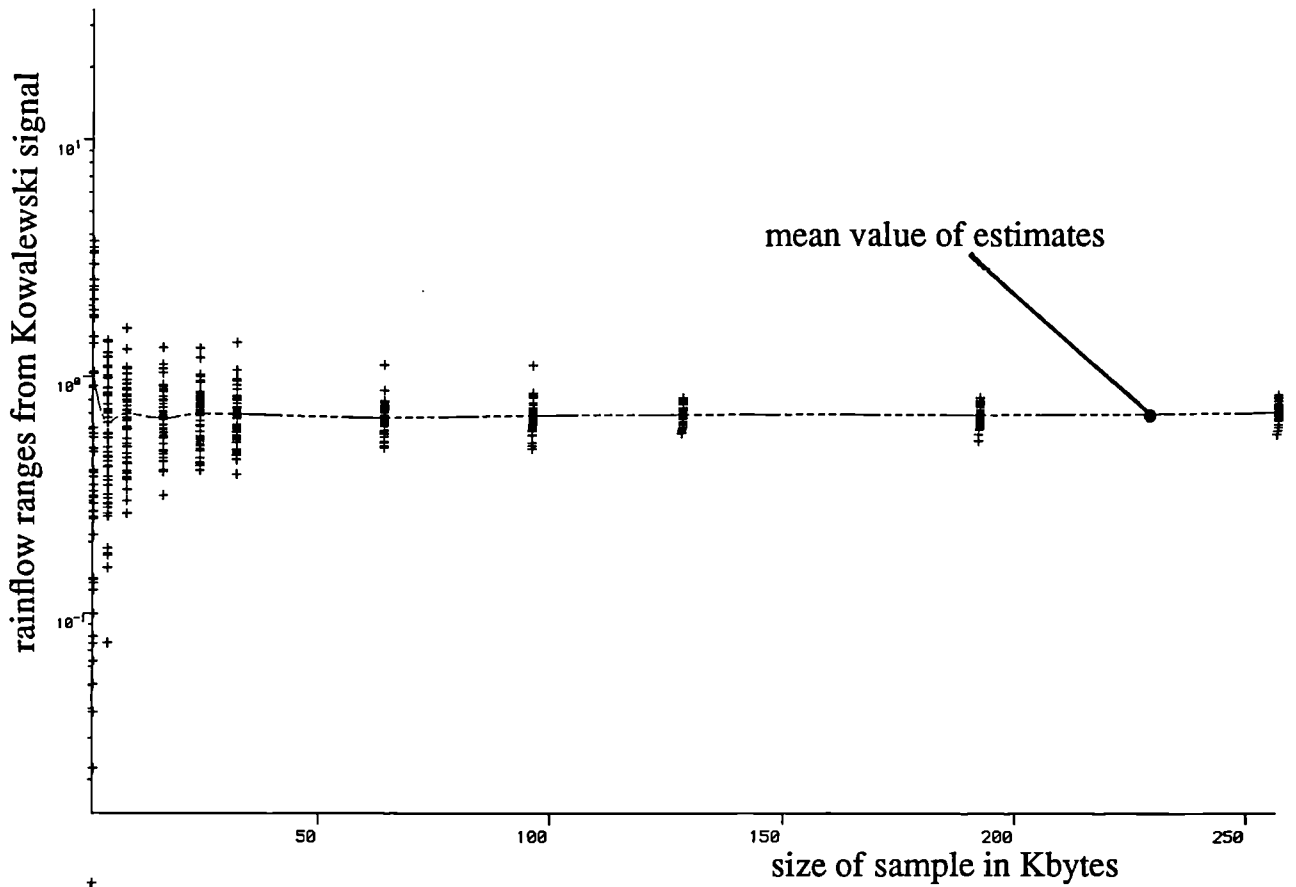


Figure 6.19(b). Rainflow range prediction of fatigue using the authors regenerated signal, normalised by rainflow range prediction on full time signal ... plotted against sample size

7. The dynamic fatigue damage analysis of fixed offshore platforms, with some examination of structures subjected to wind loading.

7.1. Introduction

As easily accessible reserves of energy on the earth become exhausted mankind will be forced to search in areas that would otherwise have been uneconomical. One such area is Offshore Engineering where structures are being built or planned in deeper water. Experience in this field is limited, so present methods of analysis are being tested and in certain cases being found to have some failings. The fatigue damage assessment of such a structure is a particularly complicated process involving many branches of engineering, including meteorology, oceanography, fluid mechanics, soil mechanics, stress analysis, materials science and signal analysis. In practice, a detailed fatigue life assessment requires the calculation of stresses in every joint for the full range of loading conditions expected during the platform's life.

There are various types of oil platforms being used at the moment. Gravity platforms are so named because they rely on their own weight for fixity to the ground. Guyed towers rely on ties to prevent excessive swaying of the structures deck. However, this report will deal with the problems associated with the fatigue analysis of steel space frame type platforms, usually called 'fixed structures'. In the past most structures have been designed on the basis of the static response to the wave loading conditions. However deeper platforms (Murchison, 156M (ref.7.1), Cognac, 310M (ref.7.2)) have meant that the dynamic response has become important. For dynamically sensitive structures fatigue considerations may predominate over the traditional maximum expected loading (first pass failure) criteria. This is because the structures are likely to resonate under the action of the more frequent but far less severe sea states with energy content near to the fundamental frequency of vibration. Therefore any method of analysis which does not fully include the dynamic characteristics of the system may be significantly in error. The dynamic behaviour of a structure is also very sensitive to the wave length/structural width interaction, therefore simplifications to the structural modelling which are often adopted for the first pass failure analysis of dynamically sensitive platforms must be used with care for a fatigue analysis. This is because the wavelengths of the more frequent

smaller waves could be near to the structural width thereby exciting higher and lower frequencies than the actual frequency of the wave.

It is the purpose of this paper to review available fatigue analysis methods which may be applied to dynamically sensitive structures. Although this report is almost entirely concerned with wave induced fatigue, one method for calculating the effects of wind is included in order to be able to highlight the advantages of the work of chapter 3 for this subject. Methods which have been reported for calculating wave induced fatigue can be broadly categorised as follows;

- (a) Deterministic,
- (b) Transient (or time domain),
- (c) Spectral,
- (d) Deterministic/spectral,
- (e) Transient/spectral,
- (f) Probabilistic.

Each method will be discussed more fully and errors with each will be highlighted. The terminology used to categorise the methods in this way is sometimes misleading because each analysis is similar and often contains aspects of the others.

The Deterministic/spectral approach is considered in more detail because it appears to be the best way of handling the random nature of the sea. This method was used to carry out a fatigue analysis in 1978 (ref.7.1) and it was claimed to be the most comprehensive fatigue analysis up to that date. Several computer runs have been carried out using this method to highlight sources of error and improvements are recommended in the way the analysis is carried out.

Following an earlier investigation by the author (ref.7.3) the rainflow method of cycle counting was shown to predict longer fatigue lives. This is also demonstrated in chapters 3 and 6. Therefore along with the normal narrow band approach this method will be used for comparison. The fatigue damage potential of separate parts of the response is also investigated using the work of chapter 3.

An extension to the work of Borgman (ref.7.4) is outlined for a more accurate representation of the loading mechanism. This will enable structural width/wave length interaction effects to be modelled in a more effective way. This is important for fatigue estimation because there is significant energy in the smaller waves(shorter wavelengths) to excite resonances in dynamically sensitive structures. Foundations, current loading and the effects of the conductor tubing will not be considered because although they do effect the fatigue life prediction they do not have a significant effect on the relative merits of each type of analysis and can easily be considered separately. It is also assumed that the structural member sizes are sufficiently small that they do not alter the incoming wave field.

A method is proposed for dealing with the loading mechanism nonlinearities which employs the concept of using 'sub PSD functions' generated from the wave spectra. This method may be applicable to general nonlinear dynamic problems.

7.2. Recap of other Authors work and relevant theory

7.2.1. Sea Environment Characterisation

The true nature of the sea is such that its statistical properties vary with time. However, for the purpose of calculating fatigue damage it can be broken down into a number of stationary sea states, each with a given probability of occurrence. One popular way of categorising these is by using the **significant wave height** (H_s) and **dominant period** (T_D). The significant wave height is defined as the mean height of the heighest third of the waves. It is possible to express this in terms of the spectral moments (ref.7.5):

$$H_s = 4\sqrt{m_0} = 4\sigma \quad (7.1)$$

Where;

σ is the root mean square value of wave height.

The dominant period is related to the frequency of the wave spectrum peak.

Several sea state classifications exist. The **Pierson Moskowitz** wave spectrum (ref.7.6) was obtained for fully developed seas and is given by;

$$S_{\eta\eta}(f) = \alpha g^2 (2\pi)^{-4} f^{-5} e^{-\beta(\frac{f}{f_D})^4} \quad (7.2(a))$$

Where;

η = distance of sea surface elevation from mean water level,

α = Philips constant = 0.0081,

g = gravitational acceleration,

β = constant = 0.74,

f_D = frequency of wave spectrum peak = $\frac{g}{2\pi U_{19.5}}$

$U_{19.5}$ = wind velocity at 19.5m above sea level,

By using equations 2.49 and 7.1 and defining the zero crossing period (T_z) as $\frac{1}{E[0]}$ the above relationship can be rearranged in terms of significant wave height and dominant period, (see reference 7.7, appendix A):

$$S_{\eta\eta}(f) = \frac{H_s^2 T_z}{8\pi^2} (f T_z)^{-5} e^{-\frac{1}{\pi} (f T_z)^4} \quad (7.2(b))$$

It is also shown that,

$$T_D = 1.408 T_z \quad (7.3)$$

The above expression allows loading data to be generated for various combinations of H_s and T_D . The data used for this investigation was generated from equation 7.2(b) and the values used are given in table 7.1.

Equation 7.2(b) represents waves from only one direction. Data is available in limited form for directional sea spectra but is not commonly used for design purposes at the moment (refs.7.8,7.9,7.10).

Traditionally, data for fatigue purposes is in the form of scatter diagrams which can either be individual wave scatter diagrams or sea state scatter diagrams.

Individual wave scatter diagrams give the numbers of waves for a given period of time which fall within certain period and height ranges. A scatter diagram could for instance contain all the waves at a particular sea location for a period of one year. In this case the scatter diagram would make no assumption about stationary sea states and in fact for a scatter diagram of such duration the waves will have come from conditions which can only be regarded as non-stationary. If individual waves generated from one

wave spectrum are stored separately then the stationary assumption still holds, (see below on the the distribution of heights and periods of sea waves).

Sea state scatter diagrams are diagrams containing the probability of occurrence of sea states within certain H_s and T_D ranges. These individual sea states are stationary, but all the sea states together are not.

Longuit Higgins (ref.7.5) derived the following empirical relationship for the distribution of the heights of sea waves;

$$P(R, Q) = \left[\frac{2}{\pi^{1/2} v} \right] \left[\frac{R^2}{Q^2} \right] e^{-R^2} \left[1 + \frac{(1 - \frac{1}{Q})^2}{v^2} \right] Y(v) \quad (7.4)$$

Where;

$$R = \frac{r}{(2m_0)^{1/2}} = \text{normalised wave height.}$$

$$Y(v) = 1 + 0.25v^2$$

$$Q = \frac{T}{\tau} = \text{normalised wave period.}$$

$$T = \text{wave period.}$$

$$\tau = \frac{2\pi m_0}{m_1}$$

$$r = \text{wave amplitude}$$

$$v = \left(\frac{m_0 m_2}{m_1^2 - 1} \right)^{1/2}$$

7.2.2. Wave Model

For the purposes of calculating the forces due to wave action it is first necessary to calculate the water particle velocities and accelerations as functions of time in terms of spatial coordinates. Several wave theories exist which have various degrees of complexity. The reason that several wave theories have been developed is that the water surface elevation can not always be regarded as sinusoidal. For instance, for large waves in deep water, the peaks of waves tend to become steeper and the troughs flatter. In this case Stokes 5th order (ref.7.11) wave theory can be applied. Similar effects occur in very

shallow water and other wave theories have been developed for this case. Airy (ref.7.12) wave theory has been developed for the case where the water surface elevation is sinusoidal and is most applicable to waves of small amplitude although it can be applied to the deepwater case above. In order to establish what is meant by 'deepwater' it is worth referring to Eagleson and Dean (ref.7.13). The following classifications were given;

$$\frac{d}{L} < \frac{1}{20} \text{ Shallow}$$

$$\frac{d}{L} > \frac{1}{20} \text{ and } < \frac{1}{2} \text{ medium}$$

$$\frac{d}{L} > \frac{1}{2} \text{ deepwater}$$

Where;

d = depth to mean water level

L = wave length

Airy wave theory is linear and more simple to apply than the higher order wave theories. Therefore, this theory will be used to illustrate the fundamental principles involved and because of its simplicity and the linear requirement of spectral analysis Airy wave theory is used in developing the spectral equations mentioned later.

For linear wave theory the sea surface elevation is defined by a simple sine wave:

$$\eta(t) = r \sin(kx - \omega t) \quad (7.5)$$

The horizontal water particle velocities and accelerations are then given by :

$$u = r\omega \left[\frac{\cosh kz}{\sinh kd} \right] \sin(kx - \omega t) \quad (7.6(a))$$

$$a = -r\omega^2 \left[\frac{\cosh kz}{\sinh kd} \right] \cos(kx - \omega t) \quad (7.6(b))$$

Where;

η = distance of sea water level from mean water level at time t,

r = half the wave height

$$k = \text{wave number} = \frac{2\pi}{L},$$

$$\omega = \text{circular wave frequency} = 2\pi f$$

$$T = \text{wave period}$$

The acceleration component lags the velocity component by 90 degrees. Similar expressions exist for the vertical components of velocity and acceleration.

The wave celerity is given by (ref.7.14);

$$c = \left[\frac{gL}{2\pi} \tanh \frac{2\pi d}{L} \right]^{\frac{1}{2}} \quad (7.7)$$

For deepwater conditions this can be simplified to;

$$c = \left[\frac{gL}{2\pi} \right]^{\frac{1}{2}} \quad (7.8)$$

Using the expression $L = cT$ we get

$$L = \frac{T^2 g}{2\pi} = 1.56T^2 \quad (7.9)$$

Observations (ref.7.15) show that there is a limiting steepness of ocean waves of about;

$$\frac{2r}{L} = \frac{1}{7} \quad (7.10)$$

In deepwater, the water particles move in a circular motion or **wave orbit**, with no long term movement (mass transport). After each wave passes the particles should be in the same position. With depth these orbits decrease exponentially according to the relationship

$$\delta = \frac{\cosh kz}{\sinh kd} \quad (7.11)$$

Where;

δ = depth decay function.

z = depth at calculation point

d = mean water depth

Figure 7.1 shows this variation for a water depth of 200m with various wave heights and frequencies. This shows that the decrease is more rapid for the smaller waves.

7.2.3. Member Force Calculation

Despite many limitations, **Morison's equation** (ref.7.16) has been widely adopted for the calculation of wave forces on slender members (i.e., $d/L < 0.2$). For structures of large dimensions which do not satisfy the above criterion methods like diffraction theory have to be used.

Morison's equation relies on the assumption that the total force on a member can be expressed as the sum of two components. The first being an inertia term dependent on the water particle accelerations and the second a drag term dependent on the water particle velocities squared;

$$F_T = F_I + F_D \quad (7.12)$$

Considerable problems arise from the second drag term because it is nonlinear. The equation also becomes more difficult to apply if 'relative' velocities and accelerations need to be accounted for. This applies where the structures own movement needs to be included in the calculation. i.e., when the structure can not be regarded as rigid.

For rigid structures the **inertia term** is given by;

$$F_I = C_I \rho \frac{\pi D^2}{4} a \quad (7.13)$$

and the **drag term** is given by;

$$F_D = C_D \rho \frac{D}{2} u |u| \quad (7.14)$$

It therefore follows that;

$$F_T = C_I \rho A a + C_D \rho \frac{D}{2} u |u| \quad (7.15)$$

Where;

C_I and C_D are the inertia and drag coefficients which are found empirically,
 A and D are the area and diameter of the incremental section of member for which the wave force is being calculated,
 a and u are the water particle acceleration and velocity.

ρ is the mass density of water

The correct choice of C_I and C_D is a very detailed subject and will not be discussed here.

If the expressions for horizontal velocity and acceleration are introduced into equation 7.15 the result is the sum of two sinusoidal components which are out of phase 90° . Nath and Harleman (ref.7.17) showed that these could be approximated by one sinusoidal function given by;

$$F_{TAPP} = \left[C_I^2 + \left[\left(\frac{8}{3\pi} \right) C_2 \right]^2 \right]^{\frac{1}{2}} \sin(\theta + \gamma_f) \quad (7.16)$$

Where;

$$\gamma_f = \tan^{-1} \left[\frac{-3\pi C_1}{8C_2} \right]$$

$$C_1 = C_I \rho A r w^2 \delta = F_I^{\max}$$

$$C_2 = C_D \rho \frac{D}{2} r^2 w^2 \delta^2 = F_D^{\max}$$

Equations 7.5, 7.6(a), 7.6(b), 7.15 and 7.16 are shown on figure 7.2(a) for comparison. Figure 7.2(b) shows the loading on one vertical member at various phase increments for a 2.4m wave.

Nath and Harleman also looked at the relative values of F_I and F_D . They derived the following expression;

$$\frac{F_D^{\max}}{F_I^{\max}} = \frac{1}{\pi} \frac{C_D}{C_I} \frac{r}{D} \left[\frac{\sinh 2kd + 2kd}{\cosh 2kd - 1} \right] \quad (7.17)$$

Putting $F_D^{\max} = F_I^{\max}$ and for $r \ll d$;

$$\frac{2r}{D} = \frac{C_I}{C_D \left(\frac{d}{L} \right)} \left[\frac{\sinh^2 kd}{1 + \frac{\sinh 2kd}{2kd}} \right] \quad (7.18)$$

This is plotted in figure 7.3. It shows that as the wave amplitude reduces, the inertia term becomes dominant.

As mentioned above, the drag term is nonlinear. This causes problems for many types of calculation including the spectral method. A linear approximation to the velocity squared term was proposed by Borgman (ref.7.18).

$$|u| = u_{rms} \left[\frac{8}{\pi} \right]^{\frac{1}{2}} \quad (7.19)$$

Where u_{rms} is the root mean square value of velocity.

7.2.4. Structural Behaviour

For any structure which exhibits dynamic characteristics, it is important to find the mode shapes (**eigenvectors**) and corresponding frequencies (**eigenvalues**) of vibration. To gain an understanding of the fundamental principles involved it is worth looking at the case of a simple cantilever which is able to move in only one direction, with stiffness K , damping C and mass M .

If we first look at the undamped case, i.e., $F = Kx$, then;

$$M\ddot{x} + Kx = 0 \quad (7.20)$$

Assuming a solution of the type;

$$x = x_0 \cos \omega_1(t-t_0) \quad (7.21)$$

results in the following result for the frequency of oscillation;

$$\omega_1 = \left[\frac{K}{M} \right]^{\frac{1}{2}} \quad \text{or} \quad f_1 = \frac{1}{2\pi} \left[\frac{K}{M} \right]^{\frac{1}{2}} \quad (7.22)$$

This very important result shows that the frequency of vibration increases with the squareroot of the stiffness and decreases with the squareroot of the mass.

Equations 7.20 and 7.21 can be written in the form;

$$(-\omega^2 M + K)x = 0 \quad (7.23)$$

If we premultiply by M^{-1} and substitute $x = M^{-\frac{1}{2}}$ and finally premultiply by $M^{-\frac{1}{2}}$, we get the standard eigenvalue form of the equation;

$$M^{-\frac{1}{2}} K M^{-\frac{1}{2}} - \omega^2 M^{-\frac{1}{2}} M M^{-\frac{1}{2}} = 0 \quad (7.24)$$

This is in the form;

$$(A - \omega^2 I)x = 0 \quad (7.25)$$

From which values for the eigenvectors (y) and eigenvalues (w^2) can be found for the non trivial solution.

Although a large offshore structure has many degrees of freedom, when the response is being governed by vibration near to a natural frequency, it can be visualised as vibration in only one dimension. Therefore if only the fundamental frequency (e.g. sway) is near to the wave loading energy, then it is possible to use the above relationships to visualise the type of response to be expected.

If more than one frequency of vibration is effecting the response then **normal mode analysis** can be used whereby energy in one mode is made independent of other modes by the coordinate transformation;

$$x = \phi z \quad (7.26)$$

Where ϕ is column-wise matrix of eigenvectors (y) obtained from equation 7.25.

The damped frequency of vibration is (ref.7.14)

$$f_d = f_n \sqrt{1 - \zeta^2} \quad (7.27)$$

Where ζ is the **damping ratio** defined by;

$$\zeta = \frac{C}{C_c} = \frac{C}{2\sqrt{MK}} \quad (7.28)$$

C_c is the critical damping value.

Therefore it can be seen that for structures with low damping, the undamped frequency is virtually the same as the damped frequency of vibration.

If it can be assumed that the loading is of the form;

$$F = F_0 \cos wt \quad (7.29)$$

Then;

$$M\ddot{x} + C\dot{x} + Kx = F_0 \cos wt \quad (7.30)$$

For which the solution for the maximum displacement is;

$$x_0 = \frac{F_0}{\sqrt{(K - Mw^2)^2 + C^2w^2}} \quad (7.31)$$

And the phase shift is;

$$\Phi = \tan^{-1} \left[\frac{Cw}{K - Mw^2} \right] \quad (7.32)$$

If we define $\Omega = \frac{w}{w_1}$ then;

$$x(t) = \left[\frac{F_0}{K \sqrt{(1 - \Omega^2)^2 + (2\zeta\Omega)^2}} \right] \cos(\omega t - \phi) \quad (7.33)$$

$$\Phi = \tan^{-1} \left[\frac{2\zeta\Omega}{1 - \Omega^2} \right] \quad (7.34)$$

If we plot equation 7.33 (figure 7.4) it is possible to visualise three distinct regions. At frequencies near to the frequency of vibration the response is governed by damping. At low frequencies the response is dominated by stiffness and at high frequencies the response is most strongly influenced by mass.

If the forcing function is not harmonic or something near to it then a time history analysis may have to be carried out. This involves a step by step solution to the equation of motion (equation 7.30) using a numerical integration routine such as Newmark-Beta or the Duhamel (or convolution) integration technique.

7.2.5. Spectral Analysis

The above equation (equation 7.31) can be obtained in a slightly different way. If we use the relationship;

$$e^{j\omega t} = (\cos\omega t + j \sin\omega t) \quad (7.35)$$

Where it is understood that only the real part of equation 7.35 is taken, then we can obtain;

$$x(j\omega) = \left[\frac{1}{(K - Mw^2) + j(Cw)} \right] F(j\omega) \quad (7.36)$$

Which is the very important relationship;

$$x(j\omega) = H(j\omega).F(j\omega) \quad (7.37)$$

$H(j\omega)$ is called a **transfer function**.

If the forcing function is not sinusoidal, it may be possible to break it down into a number of sinusoidal components using Fourier analysis in the following way;

$$F(t) = A_1 e^{j\omega_1 t} + A_2 e^{j\omega_2 t} + \dots \quad (7.38)$$

Then the response would be given by;

$$x(t) = H(j\omega_1) A_1 e^{j\omega_1 t} + H(j\omega_2) A_2 e^{j\omega_2 t} \dots \quad (7.39)$$

For random loading the above transfer function approach can be extended for use in spectral analysis, where;

$$S_{\sigma\sigma}(f) = |H(jf)|^2 S_{FF}(f) \quad (7.40)$$

This relationship is valid for any system that can be broken down into separate linear input-output relationships. It is relatively easy to obtain the transfer function of a system with few degrees of freedom, but as the system becomes more complicated the computation becomes very involved and is practically impossible to apply to systems with very many degrees of freedom without severe simplifications to the modelling.

It is important to establish what the transfer function is supposed to do. For instance, to relate the stresses at one point of a large offshore structure to the incoming waves requires more than one transfer function. However, the linear properties of the system to which these transfer functions relate means that they can be combined into one. The actual steps required are;

$$S_{FF}(f) = |H_1(jf)|^2 S_{\eta\eta}(f) \quad (7.41)$$

This relates the sea surface elevation to actual forces on the members. Care has to be taken with this step of the analysis because it includes Morison's equation containing nonlinearities which have to be linearised in some way.

The next step is from wave force to structural displacement;

$$S_{DD}(f) = |H_2(jf)|^2 S_{FF}(f) \quad (7.42)$$

This part of the analysis does not contain any significant nonlinearities apart from the soil-foundation system which is not going to be considered in this report.

Finally, to obtain information about the fatigue life of a particular point of interest, the displacements need to be related to stresses, i.e.;

$$S_{\sigma\sigma}(f) = |H_3(jf)|^2 \cdot S_{DD}(f) \quad (7.43)$$

To obtain the total response of a point, all the responses need to be summed and this involves the use of the response cross spectral density functions and a complete understanding of the processes involved becomes difficult for a system with many degrees of freedom.

It is theoretically possible to build up transfer function matrices in a manner analogous to the the one degree system. However, in practice these transfer functions are usually produced by the use of a time domain analysis (see later section 'present methods of analysis')

7.2.6. Fatigue Damage Model

Equations 2.58, 3.6 and 3.8 are used in this chapter to compute the fatigue damage based on the narrow band assumption, rainflow ranges and ordinary ranges.

Following the earlier investigation described in chapter 3, the **fatigue damage potential** is defined as the amount of fatigue damage caused by individual strips within any PSD plot. Figure 3.15(b) shows the fatigue damage potential of a rectangular plot. These damage contributions were seen to be not simply related to frequency, but dependent on other frequency bands within the PSD plot. This can be highlighted using the same rectangular plot as above to find the effects of other strips. In this way a "reduction in reduction" can be obtained for each moving strip in the presence of an "interacting" strip at any position elsewhere in the block. Therefore for this example a 20x20 matrix can be set up as plotted in figure 7.5. The notation used is that D_{IJ} equals the damage at moving strip position J , in the presence of interacting strip I .

7.3. Present Methods of Analysing Wave Loadings

7.3.1. Deterministic

A deterministic analysis makes no attempt to model the true nature of the sea. The data required for this type of analysis is (ref.7.7);

- (a) H-N curve (wave exceedence diagram),
- (b) S-H curve (stress range / wave height relationship),
- (c) S-N curve (normal fatigue data).

The data for (a) is available from oceanographers. The frequency content of the sea has been removed at this stage. Only the number of waves expected for a particular height is given, usually on semi-log paper. This data is the reverse of a wave spectrum such as equation 7.2, where the energy for a particular frequency is given regardless of height. Of course, for particular sea states, the height and frequency are strongly linked. The H-N curve can be expressed by the following relationship;

$$dN = \frac{2.303}{b_2} N_m e^{2.303 \frac{H}{b_2}} \quad (7.44)$$

Where,

N_m is the number of waves in 100 years, $= e^{2.303 \frac{H_m}{b_2}}$,

H_m is the maximum wave height in 100 years,

b_2 is the slope of the H-N curve, $= \frac{-H_m}{\log N_m}$

The static stress range/wave height relationship can be approximated by a quadratic polynomial:

$$S(H) = a_1 H + a_2 H^2 \quad (7.45)$$

Putting a_2 equal to zero results in a linear relationship.

As usual the fatigue S-N data can be put in the form;

$$N = kS^{-b} \quad (7.46)$$

Where,

N is the number of cycles to failure at stress S ,

b is the slope of the S-N curve, $= \frac{\log k}{\log S_1}$,

k and S_1 are material constants dependent on the actual S-N curve used.

Using the Binomial theorem S^b can be approximated by;

$$S^b = \left(1 + \frac{ba_2H}{a_1}\right) H^b e^{\frac{2.303H}{b^2}} dH \quad (7.47)$$

From equation 2.1 it is possible to define the damage at a particular wave height;

$$\Delta D = \frac{dN}{N} \quad (7.48)$$

Using 7.44, 7.46, 7.47, and 7.48 an expression for the total damage can be obtained by integrating over the range of wave heights.

$$D = \frac{2.303a_1^b N_m}{b_2 k} \int_0^\infty \left(1 + \frac{ba_2H}{a_1}\right) H^b e^{\frac{2.303H}{b^2}} dH \quad (7.49)$$

The above equation takes no account of any dynamic characteristics which the structure might have. An attempt at including the dynamic response can be made by using a dynamic amplification function (DAF) into equation 7.49 whereby;

$$S_d = S(H).q(H) \quad (7.50)$$

Where $q(H)$ is the DAF.

This DAF is not very satisfactory because it applies to height, not frequency. Even though T and H are strongly linked for a particular sea state, this link is not strong if a longer time period is used as in the form of a wave exceedence diagram.

An alternative approach can be used where the Rayleigh distribution is substituted for the wave exceedence diagram, i.e.;

$$p(H) = \frac{2H}{\bar{H}^2} e^{-\frac{H^2}{\bar{H}^2}} \quad (7.51)$$

Where, \bar{H}^2 is the mean value of wave heights.

By substituting $H_s = \sqrt{2\bar{H}^2}$ and using;

$$dN = N_i p(H) dH \quad (7.52)$$

Where, N_i is the number of waves in the i th sea state.

We can obtain an expression for the total damage in the i th sea state;

$$D_i = \frac{4 N_i a_i^b}{H_{si}^2 k} \int_0^\infty \left(1 + \frac{b a_2 H}{a_1}\right) a_1 H^{(1+b)} e^{-\frac{2H^2}{H_s^2}} dH \quad (7.53)$$

Again the DAF can be used if required.

7.3.2. Transient

The basis of time series analysis is to divide the forcing function up into a set of discrete time steps. Then if $x(t-\Delta t)$, $\dot{x}(t-\Delta t)$ and $\ddot{x}(t-\Delta t)$ are known, $x(t)$, $\dot{x}(t)$, and $\ddot{x}(t)$ may be calculated using numerical integration routines such as Newmark-B. This method can adequately deal with nonlinearities of loading. The relative velocities can also be kept in Morison's equation.

Data is required in the form of a time history of sea surface elevation. This could be obtained directly or by Inverse FFT methods.

The Following example is taken from (ref.7.19) and further references on this subject are (refs.7.20, 7.21 and 7.22).

If a time history of sea surface elevation is known then it is possible to use equation (7.38) to fit the actual wave profile with its sinusoidal components. The actual velocity at any point in time and space is then given by the summation of the individual velocity components. i.e.;

$$u = \sum_{i=1}^{n_c} r_i w_i \left[\frac{\cosh k_i z}{\sinh k_i d} \right] \sin(k_i x - w_i t + \phi_i) \quad (7.54)$$

Similar expressions exist for the vertical velocity and the vertical and horizontal accelerations.

The forces on the member segments are then given by;

$$F_T = C_I \rho A a_N + \rho A a_T - M_f \rho A \ddot{x}_N + C_D \rho \frac{D}{2} (u - \dot{x}_N) | (u - \dot{x}_N) | \quad (7.55)$$

Which includes the normal and tangential accelerations a_N and a_T , and the form factor M_f .

Rayleigh type damping is assumed, i.e.;

$$C = \alpha M + \beta K \quad (7.56)$$

α and β are scalar constants specifying the damping in the first two modes,

$$\alpha = \frac{2(w_1\eta_1 - w_2\eta_2)}{\left[\frac{w_2}{w_1} - \frac{w_1}{w_2} \right]} \quad (7.56(a))$$

$$\beta = \frac{2\left(\frac{\eta_2}{w_1} - \frac{\eta_1}{w_2}\right)}{\left[\frac{w_2}{w_1} - \frac{w_1}{w_2} \right]} \quad (7.56(b))$$

And the percentage of critical damping in the i th mode is given by;

$$\eta_i = \frac{\alpha}{2w_i} + \frac{\beta w_i}{2} \quad (7.57)$$

For i from 1 to the number of degrees of freedom.

Therefore if the total damping value is specified then the equations of motion can be integrated as follows;

$$x(t) = \bar{K}^{-1}\bar{F}(t) \quad (7.58(a))$$

$$\dot{x}(t) = \frac{3}{\Delta t}x(t) - B(t) \quad (7.58(b))$$

$$\ddot{x}(t) = \ddot{x}(t-\Delta t) - A(t) \quad (7.58(c))$$

Where;

$$\bar{K} = K + \frac{3}{\Delta t}C + \frac{6}{(\Delta t)^2}M \quad (7.58(d))$$

$$\bar{F}(t) = F(t) + CB(t) + MA(t) \quad (7.58(e))$$

$$A(t) = \frac{6}{(\Delta t)^2}x(t-\Delta t) + \frac{6}{\Delta t}\dot{x}(t-\Delta t) + 2\ddot{x}(t-\Delta t) \quad (7.58(f))$$

$$B(t) = \frac{3}{(\Delta t)}x(t-\Delta t) + 2\dot{x}(t-\Delta t) + \frac{\Delta t}{2}\ddot{x}(t-\Delta t) \quad (7.58(g))$$

The convergence criteria for these equations is;

$$\Delta t \leq 0.389T_{\min} \quad (7.59)$$

Where T_{\min} is the lowest natural period of the structure to be considered.

Stresses can be obtained by a linear transformation from displacements.

The main problem with the use of a transient analysis is one of cost.

7.3.3. Spectral

This type of analysis is carried out entirely in the frequency domain. This section will firstly set out a complete analysis (ref.7.14), which will be followed by the specific problem of obtaining the spectral forcing function from a spectral description of the sea surface elevation (ref.7.4), i.e. equation 7.41. (Further references on this subject are refs. 7.23, 7.24, 7.25, 7.26 and 7.27)

We can start from the description of the sum of a number of random processes ($g(t) = \sum_{i=1}^n C_i h_i(t)$) similar to the expression for sinusoidal loading components;

$$S_{gg}(f) = \sum_{r=1}^n \sum_{s=1}^n C_r C_s S_{h_r h_s}(f) \quad (7.60)$$

where C_i is a multiplying weighting constant. From equation 7.26 and assuming damping of the form $C = \alpha_1 M + \alpha_2 K$ as equation 7.56, we get;

$$\phi^T M \phi \ddot{z} + \phi^T C \phi \dot{z} + \phi^T K \phi z = \phi^T F(t) \quad (7.61)$$

From which the i_{th} uncoupled equation is;

$$M_i \ddot{z}_i + C_i \dot{z}_i + K_i z_i = \phi_{i1} F_1(t) + \phi_{i2} F_2(t) \quad (7.62)$$

The Modal receptance in mode i is defined as;

$$H_i(jf) = \frac{1}{K_i - M_i \omega^2 + j C_i \omega} \quad (7.63)$$

Direct and cross spectral densities of the generalised forces on the right hand side of equation 7.62 are given by equation 7.60;

$$S_{f_i f_j}(f) = \sum_{r=1}^n \sum_{s=1}^n \phi_{ir} \phi_{js} S_{F_r F_s}(f) \quad (7.64)$$

For i and j from 1 to n .

The spectral densities of the generalised modal coordinates are then given by;

$$S_{z_i z_j}(f) = H_i^* H_j S_{f_i f_j}(f) \quad (7.65)$$

Which can be transformed back into the original coordinates by using equations 7.26 and 7.60;

$$S_{x_r x_i}(f) = \sum_{r=1}^n \sum_{s=1}^n \phi_{ir} \phi_{is} S_{z_r z_s}(f) \quad (7.66)$$

If only a few degrees of freedom are to be considered then the system can be analysed without the above decoupling operation with the use of a transfer function matrix of elements similar to equation 7.36 (provided the individual loading components are sinusoidal). Therefore;

$$S_{x_i x_i}(f) = \sum_{r=1}^n \sum_{s=1}^n H_{ir}^* H_{is} S_{F_r F_s}(f) \quad (7.67)$$

If it is possible to calculate the cross correlation function of the loading components ($F_i F_j$) then we can obtain the cross spectral density $S_{F_i F_j}(f)$ using the fourier transform relationship equation 2.25(a).

If a further transformation to stresses is required then some knowledge of the response cross spectral densities is required.

Because of the complexity of this sort of analysis, simplifications to the model are often adopted to reduce the equations of motion to a manageable level. This is sometimes not acceptable for a fatigue damage calculation where every member needs to be checked.

A very useful result for the spectral density of wave forces on arrays of piles can be obtained as follows (ref.7.4). If we put Morison's equation in the form;

$$F(t) = \psi u(t) |u(t)| + l a(t) \quad (7.68)$$

The auto correlation function of the wave forces is given by (ref.7.18);

$$R_{FF}(\tau) = \psi^2 \sigma^4 G \left(\frac{R_{uu}(\tau)}{\sigma^2} \right) + l^2 R_{aa}(\tau) \quad (7.69)$$

Where;

$$G(r) = \frac{(2+4r^2)\sin^{-1}r+6r\sqrt{1-r^2}}{\pi} \quad (7.70)$$

$$\sigma^2 = 2 \int_0^{\infty} S_{uu}(f) df \quad (7.71)$$

For linear wave theory;

$$S_{uu}(f) = \left[\frac{(2\pi f)^2 \cosh^2 kz}{\sinh^2 kd} \right] S_{\eta\eta}(f) \quad (7.72(a))$$

$$S_{aa}(f) = \left[\frac{(2\pi f)^4 \cosh^2 kz}{\sinh^2 kd} \right] S_{\eta\eta}(f) \quad (7.72(b))$$

Although equation 7.69 produces a theoretical result for $S_{FF}(f)$, a more useful expression is obtained by using a series representation for $G(r)$. given by;

$$G(r) = \frac{1}{\pi} \left[8r + \frac{4r^3}{3} + \frac{r^5}{15} + \frac{r^7}{70} + \frac{5r^9}{1008} + \dots \right] \quad (7.73)$$

Hence;

$$R_{FF}(\tau) = \frac{\Psi^2 \sigma^4}{\pi} \left[\frac{8R_{uu}(\tau)}{\sigma^2} + \frac{4R_{uu}^3(\tau)}{3\sigma^6} + \dots \right] + l^2 R_{aa}(\tau) \quad (7.74)$$

By use of Convolution integrals it is then possible to obtain;

$$S_{FF}(f) = \frac{\Psi^2 \sigma^4}{\pi} \left[\frac{8S_{uu}(f)}{\sigma^2} + \frac{4[S_{uu}(f)]^*{}^3}{3\sigma^6} + \dots \right] + l^2 S_{aa}(f) \quad (7.75)$$

By taking only the first order approximation of equation.. we get;

$$S_{FF}(f) \approx \frac{8\Psi^2 \sigma^2}{\pi} S_{uu}(f) + l^2 S_{aa}(f) \quad (7.76)$$

Figure 7.6(a)-7.6(c) are plots of equation 7.2(b), 7.72(a), 7.72(b) and 7.76 for sea states 1, 6 and 10. This shows that at low frequencies the drag term tends to dominate but at higher frequencies the inertia term steadily increases until it becomes more dominant. Drag is more predominant in the rougher sea states. Figure 7.6(d) shows the variation of equation 7.76 with changing member diameter.

A more useful result is obtained for the total force on N piles in a similar way to above, again using the first order approximation to $G(r)$. If $Q(t)$ represents the total

force on a structure then;

$$Q(t) = \sum_{n=1}^N F_n(z, t) \quad (7.77)$$

Where;

$F_n(z, t)$ is the force at depth z on member n at time t .

The autocorrelation function is then;

$$R_{FF}^N(\tau) = E [Q(t) \cdot Q(t+\tau)] \quad (7.78)$$

By the use of various cross correlation functions and cross spectral densities, the following result is obtained (to a first order of approximation);

$$S_{QQ}^N \approx S_{\eta\eta}(f) \left[\frac{8}{\pi} \left[\frac{2\pi f \Psi}{\sinh kd} \int_0^d \sigma(z) \cosh kz \, dz \right]^2 + \left[\frac{(2\pi f)^2 l}{\sinh kd} \int_0^d \cosh kz \, dz \right]^2 \right] \times \sum_{m=1}^N \sum_{n=1}^N \cos k(x_n - x_m) \quad (7.79)$$

where x_n is the horizontal space coordinate for the n_{th} pile in an N-pile array measured in the direction of wave travel. From equation 7.79 it can be shown that;

$$S_{QQ}^N(f) \approx T_{MP}^N(f) S_{\eta\eta}(f) \quad (7.80)$$

Where;

$$T_{MP}^N(f) = \sum_{m=1}^N \sum_{n=1}^N \cos k(x_n - x_m) \quad (7.81)$$

For an L by M grid of piles spaced g and h apart equation 7.81 becomes;

$$T_{MP}^N(f) = \left[\frac{1 - \cos(kgL \cos\theta)}{1 - \cos(kg \cos\theta)} \right] \left[\frac{1 - \cos(khL \sin\theta)}{1 - \cos(kh \sin\theta)} \right] \quad (7.82)$$

At $\theta = 0$ the waves are hitting the structure square on. A three dimensional plot of T_{MP}^N against θ and k (a function of frequency given by $k = \frac{2\pi}{L}$) results.

7.3.4. Deterministic/Spectral

The fundamental principle of this type of analysis is that the transfer function is produced deterministically by a series of wave trains of different frequencies and heights (refs. 7.1, 7.2, 7.28, 7.29, and 7.30). Each point on the transfer function is obtained by comparing the response at some point with input loading in the form of a constant amplitude, constant frequency wave train. Such a transfer function is therefore required for each point of interest on the structure. Section 7.5 investigates the many assumptions inherent in this analysis procedure. Having produced the transfer function the response is then obtained by equation 7.40. The process is highlighted in figure 7.7. If the response plot is obtained in terms of stress then several methods are available for finding the fatigue damage, i.e. equations 2.58, 3.6 and 3.8.

This sort of analysis can be divided into four main stages;

- (a) Solution for the mode shapes and frequencies,
- (b) Calculation of static wave forces at several time increments for each wave that is stepped through the structure.
- (c) The reduction of forces obtained by stage (b) into harmonic loadings at each node on the structure for each base wave case being considered. This is done by sine fitting the time history of forces at each node into a sine wave. Once these harmonic loadings are produced then harmonic stress values can be calculated at chosen hot spots. These stress ranges can be divided by the wave height producing the stress to get one point on the transfer function.
- (d) Multiplication of chosen sea states by transfer functions made up of points from (c).

Stages a, b and c are used to produce the transfer function. Stage d produces the response plots and hence the fatigue damage.

This type of analysis will be investigated more fully in a later section.

7.3.5. Transient/Spectral

This sort of analysis has been so named because it uses a transient analysis to produce the transfer functions which are then used spectrally (ref.7.31). The assumption with this method is that exact transfer functions can be calculated for each sea state using the following expression;

$$T(f) = \left[\frac{S_{\sigma\sigma}(f)}{S_{\eta\eta}(f)} \right]^{\frac{1}{2}} \quad (7.83)$$

The output response is assumed to be a function of $S_{\eta\eta}(f)$, H_s and the dynamic amplification function. i.e.;

$$S_{\sigma\sigma}(f) = A(f)H_s^b(f)DAF(f)S_{\eta\eta}(f) \quad (7.84)$$

Therefore;

$$T(f) = \sqrt{a(f)H_s^b(f)} \quad (7.85)$$

Where $a(f)$ replaces the dynamic amplification function and the scaling factor $A(f)$.

The complete procedure is;

- (a) Select three or more representative sea states for which an exact transfer function is to be computed.
- (b) Simulate a random wave time history using inverse FFT methods for each chosen sea state.
- (c) Calculate the time histories of stress response using a transient analysis.
- (d) Transform these stress histories back into the frequency domain using FFT routines.
- (e) Use equation 7.83 to produce several exact transfer functions.
- (f) Use an error minimisation method to obtain values for $a(f)$ and $b(f)$ by equation 7.85.
- (g) Use the values from (e) and (f) to obtain the response plot for any sea state using interpolation.

7.3.6. Probabilistic

The Probabilistic method (refs. 7.32, 7.33 and 7.34) is a spectral method that allows for non linearities of response. At the moment only the nonlinear drag component of equation 7.15 is solvable using this technique.

7.4. One approach to the analysis of wind loading

The topic of wind induced fatigue damage is at least as big as that of wave induced damage. Therefore, no attempt will be made to fully describe the available methods. This section will only give sufficient details in order to be able to highlight the ease with

which the theories developed in earlier chapters can be applied to this area. For this purpose, a method used by Atkins Research and Development (ref.7.39,7.40) will be shown. Most of the theoretical input in terms of aerodynamic theory is detailed in references 7.41 and 7.42.

The argument used by Atkins was that the resonant and non resonant damage could be calculated separately in the following way;

Non resonant damage

Aerodynamic loading is drag dominated and will therefore be proportional to the square of the wind velocity, that is;

$$F(t) = KV(t)^2 \quad (7.86)$$

where K is a constant. The velocity term in this equation has a mean and fluctuating component. If we ignore second order terms when including the fluctuating component, we get;

$$F(t) = \bar{F} + f(t) = K(\bar{V}^2 + 2\bar{V}V(t)) \quad (7.87)$$

where; \bar{V} represents the mean wind velocity, $(V)t$ the fluctuating wind velocity, $f(t)$ the fluctuating component of force and \bar{F} the static force. The non resonant PSD of stresses used for fatigue damage calculations is then directly proportional to the $2K\bar{V}V(t)$ term in the above equation. Atkins use the following form for the PSD of wind speed fluctuations;

$$S_{uu}(f) = \frac{A_w}{(1 + B_w f^2)^{\frac{5}{6}}} = \frac{A_w}{(1 + (\frac{f}{f_R})^2)^{\frac{5}{6}}} \quad (7.88)$$

where $f_R = \sqrt{\frac{1}{B_w}}$. This comes from reference 7.41, where Von Karman's spectral equation is defined as;

$$\frac{f S_{uu}}{\sigma_u^2} = \frac{4f_u}{(1 + 70.8f_u^2)^{\frac{5}{6}}} \quad (7.89)$$

Therefore;

$$S_{uu} = \frac{4f_u \sigma_u^2 / f}{(1+70.8f_u^2)^{\frac{5}{6}}} \quad (7.90)$$

$$= \frac{4^x L_u \sigma_u^2 / V_z}{(1+70.8 \frac{[^x L_u]}{V_z})^{\frac{5}{6}}} \quad (7.91)$$

where; V_z is the hourly-mean wind speed, $f_u = \frac{^x L_u f}{V_z}$ and $^x L_u$ is the length scale of turbulence in the x direction. We therefore get;

$$A_w = \frac{4^x L_u \sigma_u^2}{V_z} \quad (7.92(a))$$

$$B_w = \frac{70.8^x L_u^2}{V_z^2} \quad (7.92(b))$$

The objective of Atkins work was to produce design curves which could be used to calculate the fatigue damage at a particular location without the need to carry out a rainflow count on a time signal generated using inverse fourier transform techniques. 'Normalised damages' and 'denormalising factors' were produced in the following way; Assume Miner's rule is given by;

$$D = \frac{n(S)}{N(S)} \quad (7.93)$$

$$= \frac{N_G p(S)}{(\frac{k}{S})^b} \quad (7.94)$$

where N_G is the total number of wind speed fluctuations. Then by defining;

$$S_n = \frac{S}{\sigma_S} \quad (7.95)$$

where σ_S is the rms of stress ranges. Then we get;

$$n(S_n) = N_G p(S_n) \quad (7.96)$$

where σ_S is the rms of the non resonant component of stress. Then if we use;

$$M_G = \frac{N_G}{f_R T} \quad (7.97)$$

where T is the duration of the fatigue damage calculation period we get;

$$E[D] = \int_0^{\infty} f_R T M_{GP}(S_n) \left(\frac{\sigma_S S_n}{k}\right)^b \quad (7.98)$$

$$= f_R T \left(\frac{\sigma_S}{k}\right)^b \int_0^{\infty} M_{GP}(S_n)^b \quad (7.99)$$

$$= F_{DN} D_N \quad (7.100)$$

where F_{DN} represents the denormalising factor and D_N the normalised damage which is therefore assumed to be independent of A_w and B_w , that is $p(S_n)$ is made to be not dependent on A_w or B_w . Then;

$$F_{DN} = f_R T \left(\frac{\sigma_S}{k}\right)^b = f_R T \left(\frac{\sigma_S}{V_{rms}}\right)^b \left(\frac{V_{rms}}{V}\right)^b \left(\frac{\bar{V}}{k}\right)^b \quad (7.101)$$

Details of the calculation of the denormalising factors can be found in reference 7.39. Then;

$$D_N = \int_0^{\infty} \frac{N}{f_R T} p(S_n) (S_n)^b \quad (7.102)$$

Using 16 combinations of A_w and B_w Atkins produced values for D_N by rainflow counting regenerated signals. For an S-N slope of 5, results were seen to span the range 1240 to 1652, with a mean value of 1466 and a standard deviation of 121.6. Using the programs developed in chapter 3, comparable results were computed for D_N with various values of A_w and B_w without making the assumption that they are independent of $p(S_n)$. The results are shown in table 7.5. This shows that D_N is only independent of A_w and not B_w . Furthermore, table 7.6. shows the sensitivity of the results to the cutoff point of both the PSD and the range distribution. Scatter caused by the cycle counting procedure on finite signals would be observed in the Atkins results. However, the addition errors with the results appear to be a result of a combination of too small an integration limit for both the PSD and the range distribution as well as an incorrect assumption about the independence of B_w .

Resonant damage

The techniques for calculating the resonant damage used by Atkins are based on the assumption that the resonant part of the damage can be calculated and included separately from the non resonant damage. In all but a few unusual situations, this is not valid and so this approach will not be discussed. However, it is important to note that the same techniques used for the non resonant damage and described in chapter 3 are also valid for calculating the total damage, including resonance. This effectively removes the need to look for a method of including the resonant damage separately.

7.5. Analysis used for this investigation

The previous section described various sorts of fatigue analysis methods that can be carried out. From this, it can be seen that the spectral method is most applicable to offshore structures exhibiting dynamic response. However, as structures become larger, with more degrees of freedom, the analysis becomes too involved for it to be practicably feasible. It is possible however, to use a mixture of time and frequency domain to provide results which retain many but not all the advantages of a frequency domain analysis over time domain calculations. This section will detail one such procedure with the aim of detecting any serious flaws in the analysis.

Deterministic/Spectral analysis method has been investigated using programs from the ASAS-Offshore suite of programs developed by Atkins Research and Development. Five programs were used. They were;

- (a) ASAS#G
- (b) ASAS#WAVE
- (c) ASAS#RESPONSE
- (d) ASAS#FATJACK
- (e) ASAS#ASDIS

(a) to (d) are the main calculation programs and #ASDIS is a graphics postprocessor. All the programs were run under one project name and were interconnected using various backing files. For large problems, considerable thought needs to be put into the handling of these files.

Two programs written by the author called N2 and N12 were used to assess the fatigue damage potential of the different frequency components making up the response. These were run in conjunction with various graph plotting programs (Ghost, ACSL and IDA) to manipulate the results into a more useful form. They were interfaced with ASAS results files using editing programs. Special options had to be used in the ASAS runs to enable the results files to be used in this way.

Each section will be discussed below. Typical data files are given in Appendix 2 and figure 7.9 shows the general layout of the programs.

7.5.1. ASAS#G

ASAS#G is used to obtain the natural frequencies and mode shapes of the structure. The first step in the analysis is to choose a suitable structural idealisation. A Finite Element mesh of tubular steel members, joined together at nodes, is used to represent the structure with a mathematical model. Each element is assigned geometrical and material properties from which the overall mass and stiffness matrices can be produced. Hence, using 7.25 the eigenvalues and eigenvectors can be calculated. Added mass can be added directly to the mass matrix to model non structural mass such as the deck. Unless otherwise restrained, each node is allowed three rotational and three translational degrees of freedom.

The effects of conductor tubing and the foundations have not been included in the ASAS#G analysis because it is not the purpose of this chapter to look at detailed ways of obtaining the mode shapes and frequencies. Many methods exist for this exercise and it is intended here to outline only one possible method.

Initially a slightly different structure with fewer elements (structure A) was analysed, but for reasons of loading computational accuracy the top of the model was later changed to a less coarse idealisation (structure B).

Structure B was 225m high and 40m wide. A tall slender structure was deliberately chosen so that the dynamic problems became important. An excessively large deck mass was added to the top of the structure (representing the mass of the deck) to force the frequency of the fundamental mode down into the frequency of loading. Figure 7.10 shows plots of structures A and B from various angles using #ASDIS. 384 members (513 d.o.f.)

were included in structure B which was analysed without condensation using the Sub Space Iteration method (ref.7.35) to obtain the first six mode shapes and frequencies. The first 8 modes for structure A were plotted using #ASDIS on figure 7.11.

Modes 1 and 2 are sway modes in the x and y directions. Mode 3 is the fundamental torsional mode. Modes 4 and 5 are second harmonic sway modes and mode six is a compression mode. By looking at the frequencies of vibration we see that only the fundamental sway and torsional modes are likely to be excited by the wave energy.

In effect each mode represents a one degree of freedom vibration with each point on the structure having a displacement relative to some specified maximum. These normal modes along with the mass and stiffness matrices are loaded onto backing files for access by ASAS#RESPONSE.

7.5.2. ASAS#WAVE

ASAS#WAVE requires a repetition of the asas#G data without the added mass deck and with an extra loading section. ASAS#WAVE is used to produce the static loading vectors for each node of the structure, which are later used to produce the harmonic loading file. Current loading can be calculated if required, but has not been included in this investigation.

The loading deck contains all the information required to calculate static wave loads for a preselected number of phase increments for each base wave case chosen. The choice of the number of increments and number of base wave cases is very important.

The number of wave increments used to calculate the static loadings is important because a sine wave fitting procedure is applied to the static loading at each node to produce a complex value or harmonic representation of the loading. This complex value has a real and imaginary part. Errors can result from this process regardless of the number of increments chosen, but the result improves as the number of increment increases. Figure 7.12 shows some typical static loading results along with the sine fitted harmonics for various numbers of increments. If the number of increments is large enough then a fairly accurate result for the magnitude of loading is obtained, but some phase problems occur. Figure 7.12(a) represents a relatively small wave. For larger waves the non linear drag term becomes important (figure 7.12(b)). For this case, actual loading may require more

than one harmonic frequency for an exact representation but the sine fitting process only uses one so some frequency information is lost. Also, members in the splash zone may experience wet/dry wave action and any sine fitting procedure for this case may be significantly in error (figure 7.12(c)).

The number of base wave cases chosen is important because each one is later used to represent a point on a transfer function. The more base wave cases, the more points on the transfer function and hence, the more accurate the result. This is particularly true for dynamically sensitive structures where sharp peaks exist in the response. There should always be one base wave case at the fundamental frequency of the structure, otherwise the dynamic response may be missed altogether. Further base wave cases should be chosen where severe changes in response are expected, and at the lowest and highest frequency of wave expected.

The choice of wave height for a particular frequency is difficult because of three main nonlinearities;

- (a) The wave theory may be nonlinear,
- (b) Programs such as ASAS#WAVE calculate the loading to local sea level not mean water level,
- (c) The nonlinear drag term in Morison's equation.

Because of this the relationship between response and wave height is nonlinear (see figure 7.13(a)). Some authors (refs.7.30,7.36) suggest using the most conservative approach which is to use the largest non breaking wave possible for any particular frequency, up to the storm wave height. Penzien (refs.7.37) suggests using a least squares technique to linearise the relationship, but this is dangerous because it can yield unconservative results (see figure 7.13(b)).

The A.P.I. code (ref.7.38) method of calculating the forces was used. That is, calculating the force normal to the member only. However, the option is available to use the method of calculating the force along the vector of velocity or acceleration. This results in an additional force along the member as well as the normal force.

Default values for the drag and inertia coefficients were used (0.7(transverse), 0.0(axial)). Various values for water depth were used ranging from 187m to 213m.

As mentioned earlier a sine fitting procedure is applied to nodal loadings. These nodal loadings result from the lumping of distributed loads from adjoining elements. The distributed loads are either linear or quadratic. A tolerance can be specified which gives the amount the loading calculated at the mid point of the member can vary from a linearly interpolated value between the end values. A second tolerance can be specified for an element subdivision. After any subdivision further loadings would be calculated at the mid points of the sub divided elements. The first tolerance could then be reapplied to the mid points of the two sub divided elements. All distributed loadings are then lumped at nodal points for subsequent sine fitting into harmonic loadcases. These are then loaded onto backing files for use by ASAS#RESPONSE.

7.5.3. ASAS#RESPONSE

The structural stiffness and mass matrices along with the mode shapes and frequencies are read from backing files produced by ASAS#G. Harmonic loadcases for each nodal point on the structure for each base wave case being considered are read from a loadfile produced by ASAS#WAVE. In addition, damping values need to be specified in the data deck for each mode shape and base wave case.

The steady state displacement is calculated for each base wave case. This involves combining the response due to all nodal loadings, taking account of the phase of each. These displacements can then be linearly transformed into stress response. These stresses are later used to form points on the transfer function.

If more than one mode shape is being used then normal mode analysis is used to find the combined response to all modes under consideration.

The nodal responses and the geometrical properties of the structure are loaded onto backing files for use by ASAS#FATJACK.

7.5.4. ASAS#FATJACK

ASAS#Fatjack reads the nodal responses for each base wave case from the backing files produced by ASAS#RESPONSE. Using this information transfer functions can be set up for specified positions around each member end. The procedure for each 'inspection point' is;

- (1) Select stress concentration factors,
- (2) Obtain the stress range for base wave case i by multiplying the values read from ASAS#RESPONSE by the values in (1) above,
- (3) Point i on the transfer function is then the stress range squared, normalised by the height of base wave case i
- (4) Repeat for $i = 1$ to the number of points on the transfer function.

Such a transfer function can be set up for each inspection point in the structure. Inspection points are chosen by default at 8 points around the circumference of each member end in the structure. Therefore, for a structure with 384 members, 6144 transfer functions have to be generated.

Figure 7.14 illustrates the process of obtaining the transfer function, although the total loading is plotted rather than the total nodal loadings.

Using these transfer functions, the response to any specified sea state can be obtained by multiplying the sea state by the transfer function to obtain a stress response spectrum (figure 7.7). ASAS#FATJACK then calculates the fatigue damage using equation 2.58 for which material S-N data needs to be specified. Additional points on the transfer function can be produced by linearly interpolating between base wave case points. This is to ensure an accurate response spectrum when there are sharp changes in the sea state spectra, i.e. at the peaks of the sea state spectra.

Several sea states can be used to obtain the damage for a given period of time using Miner's rule. These can include sea states from various directions if base wave cases for these angles are available.

By using a special option in the ASAS#FATJACK data file, output can be produced so that it can be edited by an interface file to produce the transfer function and response spectra for a critical inspection point. This was done so that fatigue programs written by the author could be used.

7.5.5. N2

N2 is a program which calculates the fatigue damage using a stress response spectrum produced by `asas#FATJACK`. As well as the conventional narrow band result the program calculates the rainflow range version and ordinary range version of fatigue damage (equations 3.6 and 3.8).

The second part of the program calculates the fatigue damage potential of individual strips within the response plot. In this way relative damage values for each part of the response plot can be estimated. It is then possible to assess the merits of structural changes with reference to the fatigue damage, e.g. the effect of removing the dynamic response altogether.

7.5.6. N12

Because the fatigue damage potential of one part of a response plot depends on other frequencies present we can say there is an interaction effect. This program is able to estimate the effect of the interaction. More details of N2 and N12 are given in chapter 3.

7.6. Results

For the purpose of distinguishing between various changes in the model shape and loading conditions, the following classifications will be used;

Model.1

Structure A, 12 base wave cases,

Model.2

Structure B, 5 base wave cases,

Model.3

Structure B, 12 base wave cases,

Model.4

Structure B, 20 base wave cases.

Model 2 was not included as a realistic design model, but was included because 5 base wave cases was considered to be the minimum that could be used to give a realistic result.

Structures A and B are plotted on figure 7.10. The corresponding mode shapes are plotted on figure 7.11. All the results are listed in Table 7.2.

In this type of analysis, added mass is included in the structure to account for non structural parts such as the deck. Equation 7.22 gives the theoretical relationship for a one degree of freedom system. The results for the natural frequencies of the structure under varying amounts of added mass confirm this (see figure 7.15).

The variation in response for different critical damping values is shown in figure 7.16. As expected the static peak is unaffected by the damping value used. The variation in the dynamic peak gives good agreement with the peak value of equation 7.31 for the same conditions.

Result H3 (figures 7.17(a-k)) is taken as an example of typical deepwater conditions. The response is two peaked. The peak on the left is at the frequency of the wave energy and is called the static peak. The peak on the right corresponds to the peak in the transfer function and is referred to as the dynamic peak.

The dynamic response is almost entirely due to the fundamental mode, i.e., translational sway. The contribution to the response from mode 3 upwards is negligible.

The dynamic peak is at the fundamental frequency (point 14, H=2.4m and T=3.3 seconds). The position of the static peak varies according to the wave spectra used, but is between points 1 and 3 (H=20m and T from 25 to 10 seconds).

Figure 7.1 illustrates that the force reduction with depth is much sharper for the smaller wave because of the shorter period, and since a large proportion of the fatigue damage results from the dynamics peak (see figures 7.18), it is important to make the vertical distance between points for which the loading is calculated sufficiently short. This was a major source of error with structure A (compare results D1 to D18 for structure A with results H3 to H17 for structure B).

Some of the ASAS results have been reanalysed using program N2. Table 7.3 lists the results. As expected, the rainflow range cycle counting method of predicting the fatigue damage consistently predicts longer fatigue lives than the conventional narrow band approach.

These results also indicate the sea states which give the most fatigue damage. PERNBD represents the percentage damage in sea state i . DISC represents the percentage difference between the narrow band and rainflow range results. By comparing the graphical results for the same computer runs as in table 7.3 (figure 7.24) it is possible to see that the biggest discrepancy occurs when the dynamic and static peaks are furthest apart and at the same time balanced with each other.

It is useful to estimate the maximum error in the fatigue result for given errors in the response spectrum. Reference 7.3 and earlier chapters showed that the relationship between a response plot change and the fatigue damage is nonlinear and a function of the S-N curve as well as other frequencies present in the response plot.

Figure 7.19 shows three methods of estimating this error;

- (1) Clip the dynamic peak by a percentage of the maximum dynamic peak value, e.g., every part of the dynamic response plot above 90% of its maximum is removed,
- (2) Reduce the whole of the dynamic peak by a certain percentage,
- (3) Reduce the whole response spectrum by a certain percentage.

Table 7.4 lists the results for an S-N slope value of 4.38 (the value used throughout this investigation).

This shows that a 20% overall reduction in the response plot gives a 60% reduction in R.R. fatigue damage. This indicates that a small error in response plot leads to a much larger error in the fatigue damage. This very important result shows that the fatigue damage result is very sensitive to errors in the response plot.

An error in the dynamics peak has been reported (ref.7.32), which results from the Pierson Moskowitz spectrum. Sea state spectra are nearly always produced with particular reference to the peak wave energy frequency and so the tails of the spectrum can have significant errors. Any error in the right hand tail is passed through the transfer function into the response plot. In effect, the dynamics peak is only as accurate as the tail of the wave spectrum, and because this is of very low amplitude, large percentage errors can result.

Another important source of error in the dynamic peak is the choice of damping value. A change from 3% to 4% critical damping results in a 66% reduction in the rainflow range fatigue damage.

A further error with the response spectrum arises because of the steady state assumption in ASAS#RESPONSE. For a wide band signal the steady state response for an isolated part of the signal is unlikely to be attained. There will therefore be an overestimate of the response around the dynamic peak.

Both directionality of waves and the height of the mean water level effect the response. Figure 7.20 shows the effect of changing the angle of wave propagation. This clearly shows that waves which hit the structure end on cause the most fatigue damage. This is very important because some authors (ref.7.1) suggest using square on waves only. This is an overconservative approach. A more realistic result can be obtained by forming a transfer function of fatigue damage against angle of propagation. Only 45° needs to be considered because the other 7 directional sectors are repetitions of the first. Unless the structure has different properties in the x and y directions, in which case 90° would need to be used.

If the area where the structure is to be built experiences tidal effects, then a further dimension needs to be added to the transfer function. Tidal variations in the mean water level result in a change in the transfer function. Figure 7.21 shows that the most dangerous place to have the mean water level is at a horizontal bracing level.

The variation of this transfer function with depth is difficult to explain at the point midway between the bracing levels, but is most likely to be a result of the way the loading is calculated, i.e., at set points along the member. Because of this, some discontinuities are created by the mathematical modelling. This is because the loading prediction is maximum just below the surface and zero above it. Therefore, as the mean water level is moved down the structure, points where the loading is calculated slowly move into the area of maximum loading and then suddenly into an area of zero loading. Real variations in the loading are only expected when the maximum loading capability of the wave increases. This is when the waves are hitting more members (when the mean water level and horizontal bracing level coincide), or hitting more members at the same time (when the wavelength and structural spacing width coincide).

If a sine wave probability density function is used to model the tidal movement, care should be taken to avoid the situation where the outside range of the function is at a bracing level. This would result in the worst loading conditions being experienced for the maximum time.

For a complete fatigue analysis a knowledge of the wave directional probabilities and tidal variations is required. This information can be combined with the 3D transfer function (figures 7.20 and 7.21) to obtain the total fatigue damage in a given period of time using Miner's rule.

As mentioned earlier, both the number of phase increments used to sine fit the loading and the sine fitting process itself, both lead to errors in the result. Figure 7.12 shows the sine fitting process for 12, 6 and 4 phase increments for both a drag dominated wave and an inertia dominated wave. This shows that if less than 12 increments are used then errors are rapidly introduced into the result.

Although a non linear wave theory is used to calculate the static loading values for drag dominated waves (figure 7.12(b)), the sine fitting procedure effectively linearises the loading history. If two terms were used to sine fit the loading history a better representation of the phase information would be obtained with a corresponding increase in the computing time required.

Another way of reducing the errors involved with the sine fitting process would be to use a Fourier analysis on the total loading rather than sine fitting individual nodal loadings. This seems justified, since for fatigue damage calculations it is the global (1st mode sway) response which is most important, and the area of concern for fatigue purposes is usually at the position of maximum moment near to the base. The n terms obtained from the fourier analysis could then be applied to the structure at the mean water level separately. The total response could be obtained by combining the steady state displacements from each of the n terms. This would also improve the result for splash zone members experiencing wet/dry wave action (figure 7.12(c)). Obviously the local response in the wave zone would have to be checked separately.

The errors involved in applying loads to the mean water level would be less important than with a design wave analysis. This is because the waves causing the fatigue damage are relatively small, so the point of loading is never too far from the mean water

level. Also, because the loading lever arm would almost always be overestimated by this method, the result would be conservative.

7.7. Conclusions

A review of available fatigue analysis methods which may be applied to dynamically sensitive structures has been carried out. These can be broadly categorised as follows;

- (a) Deterministic,
- (b) Transient (or time domain),
- (c) Spectral,
- (d) Deterministic/spectral,
- (e) Transient/spectral,
- (f) Probabilistic.

Using the results from the Atkins package and programs N2 and N12, a comprehensive review of the Deterministic/Spectral method of fatigue analysis was carried out. It was found that several problems exist with the use of this method. These are listed below;

- (a) Within ASAS#WAVE, nodal loadings are calculated at set time intervals. A sine fitting process is applied to these nodal loadings to obtain an harmonic representation of the loading time history. This effectively linearises any non linear wave theory used, so errors may be introduced into the results.
- (b) The sine fitting process can also cause significant errors in the splash zone where members are experiencing wet/dry action. Wave loadings for this type of action would be similar to an impulse function. The sine fitting process would however reduce this to an harmonic loading.
- (c) In addition to non linearities in the wave theory, the loading equation is nonlinear. This creates difficulties with the use of Spectral Analysis because the transfer function can only represent a linear system. Therefore a choice of wave heights and associated periods must be made. This choice is difficult because the link between height and period is not constant for all sea states.

- (d) ASAS#WAVE uses a set of 'base wave cases' to produce points on a transfer function. If too few waves are used, then an inaccurate response plot is obtained.
- (e) For each base wave case used, and at each time interval, loadings are calculated at set points along the member. If the variation of loading is severe, either vertically or horizontally, the overall loading may be overestimated or underestimated.
- (f) An investigation has been carried out into the fatigue damage potential of separate parts of the response plot. This showed that percentage errors in the response plot are magnified when the fatigue damage is calculated.
- (g) ASAS#FATJACK uses the traditional narrow band fatigue damage equation. This produces a conservative result when compared to the rainflow counting method.
- (h) The effect of tidal variation on response was shown to be very important. The results indicated that it is not realistic to choose one mean water level as being representative of the loading for the long term response of the structure.
- (i) In a similar way to the effect of mean water level on response, the variation in wave direction needs to be considered if an accurate results is to be obtained.
- (j) Many of the problems with the Deterministic/Spectral approach are caused by calculating nodal, rather than total loadings for the structure. A literature survey suggests that a reasonable result for fatigue purposes can be obtained by calculating only the total loads on the structure. This will be shown in the next section to be a way of improving the analysis method.
- (k) When using the Spectral method of analysis, the response plot is obtained by multiplying the input sea spectrum by the transfer function for the system. The result is a two peaked response spectrum. The static peak comes from the sea spectrum and the dynamic peak comes from the transfer function. The magnitude of these peaks is reasonably accurate in percentage terms. However, the response plot peaks are also a function of the tails of the transfer function and sea state spectra. These tails have been shown to be susceptible to various errors which are large in percentage terms because of the relatively low magnitude of the signal at these points.

From the above conclusions several areas for future work can be identified as follows

The most difficult problem with the use of the Deterministic/Spectral method is the way the transfer function is obtained. It may be possible to obtain a more complete representation of the loading problem which will remove the necessity to calculate the loadings for set base wave cases and at set points along the members. This method would also enable the overall fatigue analysis to include the very important effects of wave direction and tidal variation.

To illustrate the idea, let us assume that only the vertical members in the structure receive loading. Linear wave theory assumes that the force on a vertical member is;

$$F_T = A \cos\theta + B (\sin\theta)^2 \quad (7.118)$$

Nath and Harleman linearised this to;

$$F_T = C \sin(\theta + \phi) \quad (7.119)$$

Which tends to $A \cos\theta$ as the wave height reduces. Therefore equation 7.119 will be used to illustrate a way of obtaining the maximum loading on the structure. If F_{T1} is the maximum force on one vertical pile, then;

$$F_{TN} = \left[\sum \sin(\theta + \phi) \right] F_{T1} \quad (7.120)$$

Where;

$$(\theta) \text{ is equal to } \frac{2\pi x_l}{L} \text{ at time } t$$

x_l is the horizontal distance from some reference point.

If the waves are assumed to hit end on then figure 7.22 gives the maximum force. This can be compared with equation 7.82 (figure 7.23) for an angle of 0. An approach similar to equation 7.120 may have considerable benefits over 7.82 if it can be developed to cover the case where all the loading is not lumped into the vertical piles. This is often the case for the fatigue calculation on dynamically sensitive structures because it is important to retain all the frequency information of the loading.

The second area of research which can be developed uses the concept of 'Sub PSD' functions. This should provide a way of dealing with non linear problems while using the Spectral method of analysis.

An important flaw exists with the Deterministic/Spectral approach because of the nonlinear height against response curve. The problem arises because spectral theory requires that the system is linear. A nonlinear system can be linearised by choosing an appropriate value of loading to produce the signal. For offshore structures, the most conservative method is to use the highest possible wave for a given frequency (figure 7.13(a)). This is given justification by the strong link between the heights and periods of sea waves (equation 7.4).

For the case where the system is very nonlinear and/or there is no strong link between the magnitude and frequency of the signal the Deterministic/Spectral approach should not be used in its present form. A general solution to this problem is outlined below;

- (a) Take an input power spectral density function and inverse fourier transform it into a time series, or use an expression similar to 7.4.
- (b) Reconstitute the signal into 'Sub PSD' functions, each one containing the frequency information of only a discrete magnitude of signal. The original signal should be obtainable by simply adding the Sub PSDs together.
- (c) Use any method to produce the same number of transfer functions, with each transfer function being valid for only a discrete range of signal. i.e., a step linearisation of the nonlinear response curve.
- (d) Multiply Sub PSD i by transfer function i to get response plot i .
- (e) Obtain total response by combining the individual response plots or get fatigue damage directly from the Sub response plots. This method may be applicable in nonlinear areas where the spectral approach is preferred.

7.8. References

- (7.1) M.G. Hallam et al. Dynamic and Fatigue Analysis of Murchison Tower Structure, O.T.C. paper 3163, 1978.
- (7.2) R.K. Kinra and P.W. Marshall. Fatigue Analysis of the Cognac Platform, O.T.C. paper 3378, 1979.
- (7.3) N.W.M. Bishop and F. Sherratt. Fatigue Damage Assessment of Structures Subject to Random Loading and the Contribution to the Fatigue Damage by Discrete Frequency Intervals Within the Power Spectral Density Plot, Control Theory Center, University of Warwick, 1986.
- (7.4) L.E. Borgman. Spectral Analysis of Ocean wave Forces on Piling, Journal of the waterways and harbours division, A.S.C.E., Vol 93 no WW2, 1967.
- (7.5) M.S. Longuet-Higgins. On the Statistical Distribution of the Heights of Sea Waves, Journal of marine research, Vol XI, no 3, 1952.
- (7.6) W.J. Pierson and L. Moskowitz. A Proposed Spectral Form For Fully Developed Wind Seas Based on the Similarity Theory of S.A. Kitaigorodskii, Journal of Geophysical Research, Vol 69, no 24, 1964.
- (7.7) A.K. Williams and J.E. Rinne, Fatigue Analysis of Steel Offshore Structures, Procs I.C.E., Part 1, nov 1976.
- (7.8) L.E. Borgman. Directional Spectra for Design Use, O.T.C. paper no. 1069, 1969.
- (7.9) P.W. Marshall. Dynamic and Fatigue Analysis Using Directional Spectra, O.T.C. paper no. 2537, 1976.
- (7.10) B. Berge and J. Penzien. Three-Dimensional Stochastic Response of Offshore Towers to Wave Forces, O.T.C. paper no. 2050, 1974.
- (7.11) G.G. Stokes. On the Theory of Oscillatory Waves, Mathematical and Physical Papers, I, Cambridge University Press, 1880.
- (7.12) H. Lamb. Hydrodynamics, 6th edition, New York: Dover Publications, Inc, 1945.
- (7.13) Eagleson and Dean, Small Amplitude Wave Theory, Ch A, Estuary and Coastline Hydrodynamics, 1966

- (7.14)M.G. Hallam et al. Dynamics of Marine Structures : methods of calculating the dynamic response of fixed structures subject to wave and current action, Report UR8, CIRIA/UEG, 6 Storey's gate, London, 1977.
- (7.15)B. Kinsman. Wind Waves, Prentice Hall, Inc, New Jersey, 1965.
- (7.16)J.R. Morison et al. The force Exerted by Surface Waves on Piles, Petroleum Trans.,189, TP 2846, 1950.
- (7.17)J.H. Nath and D.R.F. Harleman. The Dynamic Response of Fixed Offshore Structures to Periodic Random Waves, M.I.T. Hydrodynamic Laboratory Report 102, 1967.
- (7.18)L.E. Borgman. A Statistical Theory For Hydrodynamic Forces on Objects, Hydraulic Engineering Laboratory Report HEL 9-6, 1965.
- (7.19)N.R. Maddox. A Deterministic Fatigue Analysis for Offshore Platforms, preliminary paper for 6th O.T.C., 1974.
- (7.20)N.F. Ebecken et al. Static and Dynamic Analysis of Offshore Structures Supported on Pile Foundations, Offshore Structures Engineering, Pentech Press, London, 1979.
- (7.21)N.R. Maddox. Fatigue Analysis for Deepwater Fixed Bottom Platforms, O.T.C. paper no. 2051, 1974.
- (7.22)N.K. Lin and W.H. Hartt. Time Series Simulations of Wideband Spectra for Fatigue Tests of Offshore Structures, Trans. of ASME, Vol 106, 1984.
- (7.23)A.K. Malhotra and J. Penzien. Nondeterministic Analysis of Fixed Offshore Structures, Eng. Mechs. Div. ASCE Vol 96 no. EM6, 1970.
- (7.24)J.R. Wallis et al. Fatigue Analysis of Offshore Structures, Trans. ASME, Vol 101, 1979.
- (7.25)A.K. Malhotra and J. Penzien. Response of Offshore Structures to Random Wave Forces, Journal of the Structural Division, ASCE Vol 96, no ST10, 1970.
- (7.26)A.E. Mansour and D.N. Millman. Dynamic Random Analysis of Fixed Offshore Platforms, O.T.C. paper no. 2049, 1974.

- (7.27)A.J. Ferrante et al. On the Fatigue Analysis of Offshore Caisons, Procs. 3rd Int. Symp. on Offshore Engineering, 1981.
- (7.28)Atkins Research and Development. Analysis of Offshore Structures with ASAS/FATJACK related programs, W.S. Atkins Group, Epsom, 1979.
- (7.29)D.J. Cronin et al. Spectral Fatigue Analysis for Offshore Structures, Ch.9, Numerical methods in offshore engineering, John Wiley and sons, Chichester, 1978.
- (7.30)N.R. Maddox. A Spectral Fatigue Analysis for Offshore Structures, O.T.C. paper no. 2261, 1975.
- (7.31)K.Y. Kan and C. Petruskas. Hybrid Time-Frequency Domain Analysis For Deep-water Platforms, O.T.C. paper no. 3965, 1981.
- (7.32)J.R. Wallis et al. An Approach to Probabilistic Fatigue Analysis of Offshore Structures, O.T.C. paper no. 3379, 1979.
- (7.33)R. Sigbjornsson. Extreme and Fatigue Response of Offshore Platforms due to Three Dimensional Stochastic Wave Fields, Eng. Structs, Vol 3, 1981.
- (7.34)P.H. Wirsching. Probabilistic Fatigue Design for Ocean Structures, Struct. Div. ASCE, Vol 103, no. ST10, 1977.
- (7.35)K.S. Bathe and E.L. Wilson. Solution Methods for Eigenvalue Problems in Structural Mechanics, Int. J. Numerical Methods in Engineering, Vol 2, 1973.
- (7.36)D.M. Pierce. Dynamic Analysis of Platforms Subjected to Ocean Waves, Exxon production research company report, EPR.21PR.73, 1973.
- (7.37)J.K. Penzien et al. Stochastic Response of Offshore Towers to Random Sea Waves and Strong Motion Earthquakes, Computers and Structures, Vol 2, Pergamon Press, 1972.
- (7.38)A.P.I. Recommended Practice for Planning, Designing and Constructing Fixed Offshore Platforms, APIRP 2A, fourth Edition, 1972.
- (7.39)A simplified approach to stress cycle counting procedure, A report prepared for BP International Ltd by Atkins Research and Development, Epsom, June 1984.
- (7.40)K. Patel and P.E. Freathy, A simplified method for assessing wind induced fatigue damage, a paper presented at Int Conf 'Design Against Wind Induced Failure',

Bristol, January 1984. To be published in 'Engineering Structures'.

(7.41)The response of flexible structures to atmospheric turbulence, ESDU sheet 76001 - Engineering Science Data Unit Ltd, ESDU International, 251-259 Regent Street, London, September 1976.

(7.42)Characteristics of atmospheric turbulence near the ground. Part II; single point data for strong winds (neutral atmosphere), ESDU sheet 85020 - Engineering Science Data Unit Ltd, ESDU International, 251-259 Regent Street, London, October 1975.

Table 7.1. Statistical properties and damage expectations computed from Wirsching's data

Sea State	Sig. Wave Ht.	Dom. Per.	Fract. of Time in Sea State i
S.S.	H _s	T _D	T
1	16.01	17.3	0.0000368
2	14.48	16.5	0.0000932
3	12.96	15.8	0.00037
4	11.43	14.7	0.0022
5	9.90	13.6	0.0073
6	8.38	12.7	0.0135
7	6.86	11.6	0.0265
8	5.53	10.3	0.08
9	3.81	9.1	0.21
10	2.28	7.7	0.49
11	0.76	4.4	0.19

Table 7.2(i). base wave cases used in ASAS#WAVE

RUN	D1-E4	E5	F1-F8	G1	G2-H1	H2	H3-H32	I1
BASE	30@24	30@24	30@24	40@24	40@24	40@24	20@25	20@25
WAVE	20@20	20@20	20@20	20@10	20@10	20@10	20@13.33	2.74@3.53
CASES	20@10	20@10	20@10	9.0@6.7	9.0@6.7	9.0@6.7	20@10	2.4@3.5
USED	9.0@6.7	9.0@6.7	9.0@6.7	3.5@4.2	3.5@4.2	3.5@4.2	14.08@8.0	2.2@3.16
TO	5.4@5.2	5.4@5.2	5.4@5.2	3.2@4.0	3.2@4.0	3.2@4.0	9.76@6.66	1.57@2.67
PRODUCE	3.5@4.2	3.5@4.2	3.5@4.2	2.9@3.86	2.9@3.85	2.9@3.85	7.17@5.71	
TRANSFER	3.2@4.0	3.2@4.0	3.2@4.0	2.7@3.7	2.7@3.7	2.2@3.3	5.5@5.0	
FUNCTION	2.9@3.86	2.9@3.86	2.9@3.86	2.4@3.5	2.4@3.5	1.9@3.1	4.34@4.44	
	2.7@3.7	2.7@3.7	2.7@3.7	2.2@3.31	2.2@3.3	1.8@3.0	3.52@4.00	
HEIGHT	2.4@3.5	2.4@3.5	2.4@3.5	1.9@3.1	1.9@3.11	1.7@2.9	3.19@3.81	
in	2.3@3.4	2.3@3.4	2.3@3.4	1.8@3.0	1.8@3.0	1.6@2.8	2.91@3.64	
m	2.2@3.3	2.2@3.3	2.2@3.3	1.7@2.9	1.7@2.9	1.5@2.7	2.74@3.53	
and(@)							2.54@3.43	
PERIOD							2.40@3.30	
in							2.31@3.24	
seconds							2.20@3.16	
							2.09@3.08	
							1.93@2.96	
							1.80@2.86	
							1.57@2.67	

Table 7.2(ii). Full ASAS results

Asas Run	Added Mass	Funda-mental Freq	Elev Rel to Hor Br Lvl	Critical Damping	Direction	TOLS	Life at Node 1002	Life at Node 1009	Struc-ture
	Tonnes	Hz	m	%	Degrees		Years	Years	
D1	81000	0.258	+6.0	3.0	0.0	NO	14.92		A
D2	81000	0.258	+4.5	3.0	0.0	NO	4.02		A
D3	81000	0.258	+3.0	3.0	0.0	NO	0.81		A
D4	81000	0.258	+1.5	3.0	0.0	NO	0.18		A
D5	81000	0.258	+0.0	3.0	0.0	NO	0.02		A
D6	81000	0.258	-1.5	3.0	0.0	NO	9.31		A
D7	81000	0.258	-3.0	3.0	0.0	NO	151.03		A
D8	81000	0.258	-4.5	3.0	0.0	NO	163.58		A
D9	81000	0.258	-6.0	3.0	0.0	NO	167.38		A
D10	81000	0.258	-7.5	3.0	0.0	NO	199.55		A
D11	81000	0.258	-9.0	3.0	0.0	NO	171.10		A
D12	81000	0.258	-10.5	3.0	0.0	NO	147.51		A
D13	81000	0.258	-12.0	3.0	0.0	NO	116.91		A
D14	81000	0.258	-13.5	3.0	0.0	NO	452.52		A
D15	81000	0.258	-15.0	3.0	0.0	NO	282.11		A
D16	81000	0.258	-16.5	3.0	0.0	NO	144.35		A
D17	81000	0.258	-18.0	3.0	0.0	NO	57.10		A
D18	81000	0.258	-19.0	3.0	0.0	NO	26.16		A
E1	81000	0.258	+6.0	1.0	0.0	NO	0.87		A
E2	81000	0.258	+6.0	2.0	0.0	NO	6.34		A
E3	81000	0.258	+6.0	4.0	0.0	NO	24.75		A
E4	81000	0.258	+6.0	5.0	0.0	NO	35.05		A
E5	81000	0.258	+6.0	3.0	0.0	NO	16.66		A
F1	81000	0.258	+6.0	3.0	2.5	NO	15.71		A
F2	81000	0.258	+6.0	3.0	5.0	NO	18.09		A
F3	81000	0.258	+6.0	3.0	10.0	NO	31.04		A
F4	81000	0.258	+6.0	3.0	15.0	NO	65.08		A
F5	81000	0.258	+6.0	3.0	20.0	NO	133.18		A
F6	81000	0.258	+6.0	3.0	25.0	NO	206.50		A
F7	81000	0.258	+6.0	3.0	35.0	NO	272.50		A
F8	81000	0.258	+6.0	3.0	45.0	NO	383.90		A
G1	54000	0.301	+6.0	3.0	0.0	NO	49.64		A
G2	45000	0.322	+6.0	3.0	0.0	NO	93.70		A
G3	63000	0.322	+6.0	3.0	0.0	NO	21.35		A
H1	27000	0.249	+6.0	3.0	0.0	NO	63.13		A
H2	27000	0.249	+6.0	3.0	0.0	NO	98.10		A
H3	36000	0.303	+6.0	3.0	0.0	YES	28.52		B
H4	36000	0.303	+2.0	3.0	0.0	YES	1.90		B
H5	36000	0.303	+4.0	3.0	0.0	YES	8.82		B
H6	36000	0.303	+1.0	3.0	0.0	YES	1.09		B
H7	36000	0.303	-2.0	3.0	0.0	YES	20.86		B
H8	36000	0.303	-4.0	3.0	0.0	YES	21.97		B
H9	36000	0.303	-6.0	3.0	0.0	YES	28.84		B
H10	36000	0.303	-8.0	3.0	0.0	YES	38.74		B

Table 7.2(ii)(cont). Full ASAS results

Asas Run	Added Mass	Funda-mental Freq	Elev Rel to Hor Br Lvl	Critical Damping	Direction	TOLS	Life at Node 1002	Life at Node 1009	Struc-ture
	Tonnes	Hz	m	%	Degrees		Years	Years	
H11	36000	0.303	-10.0	3.0	0.0	YES	45.95		B
H12	36000	0.303	-12.5	3.0	0.0	YES	7.38		B
H13	36000	0.303	+8.0	3.0	0.0	YES	57.80		B
H14	36000	0.303	+10.0	3.0	0.0	YES	89.19		B
H15	36000	0.303	+12.5	3.0	0.0	YES	3.61		B
H16	36000	0.303	-1.0	3.0	0.0	YES	0.36		B
H17	36000	0.303	+0.0	3.0	0.0	YES	0.27		B
H18	36000	0.303	-11.5	3.0	0.0	YES	22.65		B
H19	36000	0.303	+11.5	3.0	0.0	YES	6.34		B
H20	36000	0.303	+11.5	3.0	2.5	YES	6.64		B
H21	36000	0.303	+11.5	3.0	5.0	YES	8.18		B
H22	36000	0.303	+11.5	3.0	10.0	YES	12.02		B
H23	36000	0.303	+11.5	3.0	15.0	YES	18.86	37.71	B
H24	36000	0.303	+11.5	3.0	20.0	YES	48.74	69.08	B
H25	36000	0.303	+11.5	3.0	25.0	YES	70.72	89.70	B
H26	36000	0.303	+11.5	3.0	30.0	YES	122.93	100.42	B
H27	36000	0.303	+11.5	3.0	35.0	YES	159.36	101.48	B
H28	36000	0.303	+11.5	3.0	40.0	YES	160.17	74.77	B
H29	36000	0.303	+11.5	3.0	45.0	YES	200.0	68.20	B
H30	36000	0.303	+11.5	3.0	32.5	YES	152.0	109.6	B
H31	36000	0.303	+11.5	3.0	37.5	YES	153.0	87.70	B
H32	36000	0.303	+11.5	3.0	42.5	YES	205.0	88.50	B
I1	36000	0.303	+11.5	3.0	0.0	YES	0.45		B

Table 7. 3. N12 results for fatigue damage caused by sea states 1 to 11

N12 RESULTS FOR ASAS RUN D1						
RRDAM	ORDAM	NBDAM	DISCR	PERNBD		
2429	1135	2975	22.5	0.1		
4677	2330	5742	22.8	0.3		
13305	70682	16354	22.9	0.8		
58715	35163	72187	22.9	3.5		
134725	90619	165231	22.6	8.0		
162983	123754	198523	21.8	9.7		
203969	175763	244276	19.8	11.9		
330049	316953	381197	15.5	18.6		
476995	480703	526125	10.3	25.6		
388755	395255	405296	4.3	19.7		
36393	36523	36537	0.4	1.8		
181295	172880	2054443				
17.490	18.341	15.435	13.3			

N12 RESULTS FOR ASAS RUN D15						
RRDAM	ORDAM	NBDAM	DISCR	PERNBD		
635	435	684	7.7	0.6		
1091	735	1178	8.0	1.1		
2794	1860	3023	8.2	2.8		
10140	6604	11027	8.7	10.1		
18982	12247	20752	9.3	19.1		
17910	11561	19708	10.0	18.1		
15543	10293	17267	11.1	15.9		
14642	10569	16488	12.6	15.2		
11672	9668	13271	13.7	12.2		
4548	4471	5042	10.9	4.6		
231	232	232	0.4	0.2		
98188	68675	108672				
322.950	461.737	291.794	10.7			

N12 RESULTS FOR ASAS RUN D5						
RRDAM	ORDAM	NBDAM	DISCR	PERNBD		
214625	219344	239306	11.5	0.0		
531427	542987	581540	9.4	0.0		
1882950	1922050	2031170	7.9	0.1		
11987600	12205300	12673900	5.7	0.8		
38306800	38895200	39923700	4.2	2.4		
64787300	65596000	66742200	3.0	4.1		
117295000	118406000	119620000	2.0	7.3		
276285000	278150000	279569000	1.2	17.0		
521935000	524584000	525879000	0.8	31.9		
533947000	535996000	536461000	0.5	32.6		
62851500	63041300	63051200	0.3	3.8		
1630024202	1639558181	1646772016				
0.019	0.019	0.019	1.0			

N12 RESULTS FOR ASAS RUN D18						
RRDAM	ORDAM	NBDAM	DISCR	PERNBD		
1510	697	1836	21.6	0.2		
2868	1403	3500	22.0	0.3		
8058	4187	9855	22.3	0.9		
34735	20243	42556	22.5	3.8		
78131	51468	95640	22.4	8.5		
92784	69151	112994	21.8	10.0		
113421	96647	136035	19.9	12.1		
179434	171724	207658	15.7	18.4		
256046	257970	282668	10.4	25.1		
207521	210972	216218	4.2	19.2		
19065	19136	19144	0.4	1.7		
993573	903598	1128104				
31.915	35.093	28.109	13.5			

Table 7. 3(cont). N12 results for fatigue damage caused by sea states 1 to 11

N12 RESULTS FOR ASAS RUN E1						
RRDAM	ORDAM	NBDAM	DISCR	PERNBD		
9131	7225	12267	34.3	0.0		
20180	17074	26510	31.4	0.1		
65331	58044	83981	28.5	0.2		
364326	344573	450284	23.6	1.3		
1049150	1031490	1248890	19.0	3.5		
1621930	1632910	1858240	14.6	5.2		
2695150	2745380	2962260	9.9	8.4		
5891730	5999950	6224990	5.7	17.6		
10588000	10722100	10901100	3.0	30.8		
10391100	10449100	10495800	1.0	29.6		
1139290	1140630	1140700	0.1	3.2		
33835318	34148476	35405022				
0.937	0.929	0.896	4.6			

N12 RESULTS FOR ASAS RUN G1						
RRDAM	ORDAM	NBDAM	DISCR	PERNBD		
3369	1994	3769	11.9	0.5		
5878	3270	6628	12.8	0.8		
15273	8184	17337	13.5	2.2		
56706	29116	65118	14.8	8.1		
108124	55769	125428	16.0	15.6		
105532	57442	123587	17.1	15.4		
98835	60899	116787	18.2	14.5		
110669	82791	131116	18.5	16.3		
113891	101295	132637	16.5	16.5		
66776	66881	73288	9.8	9.1		
6945	7004	7025	1.2	0.9		
691998	474645	802720				
45.824	66.807	39.503	16.0			

N12 RESULTS FOR ASAS RUN E4						
RRDAM	ORDAM	NBDAM	DISCR	PERNBD		
1886	957	2175	15.3	0.2		
3505	1794	4063	15.9	0.5		
9668	5041	11234	16.2	1.3		
40061	22070	46786	16.8	5.3		
85616	50724	100391	17.3	11.5		
94767	61729	111483	17.6	12.7		
103461	76847	121816	17.7	13.9		
138300	119690	161278	16.6	18.4		
165738	159537	187918	13.4	21.5		
111109	112888	118641	6.8	13.6		
8813	8858	8864	0.6	1.0		
762924	620135	874649				
41.563	51.134	36.254	14.6			

N12 RESULTS FOR ASAS RUN G2						
RRDAM	ORDAM	NBDAM	DISCR	PERNBD		
2169	1538	2322	7.1	0.7		
3708	2561	3984	7.4	1.2		
9434	6415	10170	7.8	3.1		
33514	21965	36355	8.5	11.1		
60681	38828	66251	9.2	20.2		
54888	34484	60365	10.0	18.4		
45534	28875	50559	11.0	15.5		
41456	28241	46595	12.4	14.2		
32318	25123	36626	13.3	11.2		
11947	11239	13340	11.7	4.1		
621	628	631	1.6	0.2		
296270	199897	327198				
107.030	158.631	96.913	10.4			

Table 7.3(cont). N12 results for fatigue damage caused by sea states 1 to 11

N12 RESULTS FOR ASAS RUN G3						
RRDAM	ORDAM	NBDAM	DISCR	PERNED		
3286	1437	3921	19.3	0.3		
5917	2585	7115	20.2	0.5		
15861	7076	19190	21.0	1.3		
62701	30265	76557	22.1	5.3		
128865	69519	158302	22.8	11.0		
138146	86146	170087	23.1	11.8		
150292	112075	183932	22.4	12.8		
210984	188002	251307	19.1	17.5		
276565	271893	314227	13.6	21.9		
212163	215905	225307	6.2	15.7		
26205	26350	26391	0.7	1.8		
1230985	1011253	1436336				
25.760	31.357	22.077	16.7			

N12 RESULTS FOR ASAS RUN H3						
RRDAM	ORDAM	NBDAM	DISCR	PERNED		
2612	1187	3083	18.0	0.3		
4844	2148	5761	18.9	0.5		
13220	5831	15825	19.7	1.5		
53440	24316	64692	21.1	6.0		
109753	53850	134202	22.3	12.5		
115513	63911	142527	23.4	13.3		
118183	78850	146589	24.0	13.7		
150004	125209	183353	22.2	17.1		
181429	174710	211403	16.5	19.7		
133974	136359	143381	7.0	13.4		
20306	20423	20442	0.7	1.9		
903278	686794	1071258				
35.105	46.171	29.601	18.6			

Table 7.4. N12 results for fatigue damage potential estimation.

% Dyn. Pk. Clipping	% Overall Reduction	% Dyn. Pk. Overall Red.	Increase in Fatigue Life
10.0	0.0	0.0	1.0
20.0	0.0	0.0	4.0
30.0	0.0	0.0	9.0
50.0	0.0	0.0	32.5
100.0	0.0	0.0	209.4
0.0	10.0	0.0	24.9
0.0	20.0	0.0	59.3
0.0	30.0	0.0	109.8
0.0	50.0	0.0	320.5
0.0	0.0	10.0	12.5
0.0	0.0	20.0	25.6
0.0	0.0	30.0	43.4
0.0	0.0	50.0	87.0
0.0	0.0	100.0	209.4

Table 7.5. The variation of D_N with A_w and B_w

A_w	$B_w=800$	$B_w=1200$	$B_w=1600$	$B_w=2000$
125	1921	2056	2160	2242
250	1921	2056	2160	2242
375	1921	2056	2160	2242
500	1921	2056	2160	2242

Table 7.6. The variation of D_N with b , the slope of the S-N curve, for $A_w=500$ and $B_w=1200$

FC=10							
YTOT=	b=5.0	b=4.5	b=4.0	b=3.5	b=3.0	b=2.5	b=2.0
10	2056	939	439	212	107	59	38
8	2007					59	
7	1867					58	
5	1006					47	
3	114					20	
YTOT=10							
FC=	b=5.0	b=4.5	b=4.0	b=3.5	b=3.0	b=2.5	b=2.0
5.0	2303					66	
3.0	2500					72	
2.0	2781					80	
mean value of Atkins results	1466	785	506	248	149	96	

Figure 7.1. The variation of force with depth for different wave periods

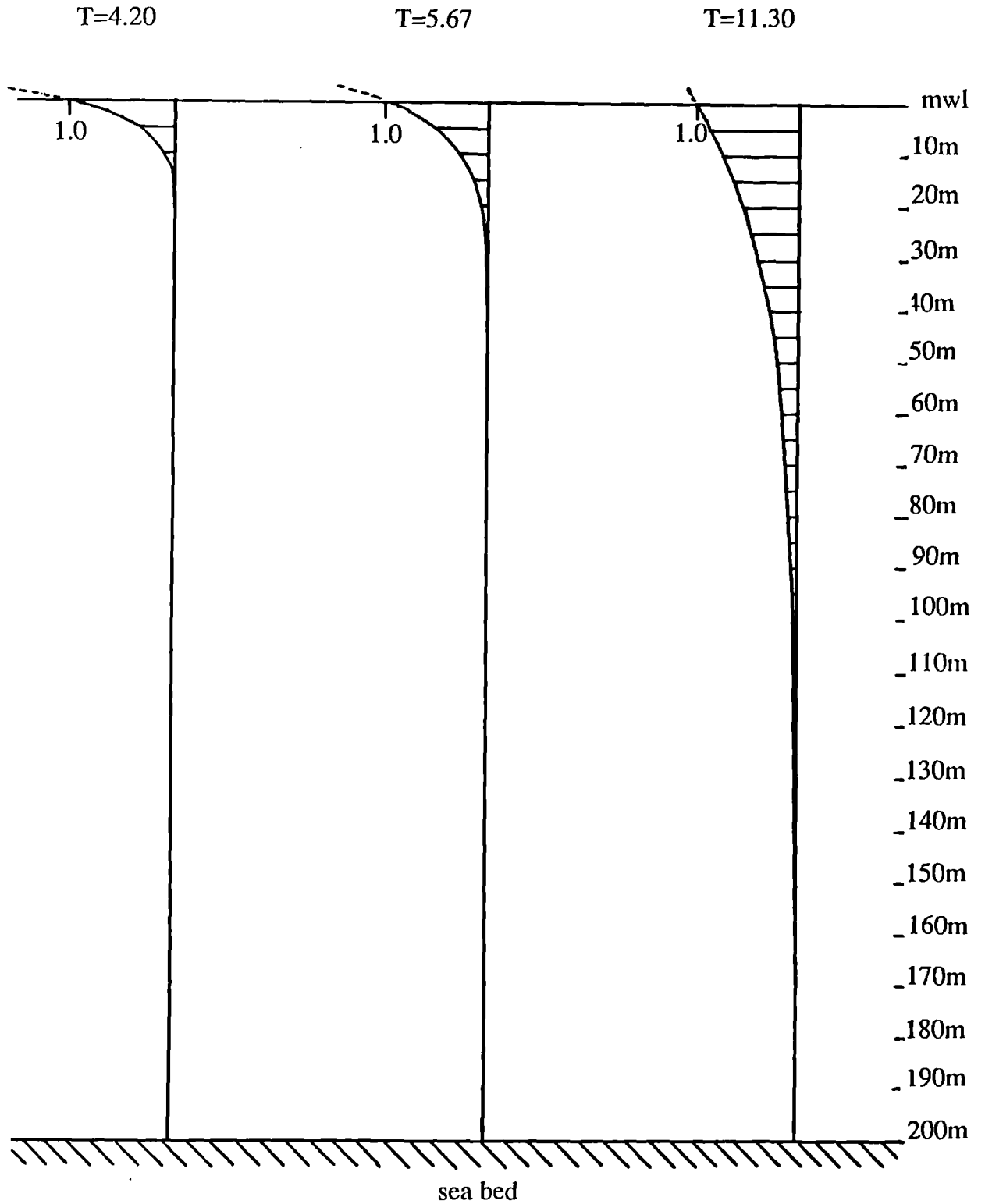


Figure 7.2(a). Velocity, acceleration and force curves along the wave profile

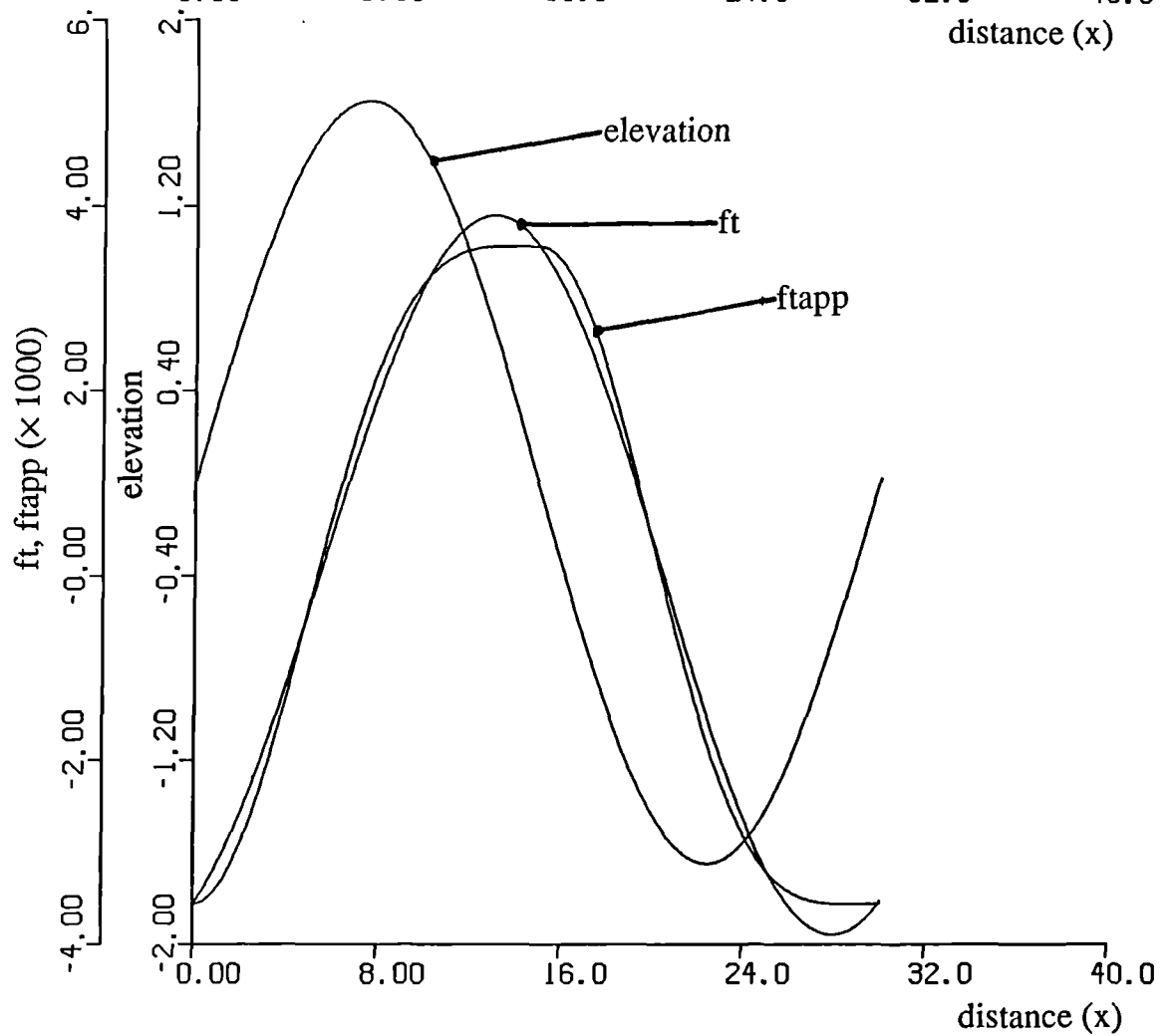
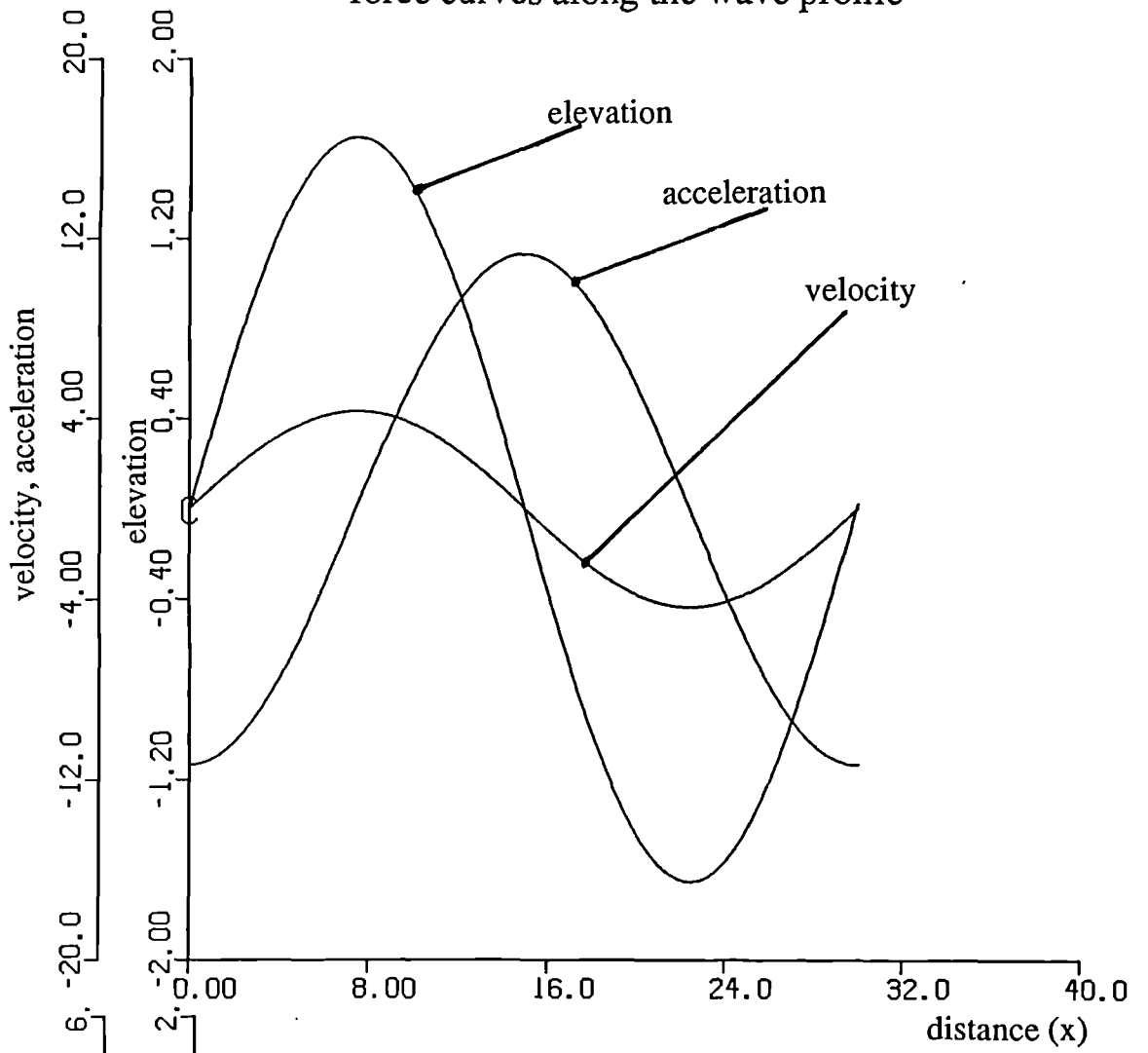


Figure 7.2(b). Results for one vertical member from an ASAS#WAVE run

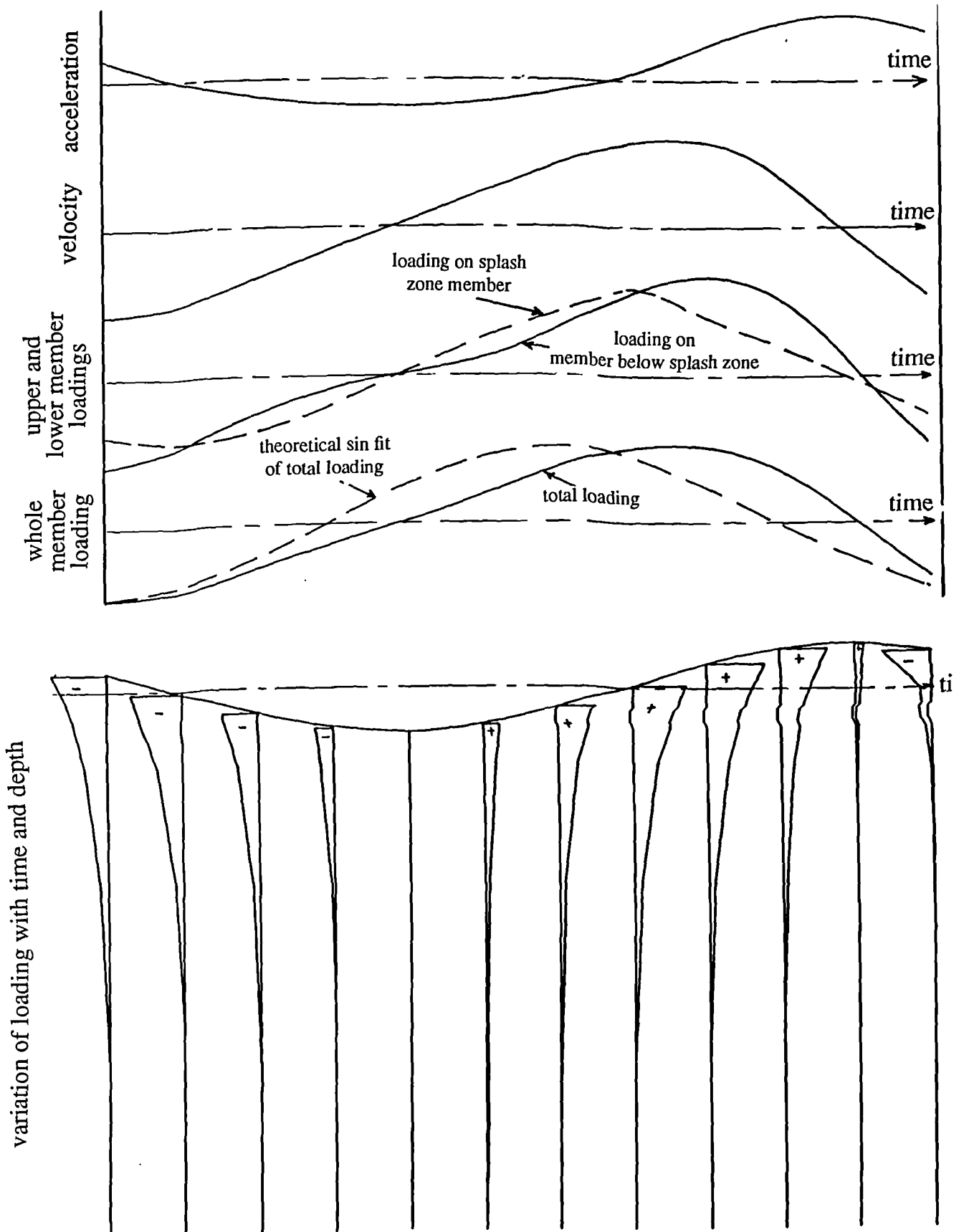


Figure 7.3. The relative effects of the drag and inertia terms on the wave force

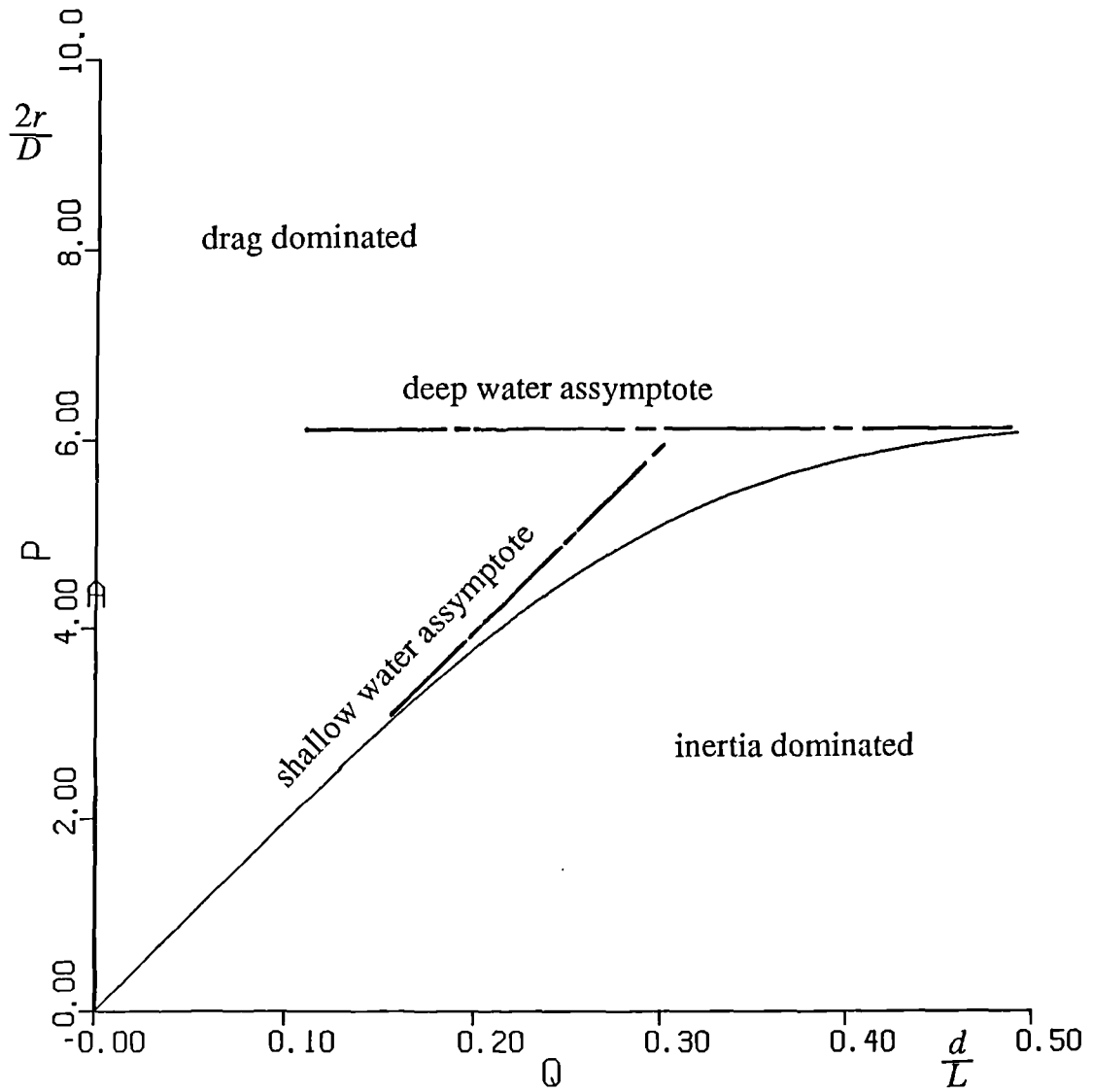


Figure 7.4. Frequency response plot for a one degree of freedom system

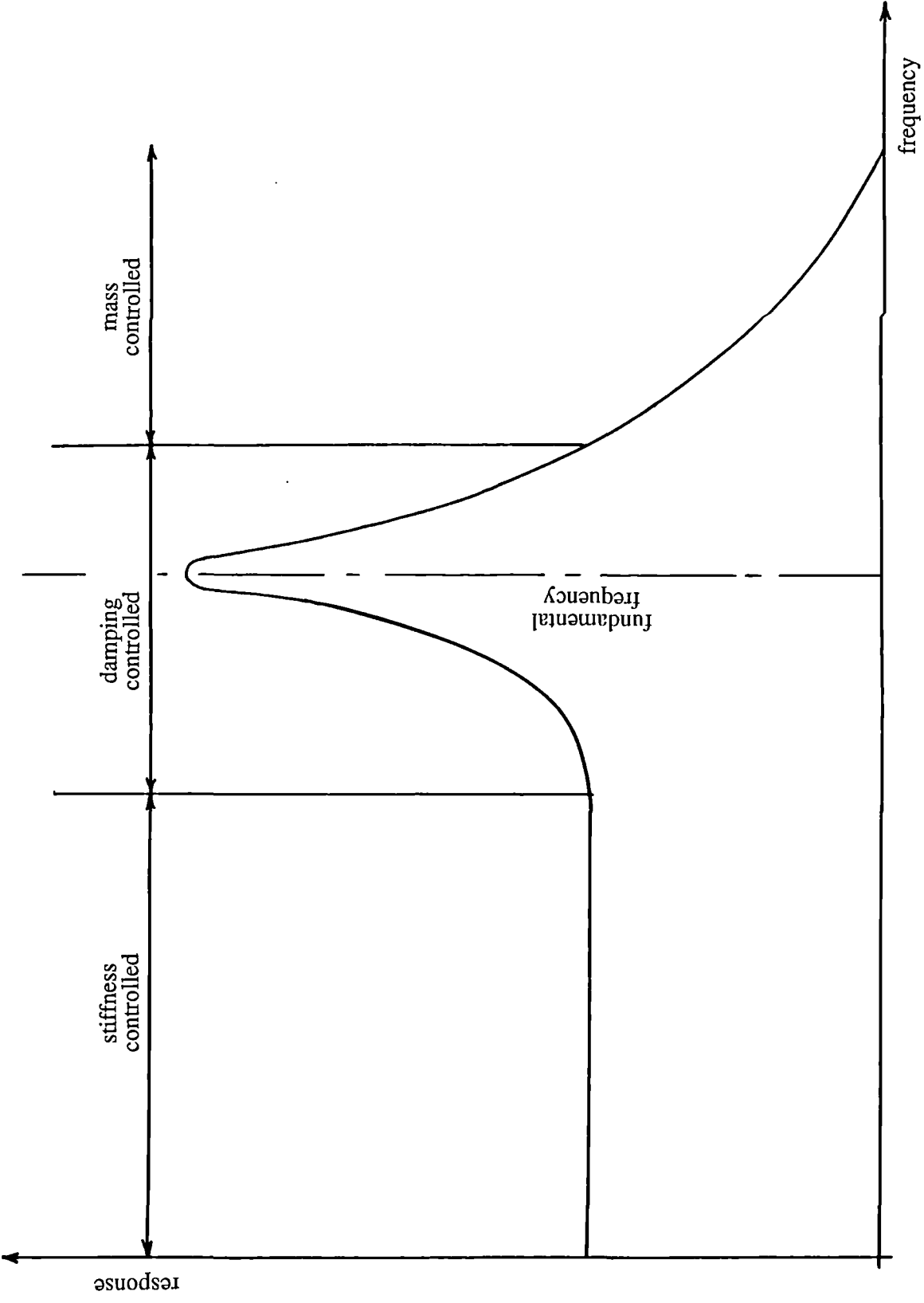


Figure 7.5. The interaction effects within any PSD plot

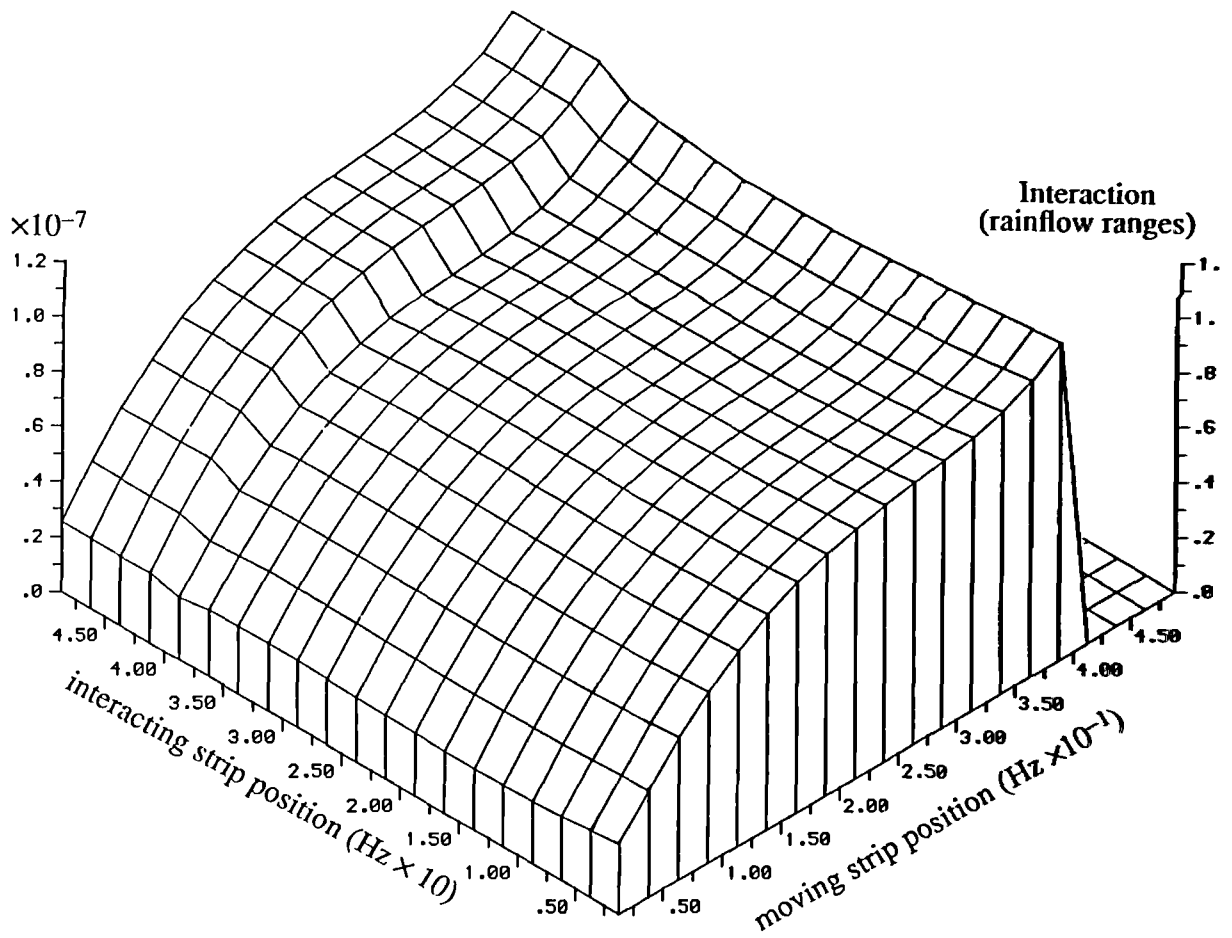
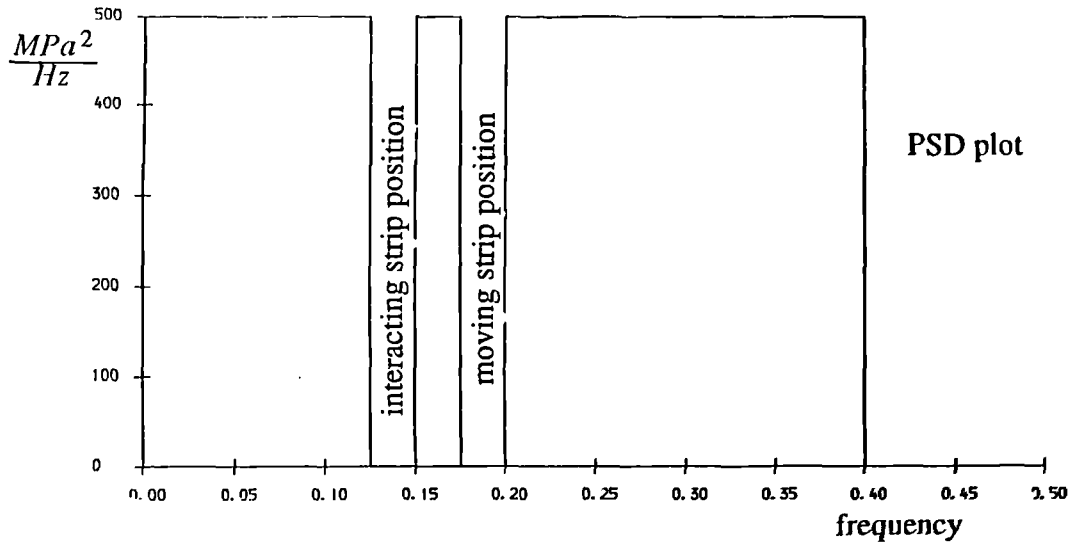


Figure 7.6(a). Velocity, acceleration and force spectra for sea state 1

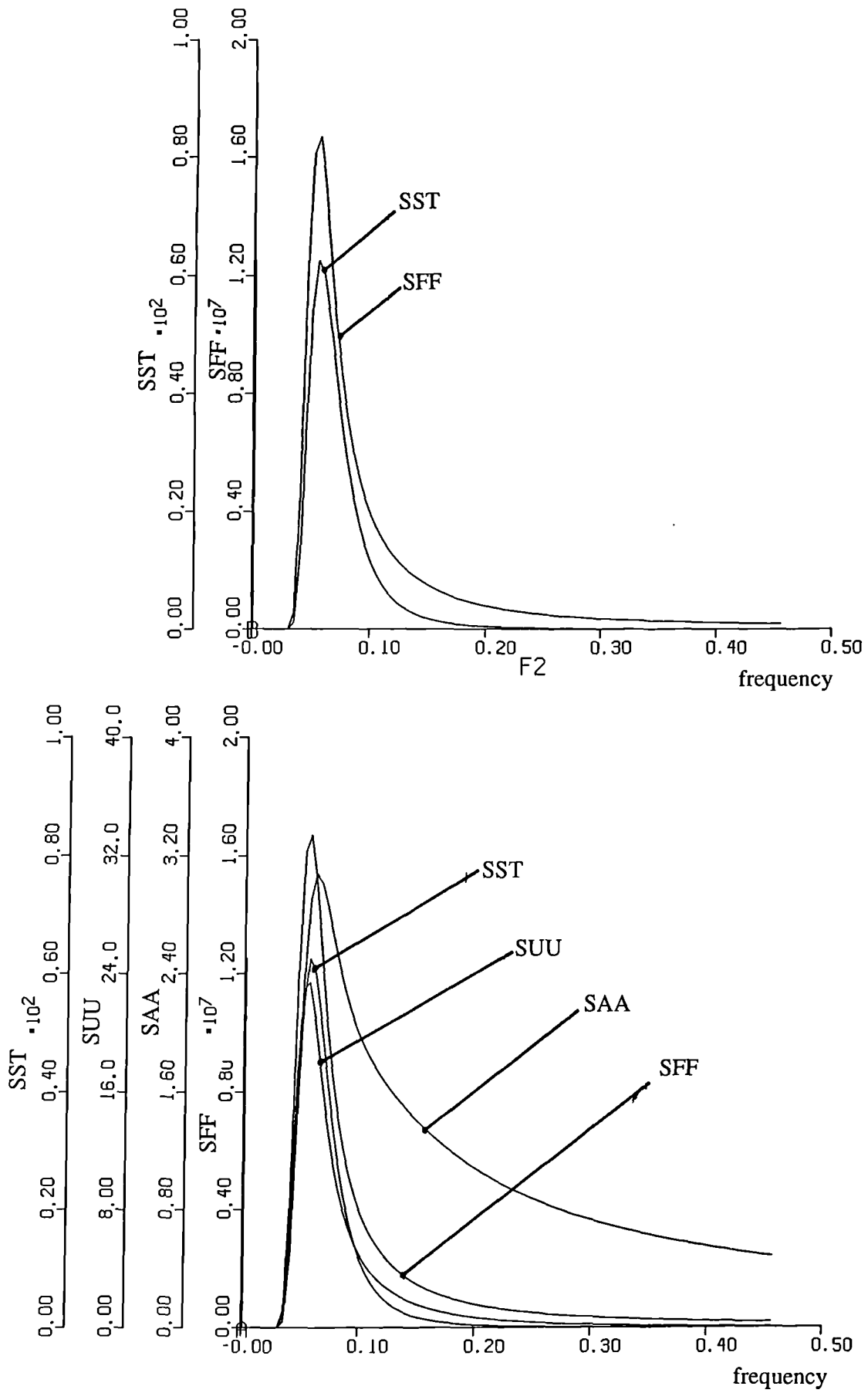


Figure 7.6(b). Velocity, acceleration and force spectra for sea state 6

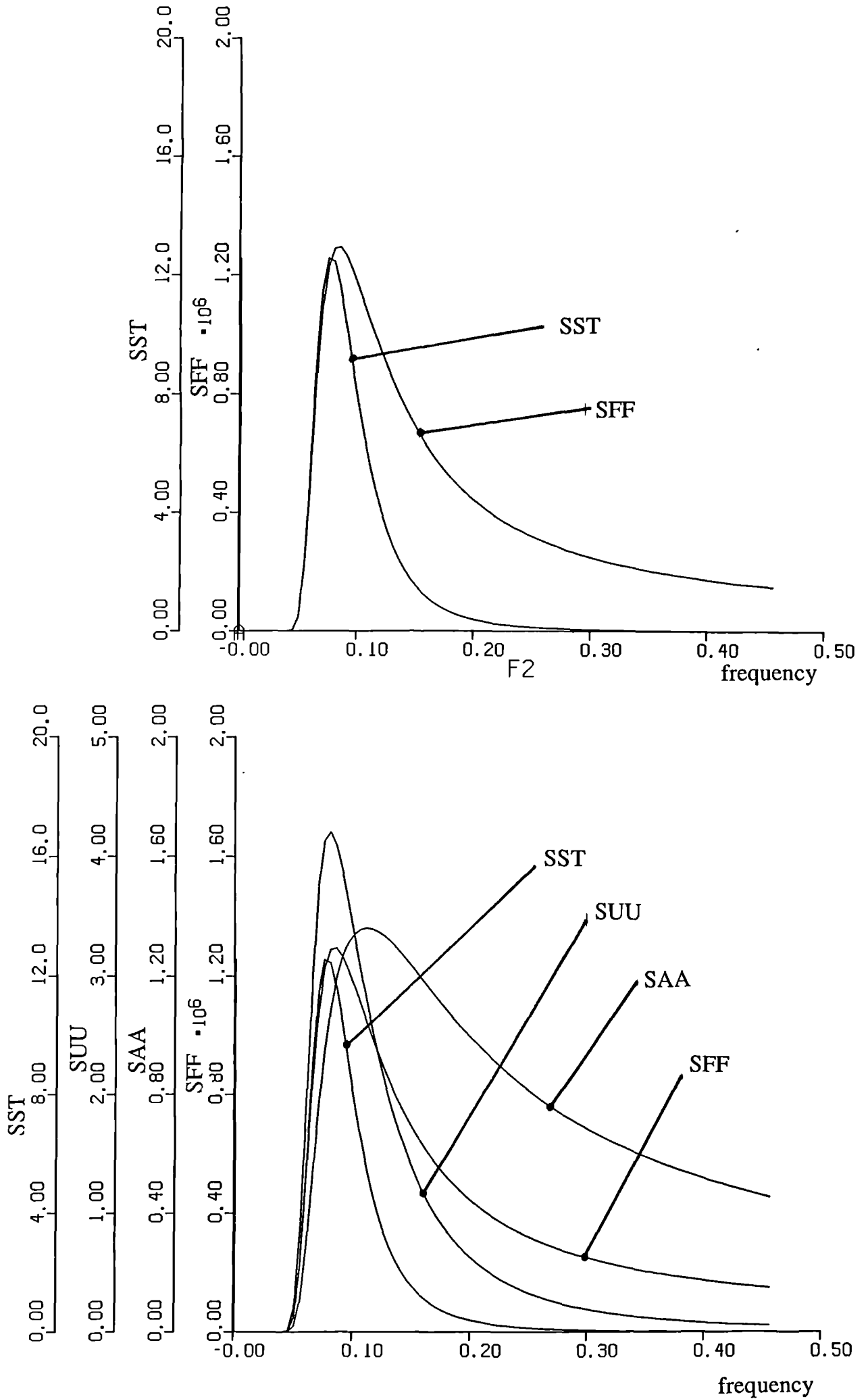


Figure 7.6(c). Velocity, acceleration and force spectra for sea state 10

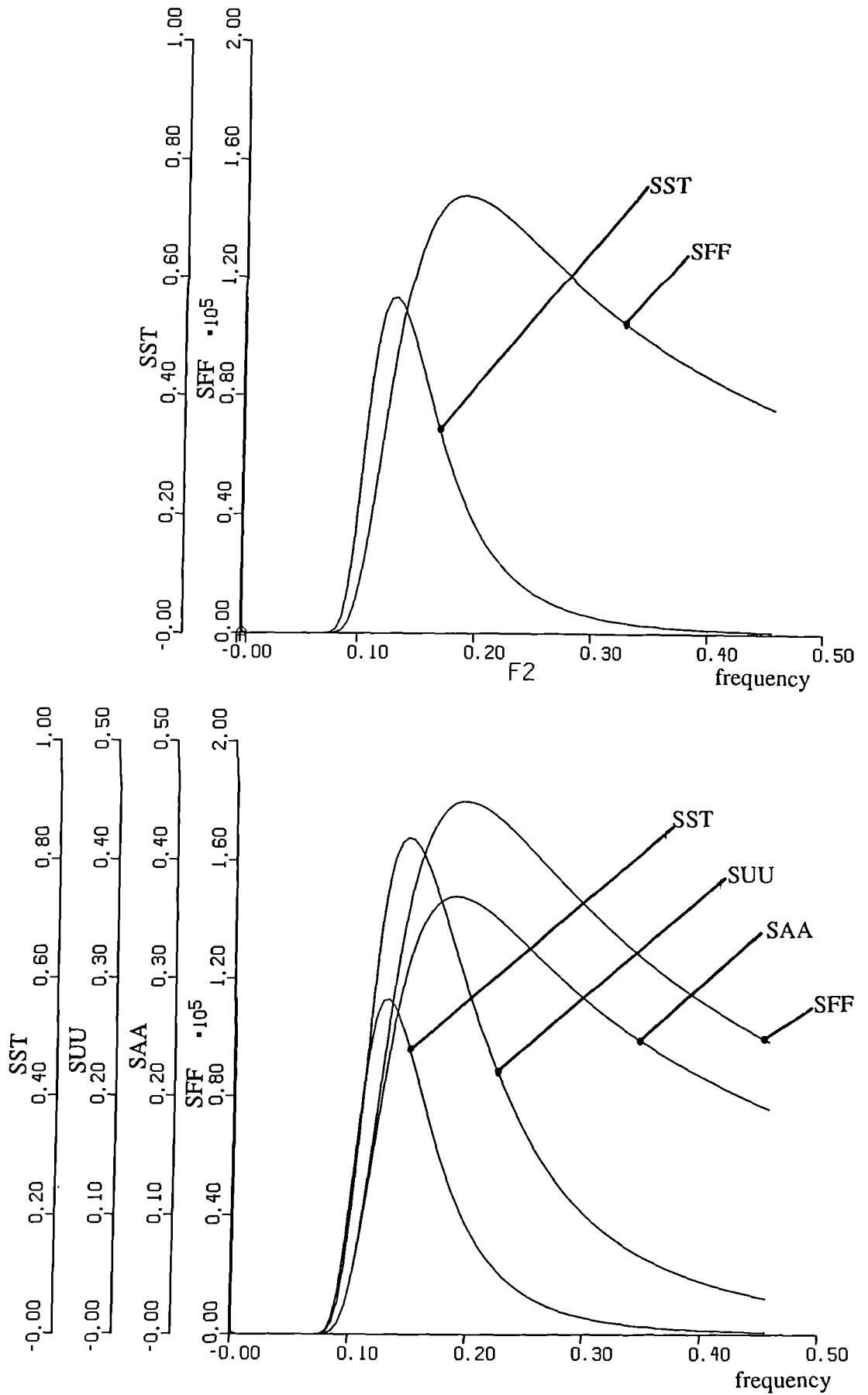


Figure 7.6(d). Velocity, acceleration and force spectra for sea state 6, with various member diameters

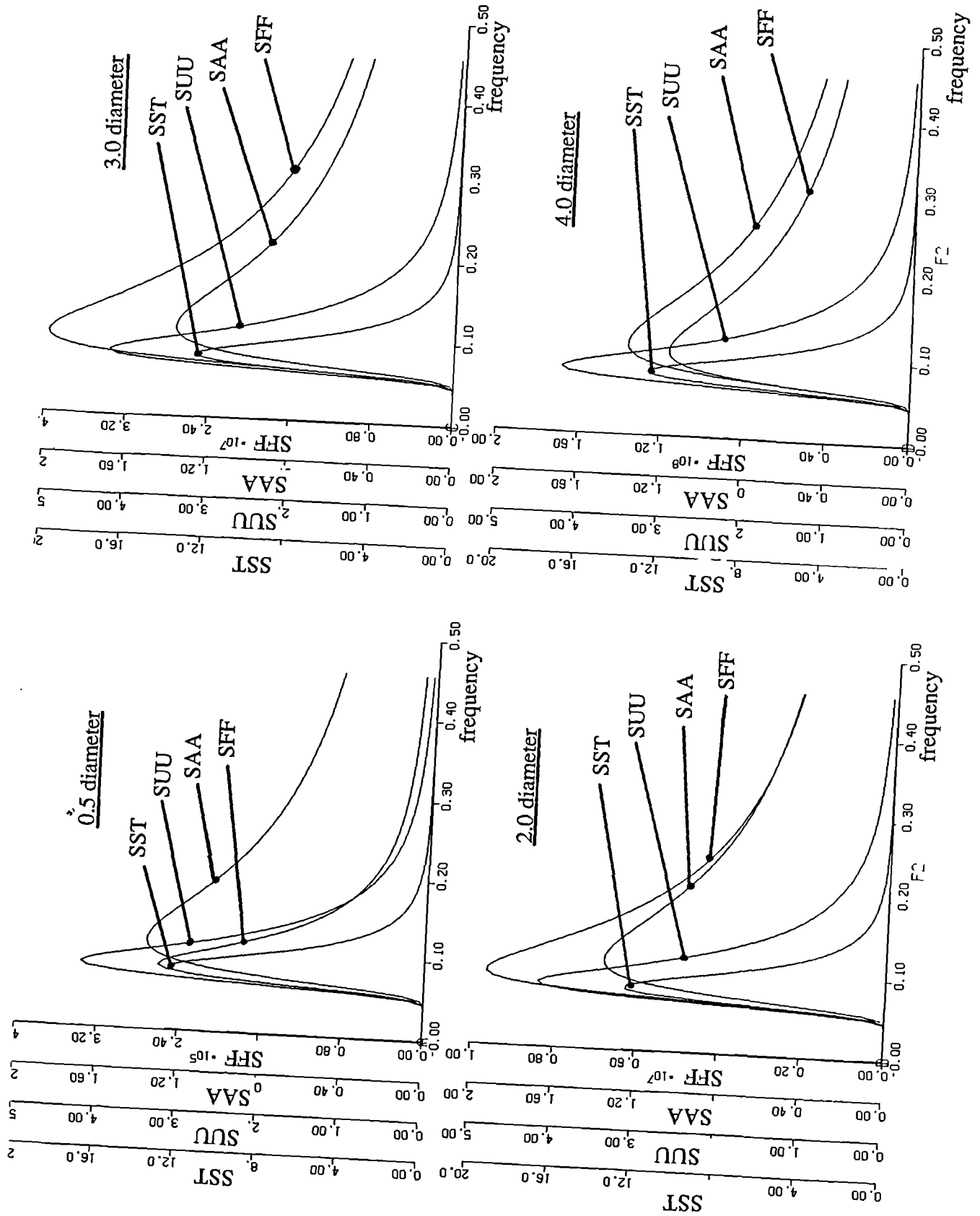


Figure 7.7. An example of the Deterministic/spectral method

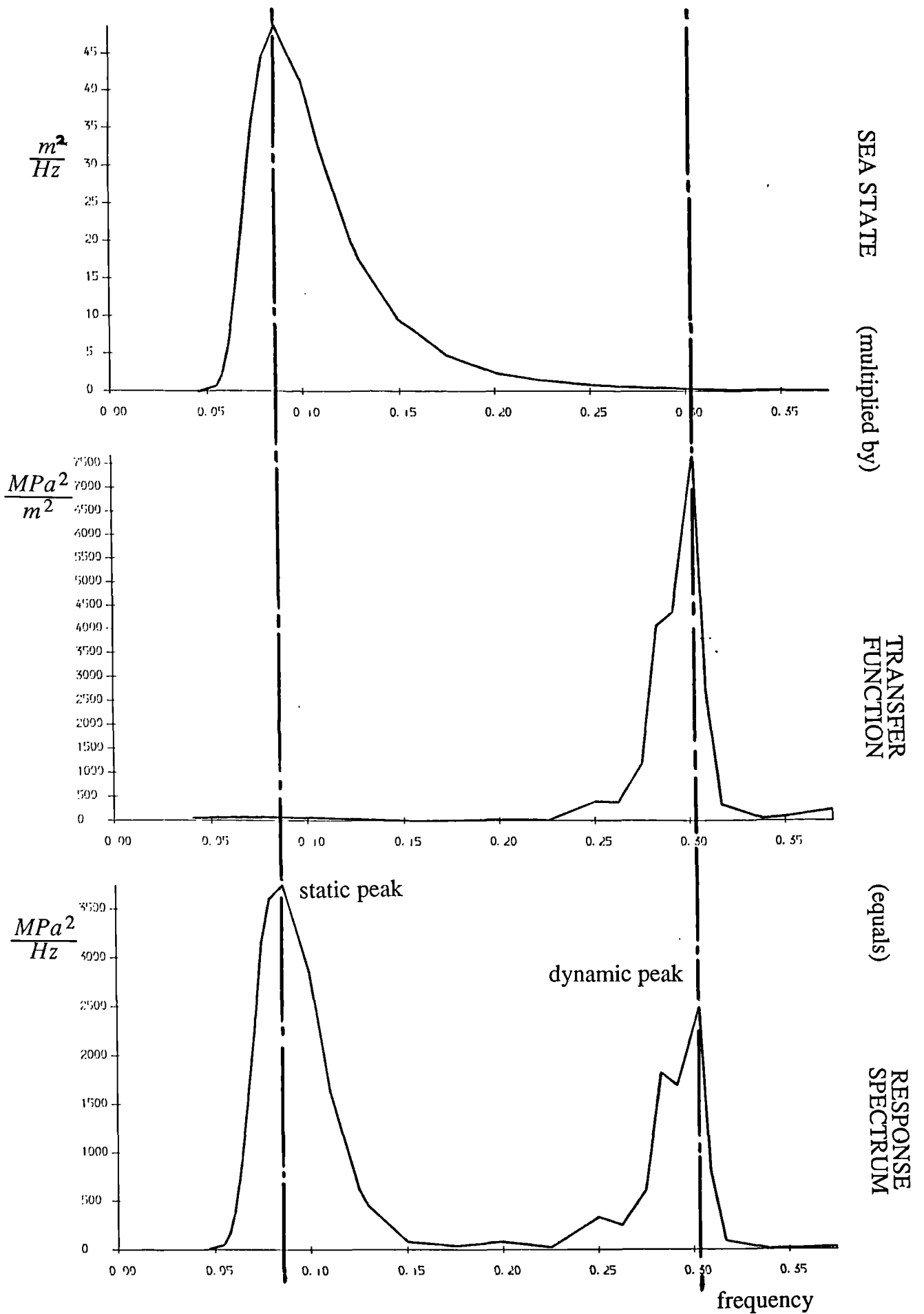


Figure 7.8. The effects of varying the parameters A_w and B_w on fatigue damage

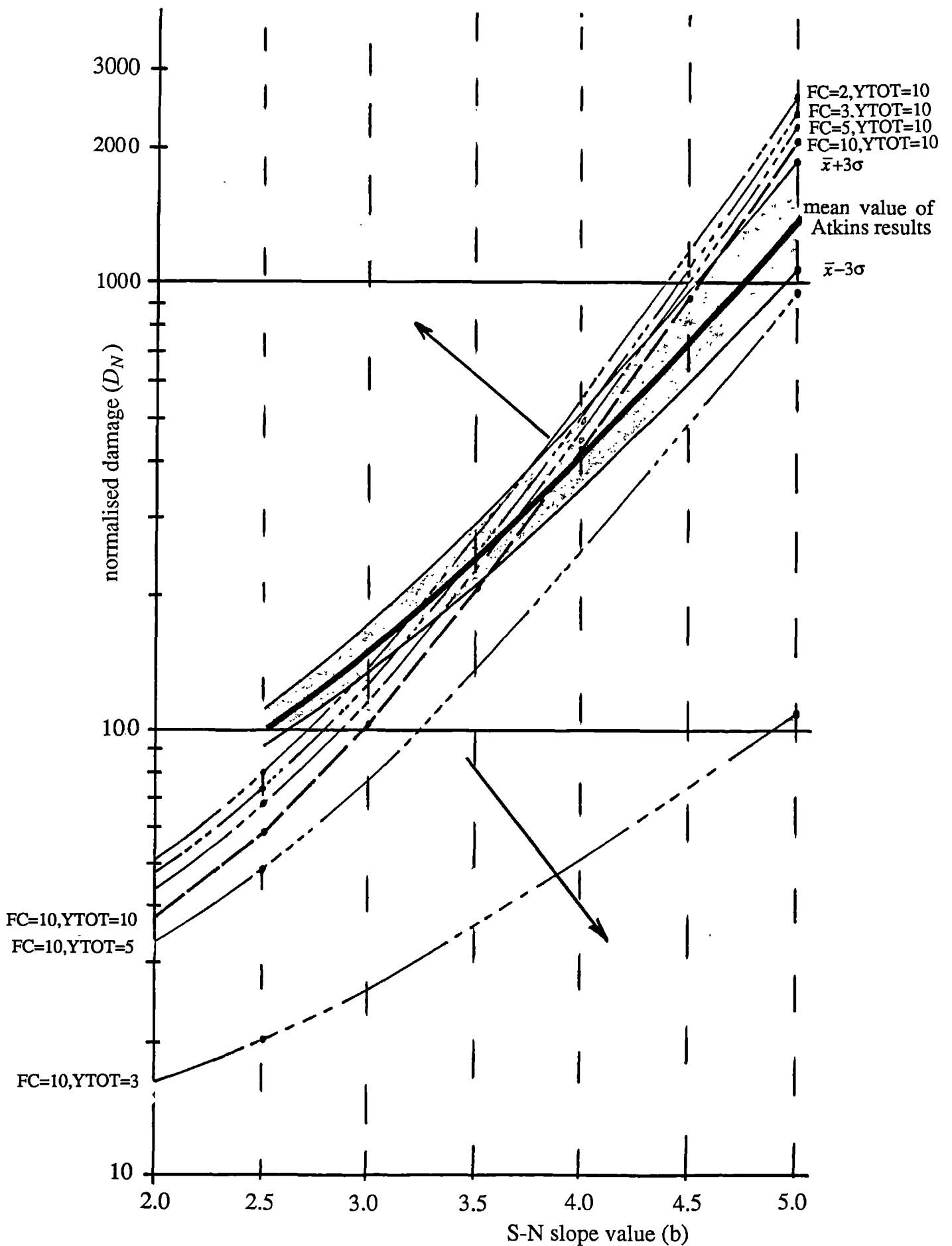


Figure 7.9. A flow chart of the programs used for analysis

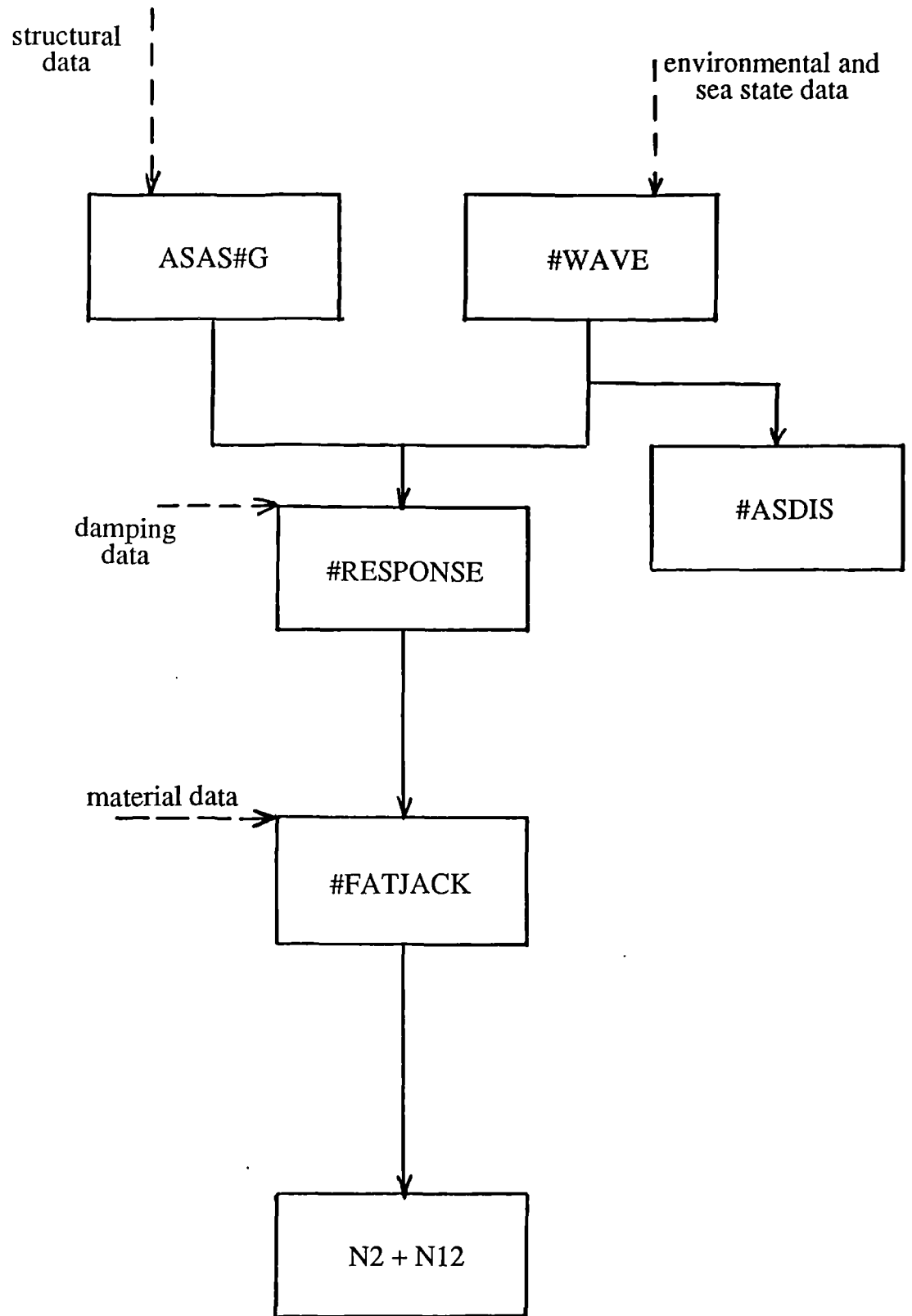


Figure 7.10. Plots of structures A and B using ASAS#ASDIS

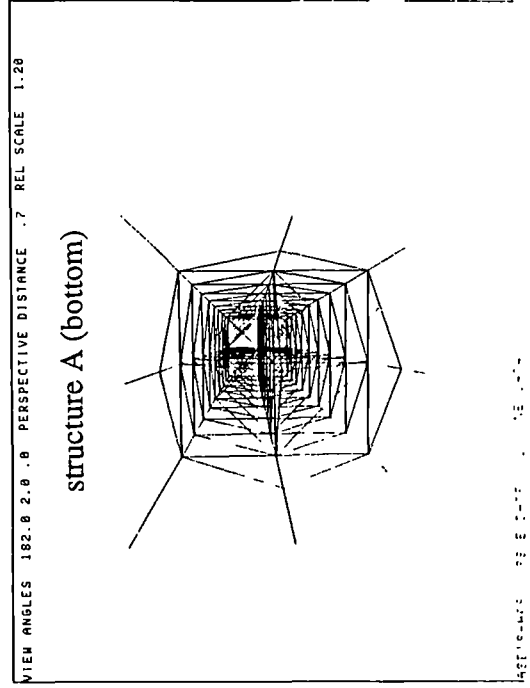
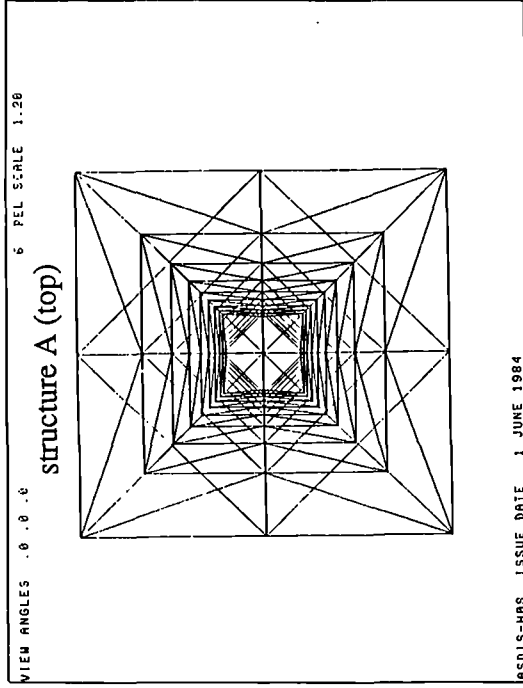
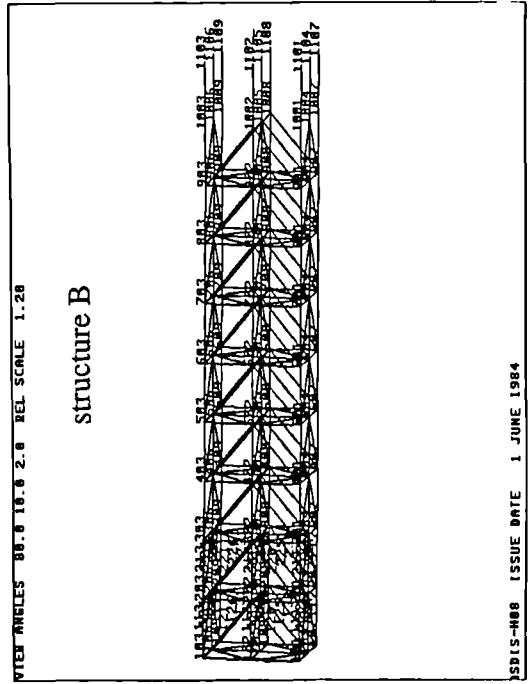
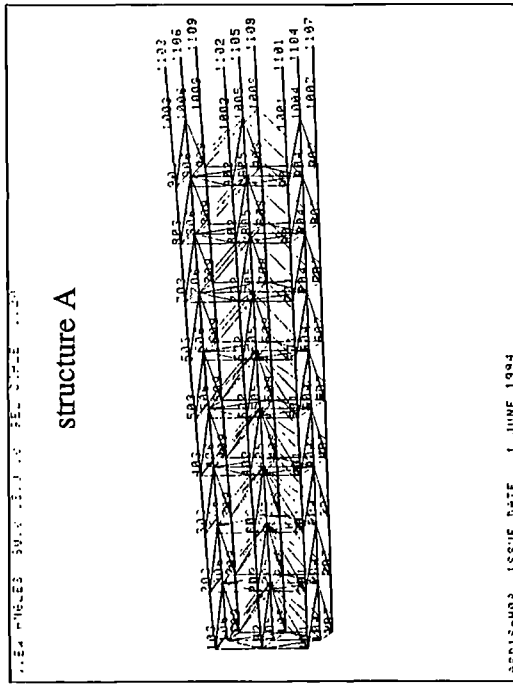


Figure 7.11. The first eight mode shapes for structure B

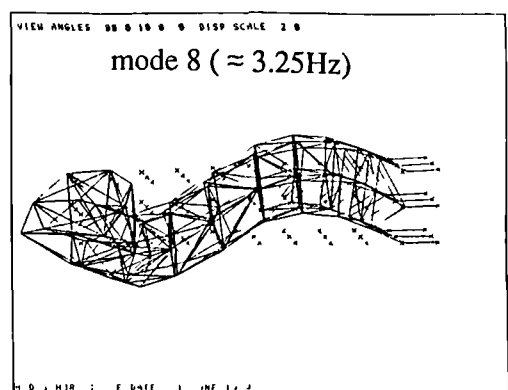
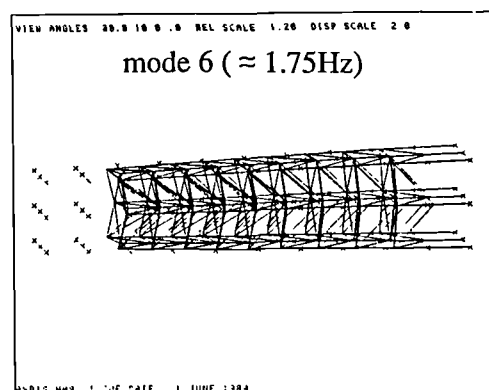
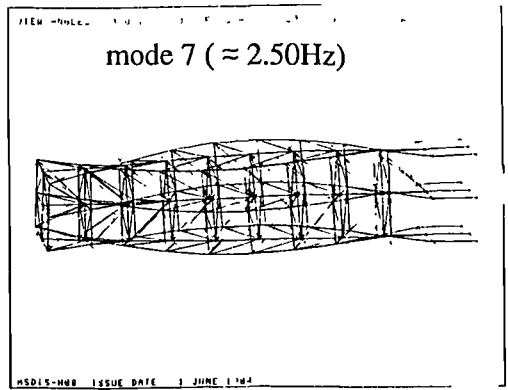
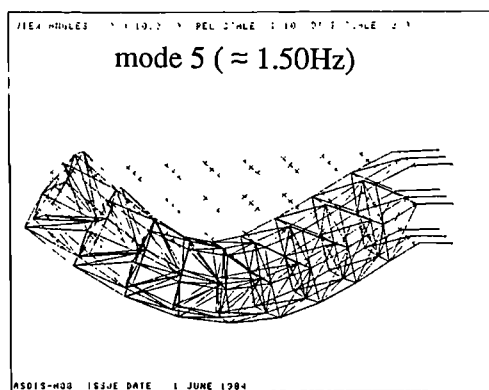
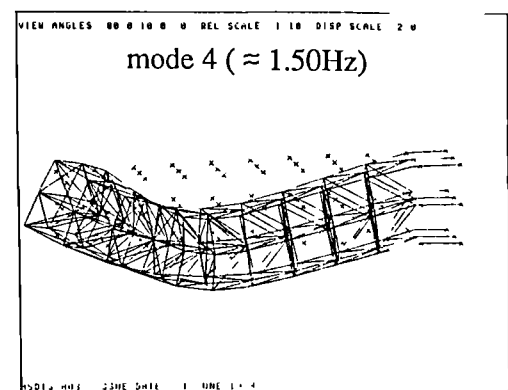
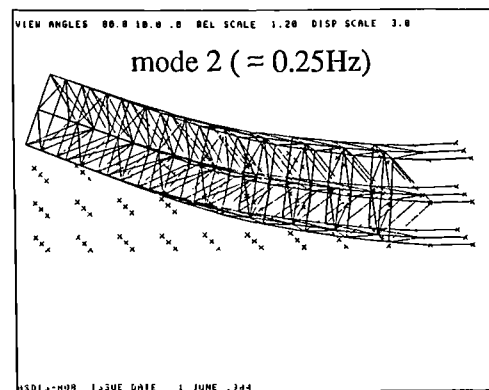
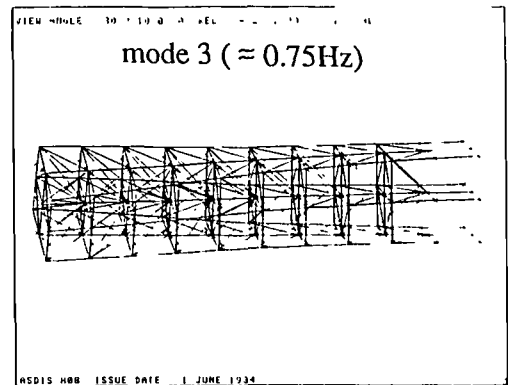
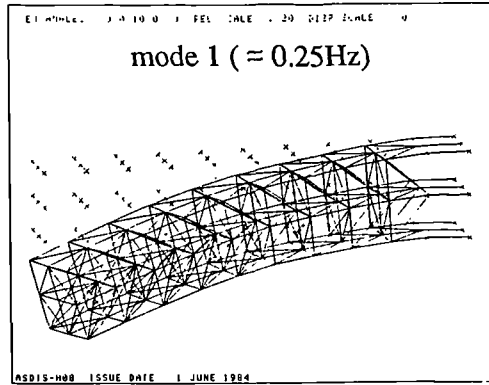


Figure 7.12(a). The sinfitting process with 12, 6 and 4 phase increments for an inertia dominated wave

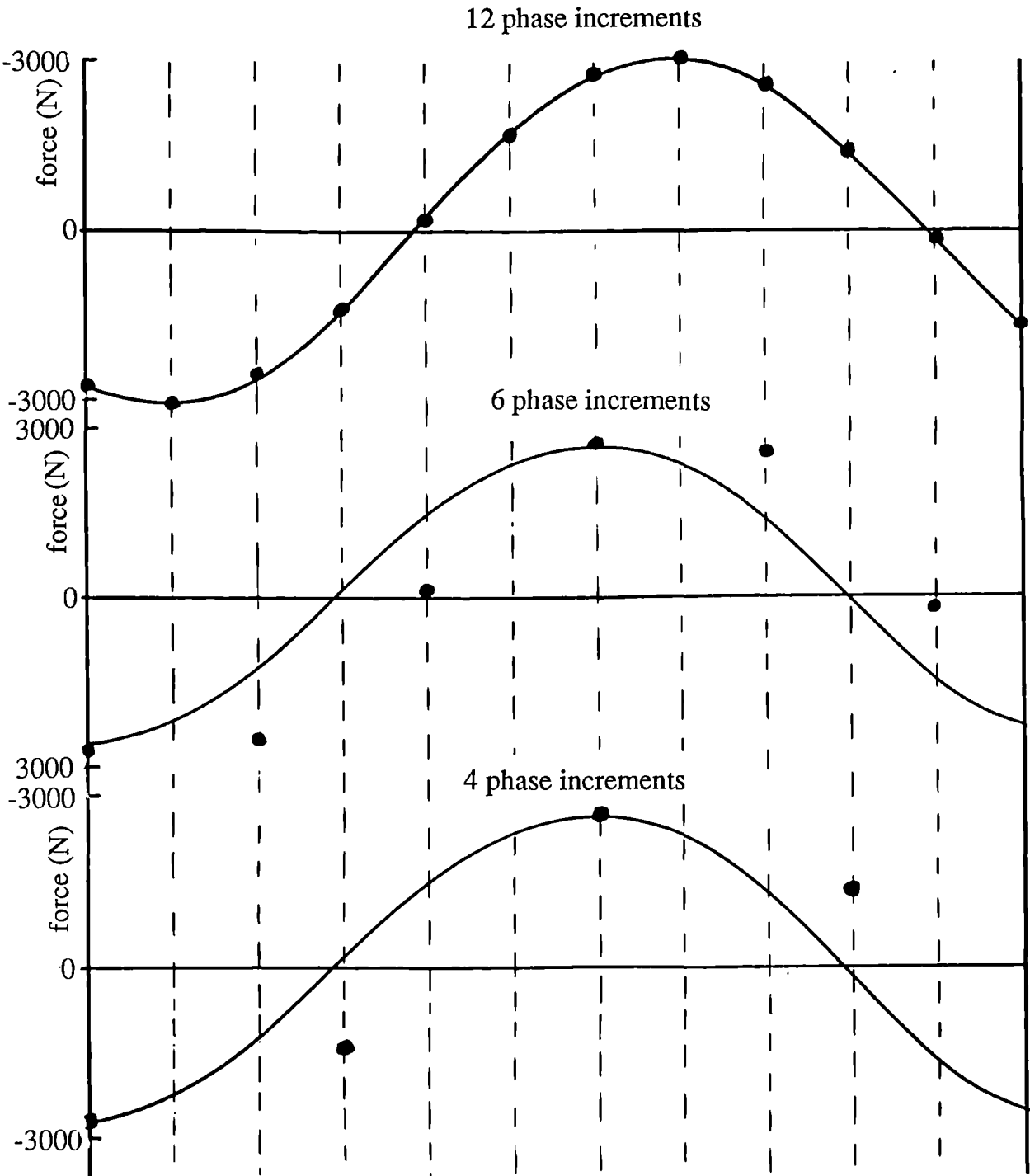


Figure 7.12(b). The sin fitting process for a drag dominated wave

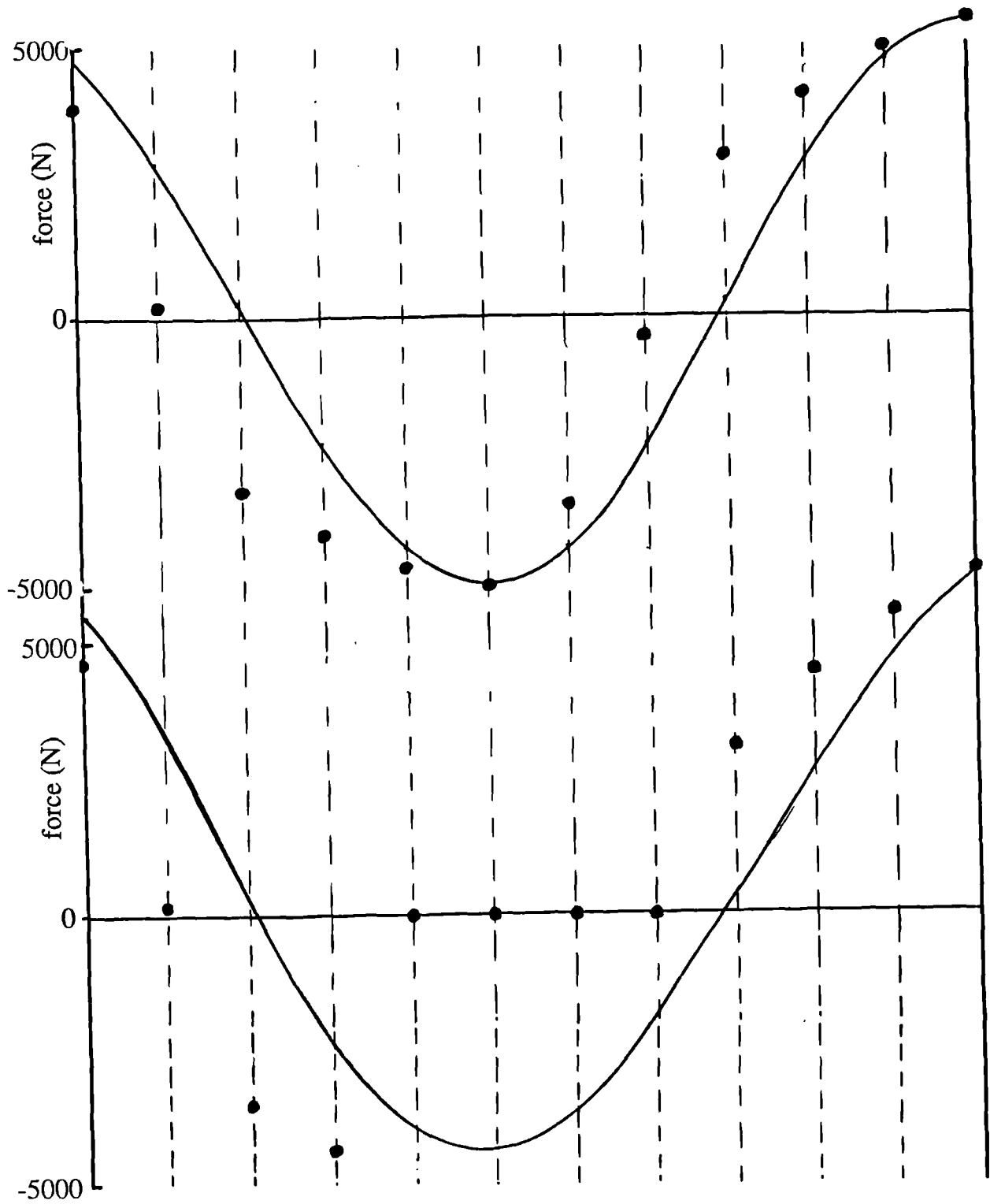


Figure 7.12(c). The sin fitting process for a drag dominated wave in the splash zone

Figure 7.13(a). Height against force. Conservative linearisation

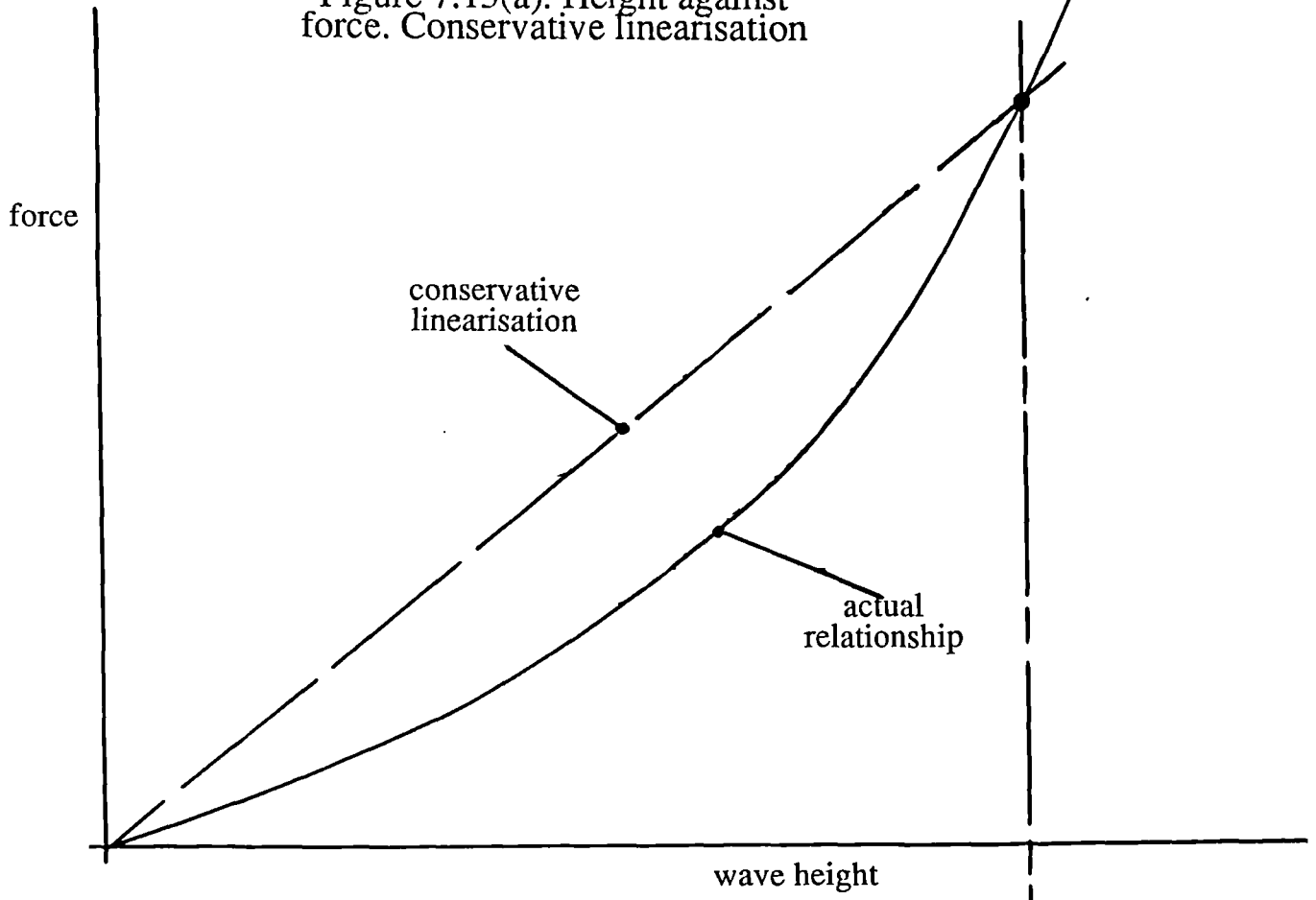


Figure 7.13(b). Height against force. Unconservative linearisation

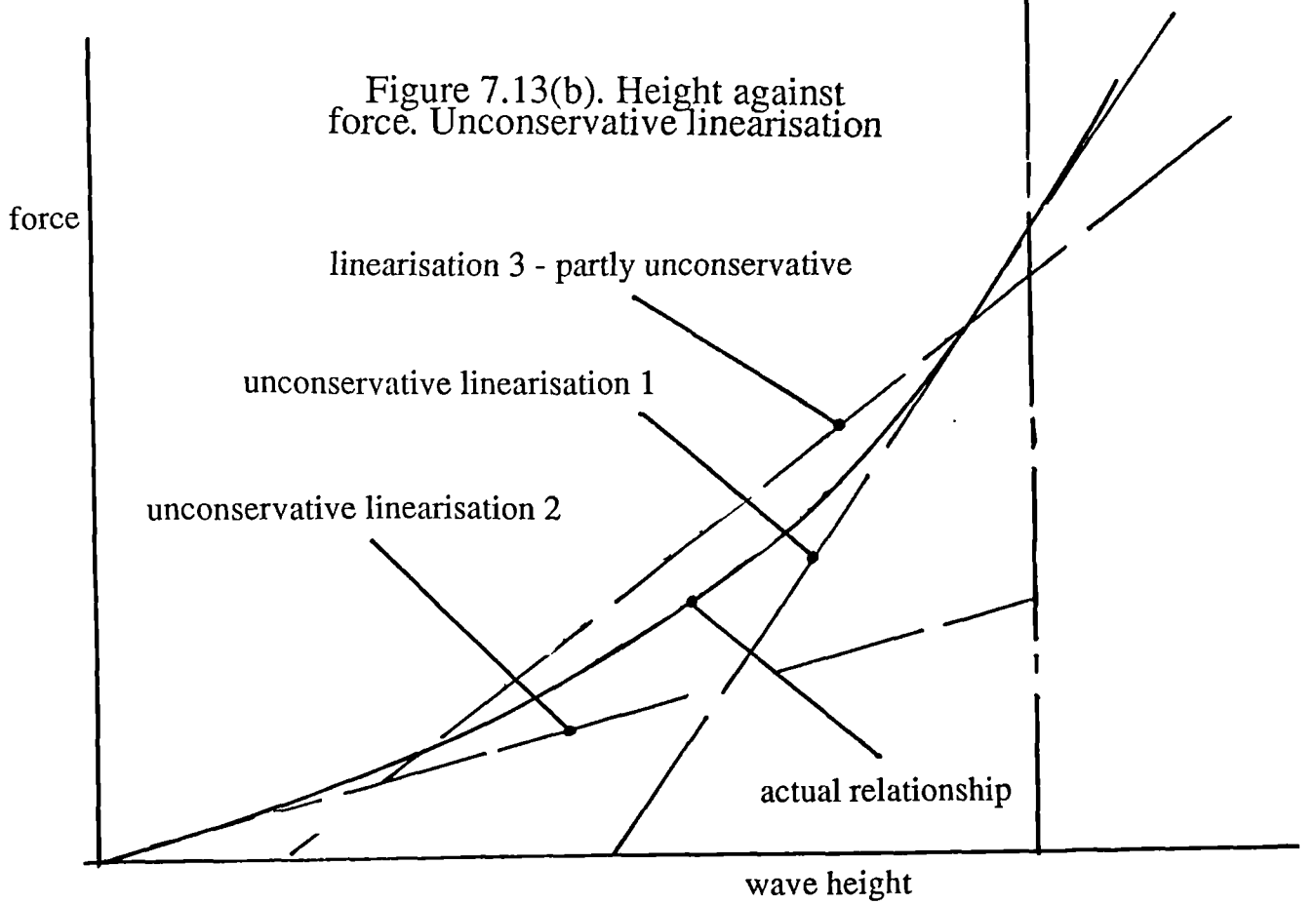


Figure 7.14. The process of obtaining the transfer function

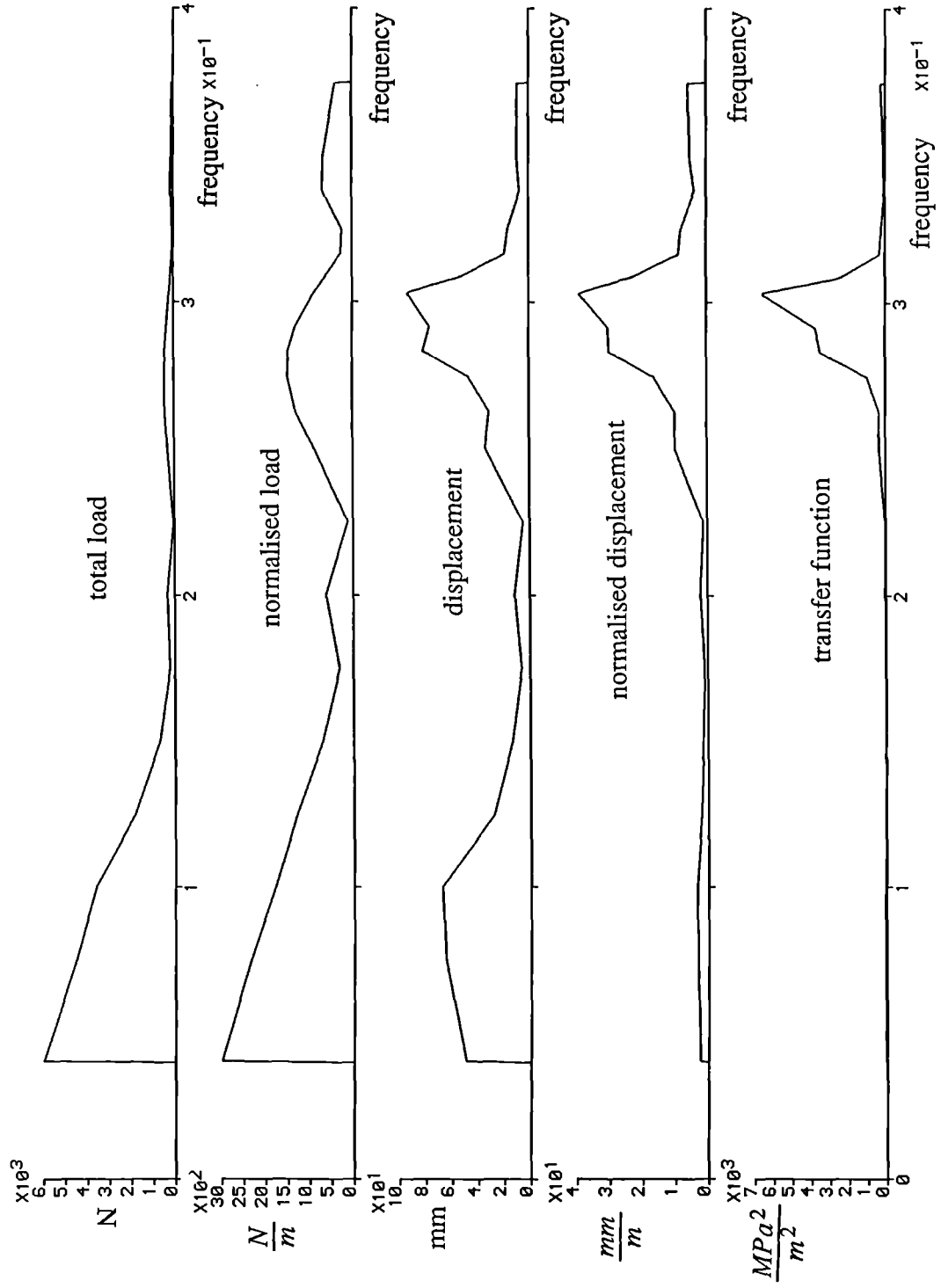


Figure 7.15. The variation of fundamental frequency with added mass

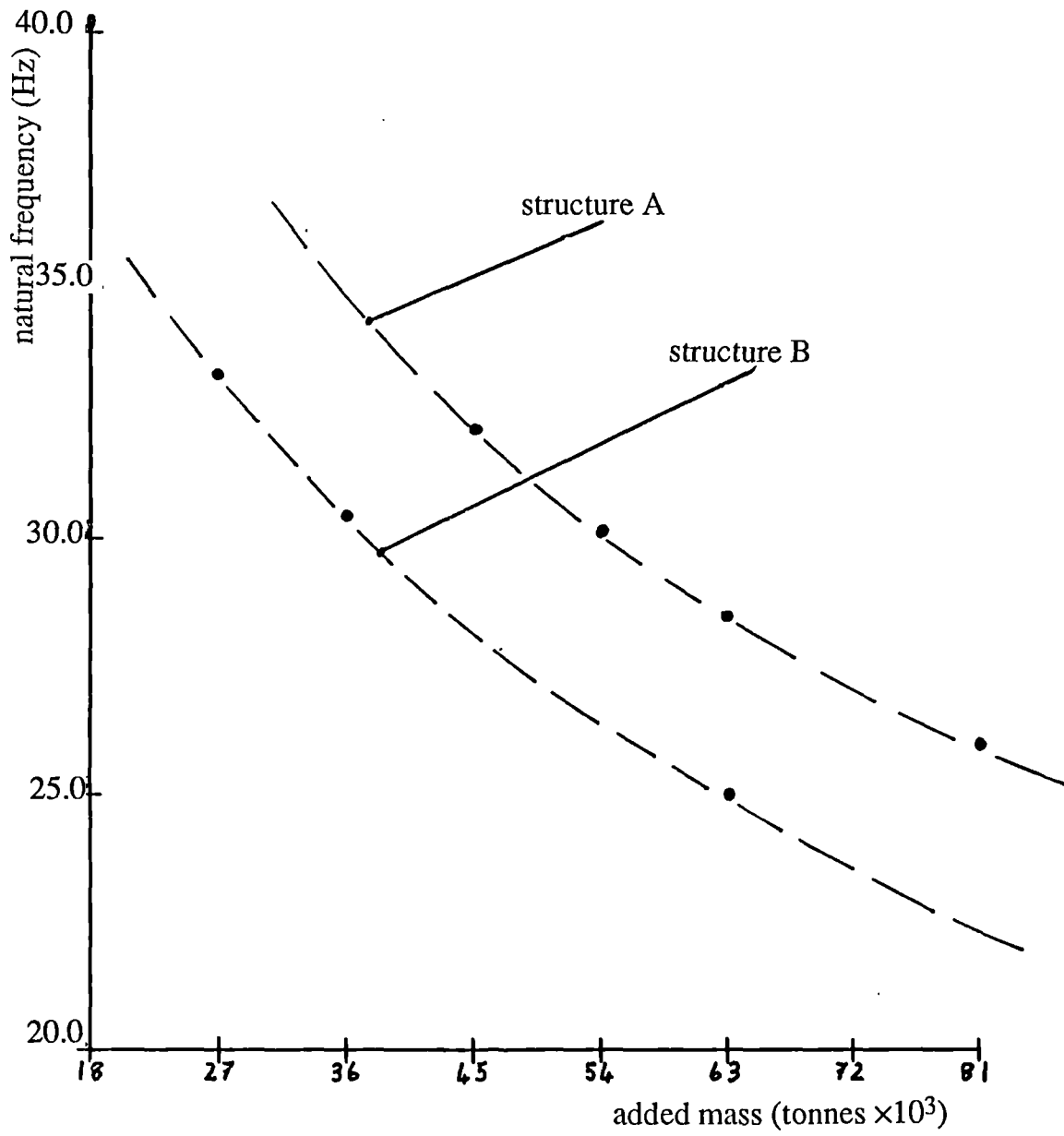


Figure 7.16. The variation of fatigue life with critical damping

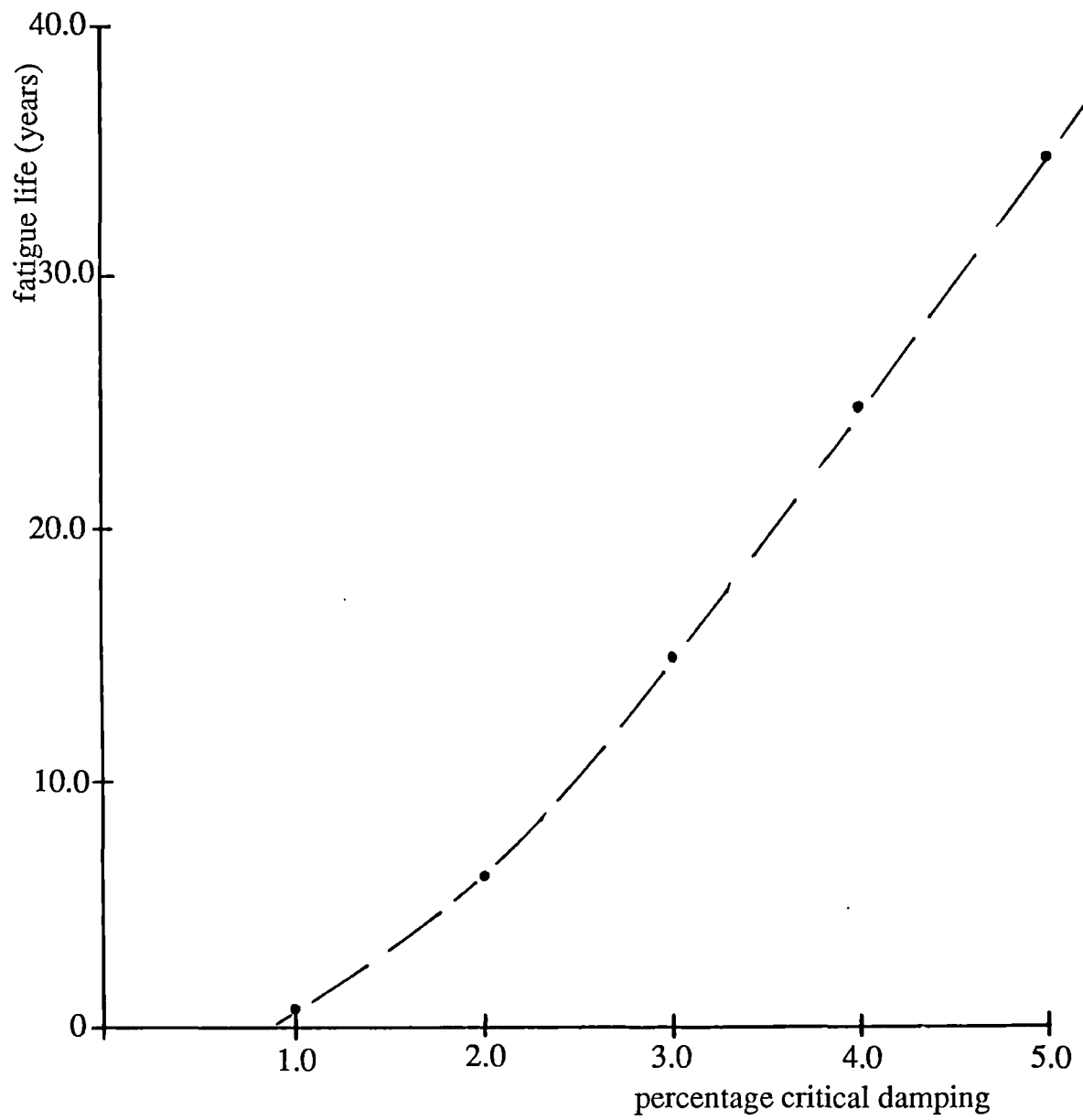


Figure 7.17(a). Results for sea state 1 with transfer function H3

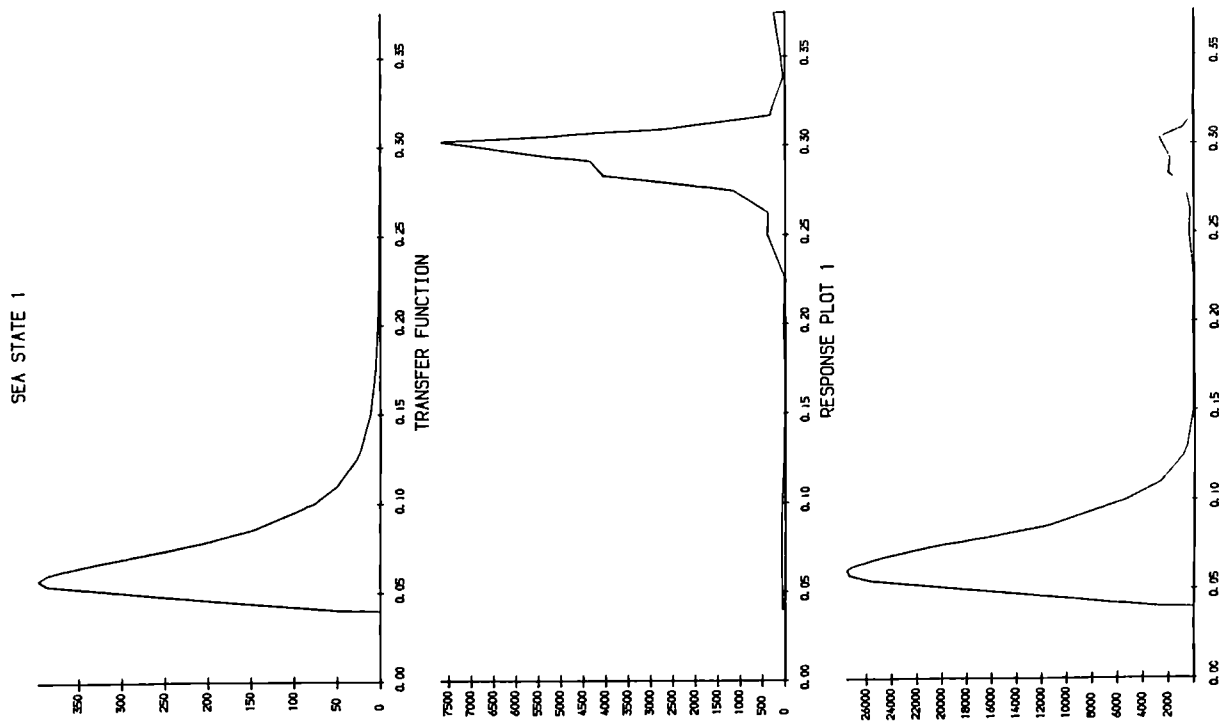


Figure 7.18(a). Fatigue damage potential for sea state 1

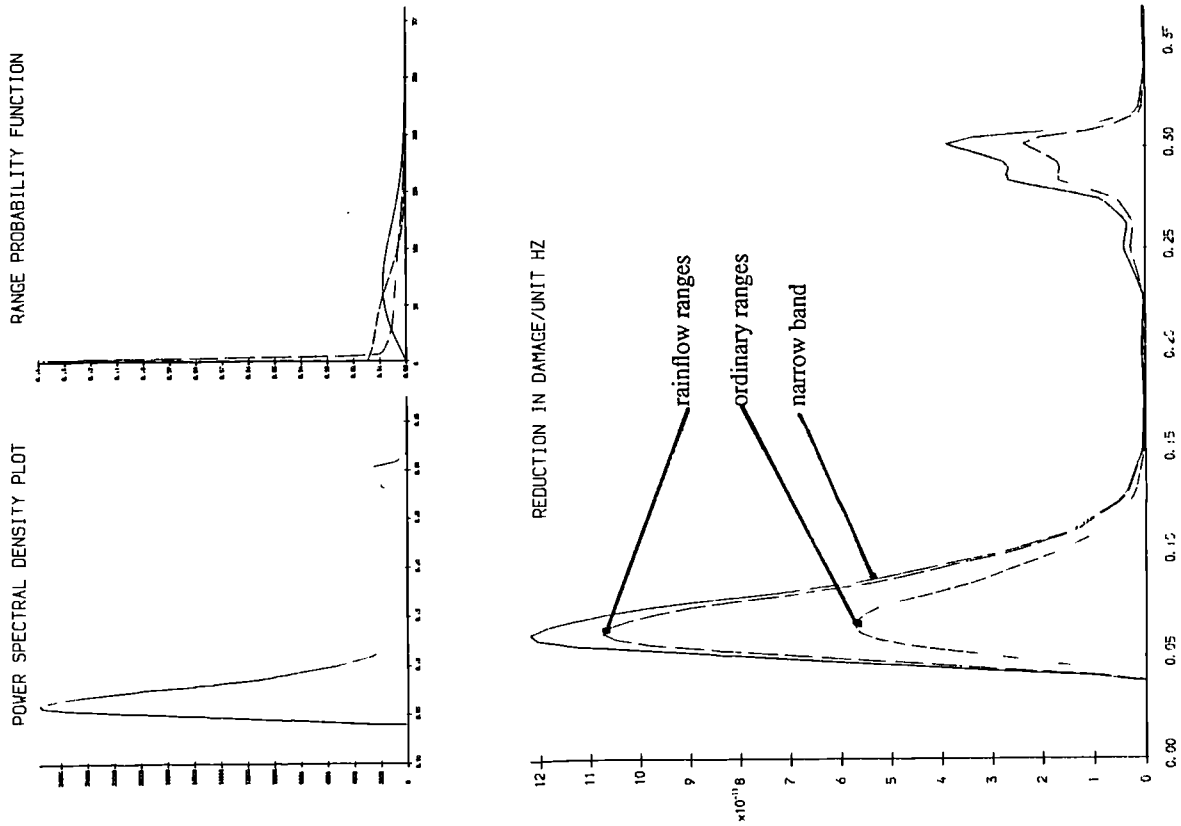


Figure 7.17(b). Results for sea state 2 with transfer function H3

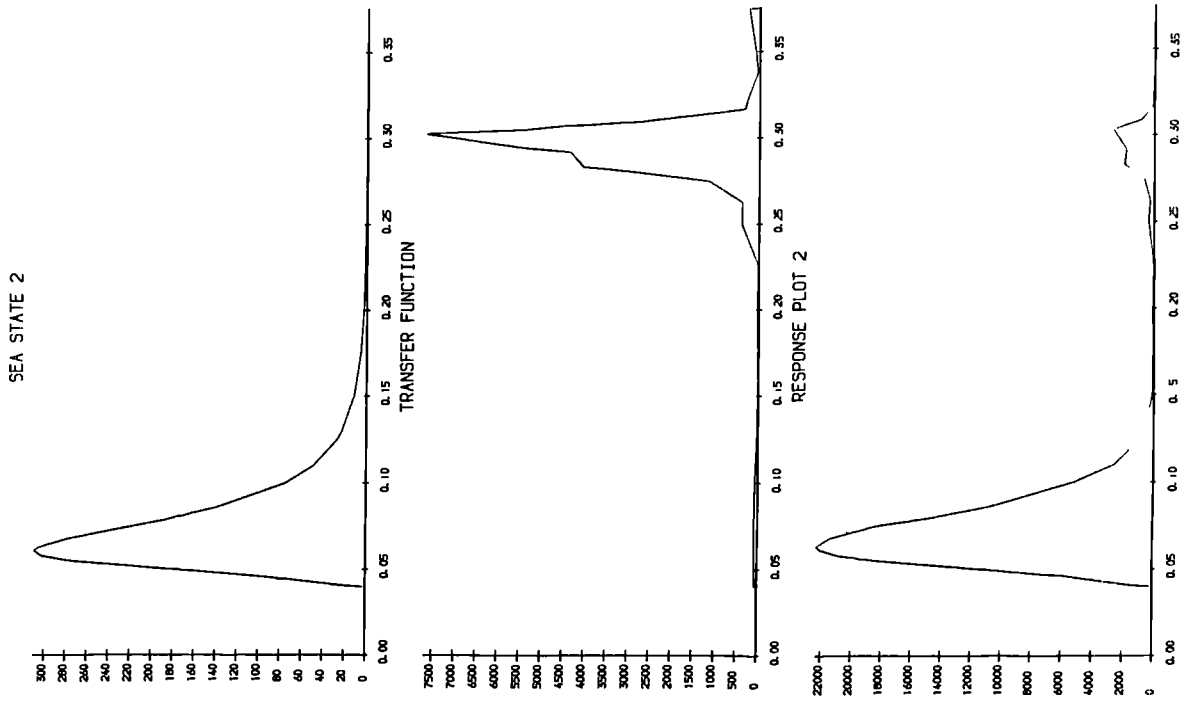


Figure 7.18(b). Fatigue damage potential for sea state 2

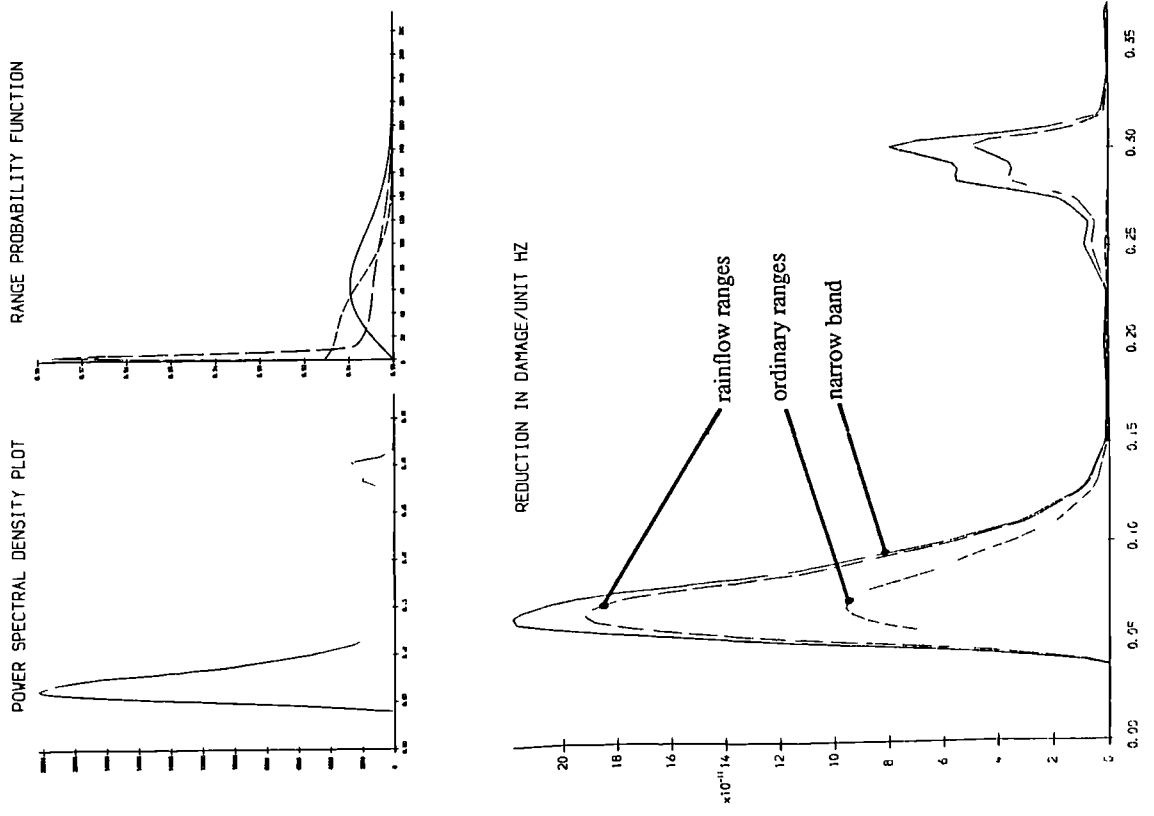


Figure 7.17(c). Results for sea state 3 with transfer function H3

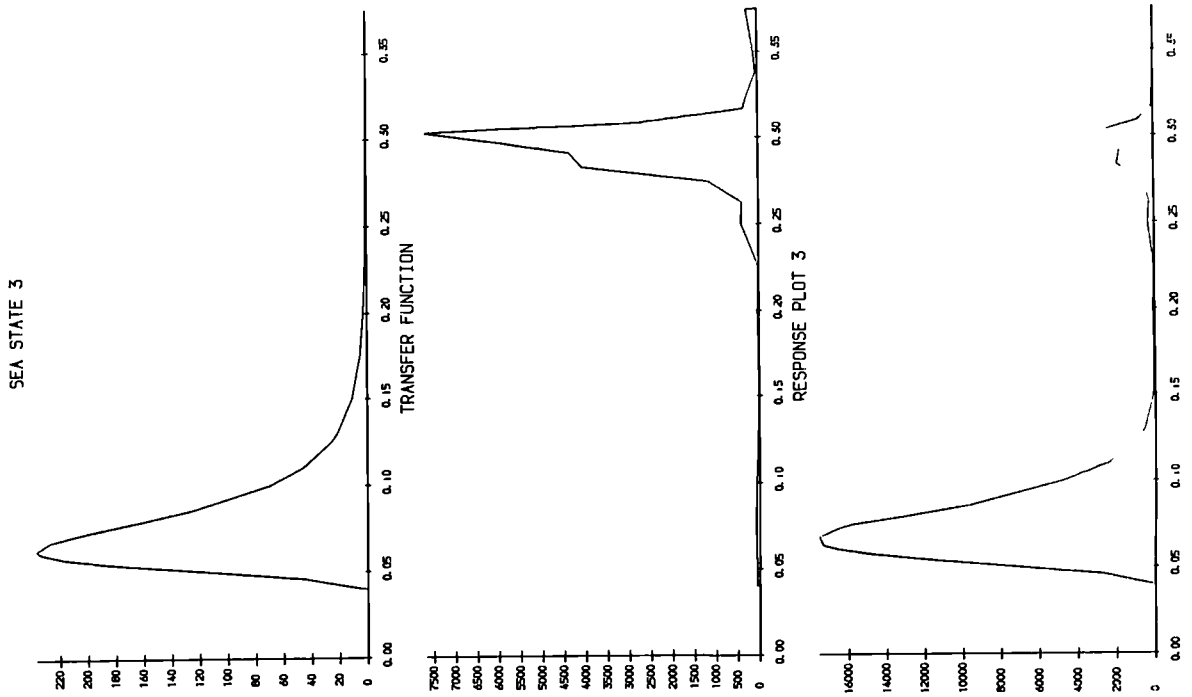


Figure 7.18(c). Fatigue damage potential for sea state 3

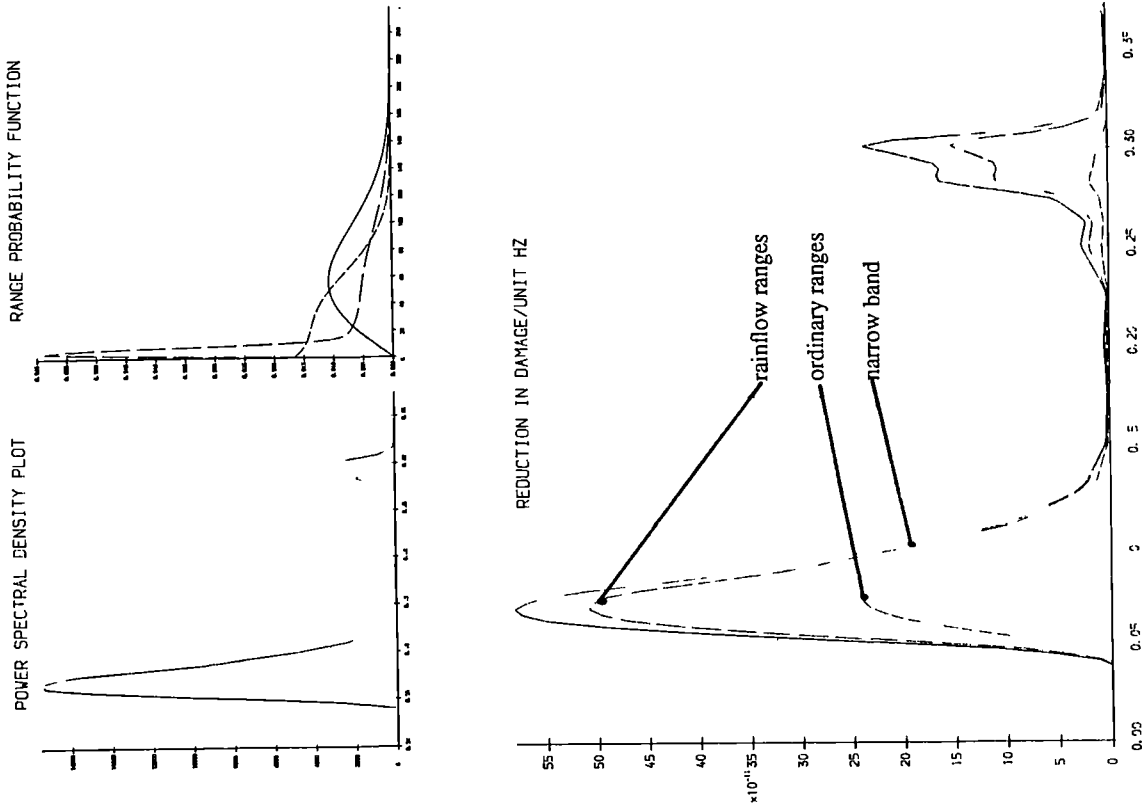


Figure 7.17(d). Results for sea state 4 with transfer function H3

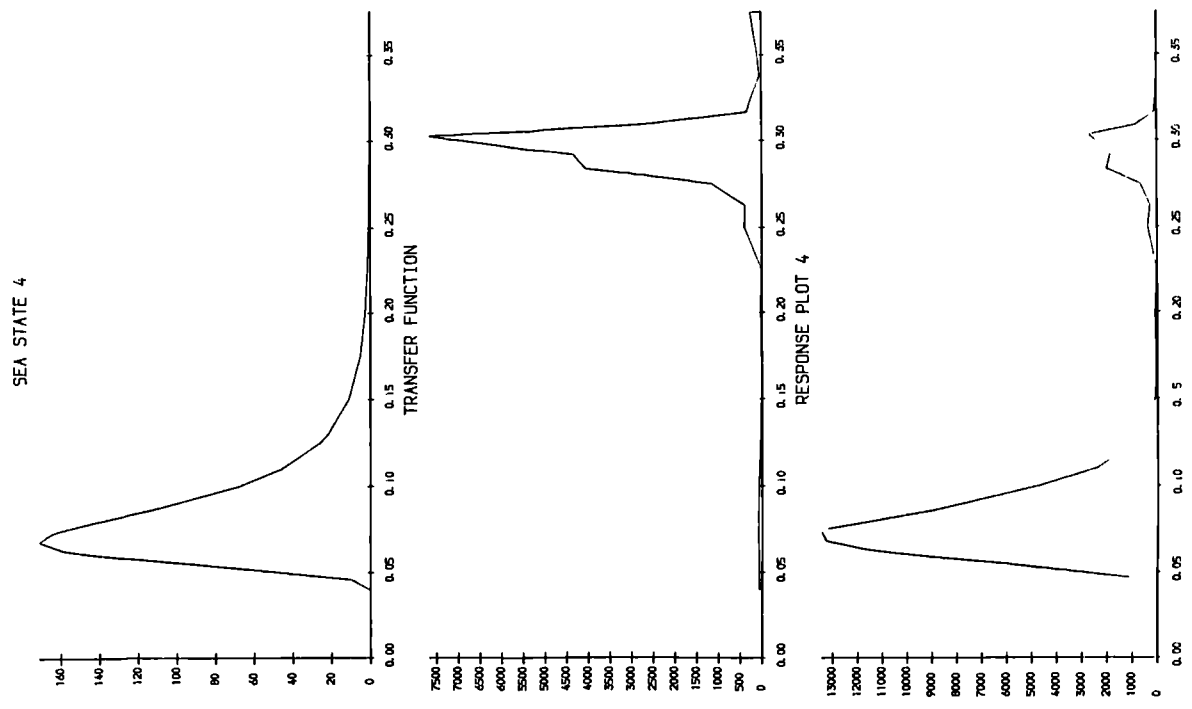


Figure 7.18(d). Fatigue damage potential for sea state 4

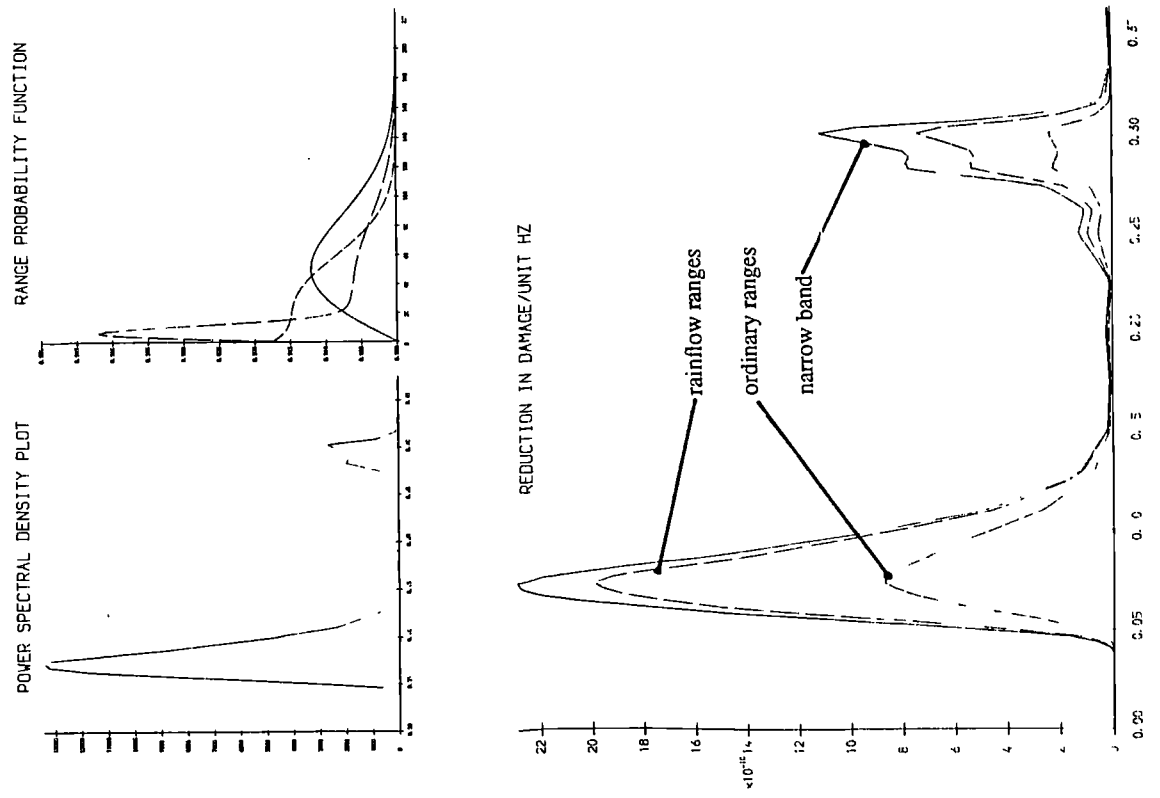


Figure 7.17(e). Results for sea state 5 with transfer function H3

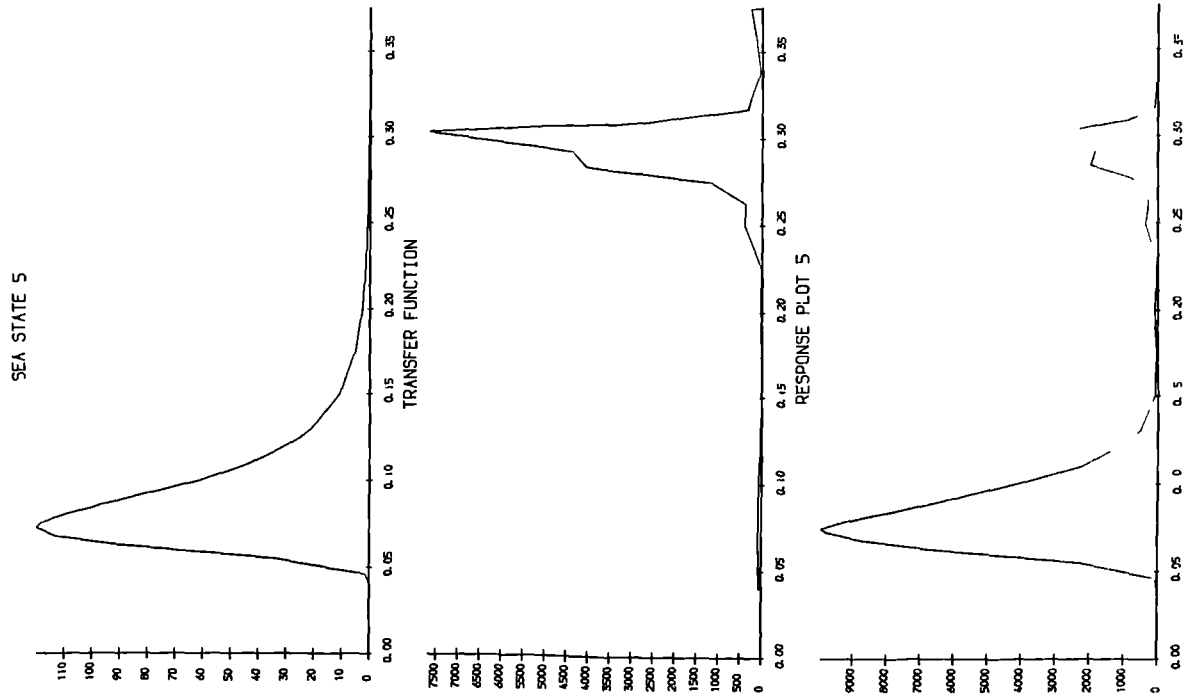


Figure 7.18(e). Fatigue damage potential for sea state 5

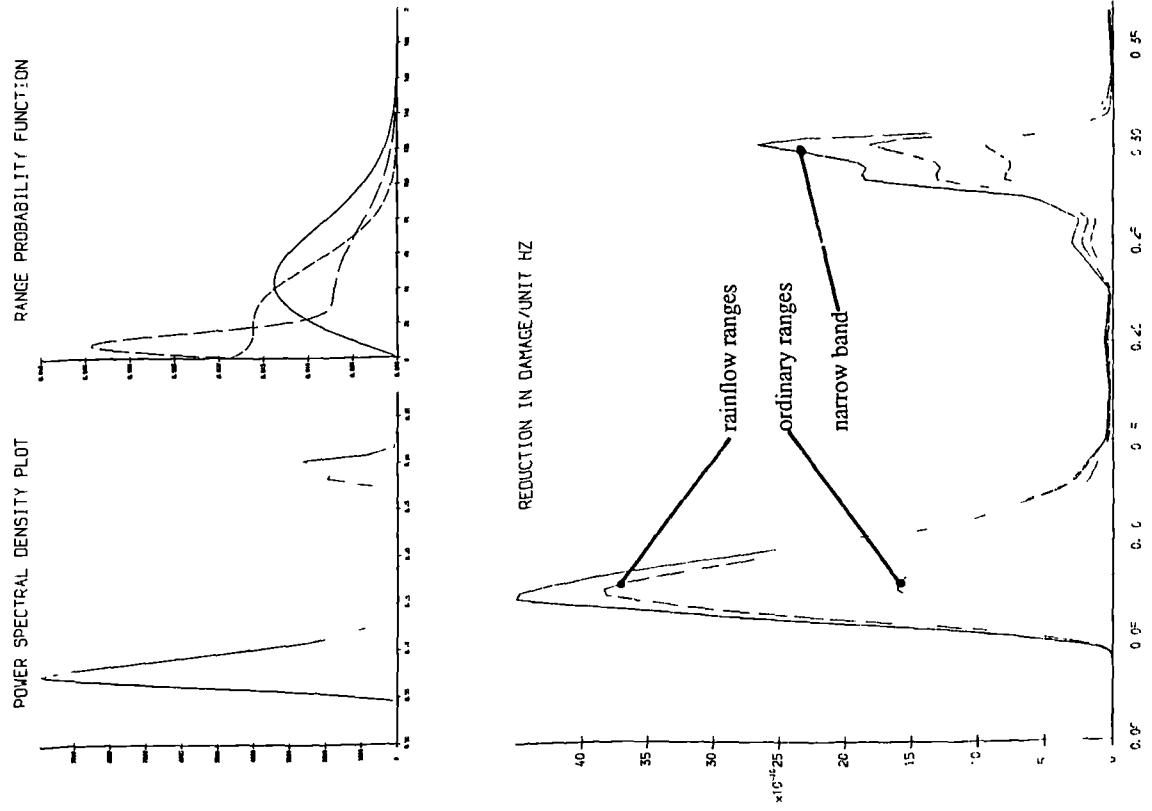


Figure 7.17(f). Results for sea state 6 with transfer function H3

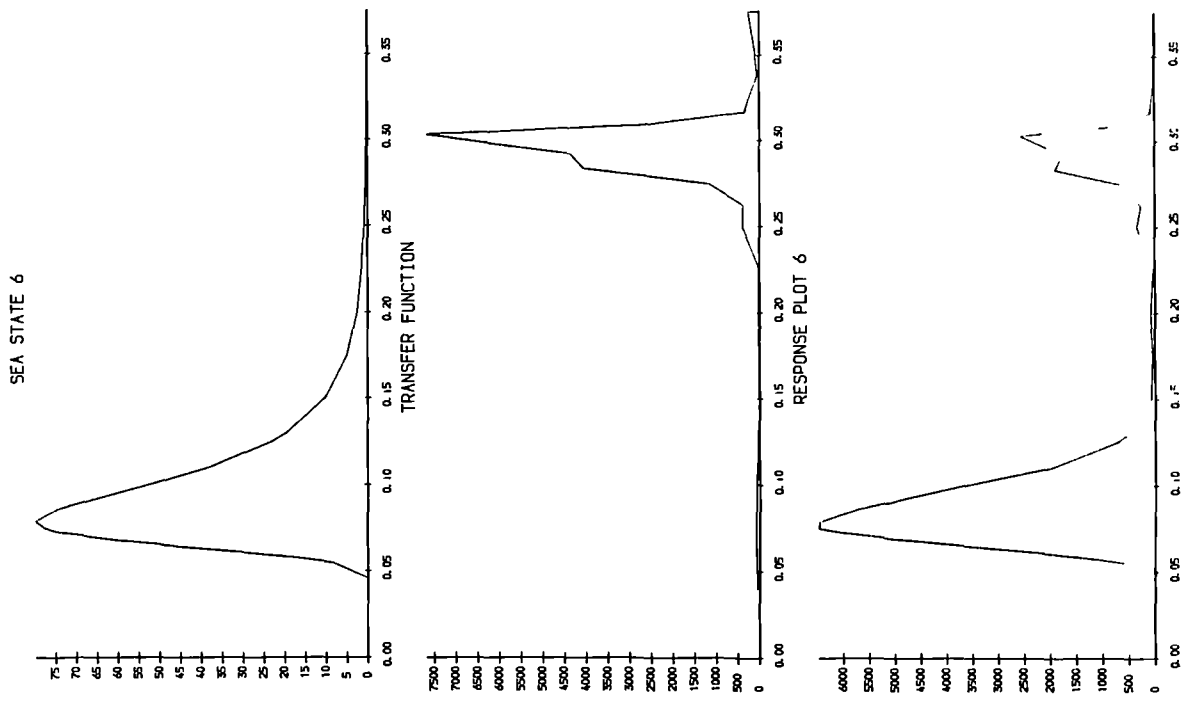


Figure 7.18(f). Fatigue damage potential for sea state 6

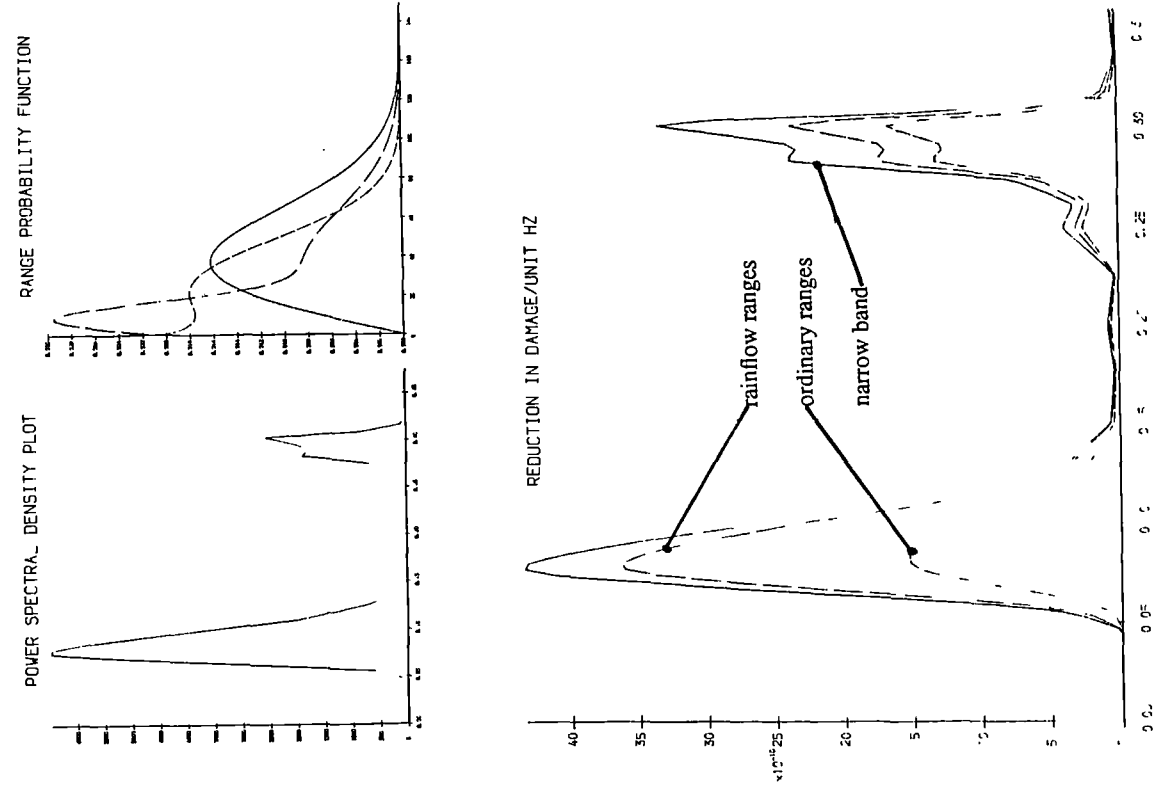


Figure 7.17(g). Results for sea state 7 with transfer function H3

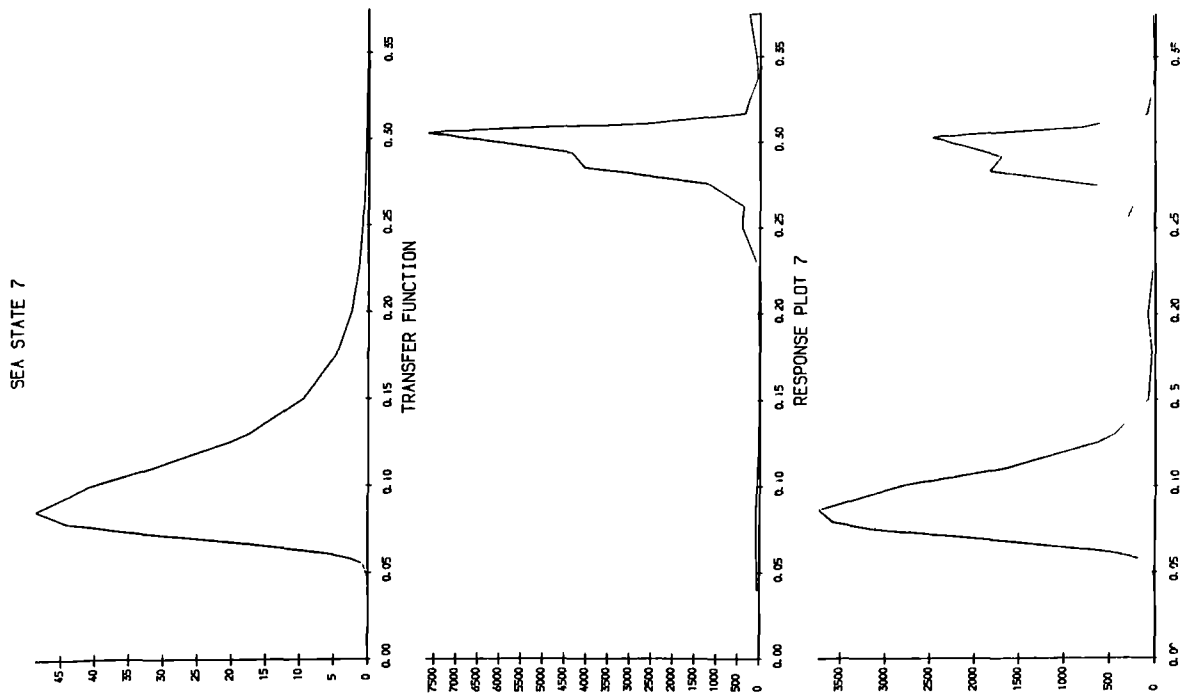


Figure 7.18(g). Fatigue damage potential for sea state 7

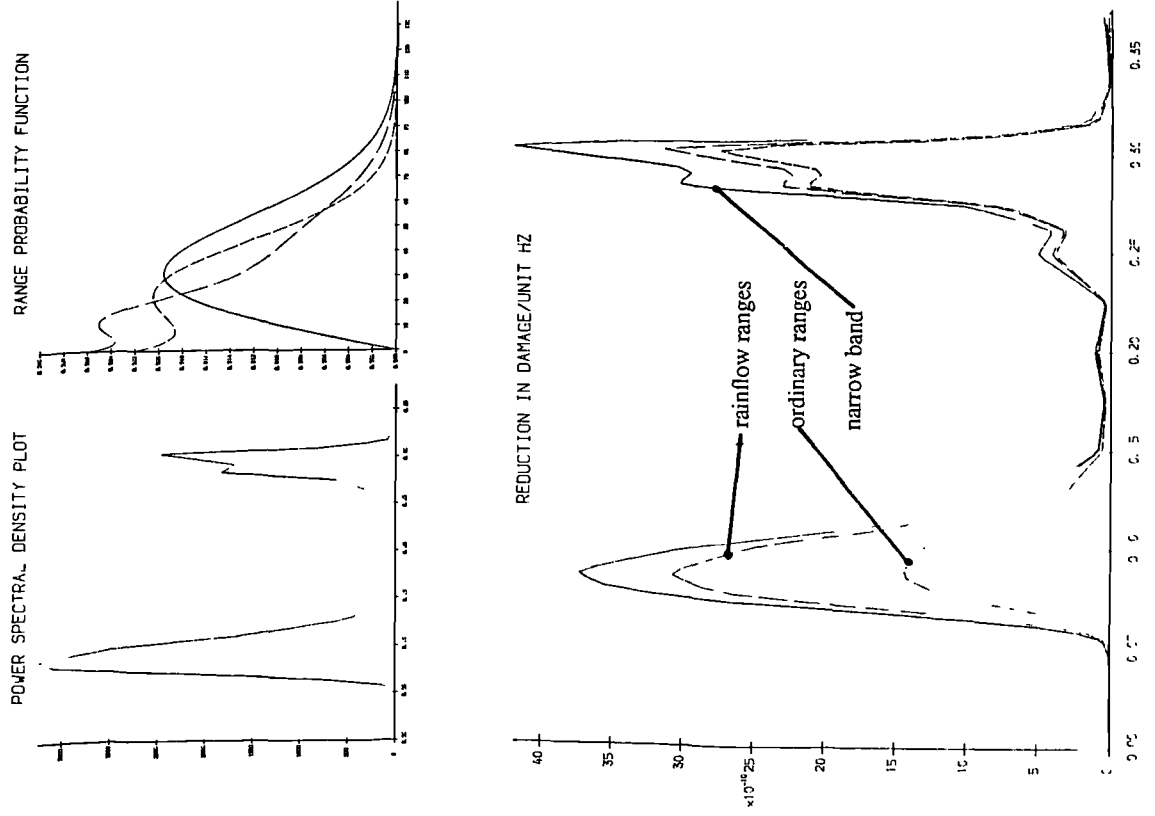


Figure 7.17(h). Results for sea state 8 with transfer function H3

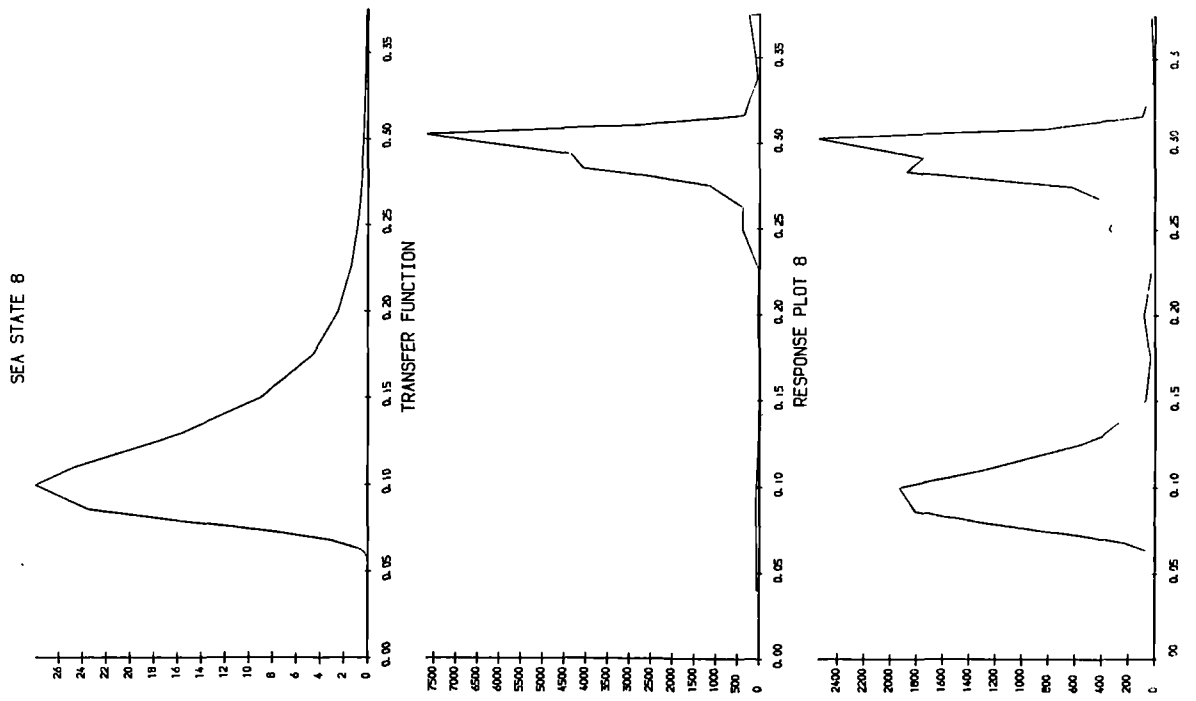


Figure 7.18(h). Fatigue damage potential for sea state 8

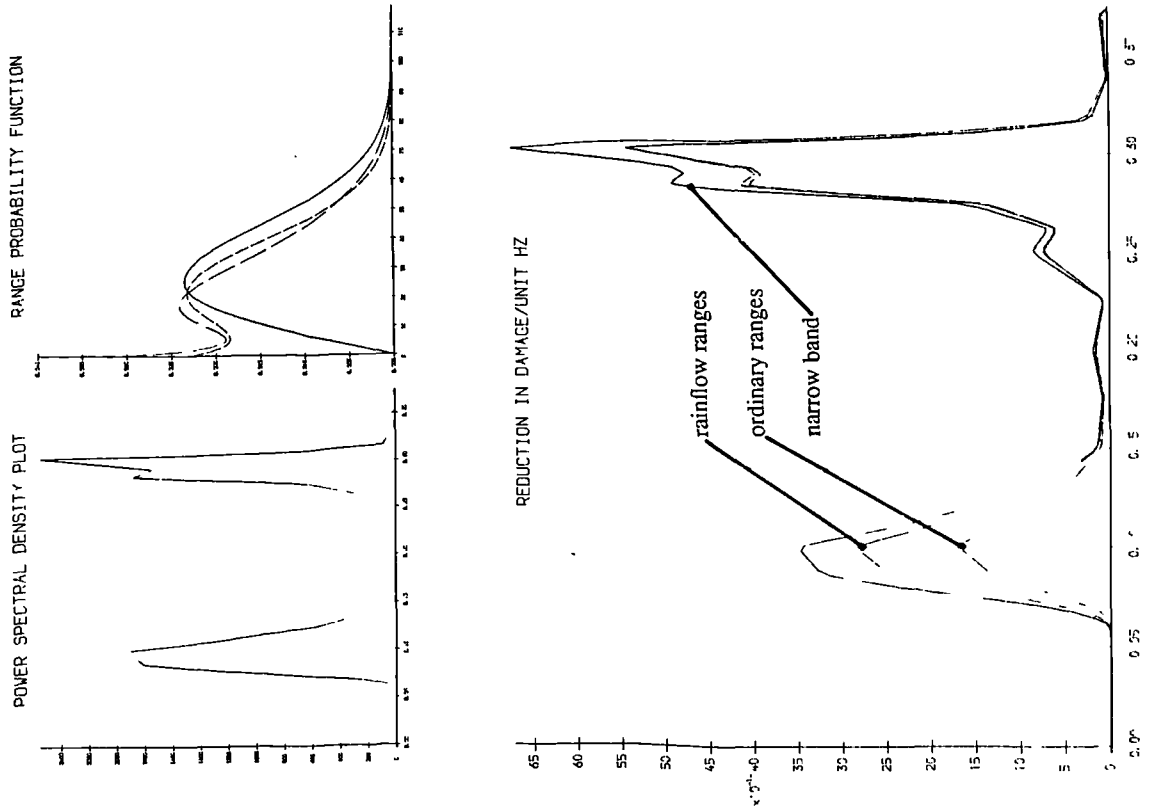


Figure 7.17(i). Results for sea state 9 with transfer function H3

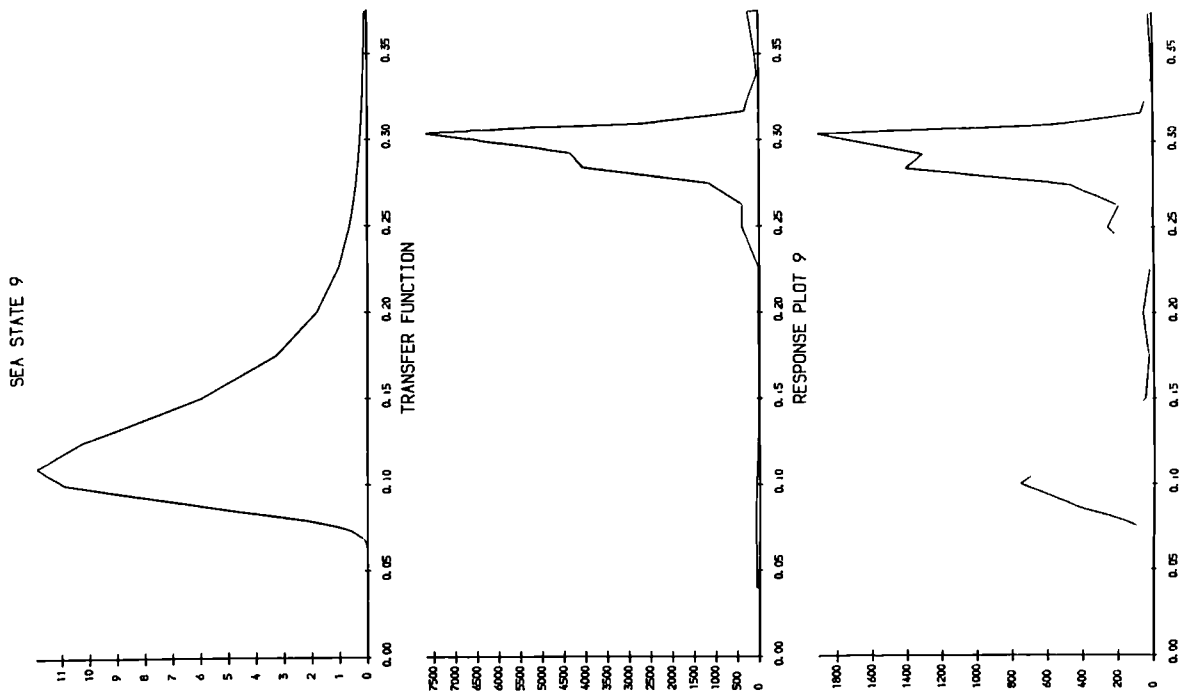


Figure 7.18(i). Fatigue damage potential for sea state 9

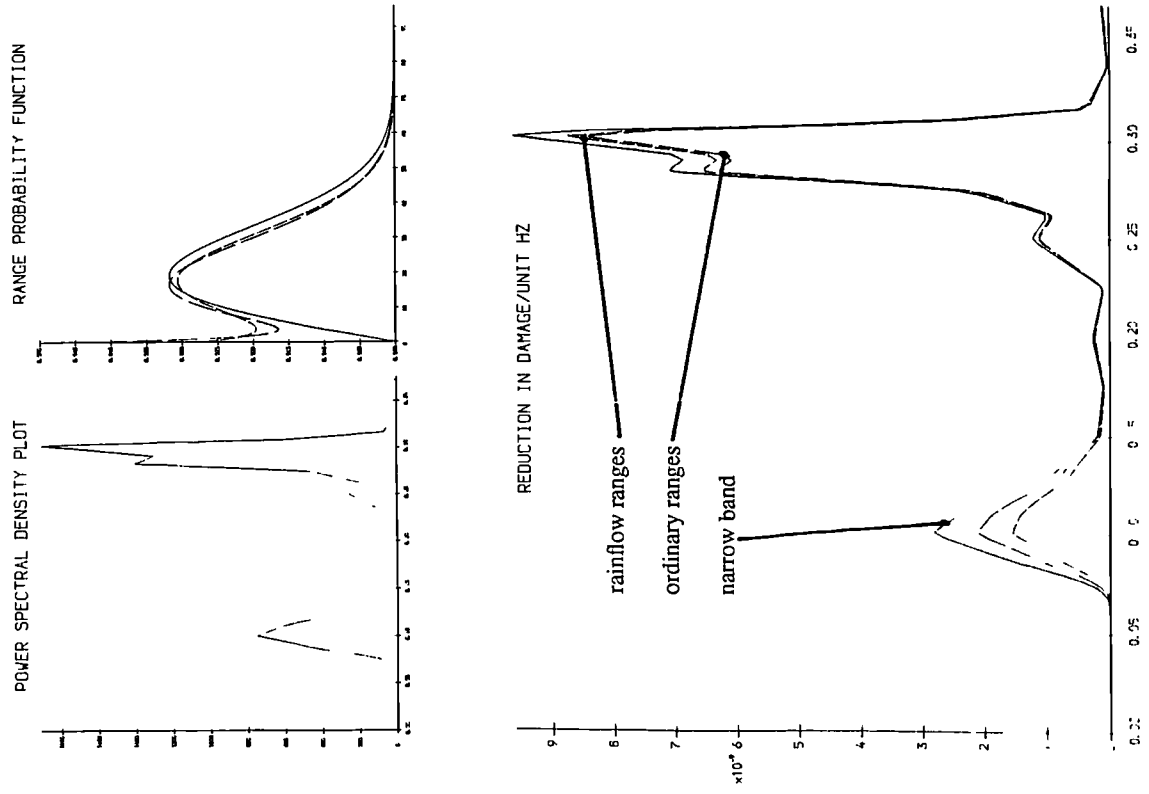


Figure 7.18(j). Fatigue damage potential for sea state 10

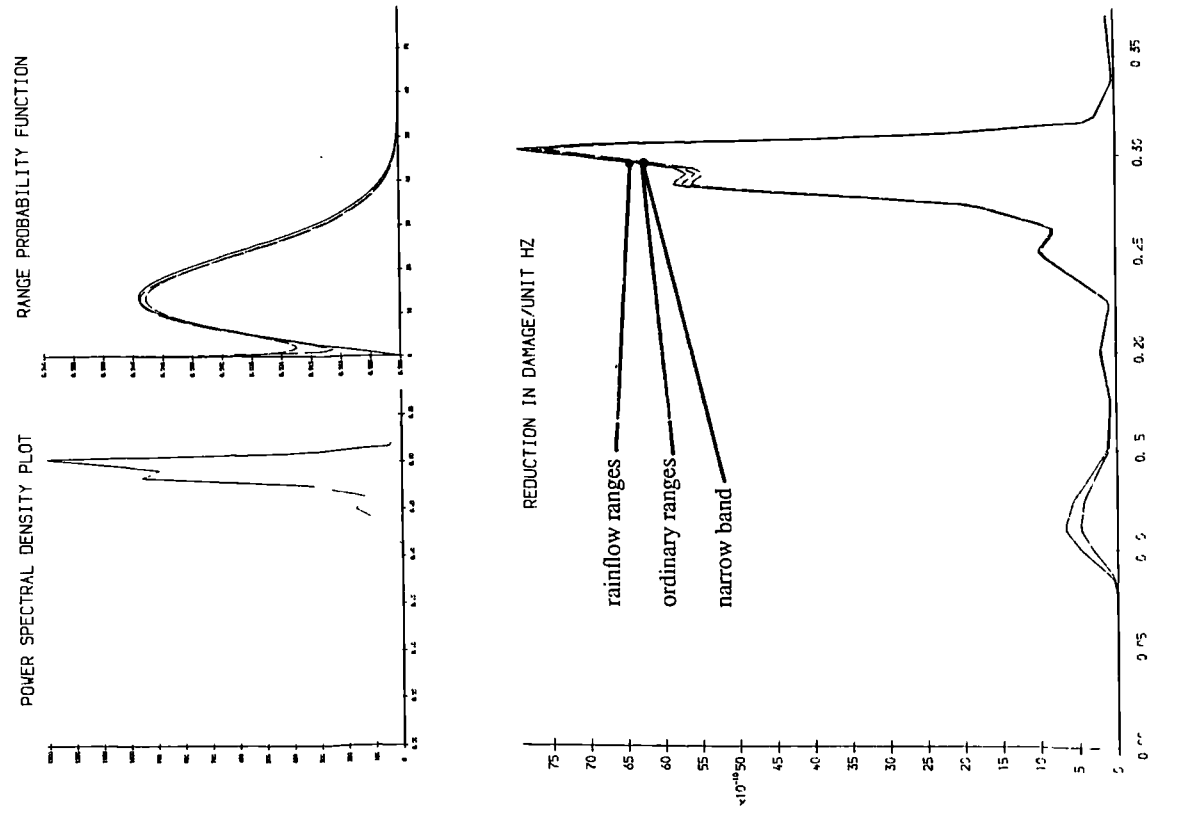


Figure 7.17(j). Results for sea state 10 with transfer function H3

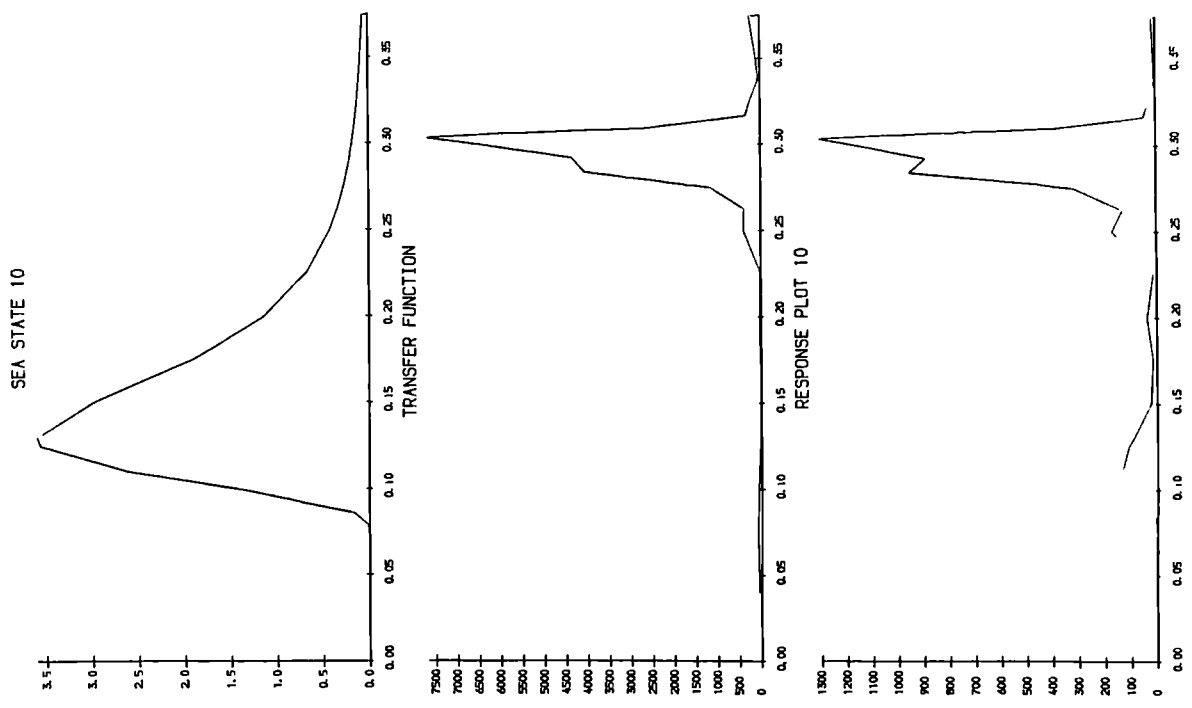


Figure 7.17(k). Results for sea state 11 with transfer function H3

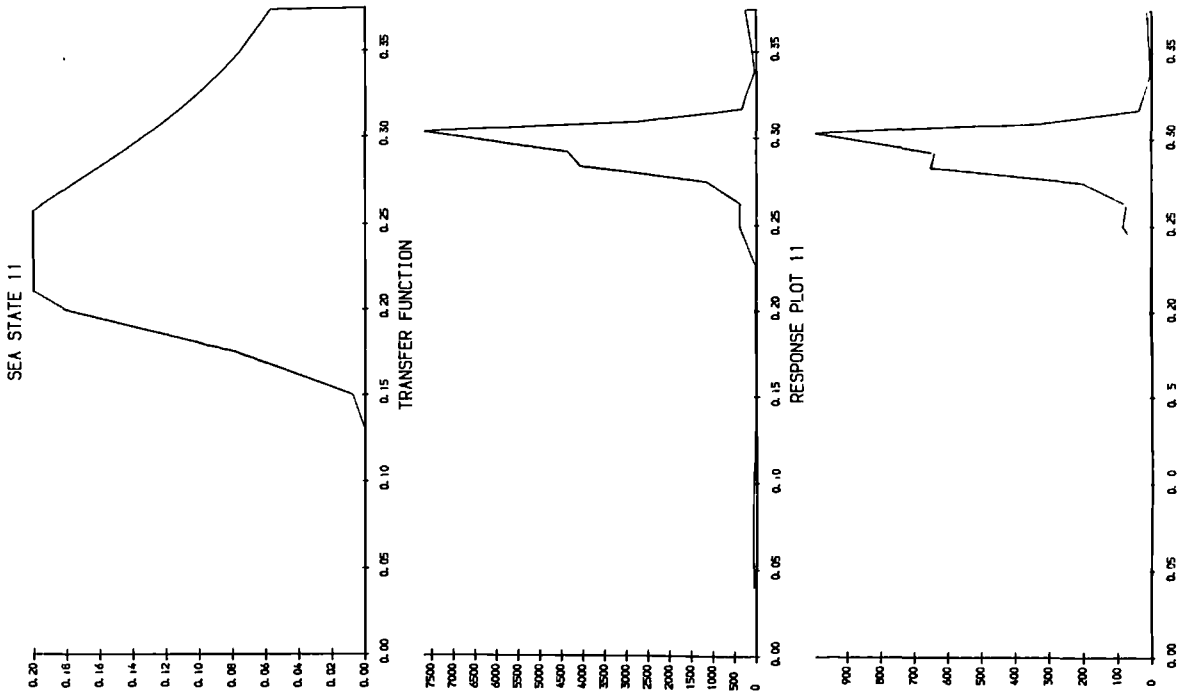


Figure 7.18(k). Fatigue damage potential for sea state 11

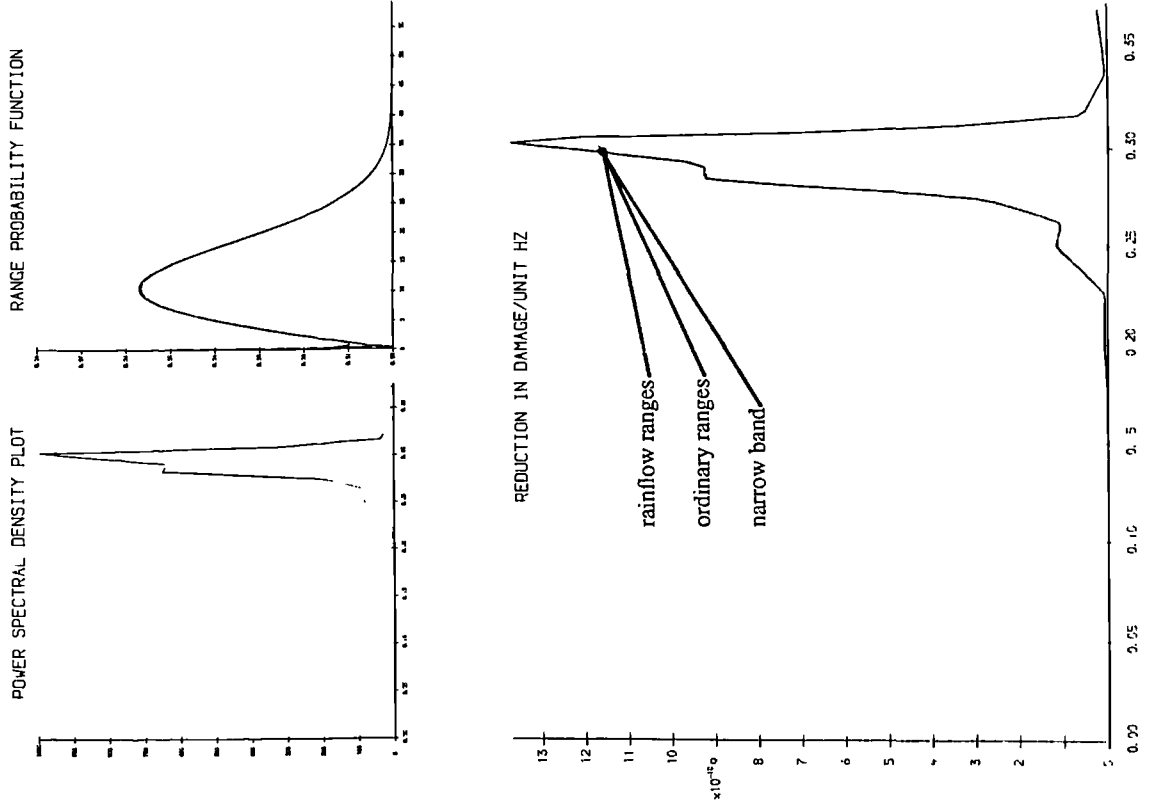


Figure 7.19. Different methods of estimating the fatigue damage potential of any response plot

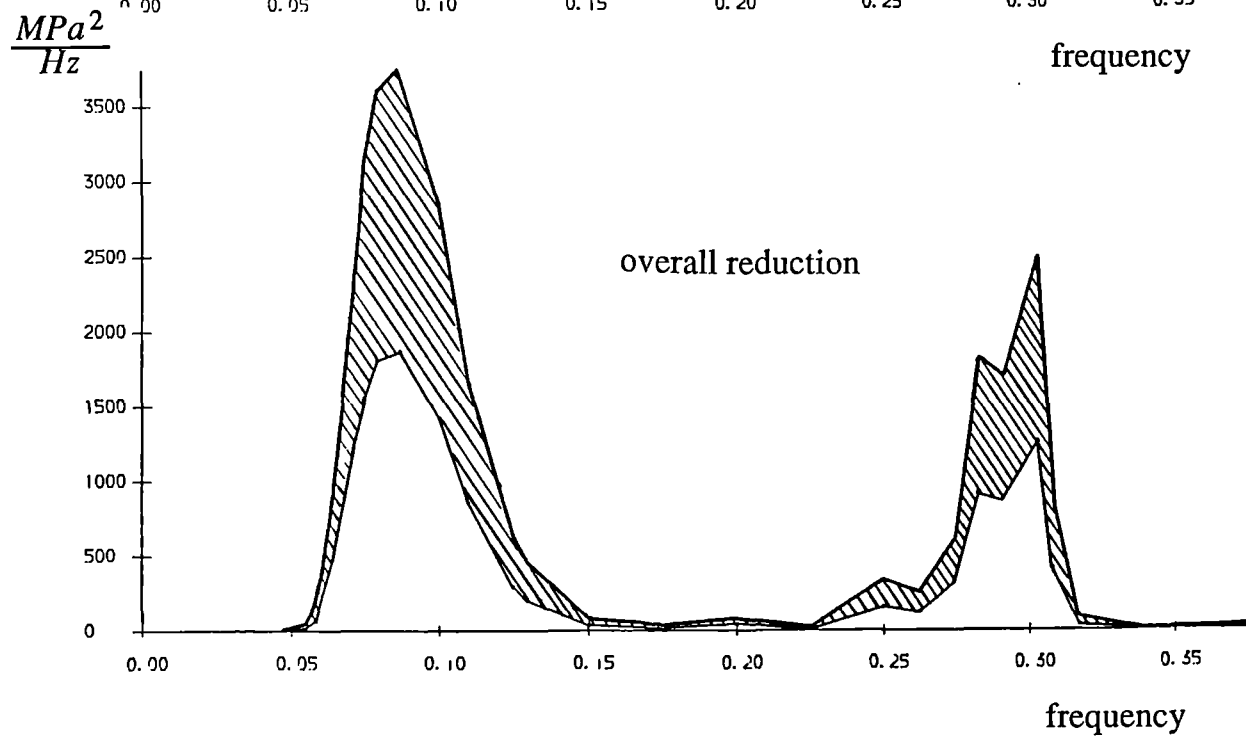
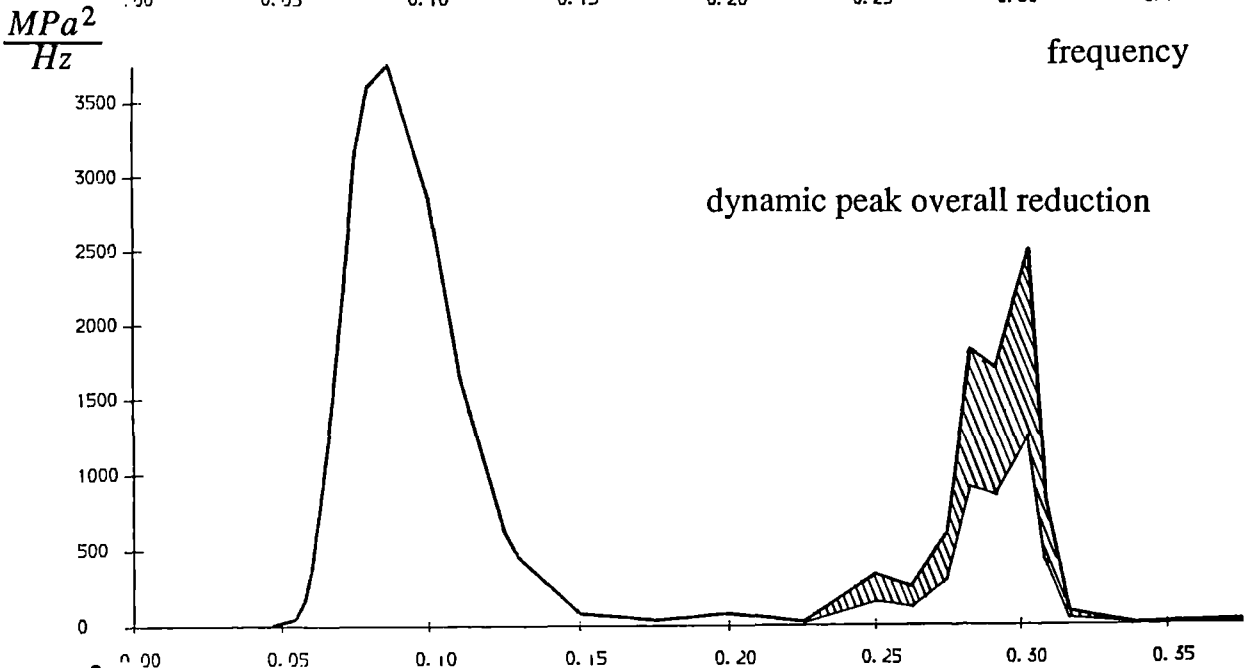
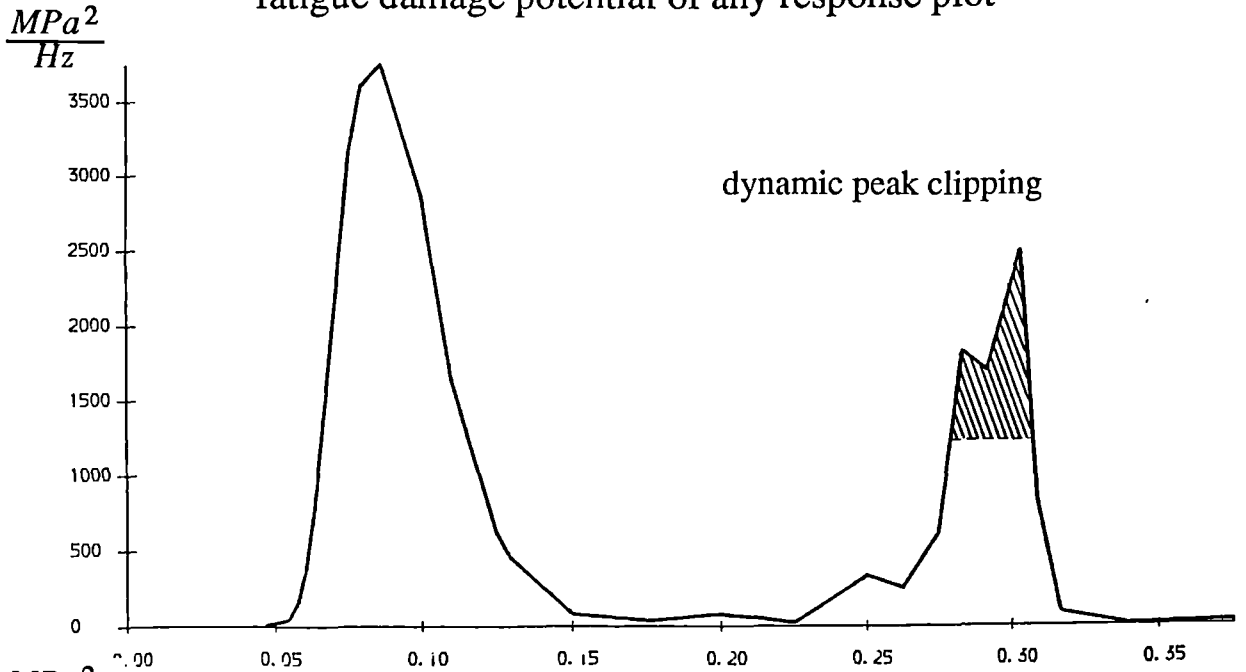


Figure 7.20. The variation of fatigue life with a wave angle of 0 degrees representing waves square on to the side

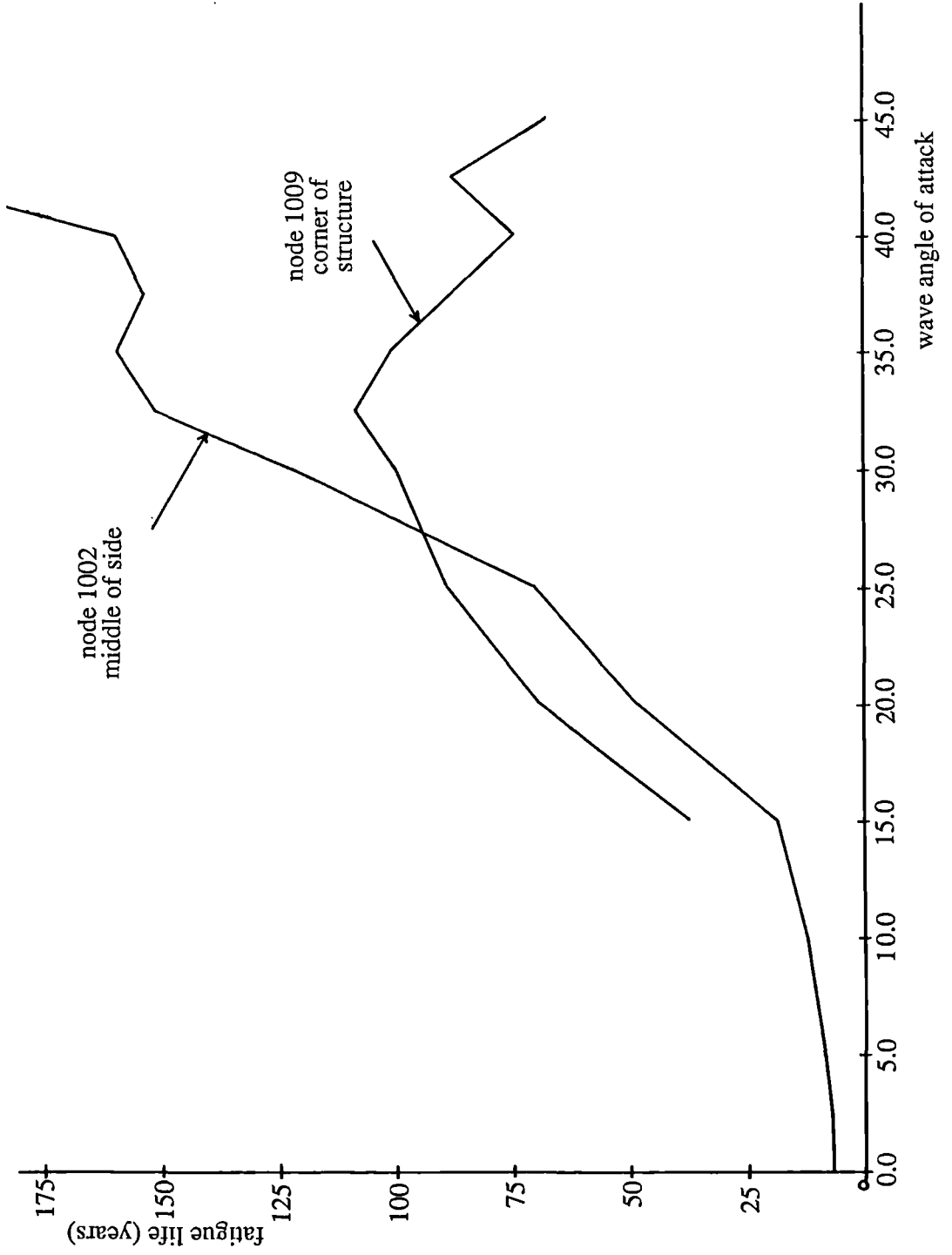


Figure 7.21. The variation of fatigue life or damage with elevation of water level at 0.0, representing a water level at a horizontal bracing level

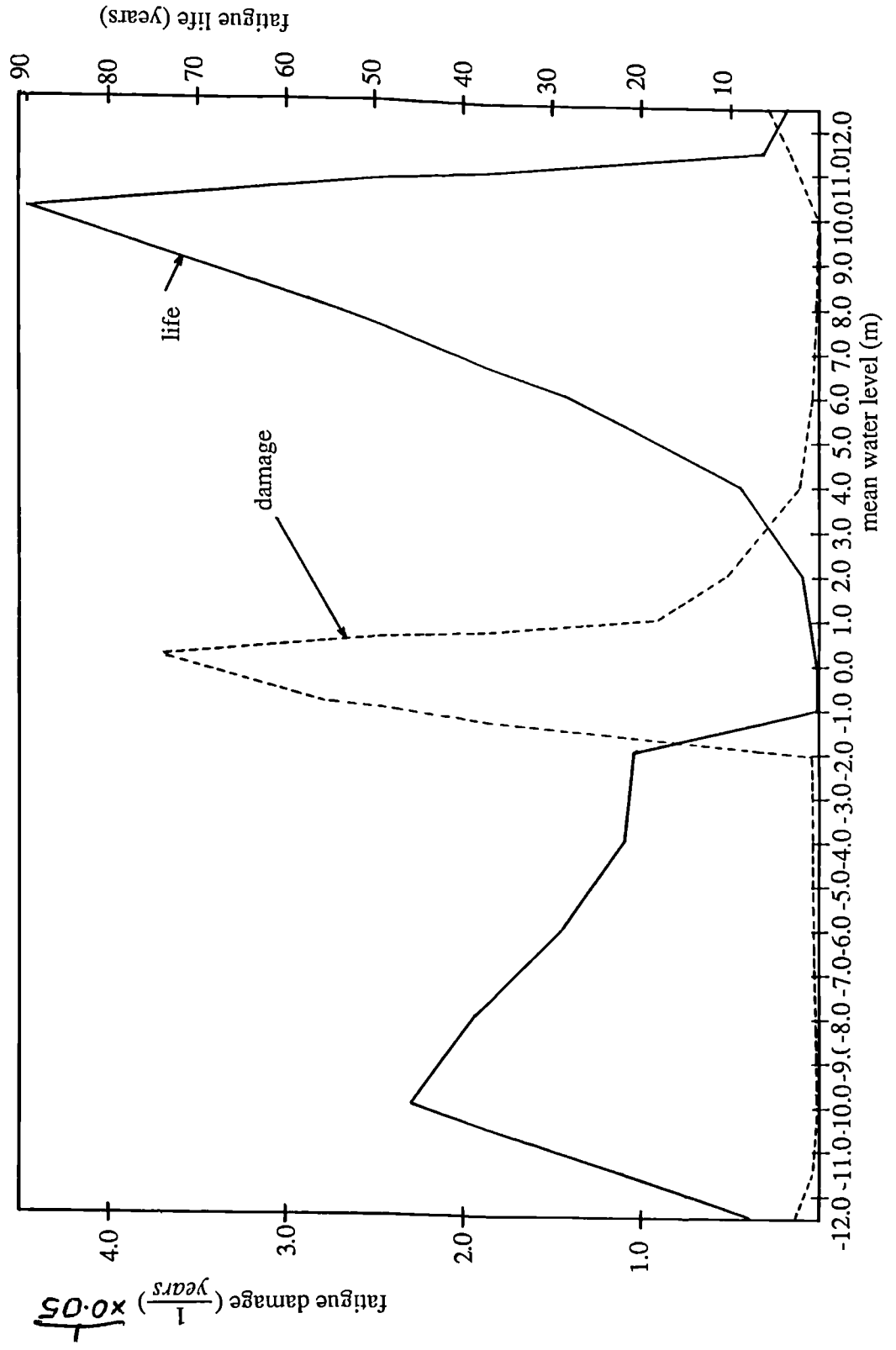


Figure 7.22. The maximum response of a structure comprising of a 3 by 3 array of piles for varying wavelength

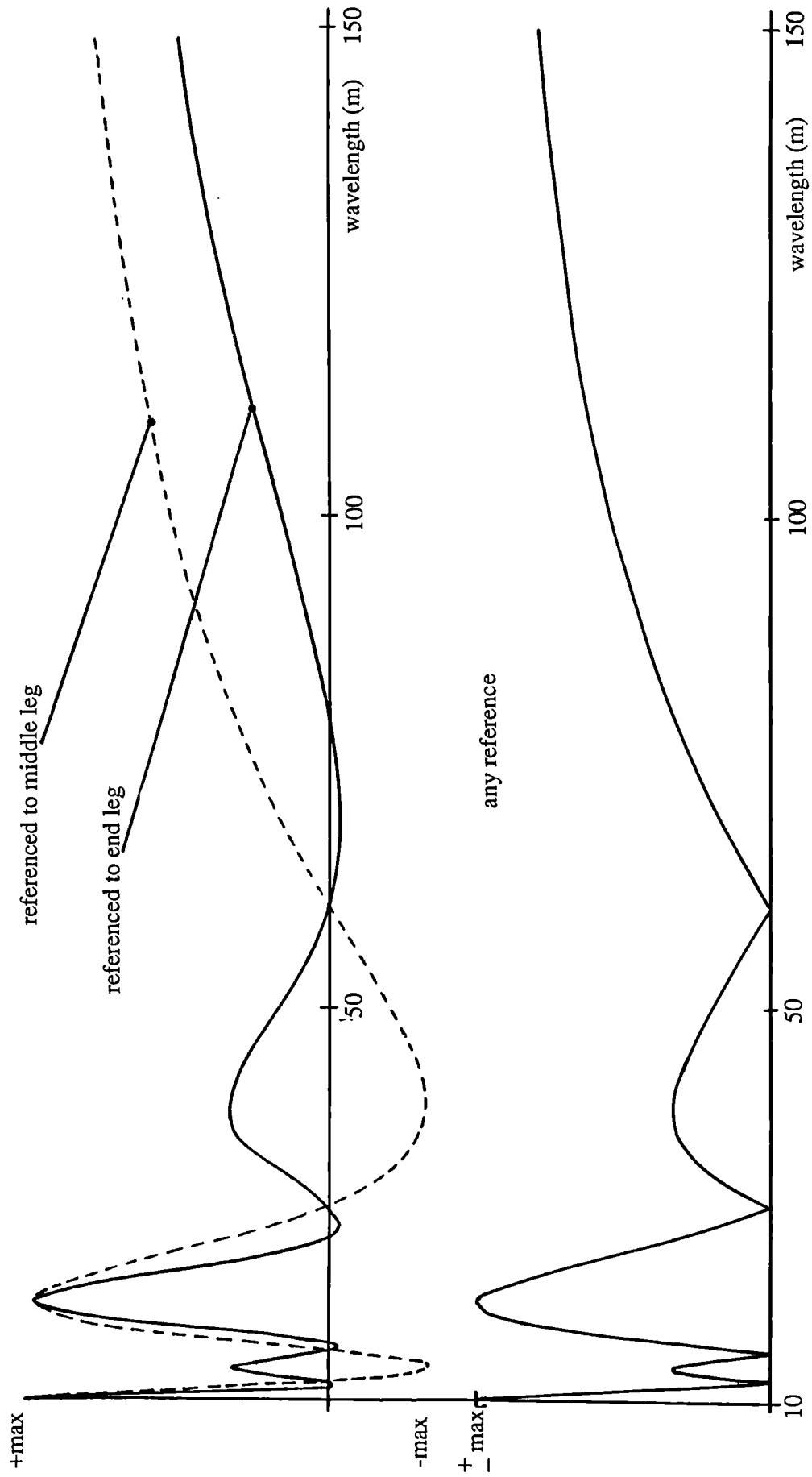


Figure 7.23. The maximum response of a structure comprising of a 3 by 3 array of piles for varying wavelength and waveangle

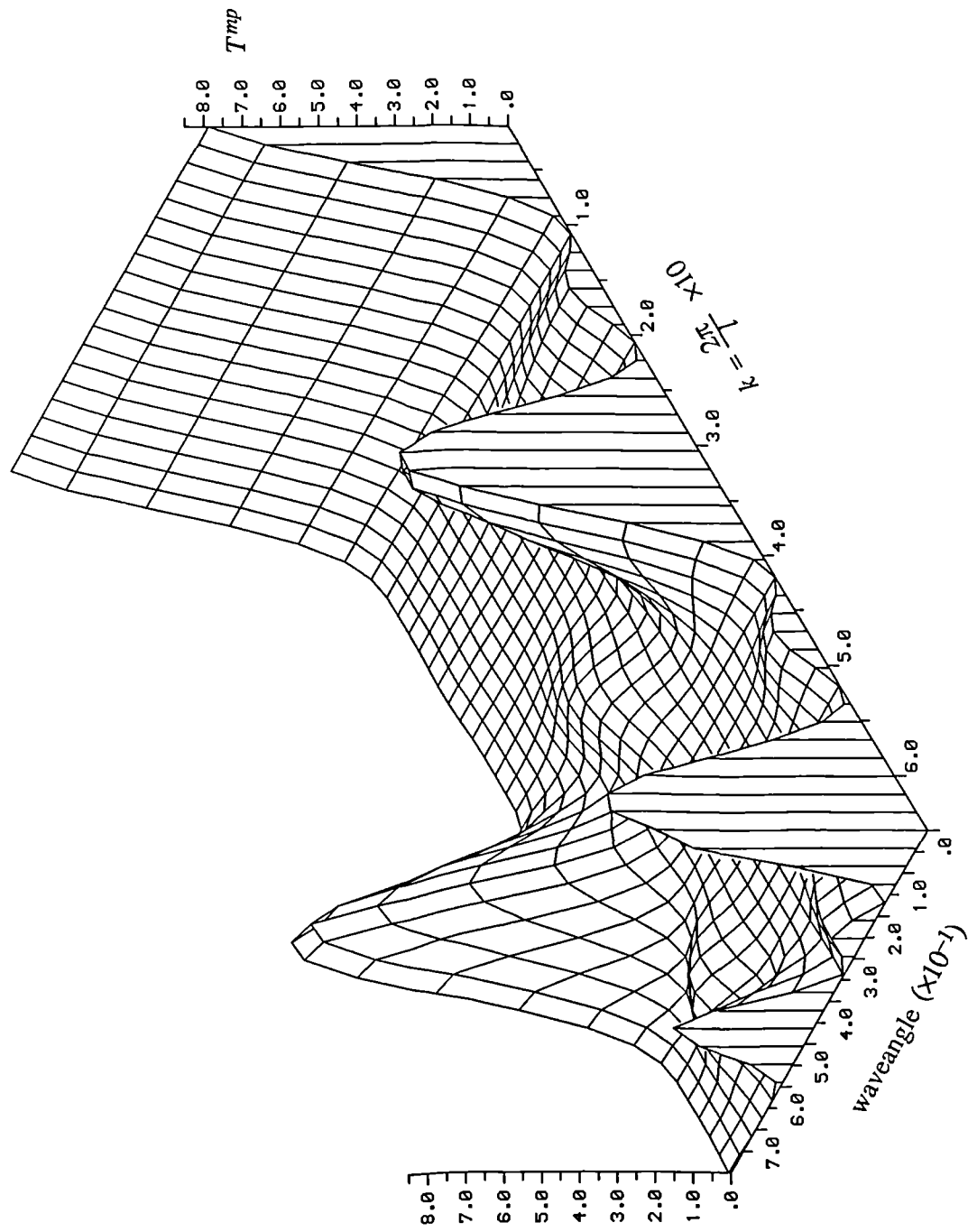


Figure 7.24(a). Results for sea state 7 with transfer function D1

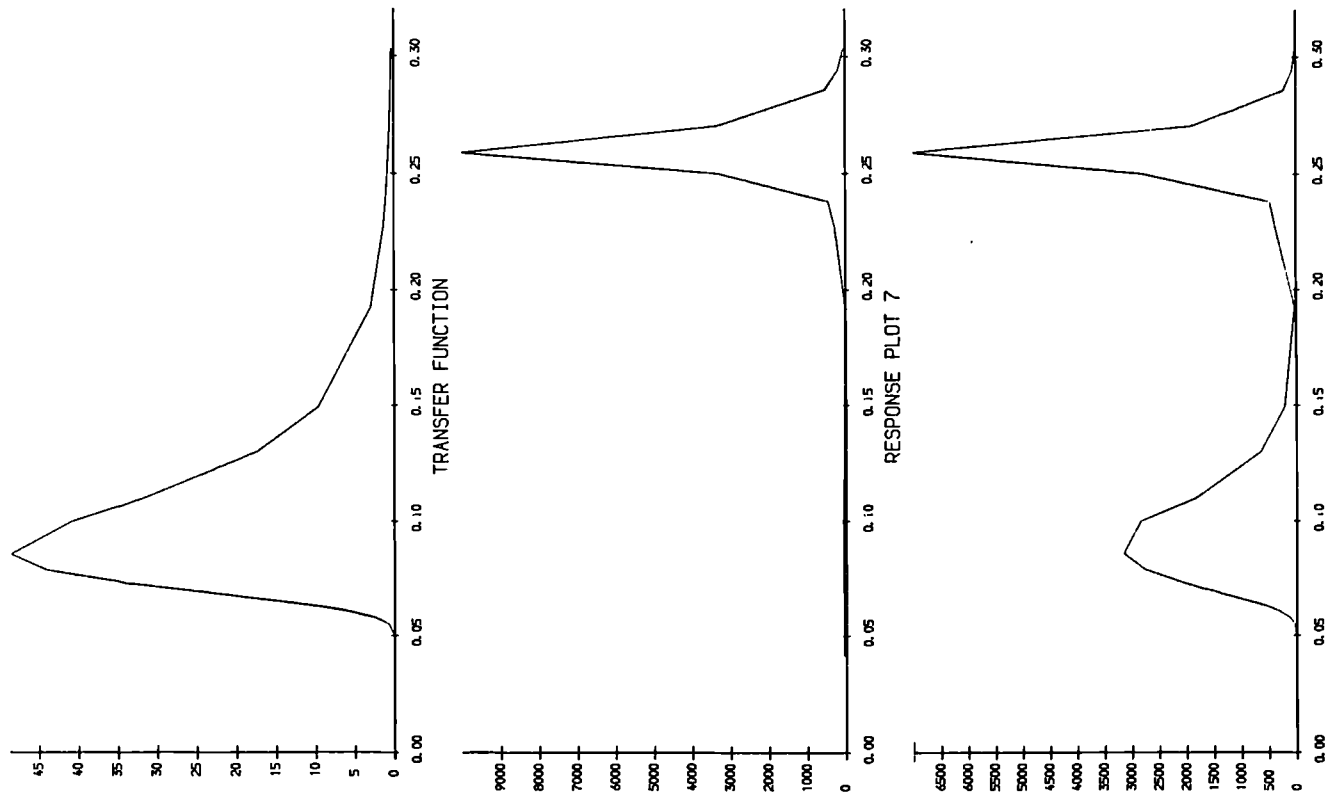


Figure 7.24(b). Results for sea state 7 with transfer function D5

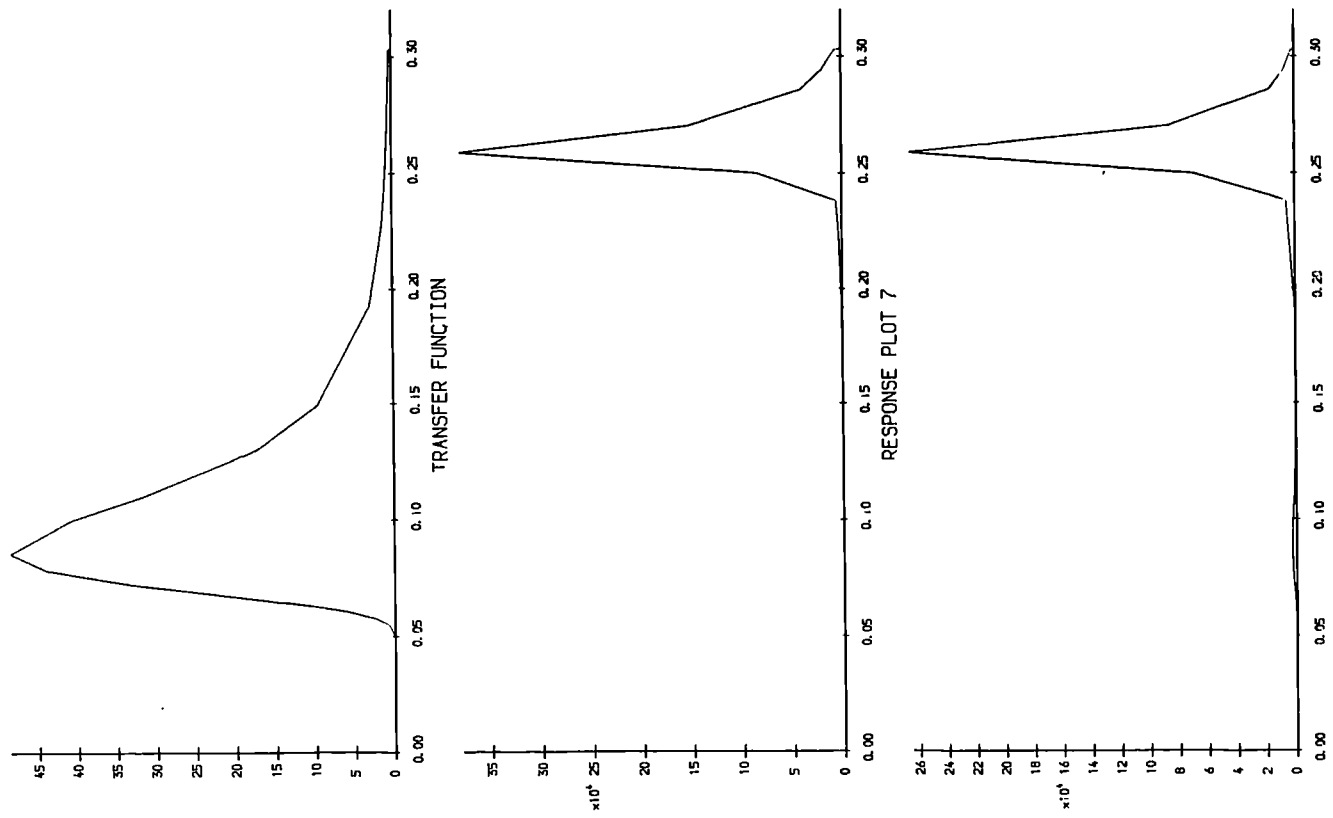


Figure 7.24(c). Results for sea state 7 with transfer function D15

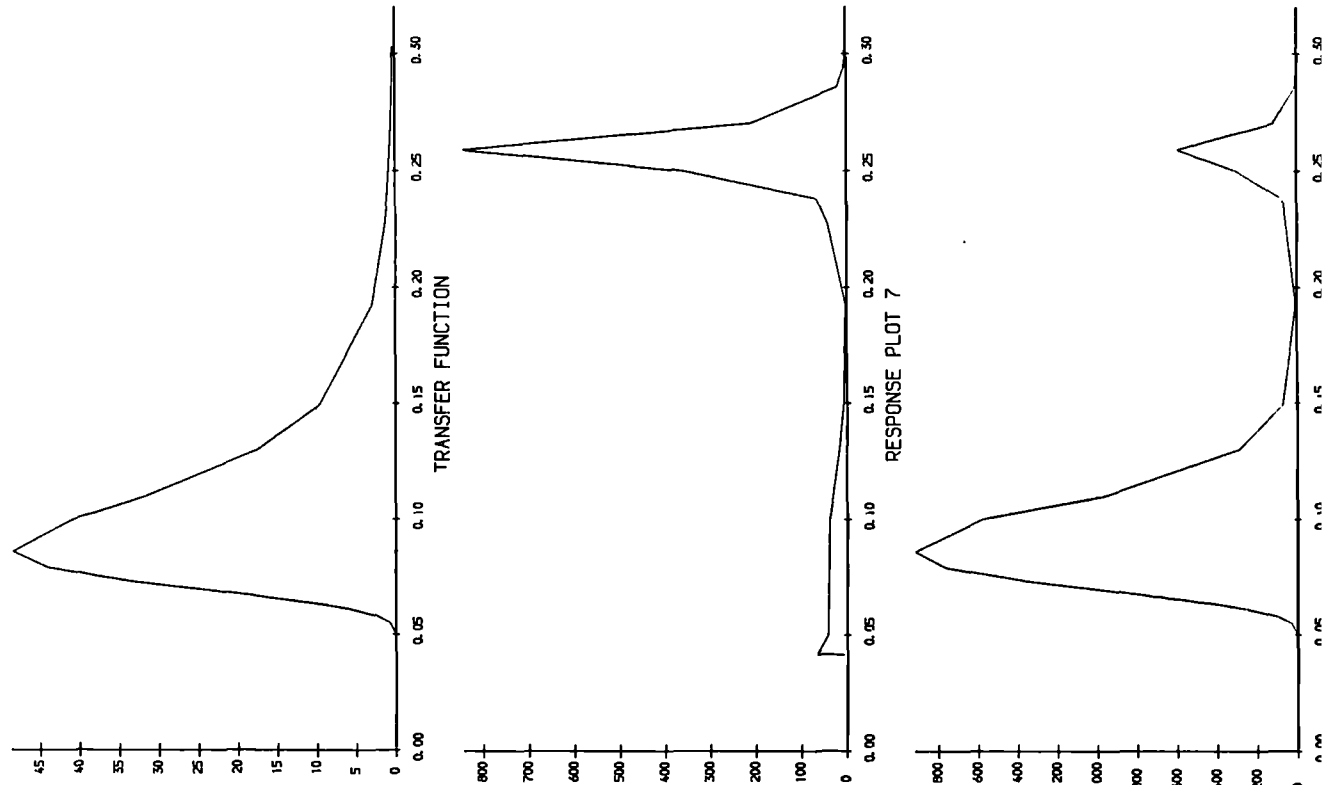


Figure 7.24(d). Results for sea state 7 with transfer function D18

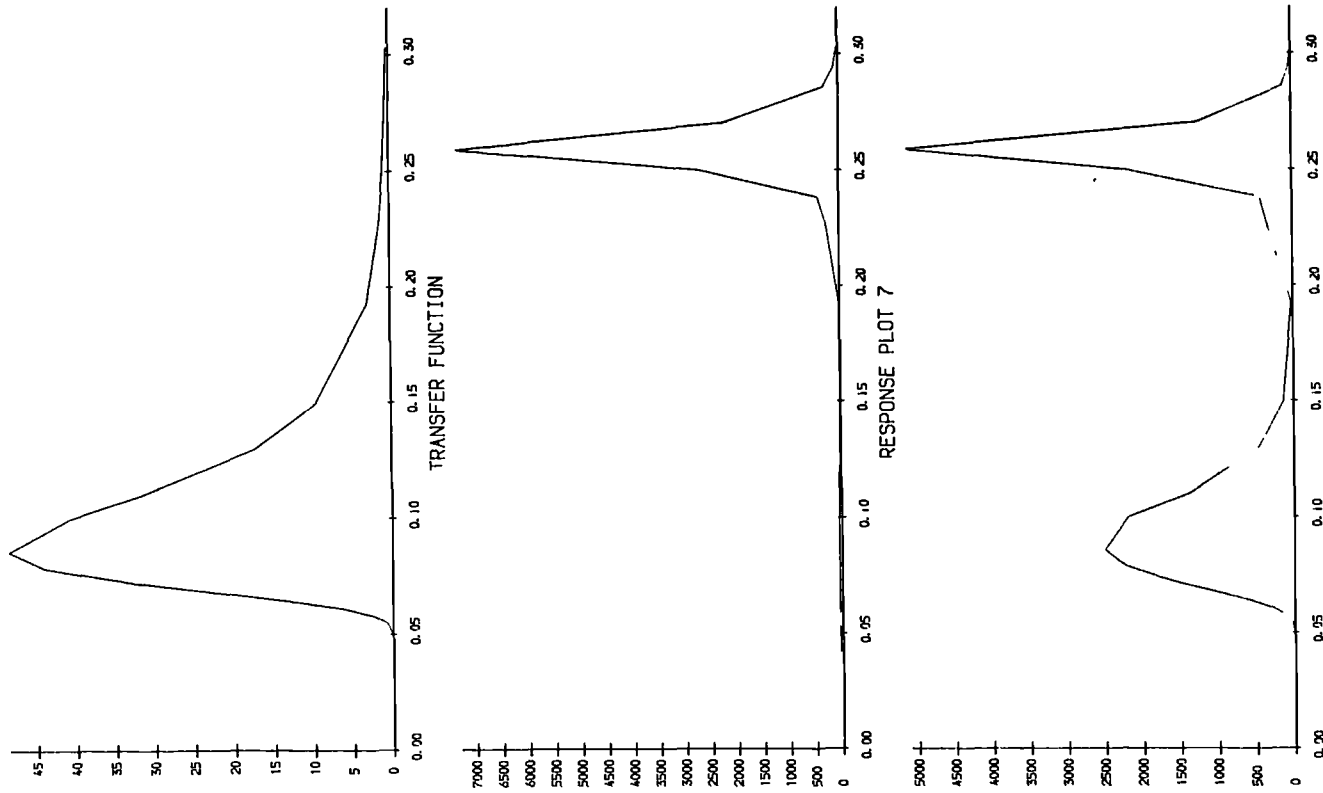


Figure 7.24(e). Results for sea state 7 with transfer function E1

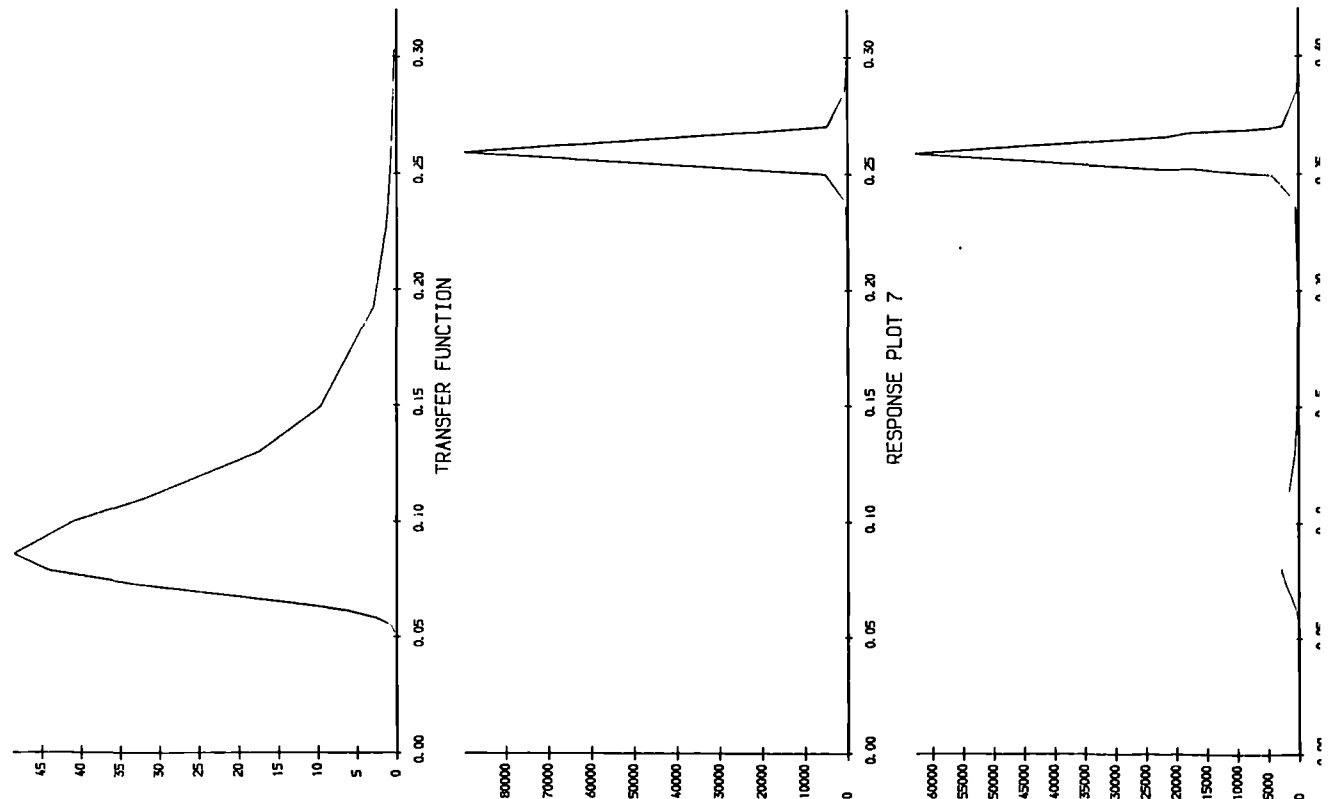


Figure 7.24(f). Results for sea state 7 with transfer function E4

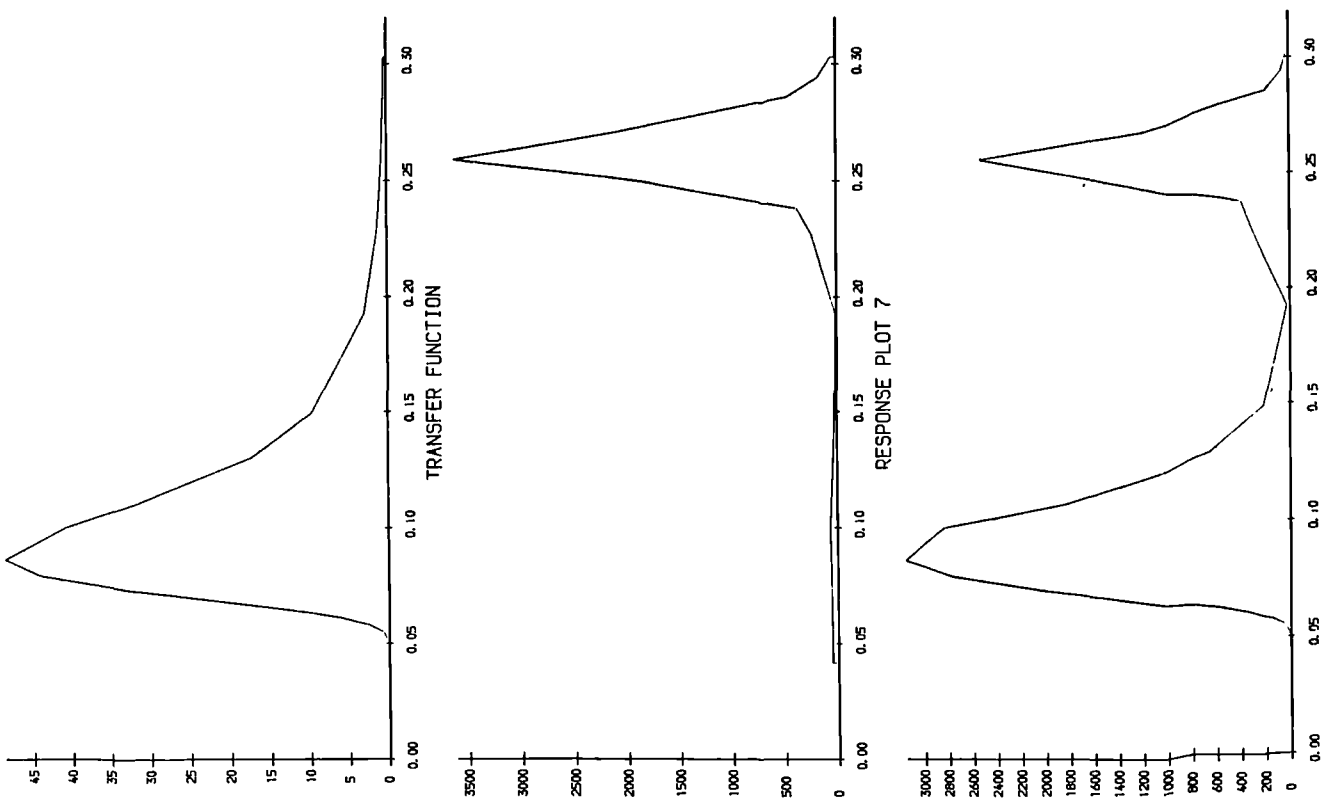


Figure 7.24(g). Results for sea state 7 with transfer function G1

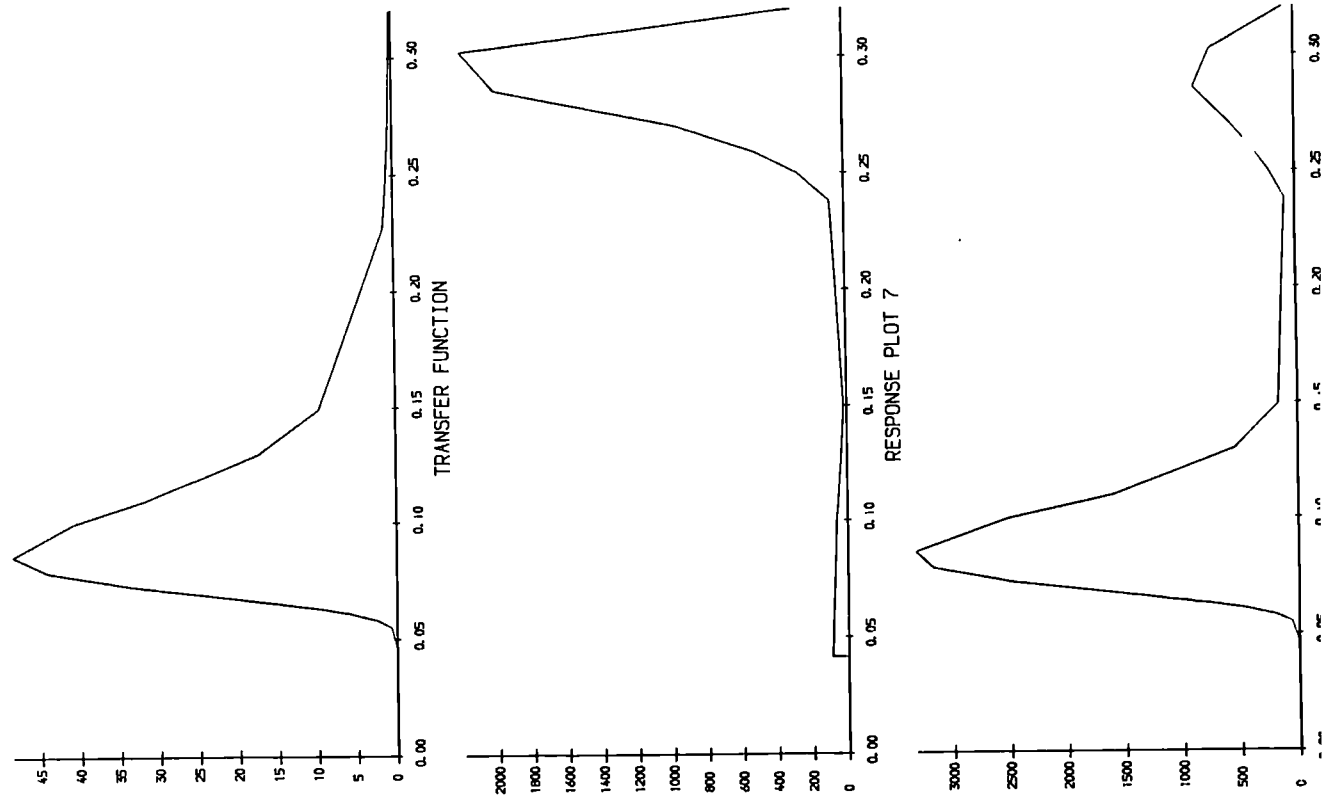


Figure 7.24(h). Results for sea state 7 with transfer function G2

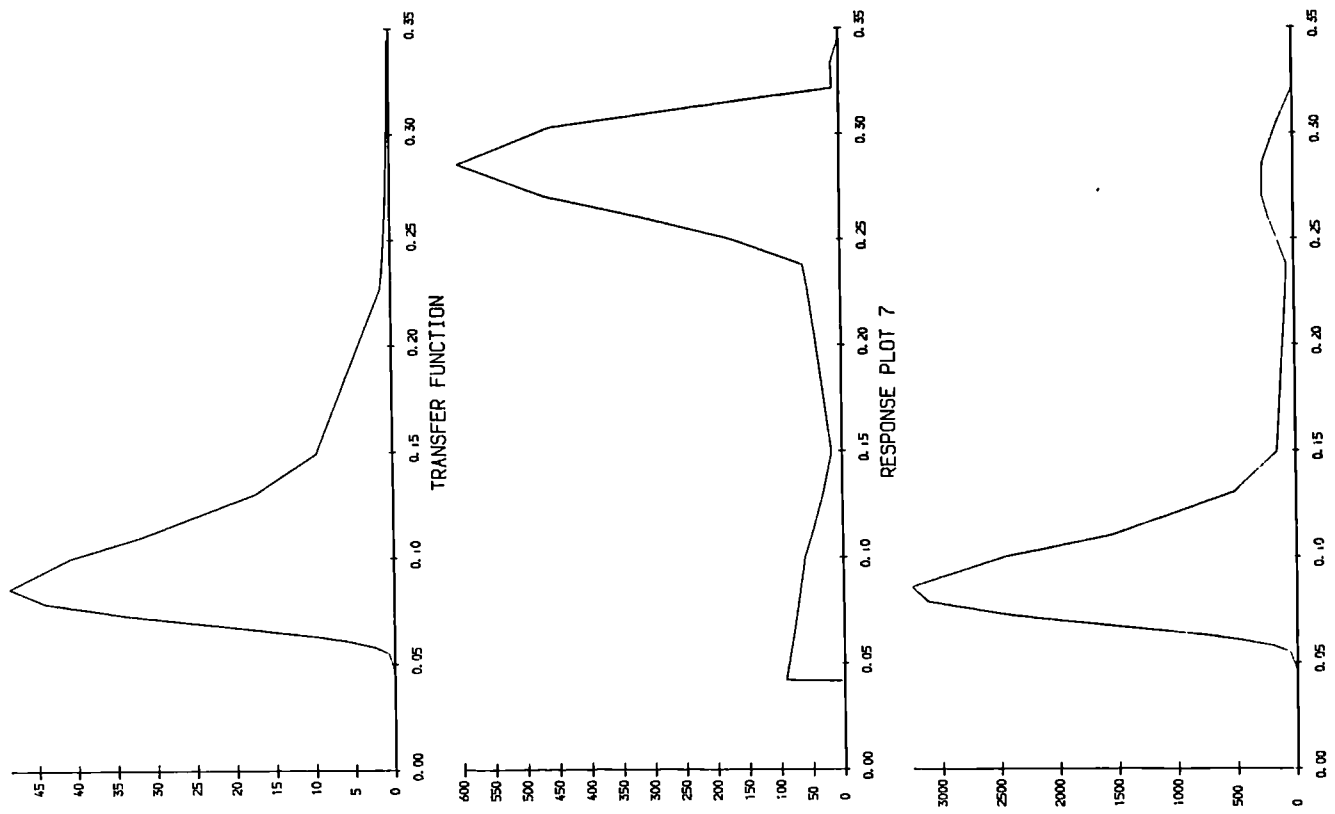


Figure 7.24(j). Results for sea state 7 with transfer function H3

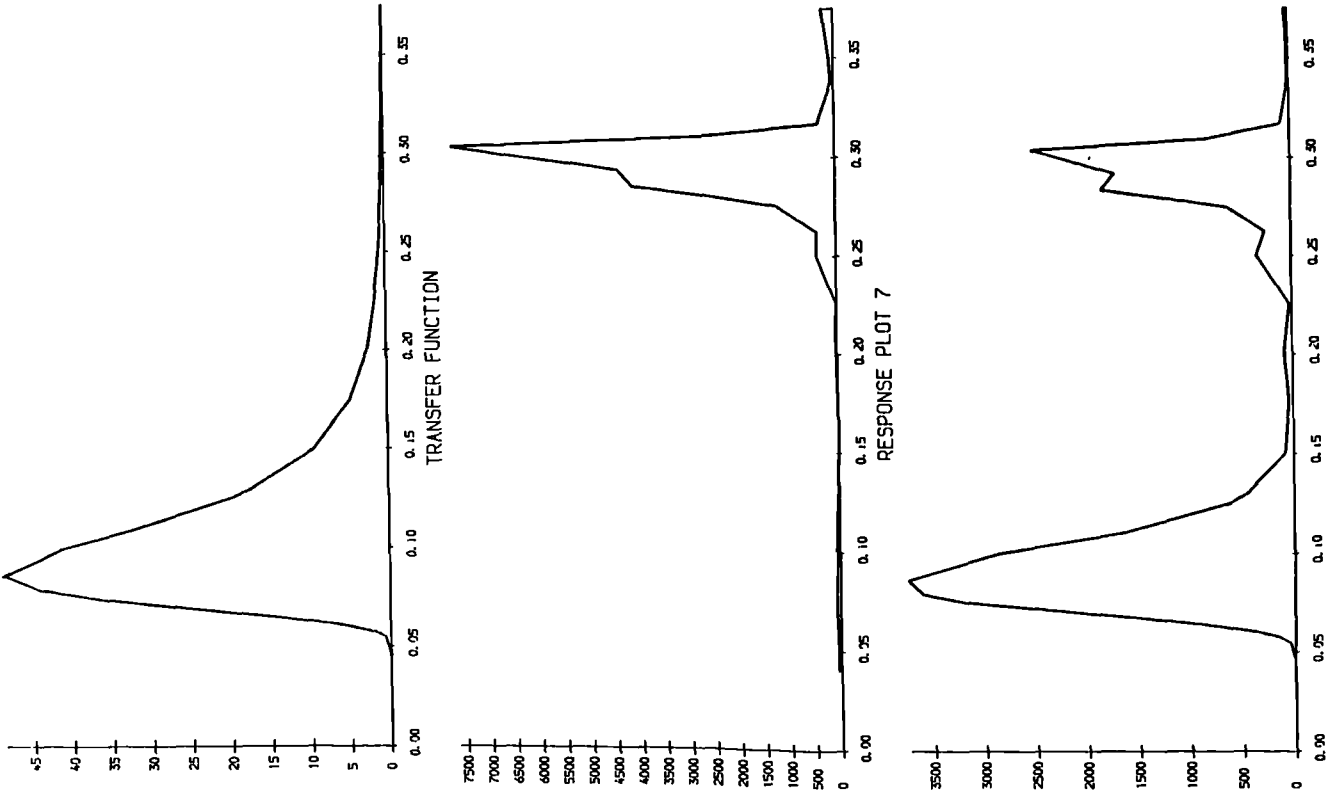
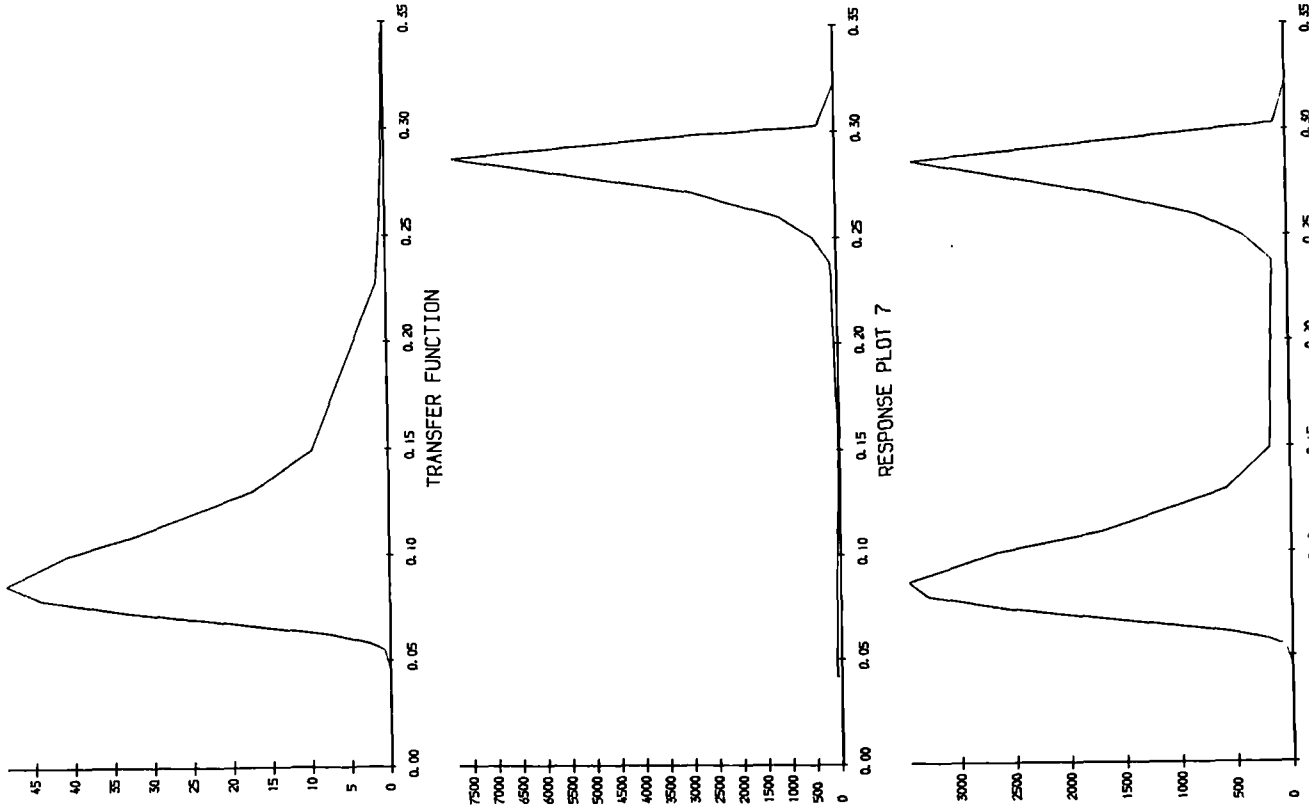


Figure 7.24(i). Results for sea state 7 with transfer function G3



8. Summary, conclusions and suggestions for future research

Summary and conclusions

The rainflow cycle counting method was introduced 20 years ago. Since then it has become widely accepted as the best method of estimating the fatigue damage caused by randomly fluctuating loading conditions. It is common for such loading conditions to be specified in the frequency domain as Power Spectral Density (PSD) data. Therefore, a theoretical link was required between this data and the rainflow range distribution. Such a theoretical solution has been obtained and is presented in chapter 5. It forms the major part of the original work presented in this thesis.

The rainflow range mechanism was broken down into a set of logical criteria and analyzed using Markov process theory. The dependence between extremes in this instance was modelled using the prediction of the joint distribution of peaks and troughs proposed by Kowalewski, and shown in chapter 4.

The solution was compared, for a variety of PSD's, with both a rainflow count on a long time signal and an earlier model produced by computer simulation. In both cases the comparison was successful.

The rest of the thesis deals with the following related subjects;

- (a) Chapter 3 investigates some empirical solutions developed by Dirlik in 1985 for estimating the ordinary and rainflow range density functions from frequency domain data. A program was developed which used these solutions along with the theoretical narrow band solution, commonly used for estimating fatigue damage from frequency domain data. The results obtained were in good agreement with those published by Chaudhury in 1985 and work in chapter 6 confirmed that Dirlik's solutions provide accurate estimates for the probability density functions. Results obtained using data from typical North Sea conditions show that the rainflow method predicts lives approximately 30% greater than the presently accepted approach for a material constant value b of 4.38.
- (b) A program was developed to determine the damage contributions from discrete frequency bands within the PSD data. These damage contributions were seen to be not

simply related to frequency, but dependent on other frequency bands within the PSD data. The work of chapter 3 showed that there is an interaction effect within PSD data. The results indicate that it is possible to quantify this interaction. Furthermore, with the aid of Finite Element programs it may be possible to obtain a direct relationship between a small change in structural geometry and the overall fatigue damage without a completely new fatigue damage analysis. In addition to applications in the offshore industry, this part of the work may be useful in areas such as automotive testing, where frequency domain control is used for the loading simulation of whole vehicles or automotive components. It should be possible to clarify the amount by which the PSD input can be allowed to vary for a maximum given error in the fatigue damage.

- (c) In order to develop the theoretical solution for the rainflow range density function which is presented in chapter 5, a theoretical solution was required for the joint distribution between adjacent extremes. This subject is dealt with in chapter 4 along with the topic of signal regeneration from peak-trough matrices. Kowalewski's expression for the dependence between adjacent peaks and troughs was used successfully for regeneration of peak-trough series. It was demonstrated that reasonable accuracy is obtained for the range distribution using this method. An improved solution for the dependence between peaks and troughs was developed by using Dirlik's ordinary range solution to correct the amplitude parameter in Kowalewski's solution. This improved solution is shown to give superior results which are less likely to be unconservative.
- (d) Chapter 6 dealt with the fatigue damage assessment and stress history determination of components when only limited samples of the service data are available. An investigation was carried out into the relative merits of time and frequency domain techniques. In particular, the effect of finite sample length was investigated with particular reference to the variance of fatigue predictions using both a rainflow count on a limited time sample and a rainflow count produced directly from a PSD of the same time sample. The frequency domain approach to rainflow cycle counting was shown to be a viable analysis technique. The acquisition rates and numbers of samples required are significantly less than the alternative time domain approach

and this may result in less computational time and storage space for on line fatigue analysis tests. Factors like the acquisition rate may be significant for high frequency fatigue work. The improved solution to Kowalewski's formulae for signal regeneration was used and shows significant improvements in terms of overall accuracy. Errors of 40% in the average value of fatigue predictions (based on the 6th moment of the rainflow ranges) were removed by this improved solution. Scatter in the fatigue predictions was shown to reduce with sample size as would be expected. The results for the frequency domain approach indicate that it is at least as good as the time domain prediction in terms of scatter. Plots of this scatter show the need for a factor of safety to be applied to any fatigue prediction which is based on a limited sample size. This applies both to time domain calculations and frequency domain solutions where a probabilistic approach is being applied.

- (e) Chapter 7 dealt with the fatigue damage assessment of dynamically sensitive offshore structures. This is a major application area for the theories presented in earlier chapters. A review of available fatigue analysis methods which may be applied to dynamically sensitive structures was carried out. Then using results from the Atkins package and programs developed in chapter 3, a comprehensive review of the Deterministic/Spectral method of fatigue analysis was carried out.

Future Work

Probably the most important area of application of the work is its significance in estimating the lives of offshore platforms. Design methods with known limitations and arbitrary correction factors are presently used. The new rainflow solution in chapter 5 allows a rational examination of these methods to be made leading to a proper choice of limiting criteria for different platform operating conditions. Development of these criteria would be a significant step forward.

Detailed points which require further investigation;

From chapter 3.

- (i) 'sizing effects' :- The effect on fatigue damage of varying the height of certain parts of the PSD plot.

- (ii) Numerical quantification of the fatigue damage potential analysis method is required in order to be able to predict the effect on fatigue damage of removing certain frequency bands. This would involve a theoretical consideration of the shapes of the curves on figures 3.18,3.19 and 3.20.

From chapter 4.

- (iii) The obvious area for future work here is the development of a better solution for the joint distribution between peaks and troughs. However, this will almost certainly require a solution to the problem of the distribution of times between zero crossings as highlighted by S.O.Rice in 1954.
- (iv) The author's version of the joint distribution of peaks and troughs (equation 4.44) is open to improvement because in modifying the range parameter of Kowalewski's Joint distribution (equation 4.42) the peak parameter is slightly affected. This work needs reconsideration to see if a joint distribution can be obtained which correctly fits both the peak and range parameters.

From chapter 5.

- (v) In order to obtain the theoretical rainflow range solution in chapter 5, use is made of Kowalewski's joint distribution of peaks and troughs. When a better joint distribution is found an immediate improvement to the rainflow range solution would be obtained. However, as stated above this will almost certainly require a solution to the problem of the distribution of times between zero crossings.
- (vi) Three events are utilised in the theoretical solution for rainflow ranges presented in chapter 5. These are highlighted in figure 5.3. When the two step peak-trough-peak transition matrix (figure 5.8(a)) is squared and resquared until the specified parts of the matrix are empty, certain convergence rates could be observed for the three events mentioned above. It would be of considerable interest to investigate the shapes and relative convergence rates of these three conditions.

From chapter 6.

- (vii) In chapter 6 the use of a factor of safety was discussed with respect to the variance of the fatigue prediction. It would be of use to quantify this factor of safety and determine which variables have an effect on its magnitude.

From chapter 7.

In addition to those listed above, two other areas for future research concerning offshore structures are dealt with at the end of chapter 7.

Appendix 1. The program used for the fatigue damage potential work in chapter 3.

```

C*****
C THIS IS A PROGRAM TO WORK OUT THE EXPECTED FATIGUE DAMAGE OF A *
C COMPONENT, GIVEN THE OUTPUT OF STRESS IN THE FORM OF A POWER SPECTRAL*
C DENSITY PLOT. TWO DIFFERENT P.S.D. PLOT INPUTS ARE ALLOWED AND THE *
C COMPUTER KNOWS WHICH ONE TO EXPECT BY THE VALUE ASSIGNED TO 'MODE'. *
C *
C MODE '5' AS MODE '4' WITH MOVING STRIP WIDTH FD (HZ). *
C *
C MODE '6' " " 3 " " " " " " *
C *
C 'BEE' EQUALS 'B', 'YAK' EQUALS 'A' AND 'END' IS THE ENDURANCE *
C LIMIT TAKEN FROM THE "N=A.S**(-B)" FATIGUE DAMAGE CURVES. "FC" IS *
C THE INTEGRATION LIMIT FOR THE POWER SPECTRAL DENSITY PLOT. "TIME" *
C IS THE PROP. OF THE TOTAL TIME THAT THE ITH SEA STATE DOMINATES. *
C "L" AND "M" ARE THE NUMBER OF POINTS INTO WHICH THE PROBABILITY *
C FUNCTIONS AND THE POWER SPECTRAL DENSITY PLOT ARE DIVIDED. "L" AND *
C "M" ARE PROVIDED INSIDE THE PROGRAM. "FD" SHOULD BE INPUT AS ZERO *
C FOR MODES '1' TO '4'. *
C THREE RESULTS SHOULD BE OUTPUT FOR THE EXPECTED FATIGUE DAMAGE. *
C THESE ARE RAINFLOW RANGE FATIGUE DAMAGE, ORDINARY RANGE FATIGUE *
C DAMAGE AND NARROW BAND FATIGUE DAMAGE. *
C*****
      IMPLICIT DOUBLE PRECISION (A-H,O-Z)
      DIMENSION G(1001),ARM(1001),PRR(201),POR(201),PNB(201)
      1,AIM(201),ADN(201),DAM(100,100),FMM(100)
      1,DAMOR(100,100),DAMNB(100,100)
      M=1000
      L=201
C READ IN DATA
      WRITE(6,999)
      PRINT*,' INPUT FC,END,TIME,A1,A2,F1,F2,Q1,Q2,BEE,YAK,MODE,FD'
      READ(5,*)FC,END,TIME,A1,A2,F1,F2,Q1,Q2,BEE,YAK,MODE,FD
      WRITE(6,984)FC,END,TIME,A1,A2,F1,F2,Q1,Q2,BEE,YAK,MODE,FD
      WRITE(6,999)
C P.S.D. PLOT INTEGRATION STEP WIDTH IS:-
      D=FC/(M)
C NUMBER OF DIVISIONS REMOVED FROM P.S.D. PLOT IN MOVING STRIP RUN IS:-
      MG=NINT(FD/D)
C POSITION WHICH MARKS LIMIT OF MOVING STRIP RUN IS:-
      ME=M-MG+1
C NUMBER OF WHOLE MOVING STRIP WIDTHS UP TO 'ME' IS:-
      MT=ME/MG
C NUMBER OF POSITIONS USED FOR MOVING STRIP IS:-
      MTI=MT+1
C LAST MOVING STRIP POINT IS:-
      MTP=1.0+MT*MG
      WRITE(6,985)MTP
      WRITE(6,88) MG
C FULL RESULTS PLOTTED WHEN MOVING STRIP IS AT POSITION 'MM'
      MMM=0.3*MT
      NNN=0.4*MT
      MM=MMM*MG+1
      NN=NNN*MG+1
      TOY=0.0
      FI=MG*D*0.5
      EP=1.0E-30
      GP=-100
C START OF DO LOOP FOR MOVING STRIP RUN
      DO 902 INO=1,MTI
      IN=(INO-1)*MG+1
      NGS=IN
      NGE=NGS+MG-1
      DO 901 IMO=1,MTI
      IM=(IMO-1)*MG+1
C "FMM(IMO)" IS THE CENTRAL FREQUENCY OF MOVING STRIP AT POSITION IM
      IF(IN.NE.1) GO TO 640

```

```

      FMM(IMO)=FI
      FI=FI+FD
640 CONTINUE
C LEFT AND RIGHT EDGES OF MOVING STRIP DEFINED BY:-
      MGS=IM
      MGE=MGS+MG-1
C*****
C
C FOR SIG. HT. SPECTRA WITH MOVING STRIP THIS SECTION ONLY IS EXECUTED.*
C
C*****
      IF(MODE.EQ.5) THEN
          TD=A2
          HS=A1
          PHI=F1
          A=F2
          FN=Q1
          ETA=Q2
          DO 24 I=1,M
              F=D*(I-0.5)
              XP=(-1050.0/((2.0*3.14159*TD*F+(EP**0.25))**4))
                  IF(I.GE.MGS .AND. I.LE.MGE) THEN
                      G(I)=EP
                  ELSE IF(I.GE.NGS .AND. I.LE.NGE) THEN
                      G(I)=EP
                  ELSE IF(XP.LT.GP) THEN
                      G(I)=EP
                  ELSE IF(I.GE.MTP) THEN
                      G(I)=EP
                  ELSE
                      G(I)=A*HS**PHI*EXP(XP)/(T
1D**4*(2.0*3.14159*F+EP)**5*((1.0-(F/FN)**2)**2+(2.0*ETA*F/FN)*
1*2))
                  END IF
          ARM(I)=F
24 CONTINUE
C*****
C
C FOR RECTANGULAR SPECTRA WITH MOVING STRIP
C
C*****
      ELSE IF(MODE.EQ.6) THEN
          F3=Q1
          F4=Q2
          DO 46 I=1,M
              F=D*(I-0.5)
              ARM(I)=F
              G(I)=EP
              IF(F.GE.F1 .AND. F.LE.F2) G(I)=A1
              IF(F.GE.F3 .AND. F.LE.F4) G(I)=A2
              IF(I.GE.MGS .AND. I.LE.MGE) G(I)=EP
              IF(I.GE.NGS .AND. I.LE.NGE) G(I)=EP
              IF(F.GT.F2 .AND. F.GT.F4) G(I)=EP
          46 CONTINUE
      END IF
C*****
C SECTION TO WORK OUT MAXIMUM G(I).
      IF(IN.NE.NN .OR. IM.NE.MM) GO TO 903
      GOY=0.0
      DO 304 J=1,M
          IF(G(J).GE.GOY) THEN
              GOY=G(J)
          END IF
304 CONTINUE
      LN=GOY/1000.0+1.0
      GOP=LN*1000.00

```

```

903 CONTINUE
C SECTION TO WORK OUT COEFFICIENTS OF P.S.D. PLOT.
  IF (IN.NE.NN .OR. IM.NE.MM) GO TO 975
  WRITE (6,999)
  PRINT*, 'VALUES OF POWER SPECTRAL DENSITY'
  WRITE (6,71) (G(K),K=1,M)
  WRITE (6,999)
  PRINT*, 'VALUES OF LEVER ARM'
C  WRITE (6,72) (ARM(K),K=1,M)
  WRITE (6,999)
975 CONTINUE
  CALL SIMP1 (G,ARM,D,M,B0,B1,B2,B4)
  SIGMAX=SQRT (B0)
  XM=B1/B0*SQRT (B2/B4)
  GAMMA=SQRT (B2**2/(B0*B4))
  UM=SQRT (B4/B2)
  AMDA=SQRT (B2/B0)
  IF (IN.NE.NN .OR. IM.NE.MM) GO TO 904
  WRITE (6,73) B0
  WRITE (6,74) B1
  WRITE (6,75) B2
  WRITE (6,76) B4
C ROOT MEAN SQUARE VALUE
  WRITE (6,77) SIGMAX
C RELATIVE MEAN
  WRITE (6,78) XM
C IRREGULARITY FACTOR
  WRITE (6,79) GAMMA
C EXPECTED NUMBER OF PEAKS
  WRITE (6,80) UM
C EXPECTED NUMBER OF POSITIVE ZEROS
  WRITE (6,801) AMDA
  WRITE (6,999)
904 CONTINUE
C INTEGRATION OF RANGE FUNCTIONS UP TO "XTOT".
  IF (IN.NE.1 .OR. IM.NE.1) GO TO 968
  JN=NINT (9.0*SIGMAX/20.0)
  XTOT=JN*20.0
968 CONTINUE
C*****
C
C START OF SECTION TO PRODUCE RAINFLOW RANGE FATIGUE DAMAGE
C
C*****
  C1=2.0*(XM-GAMMA**2)/(1+GAMMA**2)
  ALFA=(GAMMA-XM-C1**2)/(1-GAMMA-C1+C1**2)
  C2=(1-GAMMA-C1+C1**2)/(1-ALFA)
  C3=1-C1-C2
  TOR=1.25*(GAMMA-C3-(C2*ALFA))/C1
  DN=XTOT/(L-1)
  DO 22 J=1,L
  POR(J)=EP
  PNB(J)=EP
  X=DN*(J-1)
  ADN(J)=X
  AIM(J)=X**BEE
  Z=X/(2.0*SIGMAX)
  XRR=(-Z)/TOR
  YRR=(-Z)*Z/(2.0*ALFA*ALFA)
  ZRR=(-Z)*Z/2.0
  IF (XRR.LT.GP) XRR=GP
  IF (YRR.LT.GP) YRR=GP
  IF (ZRR.LT.GP) ZRR=GP
  PRR(J)=(C1/TOR*EXP (XRR)+C2*Z/(ALFA*ALFA)*EXP (YRR)
1+C3*Z*EXP (ZRR))/(2.0*SIGMAX)
  TRY=PRR(J)

```

```

        IF (TRY.GE.TOY) THEN
        TOY=TRY
C TOY IS THE MAXIMUM VALUE OF PRR(J)
        END IF
    22 CONTINUE
        IF (IN.NE.NN .OR. IM.NE.MM) GO TO 906
        MN=TOY*100.0+1.0
        TOP=MN/100.0
    906 CONTINUE
        CALL SIMP2 (PRR, DN, L, EDO, AIM, END, EDOE)
        ED=TIME*EDO*UM/YAK
        DAM (INO, IMO) =ED
C*****
C
C START OF SECTION TO PRODUCE ORDINARY RANGE FATIGUE DAMAGE
C
C*****
        XMINOR=GAMMA/ (1.0+1.25*(1.0-GAMMA) )
        C1OR=(XM-XMINOR) / (GAMMA*GAMMA)
        TOROR=0.02+2.0/GAMMA*(XM-XMINOR)
        C2OR=1.0-C1OR
        ALFAOR=GAMMA+(XM-XMINOR) /GAMMA
        DO 23 J=1, L
            Z=DN*(J-1) / (2.0*SIGMAX)
            POR(J) = (C1OR/TOROR*EXP ( (-Z) /TOROR) +C2OR*Z/ (ALFAOR*ALFAOR)
1*EXP ( (-Z) *Z/ (2.0*ALFAOR*ALFAOR) ) ) / (2.0*SIGMAX)
    23 CONTINUE
        CALL SIMP2 (POR, DN, L, EDORO, AIM, END, EDOROE)
        EDOR=TIME*EDORO*UM/YAK
        DAMOR (INO, IMO) =EDOR
C*****
C
C START OF SECTION TO PRODUCE NARROW BAND FATIGUE DAMAGE
C
C*****
        DO 59 I=1, L
            X=DN*(I-1)
            PNB (I) = (X) / (4.0*B0) *EXP ( - ( (X) **2) / (8.0*B0) )
            ADN (I) =X
    59 CONTINUE
        CALL SIMP2 (PNB, DN, L, EDNBO, AIM, END, EDNBOE)
        EDNB=TIME*EDNBO*AMDA/YAK
        DAMNB (INO, IMO) =EDNB
C*****
C SECTION TO PRODUCE DATA FOR GRAPH PLOTTER.
        IF (IN.NE.NN .OR. IM.NE.MM) GO TO 908
        WRITE (3, 804) L
        WRITE (3, 802) XTOT, TOP
        DO 63 I=1, L
            WRITE (3, 803) ADN (I) , PRR (I) , POR (I) , PNB (I)
    63 CONTINUE
            WRITE (3, 805) M
            WRITE (3, 806) FC, GOP
            DO 64 I=1, M
                WRITE (3, 807) ARM (I) , G (I)
    64 CONTINUE
    908 CONTINUE
C*****
    901 CONTINUE
    902 CONTINUE
C*****
        DOP=0.0
        DO 967 I=1, MTI
            DO 969 J=1, MTI
                DAM (I, J) = (DAM (I, MTI) -DAM (I, J) ) /FD
                DAMOR (I, J) = (DAMOR (I, MTI) -DAMOR (I, J) ) /FD

```

```

DAMNB(I,J)=(DAMNB(I,MTI)-DAMNB(I,J))/FD
IF(DAM(I,J).GT.DOP) DOP=DAM(I,J)
IF(DAMOR(I,J).GT.DOP) DOP=DAMOR(I,J)
IF(DAMNB(I,J).GT.DOP) DOP=DAMNB(I,J)
969 CONTINUE
967 CONTINUE
WRITE(3,600)MTI
WRITE(3,601)FC,DOP
WRITE(3,602)(FMM(J),(DAM(I,J),I=1,MTI),J=1,MTI)
PRINT*,'VALUES OF FMM, DAM(I,J)'
WRITE(6,990)(FMM(J),(DAM(I,J),I=1,MTI),J=1,MTI)
WRITE(3,600)MTI
WRITE(3,601)FC,DOP
WRITE(3,602)(FMM(J),(DAMOR(I,J),I=1,MTI),J=1,MTI)
PRINT*,'VALUES OF FMM, DAMOR(I,J)'
WRITE(6,990)(FMM(J),(DAMOR(I,J),I=1,MTI),J=1,MTI)
WRITE(3,600)MTI
WRITE(3,601)FC,DOP
WRITE(3,602)(FMM(J),(DAMNB(I,J),I=1,MTI),J=1,MTI)
PRINT*,'VALUES OF FMM, DAMNB(I,J)'
WRITE(6,990)(FMM(J),(DAMNB(I,J),I=1,MTI),J=1,MTI)
NEND=-1
WRITE(3,604)NEND

```

C
C
C
C
C

```

999 FORMAT(' *****
1*****
1*')
984 FORMAT(1X,2F9.3,E12.4,2F11.3,4F9.3,F8.4,E12.5,I3,F12.9)
985 FORMAT(' LAST MOVING STRIP POSITION IS',I6)
88 FORMAT(' WIDTH USED FOR MOVING STRIP IS',I5)
600 FORMAT(I4,' REDUCTION IN DAMAGE/UNIT HZ')
601 FORMAT(F10.5,E18.9)
602 FORMAT(F6.3,10E12.5,/,6X,10E12.5)
604 FORMAT(I4)
990 FORMAT(F6.3,10E12.5,/,6X,10E12.5)
802 FORMAT(F10.3,F10.7)
803 FORMAT(F10.3,3F10.7)
804 FORMAT(I4,' RANGE PROBABILITY FUNCTIONS')
805 FORMAT(I4,' POWER SPECTRAL DENSITY PLOTS')
806 FORMAT(F10.5,F10.1)
807 FORMAT(F10.5,F10.1)
808 FORMAT(F5.1)
71 FORMAT(1X,10F11.3)
72 FORMAT(1X,10F11.5)
73 FORMAT(' THE VALUE OF THE ZEROth MOMENT OF PSD IS',F18.3)
74 FORMAT(' THE VALUE OF THE FIRST MOMENT OF PSD IS',F18.3)
75 FORMAT(' THE VALUE OF THE SECOND MOMENT OF PSD IS',F18.3)
76 FORMAT(' THE VALUE OF THE FOURTH MOMENT OF PSD IS',F22.3)
77 FORMAT(' THE ROOT MEAN SQUARE VALUE IS',F14.3)
78 FORMAT(' THE RELATIVE MEAN IS',F15.5)
79 FORMAT(' THE IRREGULARITY FACTOR IS',F12.5)
80 FORMAT(' THE EXPECTED NUMBER OF PEAKS PER UNIT TIME IS',F11.4)
81 FORMAT(' ALFA IS',F12.5)
82 FORMAT(' TOR IS',F12.5)
83 FORMAT(' C1 IS',F12.5)
84 FORMAT(' C2 IS',F12.5)
85 FORMAT(' C3 IS',F12.5)
86 FORMAT(1X,10F11.5)
87 FORMAT(1X,F25.20)
201 FORMAT(' XMINOR IS',F12.5)
202 FORMAT(' C1OR IS',F12.5)
203 FORMAT(' C2OR IS',F12.5)

```

```

204 FORMAT(' ALFAOR IS',F12.5)
205 FORMAT(' TOROR IS',F12.5)
801 FORMAT(' THE EXPECTED NUMBER OF POSITIVE ZEROS IS',F11.4)
STOP
END

```

C

```

C*****
C*****

```

C

```

SUBROUTINE SIMP1(STRSS,ARMTT,DTT,MT,B0TT,B1TT,B2TT,B4TT)
IMPLICIT DOUBLE PRECISION (A-H,O-Z)
DOUBLE PRECISION STRSS,ARMTT
DIMENSION STRSS(1001),ARMTT(1001)
DT=DTT
B0T=0.0
B1T=0.0
B2T=0.0
B4T=0.0
DO 10 I=1,MT
STR=STRSS(I)
ARMT=ARMTT(I)
B0T=B0T+(STR*DT)
B1T=B1T+(STR*ARMT*DT)
B2T=B2T+(STR*ARMT**2*DT)
B4T=B4T+(STR*ARMT**4*DT)
10 CONTINUE
B0TT=B0T
B1TT=B1T
B2TT=B2T
B4TT=B4T
RETURN
END

```

C

```

C*****
C*****

```

C

```

SUBROUTINE SIMP2(STR,DNTT,LT,EDTT,AIM,END,EDTOT)
IMPLICIT DOUBLE PRECISION (A-H,O-Z)
DOUBLE PRECISION STR(201),AIM(201)
EDT=0.0
K=2
DNT=DNTT
DO 11 J=1,LT
KK=J/K
FACT=2.0
IF(J.EQ.K*KK)FACT=4.0
IF(J.EQ.1 .OR. J.EQ.LT)FACT=1.0
EDT=EDT+DNT*AIM(J)*STR(J)*FACT/3.0
11 CONTINUE
EDTT=EDT
IF(END.LE.1.0) GO TO 548
EDTO=0.0
K=2
LE=END/DNT+1.0
DO 112 J=LE,LT
KK=J/K
FACT=2.0
IF(J.EQ.K*KK)FACT=4.0
IF(J.EQ.LE .OR. J.EQ.LT)FACT=1.0
EDTO=EDTO+DNT*AIM(J)*STR(J)*FACT/3.0
112 CONTINUE
EDTOT=EDTO
548 CONTINUE
RETURN

```

```

C*****
C*****

```

END

END	X	Y	(9) (1001,1)	(9) (1101,1)
	ALL	LOAD	1	1
	1	1	TRANSFER FUNCTION POINT ONE	
	WAVE	LOA	0.000	-9.810
	GRAV		6.0	1025
	ELEV		0.1	0.000
	SLWT		20.0	0.000
	TOLS			
	WAVE			
	MAXM	12		
	OUTP	1		
	EXEC		20.0	13.33
	WAVE			0.0000
	MAXM	12		
	OUTP	1		
	EXEC		14.08	8.00
	WAVE			0.0000
	MAXM	12		
	OUTP	1		
	EXEC		9.76	6.66
	WAVE			0.0000
	MAXM	12		
	OUTP	1		
	EXEC		7.17	5.71
	WAVE			0.0000
	MAXM	12		
	OUTP	1		
	EXEC		5.50	5.00
	WAVE			0.0000
	MAXM	12		
	OUTP	1		
	EXEC		4.34	4.44
	WAVE			0.0000
	MAXM	12		
	OUTP	1		
	EXEC		3.52	4.00
	WAVE			0.0000
	MAXM	12		
	OUTP	1		
	EXEC		3.19	3.81
	WAVE			0.0000
	MAXM	12		
	OUTP	1		
	EXEC		2.91	3.64
	WAVE			0.0000
	MAXM	12		
	OUTP	1		
	EXEC		2.74	3.53
	WAVE			0.0000
	MAXM	12		
	OUTP	1		
	EXEC		2.54	3.43
	WAVE			0.0000
	MAXM	12		
	OUTP	1		

TUBE	(2)	(101,3)	(104,3)	(1)	(1)
R	(5)	(0)	(100)		
TUBE	(2)	(601,3)	(604,3)	(1)	(2)
R	(4)	(0)	(100)		
TUBE	(2)	(102,3)	(105,3)	(1)	(1)
R	(5)	(0)	(100)		
TUBE	(2)	(602,3)	(605,3)	(1)	(2)
R	(4)	(0)	(100)		
TUBE	(2)	(103,3)	(106,3)	(1)	(1)
R	(5)	(0)	(100)		
TUBE	(2)	(603,3)	(606,3)	(1)	(2)
R	(4)	(0)	(100)		
TUBE	(5)	(102,100)	(106,100)	(1)	(3)
TUBE	(5)	(104,100)	(108,100)	(1)	(3)
TUBE	(4)	(602,100)	(606,100)	(1)	(4)
TUBE	(4)	(604,100)	(608,100)	(1)	(4)
TUBE	(2)	(102,4)	(104,4)	(1)	(3)
R	(5)	(0)	(100)		
TUBE	(2)	(602,4)	(604,4)	(1)	(4)
R	(4)	(0)	(100)		
TUBE	(3)	(301,3)	(402,3)	(1)	(3)
R	(3)	(0)	(100)		
TUBE	(3)	(601,3)	(702,3)	(1)	(4)
R	(4)	(0)	(100)		
TUBE	(3)	(303,3)	(402,3)	(1)	(3)
R	(3)	(0)	(100)		
TUBE	(3)	(603,3)	(702,3)	(1)	(4)
R	(4)	(0)	(100)		
TUBE	(3)	(301,1)	(404,1)	(1)	(3)
R	(3)	(0)	(100)		
TUBE	(3)	(601,1)	(704,1)	(1)	(4)
R	(4)	(0)	(100)		
TUBE	(3)	(307,1)	(404,1)	(1)	(3)
R	(3)	(0)	(100)		
TUBE	(3)	(607,1)	(704,1)	(1)	(4)
R	(4)	(0)	(100)		
TUBE	(3)	(101,3)	(120,5)	(1)	(3)
R	(2)	(0)	(100)		
TUBE	(3)	(202,3)	(120,5)	(1)	(3)
R	(2)	(0)	(100)		
TUBE	(3)	(103,3)	(121,5)	(1)	(3)
R	(2)	(0)	(100)		
TUBE	(3)	(202,3)	(121,5)	(1)	(3)
R	(2)	(0)	(100)		
TUBE	(3)	(101,1)	(122,1)	(1)	(3)
R	(2)	(0)	(100)		
TUBE	(3)	(204,1)	(122,1)	(1)	(3)
R	(2)	(0)	(100)		
TUBE	(3)	(107,1)	(127,1)	(1)	(3)
R	(2)	(0)	(100)		
TUBE	(3)	(204,1)	(127,1)	(1)	(3)
R	(2)	(0)	(100)		

END	MATE				
END	1	2..1E11	0.300		7850
	GEOM				
	1	TUBE	2.0	0.200	
	2	TUBE	4.0	0.250	
	3	TUBE	2.0	0.150	
END	4	TUBE	3.0	0.200	
	SUPP				

SYSTEM PRIME DATA AREA 100000
 JOB POST NMWB OUT4
 TITLE TRANSFER FUNCTION RUN
 STRUCTURE OUT3
 OPTIONS TRC4 NOBL END
 END
 SPECTRAL 1 11 12

WAVE	1	11	12
1	20.0	25.0	0.0000
2	20.0	13.33	0.0000
3	20.0	10.0	0.0000
4	14.08	8.00	0.0000
5	9.76	6.66	0.0000
6	7.17	5.71	0.0000
7	5.50	5.00	0.0000
8	4.34	4.44	0.0000
9	3.52	4.00	0.0000
10	3.19	3.81	0.0000
11	2.91	3.64	0.0000
12	2.74	3.53	0.0000
13	2.54	3.43	0.0000
14	2.40	3.30	0.0000
15	2.31	3.24	0.0000
16	2.20	3.16	0.0000
17	2.09	3.08	0.0000
18	1.93	2.96	0.0000
19	1.80	2.86	0.0000
20	1.57	2.67	0.0000

END FREQ 1 0.046 0.055 0.058 0.061 0.063 0.068
 1 0.073 0.079 0.086 0.110 0.130 0.227

END ELNO 1 65 65
 END SCFS 1 5.0 5.0 5.0 5.0 5.0 5.0
 END TUBEDFLT S-N 3.7E+08 1.0E+04 4.13
 END 1 SPEC 3.7E+08 1.0E+04 4.13

ACCG 9.81
 YEAR 30.0
 TRAN 1 1.0 2 1.0 3 1.0 4 1.0 5 1.0 6 1.0 7 1.0
 TRAN 8 1.0 9 1.0 10 1.0 11 1.0 12 1.0 13 1.0 14 1.0
 TRAN 15 1.0 16 1.0 17 1.0 18 1.0 19 1.0 20 1.0
 FIN PMOS 16.01 12.3 0.0000368
 PMOS 14.48 11.7 0.0000932
 PMOS 12.96 11.2 0.00037
 PMOS 11.43 10.4 0.0022
 PMOS 9.90 9.7 0.0073
 PMOS 8.38 9.0 0.0135
 PMOS 6.86 8.2 0.0265
 PMOS 5.53 7.3 0.06
 PMOS 3.81 6.5 0.21
 PMOS 2.28 5.5 0.49
 PMOS 0.76 3.1 0.19
 END EXEC STOP